Thèse de doctorat de l'Université de Paris

Ecole doctorale BioSPC 562

Unité Biochimie des Interactions Macromoléculaires,

Institut Pasteur

Study of the translocation mechanism of the CyaA toxin from *Bordetella pertussis*

Par Alexis VOEGELE

Thèse de doctorat de Biophysique et Biochimie

Dirigée par Alexandre Chenal

Présentée et soutenue publiquement à l'Institut Pasteur à Paris le 10 Octobre 2019

Présidente du jury : Prof. Dr. Claudine Mayer, Université Paris Diderot

Rapporteur : Prof. Dr. Holger Barth, Université d'Ulm

Rapporteur : Prof. Dr. André Matagne, Université de Liège

Examinatrice : Dr. Sonia Longhi, Aix-Marseille Université

Examinatrice : Dr. Marie Béatrice Valerio-Lepiniec, Université Paris Sud

Examinateur : Prof. Dr. Nicolas Rodriguez, Sorbonne Université

Directeur de thèse : Dr. Chenal Alexandre, Institut Pasteur

Except where otherwise noted, this work is licensed under
http://creativecommons.org/licenses/by-nc-nd/3.0/

Acknowledgments

Undertake a PhD has always been a personal achievement. I think that writing a thesis to sum up all your 3 years of research in different chapters is not easy but the most difficult one is the acknowledgments part. This thesis would not have been possible without the help of people that I would like to personally thank.

To the members of the jury

Thank you very much for accepting to judge this thesis and for the time you are going to spend reading it.

To Alexandre Chenal

My first acknowledgment goes to you Alexandre. What to say Alex … A thanks would not be enough. Your advices helped me a lot throughout the project. I appreciated you were always asking whether everything was ok during the PhD. Thank for your availability, to have always "5 minutes" at any moment of the day to discuss (even if we know that it does not last few minutes !!). I learnt a lot beside you and now I can say: yes Biophysic is quite cool !

To Daniel Ladant

Thank you for your availability, the (long) scientific discussions, I learnt a lot. Also I appreciated your reminders about each conference. You were right, our experiments are not more important than those of others!

To all the people of my lab

Dorothée, I appreciate that you spread good mood in the lab even if it is not a good day for everyone ! Спасибо Gouzel for your sense of humor and our "sportive discussions". Maryline, my office neighbor, thank for your sympathy. Bénédicte, thank for your help in the administrative work.

Thanks to all the BIM members who were here these 3 years: Undine, Flora, Federica, Zayed, Mélanie, Darragh, Gabrielle, Julia, Hazel, Alice, Sacha, Samantha, Louis-Antoine.

Collaborators

This thesis would not have been possible without the help a many collaborators on the project. I thank the people from the Biophysical platform. Sylviane Hoos, Bertrand Raynal, Sébastien Brulé, Bruno Baron and Patrick England, thanks for your help and advices on AUC, ITC and CD. A special thanks to Sébastien Brier, the HDX-MS expert. Thanks for you help throughout the project. To the crystallography platform. Patrick Weber, Ariel Mechaly and Ahmed Haouz, thanks for your help and your advices for obtaining the crystals! To the Mass Spectrometry platform. Thank you Mariette Matondo and Thibault Douché. I thank Frank Wien and Matthieu Refregiers from the DISCO beamline in the Synchrotron SOLEIL for the SRCD. Thank you to Dominique Durand and Patrice Vachette for the SAXS.

To my family

This work would not have been possible without all my family. My first thoughts go to my parents. Maman papa, thank you for always being here. Since the beginning, you always supported my choices and believed in me. I owe you everything. Without you, I would not be here doing a PhD and writing a thesis.

Finally, thank to all people not mentioned here but that contributed in this thesis.

Résumé de thèse

La coqueluche est une maladie très contagieuse qui affecte les voies respiratoires. Elle a une prévalence mondiale et peut toucher des personnes de tout âge, bien que les sujets à risque restent principalement les nourrissons. Elle est à l'origine d'environ 40 millions de cas et 300 000 décès par an, principalement dans les pays en voie de développement.

Sur le plan clinique, elle est caractérisée par des quintes de toux avec des reprises inspiratoires sifflantes, qui ressemblent au "chant du coq". La contamination s'opère par voies aériennes par contact direct avec une personne infectée. Puis la coqueluche se caractérise typiquement par trois phases:

- la période d'incubation peut durer de 1 à 3 semaines. A cette étape, la bactérie colonise l'épithélium de la trachée et des bronches. Cela bloque localement les cils vibratiles et permet la multiplication des germes ainsi que l'accumulation de mucus dans le tractus respiratoire. Cette phase est marquée par de la fièvre, un écoulement nasal, une toux qui sont caractéristiques d'une rhinorrhée. Les symptômes ne sont pas spécifiques et ne permettent donc pas de diagnostiquer une coqueluche.
- la seconde phase, la phase paroxysmale, peut durer plusieurs semaines. Elle est marquée par des quintes de toux incontrôlables qui surviennent plusieurs fois par jour. C'est principalement du à la forte production du mucus qui bloque le tractus respiratoire et empêche le malade de respirer. Les toux peuvent être accompagnées d'apnée, de cyanose et de vomissements.
- la dernière phase, la convalescence, dure quelques semaines. Les quintes deviennent de moins en moins fréquentes et intenses, avec un retour à la normalité.

Les premiers vaccins contre la coqueluche dans les années 1940, puis la nouvelle génération dans les années 1980, ont permis de réduire considérablement l'incidence de la maladie. Actuellement le vaccin est tétravalent et est combiné avec la diphtérie, le tétanos et la poliomyélite (DTCP). Néanmoins, on constate une résurgence de la maladie, ce qui questionne sur les nouvelles stratégies de vaccination à aborder (Domenech de Celles et al., 2018)

Bordetella pertussis est l'agent éthologique de la coqueluche. La bactérie a été isolée en 1906 par Jules Bordet et Octave Gengou. C'est une petite bactérie Gram-négatif, aérobie d'environ 0,8 µm sur 0,4 µm. C'est une bactérie stricte de l'Homme avec aucun réservoir

connu. Elle est difficile à isoler et à cultiver car elle pousse sur un milieu particulier préparé à partir de sang enrichi.

B. pertussis produit de nombreux facteurs de virulence au cours de sa colonisation (Mattoo and Cherry, 2005). Les premières étapes de l'infection font intervenir des adhésines qui permettent l'adhésion au tractus respiratoire et la multiplication locale des bactéries. Les étapes suivantes font intervenir des toxines afin de provoquer une réaction inflammatoire en détruisant les cellules ciliées et l'accumulation de mucus. Parmi ces toxines, l'adénylcyclase (CyaA) correspond à l'un des principaux facteurs de virulence produit par la bactérie.

CyaA est une protéine de 1706 résidus avec deux régions principales. Le domaine catalytique (ACD) correspond aux 364 résidus N-terminaux et est responsable de l'activité adénylcyclase qui transforme l'ATP en AMPc. La région C-terminale, quant à elle, porte l'activité hémolytique et est indispensable pour la translocation de CyaA (Ladant and Ullmann, 1999). Ces deux activités sont indépendantes mais peuvent fonctionner en synergie pour l'intoxication de CyaA.

Le domaine C-terminal comporte plusieurs domaines (voir figure A) :

- Le domaine de translocation (TR, résidus 365 à 527) est indispensable pour la translocation de ACD.
- La région hydrophobe (HR, résidus 528 à 710) qui comprend cinq segments transmembranaires permettant l'insertion de la toxine ainsi que son activité de perméabilisation.
- La région d'acylation (AR, résidus 711 à 1005) possède deux modifications post-traductionnelles indispensables pour l'insertion et la translocation.
- Le domaine de liaison au récepteur (RD, résidus 1006 à 1706) qui lie le récepteur cellulaire. Ce domaine est composé d'environ 40 motifs RTX (Repeat in ToXin) impliqués dans la liaison au calcium.

Le mécanisme d'intoxication de CyaA sur les cellules cibles est unique parmi toutes les toxines connues. Ce processus est illustré dans la figure B. Après production par *B. pertussis*, CyaA subit deux modifications post-traductionnelles (acylations) par CyaC. La toxine est transportée à travers la membrane de la bactérie par un système de sécrétion spécifique de type I. Dans le milieu extracellulaire, CyaA lie le calcium lui permettant de se replier et d'être compétente pour lier les cellules eucaryotes par l'intermédiaire du récepteur

CD11b/CD18 exprimé par une population de leucocytes (bien que CyaA peut aussi intoxiquer des cellules ne possédant pas le récepteur). Puis la toxine s'insère dans la membrane plasmique et transloque son domaine catalytique dans le cytoplasme de la cellule cible. ACD lie son effecteur cellulaire, la calmoduline (CaM), et produit des quantités supra-physiologiques d'AMPc. Cette surproduction d'AMPc affecte les cellules immunitaires en inhibant la phagocytose, le chimiotactisme et le stress oxydatif. Cela peut aussi causer directement la mort cellulaire par apoptose ou nécrose. Par conséquent, la réponse immunitaire locale est modifiée et permet à la bactérie de se développer. CyaA est donc une toxine essentielle de *B. pertussis* pour sa défense contre l'hôte et assurer la colonisation du poumon.

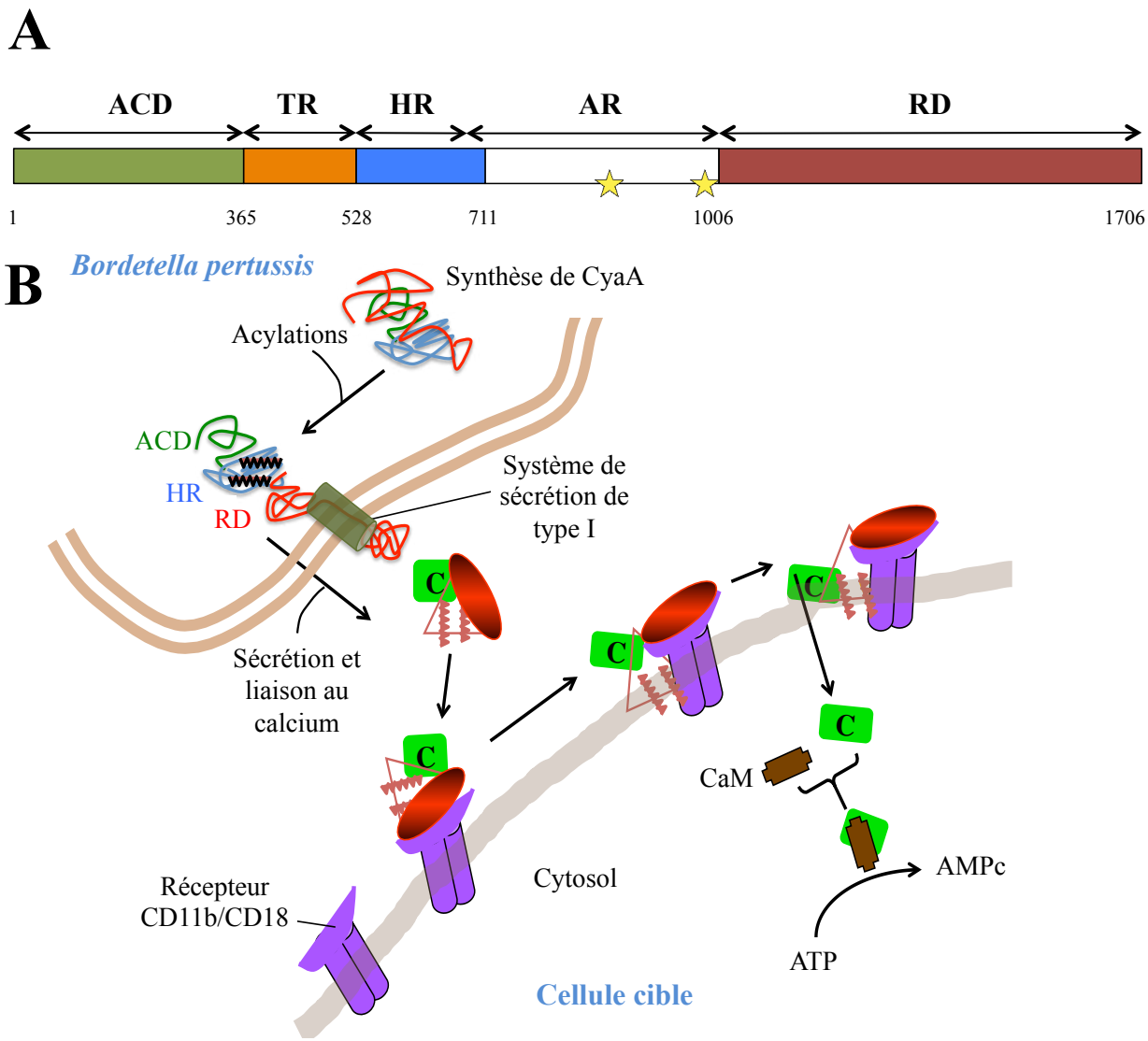

Figure: (**A**) Organisation structurale de CyaA. Les nombres représentent les résidus et les étoiles les deux modifications post-traductionnelles. ACD: domaine catalytique; TR: domaine de translocation; HR: région hydrophobe; AR: région d'acylation; RD: domaine de liaison au récepteur. (**B**) Modèle du mécanisme d'intoxication de CyaA. Voir le texte pour plus de détails.

Ce mécanisme de translocation est unique mais malheureusement peu décrit. Au cours des études réalisées sur CyaA, plusieurs mécanismes furent proposés. En 1992, Rogel et Hanski affirmaient que CyaA, *via* son activité hémolytique, pouvait créer un pore dans lequel transloquerait le domaine catalytique (Rogel and Hanski, 1992). Mais le diamètre du pore semble trop étroit pour le passage de ACD et les mutants de CyaA n'ayant pas d'activité hémolytique pouvaient toujours transloquer à travers les cellules. En 2010, Bumba et ses collègues ont proposé un nouveau model basé sur leurs études. Ils proposaient qu'après liaison avec son récepteur, CyaA s'insèrerait et déstabiliserait la membrane pour permettre le passage de calcium et le clivage du complexe CyaA-récepteur à la membrane. Puis le complexe irait dans les rafts lipidiques riches en cholestérol pour permettre la translocation (Bumba et al., 2010). Mais ce modèle n'explique pas comment CyaA peut transloquer dans des cellules dépourvues du récepteur. Récemment, Gonzalez-Bullon et ses collègues ont proposé un nouveau modèle. Ils ont reporté que CyaA possédait une activité phospholipase lui permettant de modifier localement la membrane pour former un pore dans lequel passerait le domaine catalytique (Gonzalez-Bullon et al., 2018, 2017). Mais ces résultats ont été contestés par une autre équipe et notre laboratoire a aussi démontré que CyaA ne possédait aucune activité phospholipase. Ainsi, le mécanisme permettant la translocation de CyaA reste encore mal connu.

En 2012, notre laboratoire a démontré qu'une délétion des résidus 375 à 485 dans CyaA abolit complètement la translocation du domaine catalytique sans affecter la liaison de la toxine ni son activité hémolytique (Karst et al., 2012). Cette région fut renommée le domaine de translocation et est indispensable pour la translocation de CyaA (TR, résidus 365 à 527). Des études supplémentaires ont permis d'identifier dans cette région le peptide P454 (résidus 454 à 484 de TR). Ce peptide a la capacité de lier les membranes, d'adopter une conformation en hélice α et aussi de déstabiliser et perméabiliser les membranes (Subrini et al., 2013). Ainsi un nouveau mécanisme fut proposé : après liaison à son récepteur et insertion dans la membrane, le peptide P454 pourrait interagir avec la membrane et la déstabiliser localement ce qui permettrait au domaine catalytique de transloquer. Néanmoins, beaucoup de détails moléculaires restent encore peu compris sur l'implication de P454 dans le mécanisme de translocation.

Les principaux travaux de cette thèse ont eu pour objectif de mieux comprendre le mécanisme d'intoxication de CyaA.

RESULTATS

Revue I – Le calcium est central pour la sécrétion et le repliement de la toxine CyaA de *Bordetella pertussis*, l'agent de la coqueluche.

Le domaine RD de CyaA en C-terminal (résidus 1006 à 1706) possède une quarantaine de motifs RTX qui sont impliqués dans la liaison au calcium. Le calcium est un élément crucial pour la toxicité de CyaA. Cette revue résume les récents résultats obtenus sur l'implication du calcium pour la sécrétion, le repliement et l'intoxication de CyaA.

En absence de calcium, RD possède toutes les caractéristiques d'une protéine déstructurée. En revanche, l'addition de calcium induit une stabilisation et le repliement de RD. Il est proposé que cette instabilité facilite la sécrétion de RD à travers le système de sécrétion de type I de la bactérie. La présence de calcium en extracellulaire favorise le repliement, empêchant le retour de la toxine dans la bactérie et permettrait aussi le transport du reste de la toxine.

CyaA est une protéine hydrophobe qui s'agrège et qui doit donc être conservée en présence de chaotropes. Récemment, le laboratoire a mis en place un protocole permettant d'obtenir une forme monomérique et repliée de CyaA sans chaotrope. Des études fonctionnelles ont démontré que la forme monomérique de CyaA peut hémolyser les cellules en absence de calcium libre dans le milieu mais que la translocation du domaine catalytique est dépendante de la présence calcium libre dans le milieu.

Article II – Les acylations contrôlent le repliement et les fonctions de la toxine CyaA

CyaA possède deux acylations sur les résidus lysine 860 et 983 qui sont requises pour sa translocation. Dans cet article, nous avons étudié l'effet de ces acylations sur les propriétés hydrodynamiques et structurales de CyaA et proCyaA (*i.e* CyaA sans acylation) pour comprendre comment l'acylation contribue au repliement vers un état fonctionnel de la toxine.

Nous avons d'abord caractérisé les préparations de CyaA et proCyaA par spectrométrie de masse. CyaA est acylée sur les deux lysines par différentes chaines acyles (principalement acide palmitique C16:0 et palmitoléique C16:1, avec quelques traces

d'acide myristique C14:0) alors que proCyaA est dépourvue d'acylation. Les études fonctionnelles sur érythrocytes (*i.e* hémolyse et translocation) ont montré que CyaA peut hémolyser les cellules et transloquer son domaine catalytique alors que proCyaA n'en a pas la capacité.

Par la suite, par fluorescence et ultracentrifugation analytique, nous avons montré que proCyaA est moins compacte que CyaA avec des régions hydrophobes exposées au solvant.

Pour caractériser le repliement progressif de CyaA et proCyaA, nous avons réaliser des expériences de HDX-MS (pour échange hydrogène/deutérium suivi par spectrométrie de masse) en conditions dénaturantes (*i.e* en présence d'urée). Nous avons observé qu'en absence de calcium, les deux protéines restent totalement dépliées alors qu'elles acquièrent de la structure de leur extrémité C- à N-terminale en présence de calcium. Cependant, des différences significatives sont observées dans les domaines HR et AR entre CyaA et proCyaA en présence de calcium. Nous constatons notamment que les peptides entre les résidus 798 à 958 (*i.e* dans AR) sont plus accessibles et moins repliés dans proCyaA. De plus, dans la région hydrophobe HR, le segment de 660 à 710 semble jouer un rôle central dans le repliement.

Pour résumer, le calcium est crucial pour le repliement de tous les domaines de CyaA. On propose qu'après sécrétion de CyaA, RD lie le calcium et permet le repliement successif des domaines de CyaA. Les acylations jouent aussi un rôle important dans le repliement. Les acylations favorisent l'interaction des régions hydrophobes entre les résidus 660-710 de HR, permettant un repliement plus rapide des régions AR et HR.

Article III – La toxine adénylcyclase (CyaA) de *Bordetella pertussis* n'a pas d'activité phospholipase (PLA) *in vitro*

Le mécanisme de translocation du domaine catalytique de CyaA reste encore peu décrit. Récemment, Gonzalez-Bullon et ses collègues ont proposé que CyaA possède une activité phospholipase (PLA) qui permettrait la formation d'un pore dans la membrane et le passage du domaine catalytique (Gonzalez-Bullon et al., 2018, 2017). Mais ces résultats furent contestés par une autre équipe qui affirme que CyaA ne possède aucune activité PLA (Bumba et al., 2018). Le but de cet article était de clarifier cette controverse à propos de l'activité PLA de CyaA.

Nous avons d'abord analysé les contaminations de la préparation de CyaA de notre laboratoire et de celle utilisée par Gonzalez-Bullon (aimablement fournie par Helena Ostolaza). Les 2 préparations étaient dépourvues de phospholipases provenant de *E. coli*.

Par la suite, nous avons évalué l'activité PLA de CyaA par fluorescence en utilisant des sondes spécifiques. La crotoxine, une toxine avec une activité PLA démontrée produite par un serpent, a été utilisée comme témoin positif. Les résultats obtenus ont clairement démontré que CyaA ne possède aucune d'activité PLA *in vitro* et que donc cette activité ne contribue pas à la translocation du domaine catalytique.

Revue IV – Translocation et activation par la calmoduline de la toxine adenylcyclase (CyaA) de *Bordetella pertussis*

À ce jour, CyaA est la seule toxine capable de transloquer son domaine catalytique (ACD) à travers la membrane plasmique. ACD lie ensuite la calmoduline (CaM) et produit une grande quantité d'AMPc qui conduit à la mort de la cellule. Nous avons récemment identifié le peptide P454 qui possède la capacité de lier et déstabiliser les membranes. Cette revue résume les données obtenues dans le laboratoire sur l'activité membranaire de P454 et l'activation d'ACD par la CaM. Ces résultats sont décrits plus en détails dans les articles V et VII.

Nous avons d'abord étudié les propriétés membranaires de P454. Nous avons observé que P454 était le seul peptide amphitropique de CyaA ayant la capacité de déstabiliser les membranes. Cette interaction avec les membranes est favorisée par des lipides insaturés et chargés négativement. Nous nous sommes aussi intéressés à l'implication de ses deux résidus arginine (R461 et R474). Nous avons observé que les deux résidus participent à l'interaction avec la membrane, que R474 participe au repliement et que R461 est important pour le processus de perméabilisation.

Une fois transloquée, ACD lie la CaM. Par différentes approches biophysiques, nous avons observé que ACD possède une région désordonnée de 75 résidus qui acquiert de la structure induite par la liaison à la CaM. Cette liaison contribue à des réarrangements locaux et allostériques qui permettent la stabilisation et l'activation du domaine catalytique.

Article V – Activités membranaire d'un peptide amphitropique de la région de translocation de la toxine de CyaA

Il a été démontré que la région allant des résidus 384 à 489 de CyaA était cruciale pour la translocation du domaine catalytique. Cette région fut nommée la région de translocation (TR, résidus 365-527). Dans cette région, le peptide P454 (résidus 454 à 484 de CyaA) a été identifié et possède la capacité de lier les membranes, se replier en hélice α au contact des membranes et de les perméabiliser. L'objectif de cet article était de caractériser les propriétés de P454 et de discuter de son rôle dans le processus de translocation de CyaA.

Nous avons d'abord étudié les propriétés de 11 peptides amphitropiques prédits pour s'insérer dans la membrane. Parmi ces 11, seulement 6 ont la capacité de lier et se replier en hélice α au contact de membranes. Néanmoins, seul P454 a la capacité de déstabiliser les membranes, ce qui suggère qu'il pourrait jouer un rôle dans la déstabilisation de la membrane pour l'intoxication de CyaA. Nous nous sommes donc intéressés de plus près aux propriétés de P454.

Tout d'abord, nous avons étudié l'effet du polymorphisme lipidique sur la capacité d'insertion de P454 dans les membranes. La présence de lipides favorisant la rigidité membranaire ainsi qu'une courbe négative (*i.e* invagination de la membrane) diminuent l'interaction de P454. En revanche, l'insertion de P454 est favorisée par les lipides anioniques et les lipides conférant de la fluidité aux membranes.

Nous nous sommes ensuite intéressés à la contribution des deux résidus arginines (R461 et R474) de P454. Une littérature importante indique que les arginines sont cruciales pour l'interaction et la déstabilisation membranaire. Nous les avons substitués par diffèrents acides aminés (lysine, alanine, glutamine et glutamate). Les résultats ont montré que l'interaction de P454 avec les membranes est favorisée par les forces hydrophobes et les interactions électrostatiques. Par ailleurs, les deux arginines participent distinctement à cette interaction. Concernant le repliement du peptide en hélice α, on a constaté que la substitution de R474 affecte le repliement du peptide. Nous proposons donc que cette arginine participe activement au repliement du peptide lorsqu'il interagit avec les membranes. Enfin, nous avons étudié le phénomène de perméabilisation et constaté que la substitution de R461 diminue considérablement sa capacité de déstabilisation membranaire.

Nous proposons que cette arginine soit activement impliquée dans le processus de perméabilisation.

En résumé, P454 est le seul peptide amphitropique de CyaA testé capable à la fois de s'insérer, se replier et déstabiliser les membranes. Son interaction est favorisée par des lipides dont les chaines acyles sont fluides et les têtes polaires anioniques. Les deux arginines de P454, R461 et R474, permettent l'interaction avec la membrane, avec R474 impliquée pour le repliement et R461 pour la déstabilisation membranaire. Nous proposons que le peptide P454 de la région de translocation pourrait s'insérer dans la membrane et localement la déstabiliser, ce qui permettrait au domaine catalytique de transloquer.

Article VI – Couplage des propriétés d'activité membranaire et de liaison à la CaM pour une délivrance efficace de la toxine CyaA dans les cellules

P454 partage des caractéristiques avec les AMPs (pour Peptides AntiMicrobiens). En effet, ces peptides ont la capacité de lier et déstabiliser les membranes. Certains peuvent aussi transloquer à travers les membranes pour y lier une cible intracellulaire. P454 possède des similarités avec les peptides liant la CaM et lie en effet la CaM. Cet article a pour objectif de caractériser l'interaction de P454 avec la CaM et d'étudier si la formation de ce complexe contribue à la translocation du domaine catalytique. Ces résultats sont discutés dans le contexte de la translocation de CyaA et nous ont permis de proposer mécanisme de translocation.

Nous avons d'abord caractérisé le complexe P454:CaM par différentes approches (ITC, SRCD, AUC). P454 lie la CaM avec un ratio 1:1 et une affinité de 90 nM à 25°C. Nous avons ensuite déterminé si la CaM pouvait extraire le peptide de la membrane, pour mimer l'apparition de P454 dans le cytosol. A partir des données de fluorescence et de perméabilisation, on constate que la CaM peut extraire P454 seulement en présence de calcium dans le milieu.

Notre second objectif était de démontrer que P454 pouvait transloquer à travers les membranes. Les expériences ont démontré que P454 transloque seulement si la CaM est présente de l'autre coté de la membrane. En revanche, l'hélice H (résidus 233-254 de CyaA), correspondant au segment liant la CaM dans ACD, n'a pas la capacité de transloquer dans les mêmes conditions.

La structure cristallographique du complexe P454:CaM a été obtenue. Elle montre que la partie N-terminale du peptide lie la partie C-terminale de la CaM et que la partie C-terminale du peptide lie la partie N-terminale de la CaM. Les structures indiquent que la CaM est dynamique et adopte différentes conformations. Cette diversité structurale est aussi retrouvée en SAXS. Les données SAXS du complexe H:CaM révèlent une conformation différente de la CaM comparé au complexe P454:CaM. Ces résultats montrent que, bien que P454 et l'hélice H lient la CaM, ils adoptent une conformation différente avec la CaM.

Nous avons identifié les acides aminés de P454 importants pour ses activités membranaires et de liaison avec la CaM. Ces résidus ont été mutés dans le segment P454 de CyaA. Les activités fonctionnelles (hémolyse et production d'AMPc) ont révélé que ces résidus sont essentiels pour la translocation de ACD. Ces résultats suggèrent que la formation du complexe P454:CaM favorisent la translocation de ACD.

Pour finir, nous avons réalisé le modèle structural de AC489 (résidus 1 à 489 de CyaA, contenant l'hélice H et le segment P454) avec la CaM. Les expériences HDX-MS montrent qu'une seule CaM peut à la fois lier l'hélice H et le segment P454. Les données de SAXS ont permis de modéliser le complexe AC489:CaM conformément aux données HDX-MS. On propose que la partie C-terminale de la CaM lie l'hélice H alors que la partie N-terminale lie le segment P454.

Tous ces résultats nous ont permis de proposer un modèle de translocation. Après insertion de la toxine dans la membrane de la cellule cible, le segment P454 de la région TR lie la membrane et la déstabilise localement pour transloquer. Après translocation, la CaM intracellulaire piège P454 dans le cytosol de la cellule. La formation de ce complexe agit comme une force tirant et permettant le passage du domaine catalytique à travers la membrane. Puis, lorsque l'hélice H de ACD se retrouve à sont tour dans le cytosol, elle lie la CaM, permettant l'activation du domaine catalytique (voir article VII pour plus de détails).

Article VII – La pêche à la calmoduline avec un appât structuralement désordonné active la catalyse de CyaA

Lorsque ACD est transloqué, il lie la CaM et produit de grande quantité d'AMPc conduisant à la mort de la cellule. En 2005, Guo et ses collègues ont obtenu la structure de ACD avec la partie C-terminale de la CaM (Guo et al., 2005). Néanmoins, comment la CaM

active ACD restait peu compris. Cet article a pour objectif de décrire comment la CaM régule et active ACD.

Par différentes méthodes biophysique (SAXS, SRCD et HDX-MS), nous avons constaté que la partie N-terminale de ACD (résidus 1-224) est repliée. Au contraire, la région C-terminale (résidus 225-364) est principalement dépliée avec un segment d'environ 75 résidus complètement désordonné. Ces résultats étaient inattendus car, dans la structure cristalline, cette région désordonnée est hélicale et correspond au principal contact entre ACD et la CaM. Ce contact a lieu *via* l'hélice H de ACD (résidus 233-254).

La CaM est une protéine flexible pouvant avoir différentes conformations. Elle adopte une forme "d'haltère" avec deux lobes reliés par une hélice centrale. En présence de l'hélice H, on constate que la forme globale de la CaM reste inchangée. Les données montrent aussi qu'environ 20 résidus du complexe acquièrent de l'hélicité lors de l'interaction. Les données HDX-MS affirment que liaison de l'hélice H n'induit aucune dynamique supplémentaire dans la CaM, ce qui veut dire que ce gain d'hélicité peut être attribuée à l'hélice H au moment de son interaction avec la CaM.

Finalement, le complexe ACD:CaM a été étudié par SAXS et HDX-MS. Nous observons que la partie N-terminale de ACD est stabilisée et que la région C-terminale se replie au contact de la CaM, notamment au niveau de la région de l'hélice H. Nous avons aussi observé les effets de la liaison de ACD sur la CaM. ACD stabilise la partie C-terminale de la CaM alors que la majorité de la partie N-terminale de la CaM n'est pas affectée.

En résumé, la région de 75 résidus désordonnée où se situe l'hélice H acquiert de la structure quand elle lie la CaM. Cette zone servirait d'appât pour la capture de la CaM pour le domaine catalytique dans le cytosol. La liaison permet la stabilisation et la réorganisation des segments adjacents et distants du site d'interaction ce qui permet la mise en place du site catalytique.

Table of content

Chapter I. Introduction 23

1. Whooping cough 25

1.1 Clinical symptoms 25

1.2 Diagnosis 26

1.3 Historical 27

1.3.1 Whooping cough over the centuries 27

1.3.2 Discovery of *Bordetella pertussis* 28

1.3.3 *Bordetella pertussis* 28

1.4 The genus *Bordetella* 30

1.4.1 *Bordetella parapertussis* 31

1.4.2 *Bordetella bronchiseptica* 32

1.4.3 *Bordetella holmesii* 32

1.4.4 *Bordetella avium* 32

1.4.5 *Bordetella hinzii* 33

1.4.6 *Bordetella pseudohinzii* 33

1.4.7 *Bordetella trematum* 34

1.4.8 *Bordetella petrii* 34

1.4.9 *Bordetella ansorpii* 34

1.4.10 *Bordetella muralis, tumulicola* and *tumbae* 34

1.4.11 *Bordetella bronchialis, flabilis* and *sputigena* 35

1.5 The BvgAS regulation system 35

1.6 Virulence factors 38

1.6.1 Adhesins 39

1.6.1.1 Filamentous hemagglutinin 39

1.6.1.2 Fimbriae 40

1.6.1.3 Pertactin 42

1.6.1.4 *Bordetella*-resistance-to-killing factor 43

1.6.1.5 Tracheal colonization factor 44

1.6.1.6 SphB1 44

1.6.1.7 Virulence-associated gene 8 44

1.6.2 Toxins 45

1.6.2.1 Lipopolysaccharide 45

1.6.2.2 Pertussis toxin 46

1.6.2.3 Tracheal cytotoxin 48
1.6.2.4 Dermonecrotic toxin 49
1.6.2.5 Adenylate cyclase toxin 50

Chapter II. The adenylate cyclase toxin (CyaA) from *Bordetella pertussis* 53
2. The adenylate cyclase toxin 55
2.1 Synthesis of the toxin CyaA 57
2.2 Primary structure of the CyaA toxin 59
2.2.1 The N-terminal catalytic domain 61
2.2.1.1 Structural comparison of ACD to EF and ExoY 65
2.2.2 The translocation region 68
2.2.3 The hydrophobic region 68
2.2.4 The acyl region 69
2.2.5 The receptor binding domain 73
2.2.6 The secretion signal 78
2.3 Secretion of the CyaA toxin 78
2.4 Binding of the CyaA toxin to the CD11b/CD18 receptor 81
2.5 The CyaA intoxication process 83
2.5.1 Parameters for the CyaA translocation 84
2.5.2 Translocation model 86
2.6 Hemolytic activity of the CyaA toxin 88
2.7 The CyaA toxin in vaccination 92
2.8 The CyaA toxin in biotechnology 93
2.8.1 Bacterial adenylate cyclase two-hybrid system 93
2.8.2 CyaA as a reporter for protein targeting 95
2.8.3 CyaA as a vehicle for antigen delivery 96

Chapter III. Bacterial toxin translocation in host cells 101
3. Bacterial toxins 103
3.1 Translocation from endosomal escape 107
3.1.1 Diphtheria toxin 108
3.1.2 Anthrax toxin 110
3.1.3 Botulinum neurotoxin 112
3.2 Endosomal reticulum escape 114
3.2.1 Cholera toxin 114

3.3 Forces involved in bacterial toxin translocation 115
3.3.1 Power stroke model 116
3.3.2 Brownian molecular ratchet model 117
3.3.3 Entropic pulling model 117
3.4 Identification of P454 in CyaA 118
3.4.1 P454 is an AMP-CPP-like peptide. 119
3.4.2 Antimicrobial peptides 120
3.4.3 Cell-penetrating peptides 122

Chapter IV. Aims of the doctoral thesis project 125

Chapter V. Experimental results 131

Review I. Calcium-dependent disorder-to-order transitions are central to the secretion and folding of the CyaA toxin of *Bordetella pertussis*, the causative agent of whooping cough 135

Article II. Post-translational acylation controls the folding and functions of the CyaA RTX toxin 147

Article III. The adenylate cyclase (CyaA) toxin from *Bordetella pertussis* has no detectable phospholipase (PLA) activity *in vitro* 181

Review IV. Translocation and calmodulin-activation of the adenylate cyclase toxin (CyaA) of *Bordetella pertussis* 197

Article V. Membrane-active properties of an amphitropic peptide from the CyaA toxin translocation region 211

Article VI. Coupling membrane-active and calmodulin-binding properties of the CyaA toxin translocation region for efficient delivery into cells 245

Article VII. Calmodulin fishing with a structurally disordered bait triggers CyaA catalysis 323

Chapter VI. Discussion & Perspectives 371

Chapter VII. Annex 387

Article. Bacterial kinesin light chain (Bklc) links the Btub cytoskeleton to membranes 391

Chapter VIII. Bibliography 405

Chapter I.

Introduction

Chapter I. Introduction

1. Whooping cough

Whooping cough, also named pertussis, is a highly contagious respiratory tract infection caused by *Bordetella pertussis*, a Gram-negative bacterium. It is a worldwide disease, which can infect people of any age. Nevertheless, the majority of cases and death is observed in early childhood (infancy). Whopping cough is one the most infectious diseases causing death. In fact, World Health Organization (WHO) has reported that whooping cough causes up to 40 million cases per year with about 300 000 deaths, mainly in underdeveloped countries having no access to vaccine. However, these numbers are underestimated because not all countries have implemented surveillance.

1.1 Clinical symptoms

Whopping cough is characterized by three main clinical phases. During the incubation period (also called the catarrhal phase), which can last from 7 to 21 days, *B. pertussis* colonizes the tracheal epithelium. It blocks and damages the cilia function, allowing the multiplication of germs and the accumulation of mucus in the respiratory tree. Loss of consciousness, rhinorrhea, watery eyes and cough mainly characterize this phase. At this early stage, the symptoms are close to common problems (such as upper respiratory infections or bronchitis) and do not allow the correct diagnosis of whooping cough.

The second phase, called the paroxysmal phase, is typically characterized by prolonged and uncontrollable cough episodes, followed by many hours without symptoms. This is mainly due to the overproduction of mucus that blocks the respiratory tract and prevents the patient from breathing. Patients are gasping for air and this gives rise to the characteristic “whoop” sound with 15 to 30 attacks per day. During the first two weeks of this phase, the attacks increase gradually and then remain at the same level for two to three weeks. The paroxysmal stage may usually persist for 6 weeks (up to 10). The cough can be accompanied

of vomiting and apnea or cyanosis episodes, especially in infants. Others clinical signs such as leukocytosis, lymphocytosis, weight loss might be observed (Kerr and Preston, 2001).

At this phase, *B. pertussis* triggers a disruption of the cellular function with the release of toxins, creating a local inflammation. It results in an overproduction of mucus, which, by cough episodes, eliminates cell debris and bacteria.

Moreover, serious clinical complications linked to this disease are observed in infants including otitis, convulsions, brain damage and stroke due to rupture of small blood vessels (see Figure 1) (Litvak and Gibel, 1948).

The last phase consists in a convalescent phase, lasting 1 to 3 weeks, characterized by a persistent but continuous decline of the cough before the patient returns to normality.

In the end, the whooping cough may last up to 100 days, also known as “100-day cough”.

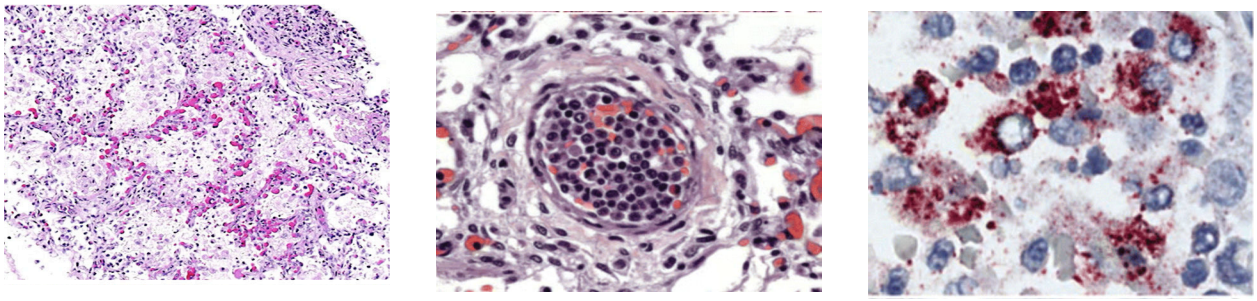

Figure 1. Left : Lung tissue from a patient with *Bordetella pertussis* infection, showing intra-alveolar infiltrates comprised predominantly of macrophages and neutrophils accompagnied by fibrin and necrotic debris. Hematoxylin and eosin stainings. Magnification ×100. Middle : Aggregates of mixed leukocytes in pulmonary arterioles. Hematoxylin and eosin stainings. Magnification ×100. Right : Abundant intra- and extracellular bacteria in alveolar infiltrates. Magnification ×158. From (Paddock et al., 2008; Tatti et al., 2006).

1.2 Diagnosis

Usually, clinical symptoms are sufficient to diagnose a whopping cough. As such, its diagnosis is expected to be simple but this is not the case. Only laboratory exams can bring a clear diagnosis and allow for the prophylaxis of the infection. One is the serology of the patient with a characteristic hyperleukocytosis and overproduction of antibodies against *B.*

pertussis toxins. Bacteria culture was the reference technic to detect the bacterium but it was needed to be rapidly done because *B. pertussis* only remains in the nasopharynx area the first 3 weeks after infection. For the genus *Bordetella*, the specific real-time polymerization chain reaction (PCR) remains by far the most sensitive, faster and practiced technic (with the same biological samples used for cultures), although a cross-reaction with others species might occur with the primers used.

1.3 Historical

1.3.1 Whooping cough over the centuries

The history of whopping cough is quite short. The first occurrence of the disease is unknown and has never been mentioned in Greek and Roman civilizations. Hippocrates describes in his book 7 some cases of people suffering for weeks of a "viscous, white and thin cough with a pain in their lower right belly", pus-like, typical symptoms of the clinical manifestations of whooping cough.

We owe the first authentic clinical description of whooping cough to Guillaume de Baillou in 1578 during an outbreak in France, who called it "*Tussis quinta*" (Lapin, 1943). Subsequently, in 1682, Willis individualized the disease, which many outbreaks appeared and were described in Europe during the XVIIIth and XIXth centuries. In the XIXth century, the precise descriptions of sick child by J.M. Goupil and A. Trousseau along with the discovery of the pertussis agent at the beginning of the XXth century helped to develop strategies. The advent of both antibiotics and vaccination has then greatly reduced the epidemics and mortality rates.

Currently, since 2010, the disease has shown a worrying upsurge in some developed countries that have full access to vaccines. It is mainly due to the asymptomatic transmission, the decrease in vaccine coverage and the incomplete coverage of current vaccines caused by emerging mutant strains (van Gent et al., 2012; Mooi et al., 2001). It has been also noted that the contagion has changed mainly due to lack of vaccination recall. Indeed, the transmission is no longer horizontal (child to child), as during the pre-vaccine era, but vertical (adolescent, adult to child), obliging to change the vaccination strategy.

1.3.2 Discovery of *Bordetella pertussis*

The causes of whooping cough were diverse: people were thinking that it was caused, for examples, by an "acrid matter that irritates lungs" or "bugs introduced in the respiratory tract". However, the agent of whooping cough is a bacterium, first observed in 1900 by Jules Bordet and Octave Gengou on a 5-month child. It was then isolated in 1906 from an extract of the own son of Jules Bordet, Paul, who had contracted whooping cough. They first though it belonged to *Hæmophilus* species, although the bacterium does not need the growth factors V (nicotinamide adenine dinucleotide, NAD) and X (haematin). Thus, the germ was called *Hæmophilus pertussis* until 1952 and then *Bordetella pertussis* in tribute to Jules Bordet (Moreno Lopez, 1990).

1.3.3 *Bordetella pertussis*

B. pertussis is a strict human pathogen with no known reservoir. It is small, Gram-negative, aerobic and immobile coccobacilli bacterium ranging from 0.5-1 µm by 0.2-0.5 µm. *B. pertussis* is particularly difficult to isolate and cultivate. It only grows on a special media called the "Bordet-Gengou medium" (see Figure 2), made of blood-rich media (a mix of salts, potato, agar and sheep blood).

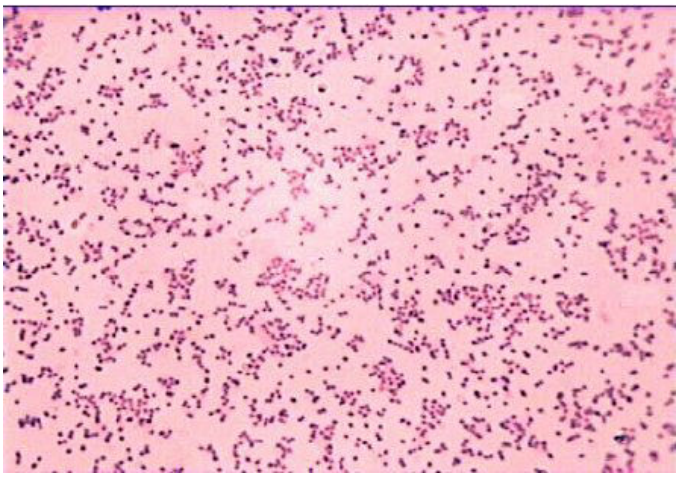

Figure 2. Microscopy view of *Bordetella pertussis* strain 134 with Gram-staining cultivated on charcoal blood agar plates at 35°C. Magnification ×1000. Adapted from (Aminian et al., 2007).

Treatments, aiming at shortening the disease, are based on antibiotics such as Erythromycin. However, some patients do not tolerate it very well and alternative antibiotics such as Azithromycin or Clarithromycin might be employed. The antibiotics are only effective during the incubation phase (phase I). A treatment beginning after the paroxysmal phase (phase II) has no effect on the cough evolution, but decreases the contagiousness by killing any remaining bacteria. Nowadays, the treatment is not totally efficient. Vaccination remains the only way to control whooping cough.

In the years after the isolation, several pertussis vaccines were developed in the XXth century. In the 1940s, the first one contained heat-killed bacteria (whole-cell vaccine, Pw). It was introduced in France in 1959 (under the name Vaxicoq®) and has shown to be very effective (more than 90% of protection) but often responsible for complications (World Health Organization, 2015). Thus, the research performed around *B. pertussis* and its virulence factors allowed for the replacement of the Pw by an acellular vaccine (Pa) in the 1980s that is better tolerated. Pa is pentavalant and contains the pertussis toxin, filamentous hemagglutinin, frimbriae (types 2 and 3) and pertactin. Pa vaccines are combined with diphtheria and tetanus ones and they have shown a protection around 85% (Sealey et al., 2016; Gabutti et al., 2015). This strategy led to a decrease in morbidity and mortality in vaccinated area. Recently, the resurgence of whooping cough raised many questions about the strategy of vaccination. Researchers call this phenomenon the "end of the honeymoon". Concretely, the vaccination has been effective over the years but incomplete. A new strategy of vaccination has to be considered (Domenech de Celles et al., 2018).

The Pa vaccines contain few toxins and adhesins from *B. pertussis* but not the adenylate cyclase (CyaA) toxin, one of the major virulence factor produced during infection and colonization (Ladant and Ullmann, 1999). CyaA is large protein exhibiting a pronounced hydrophobic character, which leads to its aggregation in multimeric forms. Thus, it imposes to extract and store CyaA in denaturing conditions (such as urea and guanidine hydrochloride), not convenient to formulate CyaA as a protective antigen. Recently, a new refolding approach based on molecular confinement on size exclusion chromatography system has permitted to generate a fully-folded, monomeric and active CyaA form in denaturant-free conditions (Karst et al., 2014). Furthermore, monomeric CyaA suggests to be the physiologically form of the active toxin. This advance would allow adding CyaA as a new protective antigen in Pa vaccines and thus increase the vaccination coverage against whooping cough.

Recently, monomeric CyaA has shown to be antigenic on Camelidae. This result paves the way to formulate CyaA as a protective antigen in a new Pa vaccine and also for *pertussis* diagnostic. These results are further discussed in part 2.7.

1.4 The genus *Bordetella*

B. pertussis belongs to the genus *Bordetella*, defined in 1952 by Manuel Moreno-Lopez in tribute to Jules Bordet (Moreno Lopez, 1990). The taxonomy of this genus was undecided until 1986. It was though that *Bordetella* belonged to multiples families (*Acinetobacter*, *Alcaligenes*, *Bacterium*, *Bacillus*, *Brucella* and *Haemophilus*) (Pittman and Wardlaw, 1981; Goodnow, 1980). Genetically, the genera *Bordetella* is related to *Alcaligenes* and is now regrouped in a new family called *Alcaligenaceae* (De Ley et al., 1986).

Bordetella species are important in veterinary and human medicine due to their ability to colonize and cause pulmonary infections. Up to now, nine different *Bordetella* species have been identified (see Figure 3). Recently, six new potential strains were proposed to be added and to belong to the genus *Bordetella* (Tazato et al., 2015; Vandamme et al., 2015). Among all of the species, three are closely related and highly studied, referred to as the classical *Bordetella* species: *B. pertussis*, *B. parapertussis* and *B. bronchiseptica*. These strains are genetically close, sharing from 73% to 85% of their DNA, indicating that these species may originate from a single same specie (Kloos et al., 1981). Genome comparisons (Diavatopoulos et al., 2005) and phylogenetic analysis (Musser et al., 1986) have shown that *B. pertussis* and *B. parapertussis* have evolved independently from a *B. bronchiseptica* ancestor. They have also in common many virulence factors and a similar regulatory system (*i.e* the BvgAS two component system, described later in part 1.5).

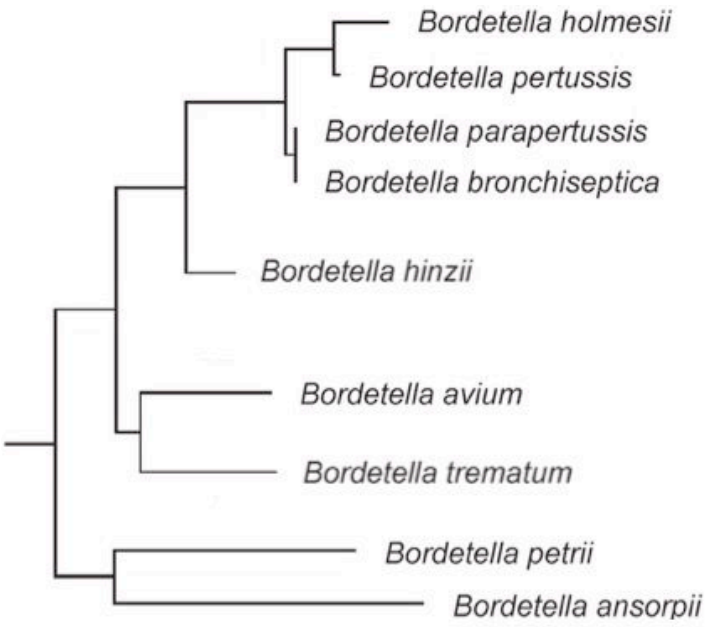

Figure 3. Phylogenetic tree of nine bacteria from genus *Bordetella* using the alignment of the 16S rRNA gene. Adapted from (Jiyipong et al., 2013).

1.4.1 *Bordetella parapertussis*

B. parapertussis was first described in 1937 (Eldering and Kendrick, 1938; Bradford and Slavin, 1937). It can cause a pertussis-like illness with middle symptoms and a less long disease. The concomitant infection with *B. pertussis* is common, which introduces difficulties to establish its clinical course. Several studies have shown a significant increase in the prevalence of *B. parapertussis* due to the failure of cross-protection by Pa vaccines (Lavine et al., 2010; Zhang et al., 2009a, 2009b). The treatments remain the same as *B. pertussis* and shorten illness duration but *B. parapertussis* evinces antibiotics resistance (Syed et al., 2016). *B. parapertussis* was thought to be a human-adapted form only until 1987 when it was detected in sheeps, causing a non-progressive pneumonia (Porter et al., 1994; Cullinane et al., 1987). Then, the discussion about zoonosis was studied and showed that *B. parapertussis* are divided in two distinct clusters, one infecting humans and another infecting ovine (Yuk et al., 1998; van der Zee et al., 1996; Porter et al., 1996). These strains come from clonal lineages that have evolved independently from *B. bronchiseptica* (van der Zee et al., 1997).

1.4.2 *Bordetella bronchiseptica*

B. bronchiseptica was first identified and isolated in 1910 as *Bacillus bronchicanis* (Ferry, 1912). It is a pathogen that infects the respiratory tree of a wide variety of wild and domestic animals. The symptoms caused can be different such as atrophic rhinitis in pigs, snuffles in rabbits and kennel cough in dogs. However, a majority of animals do not develop symptoms. In humans with a close contact of infected animals, it is seldom involved in pertussis-like disease but can occur on elderly, frail and immunocompromised patients. Compared to animals, where cross species infection of different strains can occur, *B. bronchiseptica* does not spread between humans (Woolfrey and Moody, 1991). Furthermore, actual vaccination or infection from *B. pertussis* confers immunity against *B. bronchiseptica*. This could explain the lack of transmission between humans and also infections with an immunocompromised state (Goebel et al., 2009). The comparative genome analysis has demonstrated that *B. pertussis* and *B. parapertussis* have evolved from a *B. bronchiseptica*-like ancestor. Then, the genome decay including translocation and loss of genes may explain the different host tropism (Parkhill et al., 2003).

1.4.3 *Bordetella holmesii*

B. holmesii was identified in 1995 as rare cause of bacteremia in immunosuppressed patients and lead also to arthritis, pneumonia, pericarditis, endocarditis and meningitis (Fishbain et al., 2015; Tang et al., 1998; Weyant et al., 1995). In healthy people, it is involved in pertussis-like symptoms and is often misidentified as *B. pertussis* during diagnosis (Dalby et al., 2013). Thus, epidemiological surveillance and diagnostic assays are crucial because *B. holmesii* adaptation to humans is continuing and virulence might increase (Pittet et al., 2014; Rodgers et al., 2013).

1.4.4 *Bordetella avium*

B. avium is responsible of coryza (rhinotracheitis), also called bordetellosis, in turkey poults and other birds (wild and domesticated ones), causing high morbidity and usually low mortality (Kersters et al., 1984; Filion et al., 1967). It infects the ciliated epithelium of the upper respiratory tract (Arp and Cheville, 1984). Its presence has a negative economic

impact on turkey farming, which causes a drop in their food intake and thus their gain weight. It was first identified as *Alcaligenes faecalis* (Simmons et al., 1980) but Hinz and colleagues considered it as a bacterium close to *B. bronchiseptica* (Hinz et al., 1978). Although *B. avium* shares features with *B. bronchiseptica*, the obtaining of the complete genome sequence of the strain 197N clearly demonstrated their phylogenic distance (see Figure 3) (Sebaihia et al., 2006).

It may be a rare opportunistic pathogen in humans. However, *B. avium* is now considered to be zoonotic since its discovery in people suffering from cystic fibrosis and underlying pulmonary diseases (Harrington et al., 2009; Spilker et al., 2008).

1.4.5 *Bordetella hinzii*

B. hinzii was first isolated in 1957 but misidentified as *Alcaligenes faecalis* type II (Vandamme et al., 1995). It was also referenced as *B. avium*-like, infecting the respiratory tract of turkeys and chickens but did not provide evidence of pathogenicity. *B. hinzii* is recognized as an opportunistic human pathogen in immunocompromised patients suffering from cystic fibrosis, AIDS, myelodysplastic syndrome, solid-organ transplants or Epstein-Barr virus (Hristov et al., 2008; Fry et al., 2007; Arvand et al., 2004; Coenye et al., 2002; Cookson et al., 1994). The zoonosis has never been demonstrated but aerosols from avian species reservoir or contaminated poultry products might be the source of transmission (Aude Fabre et al., 2015).

1.4.6 *Bordetella pseudohinzii*

As described before, *B. hinzii* normally infects poultry and humans but some *B. hinzii*-like strains were strictly identified in laboratory mice. Ivanov and al. (2016) proposed *B. pseudohinzii* as new a specific strain (Ivanov et al., 2016).

1.4.7 *Bordetella trematum*

Compared to others strains, which mainly infect the respiratory tract, *B. trematum* has been isolated from ear chronic and wounds infections in diabetic patients (Almagro-Molto et al., 2015; Daxboeck et al., 2004; Vandamme et al., 1996). *B. trematum* is just considered as an opportunistic pathogen because its infection is quite rare and does not necessarily require treatment.

1.4.8 *Bordetella petrii*

Among all *Bordetella* species, *B. petrii* is the only one to have an anaerobic respiration. Furthermore, it is the unique strain isolated from the environment, found in a bioreactor culture from river sediments (von Wintzingerode et al., 2001). *B. petrii* was anecdotally recovered in patients suffering from bones disease (Stark et al., 2007; Fry et al., 2005) and chronic pulmonary obstructive disease (Le Coustumier et al., 2011).

1.4.9 *Bordetella ansorpii*

B. ansorpii was recently described and isolated from a purulent exudate of a immunocompromised patient having of an epidermal cyst (Fry et al., 2007; Ko et al., 2005). It is thought to be an opportunistic strain. To date, only few data has been reported about *B. ansorpii* and its virulence.

1.4.10 *Bordetella muralis, tumulicola* and *tumbae*

Recently, new strains from a 1300-year-old mural paintings in Japan were identified (Tazato et al., 2015). Based on their gene sequence analysis, they belong to the genus *Bordetella*. These isolates are closely related to *B. petrii* at both the molecular and environmental levels and are separated into three new groups: *B. muralis, B. tumulicola* and *B. tumbae*.

1.4.11 *Bordetella bronchialis, flabilis* and *sputigena*

Over the years, with the number of respiratory samples strains from patients suffering of cystic fibrosis, researchers proposed to reclassify the taxonomy of some *Bordetella* strains (Spilker et al., 2014). Vandamme and colleagues suggest to classify four *B. hinzii*-like strains as three new genogroups: *B. bronchialis*, *B. flabilis* and *B. sputigena* (Vandamme et al., 2015).

1.5 The BvgAS regulation system

Diversity of extracellular environment plays an important role for bacterial defense, invasion and proliferation. In 1931, Leslie and Gardner showed that some *B. pertussis* strains lost their virulence capacities when cultivated *in vitro* (Leslie and Gardner, 1931). Then, in 1960, Lacey demonstrated that avirulent bacteria were observed at room temperature, in the presence of sulfate ions or nicotinic acid, calling this phenomena "phenotypic modulation" (Lacey, 1960). Genome studies allowed the identification of the *bvg* locus (for *Bordetella* virulence genes) involved in this modulation. It encodes for two proteins, BvgS and BvgA, belonging to a so-called two-component signal transduction cascade. It transduces extra and intracellular signals using a sophisticated four-step His-Asp-His-Asp phosphorelay (Uhl and Miller, 1996; Parkinson and Kofoid, 1992). BvgS acts as a membrane sensor, reacting to stimuli whereas BvgA is the cytoplasmic response regulator modulating the transcription factors.

BvgS is a 134-kDa histidine kinase composed of a N-terminal domain in the periplasm, a transmembrane domain and a linker region (PAS domain) that connects three cytoplasmic domains called transmitter, receiver and histidine-containing phosphotransfer (HPt domain) (see Figure 4) (Stibitz and Yang, 1991).

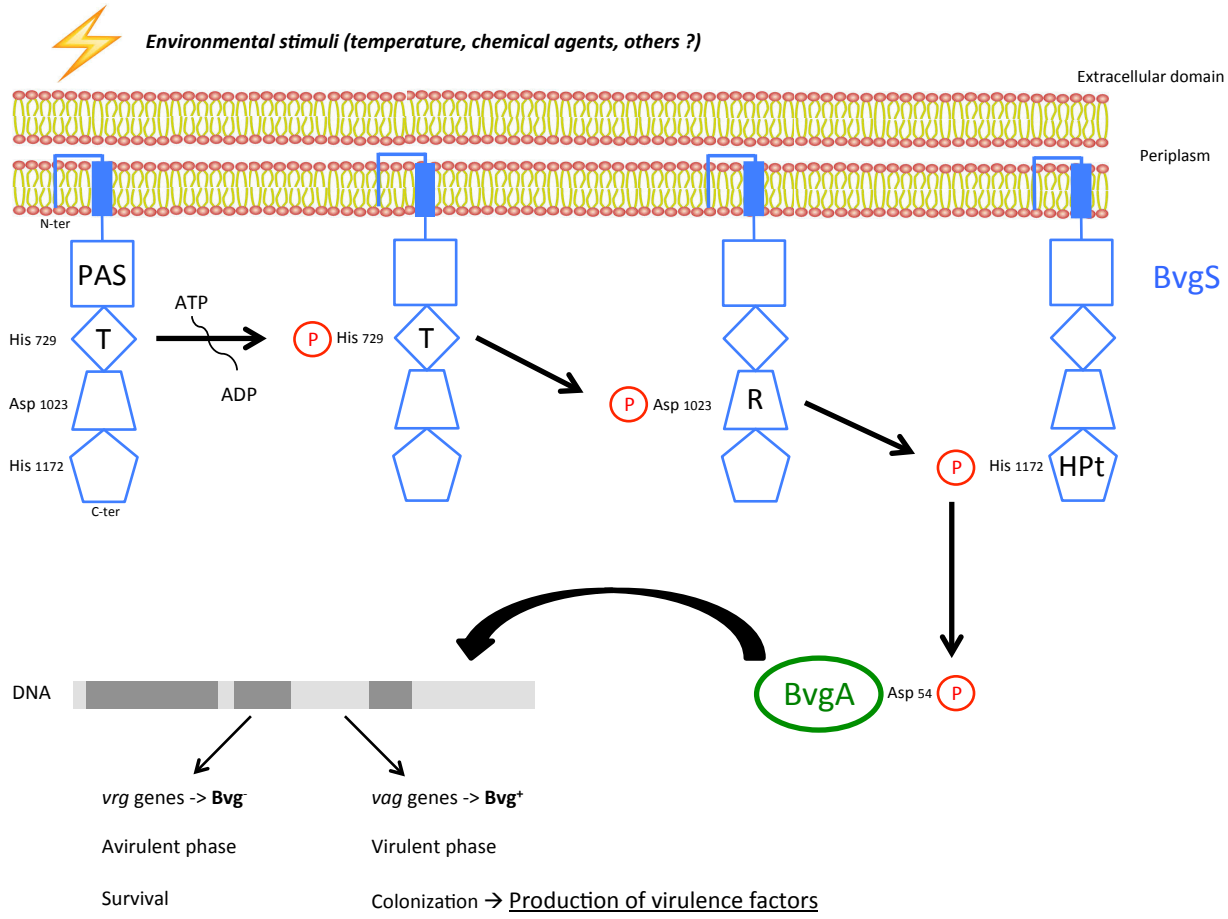

Figure 4. Structural organization of the BvgAS system in *Bordetella pertussis*. Domains of BvgS are represented in blue with PAS, T, R and HPt for linker, transmitter, receiver and histidine-containing phosphotransfer, respectively. His and Asp residues involved in phosphotransfer reactions are indicated. BvgA is phosphorylated by BvgS and activates transcription of specific genes depending on environmental stimuli. See text for more details.

BvgA is a 23-kDa response regulator with a N-terminal phosphate-receiver domain and a helix-turn-helix on its C-terminal domain characteristic of a DNA binding proteins. It activates transcription of the so-called *vag* genes (for virulence-activated genes) on the *bvg* locus coding for the adherence proteins and toxins, corresponding to the virulent phase Bvg^+, which promotes colonization of the bacterium (Bock and Gross, 2001). BvgA also activates the transcription of BvgR, a 32-kDa protein involved in the expression of *vrg* genes (for virulence-repressed genes), corresponding to the avirulent phase Bvg^- and promotes survival of the bacterium (Merkel et al., 2003; Merkel and Stibitz, 1995).

All the environmental signals regulating the BvgAS system are not identified. In BvgS, the PAS domain is able to perceive a variety of environmental stimulus that activate the BvgAS cascade. The following transmitter domain is composed of an ATP binding site and is target to autophosphorylation on a conserved His_{729}. This phosphate group is never directly transferred to BvgA (Perraud et al., 1999). It is transferred to the Asp_{1023} residue of the receiver domain which can either interrupts the phosphocascade by releasing its inorganic phosphate or transfers it to the His_{1172} residue of the HPt domain (Uhl and Miller, 1996, 1994). Finally, the HPt domain transfers its phosphate to the Asp_{54} of the response regulator BvgA (see Figure 4 for more details). Thus, an intramolecular multistep phosphorelay occurs in the BvgAS system.

Interestingly, the virulence factors from *vag* genes are transcribed in offset with "early" and "late" genes. This difference of expression is explained by a remarkable ten-fold difference in affinities of early and late promoters to the phosphorylated BvgA (Zu et al., 1996). Early promoters such as the ones coding for filamentous hemagglutinin, pertactin or fimbriae, are able to bind low amount of phosphorylated BvgA and are expressed few minutes after BvgAS activation. Conversely, later promoters including pertussis or adenylate cyclase toxins require higher concentration and are expressed hours later (Scarlato et al., 1991; Gross and Rappuoli, 1989).

Thus, the BvgAS system allows to *B. pertussis* to first express all the adhesins required for bacterial colonization and attachment to the respiratory tract. Later, the toxins are produced to locally intoxicate and destroy cells.

1.6 Virulence factors

B. pertussis adheres to tracheal epithelial cells of the respiratory tract after its entry in a new infected host. Then, it disrupts the mechanical property of ciliated cells and resists to the host immune system. To do so, *B. pertussis* triggers both infectious and toxic cascades. They are characterized by expression and secretion of adhesins and toxins. Thanks to the BvgAS system, this expression is coordinated, allowing persistence and multiplication of the bacteria in the host. The infectious syndrome is limited to the ciliated cells of the respiratory mucosa by the adhesion of bacteria thanks to adhesins, and a local bacterial multiplication. The toxinic syndrome is secondary and characterized by local destruction of ciliated cells, inflammatory reaction and accumulation of mucus.

Table 1. *Bordetella* main virulence factors of the three main members of the genus *Bordetella*. The + means gene expression; +/- gene expressed in some strains; - gene cryptic or absent. These factors are discussed below. Adapted from (Mattoo and Cherry, 2005; Parkhill et al., 2003; Smith et al., 2001; Locht, 1999).

	B. pertussis	*B. parapertussis*	*B. bronchiseptica*
Adhesins			
Filamentous hemagglutinin	+	+	+
Fimbriae	+	+	+
Pertactin	+	+	+
Brk	+	+	+/-
Tracheal colonization factor	+	-	-
SphB1	+	+	+
Vag8	+	+	+
Toxins			
LPS	+	+	+
Pertussis toxin	+	-	-
Adenylate cyclase toxin/haemolysin	+	+	+
Dermonecrotic toxin	+	+	+
Cytotracheal toxin	+	+	+

1.6.1 Adhesins

Human pathogenic *Bordetella* species produce a broad variety of different adhesins that contribute to the colonization of the respiratory tract (see Table 1). Each adhesin plays a specific role in the different steps of pathogenesis. Beside their adhesin role, some of them have immunomodulatory activities, able to subvert the immune system to the benefit of the bacterium multiplication. Thus, *B. pertussis* expends a significant quantity of energy to regulate, produce and secrete these proteins during the infection to ensure its survival.

1.6.1.1 Filamentous hemagglutinin

Filamentous hemagglutinin (FHA) is a major factor promoting the cellular adhesion step. It is encoded by the gene *fhaB*, the first virulent activated gene of a polycistronic operon activated by the BvgAS system, coding for a 367-kDa precursor FhaB (Scarlato et al., 1991). Once secreted, FhaB undergoes a protease proteolytic processing in two-steps, leading to the release of the 220-kDa mature FHA protein (Delisse-Gathoye et al., 1990; Domenighini et al., 1990). FHA is a rod-like shape protein that resembles to a "horseshoe nail" of approximately 50 nm in length and 4 nm in width, rich in β-strands secondary structures (Kajava et al., 2001; Makhov et al., 1994).

FHA is produced in large quantities on the membrane surface during the growth phase. It is first exported across the cytoplasmic membrane *via* the Sec signal peptide-dependent pathway (Chevalier et al., 2004). Then, thanks to a classical two-partner pathway, the transit of FHA from the cytoplasm to the outer membrane is mediated by the FhaC channel (Delattre et al., 2011). The FhaC channel is quite narrow, indicating that FHA is exported in an extended and unfolded conformation and folds into its native form at the cell surface (Guedin et al., 1998). FHA can remain on the cell surface or is secreted in the medium.

FHA presents several domains able to bind different cell receptors (Locht et al., 1993). The first binding domain identified is a unique carbohydrate recognition domain (CRD) that can specifically bind glycolipids present on the ciliated and macrophages cells (Liu et al., 1997; Prasad et al., 1993). The second one is a heparin-binding domain (HBD) involved in sulfated carbohydrates binding on epithelial cells and extracellular matrix, that confers its hemagglutinination properties (Hannah et al., 1994). Although CRD and HBD participate to

the binding, they do not contribute to pathogenesis and their role remain therefore unknown. The last domain is an Arg-Gly-Asp (RGD) sequence that facilitates the binding to the receptor type 3 integrin (CR3) also called $\alpha_M\beta_2$ or CD11b/CD18, present on the surface of macrophages (Relman et al., 1990). FHA would upregulate the CD11b/CD18 production through another receptor binding (Ishibashi et al., 2002, 1994). This last observation suggests cooperation during the infection process between FHA and the adenylate cyclase toxin because both bind CD11b/CD18 (see part 2.4). FHA would interact with cells, obliging them to overproduce the CD11b/CD18 receptor and would facilitate the interaction of the later produced adenylate cyclase toxin. Then, the adenylate cyclase toxin would prevent bacteria phagocytosis (Mobberley-Schuman and Weiss, 2005; Weingart and Weiss, 2000). Nevertheless, this cooperation remains to be proved.

Although FHA is not the only virulence factor implicated in the colonization, its numerous interactions with immune cells play a major role in immunomodulation for *B. pertussis* infection. Many immunomodulatory functions have been reported (Villarino Romero et al., 2014). Firstly, FHA can suppress the local pro-inflammatory interleukins production, resulting in the suppression of the immune response (McGuirk and Mills, 2000). FHA was further found to induce apoptosis on active immune cells (Abramson et al., 2001). Finally, FHA also binds and activates an inhibitor protein of the classical complement pathway, preventing bacteria phagocytosis (Berggard et al., 1997).

B. pertussis produces high amounts of FHA and its purification from bacteria supernatants is quite easy. Thus, it explains why FHA was rapidly considered as a candidate for acellular vaccines. FHA was found to induce a strong humoral immune response and is a major component of most current acellular vaccines (Locht et al., 1997; Kimura et al., 1990; Burstyn et al., 1983).

1.6.1.2 Fimbriae

B. pertussis produces fimbriae (FIM), a well widespread protein in Gram-negative bacteria. FIM, also called agglutinogens or pili, promote adhesion of bacteria on surfaces, especially for their attachment on eukaryotic cells and are partly responsible for bacterial pathogenicity (Jonson et al., 2005). *Bordetella* FIM belongs to the type 1 family of enterobacteria. It is composed of a thousand of subunits forming thin, long, hair-like

structures in the outer membrane. These structures are around 5.7 nm in diameter and get to several thousand nanometers in length. It consists of five subunits in two turns, making an axial repeat of 13 nm (Heck et al., 1996; Steven et al., 1986).

FIM from *B. pertussis* are composed of two major subunits: Fim2 (22.5 kDa) and Fim3 (22 kDa), called also serotypes 2 and 3, sharing 60% of sequence identity (Livey et al., 1987). They carry a single minor 40-kDa subunit, FimD, which serves as an adhesin. The expression of the *fim2* and *fim3* genes is positively regulated by he *bvgAS* operon, but transcriptomic analyses showed that these genes expression is also regulated by mutations in their promoter, resulting in serotype switching. In fact, the promoters contain a 15 cytosines long stretches and it appears that small deletions and insertions may occur. Theses changes regulate the transcription by changing the distance between the phosphorylated BvgA activator and the FIM promoter (Willems et al., 1990). Thus, some strains produce both FIM, some only one or not at all, contributing to the escape of the host immune response.

In bacterial disease, the role of FIM is well established but the exact function of FIM remains to be determined. *B. pertussis* FIM knockout mutants in mice and rats have shown a less persistence in trachea after infection compared to wild-type strain (Geuijen et al., 1997; Mooi et al., 1992). These observations suggest their importance for infection and colonization in the initial steps of *B. pertussis* colonization. The minor subunit FimD binds to the VLA-5 integrin receptor (for very late antigen 5), a receptor found on monocytes. As for Fim2 and Fim3, FimD also binds to sulfated sugars such as heparin, chondroitin and dextran sulfates (not dextran), ubiquitous in the respiratory tract (Hazenbos et al., 1995). FIM share sequence similarities with fibronectin and may illustrate molecular mimicry by imitating a natural ligand-receptor interaction (Geuijen et al., 1996). These bindings result in the upregulation of the CD11b/CD18 receptor expression of FHA (see part 1.6.1.1). Thus, both FIM and FHA may cooperate in *B. pertussis* adhesion, colonization and modulation of the host immune response (Scheller et al., 2015). Finally, FIM are present in most Pa vaccines and, although they induce antibody response and contribute to protect against the disease, this response remains unclear (Scheller and Cotter, 2015).

1.6.1.3 Pertactin

Pertactin (PRN) is a surface-exposed protein of the outer membrane of *B. pertussis*. PRN is a 69-kDa-protein synthetized by the BvgAS system (gene *prn*), belonging to the so-called auto-transporter proteins (Junker et al., 2006). It is also present in *B. parapertussis* and *B. bronchiseptica* strains as a 70 and 68-kDa protein, respectively. It is a polymorphic protein with 13 variants identified so far. It is synthetized as a 93-kDa polypeptide consisting of a N-terminal signal sequence, the passenger domain and a C-terminal auto-channel sequence (Charles et al., 1994). It undergoes a proteolytic digestion at its N- and C-terminus. The 69-kDa mature protein is transported through the auto-channel and is displayed at the bacterial surface where it remains not covalently bound.

The PRN fold consists of a 16-stranded parallel beta-helix with a V-shaped cross-section and a hydrophobic core (Emsley et al., 1996) (see Figure 5). It contains numerous RGD tripeptide motifs as FHA and also proline-rich regions (PRR), identified as cell-attachment in several adhesion proteins (Williamson, 1994). The PRN's role during infection is not fully understood. Several studies claimed that PRN mediates and increases the adhesion of bacteria to the ciliated cells of the upper respiratory system although its exact target receptor is still unknown (Leininger et al., 1992) (Leininger et al., 1991).

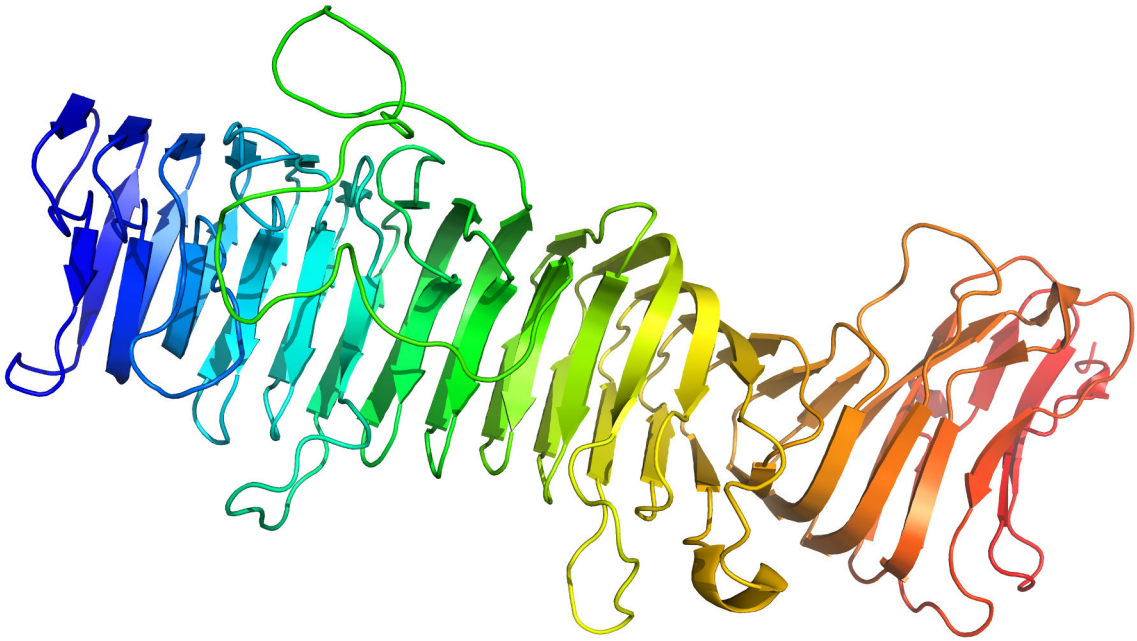

Figure 5. X-ray crystal structure of pertactin from *Bordetella pertussis*. Adapted from (Emsley et al., 1996).

PRN was initially discovered during the development of a veterinary vaccine against *B. bronchispetica* (Novotny et al., 1985). As FHA and FIM, PRN is present in the current human acellular vaccines and a study has shown that it was the only antigen inducing antibodies production crucial for *B. pertussis* opsonization by the immune system (Hellwig et al., 2003). Recently, many *B. pertussis* strains, which do not express PRN, were identified and represent up to 95% of all recent clinical isolates (Breakwell et al., 2016; Zeddeman et al., 2014). Thus, this PRN deficiency is subject to pertussis positive pressure and the probability of observing vaccinated people infected by whopping cough can greatly increase (Martin et al., 2015). Hovingh and colleagues have shown that these PRN^- strains increase pro-inflammatory response and cell death, suggesting a PRN activity in immunomodulation (Hovingh et al., 2018; Stefanelli et al., 2009).

1.6.1.4 *Bordetella*-resistance-to-killing factor

Bordetella-resistance-to-killing factor (Brk) is a protein that inhibits the bactericidal activity of the complement and may act as adhesin in *B. pertussis* colonization (Barnes and Weiss, 2001; Fernandez and Weiss, 1994). Deficiency in this gene expression leads to a less virulent bacteria compared to wild type strain and is impaired in binding to eukaryotic cells (Rambow et al., 1998; Weiss and Goodwin, 1989).

Brk is encoded by the *brk* locus, under the control of the BvgAS system. These genes code for two proteins transcribed in opposite direction: BrkA, a 103-kDa protein and BrkB, a 30-kDa protein. They are both required for serum resistance although the role of the produced cytoplasmic BrkB is not well defined. BrkA is processed during secretion through an autotransporter mechanism and yield to a 73-kDa protein that remains anchored at the bacterial surface (Oliver et al., 2003). The mature protein share 29% sequence identity with PRN, contains two RGD tripeptide motifs and harbors two binding sites for sulfated glycosaminoglycans. These similarities suggest that BrkA possesses adherence activities.

Current acellular vaccines do not contain the BrkA antigen. However, Oliver and Fernandez have shown that anti-BrkA antibodies boost existing bactericidal capacity against *B. pertussis* (Oliver and Fernandez, 2001).

1.6.1.5 Tracheal colonization factor

Tracheal colonization factor (TCF) is produced by *B. pertussis* but not by *B. parapertussis* and *B. bronchiseptica* (see Table 1). TCF is specifically involved in tracheal pertussis colonization. Indeed, TCF mutants show a reduced ability to colonize the trachea of infected mice (Finn and Stevens, 1995).

The gene encoding TCF is *tcfA* and is under the control of the BvgAS system. It is produced as a 90-kDa precursor processed to form a 68-kDa transported protein and then a 34-kDa mature protein. Sequence alignment has demonstrated that its C-terminal domain exhibits over 50% identity with PRN. It contains also three RGD motifs and high proline content. These similarities suggest that TCF is part of the autotransporter proteins. Like PRN and BrkA, TCF is found as an integral cell-associated membrane protein but TCF can be found in two forms, either as a large cell-associated protein or as a small-secreted form (Passerini de Rossi et al., 1999). Despite these similarities, the molecular mechanism of TCF remains unknown.

1.6.1.6 SphB1

SphB1 is a surface protein belonging to the subtilisin-autotransporter superfamily. It is a protease that catalyses its own proteolityc maturation at the bacterial surface. Its main function is to process the FHA precursor in order to generate a mature and active FHA form (Coutte et al., 2003, 2001). However, SphB1 knockout strains can still process FHA, suggesting that FHA can be processed by others proteases (Melvin et al., 2015).

1.6.1.7 Virulence-associated gene 8

The virulence-associated gene 8 (Vag8) is an unprocessed 95-kDa protein present at the bacterial outer membrane surface (Finn and Amsbaugh, 1998). It is encoded by the *vag8* gene, which is present as DNA homologous in both *B. parapertussis* and *B. bronchiseptica*. In *B. bronchiseptica*, Vag8 facilitates the secretion of type III proteins (Mattoo et al., 2004). Alignment analysis has shown sequence similarities with PRN, BrkA and TCF, suggesting that Vag8 may be part of the autotransporter proteins.

Recently, Marr and co-workers have shown that Vag8 binds a complement regulatory protein, C1inh (for C1 esterase inhibitor) (Marr et al., 2011). As Brka, that confers serum resistance and immunity escape to the bacteria. In fact, a Vag8 knockout mutant shows increase sensitivity to complement-mediated killing (Brookes et al., 2018).

1.6.2 Toxins

At the beginning, whopping cough was thought to be a toxin-mediated disease based on the actions of the pertussis toxin. Now, and besides the adhesins, which play a major role in attack and defense of the bacterium against the host, we know that the pathogenesis is more complicated. It is well established that *B. pertussis* invasion involves the expression of several toxins, which seem to work in a concerted manner to cause different diseases in multiple hosts.

1.6.2.1 Lipopolysaccharide

Lipopolysaccharide (LPS) is exclusively found in the outer membrane leaflet of all Gram-negative bacteria. LPS has a proper endotoxin activity, similar to enteric bacteria. It is mitogenic, pyrogenic and toxic and can induce the production of TNF (tumor necrosis factor) in macrophages (Watanabe et al., 1990; Nakase et al., 1970). Although all *Bordetella* species produce LPS, their structure differ, which may reflect their differences in the strength of biological activities (Amano et al., 1990). *B. pertussis* LPS molecules are smaller compared to the classical ones and it actually produces two types of LPS, which differ in their polysaccharide moieties (Peppler, 1984; Le Dur et al., 1980). The ratio of the two types may differ in same strains. However, the precise role of these structural differences is unclear (Ray et al., 1991). Interestingly, these LPS are regulated by the BvgAS system, which suggests a role in the respiratory tract infection (Harvill et al., 2000). LPS may also act in synergy with others toxins such as the tracheal cytotoxin or the pertussis toxin, although this cooperation remains to be confirmed. Finally, current acellular vaccines do not possess LPS but recent studies have shown that it induces immunogenic reactions (Zaitsev et al., 2014; Albitar-Nehme et al., 2013).

1.6.2.2 Pertussis toxin

This toxin had several names based on its different biological functions and was named pertussis toxin (PTX) (Pittman, 1979). Among all *Bordetella* species, PTX is exclusively synthetized by *B. pertussis* (see Table 1). In *B. parapertussis* and *B. bronchispetica*, a cryptic operon is present. However, numerous mutations in the operon make it silent (Arico et al., 1987).

PTX is considered both as an adhesin and a toxin having an important role in the establishment of infection. Mutant strains lacking PTX are defective in colonization of the respiratory tract of mice (Carbonetti et al., 2003; Khelef et al., 1994). PTX first targets resident airway macrophages and then inhibits neutrophil recruitment on the infection site, which illustrates that PTX acts as an antagonist of the host immune system and promotes immune evasion. PTX also upregulates pro-inflammatory factors such as IL-17, TNF-α and IFN-γ to enhance the influx of neutrophils to cause systemic effects and possibly boost the transmission of *B. pertussis* by cough (Andreasen et al., 2009; Mooi et al., 2009). PTX can also promote adhesion to the respiratory epithelium (Bassinet et al., 2000; Tuomanen and Weiss, 1985), induce leukocytosis (Morse and Morse, 1976) and enhance sensitization to histamine (Carbonetti, 2010; Munoz et al., 1981) . Finally, PTX is also a colonization factor with remarkable biological activities on different cells types, explaining its presence throughout infection (Connelly et al., 2012).

PTX is an ADP-ribosyltransferase toxin of 106-kDa. It is a hexameric protein with five dissimilar subunits named S1 through S5 in the ratio 1:1:1:2:1 (see Figure 6), which are encoded by *ptxA* and *ptxE* genes, respectively. The S1 subunit, also called the A promoter, possesses the enzymatic activity whereas the pentameric B comprises the S2, S3, S4 (two copies) and S5 subunits that facilitates the binding to host cells (Tamura et al., 1982). PTX is therefore a member of the A-B bacterial toxin superfamily, specifically to the A-B_5 family. Each subunit is synthetized and translated separately with a N-terminal sequence signal, suggesting that the transport into the periplasm occurs *via* a Sec dependent pathway. The PTX toxin is assembled and secreted across the outer membrane through a type IV secretion system made of nine accessory Ptl proteins (for pertussis toxin liberation) (Farizo et al., 1996; Weiss et al., 1993).

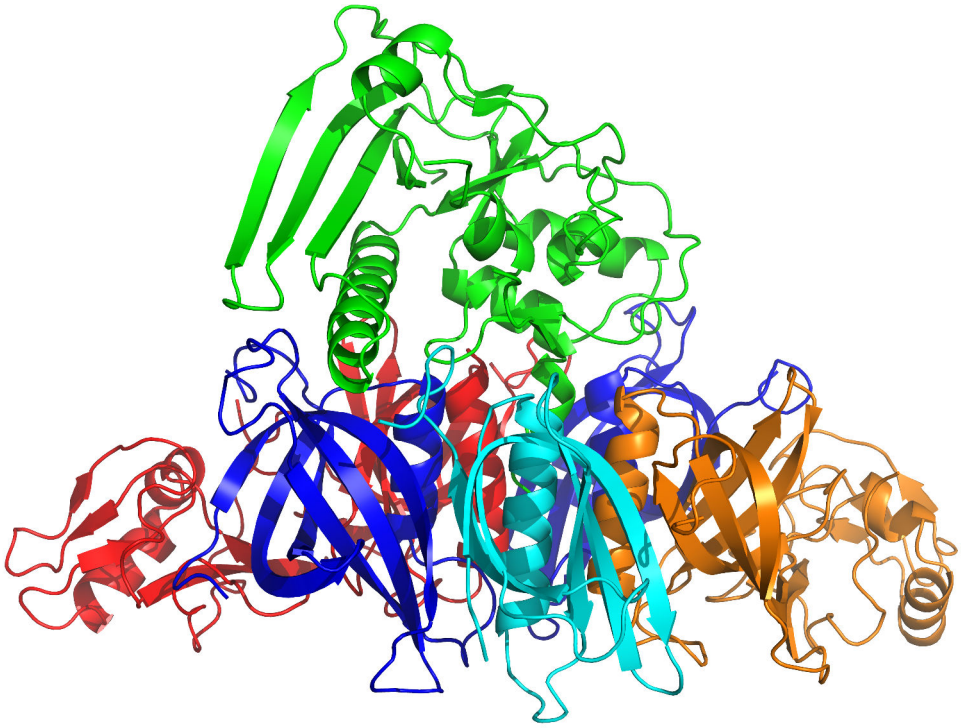

Figure 6. Crystal structure of the pertussis toxin from *Bordetella pertussis*. Subunits are colored as follows: S1, green; S2, orange; S3, red; S4, blue; S5, turquoise. Adapted from (Stein et al., 1994).

When secreted in the extracellular media, PTX binds to host ciliated cells and macrophages *via* sialic acid-containing glycoproteins receptors (Armstrong et al., 1994; Witvliet et al., 1989; Brennan et al., 1988). The binding occurs *via* the S2-S3 subunits of the B oligomer, which possesses two different carbohydrate-binding domains (Stein et al., 1994; Saukkonen et al., 1992). PTX is then endocytosed *via* a retrograde transport that involves early and late endosome, as well as Golgi apparatus, to reach the endoplasmic reticulum (ER) (Plaut and Carbonetti, 2008; Xu and Barbieri, 1995). Then, the S1 subunit is activated and released into the cytosol from the B oligomer in the presence of ATP and reducing agent. The dissociation and translocation mechanisms allow to S1 to acquire a disordered conformation which may trigger its export to the cytosol *via* the quality control of the ER-associated degradation pathway (Banerjee et al., 2016; Hazes and Read, 1997).

After reaching the cytosol, the enzymatic S1 subunit hydrolyses cellular NAD^+. The ADP-ribose released is further transferred to a cysteine residue near the C-terminal of several heterodimeric G proteins, which makes them totally inactive (Katada et al., 1983).

Consequently, the PTX enzymatic activity results in the deregulation of multiple metabolic pathways that depends on the cell type. For example, the ADP-ribosylation of G proteins blocks the inhibition of the adenylate cyclase, the activation of phosholipases A_2 and C, the activation of K^+ channels, the activation of cyclic GMP phosphodiesterase, the inactivation of Ca^+ channels and so on ... (Ui, 1990). Although most of the PTX activities consist in ADP-ribosylation, the remaining inactive B oligomer can obstruct by itself some signal transduction events and activates mitogenesis (Nasso et al., 2009; Alfano et al., 1999; Strnad and Carchman, 1987). Although it is well described, it is suggested that the B oligomer does not contribute significantly to this host-pathogen interaction. The reason thought is that the concentration of PTX reached during infection is not enough to elicit these effects (Carbonetti, 2010). However, the role of PTX in the establishment of the infection remains unclear. PTX does not seem to be involved in the main symptoms of whooping cough although this hypothesis remains controversial (Carbonetti, 2015; Mattoo and Cherry, 2005).

PTX is depicted as the major virulence factor produced by *B. pertussis*. Thus, it is part of all current acellular vaccines and induces a strong antibody response. Remarkably, a monocomponent PTX vaccine is enough to provide protection against the most severe forms of the disease (Blanchard Rohner et al., 2018; Kapil et al., 2018; Thierry-Carstensen et al., 2013; Hviid et al., 2004; Taranger et al., 2001). Therefore PTX is both an essential and sufficient antigen for vaccination (Coutte and Locht, 2015).

PTX displays strong adjuvant properties in several immunologic systems and has been proposed as a therapeutic antigen vehicle (Otto et al., 1999; Munoz et al., 1987) . It increases serum antibody responses of various antigens contributing to increase the cellular immune response and the anaphylactic sensitivity.

1.6.2.3 Tracheal cytotoxin

The tracheal cytotoxin (TCT) is a 921 Da disaccharide-tetrapeptide (1,6-anhydro-N-acetylmuramic acid-N-acetyl-glucosamine-tetrapeptide) discovered in 1982 by Goldman and colleagues (Goldman et al., 1982). It corresponds to a derivate of the cell wall peptidoglycan layer and is produced by all Gram-negative bacteria to rebuild their cell wall during growth. In contast to others bacteria, which recycle their peptidoglycan using the integral cytoplasmic protein called AmpG, *Bordetella* species secrete TCT continuously due to the

lack of AmpG (Jacobs et al., 1995; Rosenthal et al., 1987). TCT is therefore the unique virulence factor not regulated by the BvgAS system.

TCT targets and damages ciliated respiratory epithelial cells (Wilson et al., 1991; Cookson et al., 1989; Goldman et al., 1982). It has been shown that TCT acts in synergy with the LPS endotoxin for its pathogenic activity. This cooperation triggers an increase of production of pro-inflammatory cytokines (such as TNF-α, IL-1α, IL-1β and IL-6) and nitric oxide (NO^-) (Flak and Goldman, 1999; Luker et al., 1995; Heiss et al., 1993). It is proposed that TCT stimulates *in vivo* the production of IL-1α resulting in the production of high levels of NO^- that diffuses to neighboring cells causing cytopathy and preventing tissue repair (Flak and Goldman, 1996; Heiss et al., 1994). Phenotypically, it forces the infected host to cough relentlessly to remove bacteria, clear the mucus and debris that is normally done by the ciliated cells. TCT also impairs at low concentrations neutrophil function and displays a toxic activity at high concentrations (Cundell et al., 1994).

Thus, TCT seems to contribute to the survival of *B. pertussis in vivo* within the airways, although the lack of relevant animal models prevents to validate this hypothesis (Melvin et al., 2014).

1.6.2.4 Dermonecrotic toxin

Few years after the discovery of *B. pertussis*, the dermonecrotic toxin (DNT) was the first virulence factor identified as endotoxin (Bordet and Gengou, 1909). It was formerly known as “heat-labile-toxin” due to its inactivation at 56°C (Horiguchi et al., 1989; Livey and Wardlaw, 1984). As its name indicates, DNT causes local necrotic skin lesions in mice when injected intradermally and is even lethal when injected intravenously (Endoh et al., 1986; Parton, 1985; Iida and Okonogi, 1971).

The gene of DNT, *dnt*, is under the control of the BvgAS system. It has been found that DNT toxins from *B. pertussis*, *B. parapertussis* and *B. bronchiseptica* share 99% of amino acid identity (Walker and Weiss, 1994). DNT corresponds to a single polypeptide chain of 1464 amino acids with a predicted molecular mass of 160 kDa. As PTX, it belongs to the A-B toxin family. Its structure is composed of a 54-amino-acid N-terminal receptor-binding domain and 300-amino-acid C-terminal enzymatic domain. Compared to other toxins, DNT

is not secreted and remains localized in the cytoplasm, which means that its action *in vivo* may require the lysis of the bacterial cells (Nakai et al., 1985; Cowell et al., 1979). DNT is endocytosed in a dynamin-dependent manner and translocated into the cytoplasm of the host cell (Matsuzawa et al., 2004). Although its specific receptor has not been identified yet, this receptor is thought to be specific because just a subset of cells are sensitive to DNT (Matsuzawa et al., 2002; Horiguchi et al., 1995). Intracellularly, it targets GTP-binding protein Rho where DNT may deamidate or polyaminate them, which destroys GTPase activity (Fukui and Horiguchi, 2004; Masuda et al., 2000; Schmidt et al., 1999). Rho remains permanently active and sends aberrant signals to its downstream effectors, resulting in dramatic morphology change, stimulation of DNA replication and alteration of proliferation and differentiation of cells (Horiguchi et al., 1997, 1993, 1991).

DNT is considered as a virulent factor although, in mice, deficient DNT mutants exhibit the same behavior than the wild-type (Weiss and Goodwin, 1989). This may explain why DNT is not present in the current acellular vaccines. Nevertheless, recent data have shown that the production of a recombinant DNT triggers an immune response in mice and protects against *B. bronchiseptica* (Wang et al., 2015a).

1.6.2.5 Adenylate cyclase toxin

The adenylate cyclase/hemolysin toxin is a large multi-domain and bi-functional protein. It invades host immune cells *via* the translocation across the plasma membrane of its catalytic domain that possesses the enzyme activity. It results in overproduction of cyclic AMP and disruption of transduction pathways. The toxin will be described in more details in chapter II.

Chapter II. The adenylate cyclase toxin (CyaA) from *Bordetella pertussis*

Chapter II. The adenylate cyclase toxin (CyaA) from *Bordetella pertussis*

2. The adenylate cyclase toxin

The adenylate cyclase toxin (CyaA) is one of the major virulence factor produced by *B. pertussis* and plays a key role in the establishment of the infection (Ladant and Ullmann, 1999; Hewlett et al., 1976). CyaA was the first bacterial adenylate cyclase toxin demonstrated to reach the eukaryotic cell cytosol (Confer and Eaton, 1982). This toxin plays an important role in immunomodulation by impairing chemotaxis, oxidative responses and phagocytosis, which facilitate bacterial colonization during the early stages of infection. In fact, many studies have shown that strains lacking the *cyaA* gene (coding for the CyaA protein) were unable to induce lethal infections in mice and were more prone to phagocytosis by human neutrophils (Gross et al., 1992; Khelef et al., 1992; Goodwin and Weiss, 1990; Weiss et al., 1984). Furthermore, Guiso and colleagues have shown that both active and passive immunization with CyaA significantly shortens and prevents bacteria colonization of the respiratory tract in infected mice (Guiso et al., 1991, 1989).

Although CyaA is not produced by all *Bordetella* species (Sebaihia et al., 2006), it is highly conserved in those expressing strains (Donato et al., 2005; Parkhill et al., 2003). As a result, the function and role of CyaA were considered to be similar during bacterial infections. However, Fukui-Miyazaki and co-workers have recently demonstrated that *B. parapertussis* and *B. bronchiseptica* CyaA toxins exhibit a weak toxic activity in cells (Fukui-Miyazaki et al., 2018). It is due to the inactivation of CyaA by a host factor after a phosphorylation on an unconserved residue. Therefore, pathogenicity differences in *Bordetella* species can be, at least in part, assigned to the different activities of CyaA.

CyaA is a single 177-kDa bifunctional long multi-domain protein. It belongs to the RTX hemolysin family (for Repeat in ToXins) produced by many Gram-negative bacteria. The first 364 amino acids at its N-terminus carry the adenylate cyclase activity while the remaining 1342 amino acids are required for the delivery of the catalytic domain, the

binding to host cell receptor and for the hemolytic phenotype of *B. pertussis*. Both adenylate cyclase and hemolytic activities can operate independently but they may act in coordination for the overall toxicity of CyaA (Sakamoto et al., 1992). CyaA is synthetized as an inactive precursor, proCyaA, which is converted into an active CyaA form *via* specific acylation on two lysine residues by the dedicated CyaC acyltransferase (Basar et al., 2001; Westrop et al., 1996; Hackett et al., 1994; Barry et al., 1991). Then, CyaA is secreted across the bacterial envelope by a dedicated type I secretion system and can bind its specific CD11b/CD18 cellular receptor (Guermonprez et al., 2001). Interestingly, a close contact between living bacteria with target cells is important for active CyaA secretion and cell intoxication (Mattoo and Cherry, 2005; Gray et al., 2004). Compared to PTX and DNT, which are internalized *via* endocytosis after binding their receptors on host cell, CyaA is the only known toxin that directly penetrates target cells across the cytoplasmic membrane to deliver its catalytic domain. Upon receptor binding, the catalytic domain is translocated across the plasma membrane and activated by the endogenous calmodulin, leading to the overproduction of cyclic AMP (cAMP) that disrupts the cellular signaling pathways (Ladant and Ullmann, 1999; Rogel et al., 1991; Wolff et al., 1980).

CyaA can intoxicate a wide variety of eukaryotic cell types especially those expressing the CD11b/CD18 receptor such as neutrophils, macrophages, natural killer and dendritic cells. CyaA can inhibit neutrophils functions such as phagocytosis, chemotaxis and oxidative burst (Carbonetti et al., 2005; Weingart and Weiss, 2000; Friedman et al., 1987) and also induce apoptosis in macrophages both *in vitro* and *in vivo* (Gueirard et al., 1998; Khelef et al., 1993). The toxin can also upregulate MHC class II molecules on dendritic cells, resulting in a diminution of pro-inflammatory cytokine production (Boyd et al., 2005; Skinner et al., 2004). The overproduction of cAMP induces IL-23 production and IL-12 inhibition that alters the Th1/Th17 balance (Spensieri et al., 2006). It may be enhanced by promoting expression of IL-10 and suppression of interferon expression (Adkins et al., 2014; Hickey et al., 2008). Thus, CyaA contributes to bacterial and immune escapes by reducing the Th1 immune response and instead increases local inflammation with the Th17 response (Fedele et al., 2017, 2010).

The toxin can also intoxicate epithelial cells by targeting their basolateral membrane although these cells lack the CD11b/CD18 receptor (Eby et al., 2010). This interaction may upregulate the expression of both IL-6 and IL-8 cytokines but the biological consequences remain unclear (Bassinet et al., 2004; Belcher et al., 2000).

Others virulence factors may cooperate with the CyaA toxin to increase its intoxication process. In fact, FHA acts as an adhesin and also binds to the CD11b/CD18 receptor (Relman et al., 1990). It is thus suggested that FHA would upregulate CD11b/CD18 expression for the later CyaA (Ishibashi et al., 2002, 1994). These findings suggest that FHA may contribute to bring closer *B. pertussis* to the host cell *via* its interaction and may favor CyaA toxicity (Zaretzky et al., 2002; Weingart and Weiss, 2000). Another suggested cooperation is with PTX. PTX does not target neutrophils compared to CyaA but it can inhibit neutrophils recruitment on the infection site (Andreasen and Carbonetti, 2009). It is proposed that PTX acts earlier than CyaA to inhibit neutrophil influx at the site of infection (Carbonetti et al., 2005). Further, CyaA intoxicates neutrophils and others cells to increase the immune escape of *B. pertussis*.

Finally, despite the observations that CyaA is an important factor for *B. pertussis* intoxication process, it is not included in current acellular vaccines. However, several studies have shown that CyaA triggers a humoral response that enhances neutrophil phagocytosis and protects against virulent bacteria (Cheung et al., 2006; Weingart et al., 2000; Guiso et al., 1991). Thus, this toxin represents a good candidate for the next generation of acellular pertussis vaccines.

2.1 Synthesis of the CyaA toxin

The *cyaA* gene codes for CyaA (Glaser et al., 1988a). This gene belongs to the *vag* genes (virulence-activated gene) mainly expressed during the virulent phase Bvg^+ (see previously Figure 4). Therefore, *cyaA* is under the control of the BvgAS system (Gross and Rappuoli, 1989; Scarlato et al., 1991). The *cya* locus is composed of five genes, with four of them belonging to the same operon (Glaser et al., 1988a, 1988b). The last gene is transcribed in the opposite direction of the operon (see Figure 7).

The *cyaABDE* operon codes for four distinct proteins. Glaser and co-workers have cloned and sequenced the gene and found that both the adenylate cyclase and the hemolytic activities of CyaA constitute a single protein of 1706 codons (Glaser et al., 1988b). The three others genes, located downstream of *cyaA*, are denoted *cyaB*, *cyaD* and *cyaE*. The *cyaB* gene is located 77 bp downstream of *cyaA* and codes for CyaB, an ATP-binding transporter of 712 amino acids inserted into the inner membrane. *cyaD* codes for CyaD, a

440 amino acids membrane-fusion protein. Finally, *cyaE* codes for an outer membrane pore forming CyaE protein of 474 amino acids. They form a typical type I secretion system essential for the CyaA secretion (described later in part 2.3). Sequence analysis has shown that this locus organization is quite common in the RTX toxins family (Delepelaire, 2004).

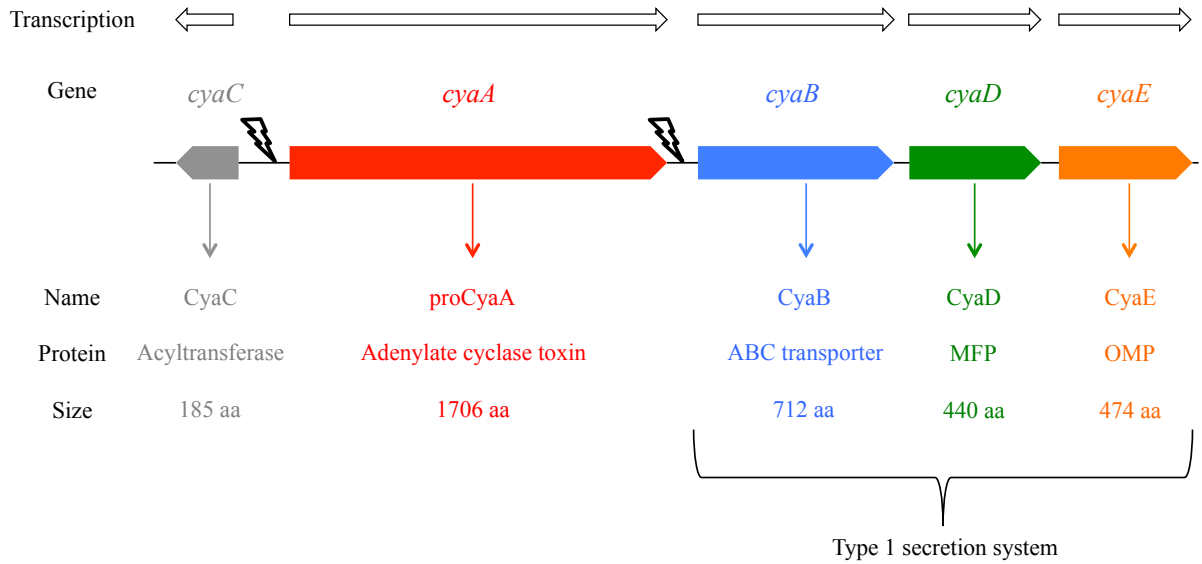

Figure 7. Organization of the *cya* locus of *Bordetella pertussis*. The *cyaABDE* genes form an operon and code for the proCyaA toxin (*cyaA* gene) and the three proteins of the type I secretion system (*cyaB*, *cyaD* and *cyaE* genes). The *cyaC* gene codes for the acyltransferase CyaC, transcribed in opposite direction. Arrows indicate the orientation of transcription of each gene. The two promoters are indicated by black lightenings. ABC: ATP-binding cassette; MFP: membrane fusion protein; OMP: outer membrane protein. See text for more details

The *cyaABDE* operon is activated by the *bvg* locus, which controls the transcription of virulent factors, as described previously. The locus promoter is located at 115 bp upstream from the translational start codon of the gene *cyaA*. It contains multiple heptamerics variants of the BvgA-binding consensus 5'-TTTCCTA-3'. These sequences extend between nucleotides -137 and -51 (Karimova et al., 1996). The *cyaA* gene does not contain any high-affinity binding site in its promoter region for the phosphorylated BvgA transcription activator (Karimova and Ullmann, 1997; Steffen et al., 1996). The *cyaA* gene requires a ten-fold concentration of the phosphorylated BvgA activator compared to the "early" promoters,

which may explain why CyaA is expressed as a relatively “later” virulence factor (Zu et al., 1996).

cyaBDE genes are contiguous to *cyaA* while there is a 77 bp intergenic region between the *cyaA* stop codon and the beginning of *cyaB* transcription (see Figure 7). It was suggested that the termination of transcription might occur in this region (Laoide and Ullmann, 1990). Interestingly, an unexpected weaker promoter was identified upstream from the *cyaB* gene and was found to be independent of the BvgAS activation system. Thus, *B. pertussis* would be able, in theory, to synthetize the secretion machinery without producing the CyaA toxin. However, the activation and the role of this second promoter remain unknown.

The last gene, *cyaC*, is transcribed in the opposite direction (see Figure 7) and codes for the 22-kDa CyaC acyltransferase. This protein is responsible for the post-translational modifications required to generate the active form of the CyaA toxin (Barry et al., 1991) (see part 2.2.4).

A clinical isolate of *B. pertussis* was identified with two copies of the *cya* locus. Up to now, it is not known whether this duplication may contribute to infection or also adaptation of *B. pertussis* (Dalet et al., 2004).

2.2 Primary structure of the CyaA toxin

The CyaA toxin is a 1706 residue-long polypeptide chain that consists of an N-terminal enzymatic domain of about 364 residues that is linked to a C-terminal hemolytic domain of about 1342 residues. The N-terminal domain possesses the catalytic activity and is able to translocate across the plasma membrane of host cells and to bind calmodulin to convert ATP into cAMP. The C-terminal domain allows CyaA binding to the host receptor and translocation of the catalytic domain. This domain can also form small cation-selective pore responsible of the hemolytic capacity of *B. pertussis* (Benz et al., 1994; Bellalou et al., 1990a; Glaser et al., 1988b).

Several domains can be identified in the 1342 C-terminal hemolysis moiety. The translocation region, spanning residues 365 to 527, is essential for the delivery of the catalytic domain into the cytosol (Subrini et al., 2013; Karst et al., 2012). The hydrophobic

region, covering residues 528 to 710, is predicted to insert into the cell membrane and has the capacity to make cation-selective pores (Basler et al., 2007; Glaser et al., 1988a). The acylation region, spanning residues 711 to 1005, has two post-translational acylation sites on two lysine residues (K860 and K983). Acylations are carried out by the dedicated CyaC acyltransferase that converts the inactive proCyaA form into the active CyaA toxin (Westrop et al., 1996; Barry et al., 1991). The last domain, spanning residues 1006 to 1706, corresponds to the cell receptor-binding domain. It consists in several copies of a calcium binding, glycine and aspartate-rich nonapeptide repeat, characteristic of the RTX (Repeat in ToXin) toxin family (Welch, 2001). Finally, a secretion signal found within the last 74 residues of CyaA, is specifically recognized by the machinery responsible of the CyaA secretion through the type I secretion system (Sebo and Ladant, 1993) (see Figure 8 for more details).

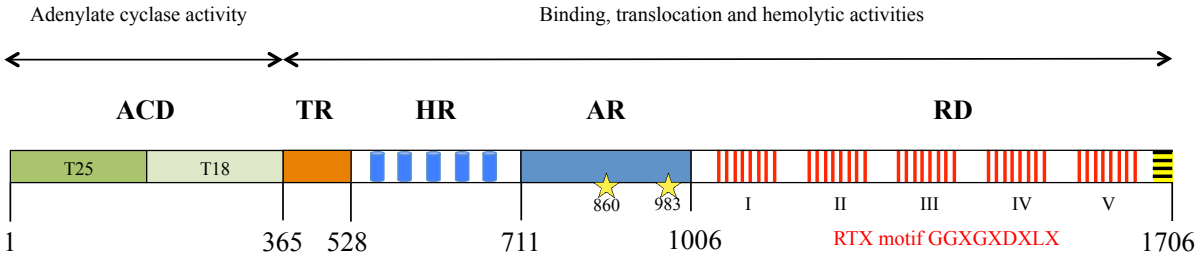

Figure 8. Structural organization of the CyaA toxin from *Bordetella pertussis*. Numbers represent amino acid residues. ACD can be cleaved by trypsin into two subdomains T25 and T18 in green and light green, respectively. The blue boxes in HR represent the five hydrophobic segments predicted to adopt α-helical structures. Yellow stars represent acylation on lysine residues K860 and K983. Each red bar within RD represents one RTX motif. The yellow box with dark bands at the C-terminal extremity represents the secretion signal. ACD: adenylate cyclase catalytic domain; TR: translocation region; HR: hydrophobic region; AR: acyl region; RD: receptor-binding domain.

2.2.1 The N-terminal catalytic domain

The adenylate cyclase catalytic domain of CyaA (ACD) is localized in the 364 amino-proximal residues. ACD belongs to the class II adenylyl cyclase family that comprises the edema factor (EF) from *Bacillus anthracis* and ExoY from *Pseudomonas aeruginosa*.

Hewlett and co-workers discovered the CyaA toxin as an extracytoplasmic enzyme present in *B. pertussis* culture media (Hewlett et al., 1976). Then, Confer and Eaton first described that human neutrophils undergo a striking increase in intracellular cAMP after exposition to *B. pertussis* extracts (Confer and Eaton, 1982). In fact, after translocating across the plasma membrane of the target cell, ACD catalyzes the reversible cyclizing reaction ATP ↔ cAMP + PP_i + H^+, which plays an important regulatory role in both eukaryotic and prokaryotic cells (Gancedo et al., 1985; Ullmann and Danchin, 1980). cAMP accumulates rapidly and without any lag period in human neutrophils, reaching a plateau within 10-20 min (Friedman et al., 1987). This uncontrolled conversion of ATP to cAMP triggers and deregulates numerous signaling pathways, subverts the cellular physiology and suppresses bactericidal functions of phagocytes (Cerny et al., 2015; Kamanova et al., 2008; Confer and Eaton, 1982). Furthermore, ATP depletion contributes to mitochondrial dysfunction that causes necrosis and apoptosis of phagocytes (Hewlett et al., 2006; Bachelet et al., 2002; Khelef and Guiso, 1995).

Besides its enzymatic and hemolytic activities, CyaA, as several other members of the RTX toxins family, was shown to increase the intracellular calcium concentration (Fiser et al., 2007). Interestingly, cAMP accumulation can also elevate intracellular calcium concentration through the activation of calcium permeable channels (Cooper et al., 1995). Thus, it remains uncertain whether this third activity is either due to cation-selective pores from CyaA or a consequence of the cAMP increase (Martín et al., 2010; Fiser et al., 2007).

The CyaA adenylate cyclase activity was up to 1000-fold higher in eukaryotic cells than *in vitro* (Hewlett et al., 1979, 1978). Then, it was suspected that its *in vivo* activity requires an endogenous activator. Wolff and colleagues have discovered that the activity of ACD was enhanced by several orders of magnitude following interaction with calmodulin (CaM) (Wolff et al., 1980). CaM is an ubiquitous protein highly conserved in the eukaryotic kingdom and absent in prokaryotes. It is made of two lobes of EF-hand calcium binding motifs connected by a flexible helix (Barbato et al., 1992; Babu et al., 1985). This flexible

linker allows both lobes to independently associate with their targets. CaM is a small protein of 16.7 kDa that interacts with a large number of enzymes and proteins in a calcium-dependent manner by a two-steps mechanism:

$$CaM + Ca^{2+} \leftrightarrow CaM\bullet\ Ca^{2+}$$

$$Enzyme_{(inactive)} + CaM\bullet\ Ca^{2+} \leftrightarrow Enzyme\bullet\ CaM\bullet\ Ca^{2+}{}_{(active)}$$

In fact, calcium binding to CaM induces conformational changes from a hydrophilic closed state to an open conformation exhibiting hydrophobic pockets (Finn et al., 1995).

ACD binds CaM with a 1:1 stoichiometry with an extremely high catalytic constant rate k_{cat} of about 2000 s^{-1} (Karst et al., 2010). It appears to be about three orders of magnitude higher than the activity of endogenous adenylate cyclases. Furthermore, ACD exhibits a very high affinity for CaM (K_d < 0.1 nM) in the presence of calcium and a lower one in its absence (K_d around 15-20 nM) (Glaser et al., 1991; Gentile et al., 1990; Ladant et al., 1989). From our results, we found that ACD exhibits a K_d at 1 nM for CaM. In cells, the free calcium is quite low (*i.e* 0.1 µM or less) which suggests the presence of abundant apoCaM (CaM without bound calcium). Thus, physiological conditions are sufficient to activate the CyaA toxin when CaM is not limiting (*i.e* 1 to 10 µM in cells) (Shen et al., 2002; Jurado et al., 1999).

Trypsin proteolysis of the ACD complexed with CaM releases two subdomains: T25 (25 kDa, residues 1-224) and T18 (18 kDa, residues 225-399) (see Figure 8). However, a proteolysis of ACD without CaM releases a T24 fragment (Ladant, 1988). Both T25 and T18 remain associated to CaM and are catalytically active as the native ACD whereas T24 does not bind CaM and is thus inactive (Munier et al., 1991). Using residue modification and mutagenesis, the catalytic site was identified in the T25 while the T18 corresponds to the main CaM binding site (Glaser et al., 1989; Ladant et al., 1989).

The catalytic core of CyaA is made of three highly conserved regions among adenylate cyclase: CR1 (for catalytic region 1, residues 54-77), CR2 (residues 184-198) and CR3 (residues 295-315). They are directly involved in ATP binding and catalysis. Mutagenesis in CR1, CR2 or CR3 segments lead to a drastic decrease, or total loss, of enzyme activity (Munier et al., 1992; Glaser et al., 1991, 1989).

Guo and colleagues have solved the crystal structure of ACD (residues 7 to 364) with the C-terminal domain of CaM (C-CaM, residues 79 to 147) (Guo et al., 2005) (see Figure 9A). It was crystallized with adefovir diphosphate, an ATP mimicker that inhibits the ACD catalytic activity with high affinity (K_i = 25 nM) (Shen et al., 2004). No electron density can be found between residues 226 to 232 of ACD, which correspond to the proteolysis-sensitive site between T25 and T18 (Ladant, 1988). Karst and colleagues have previously shown that in ACD alone, the CaM binding region adopts an extended conformation and undergoes a stabilization and compaction (Karst et al., 2010). Recently, using a combination of biophysical approaches, we showed that a 75-residue-long stretch within ACD exhibits a disorder-to-order transition upon CaM interaction (see Figure 9B and 9C). These results are further discussed in the experimental results chapter.

The main binding region of ACD to CaM is the amphipathic H-helix (spanning residues 233-254 of CyaA) of T18. This helix is mainly unfolded and flexible and adopts a stable helical conformation upon CaM binding (Karst et al., 2010). X-ray data has shown that the W242 of H is buried in a hydrophobic pocket of CaM (Guo et al., 2005; Vougier et al., 2004). This interaction is quite identical to the binding of the myosin light chain kinase (MLCK) to CaM (Ikura et al., 1992; Meador et al., 1992). Previously, studies have shown that W242 was crucial and its substitution reduced by more than 1000-fold the affinity for CaM (Gilles et al., 1990; Glaser et al., 1989).

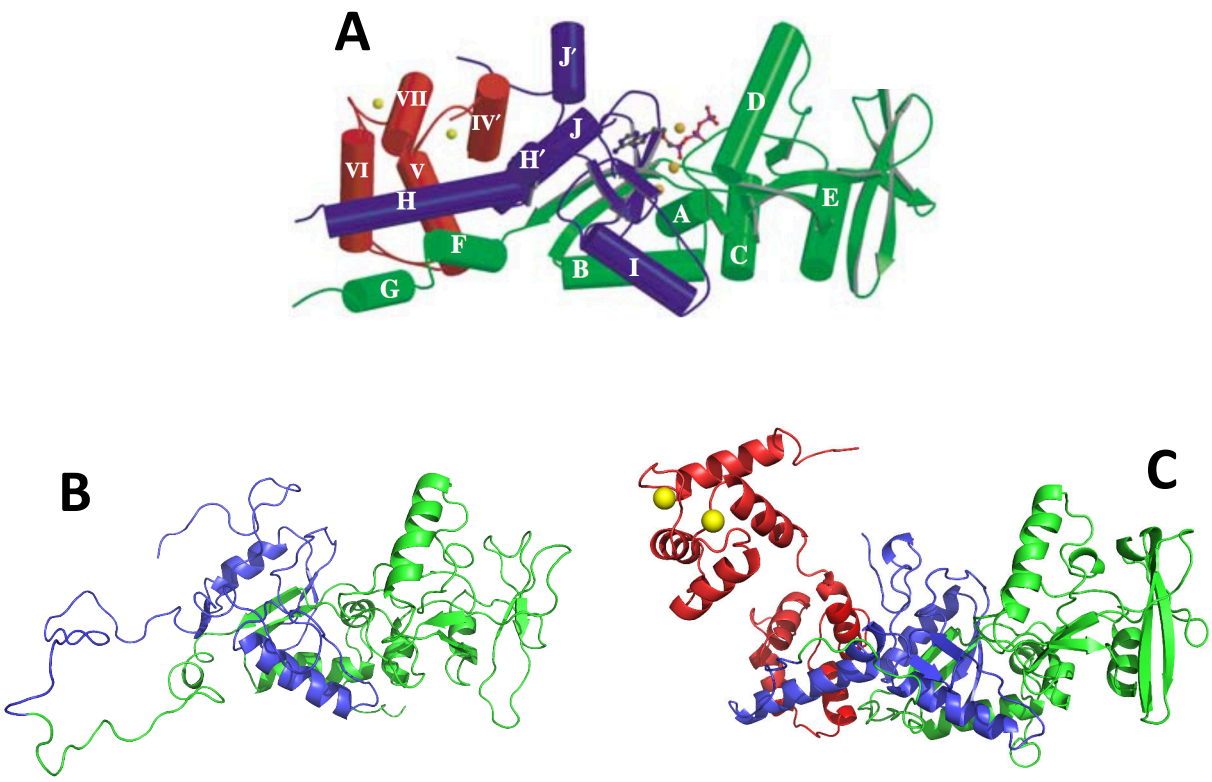

Figure 9. Structural organization of CaM with ACD (**A**) Crystal structure of ACD with C-CaM in complex with adevofir diphosphate (PDB 1YRU). (**B**) Structural model of ACD in solution. (**C**) Structural model of ACD in complex with the full length CaM. The T18 is colored in blue, the T25 in green and CaM in red. The calcium and magnesium ions are colored in yellow and orange, respectively. From (O'Brien et al., 2017) and (Guo et al., 2005).

In contrast to the CaM:MLCK complex, in which CaM adopts a compact form, the CaM:ACD complex exhibits an extended conformation (Gsponer et al., 2008; Guo et al., 2005). Recently, we solved the crystal structure of the H-helix peptide with full length CaM. We showed that both N- and C-CaM lobes can bind one H-helix peptide, leading to an extended conformation of the CaM:H 1:2 complex (Guo et al., 2005). However, the affinity of H for each lobe is quite different. Our data may explain why ACD can be both activated by N-CaM and C-CaM (Ulmer et al., 2003; Shen et al., 2002). These results and the structure will be presented in the experimental results chapter.

CaM binding to ACD depends on the reduced state of the nine methionines located in the hydrophobic pocket of CaM. Indeed, the oxidation of these methionines residues dramatically decreases the interaction (Vougier et al., 2004). Particularly, M109, M124 and

M145 are critical for binding. Interestingly, neutrophil activation results in the production of reactive oxygen species that potentially induce intracellular protein oxidation and may have consequences on ACD:CaM interaction. These results suggest that ACD can be fully activated by partially oxidized CaM and thus may contribute to its cytotoxic effect on activated neutrophils (Vougier et al., 2004).

C-CaM also interacts with a loop-helix-loop (LHL) motif (residues 341-364, helix J' on Figure 9A) located at the very C-terminal part of ACD (Guo et al., 2005). Interestingly, this LHL also directly contacts the CR3. Molecular dynamics simulations have suggested that three residues (R338, N347 and E360) might stabilize the ACD:CaM interaction (Selwa et al., 2012). Amino acids substitutions have shown that these residues act cooperatively and that R338 and E360 contribute to C-CaM binding while N347 stabilizes the CR3 (Malliavin, 2017; Selwa et al., 2014).

Taken together, these data illustrate how CaM stabilizes ACD to bring crucial residues into contact for its catalytic activation. Adjacent segments of ACD also contribute to the stabilization of the complex. However, some structural data are still missing and interesting to investigate. Firstly, no crystal structure of ACD alone is available. It would be interesting to understand how ACD is precisely organized without its ligand. Secondly, the structural information was obtained from C-CaM with ACD and not the full length one. The main difficulty that impedes the crystallization of the full length is the high flexibility of the N-CaM. Thus, the role of N-CaM is not yet clear on how it affects the structural features of ACD with CaM.

2.2.1.1 Structural comparison of ACD to EF and ExoY

CyaA belongs to the class II of nucleotidyl cyclases as EF and ExoY, which are activated upon interaction with specific cofactors. Unlike CyaA and EF, which require CaM as activator, ExoY requires filamentous actin (F-actin) (Belyy et al., 2016). Despite the fact that they need a cofactor to be activated, their intoxication process is completely different. In fact, while CyaA is directly translocated across membranes, EF uses the endocytosis pathway and ExoY is directly injected into cells *via* a type III secretion system (Hauser, 2009; Abrami et al., 2005; Ladant and Ullmann, 1999).

CyaA and EF form an extended complex with CaM (Gsponer et al., 2008; Guo et al., 2005; Drum et al., 2002). Although CyaA and EF share a similar structure, their interaction with CaM completely diverges (Shen et al., 2002). Firstly, EF has about 100-fold less affinity to CaM than ACD. This difference in affinity may be explained by the mechanism of entrance of each toxin. Their final location implies that these two enzymes compete with different sets of CaM-binding proteins (Jurado et al., 1999). Secondly, the first CaM binding site (CBS1, see Figure 10A) of EF is relatively shorter than CyaA but EF possesses an additional long C-terminal tail (*i.e* CBS2 poorly conserved in CyaA) in order to form a stable interaction with CaM. Finally, CyaA can be activated by both N- and C-CaM while EF cannot (Ulmer et al., 2003; Shen et al., 2002). Thus, these molecular details illustrate how two structurally homologous bacterial toxins bind CaM differently to be activated.

Although CyaA has a limited sequence identity with EF and ExoY (about 53% and 41%, respectively), their catalytic site share structural similarities and mechanism of activation (Belyy et al., 2016; Shen et al., 2005; Drum et al., 2002). Partial sequence alignments of their catalytic domain clearly demonstrate that they have in common the three highly conserved regions CR1, CR2 and CR3 with up to 66% similarities (see Figure 10A and 10B). These observations suggest that CyaA, EF and ExoY use common catalytic mechanism. By analogy, site-directed mutagenesis in CR1 (K58, H63 or K65), CR2 (D188, D190) or CR3 (H298, E301, N303) segments of the toxins have demonstrated that these regions are crucial for substrate binding and catalysis (Guo et al., 2005; Drum et al., 2002; Yahr et al., 1998; Munier et al., 1992; Glaser et al., 1991).

Recently, Khanppnavar and Datta obtained a partial crystal structure of ExoY and made a superposition of the three toxins (Khanppnavar and Datta, 2018) (see Figure 10C). The overall structures of all the three toxins remain more or less identical. However, it is clear that the region 1 (corresponding to the CBS1, see Figure 10A and 10C) confer to CyaA and EF their specificity to CaM as partner. Furthermore, we can observe that EF has a CBS1 shorter compared to CyaA, but uses an additional C-terminal tail poorly conserved in CyaA (CBS2) to form a stable interaction with CaM. For ExoY, the F-actin binding region is identified in its C-terminus extremity (within the region 2), which is not present in CyaA and EF (see Figure 10C) (Belyy et al., 2018). The remaining regions are exposed and disordered and may confer specificity to their binding partners and help for the stabilization of the complex (*i.e* stabilization induced by a disorder-to-order transition).

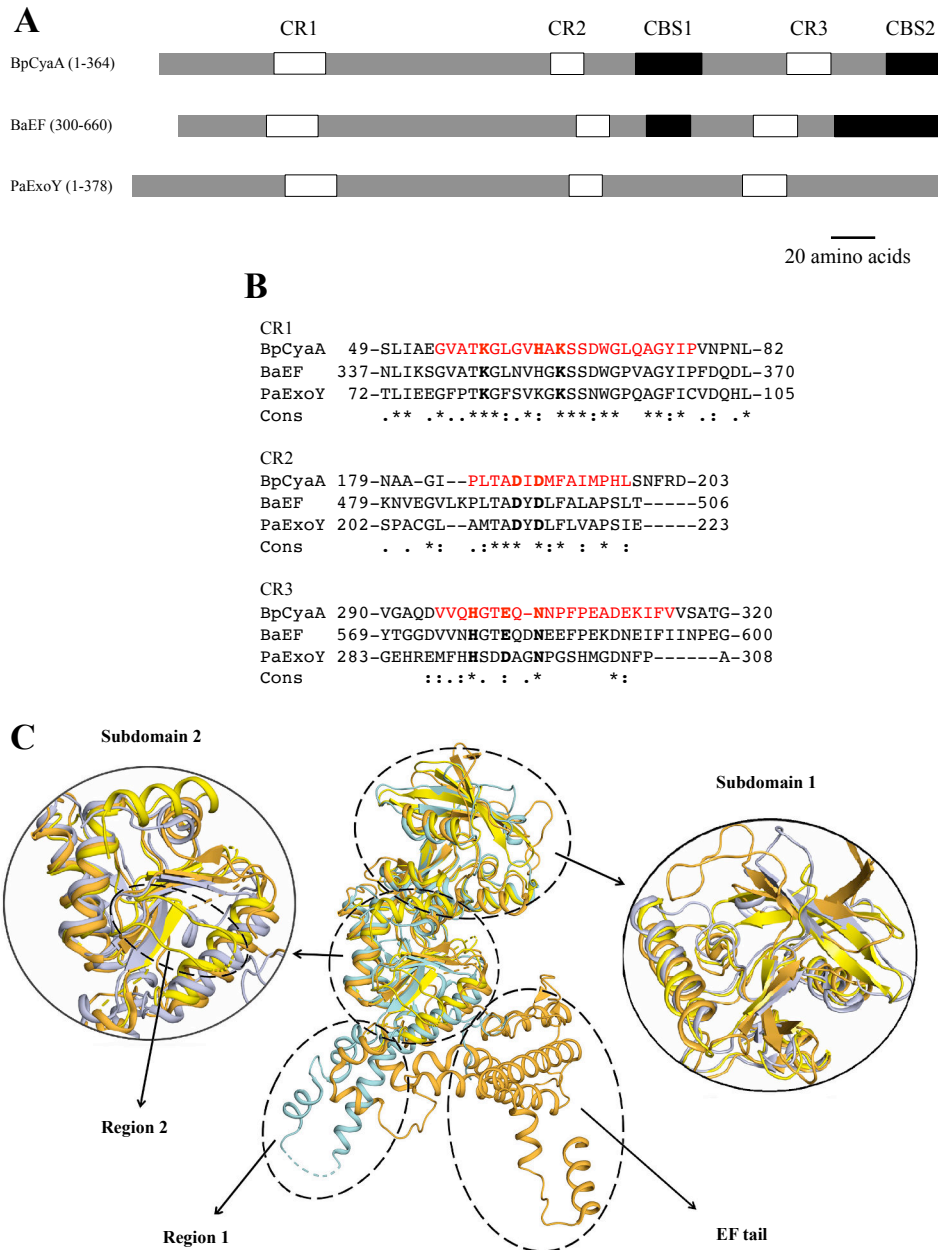

Figure 10. (**A**) Schematic organization of *Bordetella pertussis* CyaA (BpCyaA), *Bacillus anthracis* EF (BaEF) and *Pseudomonas aeruginosa* ExoY (PaExoY) catalytic domains. White boxes indicate the highly conserved catalytic regions (CR1, CR2 and CR3) while black boxes represent CaM binding sites (CBS). (**B**) Sequence alignments of the catalytic regions CR1, CR2 and CR3. The CR regions in BpCyaA are highlighted in red. Bold amino acids were characterized to be directly involved in catalysis. The alignment was performed with the T-coffee algorithm (Notredame et al., 2000). (**C**) Structural comparison of ExoY (yellow, PDB 5XNW) with EF (orange, PDB 1K8T) and CyaA (blue, PDB 2COL). Dashed lines correspond to missing flexible loops in the crystal structure. Region 1 represents the CBS1; region 2 represents the interaction site of F-actin for ExoY; subdomains 1 and 2 represent the two regions adjacent from the catalytic core of ExoY. See text for more details. Adapted from (Belyy et al., 2018; Khanppnavar and Datta, 2018).

These structural data confirm how distinct nucleotidyl cyclase toxins employ a similar disordered-to-ordered transition to regulate their activity. The few dissimilarities observed confer to these toxins their unique properties and specificity to their eukaryotic binding partner.

2.2.2 The translocation region

The translocation of the CyaA catalytic domain across the plasma membrane is unique among all known bacterial toxins but remains poorly described. The translocation model is that after binding to its receptor, the CyaA inserts into the plasma membrane to anchor the toxin. Then, ACD translocates across the membrane (Gordon et al., 1989).

Recently, a protein encompassing ACD, AC384 (residues 1-384 of CyaA), was shown to be able to bind membranes. In addition, a longer polypeptide, AC489 (residues 1-489 of CyaA) exhibits the ability to bind membranes and also to induce membrane permeabilization (Karst et al., 2012). Interestingly, the deletion of residues 375 to 485 within the full length CyaA completely abolishes the intoxication process without affecting the ability of the toxin to bind and to hemolyse targets cells. These data suggest that the region encompassing residues 375-485 plays a crucial role in the translocation process of ACD. This region was thus named the translocation region and encompasses residues 365 to 527 (TR, see Figure 8). *In silico* analyses have predicted two potential α-helical regions in TR (residues 414 to 440 and 454 to 484) that might participate in both membrane partitioning and permeabilization (Subrini et al., 2013). Using various biophysical approaches, it was shown that only the peptide covering residues 454 to 484 exhibits membrane-active properties. This peptide might insert and locally destabilize the lipid bilayer, favoring ACD translocation.

2.2.3 The hydrophobic region

The hydrophobic region (HR) is located between residues 528 to 710 and contains five hydrophobic segments predicted to adopt α-helical structures (see Figure 8). These segments are similar to the hemolytic region of the α-hemolysin from *E. coli* (Oropeza-Wekerle et al., 1992). In 1990, Bellalou and co-workers found that internal deletions in HR (623-779 and 827-886) abolish the invasive activity and severely reduce the hemolytic activity of CyaA,

suggesting that HR is involved in both CyaA delivery and pore formation (Bellalou et al., 1990a). This hemolytic activity results in cation-selective pore formation (Knapp et al., 2003; Benz et al., 1994) .

The impact of HR on the translocation and hemolytic activities of CyaA will be further discussed in part 2.6.

2.2.4 The acyl region

The acylation region (AR) follows HR and encompasses residues 711 to 1005 (see Figure 8). AR is prone to the post-translational acylation on two target sites: lysine 860 and 983. A dedicated CyaC protein performs these acylation, which are chemically called alkanoylations. They are essential for the folding and cytolytic activities of CyaA.

Rogel and colleagues were the first to propose that CyaA had post-translational modifications. Surprisingly, when CyaA was expressed in *E. coli*, the recombinant toxin was not able to produce cAMP in cells. However, the adenylate cyclase activity was still present *in vitro* (Rogel et al., 1991). In parallel, the identification of the *cya* locus (Glaser et al., 1988a, 1988b) has allowed the identification of a gene, *cyaC*, upstream to *cyaA* (Barry et al., 1991). Then, Hewlett and co-workers have shown that a mutation in the *cyaC* gene in *B. pertussis* strain lead to the production of a toxin as active as the wild type. However, this toxin was non hemolytic and had no cAMP activity in cells. Interestingly, direct injection of this mutant into the cell induced cAMP production (Hewlett et al., 1993). Thus, these results clearly showed that the *cyaC* gene needs to be co-expressed with the *cyaA* gene to produce the active form of the toxin.

The *cyaC* gene has sequence similarities with the *hlyC* gene from *E. coli*, which catalyzes the post-translational activation of the HlyA hemolysin (Wagner et al., 1988; Nicaud et al., 1985). Furthermore, the *cya* locus shares a similar organization than the *hly* locus. The *cyaA* gene is followed by two downstream genes *cyaB* and *cyaD*, which have homologs in *E. coli* (Glaser et al., 1988b) (see Figure 11). The last gene, *cyaE*, has no homologous gene in *E. coli* but shares a similar function with *tolC* for hemolysin secretion (Wandersman and Delepelaire, 1990). Finally, *cyac* and *hlyc* are upstream of the structural gene but, in contrast

to *E. coli*, the open reading frame of *cyaC* is oriented oppositely from the *cyaA* gene. Thus, CyaC acts in *trans* to active the CyaA toxin post-translationally.

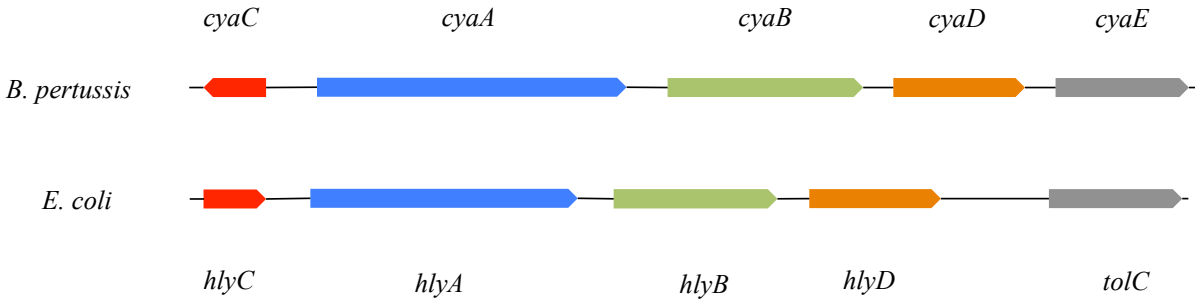

Figure 11. Schematic organization of the *cya* and *hly* locus. *cyaA* and *hlyA* correspond to the structural gene. *cyaB*, *cyaD*, *cyaE* and *hlyB*, *hlyD* and *tolC* code for the export machinery. *cyaC* and *hlyC* code for the activators. The direction of transcription is given by the orientation of the boxes.

Hackett and colleagues performed the comparison of the wild-type CyaA and a *B. pertussis* CyaC mutant. As expected, only the wild-type toxin had a post-translational modifications and exhibited both hemolytic and catalytic activities. This toxin was modified by amide-linked palmitoylation on the ε-amino group of K983 (Hackett et al., 1994). In parallel, Heveker and co-workers have tried an *in vitro* chemical approach using various acyl chains (lauric, myristic or palmitic acid chains) to confer both hemolytic and cytotoxic activities to CyaA (Heveker et al., 1994). Interestingly, it confers activities but quite lower than the *in vivo* toxin. This result suggests that acylation in *B. pertussis* is not random and is performed on specific sites (Heveker et al., 1994).

When CyaA is expressed in *B. pertussis* or *E. coli*, the pattern and chemical nature of the acylation are different. Compared to the native toxin, which is thought to be only palmitoylated, in *E. coli*, the K983 was observed to be both palmitoylated (87%) and myristoylated (13%) (Hackett et al., 1995).

RTX toxins are acylated on adjacent lysines (Stanley et al., 1994). K758 and K860 of CyaA were then investigated with respect to potential modification. Mass spectrometry analyses have shown that K758 was unmodified while two-thirds of K860 was palmitoylated on a recombinant CyaA from *E. coli* (Hackett 1995). Acylation of K860 was also CyaC dependent, which suggests that both K860 and K983 acylation occur only in the

CyaA toxins produced in *E. coli*. However, later studies have shown that K860 was fully palmitoylated in *B. pertussis* and suggests that acylation of this residue could differ among bacterial strains (Havlicek et al., 2001). Surprisingly, the recombinant toxin showed a reduced hemolytic activity. The fact is that both sites can be also acylated by palmitoleic acid (*cis* Δ9-C16:1) and not only palmitic acid (C16:0) like in the native toxin. It may explain the difference in hemolytic activity (Havlicek et al., 2001; Hackett et al., 1995).

A mono-acylation on K983 only is required and sufficient for the CyaA insertion and translocation across membrane (Basar et al., 2001). It also confers a higher hemolytic activity than the mono-acylation on K860 (Meetum et al., 2017; Masin et al., 2005). The substitution of the K983 by an arginine (K983R) drastically reduces channels formation in membranes compared to the mutant K860R, proCyaA and CyaA. K860 is also thought to be involved in membrane insertion and translocation of CyaA. In fact, substitution of K860 by an arginine (K860R) caused a ten-fold decrease of toxin activity with a five-fold reduction of cell association and two-fold reduction in cell penetration (Basar et al., 1999). In the absence of K983, the acylation of K860 allows CyaA to bind and partially intoxicate cells expressing CD11b/CD18 only (Masin et al., 2005). Then, K860 plays itself a crucial role in membrane insertion and translocation, whatever its acylation status (Basar et al., 1999). It remains not clear why CyaA is produced with two acylations. It is suggested that acylation of the two lysines is redundant in function and that one lysine acylated may be sufficient to convert proCyaA into an invasive CyaA toxin.

Therefore CyaA is synthetized as an inactive precursor proCyaA, which is acylated in two positions K860 and K983, able to intoxicate cells. As described before, CyaC shares extensive sequence homology with many RTX C proteins such as HlyC from *E. coli*, which suggests a similar mechanism of acylation (Trent et al., 1999). The CyaC enzyme catalyzes the transfer of a covalent acyl chain from an acyl-ACP (acyl-carrier protein) to the ε-amino groups of proCyaA lysines. The reaction consists of two partial reactions with an acyl-HlyC intermediate, as described by the following reaction for HlyC (Worsham et al., 2001; Issartel et al., 1991).

$$\text{Acyl-ACP} + \text{HlyC} \Leftrightarrow [\text{HlyC}\bullet\text{acyl-ACP}]_{\text{intermediate}} \Leftrightarrow \text{acyl-HlyC} + \text{ACP-SH}$$

$$\text{acyl-HlyC} + \text{proHlyA} \Leftrightarrow [\text{proHlyA}\bullet\text{acyl-HlyC}] \Leftrightarrow \text{HlyA} + \text{HlyC}$$

During the transient formation of the acyl-CyaC intermediate, the site of acylation is likely a conserved residue. Sequence homology made by Trent and co-workers identified conserved residues among the RTX toxins C protein (Trent et al., 1999). Latter data have shown that CyaC possessed an esterase activity against *p*-nitrophenyl acetate and *p*-nitrophenyl palmitate. Based on these data and sequence homology, Thamwiriyasati and colleagues identified S30, H33 and Y66 as crucial residues for CyaC acylation activity (Thamwiriyasati et al., 2010). Single substitution of these residues led to a drastic decrease in specific activity of CyaC. Thus the CyaC-acyltransferase shares a similar mechanism of hydrolysis with a serine esterase where the S30 is part of the catalytic site (Thamwiriyasati et al., 2010). Furthermore, the substitution of residue A140 of CyaC resulted in nearly complete loss of production of biacylated form of CyaA, which suggests that this alanine is a key structural residue for selection of acylation sites of CyaA (Basar et al., 2001).

The non-acylated proCyaA toxin shares comparable features with the acylated CyaA toxin: it exhibits a comparable enzyme activity, undergoes conformational changes upon calcium binding and binds to target cells (Hewlett et al., 1993). Unexpectedly, acylation is not essential for CyaA interaction with lipid membranes and the proCyaA toxin is even more active in permeabilization than the acylated CyaA (Masin et al., 2004). However, acylation is required for CyaA interaction with the CD11b/CD18 receptor and the intoxication of target cells. In fact, the proCyaA toxin binds weakly to the receptor and cannot deliver its catalytic domain, which confirms that acylation is needed for intoxication (Boyd et al., 2005; El-Azami-El-Idrissi et al., 2003). Acylation is also important for oligomerization of the toxin in solution and were shown to induce protective immunity against *B. pertussis* infection in mice (Lee et al., 2005; Betsou et al., 1993).

We recently demonstrated that the acyl chains play a key role in the folding of CyaA into a compact and functional state. These data will be further discussed in experimental results chapter.

2.2.5 The receptor binding domain

The receptor-binding domain (RD) constitutes the C-terminal part of the toxin and is located from residues 1006 to 1706 (see Figure 8). It is composed of about ~40 copies of aspartate and glycine rich repeated nonapeptide motifs GGXGXDXUX (where X is any amino acid and U a hydrophobic residue) organized in five consecutive blocks (named I to V, see Figure 12). Each block contains eight to ten repeats separated by flanking regions of different lengths (23 to 49 residues). They correspond to the main calcium binding sites and consequently are directly involved in cytotoxic activities of the toxin. These repeated sequences are characteristic of the RTX bacterial family (Welch, 2001). RTX proteins are produced by Gram-negative bacteria and constitute a large family with over a thousand of members (Linhartová et al., 2010). They also share a unique mode of secretion *via* dedicated type I secretion systems.

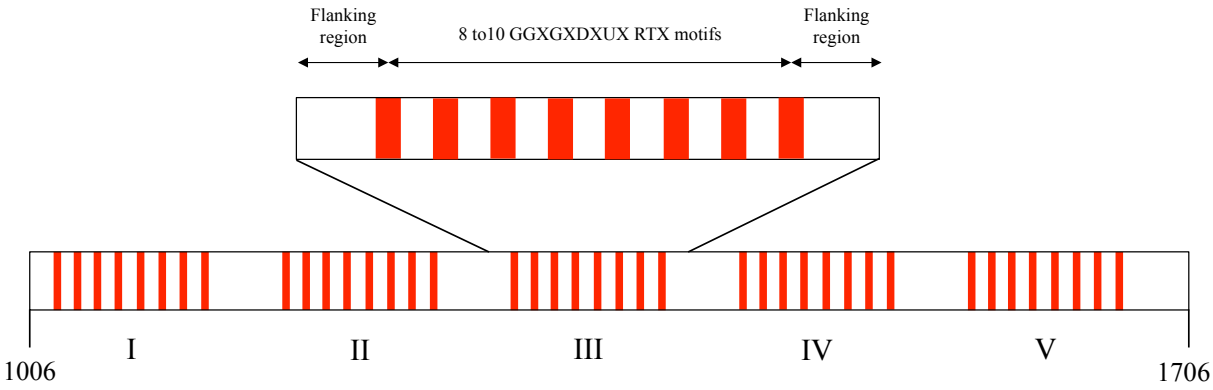

Figure 12. Structural organization of the RD domain of CyaA from *Bordetella pertussis*. RD is made of five blocks, named I to V, each composed of 8 to 10 RTX motifs (GGXGXDXUX). Each red bar represents one RTX motif. Blocks are separated by flanking regions (23 to 49 residues).

Calcium ions are required for CyaA binding to its cell receptor, cytotoxicity and hemolytic activity (Knapp et al., 2003). In fact, several studies have observed that free calcium in solution (*i.e* above 0.3 mM) is essential for the CyaA cell intoxication (Cannella et al., 2017; Hewlett et al., 1991; Gentile et al., 1990; Gordon et al., 1989). Some authors claimed that CyaA had two types of calcium binding sites with completely different affinities. They concluded that the majority of them (40 to 45) were low-affinity binding

sites for calcium and had affinity around 0.5-0.8 mM while a few (3 to 5) had high affinity in the nM range (Rhodes et al., 2001; Rose et al., 1995), although these values depended on the ionic strength used (Sotomayor Perez et al., 2010). Recently, the purification of CyaA into a monomeric state has allowed to propose another explanation about these different affinity sites (Karst et al., 2014). Cannella and colleagues found that the RTX calcium binding motifs in the monomeric CyaA are in high affinity states (Cannella et al., 2017). They proposed that the N-terminus of CyaA (residues 1 to 1005) may stabilize the RTX domain where the calcium ions would be buried into the structure and would experience a slow dissociation rate as compared to the usually CyaA toxin stored in denaturating conditions and directly diluted into buffer.

Baumann and colleagues solved the structure of one member of the RTX family, the alkaline protease from *Pseudomonas aeruginosa* (Baumann et al., 1993). They observed that addition of calcium folds the RTX region into a characteristic β-roll structure. In the structure, the first six amino acids of the repeat (*i.e* GGXGXD) form a turn while the remaining three residues (*i.e* XUX) fold into a short β-strand. The consecutive concatenation of turns and β-strand builds up a right-handed helix with parallel β-strands. Each turn consists of two consecutive RTX motifs. The calcium binds to the conserved aspartic residue of two adjacent turns (Baumann et al., 1993). In the absence of calcium, RD presents the characteristic feature of an intrinsically disordered protein while upon addition of calcium, RD exhibits major conformational changes characterized by an increase of secondary structures (Chenal et al., 2009a; Rose et al., 1995; Hewlett et al., 1991). Thus, calcium induces disorder-to-order transition in RD. Recently, Bumba and colleagues solved the crystal structure of the block V of RD (see Figure 13, residues 1529 to 1681) (Bumba et al., 2016). The overall structure of block V appears similar to the structure of the previously solved alkaline protease (Baumann et al., 1993) and the structural model published by O'Brien and colleagues (O'Brien et al., 2015).

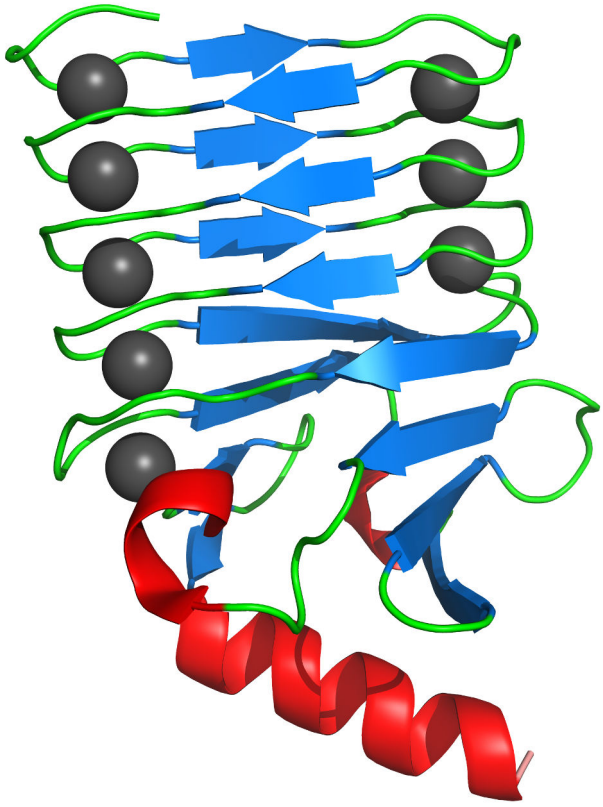

Figure 13. Crystal structure of the block V from the RD domain of CyaA (residues 1529-1681) of *Bordetella pertussis* (PDB 5CVW). The nonapeptide tandem repeats are organized in a regular right-handed helix of parallel β-strands. The first six residues form a turn with a bound calcium ion (black sphere) while the last three form a β-strand. Adapted from (Bumba et al., 2016).

Each block in the RD domain is separated by non-RTX sequences of variable length (23 to 49 residues), called flanking regions (see Figure 12). They are essential for the folding of the RTX toxins, acting as stabilizers of the β-roll structure (Sotomayor Perez et al., 2010; Bauche et al., 2006).

The calcium-induced folding completely changes the biophysical characteristics of RD (see Table 2). In the absence of calcium (*i.e* apo state), RD is characterized by structural disorder, high hydrodynamic radius, elongated shape and is highly hydrated due to the internal electrostatic repulsions between negative residues. These are the hallmarks of intrinsically disordered proteins. CyaA harbors about 40 calcium-binding sites suggesting that each RTX motifs is loaded with calcium. The calcium binding (*i.e* holo state) triggers a

strong reduction of the mean net charge, compaction, dehydration, folding and stabilization of RD (Sotomayor-Perez et al., 2011; Chenal et al., 2009a).

Table 2. Biophysical characteristics of the RD domain in absence (apo) or in presence of calcium (holo). Adapted from (Sotomayor-Perez et al., 2011; Chenal et al., 2009a).

	Apo RD	Holo RD
Molecular weight (g/mol)	72672	72638
Theoretical charges	-85	-18
Shape	Elongated	Compact and prolate
Intrinsic viscosity (mL/g)	35.1	5.5
Sedimentation coefficient (S)	2.5	4.5
Hydrodynamic radius (nm)	7.2	3.1
Hydratation (g/g)	10.3	0.3

The calcium concentration in the bacterial cytosol is quite low (*i.e* < 0.3 μM) and largely below the affinity of RD for calcium (Sotomayor Perez et al., 2010; Dominguez, 2004; Rose et al., 1995). Thus, inside the bacteria, RD adopts an elongated and unfolded conformation favorable for the secretion through the type I secretion system (T1SS) (see Figure 14). Upon reaching the extracellular calcium-rich medium (*i.e* 2 mM), RD acquires secondary and tertiary structures. The stabilization of the holo-state prevents any backtracking into the secretion channel (O'Brien et al., 2015).

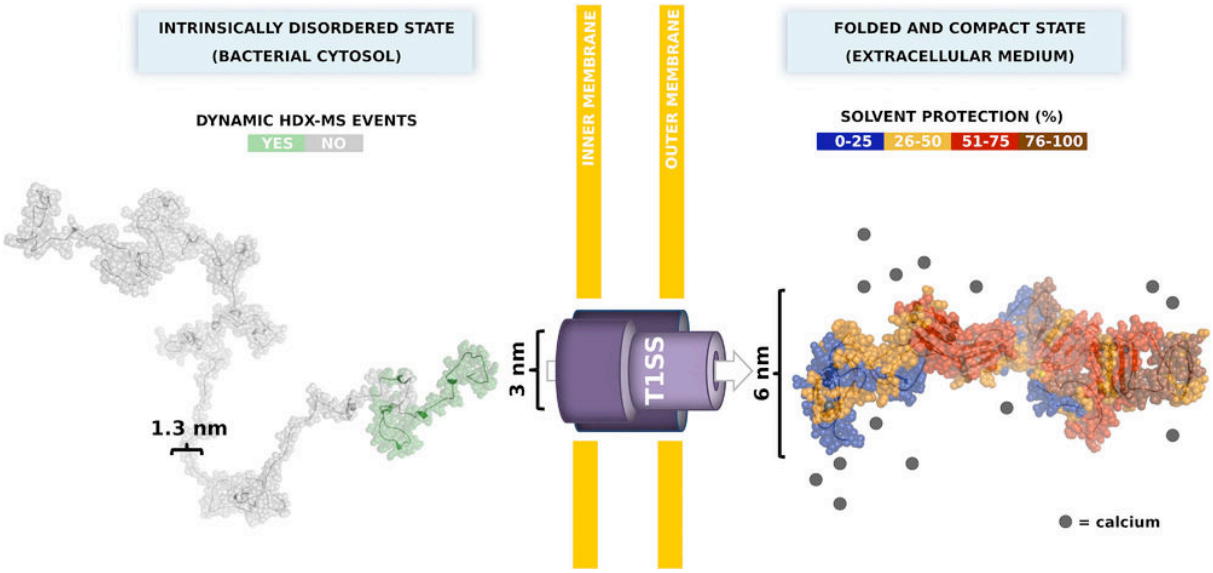

Figure 14. Structural model of the secretion of the RD domain of CyaA. Inside the bacteria, RD is flexible and has an extended conformation with a small diameter (1.3 nm) appropriate for transport through the narrow channel of the T1SS (3 nm). The extracellular calcium-rich environment induces folding of RD into a compact and stable structure larger than the T1SS (6 nm), preventing any back transport. This disorder-to-order transition is essential for the CyaA secretion. Black spheres represent calcium ions. From (O'Brien et al., 2018).

The secretion signal of CyaA is located at its C-terminal extremity (see part 2.2.6), which supposes that the block V of RD is the first part of CyaA to reach the extracellular medium. Upon secretion and calcium binding, the block V is stabilized and could act as a nucleation site for the rest of the RD domain and also for the rest of the toxin (Sotomayor-Perez et al., 2014). This cooperative reaction might improve the efficiency of the secretion process (Kloss et al., 2008) and the folding process of CyaA (Cannella et al., 2017).

Recently, Karst and colleagues were able to produce CyaA into a monomeric and fully active form using molecular confinement and denaturant-free conditions (Karst et al., 2014). Its characterization showed that once refolded, the monomeric holo-CyaA (*i.e* in presence of calcium) was remarkably stable, even in a medium depleted of calcium (Cannella et al., 2017). Furthermore, holo-CyaA displayed an efficient hemolytic activity even in the absence of free calcium in the medium. However, the translocation of the catalytic domain was only

observed in the presence of free calcium (> 0.3 mM), indicating that calcium ions are actively involved in the translocation process. Structural and hydrodynamic studies have also shown that the different regions of CyaA interact in the monomeric state, which leads to the overall stabilization of CyaA. Thus these data suggest that RD binds calcium ions with high-affinity and is somehow stabilized by the rest of the domains (and acts as a scaffold for the folding of the other domains) (Cannella et al., 2017).

2.2.6 The secretion signal

The last C-terminal residues of CyaA contains the secretion signal recognized by the type I secretion system (see Figure 8). CyaB recognizes this signal, located within the last 74 residues of CyaA. The secretion signal drives the secretion of the CyaA toxin through the channel (Sebo and Ladant, 1993).

We have investigated whether these 74 amino acids were able to interact with membranes during the secretion process but we found that the secretion signal does not interact with membranes (unpublished data).

2.3 Secretion of the CyaA toxin

As described in the previous part, the last 74 residues at the C-terminal end of CyaA correspond to the secretion signal. This signal is not processed and is recognized by a dedicated type I secretion system machinery (T1SS) (Bellalou et al., 1990b; Glaser et al., 1988b). The T1SS is encoded by the *cyaB*, *cyaD* and *cyaE* genes belonging to the *cyaABDE* operon. It implies that CyaA is produced, translated and acylated before its secretion through the T1SS (Delepelaire, 2004). These steps do not involve the formation of an intermediate and the secretion process has been proposed to be in one single step from the bacterial cytosol to the extracellular media, like others type I secreted proteins (Delepelaire and Wandersman, 1990; Holland et al., 1990; Felmlee et al., 1985).

The T1SS is composed of three proteins. CyaB is made of 712 amino acids that plays the role of an ATP binding cassette (ABC) transporter located in the inner membrane. CyaB is

in charge to recognize the secretion signal. CyaD is a 440 amino acids membrane fusion protein (MFP) located in the inner membrane with an extended periplasmic domain. Finally, CyaE is a 474 amino acids outer membrane protein. The assembly of three proteins forms a channel through the bacterial membrane (see Figure 15) (Kanonenberg et al., 2018).

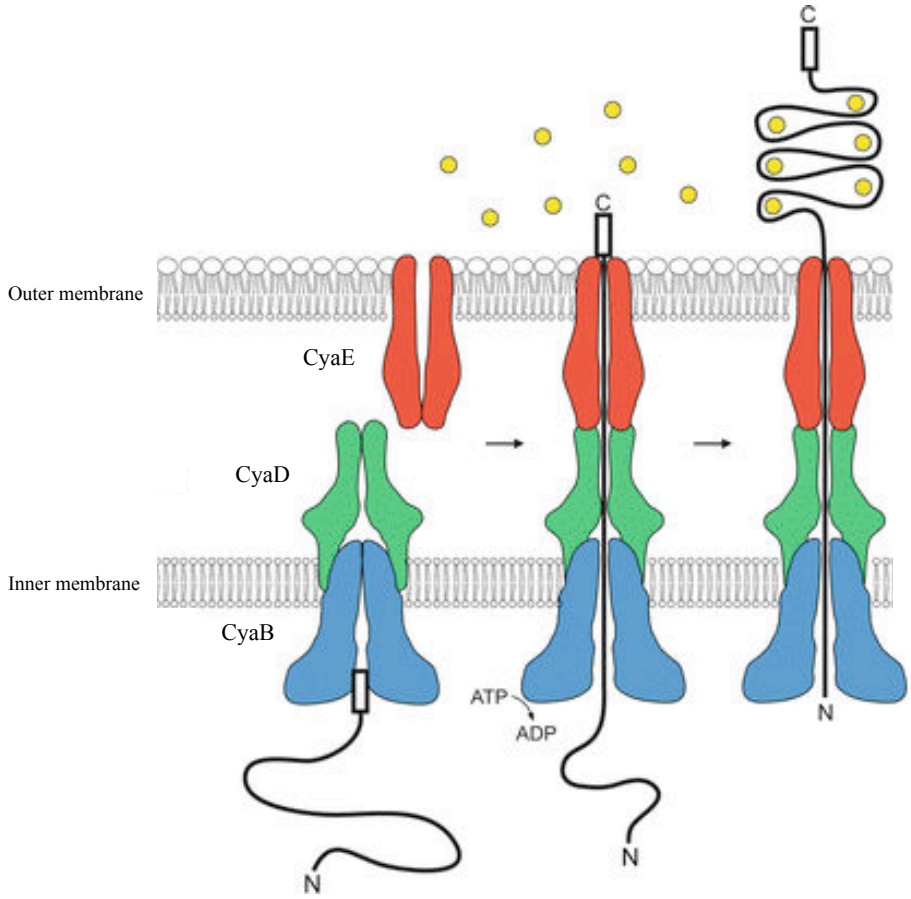

Figure 15. Schematic organization of the T1SS from *Bordetella pertussis*. Upon recognition of the C-terminal secretion signal of CyaA, the inner membrane CyaB-CyaD complex (blue and green, respectively) contacts the outer membrane CyaE (red) and form the channel. The low calcium concentration in the bacteria prevents folding of the C-terminal RTX domain. ATP hydrolysis by CyaB enables the transfer of the unfolded CyaA through the channel. The high calcium concentration (*i.e* 2 mM, yellow spots) in the extracellular environment promotes the folding and prevents back transport. Adapted from (Linhartova et al., 2016).

Many aspects of the secretion of CyaA by the T1SS remain unknown but some similarity exist with the T1SS of the α-hemolysin HlyA from *E. coli* (see Figure 11 previously), which suggests a common mechanism of secretion. CyaB and CyaD have homology with HlyB

and HlyD, sharing up to 50% and 32% of their amino acid sequence, respectively (Glaser et al., 1988b). The last protein CyaE shares sequence homology and a similar function with TolC from *E. coli* (Gross, 1995). This similar mechanism of secretion has been corroborated. In fact, Masure and colleagues showed that *E. coli* could secrete CyaA with the Hly secretion machinery (Masure et al., 1990). However, the secretion signal of HlyA is not conserved in CyaA. A truncated CyaA toxin lacking the secretion signal was not exported by the Hly machinery, suggesting that CyaA contains a specific sequence for its own secretion. Hence, these 74 C-terminal amino acids are crucial for CyaB recognition (Sebo and Ladant, 1993).

For *E. coli*, it has been shown that HlyB and HlyD both associate and form a complex in the inner membrane of the bacteria. The binding of HlyA triggers the interaction with TolC and opens the channel for HlyA secretion (Jo et al., 2019; Thanabalu et al., 1998). By analogy, the assembly of CyaB, CyaD and CyaE should occur upon interaction with the CyaA secretion signal. This latter is recognized by CyaB, which triggers the binding of CyaD and then CyaE to form the T1SS channel (see Figure 15) (Delepelaire, 2004; Létoffé et al., 1996). Once all the secretion machinery is assembled, CyaA is exported from the bacterial cytosol to the extracellular media, without passage in the periplasmic space (Koronakis et al., 2004). The process needs consumption of ATP by CyaB.

The secretion of CyaA occurs from its C- to N-terminus. Thus, RD is the first domain reaching the extracellular medium. As we described before (see part 2.2.5), RD possesses the RTX motifs that are involved in calcium binding and folding of the domain (Sotomayor-Perez et al., 2011; Chenal et al., 2009a). The calcium concentration in the bacteria is low compare to the extracellular medium (few µM and 2 mM, respectively), which allows RD to remain in an unfolded and elongated state. It is proposed that this intrinsically disordered character of RD may facilitate the secretion through the T1SS (Chenal et al., 2009a). Upon secretion, calcium binding induces stable secondary and tertiary structures to form, which may prevent back transport, hence favoring transport of the rest of the toxin (see Figure 15) (Chenal et al., 2010). These recent data will be further described in the experimental results chapter.

It was found that following secretion in *in vitro* cultures, the majority of the CyaA molecules were trapped on the bacterial cell surface due to an interaction with filamentous hemagglutinin (Zaretzky et al., 2002). At the beginning, it was suggested that the surface bound CyaA was the active form of the toxin and could either act by direct delivery to the

target cell or by internalization of the bacteria into the cell (Mouallem et al., 1990; Hewlett et al., 1989). However, it was demonstrated that the active form is not the surface bound CyaA but the secreted and released toxin (Gray et al., 2004).

2.4 Binding of the CyaA toxin to the CD11b/CD18 receptor

CyaA was first considered as a toxin without specific receptor. Indeed, CyaA can bind and intoxicate a wide variety of cells with the same virulence (Ladant and Ullmann, 1999). Additionally, CyaA can bind to erythrocytes in a nonsaturable manner, which do not possess the receptor on the cell membrane (Gray et al., 1999). Although *B. pertussis* and *B. bronchiseptica* produce a slightly different CyaA, they mainly target leukocytes (Fukui-Miyazaki et al., 2018). In fact, previously *in vivo* studies carried out on mice infected by *B. bronchiseptica* demonstrated that the major target of CyaA is macrophages and neutrophils (Harvill et al., 1999; Gueirard et al., 1998). Based on these observations, it was suggested that CyaA may possess a specific binding receptor.

In 2001, Guermonprez and colleagues demonstrated that CyaA binds specifically to the CD11b/CD18 receptor (known also as $\alpha_M\beta_2$ integrin or complement type 3 receptor CR3) with an affinity in the nM range (Guermonprez et al., 2001). Addition of anti-CD11a or anti-CD11c antibodies did not block the CyaA intoxication in sharp contrast with while anti-CD11b specifically blocked it. Furthermore, the surexpression of CD11b/CD18 in cells dramatically increases the binding and toxicity of CyaA (Guermonprez et al., 2001). This specific interaction for CD11b/CD18 may represent a strategy of evolution of the bacteria to colonize the host and avoid phagocytosis by macrophages and neutrophils.

Interaction of the toxin with its specific cell receptor depends on the folding state of the C-terminal receptor-binding domain. Calcium binding to the RTX motifs induces a conformational change that allows the binding of the toxin to the receptor (Rose et al., 1995; Rogel and Hanski, 1992). Acylation is also required for tight interaction with the receptor (El-Azami-El-Idrissi et al., 2003). Although proCyaA is able to bind to cells expressing CD11b/CD18, it is inefficient in intoxication of cells. It was shown that acylation of K983 was necessary and sufficient for toxin binding and action (Masin et al., 2005; Hackett et al., 1994). Thus, acylation is necessary for an efficient interaction of CyaA with the cells expressing the receptor to trigger cytotoxic effects.

Previous studies have shown that the filamentous hemagglutinin acts as an adhesin and also binds to the CD11b/CD18 receptor (Relman et al., 1990). It was suggested that the filamentous hemagglutinin would upregulate CD11b/CD18 expression (Ishibashi et al., 2002, 1994) and may favor later CyaA intoxication (Zaretzky et al., 2002; Weingart et al., 2000). Nevertheless, it is not clear if these two virulence factors act in cooperation.

El-Azami-El-Idrissi and colleagues showed that the N-terminal catalytic domain (residues 1-364) is not required for the binding to the receptor, while the C-terminal domain (residues 365-1706) exhibited the same activity as the full length CyaA (El-Azami-El-Idrissi et al., 2003). Hence, it was suggested that the receptor-binding site was located in the C-terminal moiety of CyaA. Further studies have identified the region spanning 1166 to 1281 (located between the second and third block of the RD domain), as the one required for interaction with the CD11b/CD18 receptor (El-Azami-El-Idrissi et al., 2003). The insertion of a FLAG epitope (sequence of 12 residues) at positions 1166, 1245, 1273 and 1281 in CyaA completely abolished the interaction with CD11b/CD18. They also observed that the binding capacity was reduced with FLAG in positions 1416, 1623 and 1648, and have suggested another interacting domain (El-Azami-El-Idrissi et al., 2003). However, addition of FLAG at different positions may locally affect the overall folding of the region and may explain why they observed a reduced binding to the receptor.

However, the binding process remains unknown. It is known that the domain I of CD11b binds ligands in a Mg^{2+} or Mn^{2+} dependent manner (Guermonprez et al., 2001). By contrast, CyaA binding occurs without the need of these two cations. A competitive inhibition has shown that the CyaA-receptor interaction depends on the recognition of N-linked oligosaccharides of CD11b/CD18 (Morova et al., 2008). The toxin binding was abolished in the presence of PNGase. Recently, Hasan and colleagues have shown that CyaA needs at least seven different N-glycosylation sites for binding (Hasan et al., 2015).

CyaA can also bind mucosal epithelial cells, which do not express the CD11b/CD18 receptor but harbor a multitude of different types of sugars in their membrane (Eby et al., 2010). Interestingly, CyaA targets these cells during the bacteria intoxication. Similarly, T cells, which do not posses the CD11b/CD18, are sensitive to CyaA (Rossi Paccani et al., 2009).

2.5 The CyaA intoxication process

CyaA can intoxicate a variety of cells, mainly those expressing the CD11b/CD18 receptor present on surface of leukocytes although it is also able to invade cells without the receptor. CyaA has this unique capacity to directly translocate its catalytic domain (ACD) across the plasma membrane (Ladant and Ullmann, 1999). When translocated, CyaA catalyzes the overproduction of cAMP that alters the cell physiology and leads to cell death. Although the precise mechanism of the CyaA internalization remains unknown, different mechanisms of intoxication have been proposed over the years.

It was first suggested that the whole *B. pertussis* bacterium could invade cells. The intoxication by the bacteria was as efficient as the CyaA toxin (Mouallem et al., 1990). However, cAMP production was observed with a lag phase of about 40-60 minutes (Khelef et al., 2001). This lag phase was not observed with the toxin alone, suggesting that the intoxication does not occur with the whole bacteria (Khelef et al., 2001).

The majority of bacterial toxins use endocytic and vesicles trafficking pathways to enter into the cytosol of their target cells (see chapter III). Then, it was suggested that the cytotoxicity of CyaA was due to internalization of the toxin (Confer and Eaton, 1982). The CD11b/CD18 receptor can be internalized and it was possible that CyaA could traffic *via* the endocytic pathway (Khelef et al., 2001). However, CyaA can also invade erythrocytes, which do not possess the receptor and organelles for endocytosis. The use of chemical agents inhibiting the endocytosis and the acidification of endosomes did not block the CyaA intoxication (Gordon et al., 1989, 1988). Furthermore, the accumulation of cAMP reached a plateau within 20-60 min, which is too fast for an endocytic pathway (Farfel et al., 1987; Friedman et al., 1987). All these data indicate that CyaA does not use the endocytic pathway to intoxicate cells.

Dal Molin and colleagues have later demonstrated that, using a fluorescent probe, cAMP accumulation occurred within few minutes underneath the plasma membrane demonstrating direct translocation of CyaA (Dal Molin et al., 2006).

2.5.1 Parameters for the CyaA translocation

Local environment plays a role for CyaA translocation. Otero and co-workers have first reported that CyaA intoxication was driven and controlled by the membrane potential (Otero et al., 1995). A membrane depolarization completely abolished intoxication. Later on, using a functional *in vitro* biomimetic membrane, Veneziano and colleagues found that translocation of the ACD was strictly dependent on the presence of calcium, acylation and application of a negative trans-membrane potential (Veneziano et al., 2013).

In fact, calcium is absolutely required for CyaA folding, binding, cytotoxicity and hemolytic activity (Gordon et al., 1988). As described before, extracellular calcium induces the folding of the receptor-binding domain harboring the RTX motifs, allowing CyaA receptor interaction and then membrane insertion of HR. Chelation of calcium by EDTA abolished penetration of the toxin (Hanski and Farfel, 1985; Confer and Eaton, 1982). However, free calcium in solution (*i.e* above 0.3 mM) is essential for ACD translocation, indicating that calcium is actively involved in the translocation of ACD (Cannella et al., 2017; Veneziano et al., 2013; Hewlett et al., 1991; Gentile et al., 1990; Gordon et al., 1989). Indeed, the recent data obtained with the CyaA into a monomeric and functional state showed that CyaA could insert and hemolyse cells in the absence of free calcium in the medium but its translocation was dependent on free calcium (Cannella et al., 2017; Karst et al., 2014).

The temperature is also an important parameter for translocation. Although CyaA can insert into the cell membrane over a wide range of temperature (*i.e* 4°C to 36°C), the toxin is not internalized when incubated with cells at 4°C (Hanski and Farfel, 1985). The internalization only occurrs above 20°C (Gray et al., 1998; Rogel and Hanski, 1992).

Although proCyaA and CyaA share similar enzymatic activity, undergo conformational changes upon calcium binding and bind to target cells, the proCyaA toxin has not the capacity to deliver its catalytic domain, which indicates that acylation is needed for intoxication (Boyd et al., 2005; El-Azami-El-Idrissi et al., 2003).

CyaA has to interact with the lipid membrane to translocate ACD. *In vitro* studies have demonstrated that CyaA can be inserted into liposomes and artificial lipids bilayers. This interaction is strongly affected by lipid/glycolipid composition (Benz et al., 1994; Gordon et

al., 1989). Thus, membrane composition could affect CyaA insertion and also pore forming activity. Martin and colleagues have demonstrated that lipids favoring nonlamellar phases, negative curvature (*i.e* membrane invagination), flip-flop and lipid scrambling, such as phosphoethanolamine and cholesterol, increased lysis (Martin et al., 2004). It was suggested that these lipids were able to lower the surface pressure of the *cis* side of the membrane and thus facilitate CyaA insertion. Further studies have shown that CyaA could insert into specific microdomains within the cell membrane called rafts and especially in cholesterol rich environment (Vojtova et al., 2006). Cholesterol depletion was found to decrease the penetration of CyaA in cells and liposomes (Bumba et al., 2010). However, it is difficult to imagine how CyaA could insert into lipids rafts, which are composed of lipids that give membrane rigidity. This local membrane composition seems to be not convenient for CyaA insertion into and translocation across the plasma membrane.

The toxin can also intoxicate epithelial cells by targeting their basolateral membrane although these cells lack the CD11b/CD18 receptor (Eby et al., 2010). Eby and co-workers have found that the apical membrane was resistant to CyaA while the basolateral membrane was sensitive. This difference may be explained by the different lipid composition at the two sites of the membrane. Interestingly, they have also shown that the intoxication occurs even in the absence of membrane potential and post-translational acylation (Eby et al., 2010).

When translocated, ACD binds to CaM. It was suggested that the energy of binding may act as the force driving the translocation (Oldenburg et al., 1992). However, CyaA mutants with low affinity for CaM were still able to translocate ACD, suggesting that this high-affinity CaM binding is not required (Heveker and Ladant, 1997). Hence, the energy that drives translocation remains unknown. Interestingly, a positive mean net charge between the residues 222 and 242 (*i.e* overlapping the H-helix, which corresponds to the main CaM binding site) appears crucial for translocation (Karimova et al., 1998a).

Some residues were identified as important for the translocation. Mutations of E509 and E516 (*i.e* in the TR) by a helix break proline blocked the translocation (Osickova et al., 1999). They suggested that the toxin might have two different conformational states in solution, one able to translocate and the other able to form channels. These two states can be obtained by varying the temperature, calcium concentration and the acylation state (Osickova et al., 1999). Basler and colleagues also found that two predicted amphipathic α-helices, located between residues 502-522 and 565-591 and comprising four glutamates

(E509, E516, E570 and E581), were critical for the translocation process (Basler et al., 2007).

Five putative CRAC motifs (for Cholesterol Recognition/interaction Amino acid Consensus) were identified in CyaA. Y632, Y658, Y725 Y738 and Y940 were characterized to play a structural role in α-helice segments that are involved in the translocation of ACD and pore formation (Masin et al., 2017). In addition, Y940 is a key amino acid for the initiation of CyaA penetration into membranes.

Finally, the deletion of regions comprising residues 623-780 and 827-887 (*i.e* in hydrophobic and acylation regions) prevented the invasive activity of the toxin, suggesting that these segments are important for CyaA translocation and hemolysis (Bellalou et al., 1990a).

2.5.2 Translocation model

Although many parameters govern the translocation of CyaA, the molecular mechanism remains poorly understood (see Figure 16).

A three steps model was proposed in erythrocytes lacking the CD11b/CD18 receptor (Rogel and Hanski, 1992). Firstly, CyaA inserts into the plasma membrane at low calcium concentrations. Secondly, it was though that the C-terminal hemolytic portion might create a channel in the membrane through which the N-terminal catalytic domain would translocate. Thirdly, ACD is cleaved by a protease and exerts its activity (Rogel and Hanski, 1992). Nevertheless, toxins lacking hemolytic activity were still competent to deliver ACD, suggesting that the hemolytic activity and the pore formation were two separate events not required for ACD translocation (Osickova et al., 2010; Bellalou et al., 1990a). Furthermore, the channel has a diameter of about 0.6-0.8 nm, suggesting that it is unlikely that ACD might not be able to pass through this narrow channel (Benz et al., 1994). Thus, ACD translocates without passage across a pore (Osickova et al., 2010).

Bumba and colleagues then proposed a revised model based on their studies with cells expressing the CD11b/CD18 receptor (Bumba et al., 2010). They suggested a two steps model: after binding to the CD11b/CD18, the hydrophobic region is inserted into the membrane. Then ACD partially forms a “translocation intermediate” that destabilizes and permeabilizes the membrane, allowing the transfer of external calcium ions. This calcium

activates the calpain protease, which in turn induces the cleavage of the talin and the liberation of the CyaA-receptor complex from the cytoskeleton. The complex diffuses into lipid rafts, in cholesterol-rich environment, where ACD translocates (Bumba et al., 2010). However, the “translocation intermediate” is undefined and this model cannot explain the translocation in erythrocytes lacking the CD11b/CD18 receptor.

Recently, Gonzalez-Bullon and colleagues proposed a novel and interesting translocation mechanism. They reported that CyaA exhibited an intrinsic calcium-dependent phospholipase activity (PLA) (Gonzalez-Bullon et al., 2018, 2017). Furthermore, they identified two residues, S606 and D1079, as part of the catalytic site for PLA. They demonstrated that both residues were important for the translocation of CyaA. Thus, they proposed that CyaA forms a toroidal pore with its PLA activity, allowing the passage of ACD. However, Bumba and colleagues contested these results and showed that CyaA was devoided of PLA activity and that S606 and D1079 were not involved in the CyaA translocation process (Bumba et al., 2018). As observed by Bumba and colleagues, we also demonstrated that the CyaA toxin does not possess any PLA activity. These results will be presented in the experimental results chapter.

Recently, the translocation region was identified as crucial for ACD translocation (Karst et al., 2012). Our recent results on this region and its involvement in the translocation process allowed us to propose a novel intoxication mechanism of CyaA. These results will be presented in the experimental results chapter.

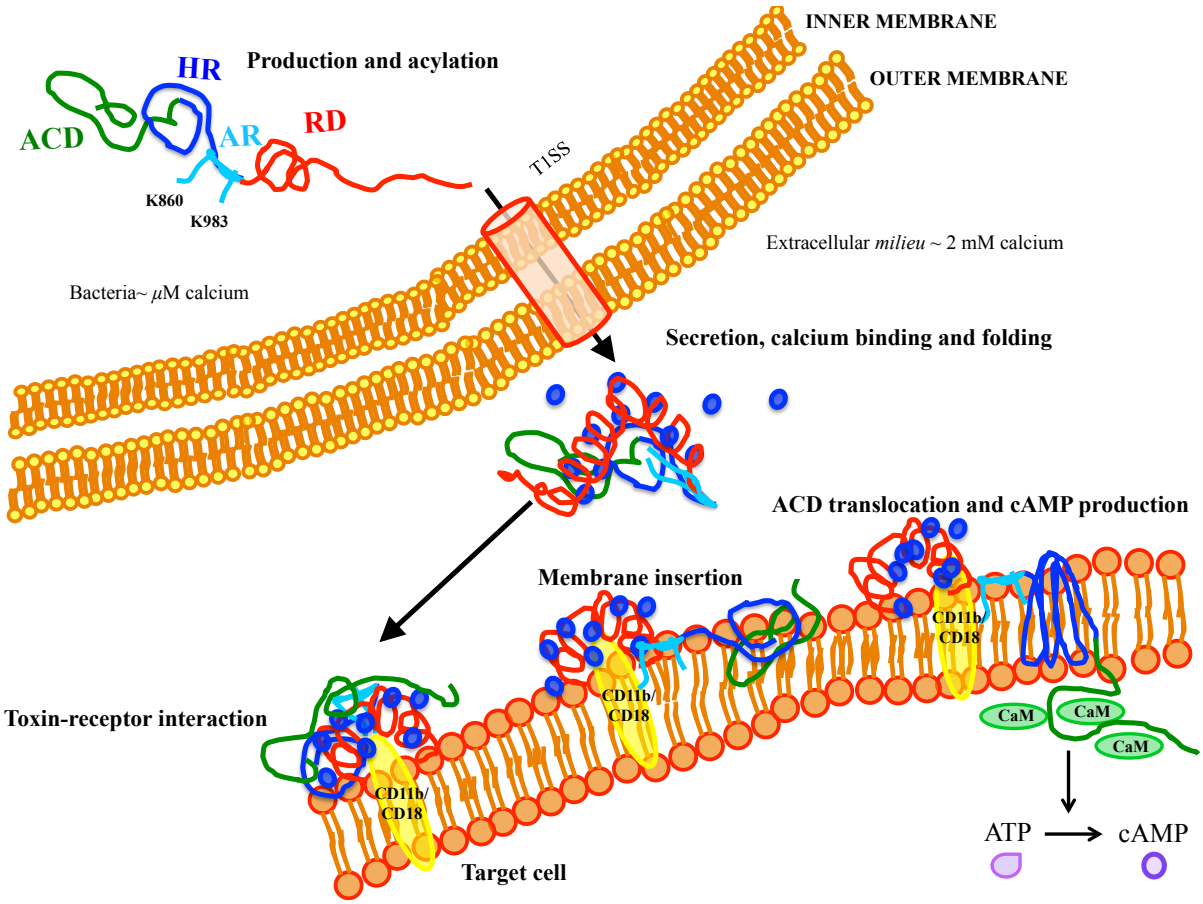

Figure 16. Schematic representation of the translocation mechanism of the CyaA toxin from *Bordetella pertussis*, based on the recent results. Calcium ions are represented by blue dots.

2.6 Hemolytic activity of the CyaA toxin

CyaA belongs to the RTX toxins family, which has the capacity to damage cells by direct formation of pores (Welch, 2001). Thus, beside its adenylate cyclase activity, CyaA was also suggested to posses a hemolytic activity comparable to that observed with HlyA of *E. coli*. Indeed, CyaA has the capacity to cause lysis of erythrocytes (Rogel et al., 1991). This hemolytic activity is located in its C-terminal part. Noteworthy, the two functions of the toxin, its enzymatic and hemolytic activities, can both operate independently but they may act in coordination for the overall toxicity of CyaA (Sakamoto et al., 1992). In fact, a truncated version of CyaA (*i.e* without the catalytic domain) displays a hemolytic activity as efficient as the intact toxin (Sakamoto et al., 1992; Ehrmann et al., 1991).

This capacity to form pore is dependent on a single exposure of calcium in the medium. In fact, an increase of almost 50 fold in hemolysis has been reported after calcium binding to the RTX motifs (Knapp et al., 2003). However, a delay was observed between the exposure to calcium and pore formation, suggesting that the toxin takes time to fold, rearrange, insert and hemolyse membranes (Knapp et al., 2003). Others divalent cations such as Mg^{2+}, Ba^{2+} and Sr^{2+} were tested and only strontium showed a similar effect than calcium. This cation selectivity is not only observed in CyaA but also in others RTX toxins (Knapp et al., 2003; Dobereiner et al., 1996). Interestingly, although the translocation of CyaA depends on free calcium in solution, the toxin is competent to hemolyse without free calcium (Cannella et al., 2017; Rogel and Hanski, 1992).

We described before that the translocation of the catalytic domain is dependent on membrane potential (Veneziano et al., 2013; Otero et al., 1995). Knapp and colleagues investigated the effect of membrane potential on the pore-forming activity of CyaA (Knapp et al., 2008). They found that, depending on the voltage applied, CyaA was able to form two different types of pores. Application of a positive potential at the *cis* side (where the toxin was added), mimicking cell membrane potential, leads to fast pore formation and a conductance of a defined size. However, for a negative potential, the pores were shortened with a very short lifetime (Knapp et al., 2008). In the absence of membrane potential, the pores were identical to those observed with a positive potential. Beside the voltage dependence, they observed that pore conductance was also dependent on the pH. Thus, local protonation and deprotonation of some residues may locally affect the overall structure of CyaA and impact its pore formation capability (Knapp et al., 2008).

CyaA can form small ion-permeable channels with a low conductance compared to that observed for others RTX toxins (Benz et al., 1994, 1989; Ropele and Menestrina, 1989). The channel was identified as cation-selective with a diameter of about 0.6-0.8 nm, up to 5 time smaller in diameter than HlyA from *E. coli* (Ehrmann et al., 1991). However, the diameter appears to be too small for the passage of the catalytic domain through (Benz et al., 1994).

Compared to others RTX toxins, CyaA is weakly hemolytic, which suggests that its main activity is to translocate its catalytic domain and catalyzes the production of cAMP (Bellalou et al., 1990a). In fact, CyaA has a lag of almost 1h for hemolysis, suggesting that it is not immediate after membrane binding. For HlyA, this lag is not observed and supposes that CyaA and HlyA do not exhibit the same mechanism of hemolysis (Fiser and Konopasek,

2009; Bakas et al., 2006; Martin et al., 2004). Furthermore, lysis requires higher toxin concentration (nM) compare to the CyaA translocation (pM), which supports that hemolysis and translocation are two distinct and independent activities of CyaA (Osickova et al., 1999; Gray et al., 1998).

The recent production of monomeric CyaA has allowed us to demonstrate that this latter was the cell-invasive toxin (Cannella et al., 2017; Karst et al., 2014). Several studies reported that the channel formation involves oligomerization of the monomeric toxin, explaining the observed lag time (Kurehong et al., 2015; Gray et al., 1998; Otero et al., 1995; Szabo et al., 1994; Benz et al., 1994). Nevertheless, the precise stoichiometry of oligomers in the membrane remains unknown, although a clear relation between toxin concentration and pore formation exists (Osickova et al., 1999; Szabo et al., 1994). Recently, Gonzalez-Bullon and colleagues demonstrated that CyaA assembles into oligomers of variable stoichiometry and different architectures leading to different size pores (Gonzalez-Bullon et al., 2019).

Acylation of K860 and K983 of CyaA is important to form hemolytic channels (Meetum et al., 2017; Benz et al., 1994; Barry et al., 1991). Indeed, the mutation of these residues have shown to decrease the hemolytic activity. Substitution of K983 drastically reduces the channels formation compared to the K860 mutants (Meetum et al., 2017; Basar et al., 1999). The non-acylated proCyaA has not the capacity to translocate across the plasma membrane. However, pores formation performed in liposomes and artificial bilayers have shown that proCyaA exhibits a higher efficiency of permeabilization than CyaA. It also depends on the nature of lipids and glycolipids and is higher in the presence of negatively charged lipids (Vojtova et al., 2006; Benz et al., 1994). Finally, the acylation modulates oligomerization and contributes to the formation of channels (Basar et al., 1999; Hackett et al., 1995). Interestingly, the hemolytic activity of CyaA is higher for toxins produced in *B. pertussis* than the recombinant forms overexpressed in *E. coli* (Sebo et al., 1991). It is speculated that this difference might be due to the different acyl chains composition when the toxin is produced in *E. coli* (Hackett et al., 1995).

Several studies have provided insights about lysis, although the identity of all segments and residues involved is still not clear. Some random mutagenesis identified that deletions of residues 623-780 and 827-887 abolish intoxication and highly reduce hemolysis, indicating

that these segments are involved in CyaA delivery and pore formation (Bellalou et al., 1990a).

The hydrophobic region (*i.e* HR encompassing residues 528-710 of CyaA) has five predicted α-helices (*i.e* $\alpha1_{(500-522)}$, $\alpha2_{(529-550)}$, $\alpha3_{(570-593)}$, $\alpha4_{(570-593)}$ and $\alpha5_{(602-627)}$). Many recent mutageneses in these regions have highlighted implication of residues. It was shown that proline replacement in each predicted helix was marked by reductions in hemolytic activity on erythrocytes, especially in helices α2 and α3 (Kurehong et al., 2017; Powthongchin and Angsuthanasombat, 2009). Recent data identified that helix α2 plays a key role in both penetration and pore-forming activity of CyaA (Roderova et al., 2019; Prangkio et al., 2018).

The pore formed by CyaA is only cation-selective (Benz et al., 1994) and appears to be controlled by pair of negatively charged glutamate residues within the segments (E509 + E516 and E570 + E581) (Basler et al., 2007; Osickova et al., 1999). Interestingly, mutation of E509 and E516 by lysine strongly enhanced the channel-forming activity of CyaA (Knapp et al., 2003). However, it reduced the cation selectivity of the channel and also modulated the frequency of pore formation (Basler et al., 2007; Osickova et al., 1999). Residue E570, but not E581, was found to be essential for cation selectivity, suggesting that E570 is close to the pore mouth and has role in cation transport (Kurehong et al., 2011; Basler et al., 2007; Osickova et al., 1999).

Additionally, a glycine motif for inter-helices interactions (G530, G533 and G537) located in the predicted helix α2 was identified. It is believed that this cluster might be implicated in stabilization of the helices during CyaA oligomerization in its channel formation in the membrane (Juntapremjit et al., 2015).

2.7 The CyaA toxin in vaccination

Following the discovery of *B. pertussis* in 1906 (Bordet, 1906), many vaccines were developed. The first whole-cell vaccine (Pw) was used for treatment (Klein, 2014; W. C. Rucker, 1912). In the 1930s, a new Pw from chemically inactivated bacteria was developed and showed efficacy for prevention of the disease (Lapin, 1943). In the beginning of 1940s, the first Pw was combined with diphtheria and tetanus. It rapidly decreased the incidence of whooping cough. In France, this vaccine was introduced under the name Vaxicoq® and has shown over 90% of effective protection but with many side effects. Since 1990s, whopping cough is reemerging. This increase of cases is thought to be linked to the switch in the 1980s from Pw to the acellular vaccine (Pa), which is better tolerated but confers a shorter, less effective and specific immune response (Sealey et al., 2016; Gabutti et al., 2015). This resurgence is called the "end of honeymoon" and required to adopt a new strategy of vaccination (Domenech de Celles et al., 2018).

The actual Pa contains some inactivated virulence factors such as pertactin, filamentous hemagglutinin, frimbriae (types 2 and 3) and pertussis toxin. However, any of the commercially Pa contains the adenylate cyclase CyaA toxin, although it is one of the major virulence factors of *B. pertussis*. Yet, it is described that *B. pertussis* strains lacking CyaA have a lower capability to survive in mice models (Cheung et al., 2006; Carbonetti et al., 2005; Goodwin and Weiss, 1990). Furthermore, CyaA can induce a strong antibodies response in naturally infected humans (Farfel et al., 1990). The epitopes targeted against CyaA are not well identified. A study performed by Wang and colleagues has shown that the majority of identified antibodies targets mainly the receptor-binding domain (RD) of CyaA (*i.e* residues 1006-1706) (Wang et al., 2015b). It was suggested that this interaction may block the binding of CyaA to its receptor *in vivo*. Therefore, RD was though to be an interesting antigen candidate for CyaA. However, in the absence of calcium, RD is flexible, disordered and not stable, which would prevent the production of an immune response.

The main problem to include CyaA in a Pa vaccine is its solubility. Indeed, CyaA is a large protein with a pronounced hydrophobic character, prone to aggregation into multimeric forms. Thus, the CyaA overproduced in *E. coli* or extracted from *B. pertussis* is usually stored in chaotropic reagents such as urea and guanidine and these reagents are non suitable for a vaccine formulation (Hewlett et al., 1989; Rogel et al., 1989). Recently, in the lab, Karst and colleagues defined the experimental conditions to obtain CyaA into a folded and monomeric

state in buffer without chaotropic reagents (Karst et al., 2014). Cannella and co-workers further characterized this form and found that the monomeric CyaA is the active form of the toxin for intoxication *in vivo* (Cannella et al., 2017). Thus, the possibility to obtain CyaA into monomeric state without chaotropic agents paves the way to use CyaA as a new antigen for vaccination. Hence, the addition of CyaA into a new generation of acellular vaccines would be definitively a step forward.

In collaboration with the plateforme d'ingénieries des anticorps of the Institut Pasteur, we recently performed a trial of immunization with the monomeric CyaA to investigate whether the monomeric form is antigenic and can induce production of VHHs. VHHs are derived from *camelidae* antibodies, also known as nanobodies. These proteins are more efficiently expressed than conventional monoclonal antibodies. Indeed, we observed that the monomeric CyaA is antigenic. After isolation, screening and production, we obtained 8 different VHHs directed against CyaA. The characterization of these VHHs on CyaA (binding sites, affinity, effects on CyaA activities...) is still under study.

2.8 The CyaA toxin in biotechnology

These last decades, a number of biotechnological applications and tools have been developed based on the biological properties of CyaA. Its unique capacity of translocation and its highly enzymatic activity has been exploited to set up methods of detection and vaccination.

2.8.1 Bacterial adenylate cyclase two-hybrid system

The catalytic domain of CyaA has a modular organization. In fact, the proteolysis of the catalytic domain complexed with calmodulin releases two subdomains: T25 (25 kDa, residues 1-224) and T18 (18 kDa, residues 225-399) (Ladant et al., 1989). The catalytic site is identified in T25 while T18 corresponds to the main calmodulin binding site (Glaser et al., 1989; Ladant et al., 1989). These two separated fragments have the capacity to be reassociated into a functional enzyme producing cAMP. This characteristic has allowed the

design of tools to study bacterial protein-protein interactions: the bacterial adenylate cyclase two-hybrid system (BACTH) developed in the lab.

Interestingly, when the two fragments are co-expressed independently in *E. coli*, they are not able to associate in the cytosol of the bacteria and do not constitute an active enzyme (Karimova et al., 1998b). However, when T25 and T18 are fused to chimeric proteins that have the capacity to interact with each other, T25 and T18 are reassembled, restoring the enzymatic activity (see Figure 17) (Dautin et al., 2002; Karimova et al., 2000a; Ladant and Ullmann, 1999).

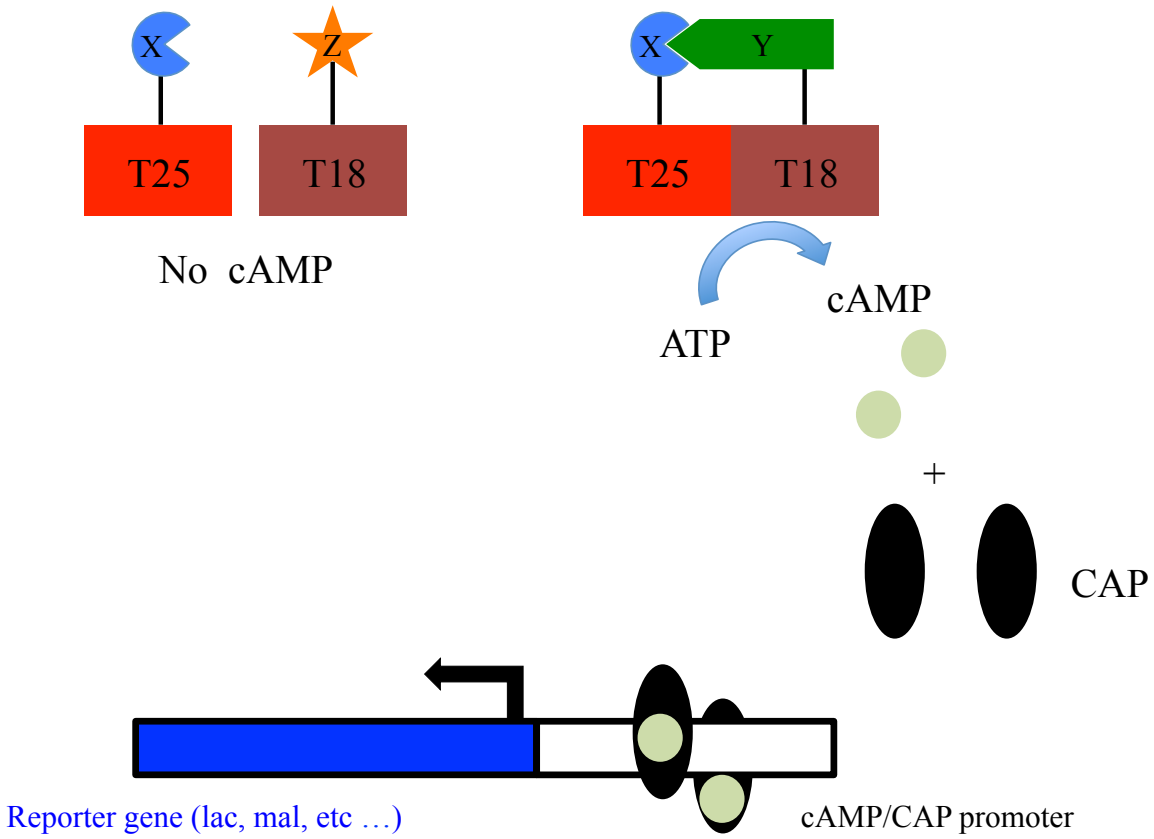

Figure 17. Schematic representation of the BACTH system. See text for more details.

In the presence of calmodulin, an extremely high catalytic constant rate k_{cat} of about 2000 s^{-1} is measured (Karst et al., 2010). However, in the absence of calmodulin (*i.e* absent in the bacteria), a residual but detectable activity of about 2 s^{-1} is detected (Karimova et al., 2000b). Nevertheless, this residual activity is sufficient because the produced cAMP is an important secondary metabolite. Indeed, cAMP binds to the catabolite activator protein CAP, a transcriptional activator, and the complex has the capacity to control the expression of

catabolic genes involved in the catabolism of carbohydrates, such as lactose and maltose (Ullmann and Danchin, 1980; Ullmann et al., 1979). Consequently, *E. coli* utilizes both lactose and maltose as a sole carbon sources, which can be determined using selective media or screening (Olson et al., 2018; Karimova et al., 2000b, 1998b).

This BACTH is possible in *E. coli* strains lacking the adenylate cyclase activity, to be sure that the functional complementation observed is only due to the physical proximity of the two proteins. BACTH allows studying interactions between proteins in the cytosol, in the inner membrane or at the level of DNA.

Nevertheless, the absence of functional complementation does not necessarily indicate that the protein-protein interaction did not occur. One of the reasons may be due to steric hindrance between T25 and T18 that can reduce or even abolishes the enzymatic activity. It depends on how the two fragments are fused to the interacting proteins. On the contrary, a weak interaction between the two proteins may lead to activation.

Hence, the BATCH offers the possibility to perform the analysis of genomes, the screening of potential interacting ligands or the design of new therapeutic agents (Karimova et al., 2009, 2005, Dautin et al., 2002, 2000).

Finally, the catalytic domain of CyaA has been employed to investigate site-specific proteolytic activities in *E. coli* (Dautin et al., 2000). Indeed, a protease-processing site is inserted between the T25 and T18 fragments. In *E. coli*, when a specific protease is expressed, it cleaves this protease-processing site and separates T25 and T18, abolishing the enzymatic activity of the toxin. The addition of a specific protease inhibitor inhibits proteolysis and the toxin remains active to produce cAMP. This technic was successfully tested for HIV-protease and may represent a tool for the screening of protease-inhibitors in patients infected by HIV (Dautin et al., 2000).

2.8.2 CyaA as a reporter for protein targeting

The enzymatic activity of the catalytic domain is activated by the binding of calmodulin. Calmodulin is only expressed in eukaryotic cells and thus the catalytic domain of CyaA may be used as reporter for translocation of a protein from the bacteria to eukaryotic cells. Some

Gram-negative bacteria deliver their virulence factors using a type III secretion system, which act as a molecular syringe (Galan and Collmer, 1999).

It is possible to make a construction of a fusion protein between the bacterial factor and the catalytic domain of CyaA. If the type III secretion system translocates the hybrid enzyme, the activation of the catalytic domain by the host calmodulin induces overproduction of cAMP that can be easily measured. Different groups used this method for type III-secreted virulence factors in, for example, *Yersinia*, *Chlamydia*, *Salmonella* or *Xanthomonas* (Gendlina et al., 2007; Iriarte and Cornelis, 1998; Sory et al., 1995; Sory and Cornelis, 1994).

2.8.3 CyaA as a vehicle for antigen delivery

CyaA has the capacity to interact *in vivo* with cells expressing the CD11b/CD18 receptor. This receptor is present on immune system cells such as dendritic, macrophages, neutrophils or natural killer cells (Guermonprez et al., 2001). Especially, dendritic cells are known to act as antigen presenting cells (APC) and are able to process antigens following the major histocompatibility complex (MHC) class I and II pathways. This induces specific $CD8^+$ and $CD4^+$ T cell responses, respectively.

APC can activate cytotoxic T lymphocytes (CTL) that recognize small peptidic fragments presented on the cell surface of APC. Activation of CTL induce lysis of cells presenting the MHC-I/$CD8^+$ epitope and therefore CTL are important to eliminate cells infected by bacteria, viruses, parasites as well as tumor associated antigens (Finn, 2018; Coulie et al., 2014). This $CD8^+$ T cell response represents an objective for an effective vaccination against many pathogens and tumor cells. With this unique translocation mechanism, the CyaA toxin has been proposed to be used as a vector to present antigens into APC and trigger immune response.

It was investigated to find permissive sites in the catalytic domain (ACD) that can tolerate amino acids insertions without affecting the translocation of CyaA or altering the rest of the toxin for receptor binding and membrane insertion (Sebo et al., 1995; Ladant et al., 1992). Many permissive sites were investigated in ACD (Osicka et al., 2000; Ladant et al., 1992). One particular was identified between the residues 224 and 225 (just between the T25 and the T18). Ability of the inserted protein to unfold is required for translocation (disulfide bound blocks translocation) and its mean net charge is also critical (acidic sequence blocks translocation) (Gmira et al., 2001; Karimova et al., 1998a).

Noteworthy, it is important to detoxify the toxin by abolishing its enzymatic activity through insertion of a dipeptide in the ATP-binding site of ACD to avoid killing APC (Osicka et al., 2000; Fayolle et al., 1996). It is also possible to insert cysteine residues in ACD to graft epitopes (*i.e* CyaA does not contain any cysteine residue) (Fayolle et al., 2004). This system could allow to couple a multitude of $CD4^+$ or $CD8^+$ T-cell epitopes on a single CyaA (Fayolle et al., 2004; Loucká et al., 2002)

Several experiments have been performed to investigate CyaA as epitope deliver. The first evidence was obtained with the lymphocytic choriomeningitis virus (LCMV) nucleoprotein, with insertion of a $CD8^+$ epitope of 15 residues in CyaA (Sebo et al., 1995). The recombinant CyaA-LCMV was able to induce a $CD8^+$ CTL response specific for the LCMV epitope. Interestingly, immunized mice were protected against virulent LCMV while non-immunized ones were rapidly killed (Saron et al., 1997).

Some similar experiments were carried out with the full length Tat of the HIV virus (Mascarell et al., 2006, 2005) and major immunogenic components from *Mycobacterium tuberculosis* (Majlessi et al., 2006). It gave encouraging results.

For the T-$CD8^+$ epitope, the detoxified and grafted CyaA toxin was found to follow the MHC-I pathway (see Figure 18). In fact, Guermonprez and colleagues used the T-$CD8^+$ antigen from ovalbumin (OVA) and found that the recombinant toxin is presented *via* the classical MHC-I pathway: it requires proteasome processing, transport from cytosol to the endoplasmic reticulum and neosynthesis of MHC-1 molecules (Guermonprez et al., 2000) (Guermonprez et al., 1999). Besides the MHC-I pathway, CyaA can also present antigens to the MHC-II pathway and induces a $CD4^+$ T cell response. The maltose-binding protein (MalE) from *E. coli* was able to induce a specific $CD4^+$ T cell response of Th1 type (Loucká et al., 2002; Dadaglio et al., 2000). Interestingly, Schlecht and colleagues used a grafted CyaA with both OVA (class I) and MalE (class II) epitopes and showed that both MHC pathways can be activated (Schlecht et al., 2004). Therefore, the ability of the recombinant CyaA to induce both a $CD4^+$ and $CD8^+$ T cell responses paves the way for further vaccine developments (Chenal and Ladant, 2018).

After the promising results obtained, Dadaglio and colleagues characterized grafted CyaA with $CD8^+$ epitopes overexpressed in melanoma cancer (Dadaglio et al., 2003). They constructed two independent CyaA carrying the HLA-A*02 haplotype, derived from either the tyrosinase or N-acetylglucosaminyltransferase V. They were able to induce a strong CTL

response in mice. *Ex vivo* assays further confirmed that these recombinant toxins are presented by dendritic cells (Dadaglio et al., 2003, 2000). The tyrosinase epitope was chosen for phase I clinical trials as vaccine candidate for melanoma patients.

Another recombinant CyaA carrying the oncogenic E7 protein from the human papillomavirus was shown to induce a specific CTL response with a Th1 $CD4^+$ response in mice (Preville et al., 2005). Although the phase I clinical trials reported promising results, no significant differences were observed between treated patients and the control group in phase II (Chenal and Ladant, 2018).

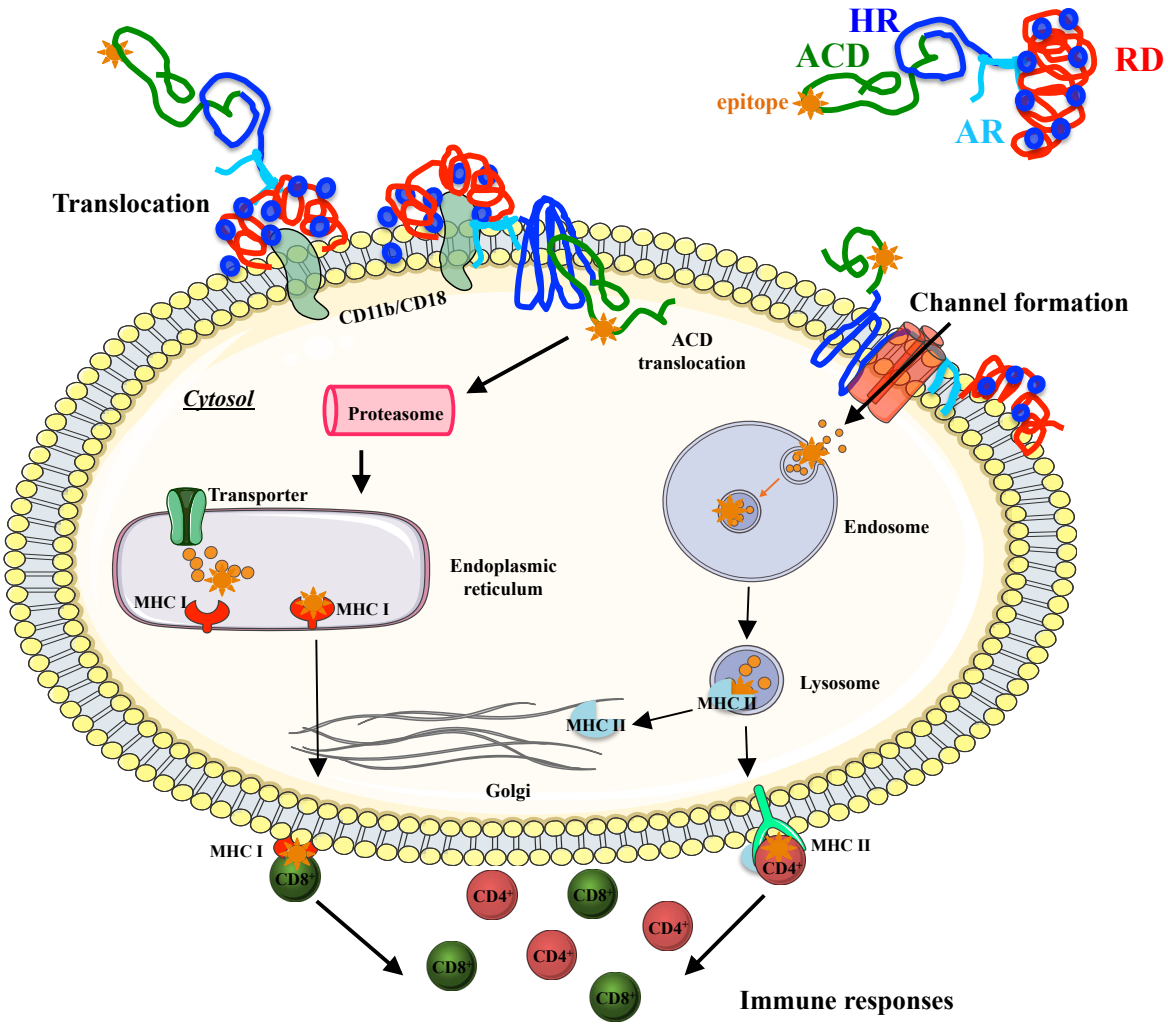

Figure 18. Schematic representation of the induction of the MHC-I and MHC-II pathways in APC. The detoxified CyaA carries an antigen in its catalytic domain. Once translocated, the recombinant CyaA follows the classical MHC-1 pathway to induce a $CD8^+$ response. Alternatively, the recombinant CyaA can enter by endocytosis following the MHC-II pathway to induce a $CD4^+$ response.

Chapter III. Bacterial toxin translocation in host cells

Chapter III. Bacterial toxin translocation in host cells

All organisms possess a biological membrane that envelops the cell, separating the interior from the extracellular environment. The membrane guaranties the maintenance of both composition and concentration of cytosolic molecules and also controls the exchange between the cell and the environment. The passage of extra- and intra-cytoplasmic proteins (those destined for organelles) involves translocation across membranes to reach their final destination. In this protein trafficking, the majority of protein translocations occurs through a protein complex, although others mechanisms exist (Agarraberes and Dice, 2001).

In this chapter, we will focus on the description of the translocation mechanism of proteins and toxins in general. To illustrate our words, selected bacterial toxins will be used as examples to describe their intoxication process and especially how they translocate across the membrane to reach their final localization.

3. Bacterial toxins

To ensure their survival in the host, pathogenic bacteria produce a cocktail of proteins that are toxic for mammalian cells. These toxins manipulate the eukaryotic cell for the benefit of the pathogen by deregulating a variety of pathways. They can act in multiple ways by activating messenger pathways, damaging cell membranes, inhibiting protein synthesis or blocking the release of neurotransmitters. It serves to establish a productive colonization. Although it exists a multitude of toxins produced by different organisms (plants, fungi, virus, animals...), we will focus on bacterial toxins in this chapter and especially on the diphtheria, anthrax, botulinum and cholera toxins.

The CyaA toxin belongs to the AB protein toxin family, which represents the most studied toxins (Ménétrey et al., 2005; Barth et al., 2004). These toxins are produced by Gram-positive and Gram-negative bacteria as well as some plants (*i.e* ricin for example).

The AB designation refers to a toxin composed of a A (Activity) domain that modifies its cellular target by an enzymatic activity upon entry into the cytosol. The B (Binding) domain is composed of one or several subunits responsible for binding to the cell receptor. It also plays the role of delivery system for the A domain within the cell. In some cases, the B domain can be composed of a receptor binding domain and a translocation domain.

AB toxins can be classified into at least three distinct groups based on their structural organization (Matsuzawa et al., 2004; Falnes and Sandvig, 2000) (see Figure 19): (i) in the first group, A and B are synthetized as a single polypeptide chain , which can be specifically separated by a protease but they remain linked by a disulfide bond (see (1) Figure 19). This group includes the diphtheria and botulinum toxins. The CyaA toxin also belongs to this group while its two AB domains are not bound by a disulfide bond (*i.e* CyaA does not posses any cysteine in its 1706 residues); (ii) In the second group, A and B are synthetized as two different subunits that are not covalently bound to each other. They are then assembled together (see (2) Figure 19). Cholera toxin belongs to this group; (iii) the third group is composed of binary toxins. A and B domains are separately produced as distinct proteins. Then, the B domain assembles on the target cell and the A domain is recruited (see (3) Figure 19). This is characteristic of the anthrax toxin.

Commonly, AB toxins are synthetized in an inactive form and are activated by proteolysis at a specific proteolytic site located between the two cysteine forming the disulfide bridge (see Figure 19). Some are processed by cellular proteases and others by the producing organism. It results in a di-chain toxin with the A and B domains linked by a disulfide bond. Interestingly, the CyaA toxin does not undergo any proteolytic processing for activation, but requires acylation as post-translational modifications.

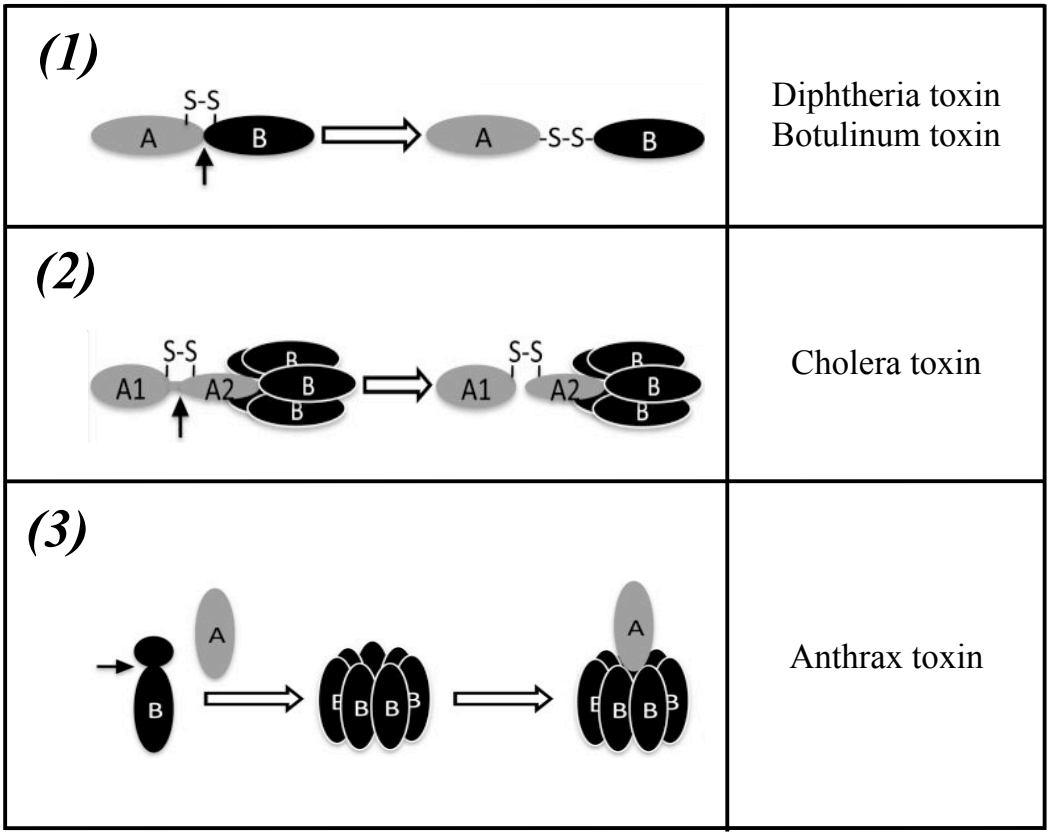

Figure 19. Molecular organization of AB toxins. Black arrows indicate the position of the proteolytic digestion sites. Group (1) corresponds to toxins produced as a single polypeptide chain. Their activation requires a proteolytic cleavage which generates two domains bound by a disulfide bridge. Group (2) contains toxins produced as separate proteins and assembled. The B domain forms a pentamere non-covalently associated with the A domain containing a disulfide bridge. A proteolytic cleavage occurs in the A domain resulting in to fragments bound by a disulfide bond. Group (3) is toxins produced as separate proteins. The B domain is activated by proteolytic cleavage and assembles into a heptameric complex in the surface of the cell that recruits the A domain. See text for more details. Adapted from (Sun, 2012; Ménétrey et al., 2005).

The fundamental property of AB toxins is to deliver their A domain into the cytosol of the target cells. Thus, toxins have developed strategies to cross the host cell membrane. Once secreted, AB toxins need to be associated with a specific cell receptor to initiate their intoxication (Lord et al., 1999). This high-affinity interaction allows toxins to preferentially target specific cells. Then, they take advantage of this interaction and are internalized into endocytic vesicles. Upon endocytosis, the entry into the cytosol can occur in one of two ways (see Figure 20). In the first pathway, toxins travel to the early and late endosomes

where they translocate through a pore to reach the cytosol. In the second pathway, they may continue their "trip" to the Golgi, and from the Golgi to the endoplasmic reticulum (ER), *i,e* the retrograde transport. Then, they translocate from the lumen to cytosol thanks to proteins channels in the ER membrane (Lord et al., 1999).

Although most of the toxins use the endocytosis cellular machinery and intracellular sorting to gain access to the cytosol, some, like the diphetria, anthrax, botulinum and CyaA toxins, carry their own translocation apparatus.

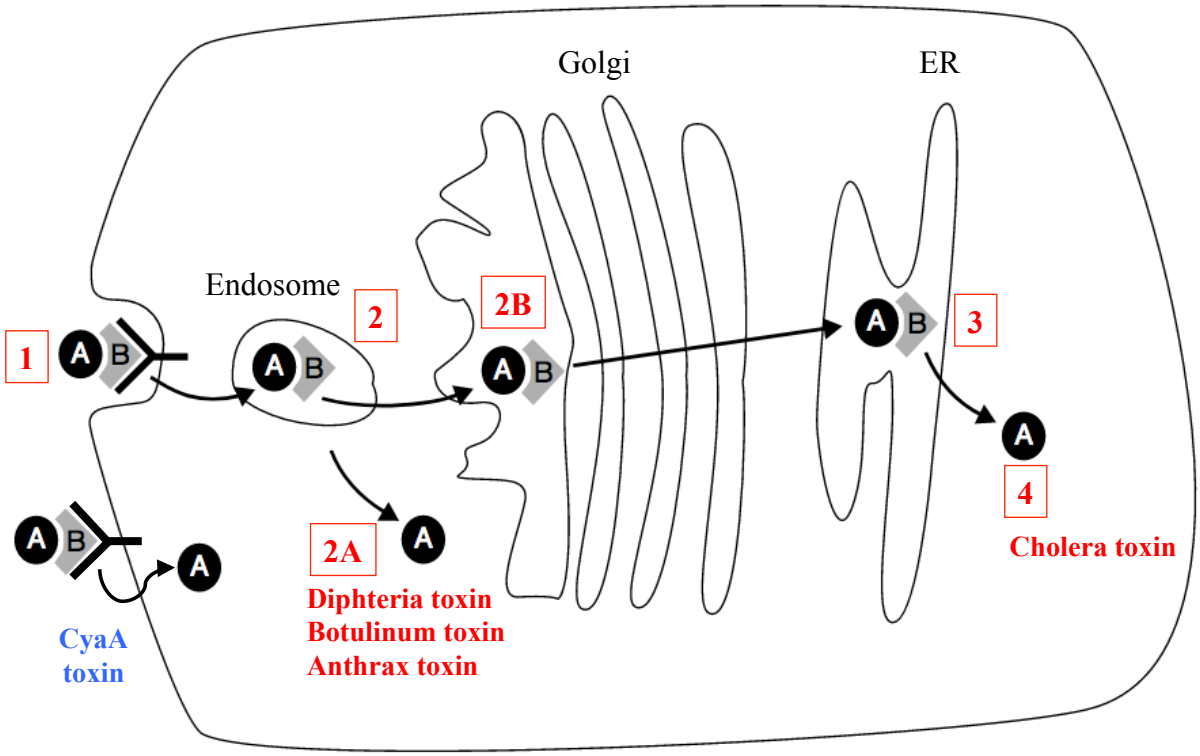

Figure 20. Schematic representation of the AB toxins transport in cells. The toxin binds to its specific cell receptor (Y shaped) through the B domain (step 1). Toxins are endocytosed in endosomes (step 2) and can be either translocated into the cytosol (step 2A) or continue their travel through the retrograde transport in the Golgi (step 2B). Then, they reach the ER (step 3) and are released into the cytosol (step 4). Each final location of the A domain of described toxins in this chapter is indicated on the scheme. In the case of CyaA, the toxin remains at the cell surface after binding to the cell receptor and the A is translocated across the plasma membrane. Adapted from (Sun, 2012; Falnes and Sandvig, 2000).

Although the above-mentioned toxins use a common mechanism of receptor-mediated endocytosis to enter into target cells, it is important to note that other pathogens use an alternative mechanism to deliver their toxins into the cytosol. In fact, some Gram-negative bacteria (such as *Pseudomonas aeruginosa*) deliver their toxins using a type III secretion system, which act as a molecular syringe (Galan and Collmer, 1999). The CyaA toxin from *B. pertussis* has a unique intoxication process: it directly translocates its catalytic domain across the plasma membrane in the presence but also in the absence of its cell receptor. Also the diphtheria toxin is able to directly translocate across the plasma membrane in the presence of an acidic pH.

As mentioned above, the A domain possesses the enzymatic activity directed toward a cytoplasmic target. To reach this target, it implies crossing a target cell membrane. Thus the selected bacterial toxins constitute excellent models to understand physico-chemical and molecular mechanisms underlying the membrane insertion and translocation across membranes and may help to decipher how the CyaA toxin from *B. pertussis* may translocate (Sandvig et al., 2013; Chenal et al., 2009b; Galloux et al., 2008; Reig and van der Goot, 2006).

3.1 Translocation from endosomal escape

Endosomes are organelles distributed in the cytoplasm of eukaryotic cells. When endocytic vesicles are formed, they bind and merge to release their content into the endosome. Then, the intravesicular pH becomes more acidic due to the action of a proton-pumping ATPase located within the endosomal membrane. When the pH progressively decreases, the toxin is dissociated from its receptor and exploits the low pH to undergo structural rearrangements (Lord et al., 1999). They adopt a partially folded state, known as molten globule (Ptitsyn, 1995), characterized by native-like secondary structures maintained but a loss of tertiary constraints and solvent-exposition of hydrophobic surfaces, which is favorable for membrane interaction.

Single-chain and binary toxins (*i.e* groups 1 and 3, respectively) use the endosomal carrier vesicles pathway. Here we will describe how the endosomal acidification triggers conformational changes, which activates the toxin to release its catalytic domain into the cell

cytoplasm. We will also focus on the cellular factors that help the passage through and extraction of the A domain from the membrane.

3.1.1 Diphtheria toxin

The diphtheria toxin (DT) is one of the most studied toxins. It is produced from toxigenic strains of *Corynebacterium diphtheriae* as a single polypeptide of 58-kDa (Kaczorek et al., 1983). The toxin is organized in three parts: the catalytic domain (C), the translocation domain (T) and the receptor-binding domain (R). From the AB designation, C corresponds to domain A and T and R to domain B (Ménétrey et al., 2005). During intoxication, the diphtheria toxin binds *via* R to the proHB-EGF receptor (for heparin-binding EGF) and is cleaved by the cell surface furin (Tsuneoka et al., 1993; Naglich et al., 1992). Then DT enters in the host cells through clathrin-coated vesicles and reaches the endosomes (Moya et al., 1985).

The role of the T domain is to assist the translocation of C. As the pH progressively decreases, some histidine residues are protonated and induce a conformational change of the T domain. T becomes partially unfolded and adopts a so-called molten globule state. As a consequence, it enables the binding to and the penetration into the endosomal membrane (Chenal et al., 2002; Malenbaum et al., 1998; London, 1992). In fact, the neutralization of acidic residues prevents the repulsion with the negatively charged membranes while basic residues drive the penetration of T into the membranes. The C domain can also partially unfold upon acidification. The unfolded state of C is crucial to cross the membrane (Falnes and Olsnes, 1995; Falnes et al., 1994). Thus, T acts as specialized a pH-dependent chaperone for C in solution and for its insertion into membranes (Chassaing et al., 2011).

Following membrane insertion, the N-terminal segment of the T helices (TH1 to TH4) has the capacity to translocate and carries the C-terminal domain of C (see Figure 21 for illustration) (Montagner et al., 2007; Chenal et al., 2002). Once in the cytosol, some cytoplasmic factors “trap“ the C and T domains. Firstly, the coatomer protein complex beta (beta-cop), a protein that participates in trafficking vesicles, binds to the T domain (Ratts et al., 2005). Then, a thioredoxin reductase reduces the disulfide bridge between C and T domains and dissociates them. Finally, C finishes its translocation and is helped by a heat shock protein (Hsp90) that uses the energy provided by the proton-pumping ATPase to

extract and refold the C domain from the membrane (Ratts et al., 2003). Finally, the catalytic domain ADP-ribosylates the elongation factor-2 and thus blocks the synthesis of proteins, which leads to cell death (Honjo et al., 1968).

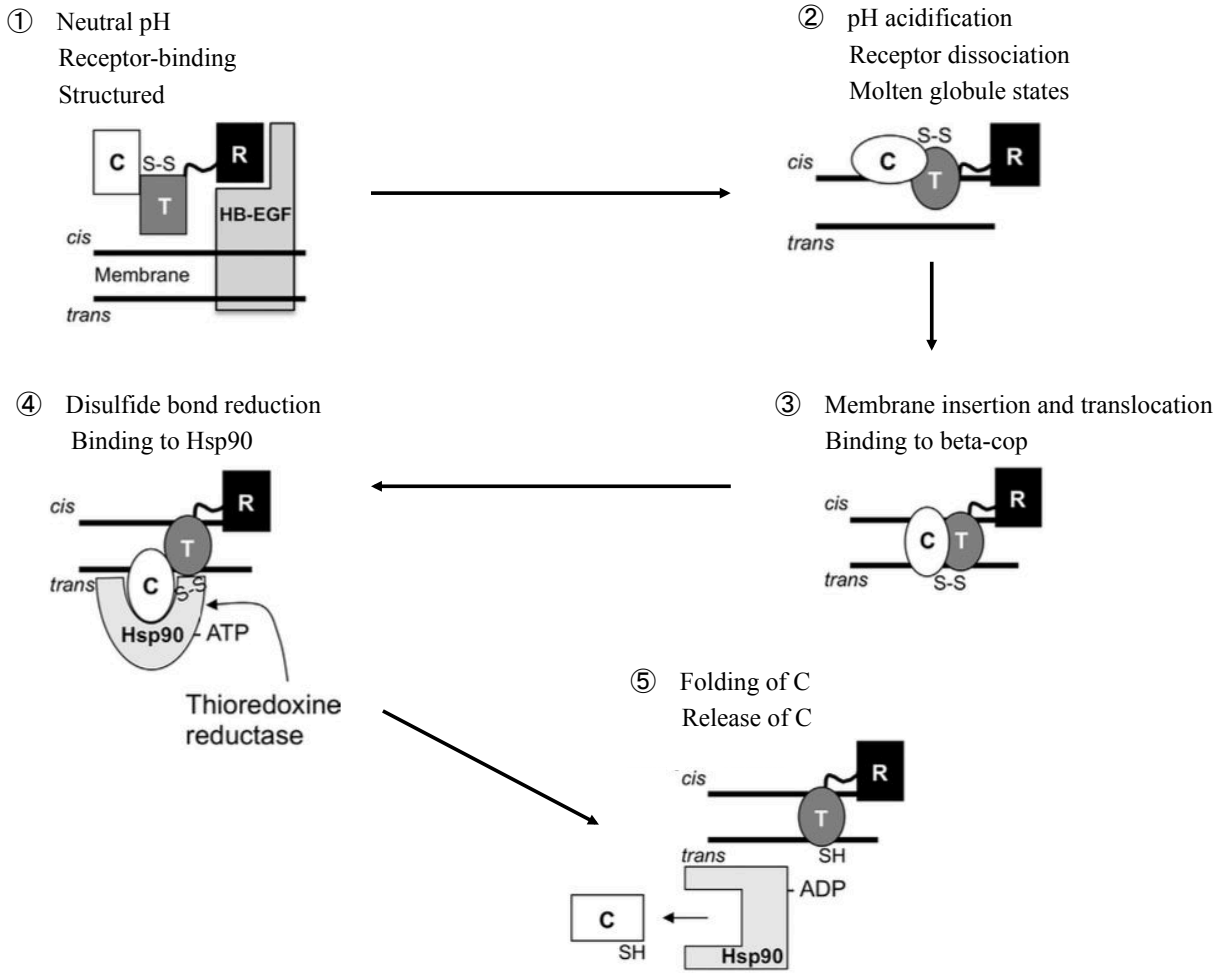

Figure 21. Schematic representation of the diphtheria toxin translocation steps through the endosome. See text for more details. Adapted from (Gillet and Barbier, 2015).

This translocation process is carried out thanks to many structural rearrangements and interactions. Firstly, the pH gradient helps to change the electrostatic balance of the protein and partially unfolds some regions. An exposition of hydrophobic surfaces favors membrane insertion and the electric membrane potential helps the pH-dependent membrane translocation. Secondly, the presence and interaction of cellular proteins with the translocated segments, such as beta-cop and Hsp90, sequester both C and T segments inside

the cytosol favoring the translocation of the C domain. All these factors would represent the energy necessary for the translocation of the catalytic domain of the diphtheria toxin. This is an example of unidirectional transport of protein across membrane.

3.1.2 Anthrax toxin

Anthrax is caused by *Bacillus anthracis* (Moayeri and Leppla, 2004). The bacterium produces a tripartite AB toxin with two alternatives A subunits, the lethal factor (LF) and the edema factor (EF), and a receptor binding B-subunit, the protective antigen (PA). LF is a zinc metalloprotease that cleaves MAP kinase proteins while EF is a calmodulin-dependent adenylate cyclase (Leppla, 1982). The three toxin proteins are individually nontoxic. Although the intoxication process of LF and EF is similar, we will focus here on EF only because it targets CaM for its enzymatic activity, as observed with CyaA.

PA binds to TEM8 (for tumor endothelial marker 8) or to CMG2 (for capillary morphogenesis gene 2), its two known receptors (Scobie et al., 2003; Bradley et al., 2001) (see Figure 22 for illustration). Then, it is cleaved at the cell surface and forms a heptametrical prepore complex in lipids rafts (Abrami et al., 2003). This oligomerization constitutes the receptor of EF. EF binds PA and the toxin-receptor complex is internalized in a clathrin-dependent manner by cellular endocytosis where it is delivered to early endosomes (Abrami et al., 2004; Liu and Leppla, 2003). EF shares similarities with DT trafficking, which suggests that EF is translocated from early endosomes to the cytosol. However, some studies showed that, depending on the nature of the receptor used for entry, EF translocation may occur at different points in the endocytic pathway (Rainey et al., 2005; Abrami et al., 2004).

The progressive acidification of the endosomal lumen induces major rearrangement in PA that inserts its amphipathic loop sequences in the membrane to create a channel. In particular, seven Phe residues form a hydrophobic environment (called Phe-clamp), which act as chaperones for the translocation of EF and maintain the proton gradient (Liu et al., 2015; Krantz et al., 2005). In parallel, acidification also induces unfolding of EF, leads to a molten globule state and confer a net positive charge. Then, the Phe-clamp interacts with the hydrophobic segments of EF. EF proceeds through the channel and neutral pH in the cytosol induces the deprotonation and prevents back transport across the Phe-clamp. Finally, EF

binds CaM in a calcium dependent manner and elevates the intracellular cAMP that imbalances the intracellular signaling pathways (Shen et al., 2005; Leppla, 1982).

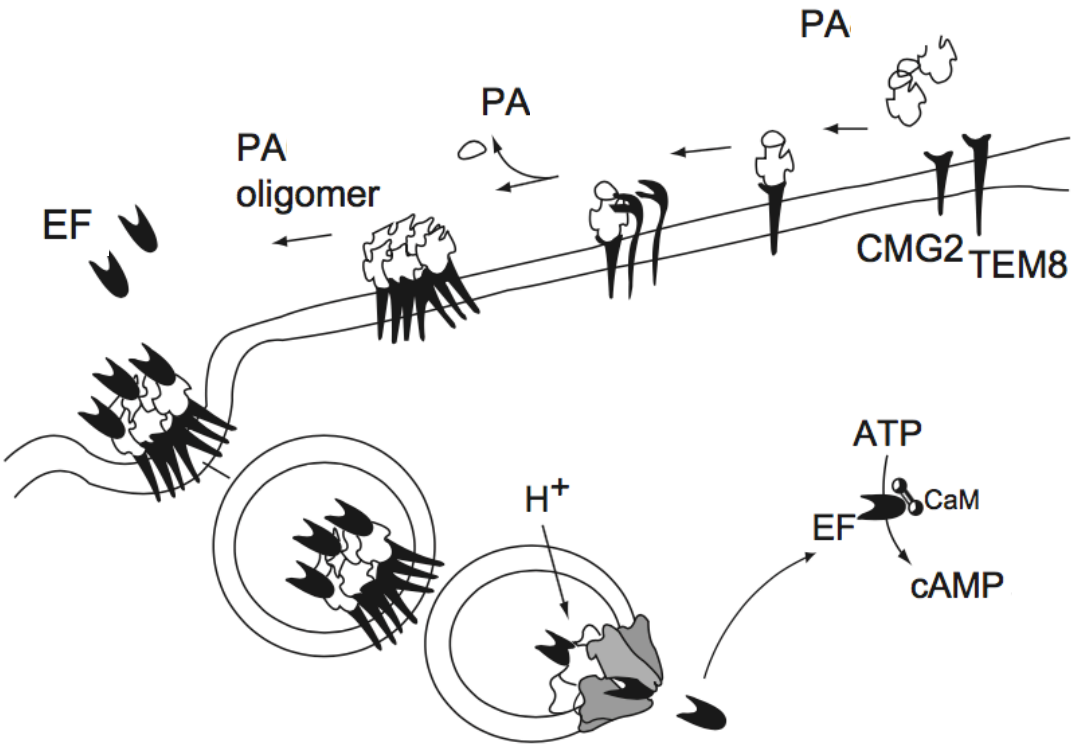

Figure 22. Schematic representation of the intoxication process of the edema factor. See text for details. Adapted from (Liu et al., 2015).

Compared to DT, which needs a pH gradient and some cytosol chaperones to assist its translocation and refolding, EF does not require the same chaperones (Dmochewitz et al., 2011). Here, the proton gradient seems to be the major energy driving the translocation of EF but the Phe-clamp is also required to promote unidirectional translocation across membrane. Furthermore, EF has a high affinity in nM ranges for CaM. Thus, CaM in the cytosol (*i.e* 1 to 10 µM in cells) might bind translocating EF and help pulling it into the cytosol.

3.1.3 Botulinum neurotoxin

Among Clostridium species, *Clostridium botulinum* and *Clostridium tetani* produce the botulinum and tetanus neurotoxins, respectively. These toxins are responsible of neuroparalytic diseases. Despite their amino acid sequence dissimilarities, they share a similar architecture and mechanism of intoxication. Here we will focus on the botulinum toxins (BoNT) only.

It exists seven isoforms of BoNT designated as BoNT/A to /G (Poulain et al., 2008). BoNT is synthetized as a unique polypeptide that is cleaved to generate two polypeptides linked by a disulfide bond (Lacy et al., 1998). From the AB designation, the A moiety corresponds to the light chain (LC), which carries the catalytic activity. The heavy H chain, corresponding to the B moiety, encompasses two domains: the translocation domain at the N-terminus (H_N) and the receptor-binding domain at the C-terminus (H_C). The three domains are required for BoNTs cell intoxication.

H_C mediates the binding to polysialoganglioside and synaptic vesicles (SV). BoNT is then endocytosed by a clathrin-dynamin dependent manner in recycling neurosecretion vesicles (see Figure 23 for illustration) (Colasante et al., 2013; Harper et al., 2011; Binz and Rummel, 2009). When endocytosis is completed, the SV lumen is acidified with the proton ATPase. Then, how LC is translocated remains largely unknown. It has been proposed that H_N could ensure a dual channel and chaperone activity. For this model, H_N forms a channel and would escort the unfolded LC through the membrane to reach the cytosol (Fischer and Montal, 2007; Koriazova and Montal, 2003). Another model suggested that H_N could act as a hydrophilic cleft allowing hydrophilic regions of LC to cross the membrane (Montecucco et al., 1989, 1988).

As observed for DT and EF, the progressive acidification triggers major conformational changes leading to a molten globule state. For BoNT, the pH decrease does not induce any major conformational change in LC and H_N, although local conformational changes may occur (Araye et al., 2016; Lai et al., 2010; Galloux et al., 2008). A recent study has shown that H_N stabilizes LC as a chaperone-like domain and limits the capacity of LC to penetrate and destabilize membrane (Araye et al., 2016). As a consequence, the proposed hydrophilic cleft model appear compatible (Montecucco et al., 1989, 1988). H_N would form a channel

where LC passes through to reach the cytosol. LC should interact with both with H_N and the membrane during its translocation.

The disulfide bond linking LC and H_N is reduced by the thioredoxin reductase to release LC from the channel. Recently, it was found that Hsp90 is also present and cooperates with the reductase to fold and active LC (Azarnia Tehran et al., 2017). Then, LC acts as a zinc-metalloprotease that cleaves SNARE proteins and thus blocks neurotransmitters release, causing flaccid paralysis.

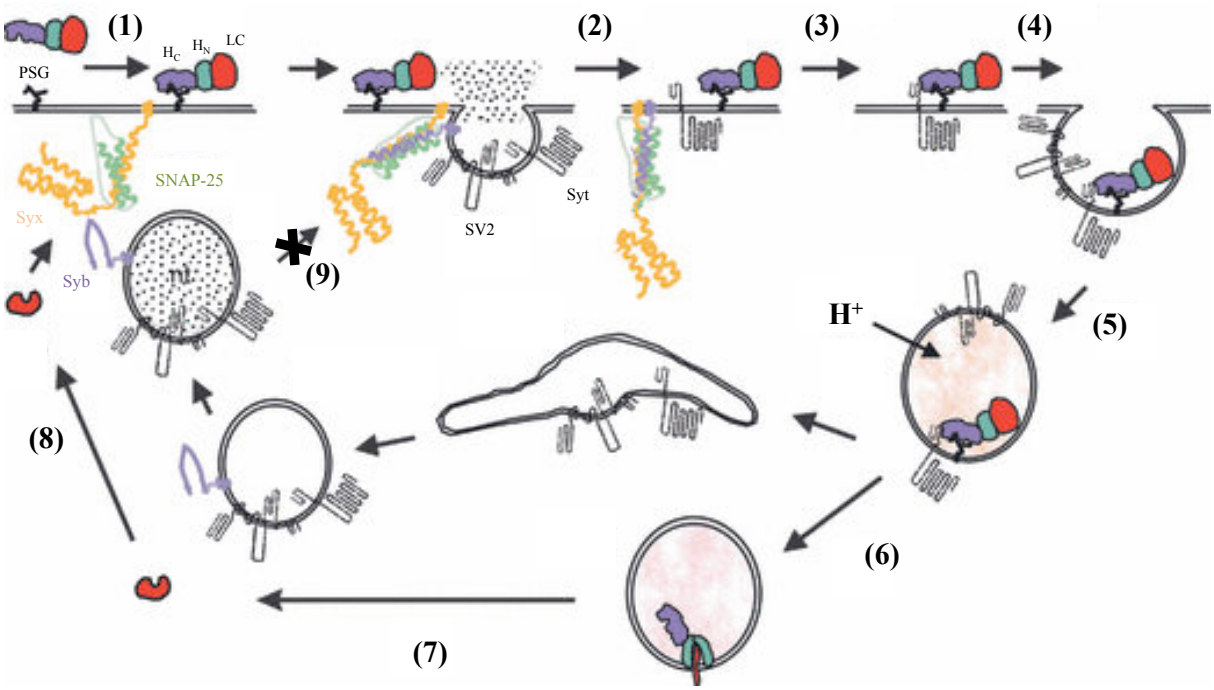

Figure 23. Model of entry of the botulinum neurotoxin. (1) BoNT binds polysialoganglioside (PSG) on cell surface with H_C. (2) Synaptic vesicles proteins are exposed on the membrane upon SNARE mediated neurotransmitter release. (3) BoNT binds synaptic vesicles *via* Syt or SV2, depending on the isoform. (4) The toxin is endocytosed *via* the recycling synaptic vesicles. (5) The lumen becomes acidified *via* the ATPase pump. (6) The acidification triggers the formation of a channel by H_N. (7) LC passes through the channel and is released into the cytosol after reduction of the disulfide bond. (8) LC cleaves SNARE proteins depending on the isoform, Syb (blue), Syx (orange) or SNAP-25 (green). (9) It blocks the synaptic vesicle cycle and the release of neurotransmitter within the synaptic cleft. See text for more details. Syt: Synaptotagmin; SV: synaptic vesicle; Synaptobrevin: Syb; Syntaxin: Syx. Adapted from (Binz and Rummel, 2009).

3.2 Endoplasmic reticulum escape

Proteins addressed to organelles or the secretion pathways traffic by the ER. These proteins arrive in an unfolded state usually through the Sec61 pore. They are then folded with some ER glycosyltransferases, oxidoreductases, lectins and chaperones. An aberrant folding and assembly can occur and generate potential toxicity. ER-associated protein degradation pathway (ERAD) exports these misfolded proteins for degradation by the ubiquitin-proteasome system (Needham and Brodsky, 2013). Interestingly, the same proteins can be involved in proteins maturation and degradation (Brodsky, 2007). Sec61 and/or also the Hrd1 pore export them into the cytosol (Smith et al., 2011).

Some toxins use the ERAD pathway to translocate into the cytosol (Teter, 2013). They exploit the ER chaperones and translocon components in ERAD. Although the general process remains the same, some details are specific of each toxin. Here we will describe how the cholera toxin hijacks the ERAD to translocate across the membrane.

3.2.1 Cholera toxin

The cholera toxin (CT) is the main virulence factor produced by *Vibrio cholerae* that induces a life threatening watery diarrhea. The A and B domains are synthetized as separate polypeptides, which are ultimately held by non-covalent interactions. The A catalytic domain of CT is produced as a pro-domain that is further activated by proteolysis leading to two fragments, CTA1 and CTA2, linked by a disulfide bond (see Figure 19 previously). CTA1 possesses the enzymatic activity while CTA2 is involved in interaction with the B domain. After the release from the bacteria, the B domain forms a pentameric ring that binds to its specific cellular receptor, the GM1-ganglioside (Merritt et al., 1994; Holmgren et al., 1975). Then CTA2 associates and inserts into the central pore of the B domain *via* non-covalent interactions (Sixma et al., 1993).

After binding to the cell receptor, the complex is endocytosed either in a clathrin-dependent or a clathrin-independent manner, depending on the cell types (Torgersen et al., 2001). In early endosomes, the CT does not follow the endosomal pathway as DT, EF and BoNT but moves directly to the trans-Golgi network *via* the retrograde transport (Chinnapen et al., 2012; Iglesias-Bartolomé et al., 2009). Then, CT is transported into the ER.

CTA1 is released from CTA2 and unfolded by the protein disulfide isomerase (PDI) in the ER lumen (Tsai et al., 2001). PDI may not be the only chaperone responsible for CTA1 unfolding. The Hsp70 chaperone BiP (heavy chain binding protein) is thought to maintain CTA1 in an unfolded, soluble and export-competent state (Winkeler et al., 2003). Then CTAI may hijack the ERAD (Cho et al., 2012). It may retro-translocate through the Sec61 channel but many questions have been raised about this mechanism and others proteins were suggested to participate in this process (Bernardi et al., 2010; Pilon et al., 1997; Wiertz et al., 1996). Interestingly, the protein Derlin-1, involved in retro-translocation, is fully dispensable for CTA1 and may play a supporting role by delivering CTA1 to the Hrd1 pore (Bernardi et al., 2008). It may form with Hrd1 a complex required for the translocation of CTA1 (Williams et al., 2013; Bernardi et al., 2010).

Ubiquitination is a cellular process leading to the successful degradation of misfolded proteins by the proteasome. Thus, ubiquitin may act as a ratchet that keeps the protein inside the cytosol and prevents its retro-transport to the ER. However, CTA1 does not undergo ubiquitination because of the scarcity of lysines (Hazes and Read, 1997). Another model implicating the Hsp90 chaperone has been suggested. Hsp90 would provide the ratchet mechanism for CTA1 and rapidly refolds it, preventing its ubiquitination and degradation (Burress et al., 2014; Taylor et al., 2010). Then CTA1 binds and uses ARF6 (for ADP-ribosylation factor 6) as an allosteric activator. The complex ADP-ribosylates G-proteins and lock them in its GTP-bound form, leading to cAMP accumulation in the cell (O'Neal et al., 2005).

3.3 Forces involved in bacterial toxin translocation

As was described in the previous part, the toxins use different mechanisms to translocate across membranes. Although their mechanisms are different, their translocation cannot be carried out without several physico-chemical parameters and the presence of eukaryotic proteins. In fact, we saw that DT, EF and BoNT exploit the pH acidification to partially unfold, allowing their interaction with the membrane. Then, their interactions with cytosolic proteins trap them into the cytosolic side and may drive their translocation, preventing the polypeptide chain from back transport. Thus, these eukaryotic proteins may act as driving forces.

To illustrate these different types of forces exerted, we will focus on the heat shock protein 70 family (Hsp70), a conserved ubiquitous chaperone. They are found in prokaryotic and eukaryotic cytosol and also in mitochondria, chloroplasts and ER. Hsp70 is implicated in protein folding, protein synthesis and degradation, assembly and disassembly of oligomeric complexes and also in pulling of translocating proteins across membranes. They are known to drive protein translocation across compartments. Here we will illustrate these forces by showing the protein import into mitochondria because it is the most studied system.

3.3.1 Power stroke model

The model corresponds to a large and rapid structural change in the protein that is used to do a mechanical work (see Figure 24). The translocating protein undergoes an unfolding force generated by Hsp70. Hsp70, while anchored to the pore, would bind the polypeptide emerging from it and would undergo a series of concerted movements using ATP. It is acting as lever arm to generate the force through conformational change and pulls the protein into the cytosol (Craig, 2018). Upon hydrolysis, Hsp70s proteins bind to proteins emerging from the pore while at the same time, detaching from it. The translocation is unidirectional because Hsp70 is anchored to the membrane and interaction with the polypeptide chain prevents backsliding (Glick, 1995; Glick et al., 1992).

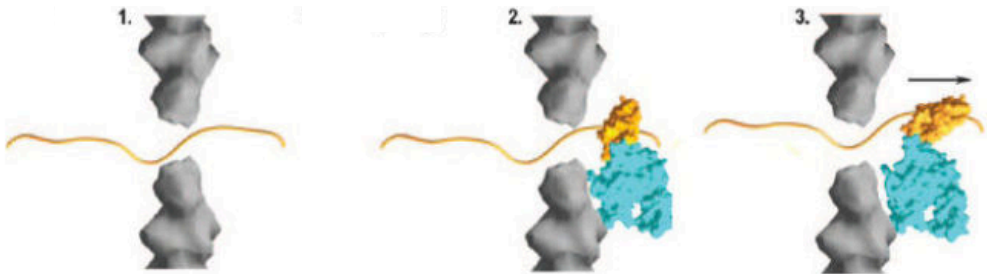

Figure 24. Power stroke model. 1) An unfolded protein moving through a pore can diffuse in both directions. 2) The protein binds Hsp70 and Hsp70 binds to the pore. 3) Hsp70 uses the pore as a fulcrum and undergoes a conformational change that pulls the protein. Adapted from (Sousa and Lafer, 2006).

3.3.2 Brownian molecular ratchet model

The Brownian ratchet is the simplest model proposed to describe the translocation mechanism (see Figure 25). The role of Hsp70 would be to simply block retro-translocation through the pore of its bound substrate. The protein moves to the downstream direction and when another protein segment for Hsp70 emerges, another Hsp70 protein binds and further blocks upstream movement (Neupert and Brunner, 2002).

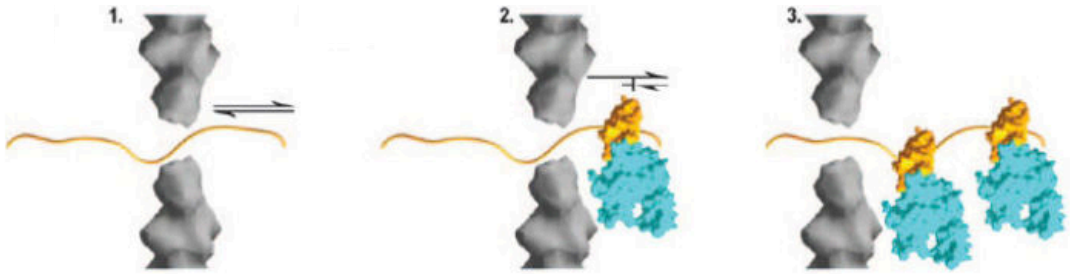

Figure 25. Brownian ratchet model. 1) An unfolded protein moving through a pore can diffuse in both directions. 2) Hsp70 binds the protein on the downstream side and blocks its upstream back. 3) Diffusion exposes another protein segment where a new Hsp70 can bind the protein. Adapted from (Sousa and Lafer, 2006)

3.3.3 Entropic pulling model

The entropic pulling corresponds to both a power stroke and a Brownian ratchet. The two models are coexisting and are inextricable manifestations of the same basic phenomenon (Goloubinoff and De Los Rios, 2007). The entropic pulling was proposed based on a more complete physical description of the system (see Figure 26) (De Los Rios et al., 2006). The binding of Hsp70 to the emerging polypeptide reduces the overall freedom of movement (thus entropy) of the two molecules, due to the volume exclusion between Hsp70 and the pore and membrane. This is equivalent to a free energy of the system that increases upon Hsp70 binding. Remarkably, the effect is progressively less pronounced as more protein is imported in the organelle, resulting in a thermodynamic force (due to a free-energy gradient) that pulls proteins inward, without the need for an anchor point and of specific conformational changes. Also, retro-translocation is inhibited by the presence of a free-energy gradient. This process does not required consumption of ATP-based energy.

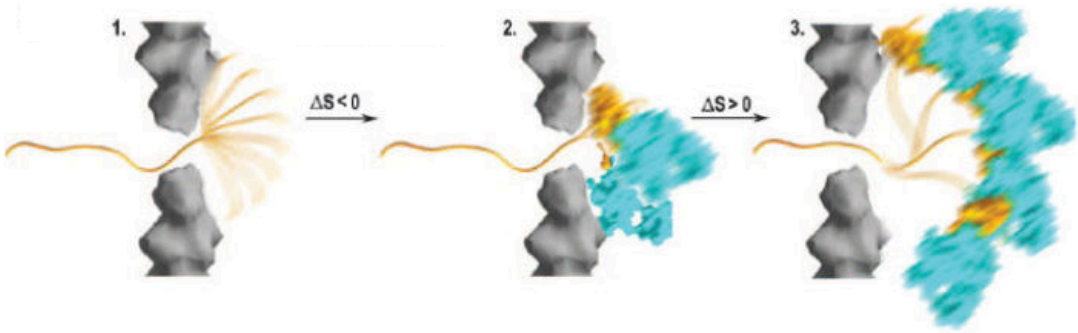

Figure 26. Entropic pulling model. 1) An unfolded protein moving through a pore can wiggle around in a volume limited only by the wall presented by the pore and membrane. 2) Binding of Hsp70 restricts the freedom of movement of the unfolded protein and it decreases the entropy ΔS. 3) Emergence of more protein increases the freedom of movement and thus entropy. Adapted from (Sousa and Lafer, 2006).

Although the forces exerted for translocation are slightly different, the binding of the eukaryotic protein to the translocating protein acts as an "import motor". Thus, as described for DT, EF, BoNT and CT, the binding to eukaryotic proteins during translocation may exert the forces necessary to pull the catalytic domain inside the cytosol. It is difficult to characterize which types of forces are exerted on these toxins. Further studies may be performed to clarify that point issue. For our study with the CyaA toxin, although the translocation process is unique among bacterial toxins, no eukaryotic protein has been identified as pulling protein for the transport of the catalytic domain so far. Recently, the identification and characterization of the so-called translocation region (encompassing residues 365 to 527 of CyaA) and especially a membrane-active peptide in this region may help to improve and decipher more precisely the translocation mechanism of CyaA.

3.4 Identification of P454 in CyaA

The precise translocation process of the CyaA toxin remains unknown. It is believed that after binding to the CD11b/CD18 receptor (although the receptor is not necessary), the hydrophobic region inserts the toxin into the plasma membrane and finally the catalytic domain is translocated across the plasma membrane (Rogel and Hanski, 1992). Recently, it has been shown that a protein covering the whole catalytic domain of CyaA, AC384

(residues 1-384 of CyaA) does not exhibit membrane-binding properties. However, a longer polypeptide, AC489 (residues 1-489 of CyaA), is able to interact with membranes and also induces permeabilization (Karst et al., 2012). Deletion of residues 375 to 485 in CyaA completely abolishes the translocation of the catalytic domain into cells but does not affect its cell binding nor its hemolytic activity. Gray and colleagues also previously showed that a monoclonal antibody recognizing an epitope between residues 373-399 blocks the translocation of the catalytic domain (Gray et al., 2001). Thus, the N-terminal 489 residues of CyaA possesses membrane binding and destabilizing properties that are directly involved in the early stages of translocation (Karst et al., 2012).

In silico predictions have allowed identifying in the region, encompassing residues 375-485, some structural disorder punctuated by several helical regions (Subrini et al., 2013; Geourjon and Deleage, 1995). Two peptides, P414 and P454 (residues 414 to 440 and 454 to 484 of CyaA, respectively) were identified to adopt α-helical structures by secondary structure prediction software. Structural and functional properties showed that only P454 was able to bind membranes and to permeabilize negatively charged membranes (Subrini et al., 2013). P454 is unfolded in solution and adopts an α-helical conformation upon membrane interaction. Biophysical studies have shown that P454 is oriented in the plane of the lipid bilayer. Thus, with these data, Subrini and colleagues proposed a new translocation model: after binding and insertion in the plasma membrane of the hydrophobic region, the segment P454 interacts with the membrane and locally destabilizes it. This local destabilization decreases the energy required to cross the membrane, favoring the translocation of the catalytic domain (Subrini et al., 2013).

3.4.1 P454 is an AMP-CPP-like peptide.

The P454 peptide exhibits membranes-active properties, *i.e*, it is able to interact with membranes, to adopt an α-helical structure upon membrane interaction and also to destabilize and permeabilize lipid vesicles. P454 is a small peptide of 31 amino acids with alternate hydrophilic and hydrophobic residues conferring amphiphilic character, which may explain its capacity to interact with membranes (see Figure 27). Mainly unfolded in solution, it adopts a α-helical conformation in the presence of negatively charged membranes (Subrini et al., 2013). The two charged arginine residues confers a positive mean net charge which may locally allow the interaction with hydrophilic head of lipids while the presence of

hydrophobic residues allows interaction with the acyl chains, thereby driving the membrane interaction of P454.

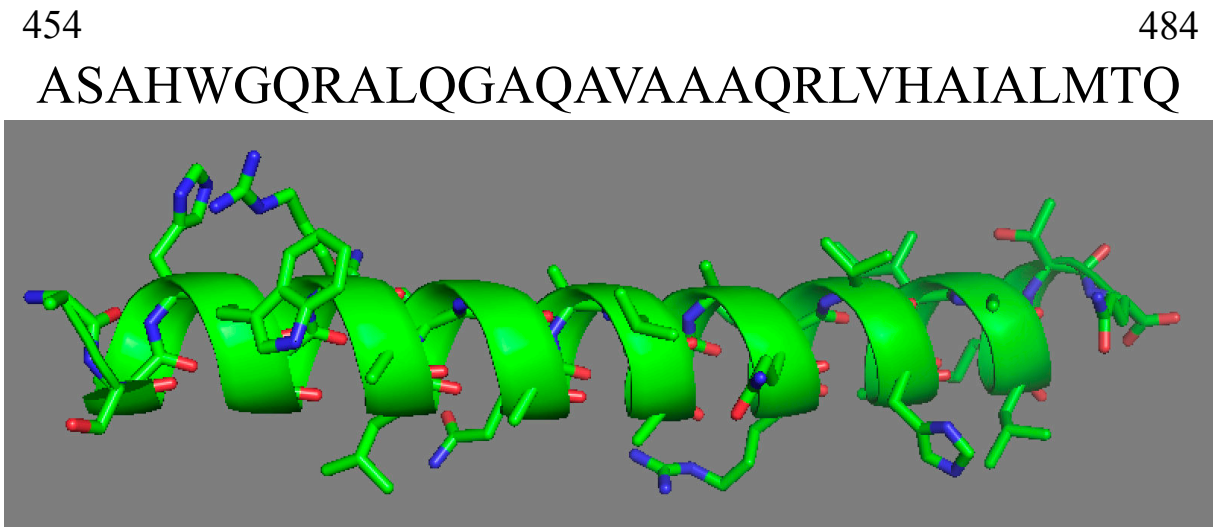

Figure 27. Sequence and structural model of P454 using the *de novo* peptide structure prediction PEP-FOLD 3 software (Shen et al., 2014). Numbering corresponds to amino acid position in the CyaA toxin.

These characteristics described here for P454 are close to two families of peptides: the antimicrobial peptides (AMPs) and the cell penetrating peptides (CPPs). These two families are further described in the next part.

3.4.2 Antimicrobial peptides

AMPs are produced by all life forms, from humans to plants to insects and to prokaryotes (Hancock, 2000; Lehrer and Ganz, 1999). They constitute an important defense mechanism in innate immunity for humans, protecting against bacteria, fungi, viruses or tumors (Marr et al., 2006; Reddy et al., 2004; Hancock and Chapple, 1999). AMPs are small peptides from 10 to 50 amino acids with an amphiphilic character. They are characterized also by a positive mean net charge due to the presence of arginine and lysine residues. Mainly unfolded in solution, they form an amphipathic secondary structure upon membrane interaction (Ebenhan et al., 2014). Then, AMPs can have different mechanisms of action on the target cell: they can cause disruption of the integrity of the microbial membrane and/or

translocate across the membrane into cytosol to act on intracellular targets (Mahlapuu et al., 2016; Hancock and Sahl, 2006).

Three membrane disruption models have been proposed and are illustrated on Figure 28. The action of AMPs leads to leakage of ions and metabolites, membrane depolarization and rapid lysis (Brogden, 2005). Translocation process of AMPs occurs *via* direct transport of the peptide across the membrane, although it has been demonstrated that local membrane destabilization is also an important parameter. They alter cell physiology in general by targeting key cellular processes such as protein synthesis, wall synthesis, DNA/RNA synthesis and protein folding (Nguyen et al., 2011; Brogden, 2005; Yeaman and Yount, 2003).

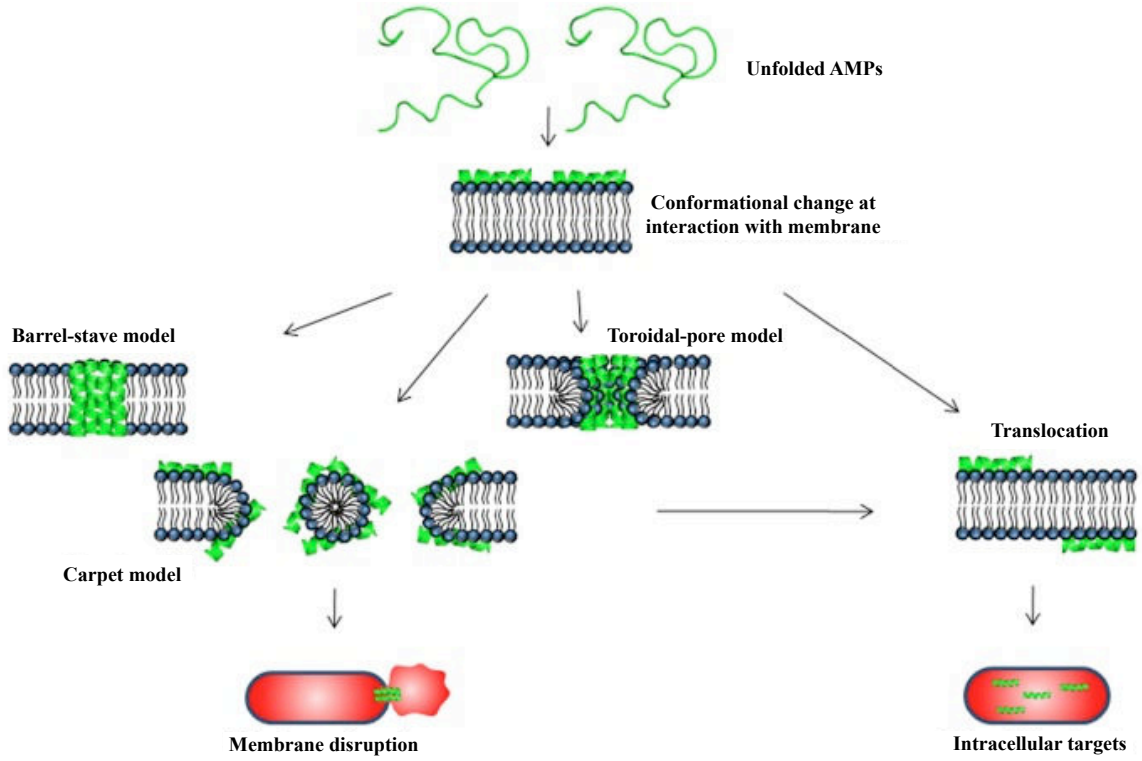

Figure 28. Schematic illustration of AMPs mechanisms. Barrel-stave model: peptides are arranged parallel to the lipids and form a channel; Carpet model: peptides interactions induce local weaknesses disintegrating the membrane structure; Toroidal-pore model: peptides binding induce a cascade aggregation that forms a continuous channel. From (Mahlapuu et al., 2016).

3.4.3 Cell-penetrating peptides

Physico-chemical characteristics of CPPs and AMPs are similar. CPPs are also short peptides not exceeding 30 residues and have the capacity to be internalized without perturbation of the membrane integrity, so-called silent translocation. They can cross the membrane with a very limited toxicity, *via* energy-dependent and/or independent mechanisms (Bechara and Sagan, 2013). CPPs are usually used as cargo to transport a variety of covalently and non-covalently molecules (*i.e* peptides, proteins, nanoparticles, RNA, DNA, antisense oligonucleotides and liposomes) and can be natural, synthetic or chimeric peptides (Lehto et al., 2012; Meade and Dowdy, 2008; Järver et al., 2007; Mäe and Langel, 2006; Gupta et al., 2005; Dietz and Bähr, 2004). CPPs may translocate directly across membranes by various mechanisms (see Figure 29). Their amphiphilic character drives membrane binding and insertion. Mostly unstructured as AMPs in solution, they adopt various secondary structures upon membrane interaction. This structural flexibility is important for membrane interaction and internalization (Deshayes et al., 2008). However, the number of basic residues in their sequence mostly governs the uptake of CPPs. Interestingly, arginine residues are more effective in terms of internalization than lysine residues (Schmidt et al., 2010; Mitchell et al., 2000; Wender et al., 2000) and their number is also crucial (Futaki et al., 2001). Furthermore, hydrophobic residues such as aromatics play a major role for membrane interaction and have been proposed to enhance peptide translocation. Particularly, tryptophan is involved in local membrane destabilization (Killian and von Heijne, 2000; White and Wimley, 1999) and is crucial for CPPs uptake (Rydberg et al., 2012; Walrant et al., 2011; Delaroche et al., 2007).

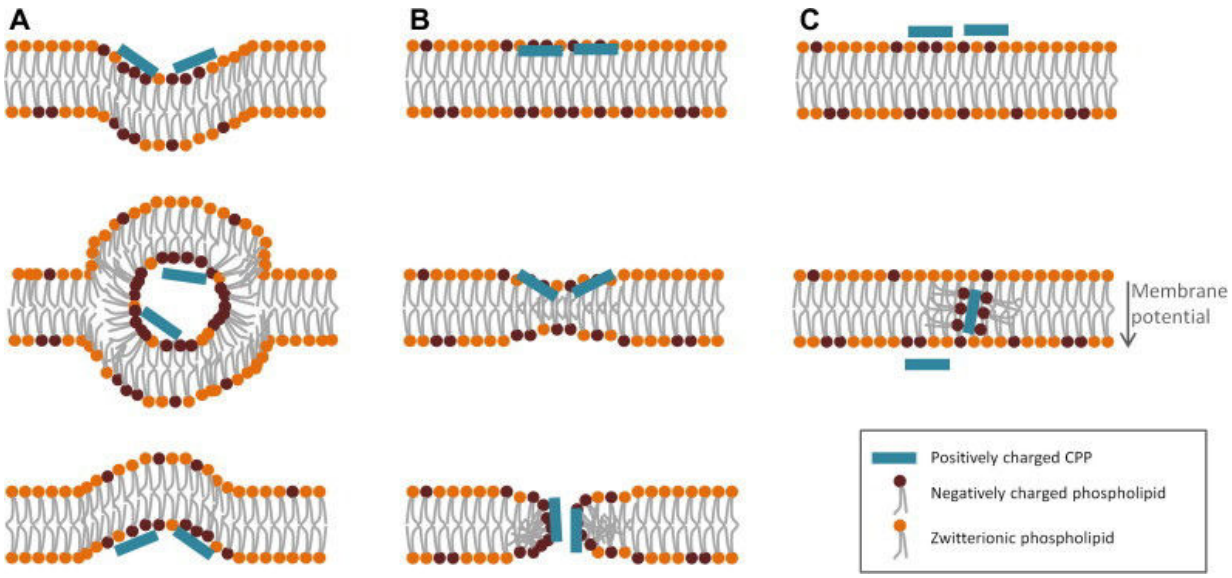

Figure 29. Examples of the proposed mechanisms for direct translocated of CPPs. (A) Inverted micelles: peptide interaction induces a local negative curvature (*i.e* invagination of the membrane) that leads to formation of an inverted micelle. Membrane disruption releases the peptide in the cytosol. (B) Pore-formation: peptides accumulation forms a transient pore through which other peptides diffuse. (C) Adaptive translocation: interaction of the guanidinium group from side chain of arginine residues and the phosphate lipid headgroups mask the peptide charge. Diffusion is driven by membrane potential and equilibrium constant in *cis*/*trans* compartments. From (Bechara and Sagan, 2013).

Chapter IV. Aims of the doctoral thesis project

Chapter IV. Aims of the doctoral thesis project

It has been demonstrated that the translocation region (*i.e* residues 365-527 of CyaA), where belongs P454, is crucial for the translocation of the catalytic domain (Subrini et al., 2013; Karst et al., 2012). Nevertheless, the contribution of P454 in the translocation process of CyaA remains unknown.

My PhD was mainly focused on the contribution of P454 in the translocation process of the catalytic domain. As described for AMPs and CPPs, the presence of certain residues contributes to their membrane activities. Especially, cationic residues are highly important for peptide-membrane interaction and destabilization. Although they have an identical charge, arginine residues are more prevalent in AMPs and CPPs and greatly enhance the peptide membrane-active activities compared to lysine residues (Cutrona et al., 2015). One of the aims of the PhD was to investigate the role of the two arginine residues of P454. We substituted them with amino acids characterized by various physico-chemical properties (lysine, glutamine, alanine, glutamate) and determined their implication for membrane binding, peptide folding and membrane permeabilization. We found that both arginine residues are highly important for all membrane activities although one was more implicated in folding and the other in membrane destabilization. Furthermore, hydrophobic residues are well known to play a major role in the interaction with the membrane. We also substituted some hydrophobic residues of P454 (tryptophan, leucine, valine and isoleucine residues) to investigate their contributions in membrane-active properties of P454. This study allowed proposing a detailed characterization of the forces and residues involved in successive steps from membrane interaction to the membrane destabilization by P454.

Knowing that P454 has the capacity to interact and to destabilize membranes, one of the goals of my PhD was also to answer the following question: does P454 have the capacity to translocate across membranes? In fact, P454 possesses all the characteristics of a translocating peptide like AMPs and CPPs. We found that indeed P454 has the capacity to translocate and reach the *trans* side of the membrane. However, this experimental

observation raises other questions about the interest of this translocation for the passage of the catalytic domain.

Previously, we described how some bacterial toxins reach the cytosol using eukaryotic partners to pull their catalytic domain inside the cytosol (see previous chapter III). Furthermore, AMPs and CPPs can translocate to reach a specific eukaryotic target in the cytosol. Thus, we hypothesized that P454 might also interact with a cytosolic partner to favor the transport of the catalytic domain. Indeed, it was found that P454 has the capacity to bind an eukaryotic protein. We propose that this interaction may constitute the pulling force based on the entropic pulling model (see part 3.3.3): it may thermodynamically reduce the free energy required for the passage of the catalytic domain across the plasma membrane.

With the previous study realized on amino acids substitutions in P454, we investigated how these substitutions also affected the binding to the eukaryotic partner. We found that some residues highly decrease the binding affinity while others have no effect. The important residues were then mutated in the P454 region in the full length CyaA. We found that some mutations did not affect translocation of the catalytic domain while others completely abolished it. Thus, these 31 residues, and especially some of P454, are essential for the translocation of CyaA.

All these data has allowed us to propose a novel translocation process of the CyaA toxin: after binding and insertion into the plasma membrane of hydrophobic and acyl regions, the peptide P454 of the translocation region may interact with the plasma membrane, be folded and locally destabilizes it. This local membrane destabilization may favor the translocation of P454 across the plasma membrane. Its eukaryotic partner may bind and trap P454 inside the cytosol and the complex may act as a pulling force for the translocation of the unstructured catalytic domain.

Upon binding of the catalytic domain to the calmodulin, it was found that a 75-residues-long stretch undergoes a disorder-to-order transition and also induces local allosteric effects. This contributes to stabilization of the catalytic site and activates the adenylate cyclase activity CyaA, which leads to cell death.

An interesting translocation mechanism was also proposed recently. A team has reported that CyaA exhibited a phospholipase activity that may be involved in destabilization of the lipid bilayer and may facilitate the translocation of the catalytic domain (Gonzalez-Bullon et

al., 2018, 2017). However, these results were contested (Bumba et al., 2018) and we tested this hypothesis and found that CyaA has no detectable phospholipase activity.

Nevertheless, it is important to note that the translocation of the catalytic domain is not only dependent of the translocation region but also of the other regions of CyaA (*i.e* hydrophobic region, acylation region and receptor binding domain). Indeed, AC489, a polypeptide encompassing the catalytic domain and the translocation region, exhibits membrane-active properties but is not able to translocate the catalytic domain across the plasma membrane (Karst et al., 2012). Furthermore, the calcium ions are crucial for folding, binding and CyaA toxicity. The acylation of the toxin is also required. Indeed, proCyaA is able to fold and interact with the cell but is unable to translocate its catalytic domain and induces production of cAMP. We recently studied the effect of the two post-translational acylation on the folding and cytotoxicity of CyaA. We found that CyaA adopts a more compact and stable form than non-acylated form proCyaA and this contributes to CyaA toxicity. Thus, acylation is not only essential for membrane translocation but also for correct folding of the toxin in particular the acyl region itself and then the hydrophobic region.

Chapter V.

Experimental results

Chapter V. Experimental results

The results obtained and my different contributions during the PhD will be presented as a set of publications and reviews. To allow a better following and understanding of these data, they will be presented not as function of the chronological dates of neither publication nor authorship but following the CyaA intoxication process (see Figure 30):

- The first publication, a review, focuses on how calcium induces conformational changes in CyaA and allows its secretion through the secretion machinery.

- The second publication provides new insights about how post-translational acylation of CyaA controls its folding and functions as an invasive toxin.

- The third publication reports our experiments demonstrated that the controversial phospholipase activity of CyaA does not exist.

- The fourth a review, introduces the data obtained in the fifth and the seventh publications.

- The fifth publication highlights on the role of the arginine residues of P454 on its membrane-active properties.

- The sixth publication describes how the region of P454 is involved in the translocation process. P454 translocation and binding to an eukaryotic partner allow to refine the model of CyaA intoxication with new steps.

- The seventh publication deciphers how calmodulin induces structural reorganization in the catalytic domain to trigger the adenylate cyclase activity.

During the PhD, I mainly contributed to the third, the fifth and the sixth publications.

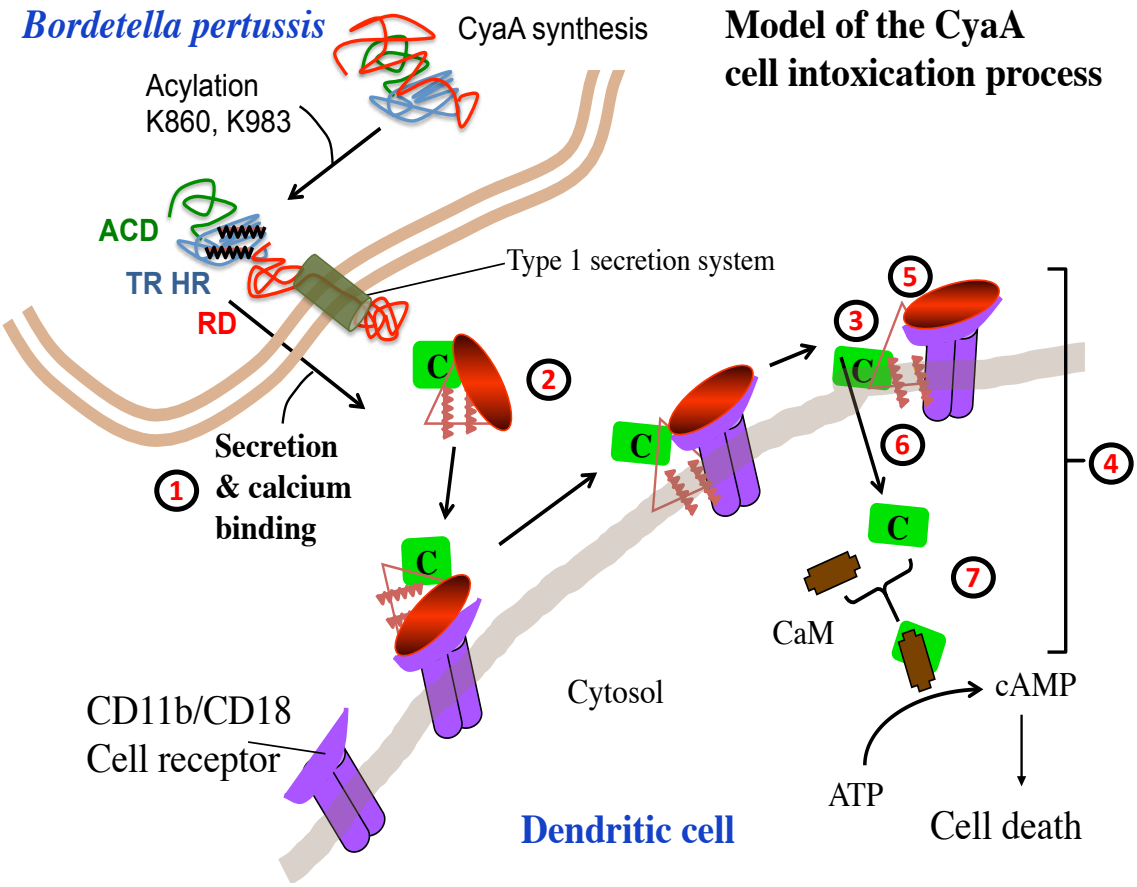

Figure 30. Model of the CyaA intoxication process. Briefly, CyaA is synthetized, acylated and secreted by the bacteria. Extracellularly, it binds calcium and folds to interact with its receptor. The toxin inserts into the membrane and translocates its catalytic domain across the membrane, which binds calmodulin and activates the adenylate cyclase activity of CyaA that leads to cell death. Numbering corresponds to the localization of the data obtained for each publication. See text for more details.

Review I

Calcium-dependent disorder-to-order transitions are central to the secretion and folding of the CyaA toxin of *Bordetella pertussis*, the causative agent of whooping cough

Darragh P. O'Brien, Ana Cristina Sotomayor Perez, Johanna Karst, Sara E. Cannella, Véronique Yvette Ntsogo Enguéné, Audrey Hessel, Dorothée Raoux-Barbot, Alexis Voegele, Orso Subrini, Marilyne Davi, J. Inaki Guijarro, Bertrand Raynal, Bruno Baron, Patrick England, Belen Hernandez, Mahmoud Ghomi, Véronique Hourdel, Christian Malosse, Julia Chamot-Rooke, Patrice Vachette, Dominique Durand, Sébastien Brier, Daniel Ladant and Alexandre Chenal

Toxicon

Volume 149

Pages 37-44

January 2018

The receptor-binding domain of CyaA (RD, encompassing residues 1006-1706) contains the RTX motifs of CyaA regrouped in five consecutive blocks (from I to V). Each one contains 8 to 10 RTX motifs separated by flanking regions (Bauche et al., 2006). These motifs represent the main calcium binding sites of the protein (Rose et al., 1995). The presence of calcium is required for the overall toxicity of CyaA. In fact, calcium induces conformational changes in CyaA allowing its folding, interaction with its cell receptor (when it is present), translocation of the catalytic domain and also its pore-forming activity. This review describes recent results obtained in our lab, describing how the calcium is crucial for CyaA secretion, folding and intoxication.

In the absence of calcium, the RTX motifs exhibit hallmarks of intrinsically disordered proteins, in particular an extended and flexible conformation (Sotomayor-Perez et al., 2012, 2011). A combination of biophysical approaches have shown that addition of calcium induces a strong overall stabilization with folding of secondary and tertiary structures (O'Brien et al., 2015; Sotomayor Perez et al., 2010; Chenal et al., 2009a). It is proposed that this structural disorder may facilitate the secretion of RD through the type I secretion system (O'Brien et al., 2015; Chenal et al., 2009a). The presence of calcium in the extracellular medium favors folding and prevents back transport through the channel. It might also favor the transport of the rest of the toxin (Chenal et al., 2010).

CyaA is a protein of 1706 amino acids residues with a pronounced hydrophobic character, which drastically limits its solubility. When produced, CyaA needs to be purified and stored in denaturing conditions (*i.e* urea or guanidine). Recently, Karst and colleagues succeeded to purify CyaA into a stable, monomeric and urea-free form in non-denaturing conditions (Karst et al., 2014). They used calcium and molecular confinement to limit intermolecular interactions. The monomeric CyaA was shown to display both hemolytic and cytotoxic activities, suggesting that it is the physiologically active form of the toxin in solution (Cannella et al., 2017). Although its hemolytic activity does not require free calcium in solution, the translocation of CyaA is calcium dependent. It indicates that the calcium loaded on monomers is not enough for translocation and supports that calcium gradient is required.

All together, these data show how calcium acts on CyaA secretion, folding and cell intoxication.

Author's Personal Copy

Toxicon 149 (2018) 37–44

Contents lists available at ScienceDirect

Toxicon

journal homepage: www.elsevier.com/locate/toxicon

Calcium-dependent disorder-to-order transitions are central to the secretion and folding of the CyaA toxin of *Bordetella pertussis*, the causative agent of whooping cough

Darragh P. O'Brien [a], Ana Cristina Sotomayor Perez [a], Johanna Karst [a], Sara E. Cannella [a], Véronique Yvette Ntsogo Enguéné [a], Audrey Hessel [a], Dorothée Raoux-Barbot [a], Alexis Voegele [a, g], Orso Subrini [a], Marilyne Davi [a], J. Inaki Guijarro [b], Bertrand Raynal [c], Bruno Baron [c], Patrick England [c], Belen Hernandez [d], Mahmoud Ghomi [d], Véronique Hourdel [e], Christian Malosse [e], Julia Chamot-Rooke [e], Patrice Vachette [f], Dominique Durand [f], Sébastien Brier [e], Daniel Ladant [a], Alexandre Chenal [a, *]

[a] *Institut Pasteur, Biochemistry of Macromolecular Interactions Unit, UMR CNRS 3528, Structural Biology and Chemistry Department, 75724 PARIS Cedex 15, France*
[b] *Institut Pasteur, Nuclear Magnetic Resonance of Biomolecules Unit, UMR CNRS 3528, Structural Biology and Chemistry Department, 75724 PARIS Cedex 15, France*
[c] *Institut Pasteur, Molecular Biophysics Platform, CITECH, UMR CNRS 3528, Structural Biology and Chemistry Department, 75724 PARIS Cedex 15, France*
[d] *Sorbonne Paris Cité, Université Paris 13, Groupe de Biophysique Moléculaire, UFR Santé-Médecine-Biologie Humaine, 93017 BOBIGNY Cedex, France*
[e] *Institut Pasteur, Mass Spectrometry for Biology Unit, USR CNRS 2000, CITECH, Structural Biology and Chemistry Department, 75724 PARIS Cedex 15, France*
[f] *Institut de Biologie Intégrative de la Cellule, UMR 9198, Université Paris-Sud, F-91405 ORSAY Cedex, France*
[g] *Université Paris Diderot Paris VII, 75013 Paris, France*

ARTICLE INFO

Article history:
Received 3 October 2017
Received in revised form
20 November 2017
Accepted 10 January 2018
Available online 12 January 2018

Keywords:
CyaA toxin
Bordetella pertussis
Whooping cough
Calcium
Disorder-to-order transition
Protein secretion
Folding

ABSTRACT

The adenylate cyclase toxin (CyaA) plays an essential role in the early stages of respiratory tract colonization by *Bordetella pertussis*, the causative agent of whooping cough. Once secreted, CyaA invades eukaryotic cells, leading to cell death. The cell intoxication process involves a unique mechanism of translocation of the CyaA catalytic domain directly across the plasma membrane of the target cell. Herein, we review our recent results describing how calcium is involved in several steps of this intoxication process. In conditions mimicking the low calcium environment of the crowded bacterial cytosol, we show that the C-terminal, calcium-binding Repeat-in-ToXin (RTX) domain of CyaA, RD, is an extended, intrinsically disordered polypeptide chain with a significant level of local, secondary structure elements, appropriately sized for transport through the narrow channel of the secretion system. Upon secretion, the high calcium concentration in the extracellular milieu induces the refolding of RD, which likely acts as a scaffold to favor the refolding of the upstream domains of the full-length protein. Due to the presence of hydrophobic regions, CyaA is prone to aggregate into multimeric forms *in vitro*, in the absence of a chaotropic agent. We have recently defined the experimental conditions required for CyaA folding, comprising both calcium binding and molecular confinement. These parameters are critical for CyaA folding into a stable, monomeric and functional form. The monomeric, calcium-loaded (holo) toxin exhibits efficient liposome permeabilization and hemolytic activities *in vitro*, even in a fully calcium-free environment. By contrast, the toxin requires sub-millimolar calcium concentrations in solution to translocate its catalytic domain across the plasma membrane, indicating that free calcium in solution is actively involved in the CyaA toxin translocation process. Overall, this data demonstrates the remarkable adaptation of bacterial RTX toxins to the diversity of calcium concentrations it is exposed to in the successive environments encountered in the course of the intoxication process.

© 2018 Elsevier Ltd. All rights reserved.

* Corresponding author.
E-mail address: alexandre.chenal@pasteur.fr (A. Chenal).

https://doi.org/10.1016/j.toxicon.2018.01.007
0041-0101/© 2018 Elsevier Ltd. All rights reserved.

Author's Personal Copy

1. Introduction

The adenylate cyclase toxin (CyaA) is one of the major virulence factors produced by *Bordetella pertussis*, the causative agent of whooping cough (Glaser et al., 1988a, 1988b; Khelef et al., 1992; Ladant et al., 1986; Weiss and Goodwin, 1989; Weiss and Hewlett, 1986). CyaA plays an important role in the early stages of respiratory tract colonization by *B. pertussis* (Harvill et al., 1999; Khelef et al., 1992; Weiss and Goodwin, 1989). The toxin uses an original intoxication mechanism: once secreted by the virulent bacteria, it is able to invade eukaryotic target cells through a unique but poorly understood mechanism that involves direct translocation of the catalytic domain across the plasma membrane. CyaA is a 1706-residue long protein organized in a modular fashion (Carbonetti, 2010; Guiso, 2017; Karst et al., 2014; Ladant and Ullmann, 1999). The ATP-cyclizing, calmodulin-activated, catalytic domain (ACD) is located in the 400 amino-terminal residues (Glaser et al., 1988b; Karst et al., 2010; Ladant, 1988), while the carboxy-terminal 1306 residues are involved in toxin binding to target cells and subsequent ACD translocation across the plasma membrane (El-Azami-El-Idrissi et al., 2003). This region also has a membrane permeabilization capacity that is responsible for the hemolytic phenotype of *B. pertussis* (see Fig. 1) (Bellalou et al., 1990; Benz et al., 1994; Glaser et al., 1988c). These activities allow CyaA to function independently as adenylate cyclase and hemolysin (Sakamoto et al., 1992). Several domains can be identified in the C-terminal region. We have recently shown that the so-called "translocation region" (TR), spanning residues 400 to 500, is crucial for the delivery of the ACD across the plasma membrane, and exhibits properties related to membrane-active peptides (Karst et al., 2012a; Subrini et al., 2013; Voegele et al., 2017). The hydrophobic region (HR), covering residues 500 to 750, contains several hydrophobic segments predicted to adopt helical structures (Glaser et al., 1988b). The acylation region (AR), spanning residues 800 to 1000, contains two post-translational modification sites that are essential for CyaA cytotoxic activities. The toxin is synthesized as an inactive precursor, proCyaA, which is converted into the active CyaA toxin upon specific acylation of Lys 860 and Lys 983 by a dedicated acyltransferase, CyaC. The CyaC enzyme catalyzes the transfer of an acyl chain from acyl-ACP (acyl-carrier protein) to the epsilon-amino groups of proCyaA lysines (Barry et al., 1991; Sebo et al., 1991; Westrop et al., 1996). The C-terminal half of CyaA is the cell receptor-binding domain (RD, residues 1000 to 1706) (El-Azami-El-Idrissi et al., 2003; Rogel et al., 1988). This domain consists of ~40 copies of a calcium-binding, glycine and aspartate-rich nona-peptide GGXGXDXUX repeat, where X is any amino-acid, and U a conserved hydrophobic residue, that is characteristic of a large family of bacterial cytolysins known as RTX (Repeat-in-ToXin) toxins. These motifs constitute the main calcium binding sites of the protein (Rose et al., 1995).

The intoxication process of CyaA can be illustrated as shown in Fig. 2. Once acylated in the bacteria, CyaA is secreted across the bacterial envelope by a dedicated type 1 secretion system (T1SS) involving CyaB, CyaD and CyaE (Glaser et al., 1988c; Masure et al., 1990). This machinery recognizes a secretion signal located at the C-terminal end of CyaA. Once secreted, the toxin binds calcium in the extracellular milieu. Although CyaA can intoxicate a variety of cell types by a process that is independent of receptor-mediated endocytosis (Angely et al., 2017; Gordon et al., 1989; Rogel and Hanski, 1992; Rogel et al., 1989), it binds in a calcium-dependent manner to a cell receptor, the CD11b/CD18 integrin, which is expressed by a subset of leukocytes including neutrophils, macrophages and dendritic cells (Angely et al., 2017; El-Azami-El-Idrissi et al., 2003; Guermonprez et al., 2001, 2002; Masin et al., 2005). Upon receptor recognition, CyaA translocates its catalytic domain directly across the plasma membrane from the extracellular medium to the host cell cytoplasm (Bumba et al., 2010; Fiser et al., 2007; Karst et al., 2012a; Veneziano et al., 2013). Binding of endogenous calmodulin (CaM) to ACD induces its stabilization into a functional state (Karst et al., 2010). Once activated by calmodulin, ACD produces supraphysiological concentrations of cAMP at the expense of ATP (Ladant and Ullmann, 1999; Sakamoto et al., 1992), which ultimately leads to cell death (Ladant and Ullmann, 1999; Vojtova et al., 2006).

Although the mechanism of translocation remains elusive, it is clearly established that calcium is required for the toxicity of CyaA. Indeed, calcium binding to CyaA is critical for its refolding, its interaction with the eukaryotic cell receptor, the translocation of the catalytic domain inside the host cell, and for the pore-forming

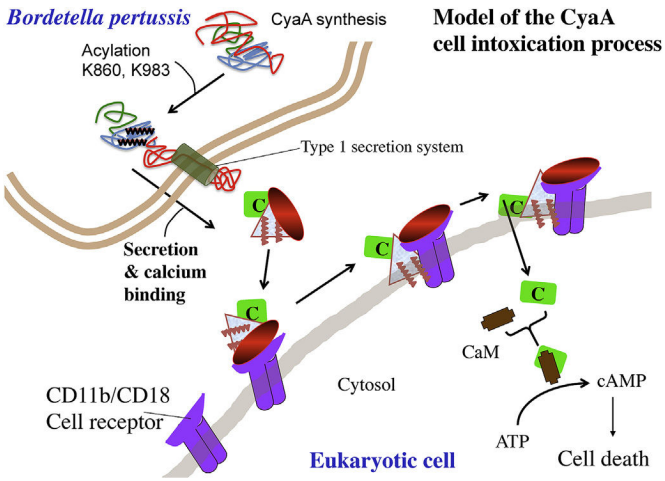

Fig. 2. Model of the intoxication process of eukaryotic cells by CyaA. CyaA is synthesized, acylated and secreted through the T1SS. Toxin folding is induced by calcium binding in the extracellular environment. Pore forming activity and ACD translocation into eukaryotic cells can both be performed in the presence and absence of the cell receptor. The color code of CyaA domains is similar to that of Fig. 1. (For interpretation of the references to color in this figure legend, the reader is referred to the Web version of this article.)

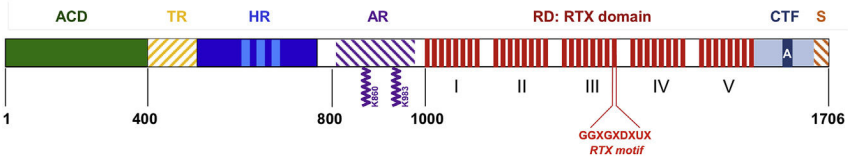

Fig. 1. Schematic representation of the CyaA toxin. CyaA is composed of five distinct regions, the adenylate cyclase catalytic domain (ACD, green), the translocation region (TR, orange hatching), the hydrophobic region (HR, blue), the acylation region (AR, purple hatching) and the C-terminal RTX domain (RD, red). RD comprises five consecutive blocks (I to V). Each red box represents one RTX motif (CTF: C-terminal flanking region; S: secretion signal). Native numbering of CyaA is given as rough indication and does not correspond to precise boundaries between CyaA regions. The two acyl-chains are represented as purple zig-zag lines. (For interpretation of the references to color in this figure legend, the reader is referred to the Web version of this article.)

Author's Personal Copy

activity of CyaA (Bauche et al., 2006; Bumba et al., 2010; Fiser et al., 2007; Karst et al., 2014; Knapp et al., 2008; Uribe et al., 2013; Veneziano et al., 2013, 2017; Vojtova-Vodolanova et al., 2009). The RTX domain (RD) of CyaA is directly involved in these calcium-dependent activities as it harbors the main calcium-binding sites of the toxin (Rose et al., 1995).

1.1. Calcium-induced folding of the CyaA toxin RD domain

In recent years, we have studied the calcium-induced conformational changes occurring within the RTX domain to try and understand the structure-function relationships of this widespread motif (Bauche et al., 2006; Chenal et al., 2009, 2010; O'Brien et al., 2015; Sotomayor Perez et al., 2010; Sotomayor-Perez et al., 2011, 2013, 2015). We have shown that, in the absence of calcium, the RTX domain exhibits the hallmarks of intrinsically disordered proteins. The unfolded state of apo-RD results in part from the internal electrostatic repulsions between negatively charged residues, as revealed by the high mean net charge (experimentally measured by electrophoretic mobility) of the apo-polypeptide (Sotomayor-Perez et al., 2011, 2012).

Calcium binding causes a strong reduction of the mean net charge, thereby triggering a global protein collapse associated with folding and stabilization of secondary and tertiary structures (Chenal et al., 2009, 2010; Sotomayor Perez et al., 2010). Calcium-induced protein collapse was initially monitored by size exclusion chromatography followed by a triple detector array (SEC-TDA) (Fig. 3), which directly provides an estimate of the molecular mass by static light scattering (no need for calibration with a set of standard globular proteins), together with information on molecular shape (Chenal et al., 2009).

The calcium-induced folding and stabilization of secondary and tertiary structures of RTX proteins were characterized by several approaches, including circular dichroism, fluorescence, infra-red, Raman and NMR spectroscopies (Figs. 4 and 5) (Chenal et al., 2009, 2010; O'Brien et al., 2015; Sotomayor Perez et al., 2010; Sotomayor-Perez et al., 2011).

Our data indicate that apo-RTX proteins adopt extended, highly flexible conformations in which the polypeptide chain is mainly disordered with residual beta-sheet elements and turns (Figs. 4 and 5). The protein also contains some residual tertiary structure elements involving aliphatic and aromatic residues, as evidenced by NMR and near-UV circular dichroism, respectively (Chenal et al., 2009, 2010). The binding of calcium induces a strong overall structural stabilization, along with dramatic secondary and tertiary structural rearrangements, characterized by the increase of beta-sheet at the expense of structural disorder (Fig. 4).

Notably, the presence of calcium is not enough to induce a disorder-to-order transition of the truncated proteins restricted to RTX motifs only: the flanking, non-RTX regions are indeed critically required to stabilize the structural elements of the holo-state (Sotomayor Perez et al., 2010). Moreover, we showed that depending on the size of the flanking regions (Sotomayor Perez et al., 2010), proper folding of the RTX polypeptides may require multimerization of the holo proteins, in addition to calcium-binding. Although not physiological (no protein with such truncated flanking regions is produced by the bacteria), this multimerization phenomenon highlights the intrinsic propensity of the RTX motifs to collapse together upon calcium binding, a property that might favor tight interactions between consecutive RTX domains once secreted by the type 1 secretion system (T1SS).

We propose that the intrinsically disordered character of the RTX proteins may facilitate their secretion through the T1SS, as illustrated in Fig. 6 (Chenal et al., 2009). Indeed, the intrinsically disordered state of apo-RTX proteins abolishes the energetic cost of polypeptide unfolding that would be needed for secretion through the duct of the T1SS, which has a diameter of approximately 3 nm, while the diameter of a globular and folded protein of 1706 amino acids is ca. 8 nm (Chenal et al., 2010; O'Brien et al., 2017; O'Brien et al., 2015). We indeed demonstrated that apo-RTX proteins are appropriately sized to pass through the T1SS channel (see below) (O'Brien et al., 2015; Sotomayor-Perez et al., 2013). Our results support the hypothesis that the folding reaction is achieved upon protein secretion and, in the case of proteins containing RTX motifs, could be finely regulated by the calcium gradient across the bacterial cell wall. Moreover, the difference in stability between the calcium-free disordered RTX polypeptide inside bacteria and the holo-state in the extra-cellular medium might favor the transport of the whole protein through the secretion machinery (Chenal et al., 2010).

Intracellular environments are crowded by biomolecules at concentrations ranging from 100 to 400 g/L (Zhou et al., 2008). In several instances, molecular crowding has been shown to induce folding of intrinsically disordered proteins and partially folded states (Minton, 2005; Perham et al., 2007; Wang et al., 2012). Molecular crowding agents (in cells, biological macromolecules themselves) occupy a large volume fraction of the solution, thereby reducing the free space available to each biomolecule. Protein

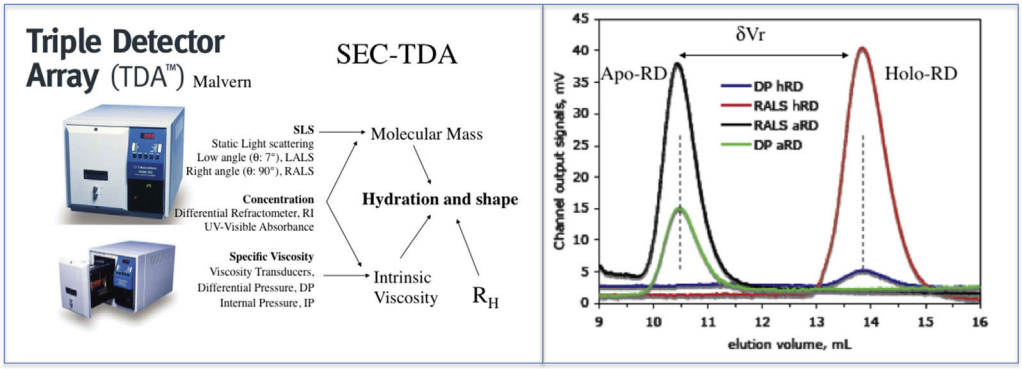

Fig. 3. Size exclusion chromatography followed by a triple detector array (SEC-TDA). Left panel: the parameters measured by the TDA instrument that combines a static light-scattering detector, a refractometer and a viscometer, allow the user to compute the molecular mass of biomolecules and to derive information about the flexibility and molecular shape of the investigated protein. Right panel: example of elution profiles of apo-RD and holo-RD showing the differential pressure (DP) and the right angle static light scattering (RALS) chromatograms used to compute the intrinsic viscosity and the molecular mass, respectively. This example illustrates that for the same amount of loaded protein, the RALS signal is similar, indicating that both species are monomeric, while the intrinsic viscosity values are significantly different, due to a major conformation difference between the apo-state and the holo-state of RD. For further details regarding the analysis of SEC-TDA data, see (Karst et al., 2012b).

Author's Personal Copy

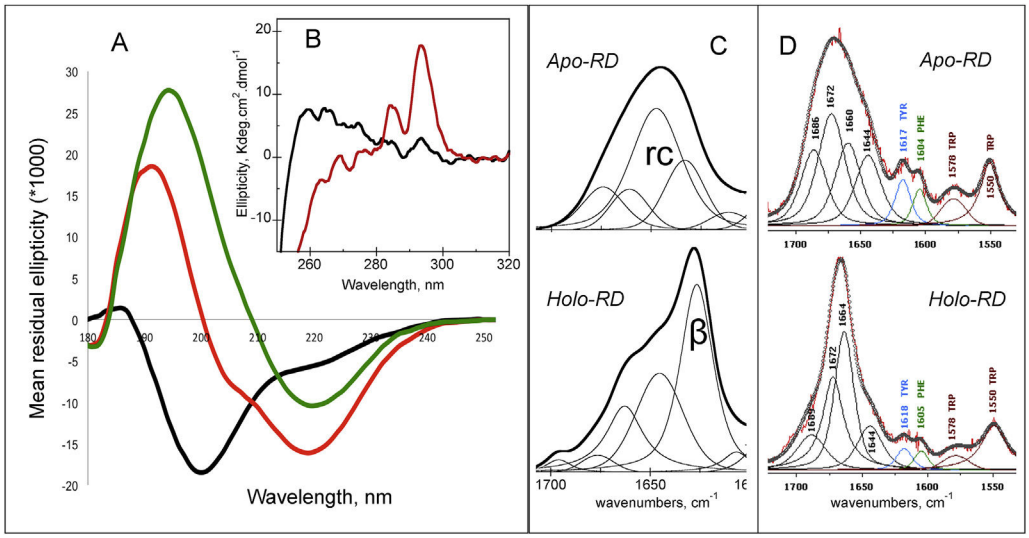

Fig. 4. Calcium-induced disorder-to-order transition of RTX proteins followed by (A) far-UV and (B) near-UV circular dichroism, (C) infra-red and (D) Raman spectroscopy. A. Apo-RD (black), holo-RD (red) and the difference spectrum (green) show that calcium binding induces a transition from a disordered to a folded protein. B. Near-UV CD of apo-RD (black) and holo-RD (red) spectra indicate that calcium binding induces tertiary structure formation involving aromatic residues. FTIR and Raman spectra provide more details on the type of secondary structure elements in both the apo- and holo-state; the apo-state is mostly populated by structural disorder (see deconvolution: random coil "rc" in C) and residual beta-sheet and turns (flanking bands), while the main contribution to the spectrum of the holo-state arises from beta-sheet structures. See original articles for detailed descriptions (Chenal et al., 2009, 2010; O'Brien et al., 2015; Sotomayor Perez et al., 2010; Sotomayor-Perez et al., 2011). (For interpretation of the references to color in this figure legend, the reader is referred to the Web version of this article.)

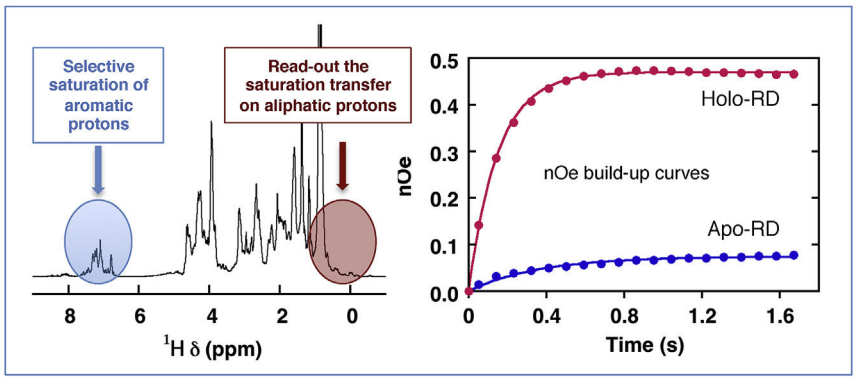

Fig. 5. Calcium-induced structural rearrangements of RTX proteins followed by NMR saturation transfer spectroscopy. Left panel: scheme of saturation transfer experiments. To probe the spatial proximity between aromatic and aliphatic residues in the tertiary structure, aromatic residues are selectively saturated and the intensity of saturation transfer is measured in the aliphatic region. Right panel: nOe build-up curves showing that aliphatic and aromatic residues are in close proximity in the holo-state of RD, while no significant saturation transfer occurs in the apo-state. See the original paper for details (Chenal et al., 2009).

conformations that occupy large hydrodynamic volumes are thus disadvantaged and, correlatively, smaller volume conformations favored, *i.e.*, the native state in the case of proteins. This is why molecular crowding is able to force proteins that are partially folded in diluted environments to adopt folded conformations in a crowded milieu. In the context of the CyaA toxin, we were interested to determine whether molecular crowding agents could significantly favor folding of apo-RTX proteins (Sotomayor-Perez et al., 2013). This issue is important, as it could question the working hypothesis, *i.e.*, that apo-RTX motifs are in a thermodynamically favorable disordered state in the calcium-poor bacterial cytoplasm prior to secretion.

We mimicked the exclusion volume effect of molecular crowding using the crowding agent Ficoll70™, a neutral, highly-branched, hydrophilic polysaccharide (Sotomayor-Perez et al., 2013). We showed that in the absence of calcium, the RTX protein adopts an intrinsically disordered state, indicating that apo-RTX proteins remain unfolded in the absence of calcium, even at high concentrations of molecular crowding agents similar (at least in terms of occupied volume fraction) to the environmental conditions prevailing in the bacterial cytoplasm. The addition of calcium induces folding and stabilization of RTX proteins. Our data further indicated that molecular crowding increases the affinity of RTX motifs for calcium (Sotomayor-Perez et al., 2013) and stabilizes the protein. We observed these molecular crowding effects on the calcium-induced folding and stabilization of two Block-V containing polypeptides, i.e., RC_L (Sotomayor-Perez et al., 2013) and RC_S ((Sotomayor Perez et al., 2010) and unpublished data), as well as on the full-length RTX domain, RD, of CyaA (unpublished data).

Recently, using an integrative approach combining Raman spectroscopy, Hydrogen Deuterium eXchange monitored by Mass Spectroscopy (HDX-MS), homology modelling and Size Exclusion Chromatography coupled to Small-Angle X-ray Scattering (SEC-SAXS) we proposed low-resolution structural models of both apo-

Author's Personal Copy

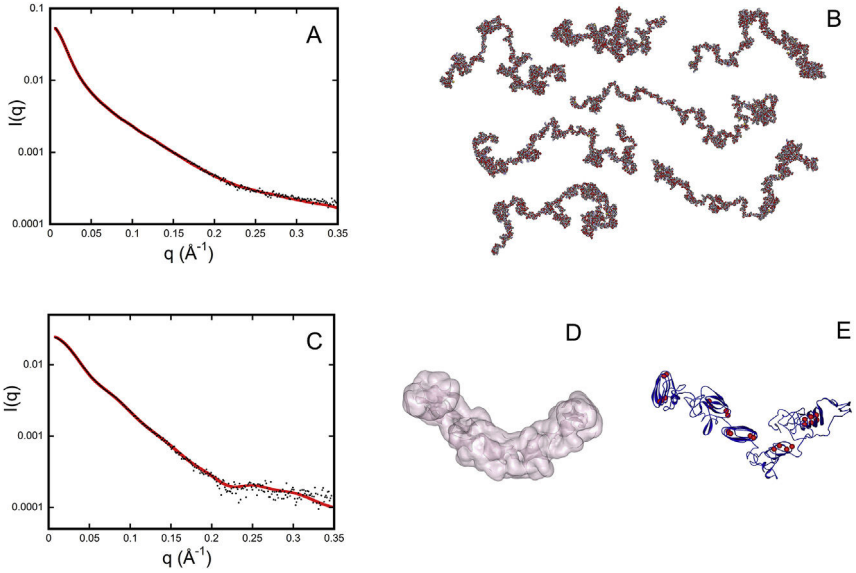

Fig. 6. SEC-SAXS data and modelling of apo- and holo-RD. A: Apo-RD SAXS pattern (black dots) and the fit obtained using EOM (red line) that is the average scattering pattern of the seven conformations shown in B. B: ensemble of seven conformations fitting the apo-RD scattering data in A. C: Holo-RD SAXS pattern (black dots) together with the calculated scattering curve of the Bunch model shown in panel E (red line). D: typical *ab initio* model of Holo-RD obtained using Gasbor. E typical Bunch model using the homology models proposed by Phyre2 for six regions of the protein identified by HDX-MS (see original paper for details). Figure assembled from figures in (O'Brien et al., 2015). (For interpretation of the references to color in this figure legend, the reader is referred to the Web version of this article.)

and holo-RD (O'Brien et al., 2017; O'Brien et al., 2015). SEC-SAXS data were recorded at the SWING beamline of SOLEIL synchrotron (David and Pérez, 2009). The structural models are in agreement with our hypothesis concerning the secretion process of CyaA: in the absence of calcium, the apo-state adopts extended and flexible conformations, typical of an intrinsically disordered protein, and well-suited for its uptake and secretion through the narrow channel of the T1SS. The central part of the apo-RD SAXS pattern was analyzed using the theory of statistical polymer chains, accounting for chain rigidity (persistence length) (Sharp and Bloomfield, 1968) and average chain thickness. This yielded a description of apo-RD in terms of a chain comprising about 10 successive statistical elements with average dimensions of 8 nm in length and 1.3 nm in diameter, *i.e.*, a diameter appropriately sized to go through the T1SS duct of 3 nm (O'Brien et al., 2015). However, these values are larger than those expected for a fully unfolded polypeptide chain, about 2 nm and 0.6 nm respectively, in agreement with the local structural elements detected by various spectroscopies (CD, NMR, *etc.*). This view is also supported by data analysis of the SAXS pattern in terms of ensemble of conformations using the program EOM (Tria et al., 2015) (Fig. 6, panel A & B). HDX-MS results show that the local structural elements mentioned above are primarily located in the C-terminal region of RD. In contrast, analysis of holo-RD SAXS pattern strongly suggests that the protein adopts a compact and stable conformation in agreement with the spectroscopic observations mentioned above. *Ab initio* modelling of the holo-state of RD using the program GASBOR (Svergun et al., 2001) yielded an elongated shape similar to a curved cylinder. Using the homology modelling Webserver Phyre2 (Kelley and Sternberg, 2009) we obtained models for six protein regions identified by HDX-MS. Refining their spatial position to fit the SAXS pattern using the program Bunch yields a global arrangement in excellent agreement with *ab initio* models (Fig. 6, panel C & D): holo-RD appears to behave like a folded multi-domain protein with flexible but fairly compact linkers. HDX-MS further revealed the existence of a C-terminal to N-terminal stability gradient, the C-terminal part, first to be secreted, being the most stable region of RD (Fig. 7).

Finally, we were interested to determine whether the C-terminal region of CyaA, from 1643 to 1706 that contains the secretion signal, exhibits the ability to interact with membranes during the secretion process. We have investigated the ability of three peptides (covering the sequences 1643–1677, 1656–1677 and 1683–1706) to bind to phospholipid bilayers and showed that none of the peptides does significantly bind to membranes (unpublished data).

1.2. CyaA refolding into a monomeric, stable and functional state

One of the most challenging aspects in the study of the full-length CyaA toxin remains the complexity of this large protein (1706 amino-acid residues), which is made up of several distinct domains, is post-translationally acylated, and which exhibits a pronounced hydrophobic character in places which drastically limits its solubility. Indeed, when over-produced in bacteria, recombinant CyaA proteins accumulate in inclusion bodies and require denaturing conditions (*i.e.*, 8 M urea) for their purification and storage (Sebo et al., 1991). Recently, we succeeded in refolding CyaA into a stable and monomeric form that is fully folded and functional, at variance with all prior procedures in which polypeptides were largely aggregated upon urea removal. Both calcium and molecular confinement are mandatory to produce the monomeric state (see Fig. 8), while CyaA acylation also strongly contributes to the efficiency of the refolding process (Cannella et al., 2017; Karst et al., 2014). Refolding intermediate species expose hydrophobic regions to the solvent, thus favoring multimerization of CyaA proteins through intermolecular hydrophobic interactions. Molecular confinement limits the intermolecular interactions occurring by diffusion and collision between partially folded CyaA proteins during the refolding process. The confinement creates "refolding cavities", providing more time for the refolding process, and decreasing inter-protein interactions. The ability to produce monomeric CyaA paves the way for both structural and functional studies.

We showed that monomeric CyaA displays hemolytic and cytotoxic activities, suggesting that it is the genuine, physiologically

Author's Personal Copy

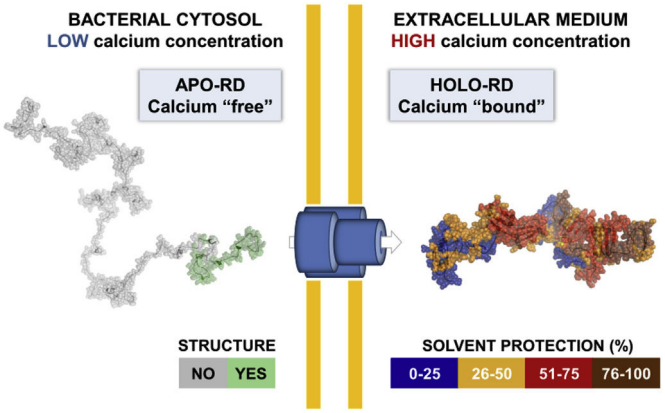

Fig. 7. Structural model for the secretion of RTX proteins inferred from HDX-MS and SEC-SAXS data. Within bacteria, Apo-RD is an extended and flexible disordered chain with a small diameter appropriately sized for transport through the narrow channel of the bacterial type 1 secretion system. The C-terminal region of RD is likely to be the first region to exit the T1SS into the calcium-rich environment of the bacterial extracellular milieu. Calcium binding to the RTX motifs induces folding of RD into a compact and stable structure larger than the T1SS conduit, thus ensuring an irreversible exit of the polypeptide. This disorder-to-order transition is essential for the secretion of CyaA and may be relevant for other RTX-containing toxins.

active form of the toxin in solution. Monomeric CyaA induces both permeabilization of lipid bilayer vesicles and erythrocyte hemolysis, even in the absence of free calcium in solution, while CyaA directly diluted from urea into the liposome or erythrocyte suspension requires calcium to acquire its lytic activities (Cannella et al., 2017). Importantly, the translocation of ACD followed by ACD:CaM complex formation and cAMP production is calcium dependent, with an apparent K_D of 0.3 mM calcium in the extracellular milieu (Cannella et al., 2017; Hewlett et al., 1991; Veneziano et al., 2013). This indicates that the calcium loaded onto CyaA monomers is not enough for ACD translocation, and that free

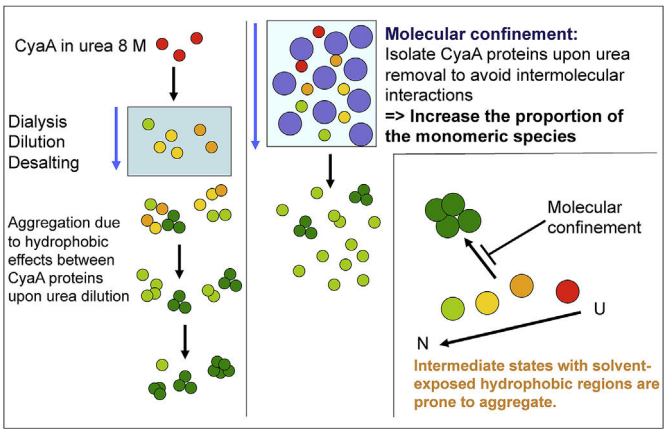

Fig. 8. Refolding of CyaA from a denaturated state in 6–8 M urea to a monomeric species by molecular confinement. Left panel: schematic diagram of the renaturation of CyaA from a urea-denaturated state (red), to a urea-free state by dialysis, dilution or desalting, leading to high proportions of multimers (complex of dark green spheres), and low proportions of monomers (individual light green spheres). Central panel: molecular confinement (here, beads of small particle radius, *i.e.*, BioSEC3, Superdex, TSK columns, *etc.*) drastically reduces the occurrence of intermolecular interactions between proteins during the refolding process, limiting CyaA aggregation due to hydrophobic effects between partially folded and solvent-exposed hydrophobic patches of CyaA proteins (orange and yellow). Right panel: color code of CyaA refolding upon urea removal. If the partially folded states are not maintained in an isolated state, they will aggregate into multimeric species (dark green), at the expense of monomeric species (light green). (For interpretation of the references to color in this figure legend, the reader is referred to the Web version of this article.)

calcium in solution is required at some stage of the translocation process. An excess of calcium may be required for cationic flux across the plasma membrane, as co-factor for protein/lipid complex formation involved in the translocation of the catalytic domain, or for the recently described phospholipase activity of CyaA (Gonzalez-Bullon et al., 2017).

We recorded SAXS data in order to propose a structural model of the monomeric CyaA in solution, again using the SEC-SAXS setup available on the SWING beamline to eliminate the contribution of larger particles (*e.g.*, aggregates), to the scattering pattern of monomeric CyaA (Cannella et al., 2017). This was essential to obtain high quality data for large proteins like CyaA, but also for soluble proteins like RD. Indeed, a recent SAXS study of holo-RD performed in batch mode (*i.e.*, by direct injection of the protein sample through the X-ray measuring cell without SEC) led to structural parameters (radius of gyration $R_g = 5.6$ nm, $D_{max} = 17.2$ nm and Vol = 275 nm^3) (Bumba et al., 2016) that are very different from these obtained in our prior structural studies of RD in both apo- and holo-states using SEC-SAXS ($R_g = 4.4$ nm, $D_{max} = 15.5$ nm and Vol = 105 nm^3 for holo-RD) (O'Brien et al., 2015). Most striking is the estimate of the volume that is 2.5 times larger than that expected for a compact protein of 72 kDa, suggesting the presence of higher molecular weight species in solution. Although we did not experience problems with apo-RD thanks to the strong repulsion between negatively charged RD proteins, we noticed that holo-RD, at the protein concentration required for SAXS experiments, mainly eluted, beyond a few oligomers, as two poorly resolved species, a dimer and monomer in equilibrium. Batch mode leads to the averaging of all species, while the use of SEC-SAXS together with data analysis using the deconvolution protocol available in the US-SOMO package (Brookes et al., 2016) allows one to recover the scattering patterns of individual species and from there to generate the structural model of the monomeric species (see (O'Brien et al., 2017) for details).

The SEC-SAXS pattern of the monomeric state of full-length CyaA indicates that it is a complex multidomain protein (Fig. 9). Moreover, the structural model of holo-RD nicely fits into the envelope of monomeric CyaA, suggesting that once RD is folded, it acts as a structural scaffold for the subsequent folding of the other domains that wrap around the RTX domain (Cannella et al., 2017; O'Brien et al., 2015).

2. Concluding remarks

Calcium-induced folding of RTX motifs represents a nice example of how basic physical forces have been harnessed by nature to produce structural modules that are finely tuned to allow efficient secretion by the T1SS machinery, as well as robust protein folding in the extracellular medium in the absence of any chaperone. The intrinsically disordered states of the RTX motifs in the low-calcium environment of the bacterial cytosol are specifically adapted for protein export through the narrow channel of the T1SS, while in the high-calcium extracellular environment, calcium binding triggers the folding of the RTX motifs into a β-roll fold that acts as a nucleus for the folding of the entire protein. These properties may explain the widespread distribution of RTX motifs in a large number of proteins secreted by a wide variety of Gram-negative bacteria, among them many RTX toxins that are key virulence factors produced by important bacterial pathogens (Chenal et al., 2015; Linhartova et al., 2010).

The calcium induced folding of the RTX motifs may also contribute to the secretion process via a molecular ratchet mechanism; indeed, the progressive folding of RTX motifs as they emerge from the T1SS channel and reach the calcium rich external medium should prevent backsliding (retrograde movement) of the

Author's Personal Copy

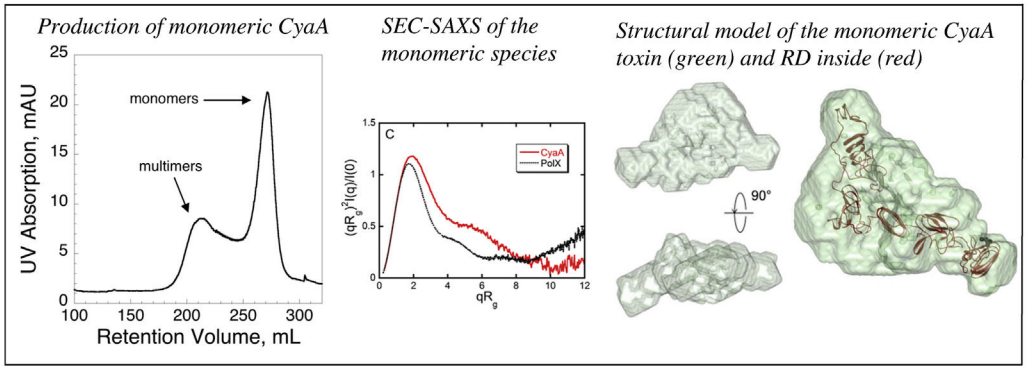

Fig. 9. Structural model of CyaA. Left panel: Example of production of high quantities of monomeric CyaA on a HiLoad superdex 200 pg column. Monomeric CyaA is concentrated on Amicon 3kD and re-loaded on a BioSEC3 column coupled to a SAXS cell. Central panel: Dimensionless Kratky representations of monomeric CyaA and PolX (a fully structured, quasi-spherical protein) SAXS patterns exhibiting a maximum at qRg = 1.9 and 1.7 respectively, indicative of a significant anisometry of CyaA shape. Right panel: typical *ab initio* bead model obtained by the program DAMMIN (Svergun, 1999) shown in light green. The model of holo-RD previously obtained by a combination of HDX-MS and SAXS is superimposed using the Supcomb routine (see the original paper for details (Cannella et al., 2017)). (For interpretation of the references to color in this figure legend, the reader is referred to the Web version of this article.)

polypeptide chain, thereby converting the stochastic movement of the translocating protein chain into an efficient vectorial transport into the extracellular medium. Yet, calcium-induced folding is not essential for active secretion, which can occur even in the complete absence of calcium in the extracellular medium ((Bumba et al., 2016) and unpublished results). Also, truncated CyaA polypeptides that cannot refold with calcium as they lack the C-terminal extremity (see above) can still be actively secreted (Sebo and Ladant, 1993). Furthermore, Schmitt and colleagues nicely demonstrated that the rate of secretion of HlyA derived substrate is independent of calcium (Lenders et al., 2016).

In contrast, several studies have established that the co-secretional calcium driven folding of CyaA at the outlet of the T1SS machinery is critical for the release of fully active toxins into the extracellular milieu. If calcium is limited, the secreted CyaA molecules cannot fold properly and may aggregate at the bacterial surface into non-toxic species, unable to invade target cells (Bumba et al., 2016; Gray et al., 2004; Karst et al., 2014). Interestingly, efficient release of active CyaA toxins is also stimulated by the presence of high concentrations of proteins such as serum albumin in the external medium, as originally shown by Bellalou et al. (1990) (Bellalou et al., 1990), and recently confirmed by Gonyar et al. (2017) (Gonyar et al., 2017). This effect highlights the contribution of molecular crowding (Cannella et al., 2017; Karst et al., 2014), occurring in the mucus layer for example, to CyaA folding into an active toxin.

Acknowledgments

Running costs were covered by Institut Pasteur, PasteurInnov (PIV15-197), PTR grant (PTR451) and the CNRS. D.O.B. was supported by PIV15-197 and PTR451. All authors were supported by CNRS and Institut Pasteur.

Transparency document

Transparency document related to this article can be found online at https://doi.org/10.1016/j.toxicon.2018.01.007.

References

Angely, C., Nguyen, N.M., Andre Dias, S., Planus, E., Pelle, G., Louis, B., Filoche, M., Chenal, A., Ladant, D., Isabey, D., 2017. Exposure to Bordetella pertussis adenylate cyclase toxin affects integrin-mediated adhesion and mechanics in alveolar epithelial cells. Biol. Cell 109, 293–311.
Barry, E.M., Weiss, A.A., Ehrmann, I.E., Gray, M.C., Hewlett, E.L., Goodwin, M.S., 1991. Bordetella pertussis adenylate cyclase toxin and hemolytic activities require a second gene, cyaC, for activation. J. Bacteriol. 173, 720–726.
Bauche, C., Chenal, A., Knapp, O., Bodenreider, C., Benz, R., Chaffotte, A., Ladant, D., 2006. Structural and functional characterization of an essential RTX subdomain of Bordetella pertussis adenylate cyclase toxin. J. Biol. Chem. 281, 16914–16926.
Bellalou, J., Sakamoto, H., Ladant, D., Geoffroy, C., Ullmann, A., 1990. Deletions affecting hemolytic and toxin activities of Bordetella pertussis adenylate cyclase. Infect. Immun. 58, 3242–3247.
Benz, R., Maier, E., Ladant, D., Ullmann, A., Sebo, P., 1994. Adenylate cyclase toxin (CyaA) of Bordetella pertussis. Evidence for the formation of small ion-permeable channels and comparison with HlyA of Escherichia coli. J. Biol. Chem. 269, 27231–27239.
Brookes, E., Vachette, P., Rocco, M., Perez, J., 2016. US-SOMO HPLC-SAXS module: dealing with capillary fouling and extraction of pure component patterns from poorly resolved SEC-SAXS data. J. Appl. Crystallogr. 49, 1827–1841.
Bumba, L., Masin, J., Fiser, R., Sebo, P., 2010. Bordetella adenylate cyclase toxin mobilizes its beta2 integrin receptor into lipid rafts to accomplish translocation across target cell membrane in two steps. PLoS Pathog. 6, e1000901.
Bumba, L., Masin, J., Macek, P., Wald, T., Motlova, L., Bibova, I., Klimova, N., Bednarova, L., Veverka, V., Kachala, M., Svergun, D.I., Barinka, C., Sebo, P., 2016. Calcium-driven folding of RTX domain beta-rolls ratchets translocation of RTX proteins through type I secretion ducts. Mol. Cell. 62, 47–62.
Cannella, S.E., Ntsogo Enguene, V.Y., Davi, M., Malosse, C., Sotomayor Perez, A.C., Chamot-Rooke, J., Vachette, P., Durand, D., Ladant, D., Chenal, A., 2017. Stability, structural and functional properties of a monomeric, calcium-loaded adenylate cyclase toxin, CyaA, from Bordetella pertussis. Sci. Rep. 7, 42065.
Carbonetti, N.H., 2010. Pertussis toxin and adenylate cyclase toxin: key virulence factors of Bordetella pertussis and cell biology tools. Future Microbiol. 5, 455–469.
Chenal, A., Guijarro, J.I., Raynal, B., Delepierre, M., Ladant, D., 2009. RTX calcium binding motifs are intrinsically disordered in the absence of calcium: implication for protein secretion. J. Biol. Chem. 284, 1781–1789.
Chenal, A., Karst, J.C., Sotomayor Perez, A.C., Wozniak, A.K., Baron, B., England, P., Ladant, D., 2010. Calcium-induced folding and stabilization of the intrinsically disordered RTX domain of the CyaA toxin. Biophys. J. 99, 3744–3753.
Chenal, A., Sotomayor Perez, A.C., Ladant, D., 2015. Structure and Function of RTX Toxins, the Comprehensive Sourcebook of Bacterial Protein Toxins, fourth ed. Elsevier.
David, G., Pérez, J., 2009. Combined sampler robot and high-performance liquid chromatography: a fully automated system for biological small-angle X-ray scattering experiments at the Synchrotron SOLEIL SWING beamline. J. Appl. Cryst. 42, 892–900.
El-Azami-El-Idrissi, M., Bauche, C., Loucka, J., Osicka, R., Sebo, P., Ladant, D., Leclerc, C., 2003. Interaction of Bordetella pertussis adenylate cyclase with CD11b/CD18: role of toxin acylation and identification of the main integrin interaction domain. J. Biol. Chem. 278, 38514–38521.
Fiser, R., Masin, J., Basler, M., Krusek, J., Spulakova, V., Konopasek, I., Sebo, P., 2007. Third activity of Bordetella adenylate cyclase (AC) toxin-hemolysin. Membrane translocation of AC domain polypeptide promotes calcium influx into CD11b+ monocytes independently of the catalytic and hemolytic activities. J. Biol. Chem. 282, 2808–2820.
Glaser, P., Danchin, A., Ladant, D., Barzu, O., Ullmann, A., 1988a. Bordetella pertussis adenylate cyclase: the gene and the protein. Tokai J. Exp. Clin. Med. 13, 239–252.
Glaser, P., Ladant, D., Sezer, O., Pichot, F., Ullmann, A., Danchin, A., 1988b. The calmodulin-sensitive adenylate cyclase of Bordetella pertussis: cloning and expression in Escherichia coli. Mol. Microbiol. 2, 19–30.
Glaser, P., Sakamoto, H., Bellalou, J., Ullmann, A., Danchin, A., 1988c. Secretion of

Author's Personal Copy

cyclolysin, the calmodulin-sensitive adenylate cyclase-haemolysin bifunctional protein of Bordetella pertussis. EMBO J. 7, 3997–4004.
Gonyar, L.A., Gray, M.C., Christianson, G.J., Mehrad, B., Hewlett, E.L., 2017. Albumin, in the presence of calcium, elicits a massive increase in extracellular Bordetella adenylate cyclase toxin. Infect. Immun. 85.
Gonzalez-Bullon, D., Uribe, K.B., Martin, C., Ostolaza, H., 2017. Phospholipase A activity of adenylate cyclase toxin mediates translocation of its adenylate cyclase domain. Proc. Natl. Acad. Sci. U. S. A. 114, E6784–E6793.
Gordon, V.M., Young Jr., W.W., Lechler, S.M., Gray, M.C., Leppla, S.H., Hewlett, E.L., 1989. Adenylate cyclase toxins from Bacillus anthracis and Bordetella pertussis. Different processes for interaction with and entry into target cells. J. Biol. Chem. 264, 14792–14796.
Gray, M.C., Donato, G.M., Jones, F.R., Kim, T., Hewlett, E.L., 2004. Newly secreted adenylate cyclase toxin is responsible for intoxication of target cells by Bordetella pertussis. Mol. Microbiol. 53, 1709–1719.
Guermonprez, P., Fayolle, C., Rojas, M.J., Rescigno, M., Ladant, D., Leclerc, C., 2002. In vivo receptor-mediated delivery of a recombinant invasive bacterial toxoid to CD11c + CD8 alpha -CD11bhigh dendritic cells. Eur. J. Immunol. 32, 3071–3081.
Guermonprez, P., Khelef, N., Blouin, E., Rieu, P., Ricciardi-Castagnoli, P., Guiso, N., Ladant, D., Leclerc, C., 2001. The adenylate cyclase toxin of Bordetella pertussis binds to target cells via the alpha(M)beta(2) integrin (CD11b/CD18). J. Exp. Med. 193, 1035–1044.
Guiso, N., 2017. Bordetella Adenylate Cyclase-hemolysin Toxins. Toxins (Basel) 9.
Harvill, E.T., Cotter, P.A., Yuk, M.H., Miller, J.F., 1999. Probing the function of Bordetella bronchiseptica adenylate cyclase toxin by manipulating host immunity. Infect. Immun. 67, 1493–1500.
Hewlett, E.L., Gray, L., Allietta, M., Ehrmann, I., Gordon, V.M., Gray, M.C., 1991. Adenylate cyclase toxin from Bordetella pertussis. Conformational change associated with toxin activity. J. Biol. Chem. 266, 17503–17508.
Karst, J.C., Barker, R., Devi, U., Swann, M.J., Davi, M., Roser, S.J., Ladant, D., Chenal, A., 2012a. Identification of a region that assists membrane insertion and translocation of the catalytic domain of Bordetella pertussis CyaA toxin. J. Biol. Chem. 287, 9200–9212.
Karst, J.C., Ntsogo Enguene, V.Y., Cannella, S.E., Subrini, O., Hessel, A., Debard, S., Ladant, D., Chenal, A., 2014. Calcium, acylation, and molecular confinement favor folding of bordetella pertussis adenylate cyclase CyaA toxin into a monomeric and cytotoxic form. J. Biol. Chem. 289, 30702–30716.
Karst, J.C., Sotomayor Perez, A.C., Guijarro, J.I., Raynal, B., Chenal, A., Ladant, D., 2010. Calmodulin-induced conformational and hydrodynamic changes in the catalytic domain of Bordetella pertussis adenylate cyclase toxin. Biochemistry 49, 318–328.
Karst, J.C., Sotomayor-Perez, A.C., Ladant, D., Chenal, A., 2012b. Estimation of intrinsically disordered protein shape and time-averaged apparent hydration in native conditions by a combination of hydrodynamic methods. Meth. Mol. Biol. 896, 163–177.
Kelley, L.A., Sternberg, M.J., 2009. Protein structure prediction on the Web: a case study using the Phyre server. Nat. Protoc. 4, 363–371.
Khelef, N., Sakamoto, H., Guiso, N., 1992. Both adenylate cyclase and hemolytic activities are required by Bordetella pertussis to initiate infection. Microb. Pathog. 12, 227–235.
Knapp, O., Maier, E., Masin, J., Sebo, P., Benz, R., 2008. Pore formation by the Bordetella adenylate cyclase toxin in lipid bilayer membranes: role of voltage and pH. Biochim. Biophys. Acta 1778, 260–269.
Ladant, D., 1988. Interaction of Bordetella pertussis adenylate cyclase with calmodulin. Identification of two separated calmodulin-binding domains. J. Biol. Chem. 263, 2612–2618.
Ladant, D., Brezin, C., Alonso, J.M., Crenon, I., Guiso, N., 1986. Bordetella pertussis adenylate cyclase. Purification, characterization, and radioimmunoassay. J. Biol. Chem. 261, 16264–16269.
Ladant, D., Ullmann, A., 1999. Bordatella pertussis adenylate cyclase: a toxin with multiple talents. Trends Microbiol. 7, 172–176.
Lenders, M.H., Beer, T., Smits, S.H., Schmitt, L., 2016. In vivo quantification of the secretion rates of the hemolysin A Type I secretion system. Sci. Rep. 6, 33275.
Linhartova, I., Bumba, L., Masin, J., Basler, M., Osicka, R., Kamanova, J., Prochazkova, K., Adkins, I., Hejnova-Holubova, J., Sadilkova, L., Morova, J., Sebo, P., 2010. RTX proteins: a highly diverse family secreted by a common mechanism. FEMS Microbiol. Rev. 34, 1076–1112.
Masin, J., Basler, M., Knapp, O., El-Azami-El-Idrissi, M., Maier, E., Konopasek, I., Benz, R., Leclerc, C., Sebo, P., 2005. Acylation of lysine 860 allows tight binding and cytotoxicity of Bordetella adenylate cyclase on CD11b-expressing cells. Biochemistry 44, 12759–12766.
Masure, H.R., Au, D.C., Gross, M.K., Donovan, M.G., Storm, D.R., 1990. Secretion of the Bordetella pertussis adenylate cyclase from Escherichia coli containing the hemolysin operon. Biochemistry 29, 140–145.
Minton, A.P., 2005. Models for excluded volume interaction between an unfolded protein and rigid macromolecular cosolutes: macromolecular crowding and protein stability revisited. Biophys. J. 88, 971–985.
O'Brien, D.P., Brier, S., Ladant, D., Durand, D., Chenal, A., Vachette, P., 2017. SEC-SAXS and HDX-MS: a powerful combination. The case of the calcium-binding domain of a bacterial toxin. Biotechnol. Appl. Biochem.
O'Brien, D.P., Hernandez, B., Durand, D., Hourdel, V., Sotomayor-Perez, A.C., Vachette, P., Ghomi, M., Chamot-Rooke, J., Ladant, D., Brier, S., Chenal, A., 2015. Structural models of intrinsically disordered and calcium-bound folded states of a protein adapted for secretion. Sci. Rep. 5, 14223.
Perham, M., Stagg, L., Wittung-Stafshede, P., 2007. Macromolecular crowding increases structural content of folded proteins. FEBS Lett. 581, 5065–5069.
Rogel, A., Farfel, Z., Goldschmidt, S., Shiloach, J., Hanski, E., 1988. Bordetella pertussis adenylate cyclase. Identification of multiple forms of the enzyme by antibodies. J. Biol. Chem. 263, 13310–13316.
Rogel, A., Hanski, E., 1992. Distinct steps in the penetration of adenylate cyclase toxin of Bordetella pertussis into sheep erythrocytes. Translocation of the toxin across the membrane. J. Biol. Chem. 267, 22599–22605.
Rogel, A., Schultz, J.E., Brownlie, R.M., Coote, J.G., Parton, R., Hanski, E., 1989. Bordetella pertussis adenylate cyclase: purification and characterization of the toxic form of the enzyme. EMBO J. 8, 2755–2760.
Rose, T., Sebo, P., Bellalou, J., Ladant, D., 1995. Interaction of calcium with Bordetella pertussis adenylate cyclase toxin. Characterization of multiple calcium-binding sites and calcium-induced conformational changes. J. Biol. Chem. 270, 26370–26376.
Sakamoto, H., Bellalou, J., Sebo, P., Ladant, D., 1992. Bordetella pertussis adenylate cyclase toxin. Structural and functional independence of the catalytic and hemolytic activities. J. Biol. Chem. 267, 13598–13602.
Sebo, P., Glaser, P., Sakamoto, H., Ullmann, A., 1991. High-level synthesis of active adenylate cyclase toxin of Bordetella pertussis in a reconstructed Escherichia coli system. Gene 104, 19–24.
Sebo, P., Ladant, D., 1993. Repeat sequences in the Bordetella pertussis adenylate cyclase toxin can be recognized as alternative carboxy-proximal secretion signals by the Escherichia coli alpha-haemolysin translocator. Mol. Microbiol. 9, 999–1009.
Sharp, P., Bloomfield, V.A., 1968. Light scattering from wormlike chains with excluded volume effects. Biopolymers 6, 1201–1211.
Sotomayor Perez, A.C., Karst, J.C., Davi, M., Guijarro, J.I., Ladant, D., Chenal, A., 2010. Characterization of the regions involved in the calcium-induced folding of the intrinsically disordered RTX motifs from the bordetella pertussis adenylate cyclase toxin. J. Mol. Biol. 397, 534–549.
Sotomayor-Perez, A.C., Karst, J.C., Ladant, D., Chenal, A., 2012. Mean net charge of intrinsically disordered proteins: experimental determination of protein valence by electrophoretic mobility measurements. Meth. Mol. Biol. 896, 331–349.
Sotomayor-Perez, A.C., Ladant, D., Chenal, A., 2011. Calcium-induced folding of intrinsically disordered repeat-in-toxin (RTX) motifs via changes of protein charges and oligomerization states. J. Biol. Chem. 286, 16997–17004.
Sotomayor-Perez, A.C., Ladant, D., Chenal, A., 2015. Disorder-to-order transition in the CyaA toxin RTX domain: implications for toxin secretion. Toxins 7, 1–20.
Sotomayor-Perez, A.C., Subrini, O., Hessel, A., Ladant, D., Chenal, A., 2013. Molecular crowding stabilizes both the intrinsically disordered calcium-free state and the folded calcium-bound state of a repeat in toxin (RTX) protein. J. Am. Chem. Soc. 135, 11929–11934.
Subrini, O., Sotomayor-Perez, A.C., Hessel, A., Spiaczka-Karst, J., Selwa, E., Sapay, N., Veneziano, R., Pansieri, J., Chopineau, J., Ladant, D., Chenal, A., 2013. Characterization of a membrane-active peptide from the Bordetella pertussis CyaA toxin. J. Biol. Chem. 288, 32585–32598.
Svergun, D.I., 1999. Restoring low resolution structure of biological macromolecules from solution scattering using simulated annealing. Biophys. J. 76, 2879–2886.
Svergun, D.I., Petoukhov, M.V., Koch, M.H., 2001. Determination of domain structure of proteins from X-ray solution scattering. Biophys. J. 80, 2946–2953.
Tria, G., Mertens, H.D.T., Kachala, M., Svergun, D.I., 2015. Advanced ensemble modelling of flexible macromolecules using X-ray solution scattering. IUCrJ 2, 207–217.
Uribe, K.B., Etxebarria, A., Martin, C., Ostolaza, H., 2013. Calpain-mediated processing of adenylate cyclase toxin generates a cytosolic soluble catalytically active N-terminal domain. PLoS One 8, e67648.
Veneziano, R., Rossi, C., Chenal, A., Brenner, C., Ladant, D., Chopineau, J., 2017. Synthesis and characterization of tethered lipid assemblies for membrane protein reconstitution (Review). Biointerphases 12, 04E301.
Veneziano, R., Rossi, C., Chenal, A., Devoisselle, J.M., Ladant, D., Chopineau, J., 2013. Bordetella pertussis adenylate cyclase toxin translocation across a tethered lipid bilayer. Proc. Natl. Acad. Sci. U. S. A. 110, 20473–20478.
Voegele, A., Subrini, O., Sapay, N., Ladant, D., Chenal, A., 2017. Membrane-active Properties of an Amphitropic Peptide from the CyaA Toxin Translocation Region. Toxins (Basel) 9.
Vojtova, J., Kamanova, J., Sebo, P., 2006. Bordetella adenylate cyclase toxin: a swift saboteur of host defense. Curr. Opin. Microbiol. 9, 69–75.
Vojtova-Vodolanova, J., Basler, M., Osicka, R., Knapp, O., Maier, E., Cerny, J., Benada, O., Benz, R., Sebo, P., 2009. Oligomerization is involved in pore formation by Bordetella adenylate cyclase toxin. Faseb. J. 23, 2831–2843.
Wang, Y., Sarkar, M., Smith, A.E., Krois, A.S., Pielak, G.J., 2012. Macromolecular crowding and protein stability. J. Am. Chem. Soc. 134, 16614–16618.
Weiss, A.A., Goodwin, M.S., 1989. Lethal infection by Bordetella pertussis mutants in the infant mouse model. Infect. Immun. 57, 3757–3764.
Weiss, A.A., Hewlett, E.L., 1986. Virulence factors of Bordetella pertussis. Annu. Rev. Microbiol. 40, 661–686.
Westrop, G.D., Hormozi, E.K., Da Costa, N.A., Parton, R., Coote, J.G., 1996. Bordetella pertussis adenylate cyclase toxin: proCyaA and CyaC proteins synthesised separately in Escherichia coli produce active toxin in vitro. Gene 180, 91–99.
Zhou, H.X., Rivas, G., Minton, A.P., 2008. Macromolecular crowding and confinement: biochemical, biophysical, and potential physiological consequences. Annu. Rev. Biophys. 37, 375–397.

View publication stats

Article II

Post-translational acylation controls the folding and functions of the CyaA RTX toxin

Darragh P. O'Brien, Sara E. Cannella, Alexis Voegele, Dorothée Raoux-Barbot, Maryline Davi, Thibaut Douché, Mariette Matondo, Sébastien Brier, Daniel Ladant and Alexandre Chenal

FASEB

June 2019

Various Gram-negative bacteria produce RTX toxins with post-translational acylation essential for their cytotoxic activities. The CyaA toxin is acylated on K860 and K983 by a dedicated CyaC acyltransferase (Bouchez et al., 2017; Hackett et al., 1994; Barry et al., 1991). The two acylations are required for translocation of the catalytic domain. Here, we report the effect of acylation on hydrodynamic and structural properties of proCyaA and CyaA monomers. This study provides new insights on how acylation drive the folding process toward a functional and folded state.

We first characterized proCyaA and CyaA by mass spectrometry. CyaA produced in the lab contains mainly palmitoleic (*cis* Δ9-C16:1) and palmitic acids (C16:0) on both lysine. Some traces of myristic acid (C14:0) were observed. As expected, proCyaA is devoid of acylation. Then, based on the method of molecular confinement developed in the team, we produced proCyaA and CyaA into monomeric state (Karst et al., 2014). Biological activities of both proteins (*i.e* hemolysis and translocation) were assessed on erythrocytes. As expected, proCyaA monomers did not hemolyse nor produce cAMP in the cell. On the other hand, CyaA monomers were able to induce hemolysis and cAMP accumulation, with higher activities than oligomers. These data confirmed that the monomeric CyaA is the physiological state of the toxin (Cannella et al., 2017).

Using ANS, we characterized solvent-exposed surfaces of both proteins. Interestingly, ANS fluorescence of CyaA was 3-fold lower than proCyaA, suggesting that the acylation allows compaction of hydrophobic regions of CyaA. Furthermore, analytic ultracentrifugation experiment suggested that proCyaA is slightly less compact than CyaA. Finally, urea denaturation indicated that CyaA is more stable than proCyaA. These data provide evidence that proCyaA is less compact and its hydrophobic regions are more exposed than CyaA.

HDX-MS (for Hydrogen/Deuterium eXchange followed by Mass Spectrometry) experiments were performed in denaturating conditions (6, 3 or 1.6 M urea) to characterize the refolding of CyaA and proCyaA. We observed that in the presence of calcium, CyaA sequentially acquires folding from C- to N-terminal extremities upon urea removal. Additionally, in the absence of calcium, CyaA remains unfolded at each urea concentration, suggesting that calcium binding to the RTX motifs is critical for both folding of the RD domain but also for the folding of the other domains. A similar sequential folding was obtained for proCyaA upon urea dilutions. However, significant differences were observed

between CyaA and proCyaA. The strongest differences were observed in the HR and AR regions.

At 3 M urea, we observed more dynamic in CyaA between the residues 658 to 719 in the HR. At 1.6 M urea, further minor differences were characterized from HR to the N-terminal part (*i.e* translocation region and catalytic domain) and also in the AR. Thus, it seems that acyl chains favor folding of the region 658-719 and that hydrophobic effects drive faster folding of CyaA than proCyaA.

In absence of urea (*i.e* in calcium buffer), the peptides between residues 798 to 958, in the AR region, were more accessible and less folded in proCyaA than CyaA. Furthermore, five peptides (539-546, 571-582, 615-622, 682-696 and 686-696), encompassing the hydrophobic segments of HR, had significant changes in HDX-MS patterns. The significant difference was observed between residues 660 and 710, which confirm that this segment may have an important role in CyaA folding.

These data show that CyaA acylation favors a hydrophobic collapse of the HR and AR domains, and is critical for folding of CyaA from 3 M urea to the monomeric state in solution.

In summary, these data show that CyaA is more compact and has hydrophobic regions less exposed than proCyaA. Independently of the acylation, HDX-MS results provide evidence that calcium is crucial for sequential folding of CyaA. In the context of CyaA secretion, the low calcium concentration in the bacteria may prevent folding while, upon secretion, RD is exposed to mM range of calcium which folds RD. Then RD may act as a scaffold for the folding of the other domains of the toxin. Finally, the comparison between CyaA and proCyaA highlights how acylation has a critical role on folding. Acylation favor hydrophobic collapse within the region encompassing residues 660-710 in HR. This region is suggested to play a central role for folding of AR and HR.

THE FASEB JOURNAL • RESEARCH • www.fasebj.org

Post-translational acylation controls the folding and functions of the CyaA RTX toxin

Darragh P. O'Brien,[*,1] Sara E. Cannella,[*,1] Alexis Voegele,[*,†] Dorothée Raoux-Barbot,[*] Marilyne Davi,[*] Thibaut Douché,[‡] Mariette Matondo,[‡] Sébastien Brier,[*,§] Daniel Ladant,[*,2] and Alexandre Chenal[*,3]

[*]Institut Pasteur, Chemistry and Structural Biology Department, and [§]Biological NMR Technical Platform, Center for Technological Resources and Research, UMR CNRS 3528, Paris, France; [†]Université Paris Diderot Paris VII, Sorbonne Paris Cité, Paris, France; and [‡]Institut Pasteur, Proteomics Platform, Mass Spectrometry for Biology Unit, USR CNRS 2000, Paris, France

ABSTRACT: The adenylate cyclase (CyaA) toxin is a major virulence factor of *Bordetella pertussis*, the causative agent of whooping cough. CyaA is synthetized as a pro-toxin, pro-CyaA, and converted into its cytotoxic form upon acylation of two lysines. After secretion, CyaA invades eukaryotic cells and produces cAMP, leading to host defense subversion. To gain further insights into the effect of acylation, we compared the functional and structural properties of pro-CyaA and CyaA proteins. HDX-MS results show that the refolding process of both proteins upon progressive urea removal is initiated by calcium binding to the C-terminal RTX domain. We further identified a critical hydrophobic segment, distal from the acylation region, that folds at higher urea concentration in CyaA than in pro-CyaA. Once refolded into monomers, CyaA is more compact and stable than pro-CyaA, due to a complex set of interactions between domains. Our HDX-MS data provides direct evidence that the presence of acyl chains in CyaA induces a significant stabilization of the apolar segments of the hydrophobic domain and of most of the acylation region. We propose a refolding model dependent on calcium and driven by local and distal acylation-dependent interactions within CyaA. Therefore, CyaA acylation is not only critical for cell intoxication, but also for protein refolding into its active conformation. Our data sheds light on the complex relationship between post-translational modifications, structural disorder and protein folding. Coupling calcium-binding and acylation-driven folding is likely pertinent for other Repeat-In-Toxin cytolysins produced by many Gram-negative bacterial pathogens.—O'Brien, D. P., Cannella, S. E., Voegele, A., Raoux-Barbot, D., Davi, M., Douché, T., Matondo, M., Brier, S., Ladant, D., Chenal, A. Post-translational acylation controls the folding and functions of the CyaA RTX toxin. FASEB J. 33, 000–000 (2019). www.fasebj.org

KEY WORDS: post-translational modification · protein folding · calcium-binding protein · adenylate cyclase · bordetella pertussis

Post-translational modifications (PTM) are involved in the regulation of many cellular processes and play a critical role in protein localization, structure, stability, and function (1, 2). Post-translational addition of acyl chains to bacterial toxins from the repeat-in-toxin (RTX) family has been shown to be essential to their cytolytic activities. RTX toxins are calcium-dependent virulence factors produced by various Gram-negative bacteria (3, 4). These cytotoxins are synthesized as nonactive precursors that require activation by selective post-translational acylation carried out by dedicated acyl-transferases that use an acyl–acyl carrier protein as fatty acid donor (5–9). Once acylated, the RTX toxins are secreted *via* dedicated type 1 secretion systems (T1SS) and exert their virulence on a variety of target cells (10). Most are cytolysins endowed with a pore-forming activity that alter the membrane integrity of their target cells (3, 4, 11), whereas few others have additional cytotoxic activities (see, for instance, the CyaA toxin below). How the acyl chains regulate the biologic activities of these RTX cytolysins has remained elusive thus far.

Here, we address this question by exploring the effects of post-translational acylation on the structure and functions of the adenylate cyclase toxin (CyaA) from *Bordetella pertussis*, the causative agent of whooping cough (12). In addition to its pore-forming activity, CyaA possesses an

ABBREVIATIONS: AC, N-terminal adenylate cyclase catalytic domain; ANS, 8-anilino-1-naphthalenesulfonic acid; AR, acylation region; AUC, analytical ultracentrifugation; CyaA, adenylate cyclase; HDX-MS, hydrogen/deuterium eXchange followed by mass spectrometry; HEPES, 4-(2-hydroxyethyl)-1-piperazineethanesulfonic acid; HR, hydrophobic region; LC, liquid chromatography; pro-CyaA, non-acylated adenylate cyclase; PTM, post-translational modifications; RD, RTX domain; RTX, repeat in toxin; T1SS, type 1 secretion system; TR, translocation region

[1] These authors contributed equally to this work.
[2] Correspondence: Institut Pasteur, Chemistry and Structural Biology Department, UMR CNRS 3528, 75724 PARIS cedex 15, France. E-mail: daniel.ladant@pasteur.fr
[3] Correspondence: Institut Pasteur, 25, rue du Dr Roux, 75015 Paris, France. E-mail: alexandre.chenal@pasteur.fr

doi: 10.1096/fj.201802442RR
This article includes supplemental data. Please visit *http://www.fasebj.org* to obtain this information.

om www.fasebj.org by Institut Pasteur - CeRIS (157.99.25.33) on June 27, 2019. The FASEB Journal Vol. ${article.issue.getVolume()}, No. ${article.issue.getIssueNumber()}, p

extra domain endowed with adenylate cyclase activity. The N-terminal CyaA catalytic domain (AC) is delivered into the cytoplasm of target cells (13, 14), where it is activated by calmodulin (15, 16) to produce high levels of cAMP, subverting host immunity (10, 17, 18). CyaA is a large, multidomain protein of 1706 amino-acid residues, with AC (residues 1–364) (16), whereas the C-terminal hemolysin region (residues 365–1706) contains several domains responsible for AC membrane translocation and pore-forming activity (19–24). The translocation region (TR; residues 365–527) is involved in AC translocation across target cell membranes (24) and membrane permeabilization (25) and exhibits features similar to membrane-active peptides (24, 26, 27). The hydrophobic region (HR) corresponds to residues 528–710, whereas the acylation region (AR) extends from residues 711 through 1005. CyaA is synthesized as an inactive precursor, nonacylated CyaA (pro-CyaA), that is converted into its active form upon specific acylation of 2 lysine residues (Lys 860 and Lys 983) by CyaC, an acyltransferase that catalyzes the transfer of an acyl chain from an acyl–acyl-carrier protein to the ε-amino groups of pro-CyaA lysines (7, 28–30). Finally, the C-terminal 701 residues (1006–1706) correspond to the cell receptor–binding domain, RTX domain (RD), which harbors ~40 copies of a glycine- and aspartate-rich nona-peptide repeat, characteristic of the RTX bacterial cytolysins. In the absence of calcium, these RTX motifs are intrinsically disordered but undergo a disorder-to-order transition upon calcium binding (4, 31–42). The RTX motifs themselves constitute the primary sites of calcium binding within the protein (3, 31, 43, 44).

It is well known that acylation is critically required for the pore-forming activity of CyaA as well as its ability to invade cells to produce high levels of cAMP (*i.e.*, cell intoxication) (45, 46). Here, we have analyzed the structural and hydrodynamic properties of both pro-CyaA and CyaA monomers to provide insights into their folding process and to identify the structural basis of the acylation-dependent gain of functions. Our biophysical data show that the acylated CyaA protein adopts a more compact and stable monomeric state than pro-CyaA, whereas hydrogen/deuterium eXchange followed by mass spectrometry (HDX-MS) studies provided direct evidence of long-range interactions between the HRs and ARs. HDX-MS results further indicate that these interactions are strongly favored in the presence of the acyl chains. We propose that these interactions may directly contribute to the folding of the acylated CyaA protein into a compact and functional monomeric state. Our data indicates that calcium-binding and post-translational acylation play a key role in the folding of CyaA into its cytotoxic form.

MATERIALS AND METHODS

Overexpression and purification of pro-CyaA and CyaA in urea and production of the monomeric species

Buffer A was composed of 20 mM 4-(2-hydroxyethyl)-1-piperazineethanesulfonic acid (HEPES) and 150 mM NaCl (pH 7.4). Production and purification of pro-CyaA and CyaA and refolding of both species into holo-monomers was performed as previously described (41 and 47). The pro-CyaA urea stock solution was loaded at 2 μM (compared with 5 μM for CyaA) on a size exclusion chromatography column (HiLoad 26/600 Superdex 200 pg, average particle size: 34 μm; column dimensions: 26 × 600 mm; Superdex 200 Increase 10/300 GL, average particle size: 8.6 μm; column dimensions: 10 × 300 mm (GE Healthcare; Chicago, IL, USA); or Agilent BioSEC-5, particle size: 5 μm, pore size: 300 Å, column dimensions: 21.2 × 300 mm) to refold the protein into a monomeric species. The monomer-to-multimer ratio increases as the particle size decreases.

Identification of the post-translational acylation of pro-CyaA and CyaA by MS

Protein digestion

CyaA (9 μM) and pro-CyaA (7 μM) in 6 M urea buffer were first digested with Lys-C (V1671; Promega, Madison, WI, USA) at a Lys-C/toxin ratio of 1/50 (w/w) at 37°C for 3 h. To ensure optimal trypsin activity, the urea concentration was decreased below 2 M with the addition of 2 volumes of buffer A, and then a second digestion was performed with Trypsin (Sequencing Grade Modified Trypsin V5111; Promega) at an enzyme/toxin ratio of 1/50 (w/w) at 37°C for 1 h. Digestion was stopped by adding formic acid to 2% final concentration. Digested peptides were desalted and concentrated with Pierce C18 Spin Columns (89870; Thermo Fisher Scientific, Waltham, MA, USA) according to the manufacturer's instructions. Peptides were vacuum centrifuged and then lyophilized. Peptides were reconstituted in 2% acetonitrile/0.1% formic acid.

LC–tandem MS analysis

A Proxeon EASY-nLC 1000 nanochromatographic system (Thermo Fisher Scientific) was coupled online to an LTQ-Orbitrap Velos Mass Spectrometer (Thermo Fisher Scientific). For each sample, 0.5 μg peptides was directly loaded onto a 15-cm home-made C4 column (5 μm particles, 300 Å pore size, ReproSil-Pur 300 C4; Dr. Maisch GmbH, Ammerbuch-Entringen, Germany) and eluted by a 1-step gradient from 3.0 to 80% solvent B (80% acetonitrile 0.1% formic acid) in 50 min at a flow rate of 250 nl/min. MS data was acquired using Xcalibur software with a survey scan (100–1800 *m/z*) analyzed into the Orbitrap mass analyzer at a resolution setting of 60,000 followed by 15 collision induced dissociation (CID) fragmentations analyzed in the linear ion trap. The Automatic Gain Control (AGC*) target for MS and tandem MS scans were set to 1E6 and 5E3, respectively. The isolation width was set to 2.5 *m/z*, and the normalized collision

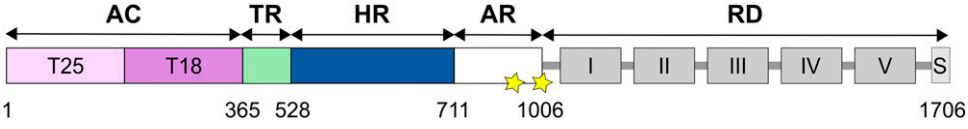

Figure 1. Schematic representation of the multidomain CyaA toxin (1706 aa residues). The toxin contains the following domains: AC (residues 1–364), TR (residues 365–527), HR (residues 528–710), AR (residues 711–1005 with acylated Lys 860 and Lys 983 marked with yellow stars), and a C-terminal RD (1006–1706) composed of 5 consecutive blocks.

om www.fasebj.org by Institut Pasteur - CeRIS (157.99.25.33) on June 27, 2019. The FASEB Journal Vol. ${article.issue.getVolume()}, No. ${article.issue.getIssueNumber()}, p

energy was set to 35. Selected ions were dynamically excluded for 15 s.

Data analysis

All raw data was analyzed using MaxQuant software v.1.5.1.2 (48) and the Andromeda search engine (49). Based on the protein expression system, data was searched against the complete *E. coli* strain K12 UniProt (*https://www.uniprot.org/*) database (4331 proteins, downloaded 2015-10-08) and CyaA protein sequence. The digestion mode was set to trypsin, and a maximum of 2 missed cleavages were allowed. Carbamidomethylation of cysteine was specified as a fixed modification. Variable modifications considered were N-terminal acetylation, oxidation of methionines, and N-acylation of lysines (Myristoyl-4H, Myristoleylation, Myristoylation, Palmitoleylation, Palmitoylation). The minimum peptide length was fixed to 5 aa, and the required false discovery rate was set to 1% at the peptide spectrum match and protein level. The main search peptide tolerance was set to 4.5 ppm and to 0.5 Da for the tandem MS match tolerance. Second peptides were enabled to identify cofragmentation events. Results of PTM identification are shown in Supplemental Fig. S2*A–C*.

HDX-MS of pro-CyaA and CyaA conformation and dynamics

We used HDX-MS to characterize the refolding process of pro-CyaA and CyaA equilibrated in 6, 3, or 1.6 M urea as well as the monomeric species in the complete absence of denaturant. The following 2 experimental conditions were analyzed: A, to monitor the effect of post-translational acylation on the refolding process of full-length pro-CyaA and CyaA at 6, 3, and 1.6 M urea; and B, to determine the effect of acylation on the full-length pro-CyaA and CyaA monomers. To achieve this, several proteins and conditions were analyzed. First, pro-CyaA and CyaA were analyzed each in the presence of 6, 3, and 1.6 M urea containing either 2 mM $CaCl_2$ or 2 mM EDTA; and second, fully folded pro-CyaA and CyaA monomers were analyzed in buffer A, complemented with 2 mM $CaCl_2$.

HDX-MS sample preparation

Prior to the addition of the deuterated buffer (100% D_2O in 20 mM HEPES, 150 mM NaCl, pD 7.4, supplemented or not with 6, 3, or 1.6 M urea), all solutions were equilibrated for 1 h at 20°C. For experiment A, labeling was initiated by diluting each sample 5-fold with the deuterated buffer and incubated for 0.16, 1, 10, 60, and 240 min at 20°C (final protein concentration of 0.3 μM during labeling); experiment B was performed using a final protein concentration of 1 μM and identical labeling conditions for 0.16, 0.5, 1, 5, 10, 30, 60, 120, 240, 480, and 1440 min, respectively.

The 80% excess of deuterium reached during labeling ensured unidirectional exchange. Aliquots of 3–10 pmol of protein were withdrawn at each experimental time point and quenched upon mixing of the deuterated sample with ice-cold 0.5% formic acid solution to achieve a final pH 2.5. For experiment A (in the presence of urea), the quench was performed by mixing 14 μl of labeled sample with 56 μl of ice-cold 0.5% formic acid (ratio 1/5, v/v, final H_2O/D_2O ratio = 20%/80%). For experiment B (monomeric species), the quench was performed by mixing 30 μl of labeled sample with 30 μl of ice-cold 0.5% formic acid (ratio 1/2, v/v, final H_2O/D_2O ratio = 50%/50%). Quenched samples were immediately snap-frozen in liquid nitrogen and stored at −80°C for ~12 h. Undeuterated controls were treated using an identical procedure. Triplicate independent technical analyses were performed for each time point and condition for all HDX-MS analyses.

HDX-MS data acquisition

Prior to MS analysis, samples were rapidly thawed. To minimize back exchange, the liquid chromatography (LC) solvent line, injection valve, and sample loop were maintained at 0°C. To achieve this, local HDX analyses were performed with the aid of a cooled HDX Manager (Waters, Milford, MA, USA). Samples were digested using an in-house prepared cartridge of immobilized pepsin beads (Thermo Fisher Scientific) for 2 min at 70 μl/min and 20°C. Peptic peptides were rapidly desalted and concentrated using a Vanguard C18 precolumn (1.7 μm, 2.1 × 5 mm; Waters) and separated using an Acquity UPLC BEH C18 column (1.7 μm, 1 × 100 mm). Pro-CyaA and CyaA peptides were separated over a 10-min gradient of 5–40% acetonitrile at 38 μl/min and at 0°C. The LC flow was directed to a Synapt G2-Si HDMS mass spectrometer (Waters), which was equipped with electrospray ionization and lock-mass correction using Glu-Fibrinogen peptide. Mass spectra were acquired in positive-ion mode over the *m/z* range of 50–1800 using a data-independent acquisition scheme (MS^E), whereby exact mass information is collected at both low and high collisional energies for collisional-induced dissociation. Unlabeled pro-CyaA and CyaA samples were digested in triplicate to build a peptide coverage map.

HDX-MS data processing

Peptide identification was *via* the Protein Lynx Global Server (PLGS) 3.0 (Waters). Oxidation of methionines and carbamylation of N-terminal and lysine residues were set as variable modifications. The sequence coverage map (Supplemental Figs. S3 and S4) was plotted using DynamX 3.0 HDX software (Waters). For the native proteins, pepsin digestion yielded 232 unique peptides identified from their accurate masses and product ion spectra. A total of 141 peptides were brought forward for HDX data analysis, corresponding to a sequence coverage of 91.0%. For the proteins in urea, 172 peptides, covering 85.7% of the protein sequence, were selected for final analysis. The reduced sequence coverage witnessed here was due to the experimental design necessitating a lower protein load on column at the 1.6-M urea concentration (down to 3 pmol, in contrast to 10 pmol for all other states), resulting in a knock-on decrease in MS sensitivity. D_2O uptake at the peptide level was extracted and visualized in uptake charts, difference plots, and heat maps performed in both DynamX and MEMHDX (50). Statistical analysis of HDX-MS results was performed with MEMHDX (Wald test, false discovery rate set to 1%).

Urea unfolding of pro-CyaA and CyaA monomers

A volume of 2.5 μl of CyaA or pro-CyaA monomers stored in 20 mM HEPES, 150 mM NaCl, and 2 mM $CaCl_2$, pH 7.5, was diluted in 20 mM HEPES, 150 mM NaCl, and 2 mM $CaCl_2$ containing urea at various concentrations to obtain a final concentration of toxin of 50 nM. A total of 22 tubes were prepared with a urea gradient from 0 to 6 M. Once diluted, the toxin was incubated at room temperature for 1 h. Emission spectra of the protein were acquired on a Jasco FP 8200 spectrofluorimeter (Jasco, Tokyo, Japan) using a 3 × 3–mm path length quartz cell (105.251.QS; Hellma Analytics, Plainview, NY, USA). The excitation wavelength was set to 280 nm, both emission and excitation slits were fixed at 5 nm, and fluorescence emission spectra were recorded from 300 to 400 nm. Spectra were acquired at 25°C. The ratio of fluorescence intensities at 340 and 380 nm were plotted against the urea concentration.

om www.fasebj.org by Institut Pasteur - CeRIS (157.99.25.33) on June 27, 2019. The FASEB Journal Vol. ${article.issue.getVolume()}, No. ${article.issue.getIssueNumber()}, p

ANS binding to CyaA and pro-CyaA monomers

Freshly prepared 8-anilino-1-naphthalenesulfonic acid (ANS) was added to pro-CyaA or CyaA monomers to reach final concentrations of 5 and 0.5 μM, respectively (molar ratio of ANS: toxin was 10:1). Excitation was fixed at 360 nm, and emission spectra were recorded between 400 and 600 nm on a Jasco FP 8200 spectrofluorimeter (Jasco) using either a 3 × 3–mm path length quartz cell (105.251.QS; Hellma Analytics) or a 10-μl drop cell. All spectra were acquired at 25°C.

Analytical ultracentrifugation analysis of pro-CyaA and CyaA monomers

Sedimentation velocity experiments were performed on a Beckman XL-A analytical ultracentrifuge (Beckman Coulter, Brea, CA, USA) in a AN60-Ti rotor at 20°C. All samples were filtered on 0.2-μm filters before experiments. Detection of the protein concentration as a function of radial position and time was performed by optical density measurements at a wavelength of 280 nm. For sample analysis, 400 μl of pro-CyaA or CyaA at 1 μM was loaded into a 1.2-mm–thick 2-channel epoxy centerpiece and spun at 20,000 rpm. Data were analyzed with SEDFIT software using a continuous size distribution c(s) model (15, 41, 51).

Hemolytic and cytotoxic activities of the different CyaA species

Toxin binding and translocation into sheep erythrocytes were assayed essentially as previously described in refs. 52 and 53. CyaA activity was measured as previously described in ref. 54; 1 U CyaA activity corresponds to 1 μmol cAMP formed per min at 30°C and pH 8.0. The different CyaA preparations were diluted directly to final concentrations of 5.6–11 nM (1–2 μg/ml) into suspensions of sheep erythrocytes (5×10^8/ml) in buffer A (20 mM HEPES-Na, pH 7.5, 150 mM NaCl) supplemented with either 2 mM $CaCl_2$ or 1 mM EDTA and incubated at 30°C for 20 min. An aliquot was removed to determine the total CyaA activity added to each sample. The cell suspensions were chilled on ice and centrifuged at 4°C, and the pelleted cells were resuspended in buffer A and separated into 2 batches. One batch was centrifuged again, and the pelleted cells were lysed with 0.1% Tween 20. The enzymatic activity measured in this extract corresponds to that of the toxin bound to the cells and was expressed as a percentage of total activity added to the cells. To the second batch, 20 μg L-1-(tosylamino)-2-phenylethyl chloromethyl ketone–treated trypsin (MilliporeSigma, Burlington, MA, USA) were added, and the mixture was incubated for 10 min at room temperature to digest the CyaA that remained at the external surface of the erythrocytes. After addition of soybean trypsin inhibitor (5-fold excess), the erythrocytes were washed again with buffer A and then lysed with 0.1% Tween 20. The CyaA activity protected from trypsin digestion, corresponding to the internalized AC activity, was then measured and expressed as a percentage of total activity added. Activities are expressed as percentages of total CyaA activity added to the erythrocytes suspension (taken as 100%) and represent the average values (with SD below 20%) from at least 2 independent measurements. The hemolytic activity of the different CyaA species was determined on sheep erythrocytes as previously described (47). Briefly, sheep erythrocytes were washed several times with buffer A and resuspended at 5×10^8 cells/ml. The hemolytic activity of pro-CyaA and CyaA was measured after overnight incubation of erythrocytes at 37°C by quantifying the amount of hemoglobin released at 540 nm (and of intracellular content release at 405 nm). Complete lysis (corresponding to 100% lysis) was obtained by the addition of 0.1% Triton.

Data availability

All data generated and analyzed during this study are included in this published article and its supplemental information files.

RESULTS

Production and MS characterization of CyaA and pro-CyaA

Pro-CyaA and CyaA (**Fig. 1**) were overexpressed in *Escherichia coli*, the latter by coexpression of pro-CyaA and CyaC (52, 55, 56), and purified to homogeneity using established methods (47). To identify the acyl chains incorporated in CyaA, the pro-CyaA and CyaA proteins were digested by Lys-C and trypsin and analyzed by MS (see Supplemental Fig. S1*A*–*C*). Two peptides (858–872 and 972–984) containing the K860 and K983 residues were identified. Both residues were primarily palmitoleylated (C16:1) in CyaA (Supplemental Fig. S1*A*, *B*). Palmitoylation (C16:0) was also identified on both K860 and K983 residues. Traces of myristoylation (C14:0) were observed on K983. Interestingly, residues K860 and K983 were always detected as modified in the CyaA sample, suggesting that the 2 lysine residues are fully acylated (see Supplemental Fig. S1*D*). However, we cannot rule out that a small fraction of CyaA remains unmodified, but the abundance of such peptides appears too low to be detected by the latest generation of the LC-MS Orbitrap instrument. Finally, as expected, no acylation was detected on K860 or K983 in pro-CyaA (Supplemental Fig. S1*C*). In summary, CyaA is primarily post-translationally modified with C16 acyl chains on both lysine residues, whereas pro-CyaA is devoid of PTM.

Refolding and functional activities of CyaA and pro-CyaA

Because of their size and hydrophobic character, both pro-CyaA and CyaA proteins are prone to aggregation. They are traditionally purified in the presence of chaotropic agents (usually urea) and stored in an unfolded state in denaturing conditions (*i.e.*, 6–8 M urea). Upon refolding by urea dilution, mixtures of multimeric and monomeric species are commonly obtained, precluding further biochemical and biophysical characterization (41). Yet, we have recently achieved to refold both pro-CyaA and CyaA into monomeric states (Supplemental Fig. S2) that remain stable in the absence of urea (41, 47), thus allowing us to investigate the relationship between the structure and function of these 2 species. The method is based on molecular confinement to prevent intermolecular interactions between HRs of proteins upon their refolding. Refolding is performed on a size-exclusion chromatography column used as molecular confinement media comprising a matrix characterized by small size particles (see Materials and Methods for details and Supplemental Fig. S2). In addition to the monomeric species, this refolding procedure also leads to the formation of a heterogeneous population of CyaA multimers. We have previously observed that

om www.fasebj.org by Institut Pasteur - CeRIS (157.99.25.33) on June 27, 2019. The FASEB Journal Vol. ${article.issue.getVolume()}, No. ${article.issue.getIssueNumber()}, p

beside molecular confinement, refolding is critically dependent on the presence of calcium and toxin acylation (41, 47). However, we succeeded to refold pro-CyaA into a monomeric protein by optimizing the procedure, essentially by decreasing the initial protein concentration, although the recovery yield was low compared with that of acylated CyaA (see Supplemental Fig. S2 and Materials and Methods for details).

The biologic activities of the refolded pro-CyaA and CyaA species were assessed on sheep erythrocytes by monitoring hemolytic activity and the ability of the toxins to invade cells (Supplemental Table S1). As expected, the monomeric CyaA species induced hemolysis and was able to bind to erythrocytes and translocate into the cytosol in a calcium-dependent manner, in agreement with prior studies (25, 47, 52, 53). In contrast, the multimeric CyaA species exhibited strongly reduced hemolytic activity and was not able to translocate into erythrocytes, whereas the pro-CyaA species were totally lacking hemolytic and cell-invasion capacities (Supplemental Table S1), which is in agreement with previous studies (55, 57). This confirms that the monomeric, acylated CyaA is the physiologic competent state of the toxin that is able to invade eukaryotic target cells.

Compactness and solvent-exposed HRs in CyaA and pro-CyaA

We then characterized the biophysical and hydrodynamic properties of pro-CyaA and CyaA. We first determined the compactness and stability of both proteins using macroscopic approaches and then characterized the proteins at medium resolution by HDX-MS. The solvent-exposed hydrophobic surfaces of pro-CyaA and CyaA monomers were probed using ANS fluorescence (58) in buffer A, complemented with 2 mM $CaCl_2$. Though a slight increase in ANS fluorescence intensity was observed in the presence of CyaA monomers, a marked increase (~3-fold) was found with the pro-CyaA monomers, suggesting that these latter expose more HRs to the solvent than the former (**Fig. 2*A***). In other words, the HRs in CyaA monomers are less accessible to ANS than those in the pro-CyaA species, suggesting that acylation favors the shielding of HRs within the protein. We then investigated the compaction state of CyaA and pro-CyaA by sedimentation velocity analysis using analytical ultracentrifugation (AUC). Both species remain essentially monomeric, with only a few aggregates observed on the time scale of the experiment (Fig. 2*B*). The analysis provided a sedimentation coefficient of 7.4 and 7.1 S, respectively, for CyaA and pro-CyaA monomers (Fig. 2*B* and Supplemental Table S2), suggesting that pro-CyaA monomers are slightly less compact than CyaA monomers. We further compared the stability of pro-CyaA and CyaA monomers by following their urea-induced unfolding by intrinsic tryptophan fluorescence. The denaturation data also indicate that CyaA is more stable than pro-CyaA at urea concentrations above 2 M (Fig. 2*C*) as highlighted by the plot of the maximum wavelength differences between the 2 proteins (Fig. 2*D*). Taken together, these results indicate that pro-CyaA monomers expose more HRs to the solvent (Fig. 2*A*) and are less compact (Fig. 2*B*) and stable (Fig. 2*C, D*) than CyaA monomers.

HDX-MS analysis of the pro-CyaA and CyaA refolding process

To further characterize the refolding process of pro-CyaA and CyaA, we used HDX-MS to probe the structure and dynamics of both full-length proteins equilibrated in 6, 3, or 1.6 M urea as well as the monomeric species in the complete absence of denaturant. **Figure 3** displays a global view of the relative deuterium fractional uptake of CyaA equilibrated in 6, 3, or 1.6 M urea in the presence of 2 mM $CaCl_2$. The relative fractional exchanges of 3 independent replicates were calculated for each peptide at each time point and plotted as a function of peptide position (CyaA peptide maps are shown in Supplemental Figs. S3 and S4). In 6 M urea (Fig. 3*B*), the protein is totally devoid of dynamic HDX-MS events, confirming that CyaA is completely denatured. In 3 M urea (Fig. 3*C*), a short segment of HR (658–719 in HR) and a large part of RD (from Block II to the C-terminal extremity of CyaA) exhibit dynamic HDX-MS behavior, whereas in 1.6 M urea (Fig. 3*D*), part of the catalytic domain (the T25 region of AC), AR, and most of HR also have dynamic HDX-MS activity. These results suggest that these regions of CyaA sequentially acquire structural elements upon progressive urea removal. This sequential folding of CyaA is further highlighted in Supplemental Fig. S5. To identify the contributions of calcium on CyaA refolding, similar HDX-MS experiments were repeated in the absence of calcium (Supplemental Fig. S6). In these conditions, the entire CyaA polypeptide remains solvent accessible and unfolded at all urea concentrations, even down to 1.6 M. The uptake difference plots between CyaA samples in the presence of calcium or EDTA at various urea concentrations are compared in **Fig. 4** (and Supplemental Figs. S7–S9 for a detailed presentation of the HDX-MS data). These HDX-MS results show that the presence of calcium is critical for the acquisition of structural elements in CyaA at 3 and 1.6 M urea. This further indicates that calcium binding to the RTX motifs is critical not only to induce folding of the C-terminal RD domain (see the effect of calcium *vs.* EDTA at 3 M urea in Fig. 4*C*) but also for the structuration of all of the upstream N-terminal domains of CyaA (see the effect of calcium *vs.* EDTA at 1.6 M urea in Fig. 4*D*).

Similar HDX-MS experiments were also performed on pro-CyaA (Supplemental Fig. S10) and revealed a comparable sequential refolding process, with RD acquiring structures at intermediate urea concentrations (3 M), followed by the refolding of AC and HR regions at lower urea concentrations (1.6 M) (Supplemental Figs. S10 and S11). As in CyaA, several regions of pro-CyaA display non-dynamic HDX-MS throughout, indicating that these regions remain largely unstructured, even at low urea concentrations. These include a large stretch of amino acids from the C-terminal end of the catalytic domain (T18 fragment), across the TR, and through the N-terminal part of HR (*i.e.*, from residues 345 to 570). Similarly, residues

om www.fasebj.org by Institut Pasteur - CeRIS (157.99.25.33) on June 27, 2019. The FASEB Journal Vol. ${article.issue.getVolume()}, No. ${article.issue.getIssueNumber()}, p

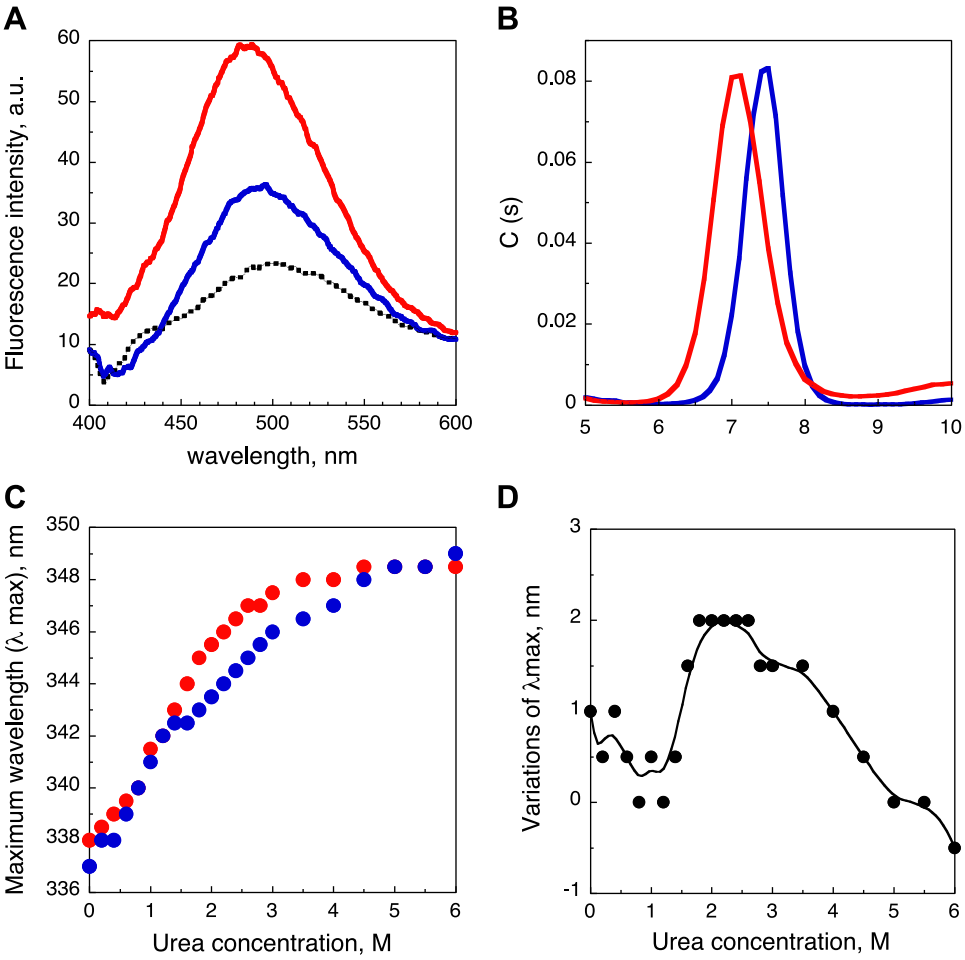

Figure 2. Macroscopic characterization of CyaA and pro-CyaA monomeric species. *A*) The emission fluorescence spectra of ANS in the absence (black) and in the presence of CyaA (blue) and pro-CyaA (red) monomers. *B*) The distribution of sedimentation coefficients c(s) of CyaA (blue) and pro-CyaA (red) monomers measured by AUC. The AUC data are presented in Supplemental Table S2. *C*) The urea-induced unfolding of CyaA (blue) and pro-CyaA (red) monomers followed by tryptophan fluorescence (SD ± 1 nm). *D*) The variation of maximum wavelength emission (λmax) between CyaA and pro-CyaA is highlighted. Buffer: buffer A, complemented with 2 mM $CaCl_2$. These experiments were performed in triplicate.

821 through 981 of the AR domain show nondynamic HDX-MS behavior throughout. However, significant differences do exist between the acylated and nonacylated proteins, as illustrated in **Fig. 5**, which shows the difference in deuterium uptake between pro-CyaA and CyaA at both 3 and 1.6 M urea. In 3 M urea (Fig. 5*B*), the differences are confined to a segment of the HR between amino acids 658 and 719. In 1.6 M urea (Fig. 5*C*), further minor structural disparities between pro-CyaA and CyaA are evidenced, extending upstream from the HR to the TR region, through to the N-terminal part of AC, and, conversely, downstream to the AR region. It therefore seems that the acyl chains at K860 and K983 of CyaA are critically involved in the folding of the segment encompassing residues 658–719 (Fig. 5*B*, *C*). We propose that the hydrophobic effects between the acyl chains and HR restrict the conformational landscape of CyaA, thus favoring a faster refolding toward the folded state compared with pro-CyaA. The present data suggest that the segment covering residues circa 660–710 of the HR can act as a hydrophobic folding nucleus, even in the presence of 3 M urea if K860 and K983 are acylated (Figs. 3 and 5*C*). In pro-CyaA, this hydrophobic collapse occurs at lower urea concentrations because of the lack of acyl chains (Supplemental Fig. S11), and consequently, the partially folded HRs may remain exposed to the solvent, thereby favoring the aggregation of pro-CyaA into multimeric species.

The relative fractional uptake maps of monomeric pro-CyaA and CyaA species (both in the absence of urea) are displayed in **Fig. 6**. Extensive dynamic HDX-MS activity, indicative of secondary structural elements, is observed throughout both proteins. Yet, segments that connect individual subdomains, such as at the boundary of the AC/TR, HR/AR, and AR/RD domains, appear to be more accessible than the adjacent domains. Equivalent HDX-MS patterns are observed between several domains of pro-CyaA and CyaA monomers as illustrated in the uptake difference plot (Fig. 6*D*), particularly the N-terminal parts of both AC and TR, and the blocks III–V of RD. These data suggest that the folding of these regions is not affected by CyaA acylation. The C-terminal part of TR (circa 454–520) and the N-terminal part of RD (mainly blocks I and II) are weakly but significantly stabilized by the presence of the acyl chains (Fig. 6*D*).

The strongest differences in HDX-MS activity between the 2 forms of CyaA are found in the HRs and ARs (Fig. 6*D*, *E*). First, peptides from the AR region (*i.e.*, residues between amino acids 798 and 958) appear to be more solvent accessible in pro-CyaA monomer than in the monomeric CyaA toxin (Fig. 6*B*, *C*, respectively). Second, significant changes in HDX-MS patterns are observed in the HR of CyaA, most notably at peptides 539–546, 571–582, 615–622, 658–672, 682–696, and 686–696 (highlighted in Figs. 6*D*, *E* and Supplemental Fig. S12), corresponding to

om www.fasebj.org by Institut Pasteur - CeRIS (157.99.25.33) on June 27, 2019. The FASEB Journal Vol. ${article.issue.getVolume()}, No. ${article.issue.getIssueNumber()},

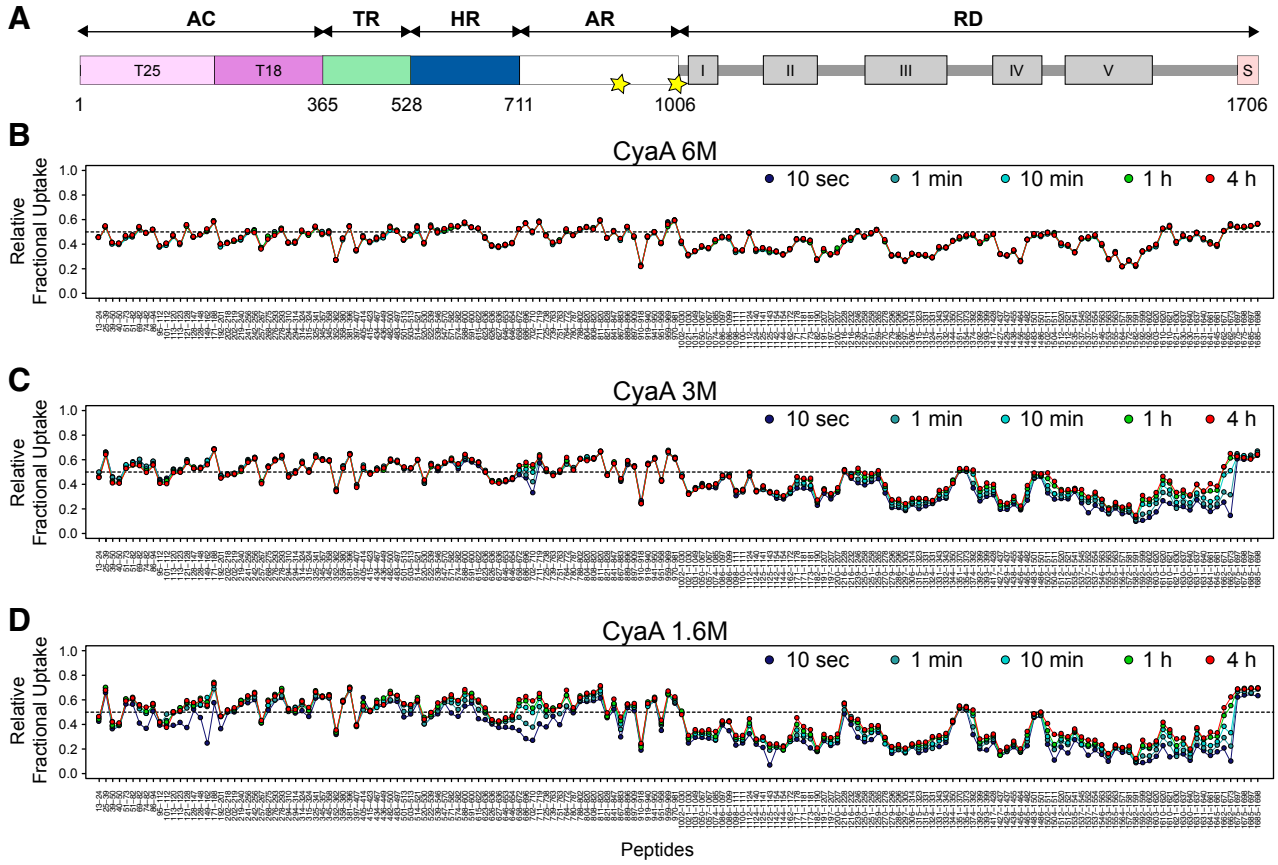

Figure 3. HDX-MS analysis of CyaA refolding. *A*) The structural organization of each domain is displayed. *B–D)* Fits to the peptide maps; the 5 blocks of RD are sized to fit to the peptide maps shown. The HDX-MS behavior of CyaA in various concentrations of urea and in the presence of 2 mM calcium is displayed. At 6 M urea (*B*), no dynamic HDX-MS behavior is observed throughout the protein. At 3 M urea (*C*), only RD and a small section of HR display dynamic activity. At 1.6 M urea (*D*), the AC, HR, and RD domains exhibit dynamic HDX-MS events. Each dot corresponds to the average value of 3 independent replicates.

the 4 hydrophobic segments of HR (Supplemental Figs. S12 and S13). Interestingly, a significant difference in HDX-MS activity is observed in all experimental conditions between pro-CyaA and CyaA for the hydrophobic segment between amino acids 660 and 710 (Figs. 5*B*, *C* and 6 and Supplemental Fig. S13). This confirms that these hydrophobic segments may indeed play an essential role in the folding process of the acylated toxin, from the initial structural elements observed at 3 M urea (Figs. 3 and 5) to the native state of the monomeric CyaA (Fig. 6). The HDX-MS data provide direct evidence that CyaA acylation favors a hydrophobic collapse of these regions that may constitute the apolar core of the protein structure.

DISCUSSION

Acylation is a requisite PTM for the cytotoxicity of RTX toxins, but the precise contribution of acyl chains to the structure and function of these cytolysins still remains largely unknown. We previously suggested that acylation may play a crucial role in the refolding of the *B. pertussis* CyaA, a prominent member of the RTX toxin family, into a monomeric and functional species (41, 47). To gain further insights into the effect of CyaA acylation, we directly compared the biophysical and functional properties of the monomeric acylated and nonacylated forms (CyaA and pro-CyaA, respectively) of this toxin.

MS analysis indicates that CyaA produced in *E. coli* in the presence of the CyaC acyltransferase is mainly modified by C16 acyl chains on K860 and K983, and, as expected, pro-CyaA is not. AUC experiments demonstrate that CyaA monomers are more compact than their pro-CyaA counterparts, whereas ANS binding studies show that HRs are less solvent-exposed in CyaA than in pro-CyaA. This indicates that the presence of acyl chains in CyaA may favor a more compact structural state. Furthermore, urea-induced unfolding experiments suggest that the acylated toxin is more stable than pro-CyaA. Together, our AUC and fluorescence data show that several hydrophobic segments may be more solvent-exposed in pro-CyaA than CyaA, leading to a less compact and stable protein.

We exploited HDX-MS to unravel the folding process of both pro-CyaA and CyaA by analyzing their structural dynamics at different urea concentrations. These studies lead to 2 important conclusions. First, we show that in both forms of the protein (*i.e.*, independently of the acylation-status), the C-terminal RTX-containing domain RD is the first region to acquire structure when the refolding is carried out in the presence of calcium (Figs. 3

om www.fasebj.org by Institut Pasteur - CeRIS (157.99.25.33) on June 27, 2019. The FASEB Journal Vol. ${article.issue.getVolume()}, No. ${article.issue.getIssueNumber()}, p

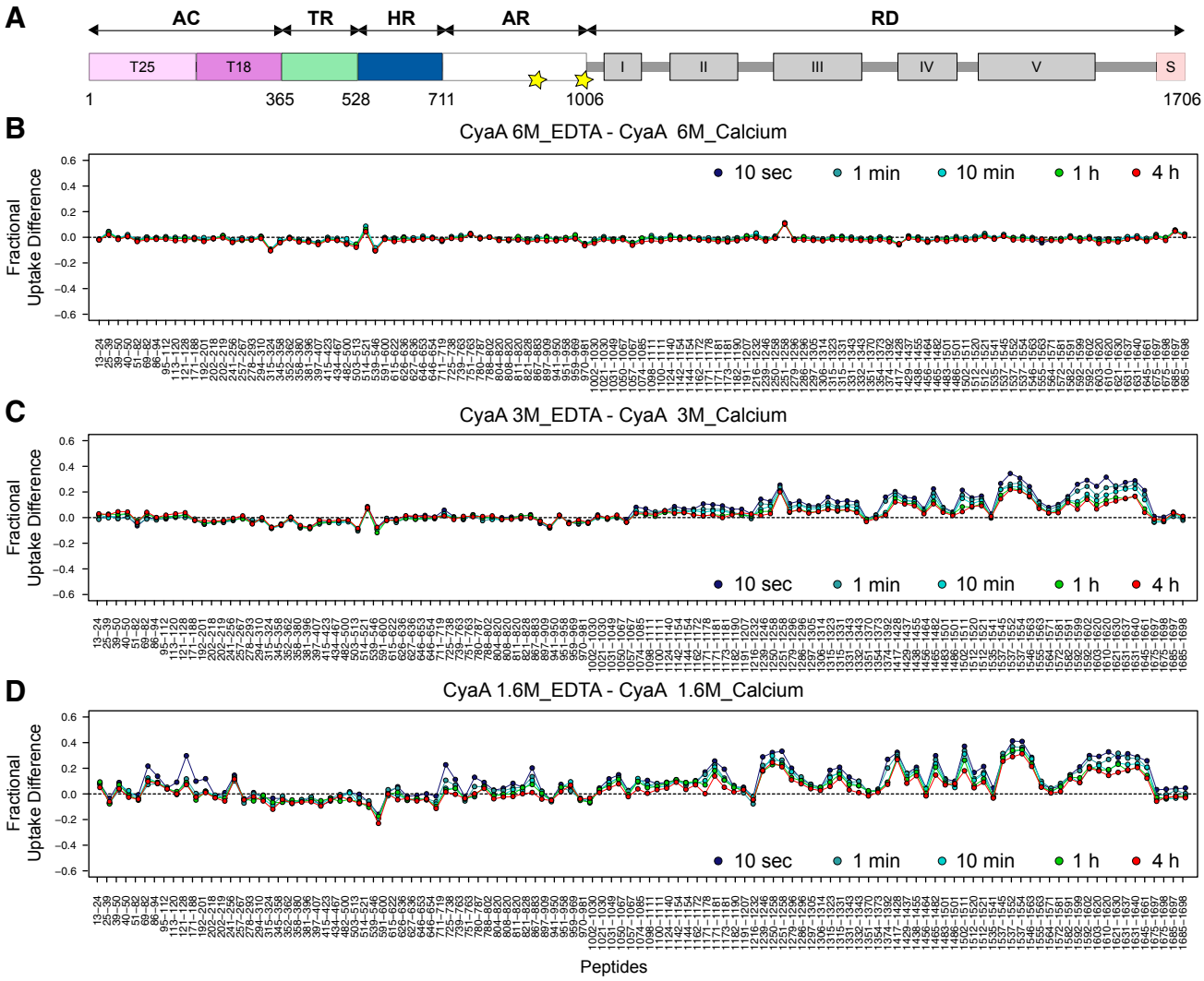

Figure 4. Deuterium uptake differences of CyaA in urea in the presence and absence of calcium. *A*) The structural organization of each domain is displayed. *B–D*) Fits to the peptide maps are shown. The fractional uptake difference plots were calculated at each urea concentration by subtracting the uptake measured in the absence (2 mM EDTA) and the presence of calcium (2 mM $CaCl_2$) for each peptide and at each time point. *C*, *D*) At 6 M urea, no difference of HDX-MS behavior is observed throughout the protein. At 3 M urea (*C*), only RD displays significant positive difference of deuterium uptake, indicative of a calcium-induced reduction of solvent accessibility (*i.e.*, protein folding in the presence of calcium). At 1.6 M urea (*D*), the AC, AR, and RD domains show a positive difference of deuterium uptake, indicating that the presence of calcium induces the folding of these domains. Each dot corresponds to the average value of 3 independent replicates.

and 4 and Supplemental Figs. S5–S11). More importantly, we found that in the absence of calcium, the entire protein remains essentially unstructured even after lowering urea concentrations down to 1.6 M urea, as indicated by the absence of any significant solvent protection across the entire CyaA polypeptide chain (Fig. 4*D* and Supplemental Figs. S6–S9). In marked contrast, in the presence of calcium, most CyaA domains do contain structural elements at 1.6 M urea and in the absence of urea, as evidenced by HDX-MS (Figs. 3*D*, 4*D*, and 6*C* and Supplemental Figs. S5*A* and S9). Our previous studies already established that RD (residues 1006–1706) is intrinsically disordered in the calcium-free apo-state and folded in the calcium-bound holo-state (4, 31–39, 41, 42, 59). A likely scenario is that in the absence of calcium, the intrinsically disordered nature of RD within the full-length protein may result in a huge entropic penalty that prevents folding of the other CyaA domains. This data has direct implications for CyaA secretion. We previously suggested that in the low calcium environment of the bacterial cytosol, RD adopts disordered conformations favorable for transport through the type 1 secretion machinery and folds upon binding calcium in the extracellular, calcium-rich environment (4, 32, 34, 39, 41, 42). Our present data now extend this model to the full-length CyaA toxin. Indeed, our HDX-MS results clearly indicate that in the low calcium environment of the bacterial cytoplasm, it is not only the RD domain but the CyaA polypeptide chain as a whole that preferentially adopts unstructured conformations that foster protein secretion through the type 1 secretion channel. Upon secretion, as the protein reaches the calcium-rich extracellular medium, RD binds calcium, folds, and may then act as a scaffold for the refolding of the upstream domains of CyaA that are

om www.fasebj.org by Institut Pasteur - CeRIS (157.99.25.33) on June 27, 2019. The FASEB Journal Vol. ${article.issue.getVolume()}, No. ${article.issue.getIssueNumber()}, p

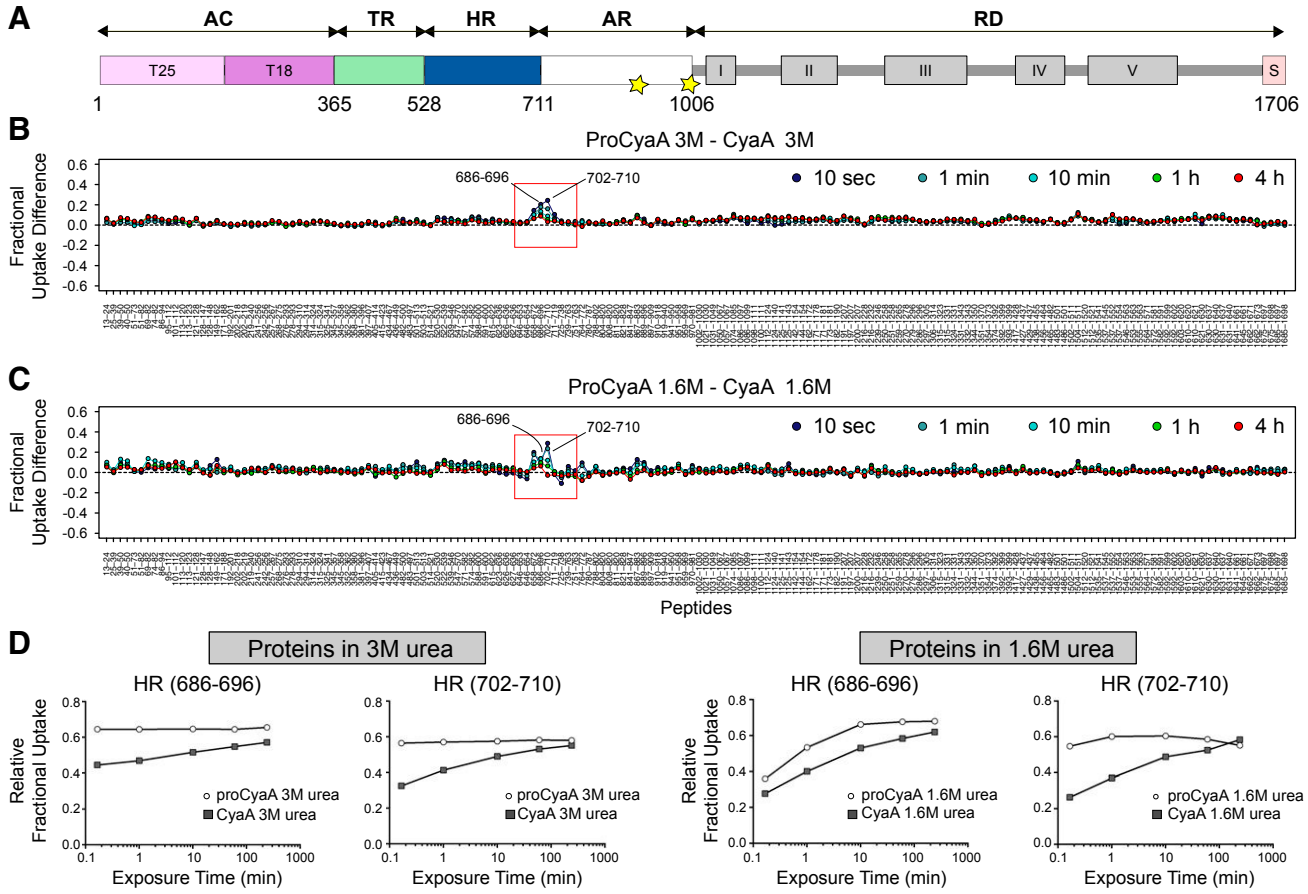

Figure 5. Unique differences in HDX-MS behavior between pro-CyaA and CyaA in the presence of calcium at 3 and 1.6 M urea. *A*) The structural organization of each domain is displayed and fits to the peptide maps. *B*, *C*) Peptide maps and the uptake difference plot between pro-CyaA and CyaA proteins at 3 and 1.6 M urea concentrations, respectively. Only a difference in HR was observed (highlighted in red boxes). Each dot corresponds to the average value of 3 independent replicates. *D*) Peptides from HR with the greatest deuterium uptake differences between the 2 proteins. Errors bars (SD) are within the size of the dots.

progressively exiting the T1SS machinery in a C- to N-terminal vectorial secretion process (39–41).

The second major finding of this study is that acylation plays a critical role in the folding of CyaA into a functional cytotoxic state. HDX-MS revealed dramatic differences in deuterium uptake between CyaA and pro-CyaA, mainly located in the hydrophobic and ARs (Figs. 5 and 6 and Supplemental Figs. S5, S11, and S12). More specifically, we identified a segment (circa residues 660–710) within the HR and distal from the acylation sites, which appears to play a central role in toxin refolding (Fig. 5*B*, *C*). We propose that in CyaA, this region may directly interact and collapse with the distant acyl chains in a process driven by hydrophobic effects. The formation of these structural elements may orient the initial CyaA folding pathway and favor toxin refolding into the monomeric state. In contrast, pro-CyaA may have to explore a broader conformational landscape because of the absence of the initial hydrophobic collapse between residues 660–710 and the acyl chains. Thus, from a kinetic point of view, the acyl chains may favor a faster folding of CyaA compared with pro-CyaA. This could also explain the higher propensity of pro-CyaA to aggregate and, consequently, the lower yield of pro-CyaA monomers compared with CyaA during the refolding process (Supplemental Fig. S2).

We propose the following calcium- and acylation-dependent refolding scheme for CyaA: as CyaA exits from the T1SS, calcium binding triggers refolding of the C-terminal RD. As previously proposed, the calcium-loaded, folded RD might act as a scaffold for the folding of other CyaA domains (*i.e.*, AR and HR) (Figs. 3 and 4 and Supplemental Figs. S7–S9). The acyl chains attached to K860 and K983 foster a hydrophobic collapse within the apolar segment spanning residues 660–710 (Fig. 5 and Supplemental Fig. S13), which acts as a nucleus for the folding into the native state (Fig. 6*D*) of both HR (residues 528–710) and AR (711–1005). Finally, TR and AC are secreted, and, interestingly, their folding appears minimally affected by the acylation status. This is in agreement with the fact that the isolated AC and AC-TR polypeptides can autonomously fold in solution (15, 16, 24). Taken together, the calcium-induced folding, coupled with hydrophobic effects between distal regions containing apolar segments and acyl chains, is likely shared with other multidomain proteins. This is probably the case of other

om www.fasebj.org by Institut Pasteur - CeRIS (157.99.25.33) on June 27, 2019. The FASEB Journal Vol. ${article.issue.getVolume()}, No. ${article.issue.getIssueNumber()}, p

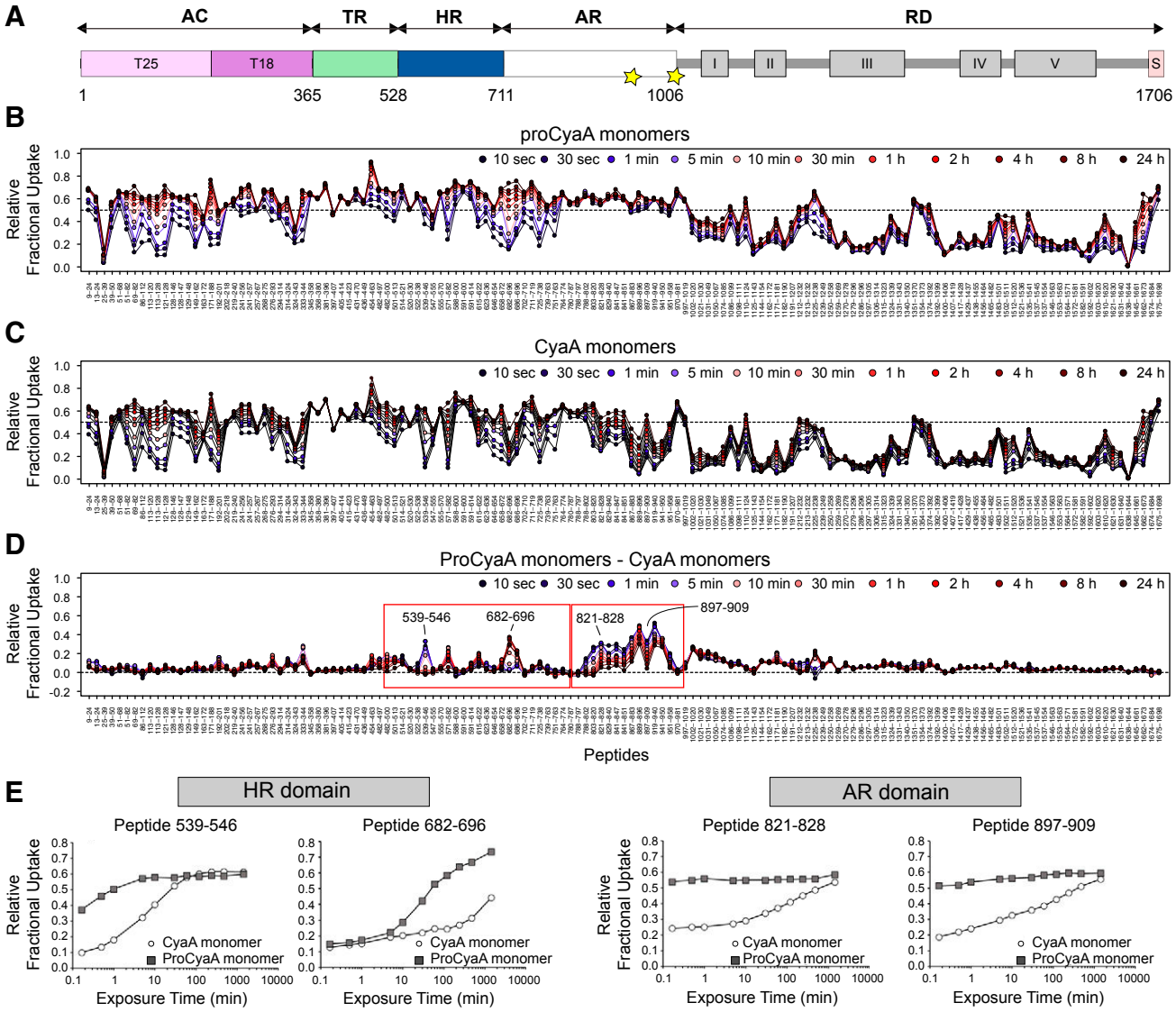

Figure 6. HDX-MS analysis of monomeric pro-CyaA and CyaA species in solution. *A*) The structural organization of each domain is displayed. *B–D*) Fits to the peptide maps are shown. The HDX-MS behaviors of full-length pro-CyaA and CyaA monomers measured in the presence of 2 mM calcium are given (*B*, *C*). Dynamic HDX-MS is observed throughout both proteins and over the time course of the reaction. *D*) The uptake difference plot between both pro-CyaA and CyaA monomers. Large differences in HDX-MS activity between the 2 proteins were observed in HR and AR (red boxes). Smaller changes were found in T18, TR, and blocks I and II of RD. Each dot corresponds to the average value of 3 independent replicates. *E*) Selected peptides from HR and AR. Errors bars (SD) are within the size of the dots.

large RTX cytolysins like CyaA, which are secreted in an unfolded state and refold in the host environment to exert their virulence (3, 4). FJ

ACKNOWLEDGMENTS

The authors thank Bertrand Raynal and Sébastien Brulé from the Plate-forme de Biophysique Moléculaire (PFBMI) for excellent technical expertise with analytical ultracentrifugation. The authors thank the CACSICE Equipex ANR-11-EQPX-0008. D.P.O'B. was supported by PasteurInnov2015-197 and PTR451 grants. S.E.C. was supported by a stipend from the Pasteur–Paris University (PPU) International PhD Program. A.V. was supported by a DIM MalInf (infectious diseases) grant from Conseil Régional Ile-de-France. Running costs were supported by Institut Pasteur, PasteurInnov (PIV15-197), PTR grant (PTR451), CNRS, and Fondation Recherche Médicale (FRM DBS20140930771). The authors declare no conflicts of interest.

AUTHOR CONTRIBUTIONS

A. Chenal designed the project; D. P. O'Brien, T. Douché, M. Matondo, S. Brier, and A. Chenal designed the experiments; D. P. O'Brien, S. E. Cannella, A. Voegele, M. Davi, T. Douché, S. Brier, and A. Chenal performed the experiments; D. P. O'Brien, S. E. Cannella, T. Douché, M. Matondo, S. Brier, D. Ladant, and A. Chenal analyzed the data; D. P. O'Brien, S. E. Cannella, S. Brier, D. Ladant, and A. Chenal wrote the manuscript; and all authors discussed the results and commented on the manuscript.

om www.fasebj.org by Institut Pasteur - CeRIS (157.99.25.33) on June 27, 2019. The FASEB Journal Vol. ${article.issue.getVolume()}, No. ${article.issue.getIssueNumber()}, p

REFERENCES

1. Siman, P., and Brik, A. (2012) Chemical and semisynthesis of posttranslationally modified proteins. *Org. Biomol. Chem.* **10**, 5684–5697
2. Ryšlavá, H., Doubnerová, V., Kavan, D., and Vaněk, O. (2013) Effect of posttranslational modifications on enzyme function and assembly. *J. Proteomics* **92**, 80–109
3. Linhartová, I., Bumba, L., Mašín, J., Basler, M., Osička, R., Kamanová, J., Procházková, K., Adkins, I., Hejnová-Holubová, J., Sadílková, L., Morová, J., and Sebo, P. (2010) RTX proteins: a highly diverse family secreted by a common mechanism. *FEMS Microbiol. Rev.* **34**, 1076–1112
4. Chenal, A., Sotomayor Perez, A. C., and Ladant, D. (2015) Structure and function of RTX toxins. In *The Comprehensive Sourcebook of Bacterial Protein Toxins*, 4th ed., Elsevier, Amsterdam, The Netherlands
5. Issartel, J. P., Koronakis, V., and Hughes, C. (1991) Activation of Escherichia coli prohaemolysin to the mature toxin by acyl carrier protein-dependent fatty acylation. *Nature* **351**, 759–761
6. Welch, R. A. (1991) Pore-forming cytolysins of gram-negative bacteria. *Mol. Microbiol.* **5**, 521–528
7. Hackett, M., Guo, L., Shabanowitz, J., Hunt, D. F., and Hewlett, E. L. (1994) Internal lysine palmitoylation in adenylate cyclase toxin from Bordetella pertussis. *Science* **266**, 433–435
8. Basar, T., Havlícek, V., Bezousková, S., Hackett, M., and Sebo, P. (2001) Acylation of lysine 983 is sufficient for toxin activity of Bordetella pertussis adenylate cyclase. Substitutions of alanine 140 modulate acylation site selectivity of the toxin acyltransferase CyaC. *J. Biol. Chem.* **276**, 348–354
9. Greene, N. P., Crow, A., Hughes, C., and Koronakis, V. (2015) Structure of a bacterial toxin-activating acyltransferase. *Proc. Natl. Acad. Sci. USA* **112**, E3058–E3066
10. Fedele, G., Schiavoni, I., Adkins, I., Klimova, N., and Sebo, P. (2017) Invasion of dendritic cells, macrophages and neutrophils by the bordetella adenylate cyclase toxin: a subversive move to fool host immunity. *Toxins (Basel)* **9**, E293
11. Benz, R. (2016) Channel formation by RTX-toxins of pathogenic bacteria: basis of their biological activity. *Biochim. Biophys. Acta* **1858**, 526–537
12. Ladant, D., and Ullmann, A. (1999) Bordatella pertussis adenylate cyclase: a toxin with multiple talents. *Trends Microbiol.* **7**, 172–176
13. Vojtova, J., Kamanova, J., and Sebo, P. (2006) Bordetella adenylate cyclase toxin: a swift saboteur of host defense. *Curr. Opin. Microbiol.* **9**, 69–75
14. Guiso, N. (2017) Bordetella adenylate cyclase-hemolysin toxins. *Toxins (Basel)* **9**, E277
15. Karst, J. C., Sotomayor Pérez, A. C., Guijarro, J. I., Raynal, B., Chenal, A., and Ladant, D. (2010) Calmodulin-induced conformational and hydrodynamic changes in the catalytic domain of Bordetella pertussis adenylate cyclase toxin. *Biochemistry* **49**, 318–328
16. O'Brien, D. P., Durand, D., Voegele, A., Hourdel, V., Davi, M., Chamot-Rooke, J., Vachette, P., Brier, S., Ladant, D., and Chenal, A. (2017) Calmodulin fishing with a structurally disordered bait triggers CyaA catalysis. *PLoS Biol.* **15**, e2004486
17. Carbonetti, N. H. (2010) Pertussis toxin and adenylate cyclase toxin: key virulence factors of Bordetella pertussis and cell biology tools. *Future Microbiol.* **5**, 455–469
18. Chenal, A., and Ladant, D. (2018) Bioengineering of *Bordetella pertussis* adenylate cyclase toxin for antigen-delivery and immunotherapy. *Toxins (Basel)* **10**, E302
19. Glaser, P., Sakamoto, H., Bellalou, J., Ullmann, A., and Danchin, A. (1988) Secretion of cyclolysin, the calmodulin-sensitive adenylate cyclase-haemolysin bifunctional protein of Bordetella pertussis. *EMBO J.* **7**, 3997–4004
20. Bellalou, J., Sakamoto, H., Ladant, D., Geoffroy, C., and Ullmann, A. (1990) Deletions affecting hemolytic and toxin activities of Bordetella pertussis adenylate cyclase. *Infect. Immun.* **58**, 3242–3247
21. Bellalou, J., Ladant, D., and Sakamoto, H. (1990) Synthesis and secretion of Bordetella pertussis adenylate cyclase as a 200-kilodalton protein. *Infect. Immun.* **58**, 1195–1200
22. Sakamoto, H., Bellalou, J., Sebo, P., and Ladant, D. (1992) Bordetella pertussis adenylate cyclase toxin. Structural and functional independence of the catalytic and hemolytic activities. *J. Biol. Chem.* **267**, 13598–13602
23. Martín, C., Requero, M. A., Masin, J., Konopasek, I., Goñi, F. M., Sebo, P., and Ostolaza, H. (2004) Membrane restructuring by Bordetella pertussis adenylate cyclase toxin, a member of the RTX toxin family. *J. Bacteriol.* **186**, 3760–3765
24. Karst, J. C., Barker, R., Devi, U., Swann, M. J., Davi, M., Roser, S. J., Ladant, D., and Chenal, A. (2012) Identification of a region that assists membrane insertion and translocation of the catalytic domain of Bordetella pertussis CyaA toxin. *J. Biol. Chem.* **287**, 9200–9212
25. Masin, J., Osickova, A., Sukova, A., Fiser, R., Halada, P., Bumba, L., Linhartova, I., Osicka, R., and Sebo, P. (2016) Negatively charged residues of the segment linking the enzyme and cytolysin moieties restrict the membrane-permeabilizing capacity of adenylate cyclase toxin. *Sci. Rep.* **6**, 29137
26. Subrini, O., Sotomayor-Pérez, A. C., Hessel, A., Spiaczka-Karst, J., Selwa, E., Sapay, N., Veneziano, R., Pansieri, J., Chopineau, J., Ladant, D., and Chenal, A. (2013) Characterization of a membrane-active peptide from the Bordetella pertussis CyaA toxin. *J. Biol. Chem.* **288**, 32585–32598
27. Voegele, A., Subrini, O., Sapay, N., Ladant, D., and Chenal, A. (2017) Membrane-active properties of an amphitropic peptide from the CyaA toxin translocation region. *Toxins (Basel)* **9**, E369
28. Barry, E. M., Weiss, A. A., Ehrmann, I. E., Gray, M. C., Hewlett, E. L., and Goodwin, M. S. (1991) Bordetella pertussis adenylate cyclase toxin and hemolytic activities require a second gene, cyaC, for activation. *J. Bacteriol.* **173**, 720–726
29. Masin, J., Basler, M., Knapp, O., El-Azami-El-Idrissi, M., Maier, E., Konopasek, I., Benz, R., Leclerc, C., and Sebo, P. (2005) Acylation of lysine 860 allows tight binding and cytotoxicity of Bordetella adenylate cyclase on CD11b-expressing cells. *Biochemistry* **44**, 12759–12766
30. Bouchez, V., Douché, T., Dazas, M., Delaplane, S., Matondo, M., Chamot-Rooke, J., and Guiso, N. (2017) Characterization of post-translational modifications and cytotoxic properties of the adenylate-cyclase hemolysin produced by various bordetella pertussis and bordetella parapertussis isolates. *Toxins (Basel)* **9**, E304
31. Bauche, C., Chenal, A., Knapp, O., Bodenreider, C., Benz, R., Chaffotte, A., and Ladant, D. (2006) Structural and functional characterization of an essential RTX subdomain of Bordetella pertussis adenylate cyclase toxin. *J. Biol. Chem.* **281**, 16914–16926
32. Chenal, A., Guijarro, J. I., Raynal, B., Delepierre, M., and Ladant, D. (2009) RTX calcium binding motifs are intrinsically disordered in the absence of calcium: implication for protein secretion. *J. Biol. Chem.* **284**, 1781–1789
33. Sotomayor Pérez, A. C., Karst, J. C., Davi, M., Guijarro, J. I., Ladant, D., and Chenal, A. (2010) Characterization of the regions involved in the calcium-induced folding of the intrinsically disordered RTX motifs from the bordetella pertussis adenylate cyclase toxin. *J. Mol. Biol.* **397**, 534–549
34. Chenal, A., Karst, J. C., Sotomayor Pérez, A. C., Wozniak, A. K., Baron, B., England, P., and Ladant, D. (2010) Calcium-induced folding and stabilization of the intrinsically disordered RTX domain of the CyaA toxin. *Biophys. J.* **99**, 3744–3753
35. Sotomayor-Pérez, A. C., Ladant, D., and Chenal, A. (2011) Calcium-induced folding of intrinsically disordered repeat-in-toxin (RTX) motifs via changes of protein charges and oligomerization states. *J. Biol. Chem.* **286**, 16997–17004
36. Sotomayor-Pérez, A. C., Karst, J. C., Ladant, D., and Chenal, A. (2012) Mean net charge of intrinsically disordered proteins: experimental determination of protein valence by electrophoretic mobility measurements. *Methods Mol. Biol.* **896**, 331–349
37. Sotomayor-Pérez, A. C., Subrini, O., Hessel, A., Ladant, D., and Chenal, A. (2013) Molecular crowding stabilizes both the intrinsically disordered calcium-free state and the folded calcium-bound state of a repeat in toxin (RTX) protein. *J. Am. Chem. Soc.* **135**, 11929–11934
38. Sotomayor-Pérez, A. C., Ladant, D., and Chenal, A. (2014) Disorder-to-order transition in the CyaA toxin RTX domain: implications for toxin secretion. *Toxins (Basel)* **7**, 1–20
39. O'Brien, D. P., Hernandez, B., Durand, D., Hourdel, V., Sotomayor-Pérez, A. C., Vachette, P., Ghomi, M., Chamot-Rooke, J., Ladant, D., Brier, S., and Chenal, A. (2015) Structural models of intrinsically disordered and calcium-bound folded states of a protein adapted for secretion. *Sci. Rep.* **5**, 14223
40. Bumba, L., Masin, J., Macek, P., Wald, T., Motlova, L., Bibova, I., Klimova, N., Bednarova, L., Veverka, V., Kachala, M., Svergun, D. I., Barinka, C., and Sebo, P. (2016) Calcium-driven folding of RTX domain β-rolls ratchets translocation of RTX proteins through type I secretion ducts. *Mol. Cell* **62**, 47–62
41. Cannella, S. E., Ntsogo Enguéné, V. Y., Davi, M., Malosse, C., Sotomayor Pérez, A. C., Chamot-Rooke, J., Vachette, P., Durand, D., Ladant, D., and Chenal, A. (2017) Stability, structural and functional

om www.fasebj.org by Institut Pasteur - CeRIS (157.99.25.33) on June 27, 2019. The FASEB Journal Vol. ${article.issue.getVolume()}, No. ${article.issue.getIssueNumber()}, p

properties of a monomeric, calcium-loaded adenylate cyclase toxin, CyaA, from Bordetella pertussis. *Sci. Rep.* **7**, 42065
42. O'Brien, D. P., Perez, A. C. S., Karst, J., Cannella, S. E., Enguéné, V. Y. N., Hessel, A., Raoux-Barbot, D., Voegele, A., Subrini, O., Davi, M., Guijarro, J. I., Raynal, B., Baron, B., England, P., Hernandez, B., Ghomi, M., Hourdel, V., Malosse, C., Chamot-Rooke, J., Vachette, P., Durand, D., Brier, S., Ladant, D., and Chenal, A. (2018) Calcium-dependent disorder-to-order transitions are central to the secretion and folding of the CyaA toxin of Bordetella pertussis, the causative agent of whooping cough. *Toxicon* **149**, 37–44
43. Rose, T., Sebo, P., Bellalou, J., and Ladant, D. (1995) Interaction of calcium with Bordetella pertussis adenylate cyclase toxin. Characterization of multiple calcium-binding sites and calcium-induced conformational changes. *J. Biol. Chem.* **270**, 26370–26376
44. Welch, R. A. (2001) RTX toxin structure and function: a story of numerous anomalies and few analogies in toxin biology. *Curr. Top. Microbiol. Immunol.* **257**, 85–111
45. Veneziano, R., Rossi, C., Chenal, A., Devoisselle, J. M., Ladant, D., and Chopineau, J. (2013) Bordetella pertussis adenylate cyclase toxin translocation across a tethered lipid bilayer. *Proc. Natl. Acad. Sci. USA* **110**, 20473–20478
46. Novak, J., Cerny, O., Osickova, A., Linhartova, I., Masin, J., Bumba, L., Sebo, P., and Osicka, R. (2017) Structure-function relationships underlying the capacity of bordetella adenylate cyclase toxin to disarm host phagocytes. *Toxins (Basel)* **9**, E300
47. Karst, J. C., Ntsogo Enguéné, V. Y., Cannella, S. E., Subrini, O., Hessel, A., Debard, S., Ladant, D., and Chenal, A. (2014) Calcium, acylation, and molecular confinement favor folding of Bordetella pertussis adenylate cyclase CyaA toxin into a monomeric and cytotoxic form. *J. Biol. Chem.* **289**, 30702–30716
48. Cox, J., and Mann, M. (2008) MaxQuant enables high peptide identification rates, individualized p.p.b.-range mass accuracies and proteome-wide protein quantification. *Nat. Biotechnol.* **26**, 1367–1372
49. Cox, J., Neuhauser, N., Michalski, A., Scheltema, R. A., Olsen, J. V., and Mann, M. (2011) Andromeda: a peptide search engine integrated into the MaxQuant environment. *J. Proteome Res.* **10**, 1794–1805
50. Hourdel, V., Volant, S., O'Brien, D. P., Chenal, A., Chamot-Rooke, J., Dillies, M. A., and Brier, S. (2016) MEMHDX: an interactive tool to expedite the statistical validation and visualization of large HDX-MS datasets. *Bioinformatics* **32**, 3413–3419
51. Karst, J. C., Sotomayor-Pérez, A. C., Ladant, D., and Chenal, A. (2012) Estimation of intrinsically disordered protein shape and time-averaged apparent hydration in native conditions by a combination of hydrodynamic methods. *Methods Mol. Biol.* **896**, 163–177
52. Karimova, G., Fayolle, C., Gmira, S., Ullmann, A., Leclerc, C., and Ladant, D. (1998) Charge-dependent translocation of Bordetella pertussis adenylate cyclase toxin into eukaryotic cells: implication for the in vivo delivery of CD8(+) T cell epitopes into antigen-presenting cells. *Proc. Natl. Acad. Sci. USA* **95**, 12532–12537
53. Gmira, S., Karimova, G., and Ladant, D. (2001) Characterization of recombinant Bordetella pertussis adenylate cyclase toxins carrying passenger proteins. *Res. Microbiol.* **152**, 889–900
54. Ladant, D. (1988) Interaction of Bordetella pertussis adenylate cyclase with calmodulin. Identification of two separated calmodulin-binding domains. *J. Biol. Chem.* **263**, 2612–2618
55. Sebo, P., Glaser, P., Sakamoto, H., and Ullmann, A. (1991) High-level synthesis of active adenylate cyclase toxin of Bordetella pertussis in a reconstructed Escherichia coli system. *Gene* **104**, 19–24
56. Westrop, G. D., Hormozi, E. K., Da Costa, N. A., Parton, R., and Coote, J. G. (1996) Bordetella pertussis adenylate cyclase toxin: proCyaA and CyaC proteins synthesised separately in Escherichia coli produce active toxin in vitro. *Gene* **180**, 91–99
57. El-Azami-El-Idrissi, M., Bauche, C., Loucka, J., Osicka, R., Sebo, P., Ladant, D., and Leclerc, C. (2003) Interaction of Bordetella pertussis adenylate cyclase with CD11b/CD18: role of toxin acylation and identification of the main integrin interaction domain. *J. Biol. Chem.* **278**, 38514–38521
58. Semisotnov, G. V., Rodionova, N. A., Razgulyaev, O. I., Uversky, V. N., Gripas', A. F., and Gilmanshin, R. I. (1991) Study of the "molten globule" intermediate state in protein folding by a hydrophobic fluorescent probe. *Biopolymers* **31**, 119–128
59. O'Brien, D. P., Brier, S., Ladant, D., Durand, D., Chenal, A., and Vachette, P. (2018) SEC-SAXS and HDX-MS: a powerful combination. The case of the calcium-binding domain of a bacterial toxin. *Biotechnol. Appl. Biochem.* **65**, 62–68

Received for publication November 14, 2018.
Accepted for publication May 13, 2019.

om www.fasebj.org by Institut Pasteur - CeRIS (157.99.25.33) on June 27, 2019. The FASEB Journal Vol. ${article.issue.getVolume()}, No. ${article.issue.getIssueNumber()}, p

Supplemental Information file

Post-translational acylation controls the folding and functions of the CyaA RTX toxin

Darragh P. O'Brien[1]#, Sara E. Cannella[1]#, Alexis Voegele[1], Dorothée Raoux-Barbot[1], Marilyne Davi[1], Thibaut Douché[2], Mariette Matondo[2], Sébastien Brier[1]*, Daniel Ladant[1]* and Alexandre Chenal[1]*

Addresses

[1] Institut Pasteur, Chemistry and Structural Biology Department, UMR CNRS 3528, 75724 PARIS cedex 15, France

[2] Institut Pasteur, Proteomics Platform, Mass Spectrometry for Biology Unit, USR CNRS 2000, 75724 PARIS cedex 15, France

# these authors contributed equally to this work

* to whom correspondence and material requests should be addressed:
sebastien.brier@pasteur.fr; daniel.ladant@pasteur.fr; alexandre.chenal@pasteur.fr

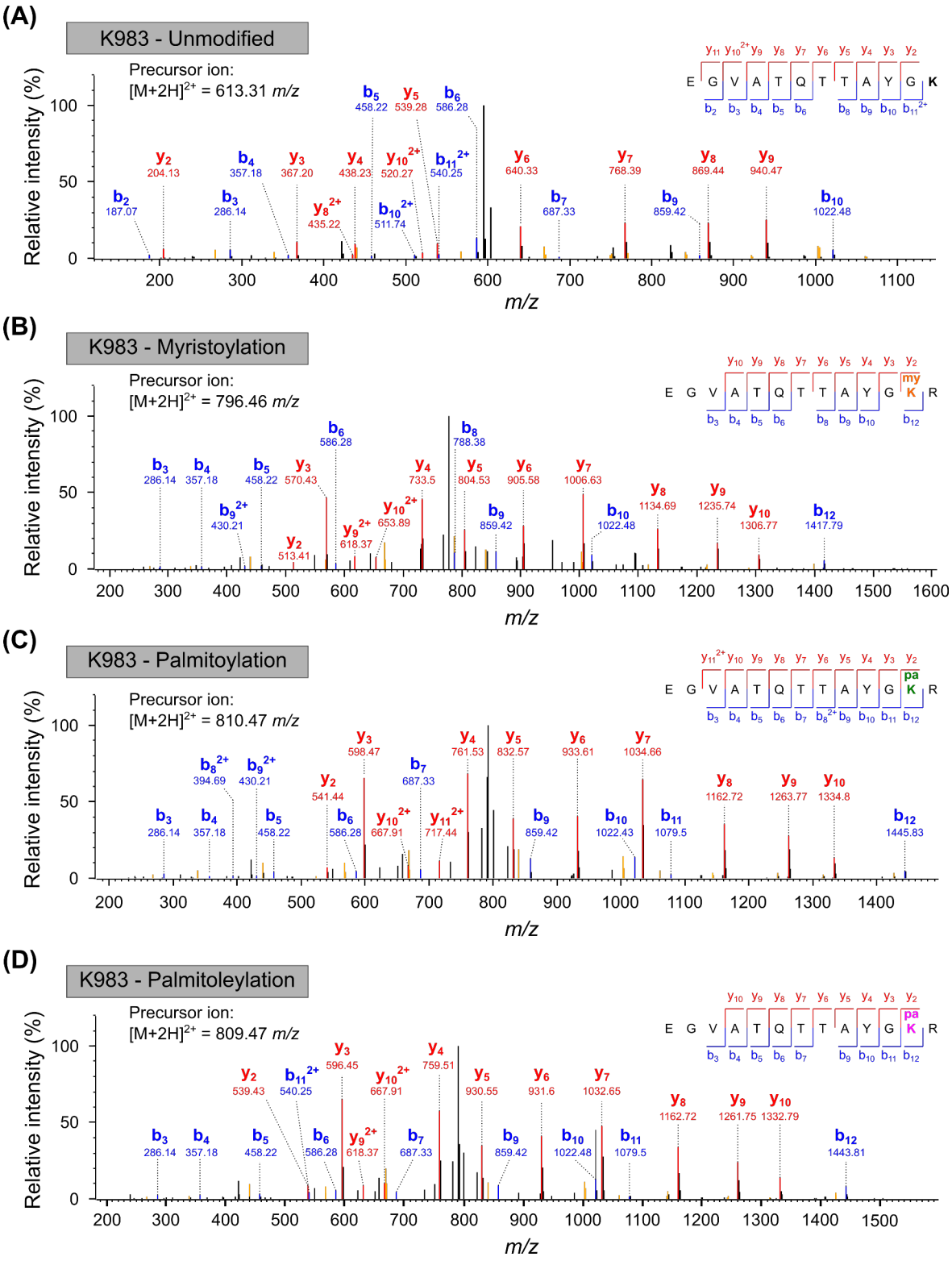

Supplemental Figure S1A: Annotated MS/MS spectrum showing the three distinct PTMs detected at residue K983 in the CyaA toxin: (A) unmodified residue, (B) myristoylated K983, (C) palmitoylated K983, and (D) palmitoleylated K983.

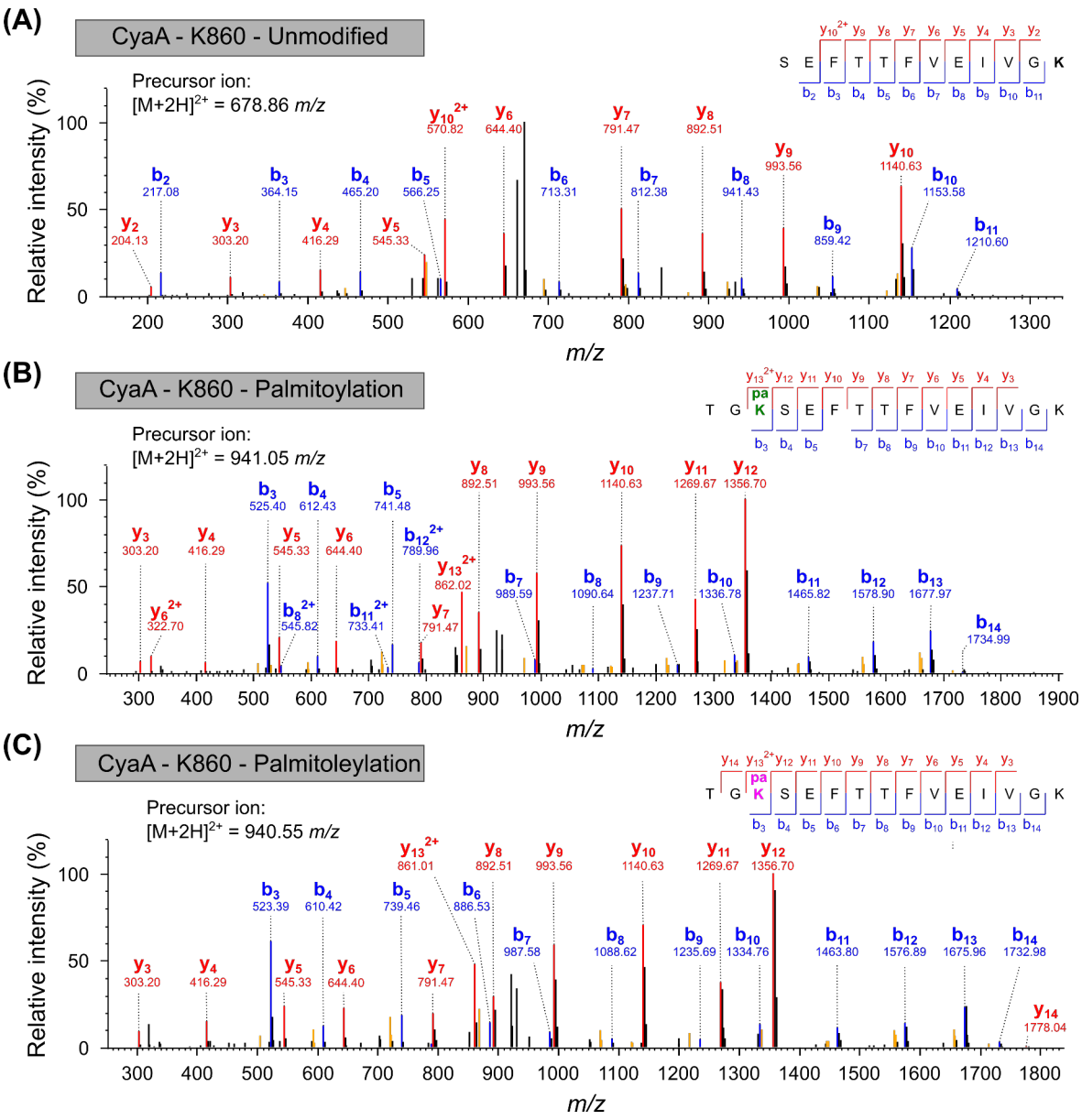

Supplemental Figure S1B: Annotated MS/MS spectrum showing the two PTMs detected at residue K860 in the CyaA toxin: (A) unmodified residue, (B) palmitoylated K860, and (C) palmitoleylated K860.

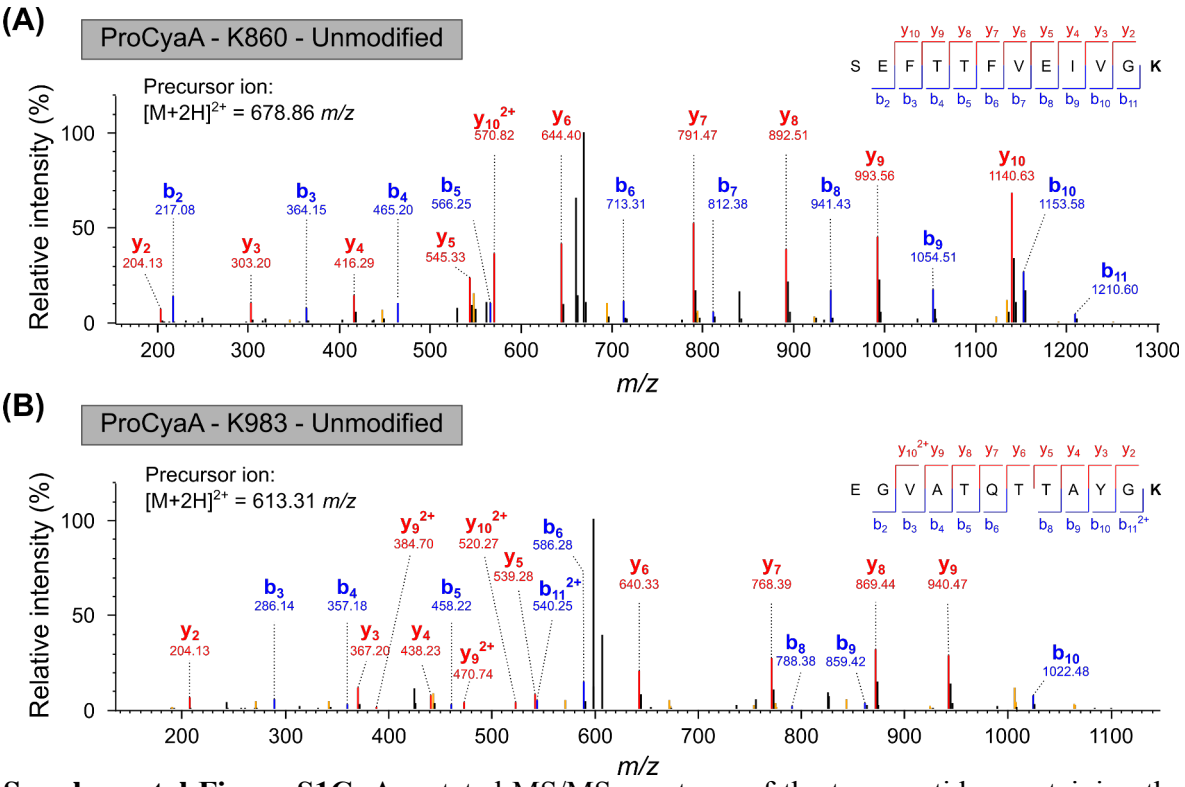

Supplemental Figure S1C: Annotated MS/MS spectrum of the two peptides containing the unmodified K860 (A) and K983 (B) residues in the pro-CyaA toxin.

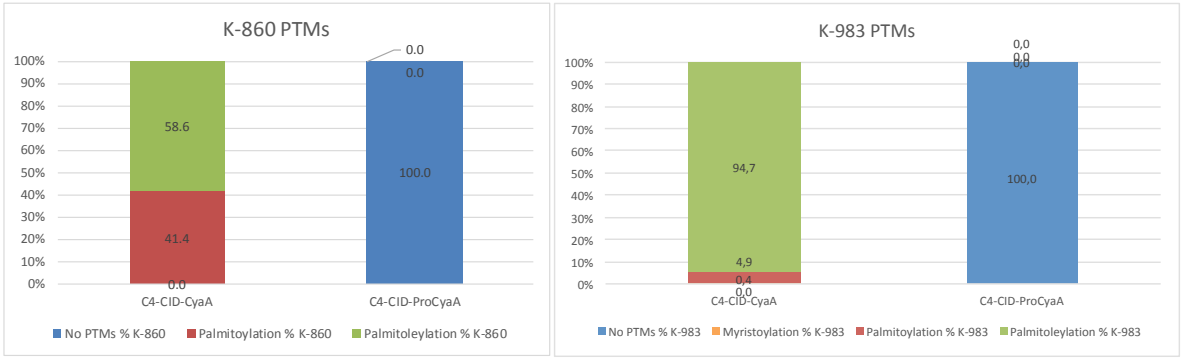

Supplemental Figure S1D: Relative quantification of the extend of K860 and K983 acetylation in pro-CyaA and CyaA monomers. Intensities of the unmodified and modified peptides were extracted. For each lysine residue (K-860 and K-983), intensities were summed by peptide form and normalized against the sum of all extracted intensities per involved lysine. These calculated percentages were plotted on the bar chart representation: Myristoylation (orange), Palmitoylation (red), Palmitoleylation (green), no PTMs (blue). The intensities of peptide ions used in the bar chart do not necessarily directly correlate with the actual amount of each corresponding peptide since ionization efficiencies can vary with the presence of post-translational modifications. However, myristoylation and palmitoylation are comparable modifications that occur on the same amino acid (Lysine), and, thus, we can postulate that the ionization efficiencies of the corresponding peptides should not be very different. The two lysine residues were found to be always unmodified in pro-CyaA and acylated in CyaA monomers.

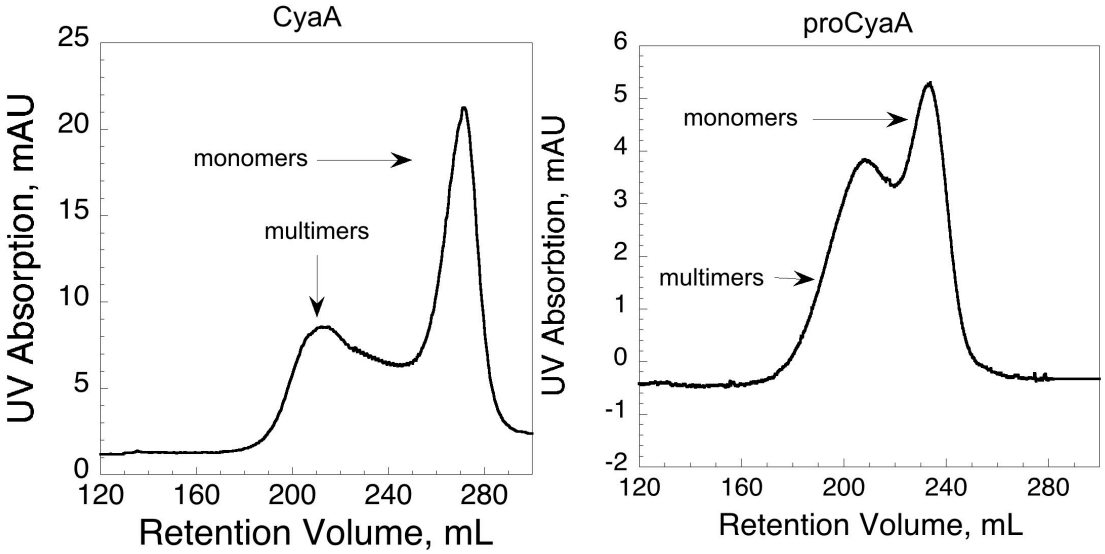

Supplemental Figure S2: Refolding of CyaA and pro-CyaA into a monomeric toxin. The protein is refolded by Size Exclusion Chromatography, using a HiLoad 16/600 Superdex 200 pg column (GE Healthcare), as described in Karst *et al.,* 2014. Briefly, the Superdex 200 pg was equilibrated with buffer A (20 mM Hepes, 150 mM NaCl, pH 7.4), complemented with 2 mM $CaCl_2$. The sample consists of 5 mL of CyaA at 5 µM or 5 mL of proCyaA at 2 µM stored in 8 mM urea, 20 mM Hepes, pH 7.4. After elution, monomers and multimers were pooled separately. Proteins were then concentrated and their hydrodynamic radius measured. Proteins were aliquoted and stored at -20°C. Note the difference of elution volume between the two monomeric species, CyaA and pro-CyaA, in agreement with the AUC data (CyaA monomers are more compact than pro-CyaA monomers).



Supplemental Figure S3: Peptide map of full-length CyaA in the presence of urea. A sequence coverage map was determined after 2 min digestion with pepsin. Each blue bar represents a single CyaA peptide. A linear sequence coverage of 85.7% was achieved. The position of the post-translational acylation sites at K860 and K983 are highlighted by gold stars.

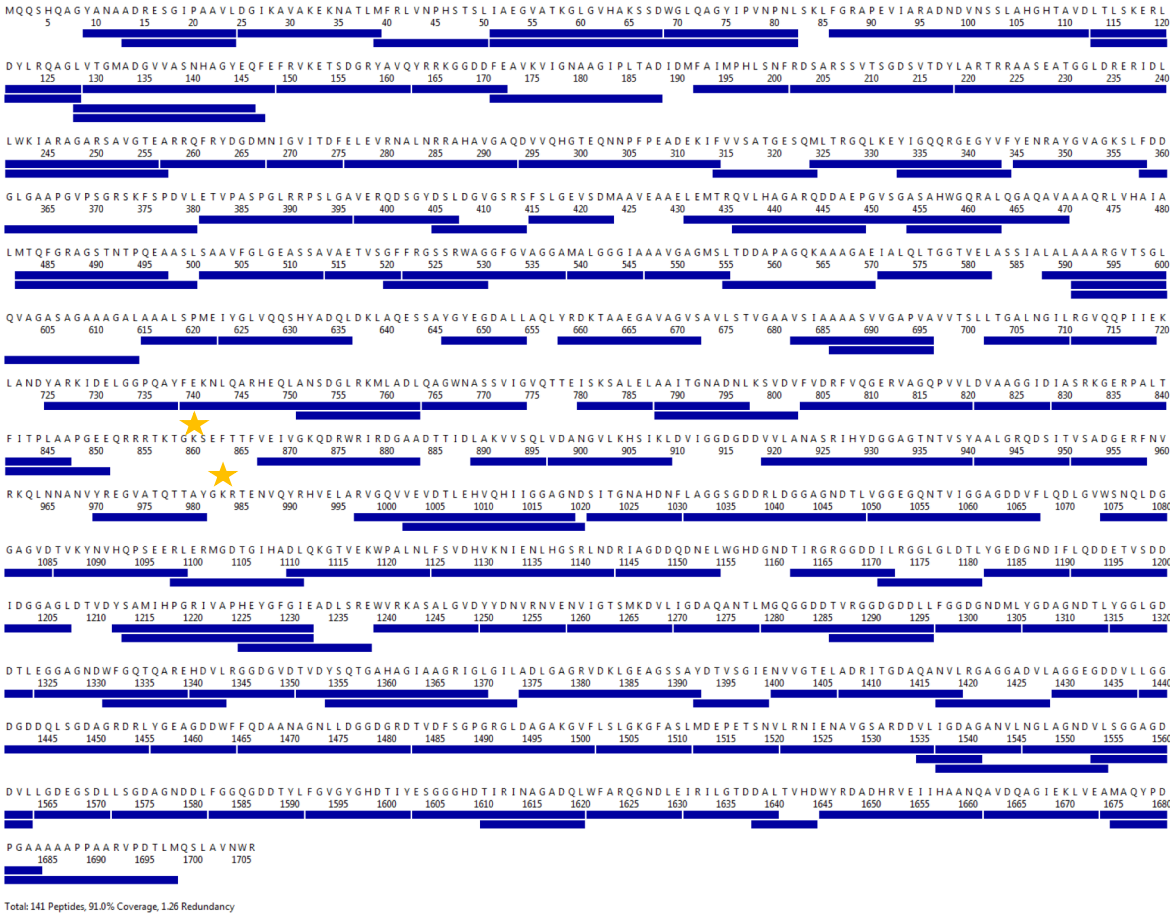

Supplemental Figure S4: Peptide map of native CyaA monomers. A sequence coverage map was determined after 2 min digestion with pepsin. Each blue bar represents a single CyaA peptide. A linear sequence coverage of 91.0% was achieved. The position of the post-translational acylation sites at K860 and K983 are highlighted by gold stars.

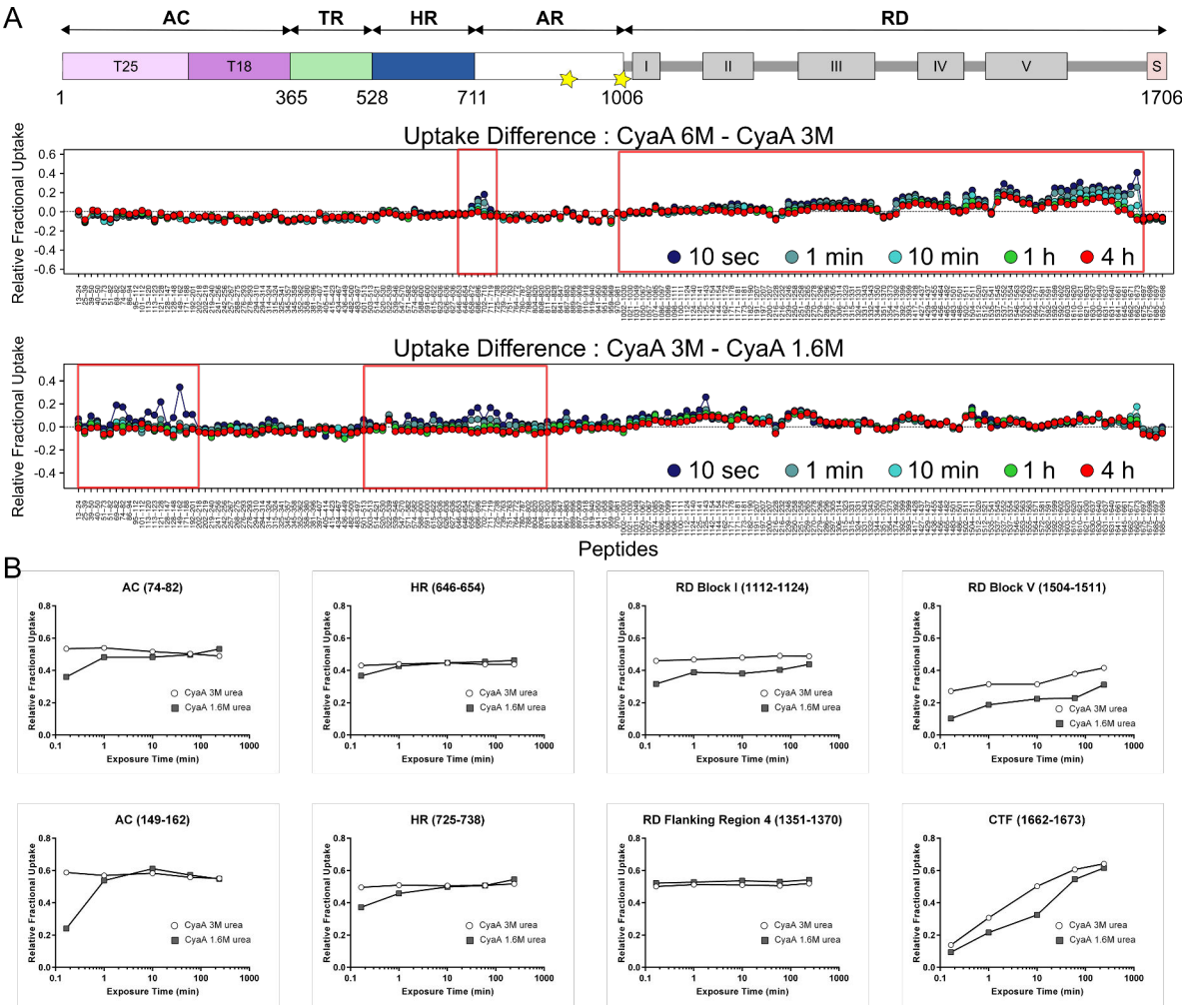

Supplemental Figure S5: Differences in amide hydrogen exchange of CyaA at varying urea concentrations. The structural organization of each domain is displayed in Panel A. Selected peptides displaying unique HDX-MS behaviors in each of the AC, HR and RD domains are given in Panel B. Buffer: buffer A, complemented with 2 mM CaCl2.

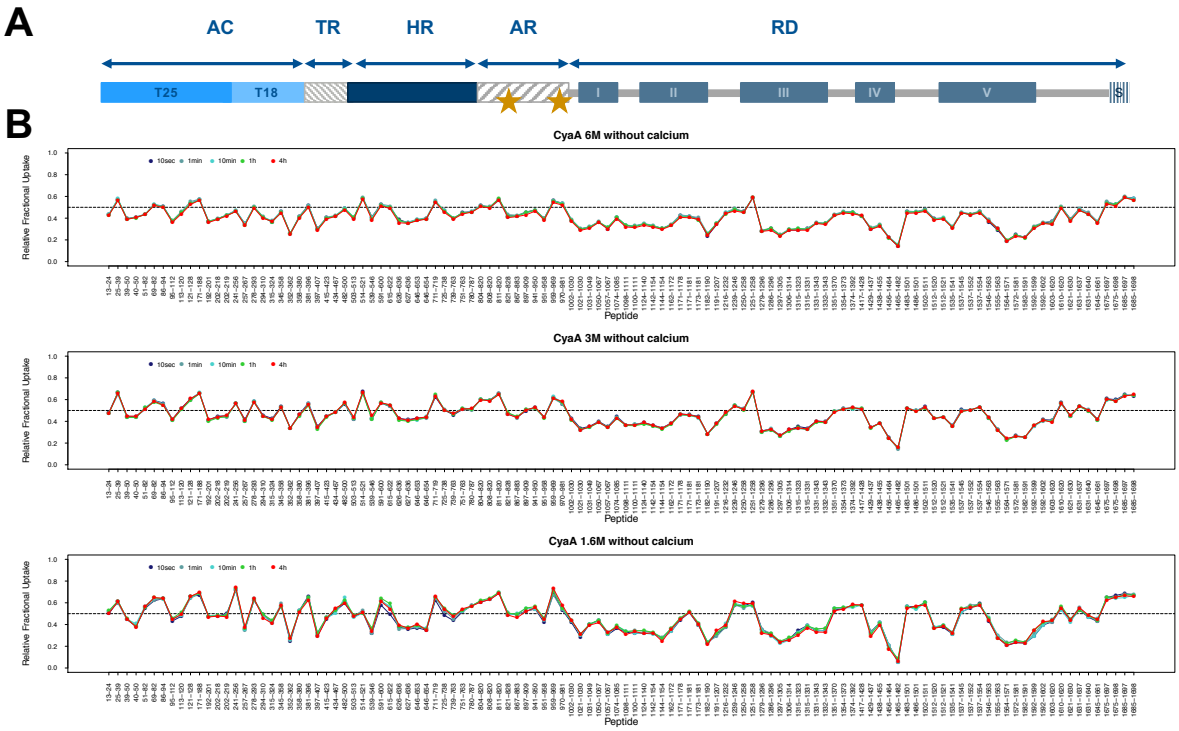

Supplemental Figure S6: Differences in amide hydrogen exchange of CyaA at varying urea concentrations in the absence of calcium. The structural organisation of each domain is displayed in Panel A. The HDX-MS behaviour of CyaA in various concentrations of urea is displayed in Panel B. It is evident that in the absence of calcium, no dynamic HDX-MS behaviour is observed in any region of the protein, regardless of the urea concentration. Buffer: buffer A (20 mM Hepes, 150 mM NaCl, pH 7.4), complemented with 2 mM EDTA.

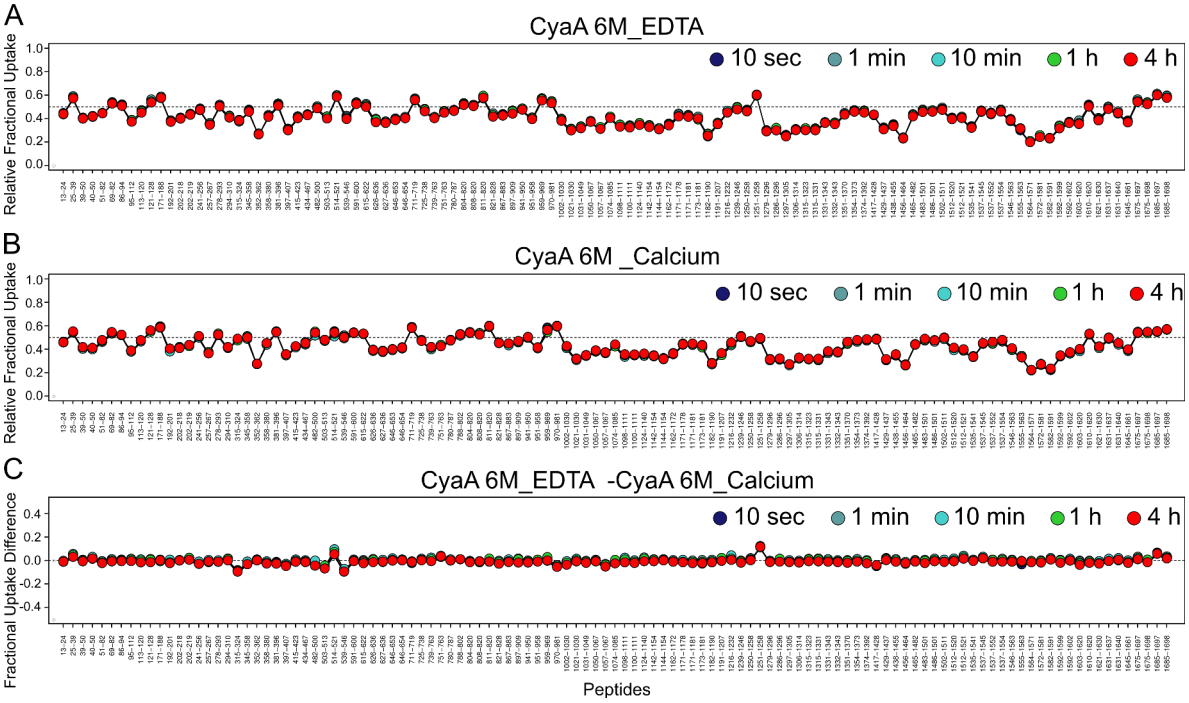

Supplemental Figure S7: Effect of Calcium on the deuterium uptake behavior of CyaA in 6M urea. (A,B) Deuterium uptake profiles of CyaA monitored for each peptide in the presence of 2 mM EDTA (A) or 2 mM Calcium (B). (C) Fractional uptake differential plot generated by subtracting the uptake measured for each peptide and at each time point in the absence (EDTA) and presence of Calcium. A positive difference value indicates a calcium-induced reduction of solvent accessibility.

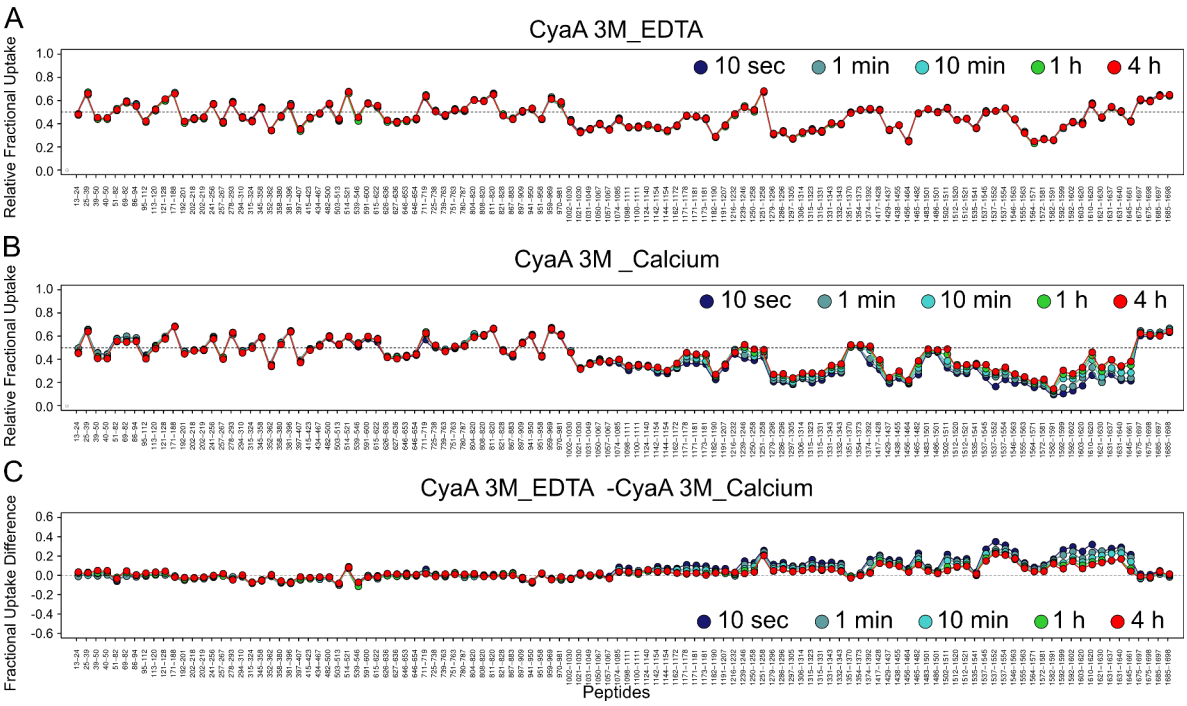

Supplemental Figure S8: Effect of Calcium on the deuterium uptake behavior of CyaA in 3M urea. (A,B) Deuterium uptake profiles of CyaA monitored for each peptide in the presence of 2 mM EDTA (A) or 2 mM Calcium (B). (C) Fractional uptake differential plot generated by subtracting the uptake measured for each peptide and at each time point in the absence (EDTA) and presence of Calcium. A positive difference value indicates a calcium-induced reduction of solvent accessibility.

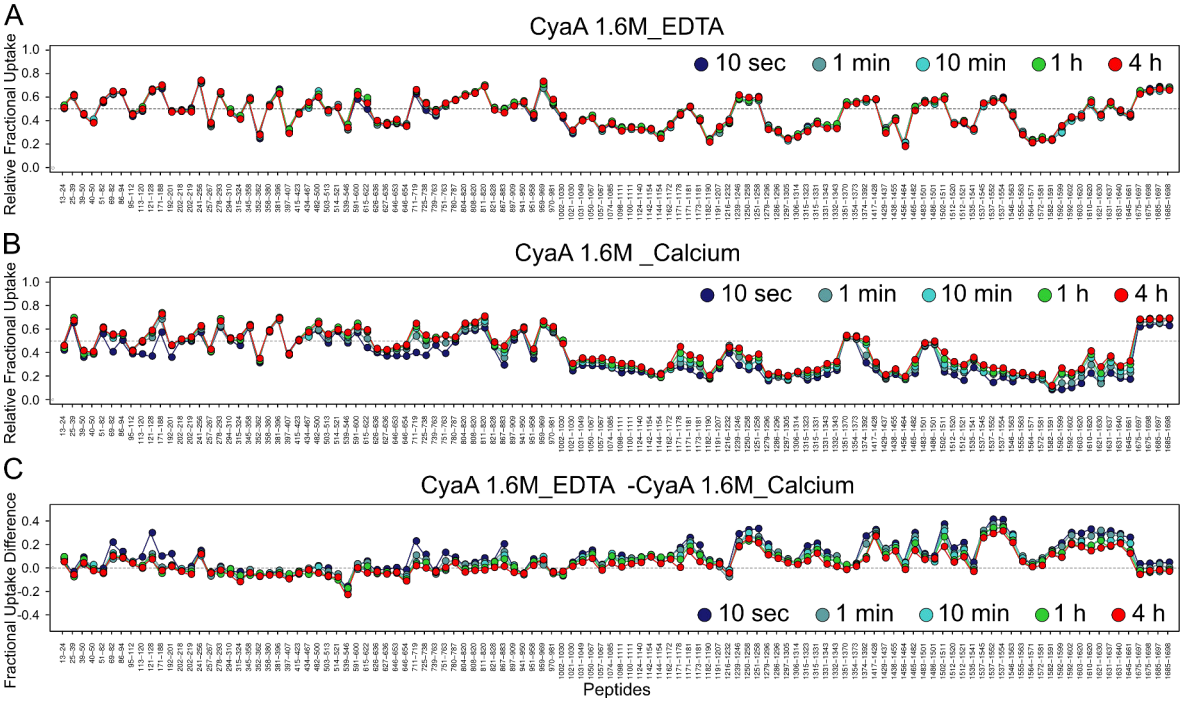

Supplemental Figure S9: Effect of Calcium on the deuterium uptake behavior of CyaA in 1.6M urea. (A,B) Deuterium uptake profiles of CyaA monitored for each peptide in the presence of 2 mM EDTA (A) or 2 mM Calcium (B). (C) Fractional uptake differential plot generated by subtracting the uptake measured for each peptide and at each time point in the absence (EDTA) and presence of Calcium. A positive difference value indicates a calcium-induced reduction of solvent accessibility.

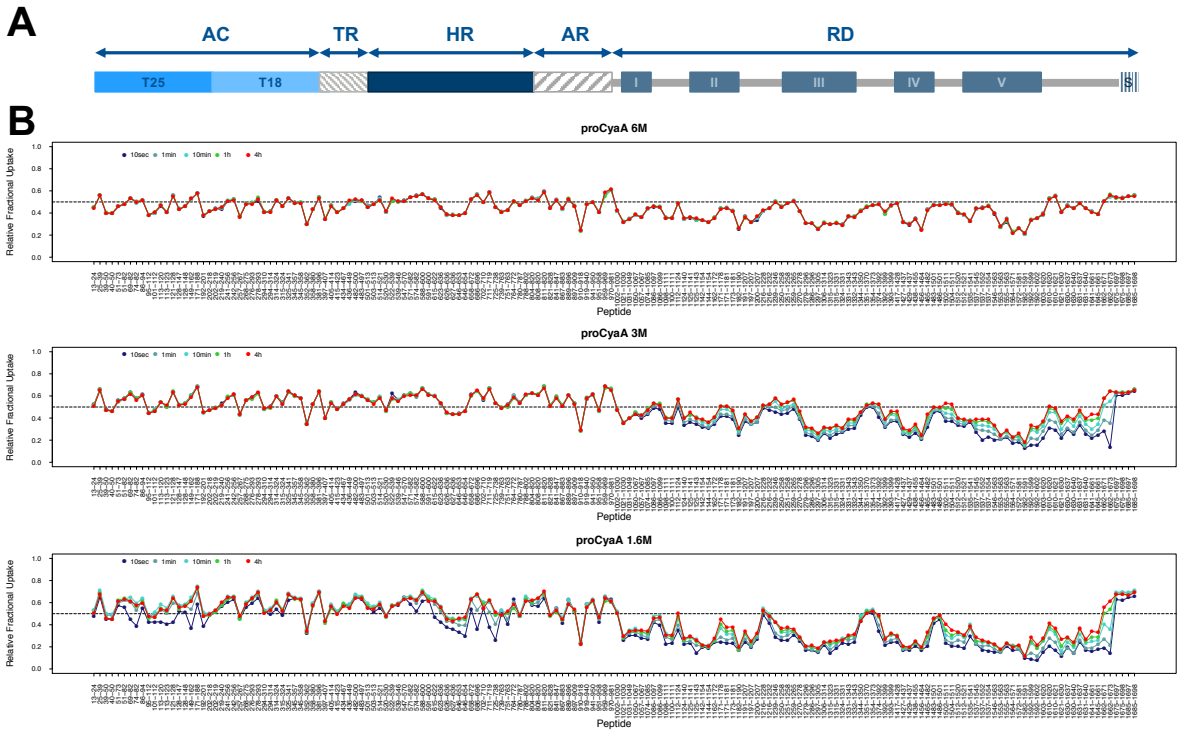

Supplemental Figure S10: Differences in amide hydrogen exchange of pro-CyaA at varying urea concentrations. The structural organisation of each domain is displayed in Panel A. The HDX-MS behaviour of pro-CyaA in various concentrations of urea is displayed in Panel B. At 6 M urea, no dynamic HDX-MS behaviour is observed throughout the protein. At 3 M urea, only the RD region displays dynamic activity. At 1.6 M urea, the AC, HR and RD domains have dynamic HDX-MS events. Buffer: buffer A, complemented with 2 mM CaCl2.

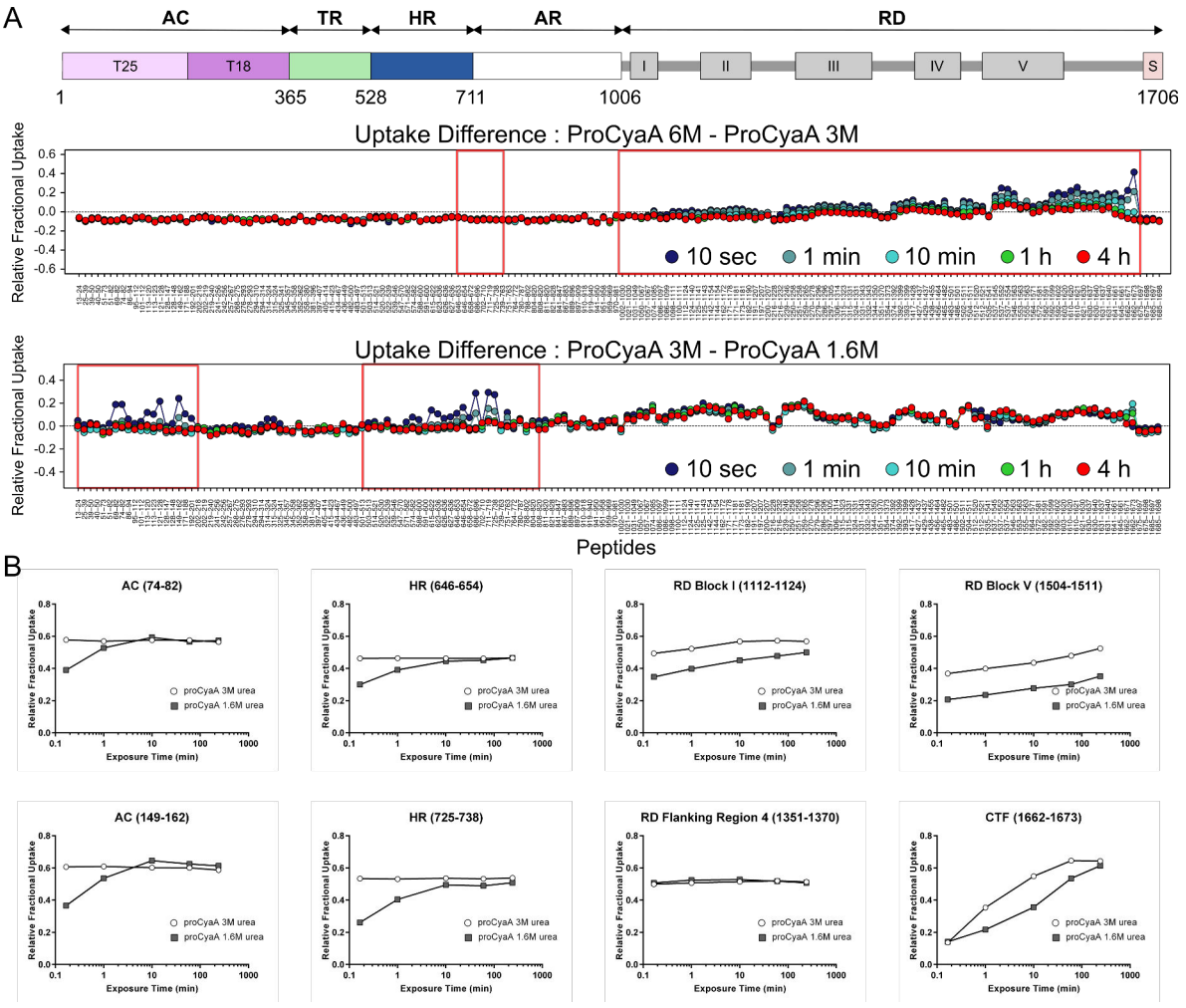

Supplemental Figure S11: Differences in amide hydrogen exchange of pro-CyaA at varying urea concentrations. The structural organization of each domain is displayed in Panel A. Selected peptides displaying unique HDX-MS behaviors in each of the AC, HR and RD domains are given in Panel B. Note that the uptake difference 6 M – 3 M in pro-CyaA shows no fractional uptake difference in HR (see the red box) while in CyaA it does (Supplemental Figure S5A). Buffer: buffer A, complemented with 2 mM CaCl2.

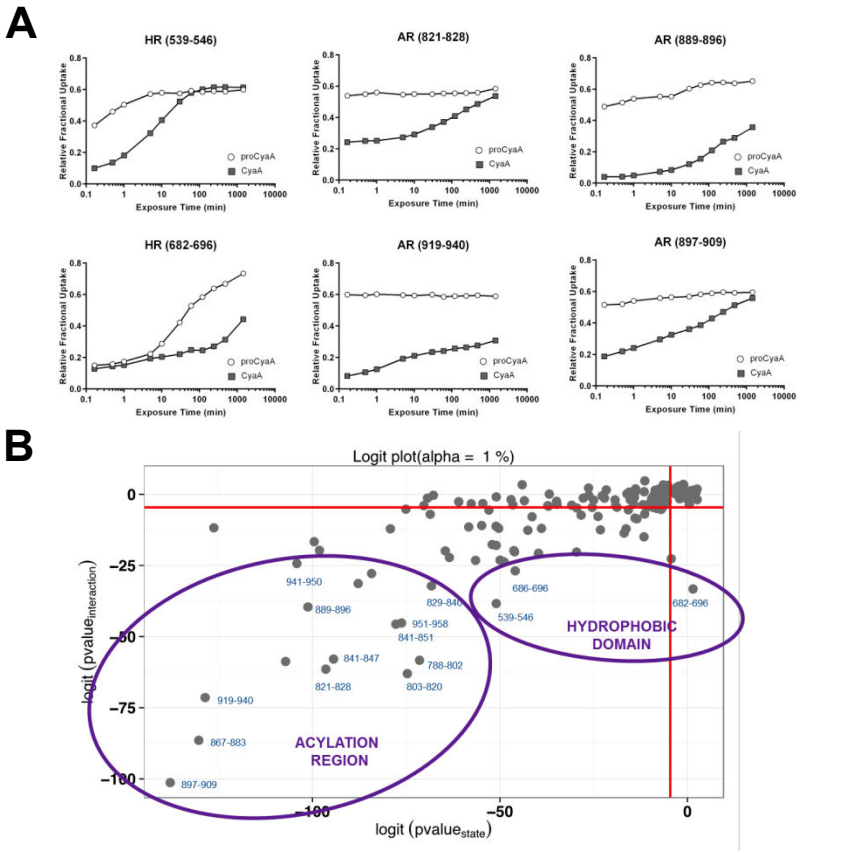

Supplemental Figure S12: Differences in HDX-MS behaviour between monomeric pro-CyaA and CyaA. Panel A displays peptides located in both the HR and AR domains and which give the greatest differences in HDX-MS activity between the two proteins. Panel B displays a Logit representation of the data. Peptides within the AR and HR domains cluster together and independently of each other, demonstrating significant and unique HDX-MS behaviours between the two.

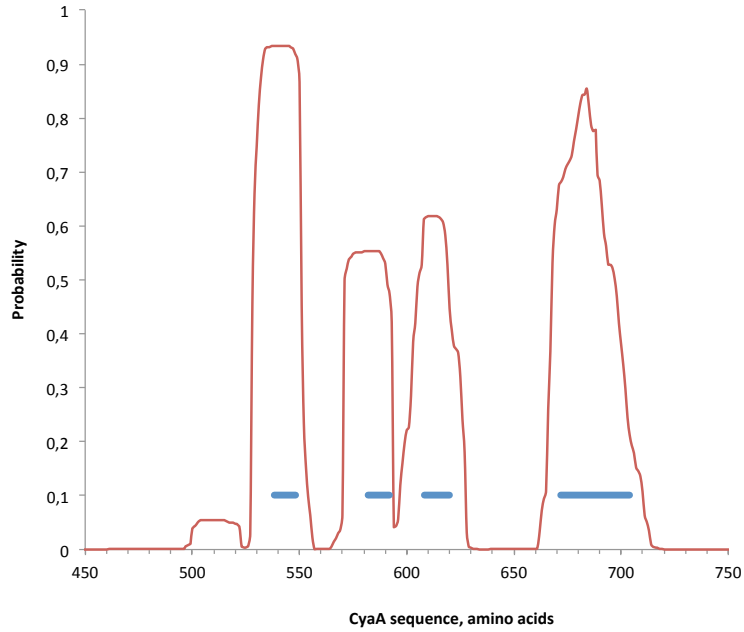

Supplemental Figure S13: Hydrophobicity of the primary structure of the CyaA toxin computed using TMHMM (red trace) and PHD transmembrane helix (blue) prediction servers (1, 2). Major changes observed by HDX-MS between the hydrophobic regions of CyaA and pro-CyaA monomers (peptides 539-546, 571-582, 615-622, 682-696, 686-696 and 702-710 see Figures 5 and 6 for details) are located within the predicted hydrophobic regions.
TMHMM is available here: http://www.cbs.dtu.dk/services/TMHMM/
PHD transmembrane helix prediction is available here:
https://npsa-prabi.ibcp.fr/cgi-bin/npsa_automat.pl?page=/NPSA/npsa_htm.html

	Proteins	Assay conditions	Hemolysis (%)	Bound Activity (% total)	Internalized Activity (% total)
1	CyaA in urea	$CaCl_2$	87 ± 8	2.14	1.55
		EDTA	< 2.0	0.02	< 0.01
2	Monomeric CyaA	$CaCl_2$	100 ± 6	2.70	0.85
		EDTA	< 2.0	0.34	< 0.01
3	Multimeric CyaA	$CaCl_2$	14 ± 9	2.93	< 0.01
		EDTA	< 2.0	0.39	< 0.01
4	Pro-CyaA in urea	$CaCl_2$	< 2.0	0.03	< 0.01
		EDTA	< 2.0	< 0.01	< 0.01

Supplemental Table S1: Hemolytic and cytotoxic activities of the different CyaA species. Toxin binding and translocation into sheep erythrocytes were assayed as described in Materials and Methods. The indicated CyaA solutions were directly diluted (final concentrations of 5.6 - 11 nM) into sheep erythrocytes (5×10^8/mL) suspended in buffer A supplemented with 2 mM $CaCl_2$ or 1 mM EDTA. Bound and internalized activities are expressed as percentages of total CyaA activity added to the erythrocyte suspension (taken as 100%) and represent the average values (with standard deviations below 20 %) from at least two independent measurements. Results are in good agreement with prior studies that showed that about 2-3 % of total CyaA can bind to erythrocytes while 0.5-1.5 % can be internalized in the presence of calcium (3, 4). The hemolytic activity was measured after overnight incubation at 37°C with 60 nM of indicated proteins as described in Materials and Methods.

Protein species	CyaA monomers	Pro-CyaA monomers
Sedimentation coefficient, S	7.4 ± 0.1	7.1 ± 0.1
R_H, nm	5.5 ± 0.1	5.8 ± 0.1
Solvent density, $g.mL^{-1}$	1.006	1.006
Solvent viscosity, $g.cm^{-1}.s^{-1}$	0.013	0.013
Molecular mass, kDa	177	177
Partial specific volume, $mL.g^{-1}$	0.725	0.725

Supplemental Table S2: Hydrodynamic parameters of CyaA and pro-CyaA monomers measured by AUC. AUC velocity analysis was performed at 20°C as described in Material and Methods. Buffer: 20 mM Hepes, 150 mM NaCl, 2 mM $CaCl_2$, pH 7.4. Experimental details are provided in the material and methods section.
Units used for AUC experiments:
Sedimentation coefficient, S, Svedberg, 10^{-13} sec
Hydrodynamic radius of the protein, R_H, nm
Solvent density, ρ, g/mL
Solvent viscosity, η, poise ($g.cm^{-1}.s^{-1}$)
Molecular Mass, M, kDa
Partial specific volume, $\bar{v}$, mL/g

Supplemental references

1. Combet, C., Blanchet, C., Geourjon, C., and Deleage, G. (2000) NPS@: network protein sequence analysis. *Trends Biochem Sci* **25**, 147-150
2. Krogh, A., Larsson, B., von Heijne, G., and Sonnhammer, E. L. (2001) Predicting transmembrane protein topology with a hidden Markov model: application to complete genomes. *Journal of molecular biology* **305**, 567-580
3. Karimova, G., Fayolle, C., Gmira, S., Ullmann, A., Leclerc, C., and Ladant, D. (1998) Charge-dependent translocation of Bordetella pertussis adenylate cyclase toxin into eukaryotic cells: implication for the in vivo delivery of CD8(+) T cell epitopes into antigen-presenting cells. *Proc Natl Acad Sci U S A* **95**, 12532-12537
4. Gmira, S., Karimova, G., and Ladant, D. (2001) Characterization of recombinant Bordetella pertussis adenylate cyclase toxins carrying passenger proteins. *Res Microbiol* **152**, 889-900

Article III

The adenylate cyclase (CyaA) toxin from *Bordetella pertussis* has no detectable phospholipase (PLA) activity *in vitro*

Alexis Voegele, Mirko Sadi, Dorothée Raoux-Barbot, Thibaut Douché, Mariette Matondo, Daniel Ladant and Alexandre Chenal

Toxins
Volume 11(2)
February 2019

The translocation mechanism of the CyaA toxin remains largely unknown. Recently, Gonzalez-Bullon and colleagues reported an interesting mechanism of translocation. They identified that CyaA exhibited an intrinsic calcium-dependent phospholipase activity (PLA) (Gonzalez-Bullon et al., 2018, 2017). They identified residues S606 and D1079 as two crucial residues for enzymatic PLA activity and also important for translocation of the catalytic domain. Their data supported that generation of lysophospholipids (*i.e* lipids with only one acyl chain) into the cell membrane would form a proteolytic toroidal pore through which the catalytic domain could be transported. Bumba and colleagues later contested these results. They showed that CyaA did not possess a PLA activity and that the two residues S606 and D1079, claimed to be crucial for PLA activity and translocation, were not involved in CyaA translocation (Bumba et al., 2018). The aim of our study was to clarify this controversy about the CyaA PLA activity.

We first analyzed the CyaA preparations from our lab and the CyaA used by Gonzalez-Bullon (kindly provided by Helena Ostolaza). We found that both proteins were able to induce cells hemolysis and cAMP accumulation. Proteomic analysis further showed that they were devoid of any contamination from *E. coli* phospholipases.

We then investigated the CyaA PLA activity using PED6, a specific probe for PLA2 activity. The cleavage of PED6 was monitored by fluorescence recovery. We used crotoxin, a neurotoxin from *Crotalus durissus terrificus* with a potent PLA activity, as positive control (Ostrowski et al., 2016). Data clearly showed that only crotoxin exhibited a PLA activity (up to 15 fold increase in fluorescence emission) and that the CyaA proteins did not exhibit any PLA activity.

We used also the B3781 fluorescent probe, which reports PLA1 and PLA2 activity. As observed with PED6, only crotoxin exhibited a potent PLA activity while CyaA proteins did not.

All together, these data showed unambiguously that CyaA has no detectable PLA activity *in vitro* and thus does not contribute to the translocation process of the catalytic domain.

toxins

MDPI

Brief Report

The Adenylate Cyclase (CyaA) Toxin from *Bordetella pertussis* Has No Detectable Phospholipase A (PLA) Activity In Vitro

Alexis Voegele [1,2], Mirko Sadi [1], Dorothée Raoux-Barbot [1], Thibaut Douché [3], Mariette Matondo [3], Daniel Ladant [1,*] and Alexandre Chenal [1,*]

1 Chemistry and Structural Biology Department, Institut Pasteur, UMR CNRS 3528, CEDEX 15, 75724 Paris, France; alexis.voegele@pasteur.fr (A.V.); mirko.sadi@outlook.de (M.S.); dorothee.raoux-barbot@pasteur.fr (D.R.-B.)
2 Université Paris Diderot Paris VII, 75013 Paris, France
3 Mass Spectrometry for Biology Unit, Proteomics Platform, Institut Pasteur, USR CNRS 2000, CEDEX 15, 75724 Paris, France; thibaut.douche@pasteur.fr (T.D.); mariette.matondo@pasteur.fr (M.M.)
* Correspondence: daniel.ladant@pasteur.fr (D.L.); alexandre.chenal@pasteur.fr (A.C.)

Received: 28 January 2019; Accepted: 11 February 2019; Published: 13 February 2019



Abstract: The adenylate cyclase (CyaA) toxin produced in *Bordetella pertussis* is the causative agent of whooping cough. CyaA exhibits the remarkable capacity to translocate its N-terminal adenyl cyclase domain (ACD) directly across the plasma membrane into the cytosol of eukaryotic cells. Once translocated, calmodulin binds and activates ACD, leading to a burst of cAMP that intoxicates the target cell. Previously, Gonzalez-Bullon et al. reported that CyaA exhibits a phospholipase A activity that could destabilize the membrane to facilitate ACD membrane translocation. However, Bumba and collaborators lately reported that they could not replicate these results. To clarify this controversy, we assayed the putative PLA activity of two CyaA samples purified in two different laboratories by using two distinct fluorescent probes reporting either PLA2 or both PLA1 and PLA2 activities, as well as in various experimental conditions (i.e., neutral or negatively charged membranes in different buffers.) However, we could not detect any PLA activity in these CyaA batches. Thus, our data independently confirm that CyaA does not possess any PLA activity.

Keywords: adenylate cyclase toxin; CyaA toxin; bordetella pertussis; phospholipase A; fluorescence

Key Contribution: The present communication aims at clarifying the controversy on the recently reported PLA activity of CyaA, by using fluorescent probes reporting either PLA2 or both PLA1 and PLA2 activities in various experimental conditions. We could not detect PLA activity in two CyaA samples purified in two different laboratories, confirming that CyaA does not possess any PLA activity.

1. Introduction

The adenylate cyclase (CyaA or ACT) toxin is secreted by *Bordetella pertussis*, the causative agent of whooping cough. The CyaA toxin is one of the major virulence factors produced by *B. pertussis* and is involved in the early stages of respiratory tract colonization [1–5]. CyaA invades eukaryotic target cells, where it is activated by calmodulin (CaM) to produce supra-physiological cAMP concentrations. It is a 1706-residue long protein that belongs to the Repeat-in-ToXin (RTX) family of cytolysins [6–10]. CyaA is a multi-domain protein [11,12], harboring from the N- to C-terminus, that has (i) a calmodulin-activated catalytic domain, ACD, located in the first 364 N-terminal residues [13–15]; (ii) a translocation region (TR, residues 365 to 527) that is essential for ACD translocation into target

cells [16–19]; (iii) a hydrophobic region (HR, residues 528 to 710) that inserts into the cell membrane and makes cation-selective pores leading to cell lysis [10,20,21]; (iv) an acylation region (AR, residues 711 to 1005) that contains two post-translational acylation sites on K860 and K983 [22–24] (modifications are required for the proper refolding and activity of CyaA) [5,12,22,23,25]; and (v) a C-terminal domain (RD, residues 1006 to 1706) made of about 40 copies of calcium-binding RTX motifs [8–10,26] that are required for RD and subsequently CyaA folding [27–35] and interaction with the CyaA cell receptor, CD11b/CD18 [36,37]. CyaA uses an original intoxication mechanism: once secreted by *B. pertussis*, it invades eukaryotic cells through a unique molecular mechanism that involves a direct translocation of its ACD catalytic domain across the plasma membrane. Yet, the molecular mechanisms of this unique entry process remain largely unknown.

Recently, H. Ostolaza et al. reported that CyaA exhibits a phospholipase A (PLA) activity [38,39] that is involved in destabilizing the lipid bilayer to facilitate ACD translocation across the plasma membrane. These results were contested by Bumba et al., who subsequently reported that CyaA has no PLA1 activity and showed that the two residues Ser606 and Asp1079 claimed to be critical for the putative PLA activity of CyaA, were not involved in CyaA translocation [40].

To clarify this controversy, we examined the PLA activity of two purified CyaA samples, one from our laboratory ($CyaA_{IP}$) and the second provided by Ostolaza's team ($CyaA_{UBC}$). Mass spectrometry data revealed that both CyaA batches were devoid of contaminating *E. coli* phospholipase. Using two distinct fluorescent probes of PLA activity, PED6 (specific to PLA2 activity) and B3781 (for both PLA1 and PLA2 activities), we could not detect any PLA activity in these CyaA preparations. This unambiguously indicates that CyaA has no detectable phospholipase A activity in vitro, which agrees with the prior results of Bumba et al. [40]. We discuss potential artifacts that might have blurred the conclusions of the Ostolaza team.

2. Results

2.1. Characterization of the $CyaA_{IP}$ and $CyaA_{UBC}$ Preparations

The CyaA preparations used in this study, $CyaA_{IP}$ from our laboratory and $CyaA_{UBC}$ from Ostolaza's team, were recombinantly produced in *E. coli* and purified using previously described protocols [12,38,41]. Both protein samples showed potent hemolytic activity and cell invasive capacities when tested on sheep erythrocytes (data not shown). Proteomic analysis of the CyaA batches was then performed to determine the extent of contamination of the samples by *E. coli* host phospholipases. The total *E. coli* contaminant proteins from both CyaA batches were identified using liquid chromatography–mass spectrometry (LC-MS/MS) (see supporting files: CyaA_IP_MS_result and CyaA_UBC_MS_result). The *E. coli* phospholipases (protein references EC 3.1.1.32 and EC 3.1.1.4) were not detected among contaminants in both CyaA samples. A lysophospholipase (EC 3.1.1.5), however, was identified in $CyaA_{UBC}$ but at very low abundance (see supporting file CyaA_UBC_MS_result). Hence, we can conclude that both $CyaA_{IP}$ and $CyaA_{UBC}$ are devoid of any contaminating PLA from *E. coli*.

2.2. PLA Activity Measurements as Monitored with the PED6 Fluorescent Probe

We first investigated PLA activity using a fluorescent probe, PED6, which is specific for PLA2 activity. In PED6, a 4,4-Difluoro-5,7-Dimethyl-4-Bora-3a,4a-Diaza-s-Indacene group linked to the acyl chain is quenched with a 2,4-Dinitrophenyl group linked to the lipid headgroup. The cleavage of PED6 using a PLA2 enzyme is monitored by the fluorescent recovery of the indacene group (excitation at 480 nm; emission at 490–650 nm; full spectra are shown in supplementary Figure S1). Figure 1A shows a time course recording of the fluorescence emission at 515 nm (F_{515}) of PED6 in the presence of LUV (DOPC:PED6 at a 8:2 molar ratio) in buffer alone or after addition of various proteins. Further, the addition of 10 nM crotoxin, a neurotoxin from *Crotalus durissus terrificus* [42,43] with a potent PLA activity, induced a large increase (up to 15 fold) in fluorescence emission (Figure 1A,B, black trace).

In contrast, no detectable PED6 fluorescence changes were observed after the addition of 10 nM BSA, a control protein lacking PLA activity, or, more importantly, of 10 nM of either $CyaA_{IP}$ or $CyaA_{UBC}$ (Figure 1A, orange and red traces, respectively). This indicates that the two CyaA proteins do not exhibit PLA2 activity. Figure 1B shows the same kinetics of fluorescence emission after normalization to the fluorescence intensity at a time of zero. While a high increase in fluorescence is observed with crotoxin (black trace), the fluorescence intensity variations observed with the two CyaA samples over a 30 min course are within a few percent of the initial F_{515} (Figure 1B, inset) and are essentially indistinguishable from that recorded with the buffer alone, or upon addition of BSA or of 60 mM urea (corresponding to the residual urea concentration obtained after addition of 10 nM CyaA proteins, as the toxins were stored in concentrated urea solutions). These data unambiguously indicate that the CyaA samples had no detectable PLA2 activity in these conditions.

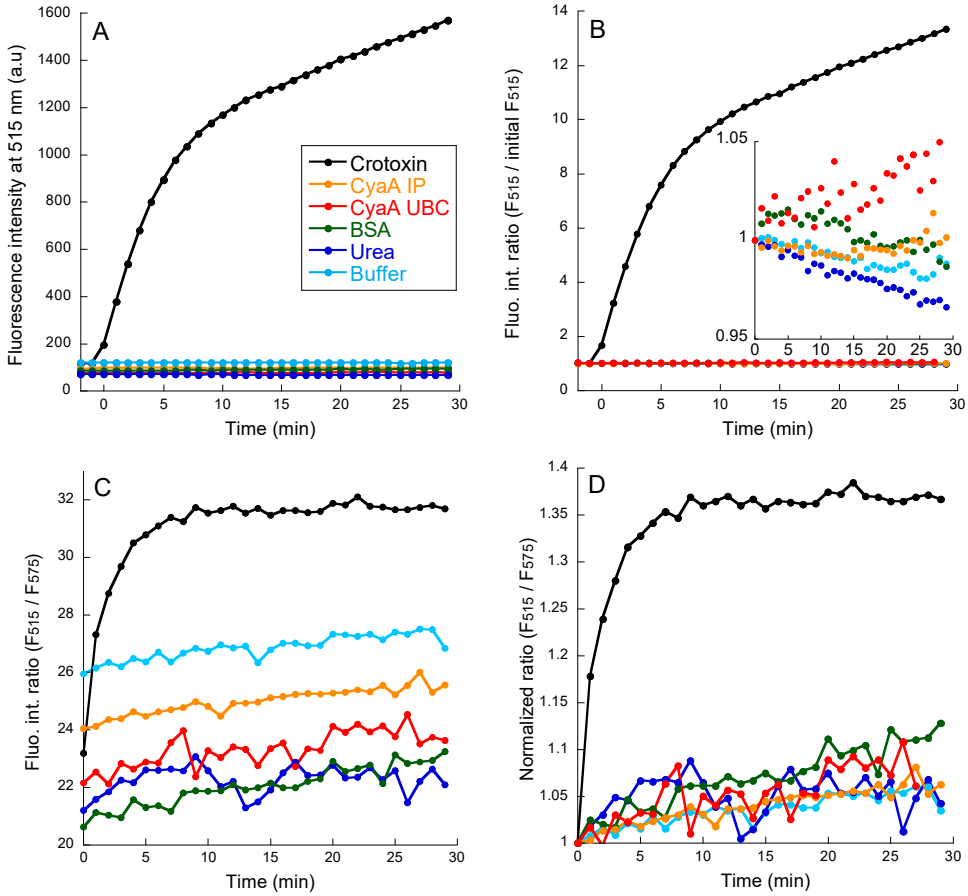

Figure 1. The kinetics of fluorescence changes of PED6 incorporated in DOPC:PED6 8:2 LUV (data from Figure S1). The time 0 min corresponds to the addition of the following samples: buffer (light blue), urea (dark blue), BSA (green), Crotoxin (black), $CyaA_{IP}$ (orange), and $CyaA_{UBC}$ (red). (**A**) Increase of fluorescence emission intensity at 515 nm. (**B**) Ratio of fluorescence intensity at 515 nm, F_{515}, at time t normalized by initial fluorescence at 515 nm. Inset shows same data with an expanded *Y*-axis (from 0.95 and 1.05). (**C**) Ratio of fluorescence intensity at 515 nm over fluorescence intensity at 575 nm: F_{515}/F_{575}. (**D**) The F_{515}/F_{575} values are normalized to the initial F_{515}/F_{575} value at 0 min (see methods for details).

Figure 1C,D show a different representation of the same data, plotted as relative ratio of fluorescence intensity at 515 nm over fluorescence intensity at 575 nm (F_{515}/F_{575}) for all samples. These plots (before, Figure 1C, and after, Figure 1D, normalization of baseline to 1 at time t = 0, respectively) fully confirm that only the crotoxin sample displays a significant PLA2 activity, while with

other protein samples, $CyaA_{IP}$, $CyaA_{UBC}$, or BSA, the basal, random drifts of F_{515}/F_{575} fluorescence ratio are indistinguishable from that recorded with the buffer alone or 60 mM urea.

2.3. PLA Activity Measurements as Monitored with the B3781 Fluorescent Probe

We then investigated the PLA activity using the B3781 fluorescent probe that reports both PLA1 and PLA2 phospholipase activities (Figure 2). Fluorescence excitation was fixed at 342 nm and the emission spectra of the B3781 probe were recorded from 350 to 600 nm each minute for 30 min (see Figure S2). The 1-pyrenebutanoyl groups linked to the lipid acyl chains form excimers was characterized using a maximum fluorescence emission near 480 nm. Hydrolysis of lipid acyl chains using a phospholipase releases a pyrene fatty acid that diffuses away from the pyrene lysophospholipid. These two pyrene derivatives exhibit a maximum emission of fluorescence between 380 and 400 nm [44,45].

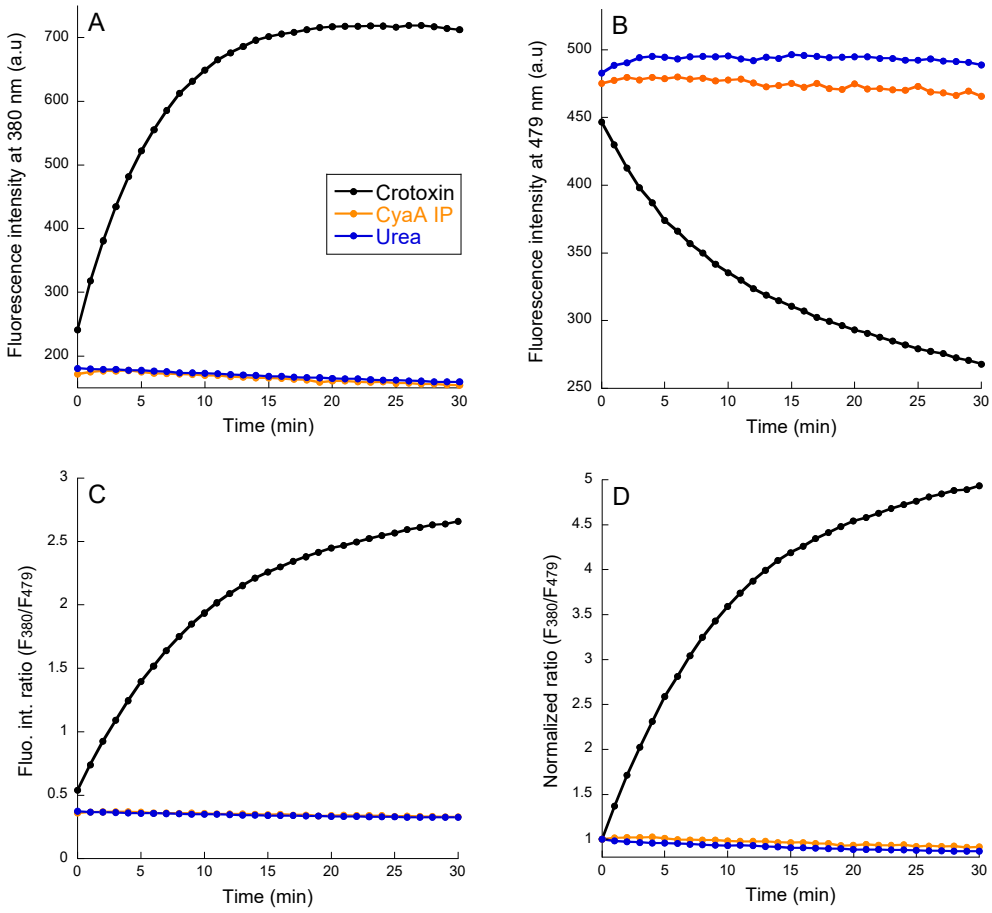

Figure 2. Kinetics of fluorescence changes of B3781 incorporated in POPC:POPG:B3781 79:20:1 LUV (data from Figure S2) upon addition of 100 nM crotoxin (black), 600 nM $CyaA_{IP}$ (orange), and 180 mM urea (dark blue). (**A**) Increase of fluorescence intensity emitted at 380 nm. (**B**) Decrease of fluorescence emission intensity at 479 nm. (**C**) Ratio of fluorescence intensity at 380 nm over fluorescence intensity at 479 nm: F_{380}/F_{479}. (**D**) F_{380}/F_{479} values are normalized to the initial F_{380}/F_{479} value at 0 min.

Figure 2 shows a time course recording of the fluorescence emission changes (at 380 nm, F_{380}, Panel A, or 479 nm, F_{479}, Panel B) of B3781 (in LUV composed of POPC:POPG:B3781 at a lipid ratio 79:20:1) after the addition of crotoxin, $CyaA_{IP}$, or urea (180 mM final concentration; full spectra are shown in Figure S2). Large changes in fluorescence, typical of excimer-to-monomer conversion of the B3781 probe, were observed with crotoxin (100 nM) as a result of its PLA activity. However, no detectable changes were noticed with up to 600 nM of purified CyaA, demonstrating the total

lack of phospholipase activity of the toxin. Panels C and D in Figure 2 show the same results, as a ratio of fluorescence intensity at 380 nm over fluorescence intensity at 479 nm, F_{380}/F_{479}, before and after normalization to the initial F_{380}/F_{479} value at a time of zero. All data representations clearly indicate that the CyaA toxin does not exhibit any detectable phospholipase A activity in these in vitro conditions.

3. Discussion

It is clear from our present data that no significant PLA1 or PLA2 activity can be detected for highly purified CyaA proteins using fluorescent probes classically used for measuring phospholipase A activity. These experiments were repeated several times, using several distinct CyaA batches, as well as different batches of LUV of different composition—in the absence (POPC:PED6 at 8:2 molar ratio) or in the presence of anionic lipids (POPC:POPG: B3781 at 79:20:1 molar ratio)—and different buffer conditions (Tris-HCl instead of HEPES-Na, data not shown). Our PLA assays were validated using crotoxin, a venom neurotoxin with potent PLA activity, and BSA as positive and negative controls, respectively. We therefore concluded that CyaA has no detectable PLA activity in vitro. These data corroborate the prior results found by Bumba et al. [40], who likewise could not detect PLA activity in their purified batches of CyaA.

Yet, how can these results be reconciled with the claims of the Ostolaza study? These authors used a similar fluorescent probe, PED1 to monitor the PLA1 activity of CyaA. In their reported experiments, only very small changes in fluorescent intensity of the probe (<1.1–1.4 relative ratio) were observed after the addition of CyaA. Moreover, the kinetic experiments presented in their recent paper [39] revealed odd profiles that question the validity of interpretation of the fluorescence changes as signatures of a PLA enzymatic activity. Indeed, they observed an abrupt, yet limited, change of fluorescence intensity just after addition of the CyaA sample (i.e., at the first recording point) with no further changes during the following 30 min of incubation. Strikingly, all assays at various concentrations of CyaA showed an identical profile: an abrupt initial change followed by a constant plateau over the whole course of the kinetics. Only the plateau values were different and roughly proportional to the amount of added proteins. Surprisingly, the authors were able to derive "velocities" (i.e., fluorescent change per minute) from these odd kinetic data, as shown in their plot of Figure 2C in [39].

The authors did notice the singular feature of the CyaA PLA activity. To explain this, as well as the very weak lipid hydrolytic activity as compared to that of other known phospholipases A, they proposed that a local accumulation of the lysophospholipidic product around the toxin molecules in the membrane could inhibit its PLA catalytic activity. Yet, it is hard to understand why the lysophospholipid could not continuously diffuse out in the membranes while being replaced by new substrates, i.e., unprocessed phospholipidic PLA probes. Furthermore, this hypothesis would require that the CyaA toxin binds to the lipid vesicles and hydrolyzes the PLA fluorescent probes within seconds after being added to the membrane with no further interaction and/or hydrolytic events occurring during the further 30 min of incubation. This is obviously not the case as all prior kinetic measurements of CyaA activities (including in prior publications from Ostolza and collaborators) clearly showed a progressive time-dependent accumulation of cAMP, hemolysis, or membrane permeabilization over a 5–30 min time scale. Therefore, it is more reasonable to assume that the weak and fast fluorescence increase observed by Gonzalez-Bullon et al. was an artifact, due to photon counting variations induced by light scattering as a result of the CyaA sample addition to the solution rather than to the consequence of a putative enzymatic cleavage of the probe by the PLA activity of CyaA. Indeed, in our experiments we did not observe any similar small burst of fluorescence after adding CyaA, but only a very limited random drift that was not different from that observed with the negative control BSA protein. In summary, on the basis of our in vitro assays with fluorescent PLA probes, we can unambiguously conclude that CyaA has no detectable PLA activity in vitro, which agrees with the prior studies of Bumba et al. [40].

4. Material and Methods

4.1. Buffers

Buffer A is composed of 20 mM HEPES, 150 mM NaCl and 10 mM $CaCl_2$ pH 7.4. Buffer B is composed of 20 mM HEPES, 150 mM NaCl, and 2 mM $CaCl_2$ pH 7.4.

4.2. Protein Samples

CyaA is expressed in *E. coli*, purified to homogeneity by established procedures [12,41]. CyaA was stored in 20 mM HEPES, 6 M urea, pH 7.4. CyaA was purified in our laboratory at Institut Pasteur and is hereafter called $CyaA_{IP}$. The second batch of CyaA used in this study was a kind gift from Helena Ostolaza, from the University of Basque Country, hereafter named $CyaA_{UBC}$. The crotoxin protein from *Crotalus durissus terrificus* is a kind gift from G. Faure [42,43]. Crotoxin was resuspended in 0.1% BSA in buffer B. BSA (from Sigma, St Louis, MI, USA, reference A0281) was resuspended in buffer B.

4.3. Mass Spectrometry Analysis

Sample Preparation

The protein digestion of the $CyaA_{IP}$ batch was performed as follows: CyaA was placed in 20 mM HEPES, 6 M in urea, and the pH 7.4 was digested by Lys-C (V1671, Promega, Madison, WI, USA) at a Lys-C/CyaA ratio 1/50 (w/w), which corresponded to a 1/7 molar ratio (mol/mol). The sample was vortexed and centrifuged for 1 min at 3000 rpm then incubated for 3 h at 37 °C under agitation (500 rpm). Urea concentration decreased to 2 M with the addition of 20 mM HEPES, which optimized trypsin digestion. Trypsin (V5111, Promega, Madison, WI, USA) was added at a trypsin/CyaA ratio of 1/50 (w/w). The sample was vortexed and centrifuged for 1 min at 3000 rpm then the digestion was carried out for 1 h at 37 °C under agitation (500 rpm). The digestion stopped with 2% formic acid (FA) (Fluka, 94318) and digested peptides were desalted on reversed phase C_{18} Sep-Pak Cartridge (WAT054955, Waters Corporation, Milford, MA, USA). Peptides were eluted with a final 80% Acetonitrile (ACN)/0.1% Formic acid (FA). Resulting peptides were vacuum centrifuged to evaporate ACN and then lyophilized. Peptide samples were reconstituted in 2% ACN/0.1% FA.

Protein digestion of the $CyaA_{UBC}$ batch was performed as follows: 15 µg of the purified fraction containing $CyaA_{UBC}$ were diluted with Urea 8 M/NH_4HCO_3 100 mM. The samples were reduced with 5 mM TCEP over 1 h and alkylated with 20 mM iodoacetamide over 1 h. The sample was digested with rLys-C (Promega, Madison, WI, USA, V1671), ratio 1:50 (enzyme:protein/w:w) for 4 h at 37 °C and then with Sequencing Grade Modified Trypsin (Promega, Madison, WI, USA, V5111), ratio 1:50 (enzyme:protein/w:w) overnight at 37 °C. The digestion stopped with 2% formic acid (FA) (Fluka, 94318) and digested peptides were purified with C_{18} Spin Columns Pierce™ (ThermoFisher Scientific, Waltham, MA, USA, 89870). Peptides were eluted with 80% ACN/0.1% FA. Resulting peptides were vacuum centrifuged to evaporate ACN and then lyophilized. Peptide samples were reconstituted in 2% ACN/0.1% FA.

4.4. LC-MS/MS Analysis of the CyaA Batches

LC-MS/MS analysis of the $CyaA_{IP}$ batch was performed on a U3000-Velos mass spectrometer. A nanochromatographic system Ultimate 3000 system (Dionex, Amsterdam, The Netherlands) was coupled on-line to a LTQ-Orbitrap Velos Mass Spectrometer (Thermo Fisher Scientific, Waltham, MA, USA) using an integrated column oven (PRSO-V1, Sonation GmbH, Biberach, Germany). For each sample, 1.0 µg of peptides were loaded onto a C_{18} pre-column (300 µm inner diameter × 5 mm; Dionex, Sunnyvale, CA, USA) at 30 µL/min in 2% ACN, 0.1% FA. After 5 min of desalting, the pre-column was switched online to an in-house packed 15 cm nano-HPLC column (75 µm inner diameter) with C_{18} resin (3 µm particles, 100 Å pore size, ReproSil-Pur Basic C18, Dr. Maisch GmbH, Ammerbuch-Entringen, Germany). Peptides were then separated with a multi-step gradient from 2% to 9% buffer B (80%

ACN/0.1% FA) in 5 min, 9% to 29% buffer B in 70 min, 29% to 56% buffer B in 30 min, and 56% to 100% buffer B in 5 min at a flow rate of 300 nL/min over 132 min. The column temperature was set to 40 °C. MS data were acquired using Xcalibur software with a survey scan (300–2000 m/z) analyzed into the Orbitrap mass analyzer at a resolution setting of 60,000, followed by 10 CID fragmentations analyzed into the linear ion trap. The AGC targets for MS and MS/MS scans were set to 1E6 and 5E3 respectively. The isolation width was set to 2.5 m/z and the normalized collision energy was set to 35. Selected ions were dynamically excluded for 30 s.

LC-MS/MS analysis of the $CyaA_{UBC}$ batch was performed on a Proxeon 1200-Q Exactive mass spectrometer. A nanochromatographic system (Proxeon EASY-nLC 1200, Thermo Fisher Scientific, Waltham, MA, USA) was coupled on-line to a Q ExactiveTM Plus Mass Spectrometer (Thermo Fisher Scientific, Waltham, MA, USA) using an integrated column oven (PRSO-V1, Sonation GmbH, Biberach, Germany). For each samples, 1.0 µg of peptides was injected onto a 46 cm homemade C_{18} column (1.9 µm particles, 100 Å pore size, ReproSil-Pur Basic C18, Dr. Maisch GmbH, Ammerbuch-Entringen, Germany) and separated with a multi-step gradient from 2% to 7% buffer B (80% ACN/0.1% FA) in 5 min, 7% to 23% buffer B in 70 min, 23% to 45% buffer B in 30 min, and 45% to 95% buffer B in 5 min at a flow rate of 250 nL/min over 132 min. The column temperature was set to 60 °C. MS data were acquired using Xcalibur software and a data-dependent Top 10 method with survey scans (300–1700 m/z) at a resolution of 70,000 and a MS/MS scans (fixed first mass 100 m/z) at a resolution of 17,500. The AGC target and maximum injection time for the survey scans and the MS/MS scans were set to 3E6, 20 ms, and 1E6, 60 ms, respectively. The isolation window was set to 1.6 m/z and normalized collision energy fixed to 28 for HCD fragmentation. We used a minimum AGC target of 1.0E4 for an intensity threshold of 1.7E5. Unassigned precursor ion charge states as well as 1, 7, 8, and >8 charged states were rejecte and the peptide match was disabled. Excluded isotopes were enabled and selected ions were dynamically excluded for 45 s.

4.5. MaxQuant Analysis

Raw data were analyzed using MaxQuant software version 1.5.1.2 [46] using the Andromeda search engine [47]. Based on the protein expression system, the MS/MS spectra were searched against the *Escherichia coli* strain BL21DE3 UniProt database containing 4,156 proteins plus the CyaA sequence. The digestion mode was set to trypsin and a maximum of two missed cleavages were allowed. N-terminal acetylation, Methionine oxidation, and Lysine N-acylations (Myristoyl-4H, Myristoleylation, Myristoylation, Palmitoleylation, Palmitoylation) were set to variable modifications while Cystein Carbamidomethylation was set as fixed modification. The minimum peptide length was fixed to amino acids and the required false discovery rate was set to 1% at the PSM level and protein level. The main search peptide tolerance was set to 4.5 ppm and to 0.5 Da for the MS/MS match tolerance. Second peptide was enabled to identify co-fragmentation events.

4.6. Fluorescent Probes

PED6 (N-((6-(2,4-Dinitrophenyl)amino)hexanoyl)-2-(4,4-Difluoro-5,7-Dimethyl-4-Bora-3a, 4a-Diaza-s-Indacene-3-Pentanoyl)-1-Hexadecanoyl-sn-Glycero-3-Phosphoethanolamine, Triethylammonium Salt), and B3781 (1,2-Bis-(1-pyrenebutanoyl)-sn-glycero-3-phosphocholine) probes were purchased from Thermo Scientific. The PED6 and B3781 probes were resuspended in chloroform and stored at −20 °C under Argon.

4.7. Preparation of PED6-Containing LUV

Large unilamellar vesicles (LUV) were composed of DOPC:PED6 at a 8:2 molar ratio and prepared by reverse phase evaporation followed by extrusion of the multi-lamellar vesicles (MLV) suspension through 200 nm pore size polycarbonate filters [19]. A solution of 1 mL of LUVs was prepared at a lipid concentration of 500 µM in buffer A. Size, polydispersity, and electrophoretic mobility of LUV suspensions were measured on a Zetasizer NanoZS (Malvern, UK). All proteins (CyaA samples,

BSA, and crotoxin) were assayed for PLA activity at a final protein concentration of 10 nM. Lipid concentration of LUV in the cuvette was 10 μM, i.e., a lipid:protein molar ratio of 1000. Experiments were performed under constant stirring at 37 °C using a 109 004F cuvette (Hellma) in a Jasco fluorometer. Fluorescence excitation was fixed at 480 nm and the emission spectra were recorded from 490 to 650 nm each minute for 30 min. The 2,4-Dinitrophenyl group linked on the lipid headgroup does quench the 4,4-Difluoro-5,7-Dimethyl-4-Bora-3a,4a-Diaza-s-Indacene group linked to the acyl chain. PLA2 activity will allow fluorescence recovery of the indacene derivative released in the membrane and diffusing away from the 2,4-Dinitrophenyl group liked to the lysophospholipid.

4.8. Preparation of B3781-Containing LUV

Large unilamellar vesicles (LUV) were composed of POPC:POPG:B3781 at a 79:20:1 molar ratio and prepared by reverse phase evaporation followed by extrusion of the multi-lamellar vesicles (MLV) suspension through 200 nm pore size polycarbonate filters [19]. A solution of 2 mL of LUVs was prepared at a lipid concentration of 2 mM in buffer B. Size, polydispersity, and electrophoretic mobility of LUV suspensions were measured on a Zetasizer NanoZS (Malvern). CyaA and crotoxin were assayed for PLA activity at a final protein concentration of 600 nM and 100 nM, respectively. Lipid concentration of LUV in the cuvette was 200 μM, i.e., a lipid:protein molar ratio of 333 for CyaA and 2000 for crotoxin. Experiments were performed under constant stirring at 37 °C using a 109 004F cuvette (Hellma) in a Jasco fluorometer. Fluorescence excitation was fixed at 342 nm and the emission spectra were recorded from 350 to 600 nm each minute for 30 min. The 1-pyrenebutanoyl groups linked to the lipid acyl chains form excimers characterized by a maximum emission of fluorescence near 480 nm. Hydrolysis of acyl chains by a phospholipase releases a pyrene fatty acid that diffuses away from the pyrene lysophospholipd. These two pyrene derivatives exhibit a maximum emission of fluorescence between 380 and 400 nm [44,45].

Supplementary Materials: The following are available online at http://www.mdpi.com/2072-6651/11/2/111/s1, The supporting information contains two figures and two files that report the lists of the contaminant proteins identified by mass spectrometry in the IP CyaA samples, $CyaA_{IP}$, CyaA_IP_MS_result, and in the UBC CyaA sample, $CyaA_{UBC}$, CyaA_UBC_MS_result.

Author Contributions: Conceptualization, D.L. and A.C.; methodology, A.V., M.M., D.L. and A.C.; validation, M.M. and A.C.; investigation, A.V., M.S., D.R.-B. and T.D.; data curation, A.V. and T.D.; writing—original draft preparation, A.C.; writing—review and editing, A.V., D.L. and A.C.; visualization, A.V.; supervision, A.C.; project administration, A.C.

Funding: A.V. was supported by a DIM MalInf (infectious diseases) grant. M.S. was supported by the Erasmus+ program from the European Commission. We thank the CACSICE Equipex ANR-11-EQPX-0008. This research was funded by Institut Pasteur and CNRS. The APC was funded by Institut Pasteur.

Acknowledgments: We thank Helena Ostolaza for sharing her biological material, the CyaAUBC sample, and G. Faure for providing us purified crotoxin.

Conflicts of Interest: The authors declare no competing interests.

References

1. Ladant, D.; Brezin, C.; Alonso, J.M.; Crenon, I.; Guiso, N. Bordetella pertussis adenylate cyclase. Purification, characterization, and radioimmunoassay. *J. Biol. Chem.* **1986**, *261*, 16264–16269. [PubMed]
2. Glaser, P.; Danchin, A.; Ladant, D.; Barzu, O.; Ullmann, A. Bordetella pertussis adenylate cyclase: The gene and the protein. *Tokai J. Exp. Clin. Med.* **1988**, *13*, 239–252. [PubMed]
3. Glaser, P.; Ladant, D.; Sezer, O.; Pichot, F.; Ullmann, A.; Danchin, A. The calmodulin-sensitive adenylate cyclase of Bordetella pertussis: Cloning and expression in Escherichia coli. *Mol. Microbiol.* **1988**, *2*, 19–30. [CrossRef] [PubMed]
4. Guiso, N. Bordetella Adenylate Cyclase-Hemolysin Toxins. *Toxins* **2017**, *9*, 277. [CrossRef] [PubMed]
5. Novak, J.; Cerny, O.; Osickova, A.; Linhartova, I.; Masin, J.; Bumba, L.; Sebo, P.; Osicka, R. Structure-Function Relationships Underlying the Capacity of Bordetella Adenylate Cyclase Toxin to Disarm Host Phagocytes. *Toxins* **2017**, *9*, 300. [CrossRef] [PubMed]

6. Coote, J.G. Structural and functional relationships among the RTX toxin determinants of gram-negative bacteria. *FEMS Microbiol. Rev.* **1992**, *8*, 137–161. [CrossRef]
7. Welch, R.A. RTX toxin structure and function: A story of numerous anomalies and few analogies in toxin biology. *Curr. Top. in Microbiol. and Immunol.* **2001**, *257*, 85–111.
8. Linhartova, I.; Bumba, L.; Masin, J.; Basler, M.; Osicka, R.; Kamanova, J.; Prochazkova, K.; Adkins, I.; Hejnova-Holubova, J.; Sadilkova, L.; et al. RTX proteins: A highly diverse family secreted by a common mechanism. *FEMS Microbiol. Rev.* **2010**, *34*, 1076–1112. [CrossRef] [PubMed]
9. Chenal, A.; Sotomayor Perez, A.C.; Ladant, D. Structure and function of RTX Toxins. In *The Comprehensive Sourcebook of Bacterial Protein Toxins*, 4th ed.; Elsevier: Amsterdam, The Netherlands, 2015.
10. Benz, R. Channel formation by RTX-toxins of pathogenic bacteria: Basis of their biological activity. *Biochim. Biophys. Acta.* **2016**, *1858*, 526–537. [CrossRef] [PubMed]
11. Ladant, D.; Ullmann, A. Bordatella pertussis adenylate cyclase: A toxin with multiple talents. *Trends Microbiol.* **1999**, *7*, 172–176. [CrossRef]
12. Karst, J.C.; Ntsogo Enguene, V.Y.; Cannella, S.E.; Subrini, O.; Hessel, A.; Debard, S.; Ladant, D.; Chenal, A. Calcium, Acylation, and Molecular Confinement Favor Folding of Bordetella pertussis Adenylate Cyclase CyaA Toxin into a Monomeric and Cytotoxic Form. *J. Biol. Chem.* **2014**, *289*, 30702–30716. [CrossRef] [PubMed]
13. Ladant, D. Interaction of Bordetella pertussis adenylate cyclase with calmodulin. Identification of two separated calmodulin-binding domains. *J. Biol. Chem.* **1988**, *263*, 2612–2618. [PubMed]
14. Karst, J.C.; Sotomayor Perez, A.C.; Guijarro, J.I.; Raynal, B.; Chenal, A.; Ladant, D. Calmodulin-induced conformational and hydrodynamic changes in the catalytic domain of Bordetella pertussis adenylate cyclase toxin. *Biochemistry* **2010**, *49*, 318–328. [CrossRef] [PubMed]
15. O'Brien, D.P.; Durand, D.; Voegele, A.; Hourdel, V.; Davi, M.; Chamot-Rooke, J.; Vachette, P.; Brier, S.; Ladant, D.; Chenal, A. Calmodulin fishing with a structurally disordered bait triggers CyaA catalysis. *PLoS Biol.* **2017**, *15*, e2004486. [CrossRef]
16. Karst, J.C.; Barker, R.; Devi, U.; Swann, M.J.; Davi, M.; Roser, S.J.; Ladant, D.; Chenal, A. Identification of a region that assists membrane insertion and translocation of the catalytic domain of Bordetella pertussis CyaA toxin. *J. Biol. Chem.* **2012**, *287*, 9200–9212. [CrossRef] [PubMed]
17. Subrini, O.; Sotomayor-Perez, A.C.; Hessel, A.; Spiaczka-Karst, J.; Selwa, E.; Sapay, N.; Veneziano, R.; Pansieri, J.; Chopineau, J.; Ladant, D.; et al. Characterization of a membrane-active peptide from the Bordetella pertussis CyaA toxin. *J. Biol. Chem.* **2013**, *288*, 32585–32598. [CrossRef] [PubMed]
18. Masin, J.; Osickova, A.; Sukova, A.; Fiser, R.; Halada, P.; Bumba, L.; Linhartova, I.; Osicka, R.; Sebo, P. Negatively charged residues of the segment linking the enzyme and cytolysin moieties restrict the membrane-permeabilizing capacity of adenylate cyclase toxin. *Sci. Rep.* **2016**, *6*, 29137. [CrossRef] [PubMed]
19. Voegele, A.; Subrini, O.; Sapay, N.; Ladant, D.; Chenal, A. Membrane-Active Properties of an Amphitropic Peptide from the CyaA Toxin Translocation Region. *Toxins* **2017**, *9*, 369. [CrossRef]
20. Knapp, O.; Maier, E.; Masin, J.; Sebo, P.; Benz, R. Pore formation by the Bordetella adenylate cyclase toxin in lipid bilayer membranes: Role of voltage and pH. *Biochim. Biophys. Acta* **2008**, *1778*, 260–269. [CrossRef]
21. Basler, M.; Knapp, O.; Masin, J.; Fiser, R.; Maier, E.; Benz, R.; Sebo, P.; Osicka, R. Segments crucial for membrane translocation and pore-forming activity of Bordetella adenylate cyclase toxin. *J. Biol. Chem.* **2007**, *282*, 12419–12429. [CrossRef]
22. Barry, E.M.; Weiss, A.A.; Ehrmann, I.E.; Gray, M.C.; Hewlett, E.L.; Goodwin, M.S. Bordetella pertussis adenylate cyclase toxin and hemolytic activities require a second gene, cyaC, for activation. *J. Bacteriol.* **1991**, *173*, 720–726. [CrossRef]
23. Hackett, M.; Guo, L.; Shabanowitz, J.; Hunt, D.F.; Hewlett, E.L. Internal lysine palmitoylation in adenylate cyclase toxin from Bordetella pertussis. *Science* **1994**, *266*, 433–435. [CrossRef] [PubMed]
24. Westrop, G.D.; Hormozi, E.K.; Da Costa, N.A.; Parton, R.; Coote, J.G. Bordetella pertussis adenylate cyclase toxin: proCyaA and CyaC proteins synthesised separately in Escherichia coli produce active toxin in vitro. *Gene* **1996**, *180*, 91–99. [CrossRef]
25. Veneziano, R.; Rossi, C.; Chenal, A.; Devoisselle, J.M.; Ladant, D.; Chopineau, J. Bordetella pertussis adenylate cyclase toxin translocation across a tethered lipid bilayer. *Proc. Natl. Acad. Sci. USA* **2013**, *110*, 20473–20478. [CrossRef] [PubMed]

26. Rose, T.; Sebo, P.; Bellalou, J.; Ladant, D. Interaction of calcium with Bordetella pertussis adenylate cyclase toxin. Characterization of multiple calcium-binding sites and calcium-induced conformational changes. *J. Biol. Chem.* **1995**, *270*, 26370–26376. [CrossRef]
27. Chenal, A.; Guijarro, J.I.; Raynal, B.; Delepierre, M.; Ladant, D. RTX calcium binding motifs are intrinsically disordered in the absence of calcium: Implication for protein secretion. *J. Biol. Chem.* **2009**, *284*, 1781–1789. [CrossRef] [PubMed]
28. Sotomayor Perez, A.C.; Karst, J.C.; Davi, M.; Guijarro, J.I.; Ladant, D.; Chenal, A. Characterization of the regions involved in the calcium-induced folding of the intrinsically disordered RTX motifs from the bordetella pertussis adenylate cyclase toxin. *J. Mol. Biol.* **2010**, *397*, 534–549. [CrossRef] [PubMed]
29. Chenal, A.; Karst, J.C.; Sotomayor Perez, A.C.; Wozniak, A.K.; Baron, B.; England, P.; Ladant, D. Calcium-induced folding and stabilization of the intrinsically disordered RTX domain of the CyaA toxin. *Biophys. J.* **2010**, *99*, 3744–3753. [CrossRef] [PubMed]
30. Sotomayor-Perez, A.C.; Ladant, D.; Chenal, A. Calcium-induced folding of intrinsically disordered repeat-in-toxin (RTX) motifs via changes of protein charges and oligomerization states. *J. Biol. Chem.* **2011**, *286*, 16997–17004. [CrossRef] [PubMed]
31. Sotomayor-Perez, A.C.; Subrini, O.; Hessel, A.; Ladant, D.; Chenal, A. Molecular Crowding Stabilizes Both the Intrinsically Disordered Calcium-Free State and the Folded Calcium-Bound State of a Repeat in Toxin (RTX) Protein. *J. of the Am. Chem. Soc.* **2013**, *135*, 11929–11934. [CrossRef]
32. Sotomayor-Perez, A.C.; Ladant, D.; Chenal, A. Disorder-to-order transition in the CyaA toxin RTX domain: Implications for toxin secretion. *Toxins* **2015**, *7*, 1–20. [CrossRef] [PubMed]
33. O'Brien, D.P.; Hernandez, B.; Durand, D.; Hourdel, V.; Sotomayor-Perez, A.C.; Vachette, P.; Ghomi, M.; Chamot-Rooke, J.; Ladant, D.; Brier, S.; et al. Structural models of intrinsically disordered and calcium-bound folded states of a protein adapted for secretion. *Sci. Rep.* **2015**, *5*, 14223. [CrossRef] [PubMed]
34. Bumba, L.; Masin, J.; Macek, P.; Wald, T.; Motlova, L.; Bibova, I.; Klimova, N.; Bednarova, L.; Veverka, V.; Kachala, M.; et al. Calcium-Driven Folding of RTX Domain beta-Rolls Ratchets Translocation of RTX Proteins through Type I Secretion Ducts. *Mol. Cell* **2016**, *62*, 47–62. [CrossRef] [PubMed]
35. O'Brien, D.P.; Perez, A.C.S.; Karst, J.; Cannella, S.E.; Enguene, V.Y.N.; Hessel, A.; Raoux-Barbot, D.; Voegele, A.; Subrini, O.; Davi, M.; et al. Calcium-dependent disorder-to-order transitions are central to the secretion and folding of the CyaA toxin of Bordetella pertussis, the causative agent of whooping cough. *Toxicon* **2018**, *149*, 37–44. [CrossRef] [PubMed]
36. El-Azami-El-Idrissi, M.; Bauche, C.; Loucka, J.; Osicka, R.; Sebo, P.; Ladant, D.; Leclerc, C. Interaction of Bordetella pertussis adenylate cyclase with CD11b/CD18: Role of toxin acylation and identification of the main integrin interaction domain. *J. Biol. Chem.* **2003**, *278*, 38514–38521. [CrossRef] [PubMed]
37. Fedele, G.; Schiavoni, I.; Adkins, I.; Klimova, N.; Sebo, P. Invasion of Dendritic Cells, Macrophages and Neutrophils by the Bordetella Adenylate Cyclase Toxin: A Subversive Move to Fool Host Immunity. *Toxins* **2017**, *9*, 293. [CrossRef] [PubMed]
38. Gonzalez-Bullon, D.; Uribe, K.B.; Martin, C.; Ostolaza, H. Phospholipase A activity of adenylate cyclase toxin mediates translocation of its adenylate cyclase domain. *Proc. Natl. Acad. Sci. USA* **2017**, *114*, E6784–E6793. [CrossRef] [PubMed]
39. Gonzalez-Bullon, D.; Martin, C.; Ostolaza, H. Characterization of the Intrinsic Phospholipase A1 Activity of Bordetella pertussis Adenylate Cyclase Toxin. *Toxins* **2018**, *10*, 514. [CrossRef] [PubMed]
40. Bumba, L.; Masin, J.; Osickova, A.; Osicka, R.; Sebo, P. Bordetella Pertussis Adenylate Cyclase Toxin Does Not Possess a Phospholipase A Activity; Serine 606 and Aspartate 1079 Residues Are Not Involved in Target Cell Delivery of the Adenylyl Cyclase Enzyme Domain. *Toxins* **2018**, *10*, 245. [CrossRef]
41. Cannella, S.E.; Ntsogo Enguene, V.Y.; Davi, M.; Malosse, C.; Sotomayor Perez, A.C.; Chamot-Rooke, J.; Vachette, P.; Durand, D.; Ladant, D.; Chenal, A. Stability, structural and functional properties of a monomeric, calcium-loaded adenylate cyclase toxin, CyaA, from Bordetella pertussis. *Sci. Rep.* **2017**, *7*, 42065. [CrossRef]
42. Ostrowski, M.; Porowinska, D.; Prochnicki, T.; Prevost, M.; Raynal, B.; Baron, B.; Sauguet, L.; Corringer, P.J.; Faure, G. Neurotoxic phospholipase A2 from rattlesnake as a new ligand and new regulator of prokaryotic receptor GLIC (proton-gated ion channel from G. violaceus). *Toxicon* **2016**, *116*, 63–71. [CrossRef] [PubMed]
43. Hendrickson, H.S.; Rauk, P.N. Continuous fluorometric assay of phospholipase A2 with pyrene-labeled lecithin as a substrate. *Anal. Biochem.* **1981**, *116*, 553–558. [CrossRef]

44. Cox, J.; Mann, M. MaxQuant enables high peptide identification rates, individualized p.p.b.-range mass accuracies and proteome-wide protein quantification. *Nat. Biotechnol.* **2008**, *26*, 1367–1372. [CrossRef] [PubMed]
45. Faure, G.; Xu, H.; Saul, F.A. Crystal structure of crotoxin reveals key residues involved in the stability and toxicity of this potent heterodimeric beta-neurotoxin. *J. Mol. Bio.* **2011**, *412*, 176–191. [CrossRef] [PubMed]
46. Aarsman, A.J.; Vandeenen, L.L.M.; Vandenbosch, H. Studies on Lysophospholipases VII. Synthesis of Acylthioester Analogs of Lysolecithin and Their Use in a Continuous Spectrophotometric Assay for Lysophospholipases, a Method with Potential Applicability to Other Lipolytic Enzymes. *Bioorg. Chem.* **1976**, *5*, 241–253. [CrossRef]
47. Cox, J.; Neuhauser, N.; Michalski, A.; Scheltema, R.A.; Olsen, J.V.; Mann, M. Andromeda: A peptide search engine integrated into the MaxQuant environment. *J. Proteome Res.* **2011**, *10*, 1794–1805. [CrossRef] [PubMed]



© 2019 by the authors. Licensee MDPI, Basel, Switzerland. This article is an open access article distributed under the terms and conditions of the Creative Commons Attribution (CC BY) license (http://creativecommons.org/licenses/by/4.0/).

Supplementary Materials: The Adenylate Cyclase (CyaA) Toxin from Bordetella pertussis Has No Detectable Phospholipase A (PLA) Activity *in Vitro*

Alexis Voegele, Mirko Sadi, Dorothée Raoux-Barbot, Tohibaut Douché, Mariette Matondo, Daniel Ladant and Alexandre Chenal

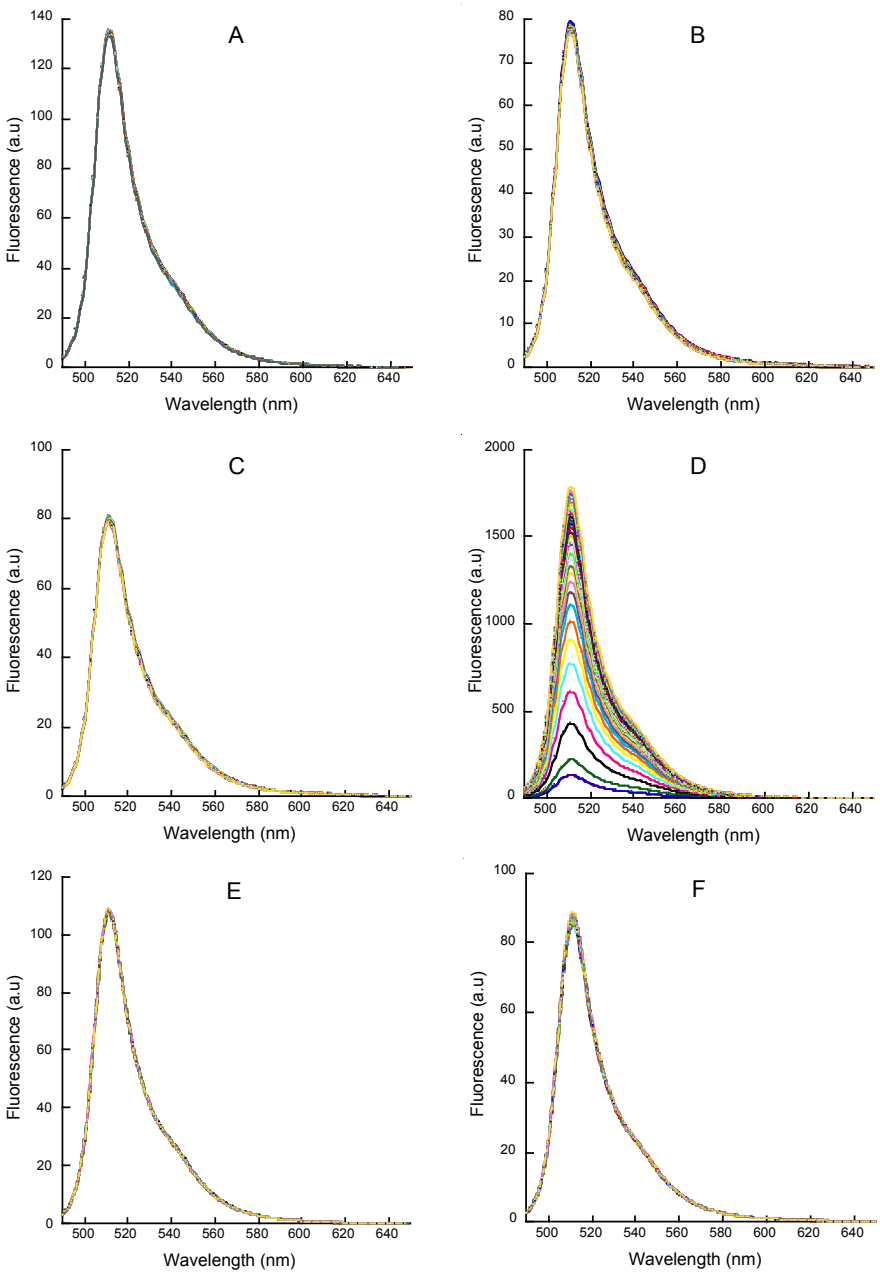

Figure S1. Phospholipase assay using PED6 as fluorogenic substrate for PLA2 activity. LUV made of DOPC: PED6 at a molar ratio 8:2 were incubated at 37 °C under constant stirring in (**A**) buffer 20 mM HEPES, 150 mM NaCl, 10 mM $CaCl_2$ pH 7,4, completed with: (**B**) urea at 60 mM final concentration, (**C**) BSA at 10 nM, (**D**) Crotoxin at 10 nM, (**E**) CyaA$_{IP}$ at 10 nM and (**F**) CyaA$_{UBC}$ at 10 nM. Excitation was set at 480 nm and fluorescence emission spectra were recorded from 490 to 650 nm, every minute for 30 min.

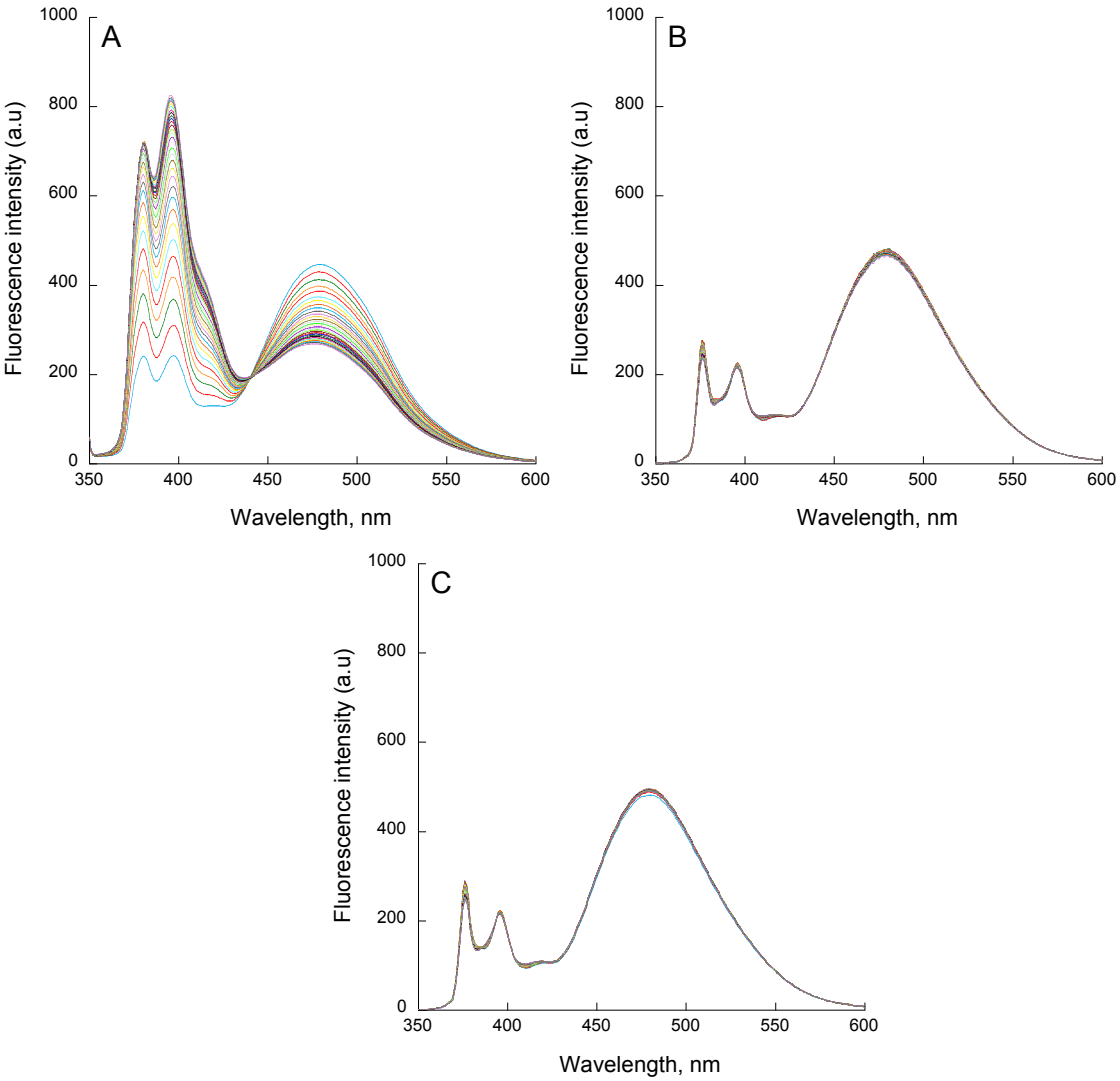

Figure S2. Phospholipase assay using B3781 as fluorogenic substrate for PLA2 activity. LUV made of POPC: POPG: B3781 79:20:1 were incubated at 37 °C under constant stirring in presence of (**A**) Crotoxin at 100 nM, (**B**) CyaA$_{IP}$ at 600 nM, (**C**) urea at 180 mM final concentration. Excitation was set at 342 nm and fluorescence emission spectra were recorded from 350 to 600 nm, every minute for 30 min. The excimer band at 480 nm decreases while the monomeric bands (in between 360–400 nm) of acylated pyrene derivatives increases over the time course of the experiment.

Review IV

Translocation and calmodulin-activation of the adenylate cyclase toxin (CyaA) of *Bordetella pertussis*

Alexis Voegele, Darragh P. O'Brien, Orso Subrini, Nicolas Sapay, Sara E. Cannella, Véronique Yvette Ntsogo Enguéné, Audrey Hessel, Johanna Karst, Rémi Veneziano, Joel Chopineau, Patrice Vachette, Dominique Durand, Sébastien Brier, Daniel Ladant and Alexandre Chenal

Pathogens and disease
Volume 76(8)
November 2018

The CyaA toxin has the unique capacity to translocate its catalytic domain (ACD) across the plasma membrane. Once in the cell, ACD binds to calmodulin (CaM) and produces high levels of cAMP, leading to cell death. Although several mechanisms of translocation of the toxin have been proposed over the years, it remains poorly understood. In the lab, we identified the segment P454 (*i.e* residues 454-484) in the translocation region, exhibiting membrane-active properties (*i.e* insertion, folding and permeabilization upon membrane interaction) (Subrini et al., 2013; Karst et al., 2012). This review introduces recent data obtained in our lab about the P454 peptide and its membrane-active properties. It also describes what are the parameters needed for ACD translocation and how ACD is activated by CaM upon translocation. All these data will be described in more details in the following articles V and VII.

We first investigated the membrane interaction properties of P454. We found that P454 partition is favored by negatively charged and unsaturated lipids. We also focused on the contribution of the two arginine residues of P454 (R461 and R474) on its membrane active properties. We found that both arginine are involved in membrane partition. We further identified that R474 contributes to α-helix formation and R461 to the permeabilization process.

We studied other amphipathic regions of CyaA suggested to have membrane-active properties. Interestingly, we identified P454 as the unique peptide able to interact with membranes, adopting a helical structure upon interaction and permeabilize membranes. We propose that P454 may locally destabilize membrane integrity to favor ACD translocation.

The translocation of ACD is dependent on several parameters. Using an *in vitro* tethered lipid bilayer, it has been found that CyaA can deliver ACD without any eukaryotic components except CaM. Furthermore, the translocation is dependent on negative membrane potential, acylation of CyaA and also calcium ions in solution. In fact, calcium is critical for the CyaA folding. In absence of calcium, CyaA does not (i) fold, (ii) interact with membranes and (iii) translocate ACD. Free calcium in solution is also required for ACD translocation.

Finally, when translocated, ACD binds to CaM to produce cAMP. Using a combination of biophysical approaches, we showed that ACD possesses a region of over 75 disordered residues. The complex formation is associated with disorder-to-order transition of this region and also allosteric effects in other regions. We propose that upon ACD:CaM interaction, this

disordered region binds CaM and contributes to structural rearrangement of ACD and stabilization of the catalytic site.

In summary, we propose that P454 may locally destabilize the membrane, decreasing the energy required for ACD translocation. Inside cell, the binding of ACD to CaM induced structural rearrangements that stabilize the catalytic site, leading to overproduction of cAMP.

Pathogens and Disease, 76, 2018, fty085

doi: 10.1093/femspd/fty085
Advance Access Publication Date: 18 November 2018
Minireview

MINIREVIEW

Translocation and calmodulin-activation of the adenylate cyclase toxin (CyaA) of *Bordetella pertussis*

Alexis Voegele[1,2,†], Darragh P. O'Brien[1,3], Orso Subrini[1], Nicolas Sapay[4], Sara E Cannella[1,3], Véronique Yvette Ntsogo Enguéné[1], Audrey Hessel[1], Johanna Karst[1], Véronique Hourdel[1], Ana Cristina Sotomayor Perez[1], Marilyne Davi[1], Rémi Veneziano[5,6], Joel Chopineau[5], Patrice Vachette[7], Dominique Durand[7], Sébastien Brier[1], Daniel Ladant[1] and Alexandre Chenal[1,*,‡]

[1]Département de Biologie Structurale et Chimie, Institut Pasteur, CNRS UMR 3528, 28 Rue du Dr Roux, 75724 Paris, CEDEX 15, France, [2]Université Paris Diderot Paris VII, 75013 Paris, France, [3]University of Oxford, United Kingdom, [4]Bioaster Technology Research Institute, 69007 Lyon, France, [5]ICGM, UMR 5253 Univ Montpellier, CNRS, ENSCM, Montpellier 34095, France, [6]Department of Bioengineering, Volgenau School of Engineering, George Mason University, Fairfax, VA 22030-4422, USA and [7]Institute for Integrative Biology of the Cell (I2BC), CEA, CNRS, Univ. Paris-Sud, Université Paris-Saclay, Gif-sur-Yvette cedex 91198, France

[*]**Corresponding author:** Tel: 00 33 1 44 38 92 12; E-mail: chenal@pasteur.fr
One sentence summary: The studies performed in our lab on the mechanism of translocation and calmodulin-activation of the CyaA catalytic domain are presented in this review.
Editor: Michel Popoff
[†]Alexis Voegele, http://orcid.org/0000-0002-0452-6814
[‡]Alexandre Chenal, http://orcid.org/0000-0002-4959-1003

ABSTRACT

The adenylate cyclase toxin (CyaA) is a multi-domain protein secreted by *Bordetella pertussis*, the causative agent of whooping cough. CyaA is involved in the early stages of respiratory tract colonization by *Bordetella pertussis*. CyaA is produced and acylated in the bacteria, and secreted via a dedicated secretion system. The cell intoxication process involves a unique mechanism of transport of the CyaA toxin catalytic domain (ACD) across the plasma membrane of eukaryotic cells. Once translocated, ACD binds to and is activated by calmodulin and produces high amounts of cAMP, subverting the physiology of eukaryotic cells. Here, we review our work on the identification and characterization of a critical region of CyaA, the translocation region, required to deliver ACD into the cytosol of target cells. The translocation region contains a segment that exhibits membrane-active properties, i.e. is able to fold upon membrane interaction and permeabilize lipid bilayers. We proposed that this region is required to locally destabilize the membrane, decreasing the energy required for ACD translocation. To further study the translocation process, we developed a tethered bilayer lipid membrane (tBLM) design that recapitulate the ACD transport across a membrane separating two hermetic compartments. We showed that ACD translocation is critically dependent on calcium, membrane potential, CyaA acylation and on the presence of

Received: 6 September 2018; **Accepted:** 16 November 2018
© FEMS 2018. All rights reserved. For permissions, please e-mail: journals.permissions@oup.com

Downloaded from https://academic.oup.com/femspd/article-abstract/76/8/fty085/5188676 by Institut Pasteur user on 08 March 2019

calmodulin in the trans compartment. Finally, we describe how calmodulin-binding triggers key conformational changes in ACD, leading to its activation and production of supraphysiological concentrations of cAMP.

Keywords: adenylate cyclase; CyaA; Bordetella pertussis; membrane translocation; membrane-active properties; protein folding; intrinsically disordered protein; ATP; cAMP; calmodulin

INTRODUCTION

The adenylate cyclase (CyaA) toxin produced by *Bordetella pertussis*, the causative agent of whooping cough, is one of the major virulence factors of this bacterium (Ladant *et al.* 1986; Glaser *et al.* 1988a,b; Guiso 2017; Novak *et al.* 2017). CyaA plays a central role in the early stages of respiratory tract colonization by *B. pertussis*. This toxin uses an original intoxication mechanism, secreted by the virulent bacteria, and it is able to invade eukaryotic target cells through a unique but poorly understood mechanism that involves a direct translocation of the catalytic domain across the plasma membrane. CyaA is a 1706-residue long multi-domain protein (Ladant and Ullmann 1999; Karst *et al.* 2014). The ATP-cyclizing, calmodulin-activated, catalytic domain (adenylate cyclase domain, ACD) is located in the 364 N-terminal residues (Ladant 1988; Karst *et al.* 2010; O'Brien *et al.* 2017), while. the C-terminal part of the toxin is required for ACD translocation and responsible for the hemolytic phenotype of *B. pertussis*. The domains of CyaA are presented in Fig. 1, and their boundaries are proposed based on functional, structural and *in silico* analyses. The translocation region (TR, residues 365–527) is essential for ACD translocation into target cells and exhibits properties related to membrane-active peptides (Karst *et al.* 2012; Subrini *et al.* 2013; Voegele *et al.* 2017). The hydrophobic region, HR, located between residues 528 and 710 of CyaA, is able to insert into the cell membrane and make cation-selective pores (Basler *et al.* 2007; Knapp *et al.* 2008; Benz 2016). The acylation region, spanning residues 711 to 1005, contains two post-translational acylation sites required for efficient CyaA refolding (Karst *et al.* 2014) and ACD translocation (Barry *et al.* 1991; Hackett *et al.* 1994; Veneziano *et al.* 2013; Novak *et al.* 2017). The toxin is synthesized as an inactive precursor, pro-CyaA, which is unable to translocate the catalytic domain across the plasma membrane of target cells. The CyaC protein, a dedicated acyltransferase, catalyzes the transfer of an acyl chain from acyl-ACP (acyl-carrier protein) to the epsilon-amino groups of pro-CyaA lysines K860 and K983 (Barry *et al.* 1991; Hackett *et al.* 1994; Westrop *et al.* 1996). This specific acylation converts the pro-CyaA species into the active CyaA toxin. The C-terminal part of the toxin corresponds to the cell receptor-binding domain (RD, residues 1006–1706; El-Azami-El-Idrissi *et al.* 2003; see Fedele *et al.* (2017) for a review). RD is made of about 40 copies of a calcium-binding, glycine and aspartate-rich nonapeptide repeat that is characteristic of a large family of bacterial cytolysins known as RTX (Repeat-in-ToXin) toxins (Linhartova *et al.* 2010; Chenal, Sotomayor Perez and Ladant 2015; Benz 2016). These motifs constitute the main Ca^{2+} binding sites of the protein that binds up to ≈40 calcium ions with sub-millimolar affinity (Rose *et al.* 1995). Calcium binding is critical for the proper folding of CyaA into its cytotoxic form (for a review see O'Brien *et al.* (2018b)).

Figure 2 illustrates the intoxication process of target cells by CyaA. Once produced and acylated in the bacteria, CyaA is secreted across the bacterial envelope by a dedicated type I secretion system (T1SS) made of CyaB, CyaD and CyaE proteins (Glaser *et al.* 1988c; Masure *et al.* 1990). The T1SS recognizes a secretion signal located at the C-terminal end of CyaA (Fig. 1). Once secreted through the narrow channel of the T1SS, the toxin binds calcium and folds in the extracellular milieu. RD exhibits the hallmarks of intrinsically disordered proteins, and the binding of calcium induces a disorder-to-order transition (Bauche *et al.* 2006; Chenal *et al.* 2009, 2010; Sotomayor Perez *et al.* 2010; Sotomayor-Perez, Ladant and Chenal 2011; Sotomayor-Perez *et al.* 2013; O'Brien *et al.* 2015; Sotomayor-Perez, Ladant and Chenal 2015; O'Brien *et al.* 2017, 2018b). We proposed that this conformational transition occurs upon secretion of the toxin through the T1SS, from the low-calcium environment (i.e. μM) of the bacterial cytosol to the calcium-rich extracellular environment (i.e. mM). Holo-RD may then act as a structural template for the refolding of CyaA (Karst *et al.* 2014; Cannella *et al.* 2017). CyaA can intoxicate various cell types such as erythrocytes in a calcium-dependent manner and in the absence of specific receptor. CyaA, however, binds with high affinity to a subset of leukocytes (neutrophiles, dendritic cells (DC) and macrophages) via a cell receptor, the CD11b/CD18 integrin (Guermonprez *et al.* 2001, 2002; Masin *et al.* 2005; Fiser *et al.* 2007; Svedova *et al.* 2016). This specific interaction between CyaA and DC via the CD11b/CD18 integrin paved the road for the use of CyaA as an antigen-delivery vehicle for immunotherapy (Adkins *et al.* 2012; Chenal and Ladant 2018). Irrespective of the presence of the CD11b/CD18 integrin, CyaA does translocate its ACD directly across the plasma membrane into the cytoplasm of the target cell (Fiser *et al.* 2007; Bumba *et al.* 2010; Karst *et al.* 2012; Uribe *et al.* 2013a,b; Veneziano *et al.* 2013). The high-affinity binding of endogenous calmodulin (CaM, located into the cytosol of the intoxicated cell) to ACD induces its stabilization into its active state that displays a very high catalytic turnover (Karst *et al.* 2010; O'Brien *et al.* 2017). The ACD:CaM complex produces supraphysiological levels of cAMP at the expense of ATP (Sakamoto *et al.* 1992; Ladant and Ullmann 1999), thus subverting the cell physiology and eventually leading to cell death (Ladant and Ullmann 1999; Vojtova, Kamanova and Sebo 2006).

In this review, we discuss our recent results focusing on the mechanisms of translocation of the catalytic domain and the calmodulin-induced conformational changes leading to the activation of its enzymatic activity.

THE TR OF CYAA EXHIBITS MEMBRANE-ACTIVE PROPERTIES

The most original property of CyaA is its ability to translocate its ACD across the plasma membrane into the cytoplasm of the target cells (Ladant and Ullmann 1999). The current translocation model posits that after binding to the CD11b/CD18 receptor, HR may insert into the plasma membrane to irreversibly anchor the toxin to the target cells. Then, ACD is directly translocated across the plasma membrane of these cells into the

Downloaded from https://academic.oup.com/femspd/article-abstract/76/8/fty085/5188676 by Institut Pasteur user on 08 March 2019

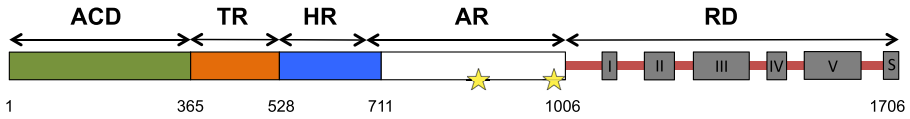

Figure 1. Schematic representation of the CyaA toxin. CyaA comprises five main regions, the adenylate cyclase catalytic domain (ACD), the translocation region (TR), the hydrophobic region (HR), the acylation region (AR) and the C-terminal RTX domain (RD). Native numbering of CyaA is given as rough indication and does not correspond to precise boundaries between CyaA regions. The two acyl-chains are represented by yellow stars

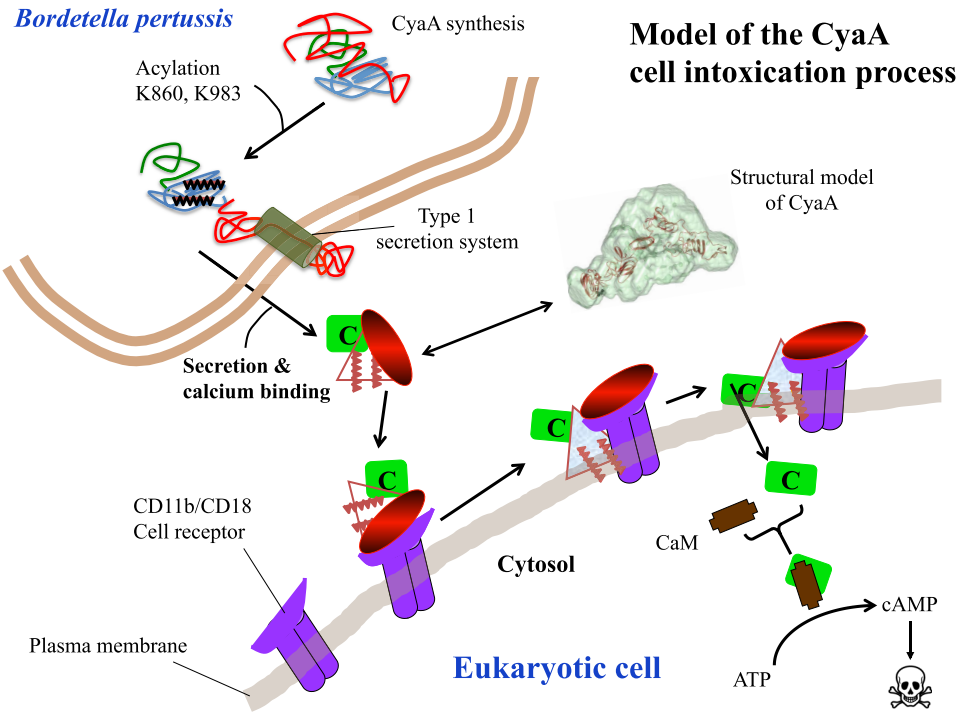

Figure 2. Model of the intoxication process of eukaryotic cells by CyaA. CyaA is produced, acylated and secreted through the T1SS. The folding of the toxin is induced by calcium binding in the extracellular environment. Pore-forming activity and ACD translocation into eukaryotic cells can be both performed in the absence and in the presence of its cell receptor. The molecular envelope of the monomeric CyaA species is shown in green and the structural model of holo-RD in red.

cytosol. In recent years, we provided direct evidence that a region located between ACD and HR (i.e. residues 365–527), which we named the translocation region, TR, is crucial for the translocation of ACD across the plasma membrane (Karst *et al.* 2012). Indeed, the deletion of this region abolishes the ability of CyaA to translocate ACD while it does not affect its ability to bind to target cells nor its hemolytic activity (Karst *et al.* 2012).

In silico predictions suggest that TR contains structural disorder, punctuated by several helical regions, as shown in Fig. 3 with the secondary structure prediction software SOPMA (Geourjon and Deleage 1995). We produced four peptides covering these predicted helical sequences and showed that only the P454 peptide (residues 454–484 of CyaA) exhibits properties related to membrane-active peptides (Subrini *et al.* 2013; Voegele *et al.* 2017). We characterized the membrane-active properties of P454 by various biophysical approaches and showed that P454 (i) binds to membranes, (ii) adopts a helical structure oriented in plane with respect to the lipid bilayer and (iii) permeabilizes lipid vesicles (Figs 4 and 5). These experimental observations were supported by molecular dynamics computations (Fig. 5).

We have also investigated the effect of lipid composition on P454 membrane partitioning. We observed that the lipid headgroup charge, acyl chain fluidity (i.e. acyl chain length and degree of saturation) and lipid polymorphism regulate P454 membrane binding. Indeed, negatively charged and unsaturated acyl chains favor P454 membrane partitioning, while negative membrane curvature and increased membrane rigidity (i.e. saturated acyl chains and cholesterol) decrease the partition of P454.

EFFECT OF ARGININE RESIDUES ON THE MEMBRANE-ACTIVE PROPERTIES OF P454

The affinity of P454 for negatively charged membranes (generally comprising 80% neutral lipids and 20% anionic lipids) may be explained by the presence of two arginine residues, R461 and R474. We characterized their respective

Downloaded from https://academic.oup.com/femspd/article-abstract/76/8/fty085/5188676 by Institut Pasteur user on 08 March 2019

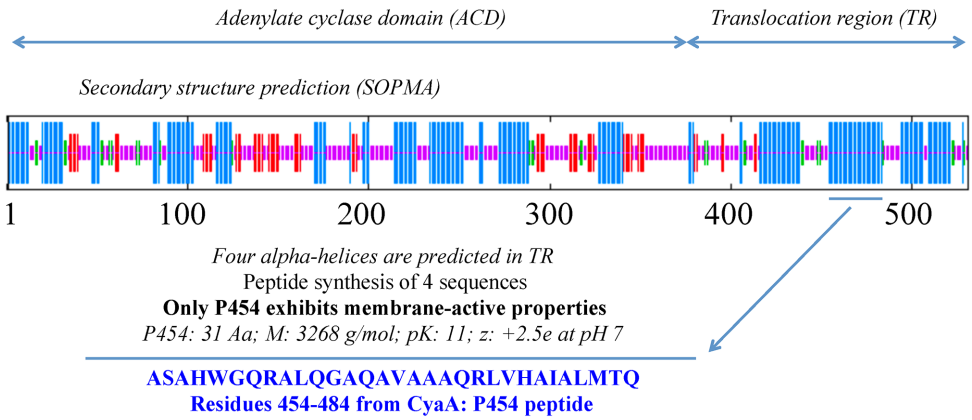

Figure 3. Secondary structure prediction of the ACD and TR regions of CyaA using the SOPMA software (Geourjon and Deleage 1995). The amino-acid sequence of P454 and some of its properties are highlighted.

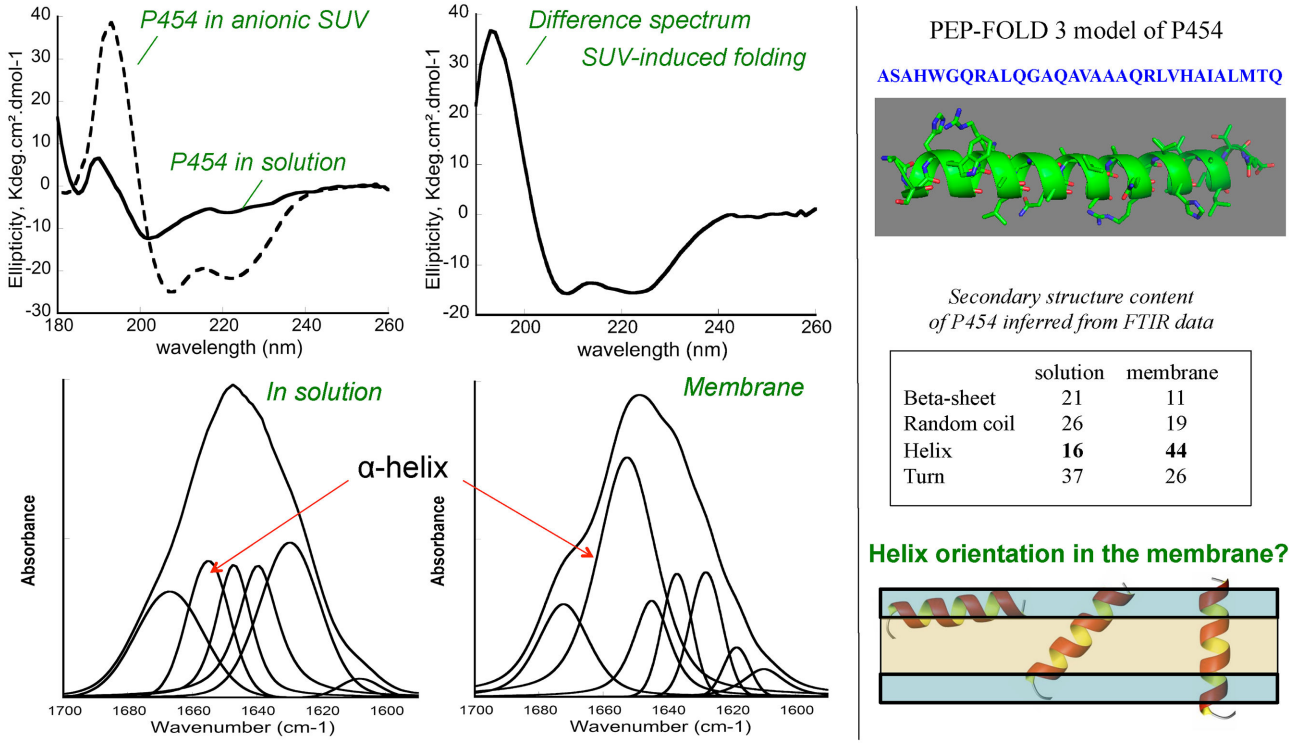

Figure 4. Structural characterization of the P454 peptide. Far-UV CD and FTIR data show that P454 is rather unfolded in solution and adopts a helical conformation once inserted into membranes. A structural model of P454 is shown using the *de novo* peptide structure prediction PEP-FOLD 3 software (Shen *et al.* 2014).

contributions to lipid bilayer insertion, membrane-induced secondary structure formation and membrane permeabilization. We found that both arginines are involved in membrane-active properties: the charge and permeabilization efficiency of the peptides correlate with the free energy of partitioning from the solution to membrane (Fig. 6). We further showed that R474 significantly contributes to helix formation, while R461 is primarily involved in the membrane permeabilization process (Fig. 6B).

We analyzed other regions of CyaA exhibiting amphiphilic properties. Based on their hydrophobicity, hydrophobic moment and helical propensity, we identified 10 amphiphilic sequences that might have membrane-active properties (Fig. 7). We produced these peptides, measured their membrane-binding propensity and their ability to permeabilize membranes (Subrini *et al.* 2013; Voegele *et al.* 2017). Interestingly, we noticed that some of them are not able *per se* to interact with membranes (yellow boxes, Fig. 7), some of them interact with membranes (orange boxes, Fig. 7), while P454 is the only one that interacts and permeabilizes membranes (red box, Fig. 7). Hence, P454 is the unique amphiphilic peptide from CyaA-derived peptides exhibiting membrane-active properties so far.

Taken together, our results suggest that the region encompassing the helix 454–484 of CyaA inserts into membrane and

Downloaded from https://academic.oup.com/femspd/article-abstract/76/8/fty085/5188676 by Institut Pasteur user on 08 March 2019

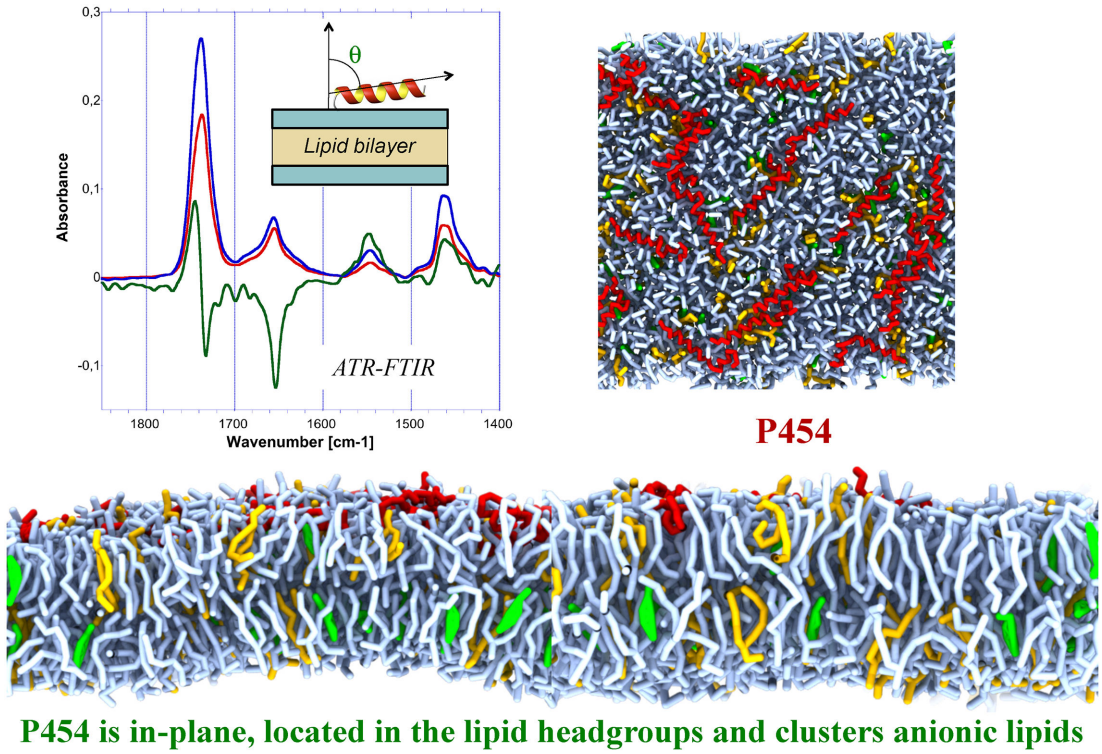

Figure 5. ATR-FTIR and molecular dynamics of the P454 peptide. ATR-FTIR of P454 in membrane indicates that the peptide adopts an in-plane orientation on the membrane. Molecular dynamics of P454 inserted into an anionic lipid bilayer. Snapshot of the system after 1 μs of molecular dynamics simulation at constant temperature (323.15 K) and pressure (1 bar). Red, P454 peptides; light blue, DOPC; green, cholesterol; yellow-orange, DOPG. For clarity, water is not depicted.

induces a local destabilization of the lipid bilayer. We propose that this local destabilization favors the initial steps of ACD translocation across the plasma membrane by decreasing the energy required for the polypeptide chain to cross the lipid bilayer.

TRANSLOCATION OF THE CATALYTIC DOMAIN ACROSS MEMBRANES

We have developed a method allowing us to follow *in vitro* the translocation of ACD across a single tethered lipid bilayer separating two aqueous compartments. This method is based on a home-made SPR sample cell housing a tethered bilayer lipid membrane (tBLM; Fig. 8). This device provides the opportunity to monitor protein membrane insertion and translocation across a lipid bilayer in the absence of the CD11b/CD18 toxin receptor (Veneziano *et al.* 2013, 2017). The compositions of the lipid bilayer, the buffers in the cis and trans compartments as well as the membrane potential are controlled.

In particular, using this tBLM/CaM system, we showed that CyaA is able to deliver its ACD across a biological membrane with no need for any eukaryotic component except CaM. Moreover, our data indicate that the presence of calcium in solution and CyaA acylation are crucial for ACD translocation. Finally, the translocation process is strictly dependent on the presence of a negative membrane potential established across the tethered lipid bilayer (Veneziano *et al.* 2013). Besides CyaA, this biomimetic tBLM/CaM design provides an opportunity to explore *in vitro* the molecular mechanisms of protein translocation across biological membranes in precisely defined conditions.

CALCIUM IS REQUIRED FROM CYAA FOLDING TO CYTOTOXIC ACTIVITY

Although the mechanism of translocation remains elusive, it is well established that calcium is required for the toxicity of CyaA. Indeed, calcium binding to CyaA is critical for its folding, its interaction with the eukaryotic cell receptor, for the translocation of the catalytic domain inside the host cell and for the pore-forming activity of CyaA (Bauche *et al.* 2006; Fiser *et al.* 2007; Knapp *et al.* 2008; Vojtova-Vodolanova *et al.* 2009; Bumba *et al.* 2010; Uribe *et al.* 2013; Veneziano *et al.* 2013; Karst *et al.* 2014; Cannella *et al.* 2017). The RTX domain (RD) of CyaA is directly implicated in these calcium-dependent activities as it harbors the main calcium-binding sites of the toxin.

CyaA, because of its large size and hydrophobicity, is prone to aggregation into multimeric and inactive forms. These constraints have seriously impeded reliable biophysical characterizations of the purified CyaA molecule. As a matter of fact, in most studies carried out up to now, CyaA has been extracted, purified and stored in denaturing conditions (usually in 6–8 M urea), and for functional studies on target cells, it is commonly refolded by directly diluting the protein stock solution into the cell medium.

Recently, we succeeded to fold CyaA in solution into a stable, monomeric and functional form by exploiting a molecular confinement strategy that efficiently prevented the aggregation of the polypeptide chains (at variance with prior procedures

Downloaded from https://academic.oup.com/femspd/article-abstract/76/8/fty085/5188676 by Institut Pasteur user on 08 March 2019

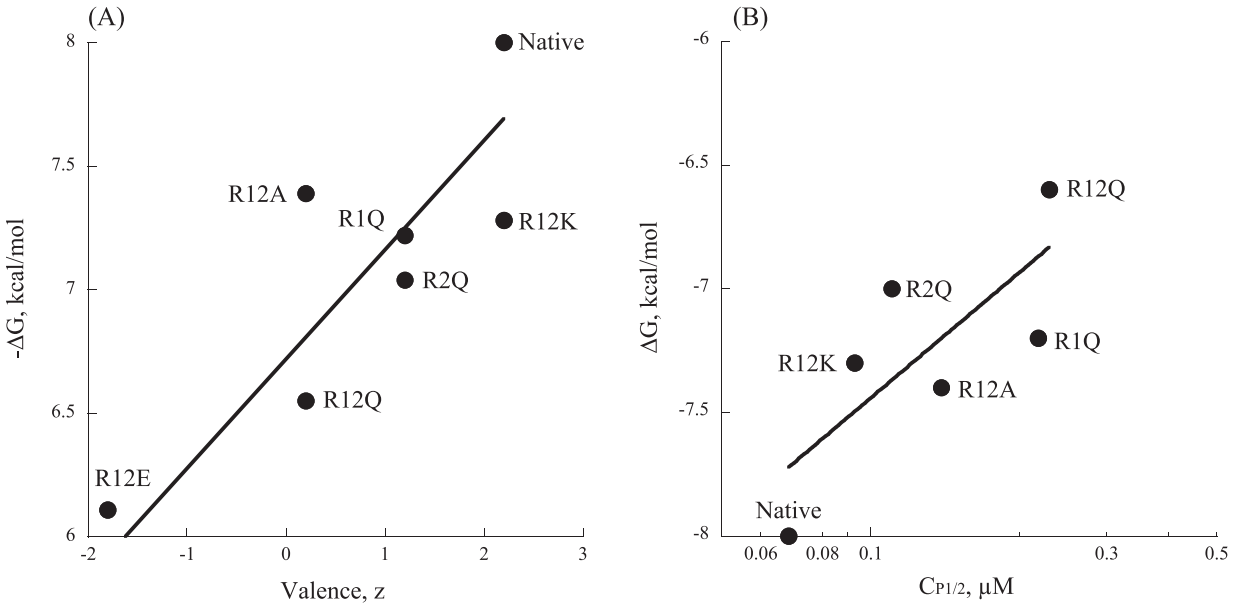

Figure 6. Contributions of the two arginines to membrane-active properties of P454. The free energy of membrane partitioning (**A**), membrane-induced helical formation (not shown here) and membrane permeabilization (**B**) was investigated. R461 (R1), R474 (R2) and both (R12) substitutions were introduced in P454. The two arginines (R1, R2 or both: R12) were substituted by lysines (R12K), glutamines (R1Q, R2Q and R12Q), alanines (R12A) and glutamates (R12E). In panel B, the CP1/2 values correspond to the peptide concentration inducing half permeabilization. See the original article for details (Voegele *et al.* 2017).

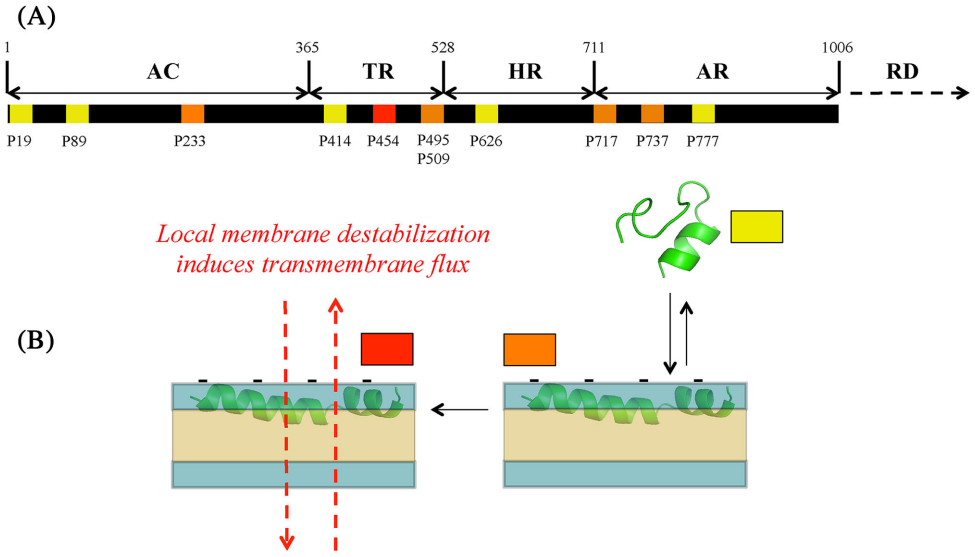

Figure 7. Schematic summarizing the amphiphilic peptides investigated so far. Some peptides do not interact by themselves with membranes (yellow boxes), most of them partition into membranes (orange boxes), while only P454 exhibits the ability to permeabilize membranes (red box). Some of the orange peptides are able to permeabilize membranes in the presence of a chemical gradient across the membrane (data not shown).

that generated mainly aggregated forms). We found that calcium ions are absolutely mandatory to allow refolding of CyaA into the monomeric state, while CyaA acylation strongly enhances the efficiency of the refolding process (Karst *et al.* 2014; Cannella *et al.* 2017; O'Brien *et al.* 2018b). The opportunity to produce a monomeric CyaA species opened the way to both structural and functional studies of the cytotoxic form.

Remarkably, we found that the monomeric, calcium-loaded CyaA form is able to induce both permeabilization of lipid bilayer vesicles and erythrocyte hemolysis even in the complete absence of free calcium in the medium, while the translocation of ACD into erythrocyte is strictly calcium dependent (with a half-maximum calcium concentration of ≈0.3 mM; Cannella *et al.* 2017).

This indicates that the calcium ions bound to CyaA monomer during its refolding process allow efficient binding of the toxin to erythrocytes and subsequent formation of cation-selective pores, but are not enough for ACD translocation that specifically requires free calcium in solution to proceed. Possibly, a chemical gradient of calcium across the membrane may contribute

Downloaded from https://academic.oup.com/femspd/article-abstract/76/8/fty085/5188676 by Institut Pasteur user on 08 March 2019

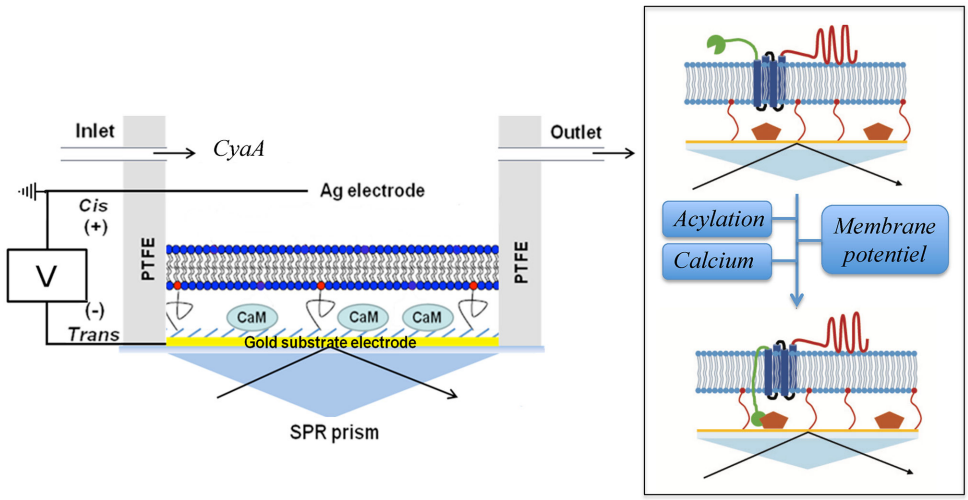

Figure 8. CyaA translocation across a tethered lipid bilayer. Principle of CyaA translocation assay on tBLM/CaM assembly. Schematic representation of the home-made SPR sample cell cross-section and tBLM/CaM construction. A tethered lipid bilayer (tBLM) is assembled on an amine–gold surface derivatized with calmodulin (CaM). The assembled bilayer forms a continuous and protein-impermeable boundary. CyaA binding to the immobilized CaM, revealed by enzymatic activity, serves as a highly sensitive reporter of toxin translocation across the bilayer. See Veneziano *et al.* (2013, 2017) for details.

part of the energy required for transport of ACD across the bilayer, in a process that might be defined as an ACD:Ca^{2+} influx as previously observed (Fiser *et al.* 2007). Besides, a calcium influx might also contribute to enhance ACD binding to intracellular CaM, although prior studies showed that the high affinity of ACD for its activator is not mandatory for translocation (Heveker and Ladant 1997). Further studies are needed to elucidate the precise structural and energetic contribution of calcium ions in the ACD translocation process.

A CALMODULIN-INDUCED DISORDER-TO-ORDER TRANSITION REGULATES ACD ACTIVATION

Once in the cytosol, ACD binds to calmodulin and produces supraphysiologic levels of cAMP (Sakamoto *et al.* 1992; Ladant and Ullmann 1999). We showed that calmodulin binding had a pronounced effect on the hydrodynamic properties of ACD (Karst *et al.* 2010). Recently, we used a combination of SEC-SAXS, SR-CD and HDX-MS data to generate structural models of the isolated ACD and CaM proteins and the ACD:CaM complex (O'Brien *et al.* 2018a). These data allowed us to propose a molecular model of the structural transition between the calmodulin-free and calmodulin-bound ACD (O'Brien *et al.* 2017). SEC-SAXS, SR-CD and HDX-MS provide direct evidence that the isolated ACD protein contains a region of 70 amino-acid residues characterized by structural disorder (Fig. 9). Noteworthy, this intrinsically disordered region (IDR) contains the molecular recognition feature (MoRF) motif required for the recruitment of CaM by ACD. The formation of the ACD:CaM complex is associated with a disorder-to-order transition of the MoRF, corresponding to the H-helix of ACD. This MoRF is a molecular hook, flanked by disordered regions, allowing a maximal flexibility and optimizing the fishing of the C-terminal lobe of CaM. Upon ACD:CaM complex formation, the region involved in binding is not the only affected by the interaction; allosteric effects are monitored in distal regions of the ACD:CaM complex, including the catalytic site of ACD that is significantly stabilized. The catalytic loop remains, however, largely dynamic, allowing for the fast uptake and release—on a sub-millisecond time scale—of substrate (ATP) and products (cAMP + PPi), needed to achieve high catalytic rates (higher than 1000 s^{-1}).

The presence of a large IDR in AC has major implications for the biological functions of the molecule. Firstly, the IDR and global structural disorder of the T18 moiety may contribute, via an 'entropic chain effect,' to destabilize the catalytic site and thus prevent cAMP synthesis, in the absence of the activator, most importantly when CyaA is synthesized in *Bordetella pertussis* (any significant basal activity would be toxic for the bacterial host). Secondly, the weak stability of the AC polypeptide should be favorable for delivery of the toxin from the bacterial host to the eukaryotic target cells; indeed, both CyaA secretion through the dedicated T1SS and AC translocation across the plasma membrane of target cells are dependent upon partial unfolding of the polypeptide chain (Gmira, Karimova and Ladant 2001; O'Brien *et al.* 2015). Thirdly, the intrinsic disorder of the central region of AC encompassing the main CaM-binding site could facilitate the efficient capture of the intracellular CaM through a 'fly-casting' mechanism. Hence, the CyaA toxin illustrates nicely how disorder-to-order transitions can be harnessed to finely tune protein activities to the different environments it encounters during its biogenesis and mode of action (O'Brien *et al.* 2017, 2018b).

CONCLUSION

We have reviewed here recent progresses in the study of the CyaA toxin. These results highlight the crucial role played by various conformational transitions at different stages of the toxin path from bacteria to the target cell cytosol. Inside the bacterial cell with a sub μM Ca^{2+} concentration, the protein is inactive and ready for secretion through the T1SS channel starting with the C-terminus. As soon as it reaches the Ca^{2+} rich extracellular milieu, the protein folds in structural units wide enough to prevent backward chain movements. In the extracellular milieu, full-length CyaA exhibits a compact structure. Once

Downloaded from https://academic.oup.com/femspd/article-abstract/76/8/fty085/5188676 by Institut Pasteur user on 08 March 2019

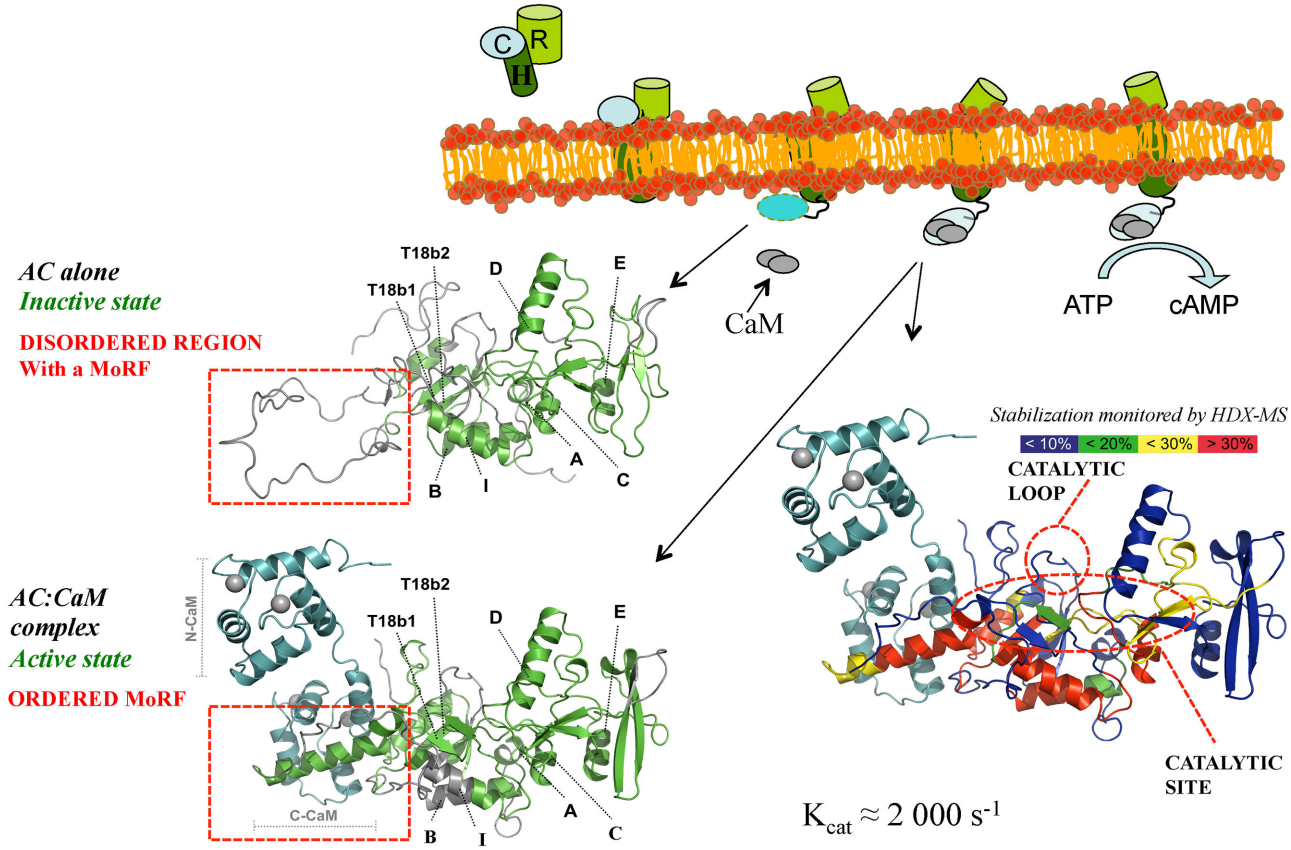

Figure 9. Disorder-to-order transition induced by CaM binding activates ACD. Using a combination of HDX-MS, SAXS and SR-CD, we build up structural models of ACD, CaM and the ACD:CaM complex. CaM binding induces local and distal stabilization effects in ACD, leading to its enzymatic activation. The intrinsically disordered region prevents bacterial intoxication. After translocation, the molecular recognition features (MoRF) is involved in CaM binding, folding, stabilization and activation of AC, leading to cAMP production and to cell death.

bound to the membrane, the TR may contribute to locally destabilize the lipid bilayer, decreasing the energy required to transport ACD into the cytoplasm of target cells. Once translocated, ACD adopts a folded structure that accommodates a large intrinsically disordered region. This latter encompasses the main CaM-binding site and may favor a dynamic exploration of the intracellular environment for CaM-'fishing.' CaM binding finally induces an allosteric stabilization of ACD. Effectors such as Ca^{2+} and CaM finely tune a subtle balance between highly flexible loops and well-structured regions within the ACD:CaM complex. The adenylate cyclase activity leads to a massive production of cAMP, which subverts the cell physiology and ultimately induces cell death.

Conflict of interest. None declared.

REFERENCES

Adkins I, Holubova J, Kosova M *et al.* Bacteria and their toxins tamed for immunotherapy. *CPB* 2012;**13**:1446–73.

Barry EM, Weiss AA, Ehrmann IE *et al. Bordetella pertussis* adenylate cyclase toxin and hemolytic activities require a second gene, cyaC, for activation. *J Bacteriol* 1991;**173**:720–6.

Basler M, Knapp O, Masin J *et al.* Segments crucial for membrane translocation and pore-forming activity of *Bordetella* adenylate cyclase toxin. *J Biol Chem* 2007;**282**:12419–29.

Bauche C, Chenal A, Knapp O *et al.* Structural and functional characterization of an essential RTX subdomain of *Bordetella pertussis* adenylate cyclase toxin. *J Biol Chem* 2006;**281**:16914–26.

Benz R. Channel formation by RTX-toxins of pathogenic bacteria: basis of their biological activity. *Biochim Biophys Acta* 2016;**1858**:526–37.

Bumba L, Masin J, Fiser R *et al. Bordetella* adenylate cyclase toxin mobilizes its beta2 integrin receptor into lipid rafts to accomplish translocation across target cell membrane in two steps. *PLoS Pathog* 2010;**6**:e1000901.

Cannella SE, Ntsogo Enguene VY, Davi M *et al.* Stability, structural and functional properties of a monomeric, calcium–loaded adenylate cyclase toxin, CyaA, from *Bordetella pertussis*. *Sci Rep* 2017;**7**:42065. doi: 10.1038/srep42065.

Chenal A, Guijarro JI, Raynal B *et al.* RTX calcium binding motifs are intrinsically disordered in the absence of calcium. *J Biol Chem* 2009;**284**:1781–9.

Chenal A, Karst JC, Sotomayor Perez AC *et al.* Calcium-induced folding and stabilization of the intrinsically disordered RTX domain of the CyaA toxin. *Biophys J* 2010;**99**:3744–53.

Chenal A, Ladant D. Bioengineering of *Bordetella pertussis* adenylate cyclase toxin for antigen-delivery and immunotherapy. *Toxins* 2018;**10**. doi: 10.3390/toxins10070302.

Chenal A, Sotomayor Perez AC, Ladant D. Structure and function of RTX Toxins. *The Comprehensive Sourcebook of Bacterial Protein Toxins*, 4th edn. Amsterdam: Elsevier, 2015, 677–718.

El-Azami-El-Idrissi M, Bauche C, Loucka J *et al.* Interaction of *Bordetella pertussis* adenylate cyclase with CD11b/CD18: role of

Downloaded from https://academic.oup.com/femspd/article-abstract/76/8/fty085/5188676 by Institut Pasteur user on 08 March 2019

toxin acylation and identification of the main integrin interaction domain. *J Biol Chem* 2003;**278**:38514–21.

Fedele G, Schiavoni I, Adkins I *et al.* Invasion of dendritic cells, macrophages and neutrophils by the *Bordetella* adenylate cyclase toxin: a subversive move to fool host immunity. *Toxins* 2017;**9**. doi: 10.3390/toxins9100293.

Fiser R, Masin J, Basler M *et al.* Third activity of *Bordetella* adenylate cyclase (AC) toxin-hemolysin. Membrane translocation of AC domain polypeptide promotes calcium influx into CD11b+ monocytes independently of the catalytic and hemolytic activities. *J Biol Chem* 2007;**282**:2808–20.

Geourjon C, Deleage G. SOPMA: significant improvements in protein secondary structure prediction by consensus prediction from multiple alignments. *Comput Appl Biosci* 1995;**11**:681–4.

Glaser P, Danchin A, Ladant D *et al.* *Bordetella pertussis* adenylate cyclase: the gene and the protein. *Tokai J Exp Clin Med* 1988a;**13** Suppl:239–52.

Glaser P, Ladant D, Sezer O *et al.* The calmodulin-sensitive adenylate cyclase of *Bordetella pertussis*: cloning and expression in *Escherichia coli*. *Mol Microbiol* 1988b;**2**:19–30.

Glaser P, Sakamoto H, Bellalou J *et al.* Secretion of cyclolysin, the calmodulin-sensitive adenylate cyclase-haemolysin bifunctional protein of *Bordetella pertussis*. *EMBO J* 1988c;**7**:3997–4004.

Gmira S, Karimova G, Ladant D. Characterization of recombinant *Bordetella pertussis* adenylate cyclase toxins carrying passenger proteins. *Res Microbiol* 2001;**152**:889–900.

Guermonprez P, Fayolle C, Rojas MJ *et al.* In vivo receptor-mediated delivery of a recombinant invasive bacterial toxoid to CD11c + CD8 alpha -CD11bhigh dendritic cells. *Eur J Immunol* 2002;**32**:3071–81.

Guermonprez P, Khelef N, Blouin E *et al.* The adenylate cyclase toxin of *Bordetella pertussis* binds to target cells via the alpha(M)beta(2) integrin (CD11b/CD18). *J Exp Med* 2001;**193**:1035–44.

Guiso N. *Bordetella* adenylate cyclase-hemolysin toxins. *Toxins* 2017;**9**. doi: 10.3390/toxins9090277.

Hackett M, Guo L, Shabanowitz J *et al.* Internal lysine palmitoylation in adenylate cyclase toxin from *Bordetella pertussis*. *Science* 1994;**266**:433–5.

Heveker N, Ladant D. Characterization of mutant *Bordetella pertussis* adenylate cyclase toxins with reduced affinity for calmodulin. Implications for the mechanism of toxin entry into target cells. *Eur J Biochem* 1997;**243**:643–9.

Karst JC, Barker R, Devi U *et al.* Identification of a region that assists membrane insertion and translocation of the catalytic domain of *Bordetella pertussis* CyaA toxin. *J Biol Chem* 2012;**287**:9200–12. doi: 10.1074/jbc.M111.316166.

Karst JC, Ntsogo Enguene VY, Cannella SE *et al.* Calcium, acylation, and molecular confinement favor folding of *Bordetella pertussis* adenylate cyclase CyaA toxin into a monomeric and cytotoxic form. *J Biol Chem* 2014;**289**:30702–16. doi: 10.1074/jbc.M114.580852.

Karst JC, Sotomayor Perez AC, Guijarro JI *et al.* Calmodulin-induced conformational and hydrodynamic changes in the catalytic domain of *Bordetella pertussis* adenylate cyclase toxin. *Biochemistry* 2010;**49**:318–28. doi: 10.1021/bi9016389.

Knapp O, Maier E, Masin J *et al.* Pore formation by the *Bordetella* adenylate cyclase toxin in lipid bilayer membranes: role of voltage and pH. *Biochim Biophys Acta* 2008;**1778**:260–9.

Ladant D. Interaction of *Bordetella pertussis* adenylate cyclase with calmodulin. Identification of two separated calmodulin-binding domains. *J Biol Chem* 1988;**263**:2612–8.

Ladant D, Brezin C, Alonso JM *et al.* *Bordetella pertussis* adenylate cyclase. Purification, characterization, and radioimmunoassay. *J Biol Chem* 1986;**261**:16264–9.

Ladant D, Ullmann A. *Bordetella pertussis* adenylate cyclase: a toxin with multiple talents. *Trends Microbiol* 1999;**7**:172–6.

Linhartova I, Bumba L, Masin J *et al.* RTX proteins: a highly diverse family secreted by a common mechanism. *FEMS Microbiol Rev* 2010;**34**:1076–112.

Masin J, Basler M, Knapp O *et al.* Acylation of lysine 860 allows tight binding and cytotoxicity of *Bordetella* adenylate cyclase on CD11b-expressing cells. *Biochemistry* 2005;**44**:12759–66.

Masure HR, Au DC, Gross MK *et al.* Secretion of the *Bordetella pertussis* adenylate cyclase from *Escherichia coli* containing the hemolysin operon. *Biochemistry* 1990;**29**:140–5.

Novak J, Cerny O, Osickova A *et al.* Structure–function relationships underlying the capacity of *Bordetella* adenylate cyclase toxin to disarm host phagocytes. *Toxins* 2017;**9**. doi: 10.3390/toxins9100300.

O'Brien DP, Brier S, Ladant D *et al.* SEC-SAXS and HDX-MS: a powerful combination. The case of the calcium-binding domain of a bacterial toxin. *Biotechnol Appl Biochem* 2018a;**65**:62–68.

O'Brien DP, Durand D, Voegele A *et al.* Calmodulin fishing with a structurally disordered bait triggers CyaA catalysis. *PLoS Biol* 2017;**15**:e2004486. doi: 10.1371/journal.pbio.2004486.

O'Brien DP, Hernandez B, Durand D *et al.* Structural models of intrinsically disordered and calcium-bound folded states of a protein adapted for secretion. *Sci Rep* 2015;**5**:14223. doi: 10.1038/srep14223.

O'Brien DP, Perez ACS, Karst J *et al.* Calcium-dependent disorder-to-order transitions are central to the secretion and folding of the CyaA toxin of *Bordetella pertussis*, the causative agent of whooping cough. *Toxicon* 2018b;**149**:37–44.

Rose T, Sebo P, Bellalou J *et al.* nteraction of calcium with *Bordetella pertussis* adenylate cyclase toxin. Characterization of multiple calcium-binding sites and calcium-induced conformational changes. *J Biol Chem* 1995;**270**:26370–6.

Sakamoto H, Bellalou J, Sebo P *et al.* *Bordetella pertussis* adenylate cyclase toxin. Structural and functional independence of the catalytic and hemolytic activities. *J Biol Chem* 1992;**267**:13598–602.

Shen YM, Maupetit J, Derreumaux P *et al.* Improved PEP-FOLD approach for peptide and miniprotein structure prediction. *J Chem Theory Comput* 2014;**10**:4745–58.

Sotomayor Perez AC, Karst JC, Davi M *et al.* Characterization of the regions involved in the calcium-induced folding of the intrinsically disordered RTX motifs from the *Bordetella pertussis* adenylate cyclase toxin. *J Mol Biol* 2010;**397**:534–49.

Sotomayor-Perez AC, Ladant D, Chenal A. Calcium-induced folding of intrinsically disordered repeat-in-toxin (RTX) motifs via changes of protein charges and oligomerization states. *J Biol Chem* 2011;**286**:16997–7004.

Sotomayor-Perez AC, Ladant D, Chenal A. Disorder-to-order transition in the CyaA toxin RTX domain: implications for toxin secretion. *Toxins* 2015;**7**:1–20.

Sotomayor-Perez AC, Subrini O, Hessel A *et al.* Molecular crowding stabilizes both the intrinsically disordered calcium-free state and the folded calcium-bound state of a repeat in toxin (RTX) protein. *J Am Chem Soc* 2013;**135**:11929–34.

Subrini O, Sotomayor-Perez AC, Hessel A *et al.* Characterization of a membrane-active peptide from the *Bordetella pertussis* CyaA toxin. *J Biol Chem* 2013;**288**:32585–98.

Downloaded from https://academic.oup.com/femspd/article-abstract/76/8/fty085/5188676 by Institut Pasteur user on 08 March 2019

Svedova M, Masin J, Fiser R *et al*. Pore-formation by adenylate cyclase toxoid activates dendritic cells to prime CD8+ and CD4+ T cells. *Immunol Cell Biol* 2016;**94**:322–33.

Uribe KB, Etxebarria A, Martin C *et al*. Calpain-mediated processing of adenylate cyclase toxin generates a cytosolic soluble catalytically active N-terminal domain. *PLoS One* 2013a;**8**:e67648.

Uribe KB, Martin C, Etxebarria A *et al*. Ca2+ influx and tyrosine kinases trigger *Bordetella* adenylate cyclase toxin (ACT) endocytosis. Cell physiology and expression of the CD11b/CD18 integrin major determinants of the entry route. *PLoS One* 2013b;**8**:e74248.

Veneziano R, Rossi C, Chenal A *et al*. *Bordetella pertussis* adenylate cyclase toxin translocation across a tethered lipid bilayer. *P Natl Acad Sci U S A* 2013;**110**:20473–8.

Veneziano R, Rossi C, Chenal A *et al*. Synthesis and characterization of tethered lipid assemblies for membrane protein reconstitution (review). *Biointerphases* 2017;**12**:04E301. doi: 10.1116/1.4994299.

Voegele A, Subrini O, Sapay N *et al*. Membrane-active properties of an amphitropic peptide from the CyaA toxin translocation region. *Toxins* 2017;**9**. doi: 10.3390/toxins9110369.

Vojtova J, Kamanova J, Sebo P. *Bordetella* adenylate cyclase toxin: a swift saboteur of host defense. *Curr Opin Microbiol* 2006;**9**:69–75.

Vojtova-Vodolanova J, Basler M, Osicka R *et al*. Oligomerization is involved in pore formation by Bordetella adenylate cyclase toxin. *FASEB J* 2009;**23**:2831–43.

Westrop GD, Hormozi EK, Da Costa NA *et al*. *Bordetella pertussis* adenylate cyclase toxin: proCyaA and CyaC proteins synthesised separately in *Escherichia coli* produce active toxin in vitro. *Gene* 1996;**180**:91–99.

Downloaded from https://academic.oup.com/femspd/article-abstract/76/8/fty085/5188676 by Institut Pasteur user on 08 March 2019

Article V

Membrane-active properties of an amphitropic peptide from the CyaA toxin translocation region

Alexis Voegele, Orso Subrini, Nicolas Sapay, Daniel Ladant and Alexandre Chenal

Toxins
Volume 9(11)
November 2017

It has been previously shown that the region encompassing residues 384-489 of CyaA, belonging to the translocation region (TR), was crucial for the transport of the catalytic domain across the membrane (Karst et al., 2012). Subsequently, the peptide P454 (residues 454 to 484 of CyaA) was identified and exhibited membrane-active properties (Subrini et al., 2013). In fact, this peptide is able to interact with membranes, acquire a α-helical structure upon membrane interaction and also induce lipid bilayer permeabilization. Recently, it was reported that most of the TR, from residues 411 to 490, was inserted into the membrane. Furthermore, it was shown that substitutions of arginine residues in TR affect the translocation of CyaA (Masin et al., 2016). The aim of the present study was to characterize the membrane-active properties of various amphitropic regions of CyaA. Only P454 was able to interact with membrane, fold upon membrane interaction and also permeabilize membranes. We further characterized the effect of lipid polymorphism and contribution of its arginine residues in its membrane-active properties to discuss these results in the context of the CyaA translocation.

We first investigated the properties of 11 predicted membrane-active regions of CyaA, based on *in silico* studies. Using tryptophan fluorescence and circular dichroism (CD), we found that only 6 among these 11 peptides were able to interact with membrane and adopt a structure upon membrane interaction.

Molecular dynamics simulations highlighted the diversity of conformations, depths of penetration and thermodynamics of the CyaA-derived peptides investigated.

Finally, we investigated the ability of these peptides to permeabilize membranes. As expected, non-interacting peptides did not show any permeabilization activity. Surprisingly, among the 6 interacting peptides, only P454 was able to destabilize the lipid bilayer. This suggests that P454 might be involved in local destabilization of the membrane in the CyaA intoxication. Therefore, P454 properties were further investigated.

We then examined the effect of lipid polymorphism and charge on the partition of P454 using different membranes compositions by tryptophan fluorescence. We used the neutral lipid DOPC as reference, which confers plane membrane and we combined it with the negatively charged lipid DOPG. We also tested the effect of the neutral DOPE and cholesterol, which increase membrane rigidity and local negative curvature (*i.e* membrane invagination) (see Figure 31). We found that negatively charged lipids increase P454 affinity for membrane while rigidity and negative membrane curvature decreased it. We also tested how positive curvature could affect the P454 membrane interaction, using lysoPC (see Figure

31). Interestingly, we found that compared to negative curvature, positive curvature considerably increased P454 partition (unpublished data). These preliminary results were interesting and the potential phospholipase activity described by Gonzalez-Bullon and colleagues might have explained why P454 can bind such membranes. However, CyaA does not possess a phospholipase activity (see previous article III) and any model can be built up using PLA activity.

Finally, we investigated the effect of lipid acyl chain. We replaced DOPC (fluidic lipid) by POPC (more rigid lipid) and observed that P454 partition was reduced and even abolished with “rigid” lipids.

Taken together, P454 membrane interaction is favored by negatively charged lipid, positive curvature and fluidic membrane. We propose that recruitment of such lipids may favor P454 membrane interaction.

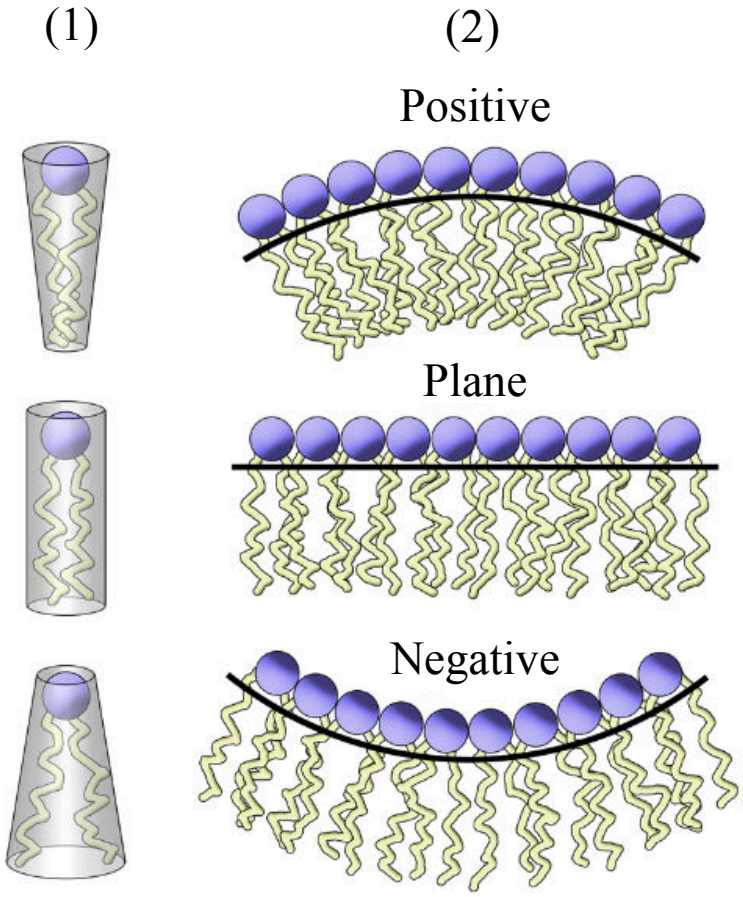

Figure 31. Phospholipid form and spontaneous membrane curvature. (1) Schematic illustration of the different lipid geometrical shapes. The shape is given by the lipid headgroup and by the acyl chain length and insaturations. (2) Phospholipid shapes govern the membrane curvature. When the headgroup becomes progressively smaller compared to the acyl chains, the curvature follows a sequence from positive through plane to negative. Adapted from (Brown, 2012).

After determining the main lipid properties favoring P454 membrane interaction, we focused on the contribution of the two native arginines residues R461 and R474. They were substituted by lysines, glutamines, alanines and glutamates.

Using tryptophan fluorescence, we observed that arginine substitutions affect peptide-membrane interaction. Interestingly, the interaction depended on membrane composition, as observed before for the native P454. We observed that hydrophobic forces and attractive electrostatic interactions contribute to P454 membrane interaction. Furthermore, both arginine residues distinctly contribute to membrane interaction.

Secondary structure content upon membrane interaction of P454-derived peptides was studied by synchrotron radiation circular dichroism in far-UV. The data showed that peptides were mainly characterized by structural disorder in solution and addition of membranes induced a variable increase in helical content of the different P454 peptides. As observed for partition, α-helical content depended on membrane composition and was correlated to partition. Interestingly, substitution of the second arginine R474 affected folding and this residue was proposed to significantly contribute to the formation of α-helix upon membrane partitioning.

Finally, we studied membrane permeabilization induced by the P454 derived peptides. All the peptides, expected the glutamate substitutions, were able to permeabilize membrane in a concentration-dependent manner. As observed for the α-helical content, permeabilization was correlated to membrane partitioning. Substitution of the first arginine R461 of P454 strongly decreased its efficiency to destabilize membrane. This residue was proposed to specifically contribute to membrane permeabilization.

Taken together, these data provide direct evidence that P454 is a major amphipathic peptide from CyaA exhibiting membrane-active properties and especially membrane permeabilization. We showed that negatively charged lipids and fluidic membrane as well as lipids promoting positive curvature, favor P454-membrane interaction. We then demonstrated that its two arginine residues, R461 and R474, contribute to its membrane-active properties: R474 is primarily involved in helix formation upon membrane association while R461 is important for membrane permeabilization. These results allowed us to propose a model of translocation of CyaA: once inserted into the membrane with the hydrophobic and acyl regions, the C-terminal segment of P454, with the R474, might insert and be folded into the membrane and allows the N-terminal segment, with the R461, to locally disrupt the membrane. This local perturbation may help to decrease the energy required for the translocation of the catalytic domain.

toxins

MDPI

Article

Membrane-Active Properties of an Amphitropic Peptide from the CyaA Toxin Translocation Region

Alexis Voegele [1,2], Orso Subrini [1,3], Nicolas Sapay [4], Daniel Ladant [1,*] and Alexandre Chenal [1,*]

1 Département de Biologie Structurale et Chimie, Institut Pasteur, Unité de Biochimie des Interactions Macromoléculaires, CNRS UMR 3528, 28 Rue du Dr Roux, 75724 Paris, CEDEX 15, France; alexis.voegele@outlook.fr (A.V.); orso.subrini@gmail.com (O.S.)
2 Université Paris Diderot Paris VII, 75013 Paris, France
3 Institut de Biologie Structurale, 71 Avenue des Martyrs, 38044 Grenoble, CEDEX 9, France
4 Bioaster Technology Research Institute, 69007 Lyon, France; nicolas.sapay@bioaster.org
* Correspondence: daniel.ladant@pasteur.fr (D.L.); alexandre.chenal@pasteur.fr (A.C.); Tel.: +33-1-45-68-84-00 (D.L.); +33-1-44-38-92-12 (A.C.)

Academic Editor: Holger Barth
Received: 18 October 2017; Accepted: 10 November 2017; Published: 14 November 2017

Abstract: The adenylate cyclase toxin CyaA is involved in the early stages of infection by *Bordetella pertussis*, the causative agent of whooping cough. CyaA intoxicates target cells by a direct translocation of its catalytic domain (AC) across the plasma membrane and produces supraphysiological levels of cAMP, leading to cell death. The molecular process of AC translocation remains largely unknown, however. We have previously shown that deletion of residues 375–485 of CyaA selectively abrogates AC translocation into eukaryotic cells. We further identified within this "translocation region" (TR), P454 (residues 454–484), a peptide that exhibits membrane-active properties, i.e., is able to bind and permeabilize lipid vesicles. Here, we analyze various sequences from CyaA predicted to be amphipatic and show that although several of these peptides can bind membranes and adopt a helical conformation, only the P454 peptide is able to permeabilize membranes. We further characterize the contributions of the two arginine residues of P454 to membrane partitioning and permeabilization by analyzing the peptide variants in which these residues are substituted by different amino acids (e.g., A, K, Q, and E). Our data shows that both arginine residues significantly contribute, although diversely, to the membrane-active properties of P454, i.e., interactions with both neutral and anionic lipids, helix formation in membranes, and disruption of lipid bilayer integrity. These results are discussed in the context of the translocation process of the full-length CyaA toxin.

Keywords: membrane-active peptide; adenylate cyclase; CyaA toxin; repeat in toxin; membrane partitioning-folding coupling; membrane disruption; arginine side chain

1. Introduction

The adenylate cyclase toxin (CyaA or ACT) is one of the major virulence factors produced by *Bordetella pertussis*, the causative agent of whooping cough [1,2]. CyaA plays a crucial role in the early stages of respiratory tract colonization by *B. pertussis* [3]. CyaA is a 1706-residue long multi-functional, and multi-domain protein [4–7], composed of a catalytic domain (AC, residues 1–364) [8–10], a translocation region (TR, approx. 370–500) [10,11], a hydrophobic region (HR, residues 500–750), an acylation region (AR, residues 750–1000), and a C-terminal Repeats-in-ToXin (RTX) calcium-binding domain (RD, residues 1000–1706). After synthesis, CyaA is acylated intra-cellularly by the CyaC transacylase and secreted in unfolded conformations through a dedicated type 1 secretion

system. Upon secretion, calcium binding to the RTX motifs triggers the cooperative folding of the RD domain followed by the whole CyaA toxin [12–21]. Indeed, calcium is an essential cofactor of CyaA cytotoxic activities [5–7]. After binding to its cell receptor CD11b/CD18 [22–25], or upon direct interaction with the membrane, CyaA inserts its hydrophobic region HR into the plasma membrane of eukaryotic target cells. The AC domain is then directly translocated across the plasma membrane into the cytosol of the target cells [4,6,26], where it is activated by calmodulin to produce supra-physiological levels of cAMP. Accumulation of cAMP alters cell physiology and may ultimately lead to cell death. Besides this, as with many other RTX cytolysins, CyaA is endowed with a pore-forming activity, which is able to induce cell lysis, an activity that is usually monitored by hemolysis of erythrocytes [27–30].

The mechanisms by which the AC of CyaA is translocated across the plasma membrane of eukaryotic target cells still remain largely unknown at the molecular level. The translocation process, however, is known to be dependent on several parameters, including the presence of free calcium in the extracellular medium [7,22], the CyaC-mediated post-translational acylation of CyaA on two lysines (K860 and K983) [31–35], the membrane potential [36,37], and temperature (required for membrane fluidity) [22]. Besides, it was recently suggested that CyaA may be endowed with a phospholipase activity that seems to be required for the AC domain translocation [26].

We have previously shown that the translocation region (TR), encompassing residues 384–489 of CyaA, is essential for transport of the AC domain across the cell membrane. We demonstrated that the deletion of TR selectively abrogated the ability of CyaA to trigger cAMP accumulation in target cells, while it did not affect CyaA cell binding nor its hemolytic activity [10]. Furthermore, while the AC domain alone cannot bind membranes, a longer polypeptide, AC489 (residues 1 to 489 of CyaA), encompassing AC and TR, is able to bind and permeabilize membranes. We subsequently identified within TR a polypeptide segment (residues 454 to 484), which exhibits membrane-active properties [11]. The peptide corresponding to this sequence, called P454, partitions into membranes, acquires a helical conformation, and induces lipid bilayer permeabilization. We proposed that this region may locally destabilize the lipid bilayer and thus favor AC translocation across the plasma membrane [11]. Recently, Masin et al. reported that most of the TR region from residues 411 to 490 is inserted into membrane [30]. They further showed that substitutions of arginine residues in the TR region decreased the translocation efficiency of CyaA, while neutralization of negatively charged aspartate and glutamate residues affected CyaA pore-forming activity [30].

In the present article, we characterize the membrane interacting properties of various predicted amphitropic regions of CyaA. Amphitropic regions are involved in the regulation of both the folding and functions of peripheral proteins and membrane proteins [38,39]. We show that several of these amphitropic CyaA peptides are able to interact with membranes and fold upon membrane interaction. However, only P454 is able to permeabilize membranes. We further analyze the contribution of the arginine residues of P454, R461, and R474, and characterize their involvement in lipid bilayer insertion, membrane-induced secondary structure formation, and membrane permeabilization. We show that P454 does exhibit several characteristics of antimicrobial peptides, in particular, the contribution of arginine residues to membrane-active properties, such as folding upon membrane insertion and disruption of the lipid bilayer packing. We discuss these results in the context of the CyaA toxin.

2. Results

2.1. Experimental Determination of Membrane Partition of CyaA-Derived Peptides

To characterize the properties of predicted membrane-active regions of CyaA, 11 peptides were produced by peptide synthesis, corresponding to short sequences exhibiting amphiphilic properties identified in silico and with hydrophobicity, and hydrophobic moments located within the Surface-Membrane area of the <H>-μH plot of Eisenberg et al. [40]. The properties of these

peptides (designated by the residue number of their N-terminal extremity in Figure 1A) are described in ''Materials and Methods" and Tables S1 and S2 and Figure S1.

We have analyzed their ability to (i) partition from the solution to the membrane (SUVs made of DOPC/DOPE/DOPG/Chol 4:3:2:1, i.e., the lipid composition used in our previous studies [10,11]) by tryptophan intrinsic fluorescence; (ii) fold upon membrane partitioning by far-UV circular dichroism; and (iii) induce a local destabilization of lipid bilayers as monitored by permeabilization assay. We have further investigated these peptides by molecular dynamics to get more insights into their conformations in membranes.

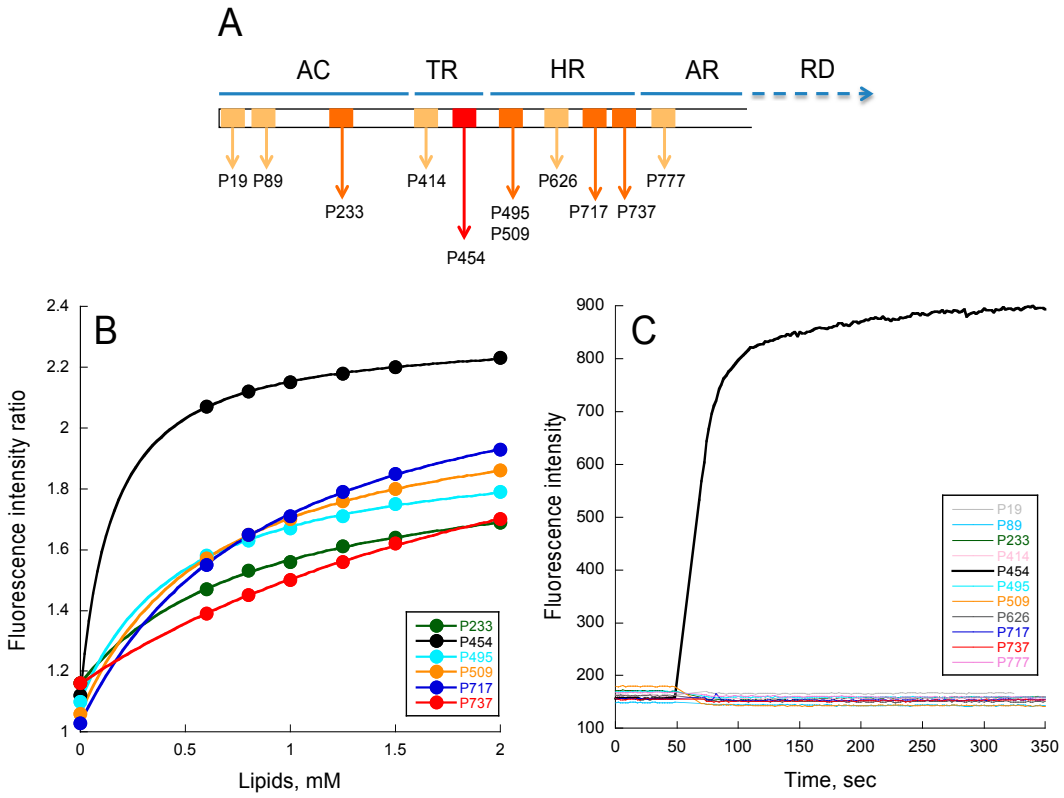

Figure 1. Peptide membrane partition followed by tryptophan intrinsic fluorescence. (**A**) Localization of CyaA-derived peptides on the full-length toxin. Each box represents a peptide. Light orange boxes correspond to peptides unable to interact with membranes (P19, P89, P414, P626, and P737); orange boxes (P233, P495, P509, P717, and P737) correspond to peptides able to partition into membranes but that do not permeabilize membranes; the red box corresponds to the unique P454 peptide able to interact and permeabilize membranes; (**B**) Ratio of fluorescence intensity (340 nm/380 nm, excitation at 280 nm) as a function of lipid concentration. The negatively charged small unilamellar vesicles (SUVs) were made of dashed blue (DOPC/DOPE/DOPG/Chol at ratio 4:3:2:1); (**C**) Membrane permeabilization assay. Time course of fluorophore probe (ANTS) and quencher (DPX) efflux (excitation at 390 nm and emission at 515 nm) from negatively charged LUVs (0.45 mM lipids) were prepared at a molar ratio DOPC/DOPE/DOPG/Chol 4:3:2:1. Experiments were performed in the presence of 1 μM of P454 (black) and 10 μM for all other CyaA-derived peptides. Standard deviations (S.D.) are within the size of the dots.

From tryptophan fluorescence and circular dichroism (CD) data (Figures 1B and S2 respectively), we found that the following peptides were able to interact with membranes: P233, P454, P495, P509, P717, and P737. For P19, P89, P414, P626, and P777 peptides, no detectable change of tryptophan fluorescence or CD signature was observed upon addition of membranes (data not shown). The six peptides interacting with membranes display various free energy (ΔG) values calculated from their partition coefficients (K_X, see Table S3), obtained from fluorescence titrations (see Material and Methods

for details). They also exhibit various membrane-induced secondary structure changes: the P454, P717, and P233 peptides show a higher helical content than P737, P495, and P509. The low alpha-helical content of P737 is likely related to its low K_X, while P495 and P509, which both exhibit relatively high K_X, are likely to adopt non-canonical structures in membranes, as suggested by far-UV CD and molecular dynamics (see Figure 2).

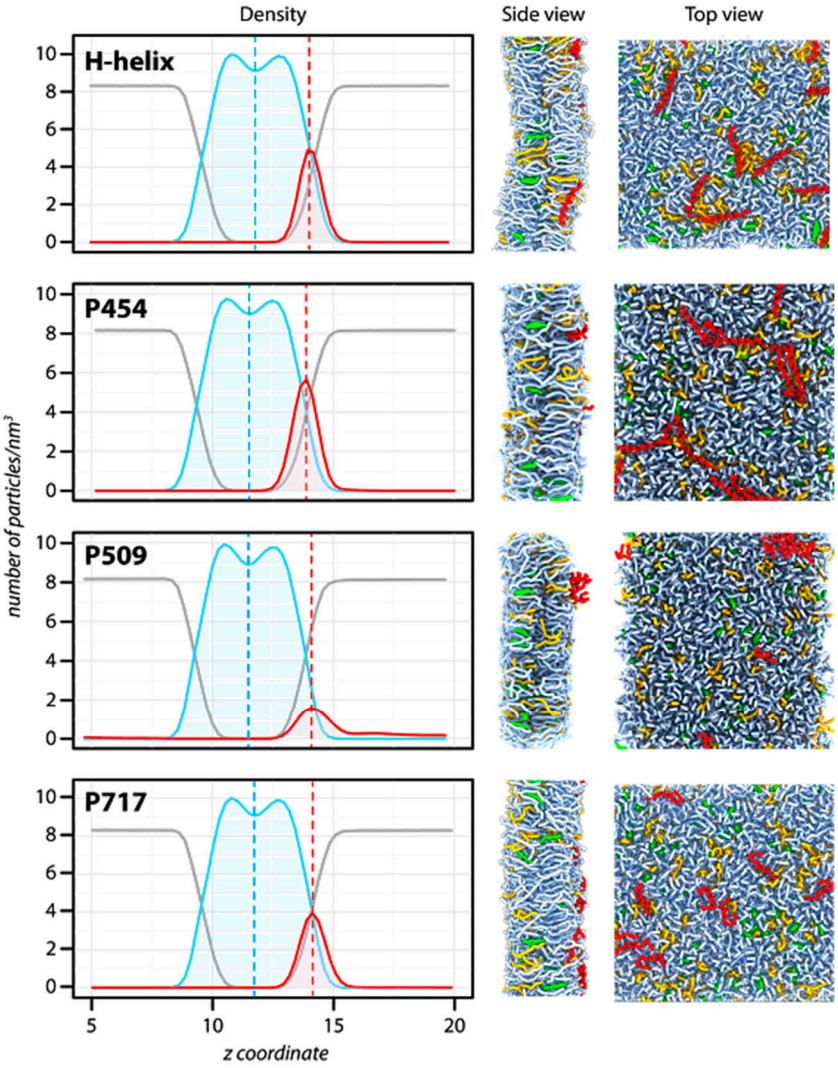

Figure 2. Molecular dynamics of CyaA-derived peptides in the presence of membrane. Summary of the molecular dynamics simulations in the presence of dashed green (DOPG), including the particle density along the trans-membrane axis (**left**), the side (**middle**), and the top (**right**) views of the systems after 1 µs of simulation. *Left panel*: The density is calculated for water (grey), lipids (blue), and peptides (red). The center of the bilayer is indicated by a blue dashed line. The average position of each peptide is indicated by a dashed red line. The peptide density is four times magnified to better visualize the position of each peptide. *Middle and right panels*: Snapshots of the systems after 1 µs of molecular dynamics simulation at constant temperature (323.15 K) and pressure (1 bar). The peptides are depicted in red, DOPC molecules in light blue, cholesterol molecules in green, and DOPG molecules in orange. For clarity, water is not depicted.

2.2. Molecular Dynamics of CyaA-Derived Peptides in Lipid Bilayers

We performed molecular dynamics simulations of DOPC/DOPG/Chol 8:1:1 lipid mixture with the following peptides: P233 (H-helix), P454, P509, and P717. Snapshots of the systems after 1 µs

of molecular dynamics simulation are shown in Figure 2 to illustrate the general organization of the peptide/lipid mixtures following the simulations. To better characterize the peptide partition in the bilayer, the density of lipids, peptides, and water was determined along the transmembrane axis *z* (Figure 2, left panels). The size of the bilayer, corresponding to the width of the lipid density, is almost identical in all the simulated systems (peak-to-peak distance ≈ 2.0 nm, corresponding to the approximate acyl chain thickness), as well as the lipid bilayer hydration. The position of the peptide density significantly changes between systems, however. P509 is located on average at 2.6 nm from the bilayer center, while P233, P454, and P717 are located at 2.2, 2.35, and 2.4 nm, respectively. Therefore, P233, P454, and P717 are more embedded in the bilayer than P509. Notably, P233, P454, and P717 exhibit regular helical conformations, while P509 adopts non-canonical conformations, as observed on the system top view (Figure 2), and as suggested by circular dichroism data (Figure S2). These observations highlight the diversity of conformations, depths of penetration, and thermodynamics of the CyaA-derived peptides investigated herein.

2.3. Lipid Vesicle Permeabilization

We then investigated the ability of the peptides to permeabilize LUVs composed of DOPC/DOPE/DOPG/Chol 4:3:2:1 (Figure 1C). Permeabilization was monitored using the ANTS/DPX assay (see methods). As expected, peptides such as P19, P89, P414, P626, and P777, which are not able to partition into membrane, do not show any permeabilization activity, even at high peptide concentrations up to 10 μM (Figure 1C). Surprisingly, among the peptides P233, P454, P495, P509, P717, and P737, which partition into membranes, only P454 was able to permeabilize LUVs. Hence, P454 is the unique peptide from the CyaA-derived peptide series able to destabilize the lipid bilayer of LUVs, suggesting that it has a specific role in CyaA invasive activity. We therefore decided to investigate more thoroughly the properties of the P454 peptide.

2.4. Effects of Non-Lamellar Lipids, Charge, and Acyl Chains Fluidity on P454 Membrane Partition

We examined the effect of lipid polymorphism and charge on the partition of P454. The lipid of reference is DOPC, a neutral, lamellar-forming lipid with a cylindrical shape in liquid-disordered state at room temperature, to which we added anionic, lamellar bilayer forming DOPG lipid. We also tested the effect of neutral DOPE and cholesterol, which increase membrane rigidity and DOPC acyl chains straightening [41–43], as well as promote inverted hexagonal structures (H_{II}) in PC lipid bilayers [44,45].

The partition of P454 into DOPC (green trace) is shown in Figure 3A. The addition of the negatively charged DOPG (green dash trace) to DOPC membranes increases the affinity of P454 for membranes. On the contrary, addition of DOPE (purple trace) or cholesterol (grey trace) or both (blue trace) to DOPC membranes progressively decreases the affinity of P454 for these membranes. The addition of DOPG (blue dash trace) to DOPC/DOPE/Chol (blue trace) partially compensates for the effects of DOPE and cholesterol.

Cholesterol and DOPE, which undergo lamellar/inverse hexagonal ($L\alpha$–H_{II}) phase transition below 10 °C [46], both favor non-lamellar bilayer structures at 25 °C. This suggests that negative curvatures may be unfavorable for P454 membrane partition. PE and cholesterol also decrease the fluidity of liquid-disordered lipid bilayers [42,43], and the increased membrane rigidity may likewise disfavor P454 partitioning into membranes.

We further investigated the effect of the hydrocarbon core fluidity on P454 membrane partition by increasing acyl chain rigidity. DOPC and DOPG lipids were substituted by POPC and POPG, which are characterized by higher phase transition temperatures. Figure 3B shows that the membrane partition of P454 is reduced in POPC membranes (orange trace) as compared to DOPC (green trace) lipid bilayers. The addition of POPG in POPC membranes (dash orange trace) does increase the membrane partition of P454, as observed for DOPC/DOPG (dash green trace). Finally, the addition of both POPE and cholesterol to POPC totally abolishes the partition of P454 (not shown), in agreement

with the effects of PE and cholesterol observed with DO-phospholipids. Taken together, P454 partition is favored in the presence of lamellar-structure forming lipids, and in negatively charged membranes in the liquid-disordered state (see Table S4).

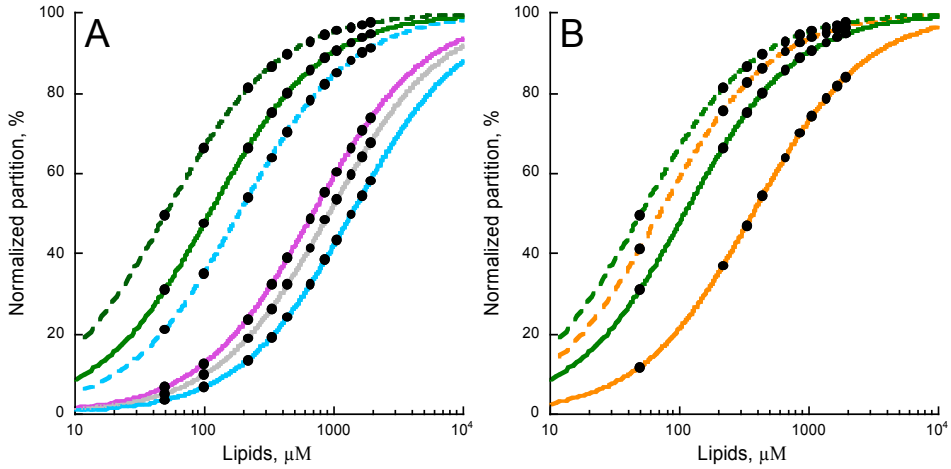

Figure 3. Effects of lipid composition on P454 membrane partition. (**A**) P454 membrane partition in DOPC (green), DOPC/DOPG 8:2 (dashed green), DOPC/DOPE 7:3 (purple), DOPC/Chol 7:3 (grey), DOPC/DOPE/Chol 6:3:1 (blue), and DOPC/DOPE/DOPG/Chol 4:3:2:1 (dashed blue) SUVs. (**B**) P454 membrane partition in DOPC SUVs in the absence (green) and in the presence of DOPG (dashed green); in POPC SUVs in the absence (orange) and in the presence of POPG (dashed orange). Data sets of K_X and ΔG values are given in Table S4. S.D. are within ±5%.

2.5. Membrane Partition of P454-Derived Peptides

After determining the main lipid properties favoring peptide membrane partition, we have investigated the contribution of the two native arginines of P454, R461, and R474 (hereafter referred to R1 and R2, respectively), to membrane partitioning, membrane-induced helical formation, and membrane permeabilization. The two arginines (R1, R2, or both: R12) were substituted by (i) lysines, (R12K) to preserve the positive charge, while removing the guanidinium group at the extremity of arginine side chains; (ii) glutamines (R1Q, R2Q, and R12Q), to neutralize the side chains and keep similar bulky side chains; (iii) alanines (R12A), to neutralize the side chains and reduce the bulkiness of arginine side chains, and (iv) glutamates (R12E), to reverse the charge.

The partition coefficients K_X and the ΔG values (Table S5) of the seven peptides were obtained from titration experiments followed by tryptophan fluorescence (Figure S3). Figure 4 shows the ΔG values reported as a function of the peptide valence, z, in the presence of POPC ± POPG (Figure 4A) and DOPC ± DOPG (Figure 4B). A correlation between the peptide valence and the ΔG of membrane partition is observed. Linear regressions (red and black dash lines in Figure 4) show that membrane partition of peptides is favored in the presence of membranes containing anionic PG lipids (red lines vs black lines) and in the more fluidic DO-phospholipids (Figure 4B) than in the PO-phospholipids (Figure 4A). However, no correlation was observed between the hydrophobic moment, the mean hydrophobicity, and free energy of membrane partition (ΔG) among the P454 peptide series (Figure S4), indicating that their amphiphilicity is not a primary criterion for membrane affinity.

Arginine substitutions significantly affect the ΔG of partition, with ΔG ranging from −5 to −8 kcal/mol. The peptides follow a ΔG-valence dependency from the negatively charged R12E (z = −1.8 e) to the native (N) P454 peptide (z = +2.2 e). The three peptides with arginine to glutamine substitutions (R1Q, R2Q, and R12Q) nicely follow the ΔG-valence dependency, providing further evidence that membrane partitioning correlates with peptide charge (Figure 4A,B).

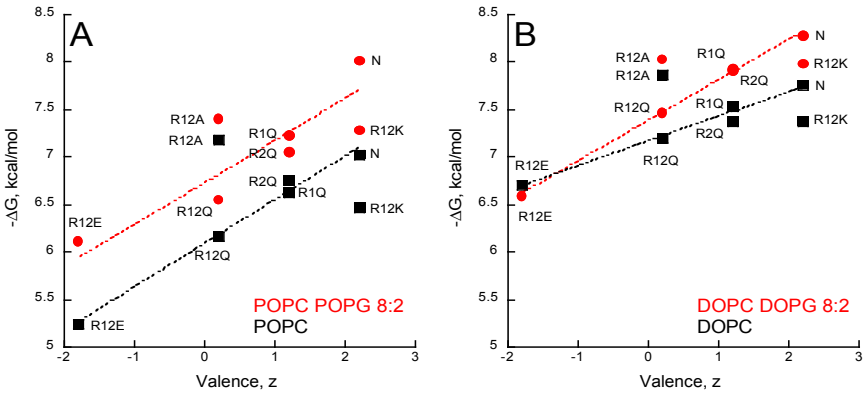

Figure 4. Valence-dependent solution-to-membrane partitioning of P454-derived peptides. (**A**) Free energy of membrane partitioning for peptides in POPC/POPG 8:2 (circles) and POPC (squares) SUVs. (**B**) Free energy of membrane partitioning for peptides in DOPC/DOPG 8:2 (circles) and DOPC (squares) SUVs. Solution-to-membrane partition of peptides was recorded by tryptophan intrinsic fluorescence. Titration data sets are shown in Figure S3 and were used to determine the K_X and ΔG values (see Table S5). The valence of peptides is given in Table S1. S.D. are $\pm$0.1 kcal/mol.

The membrane partition of R12A depends on the charge of the membrane. R12A is slightly more efficient than WT P454 to partition into neutral DOPC and POPC membranes, while in negatively charged membranes (DOPC/DOPG and POPC/POPG) its ΔG values are lower than those measured for the native P454 peptide. This further highlights the contribution of electrostatic interactions between P454 and anionic membranes. Notably, the R12A peptide has the same valence as R12Q (z = +0.2 e). The R12A ΔG values are higher than R12Q ΔGs for all membrane lipid compositions tested, suggesting that the substitution from glutamine to alanine favors membrane interaction, in agreement with the White-Wimley interfacial scale [47].

The White-Wimley scales predict [47] that substitutions of arginine to glutamine or alanine should significantly favor membrane binding, but our experimental data shows that R1Q, R2Q, R12Q, and R12A have a reduced affinity for membranes (or slightly improved for R12A in neutral membranes) compared to WT P454. This observation supports the view that arginine favors membrane partitioning, in agreement with recent data on arginine in membranes [48].

The R12K ΔG values are lower than those of the native P454 peptide for all membrane lipid compositions tested, indicating that, for the same valence, arginine residues provide a significant net contribution of about $\Delta\Delta G = 0.5 \pm 0.2$ kcal/mol to the partition compared to the lysine residues of R12K. From a thermodynamic perspective, this $\Delta\Delta G$ fits nicely with the White-Wimley interfacial scale: the ΔG from water to interface is 0.81 and 0.99 kcal/mol for arginine and lysine, respectively, and 0.4 kcal/mol for two substitutions. From a structural point of view, this is likely due to the guanidinium-phosphate bidentate complex establishing hydrogen bonds between the guanidinium group of arginine side chains and the phosphate group of phospholipids (see discussion). To summarize, this data suggests that hydrophobic forces, attractive electrostatic interactions, and hydrogen bonds contribute to P454 membrane insertion.

2.6. Synchrotron Radiation Circular Dichroism of P454-Derived Peptides

Secondary structure content changes of P454-derived peptides upon membrane partition were studied in the far-UV range (Figure S5) by synchrotron radiation circular dichroism (SRCD). CD spectra were deconvoluted using BestSel [49] to estimate the alpha helical content in each experimental condition (Table S6 and Figure S6). The data shows that P454 peptides are mainly characterized by structural disorder in solution, with the exception of R12A, which exhibits a slightly higher helical content than the native P454 peptide in solution. The structural disorder was evidenced by the presence of a negative π-π band (190–210 nm) and the low intensity of the n-π band (210–230 nm). The addition

of TFE induced a large increase of helical content for all peptides, as evidenced by the splitted π-π band and the strong negative n-π band (Figure S5). This data indicates that the P454-derived peptides exhibit an intrinsic propensity to fold in low dielectric constant environments, such as in lipid bilayers.

The addition of neutral membranes induced a variable increase in helical content of the different P454 peptides. This increase was further enhanced in the presence of negatively charged membranes, especially for the native and R12K peptides (Table S6 and Figure S6). This data indicates that the P454-derived peptides acquire secondary structures upon partitioning from the solution to the membrane, following a classical partitioning-folding coupling process [47,50].

The increase in alpha-helical content of the different peptides in neutral membranes (POPC and DOPC) nicely correlates with the helix propensity scale of amino acids A, R, K, Q, and E (0, 0.21, 0.26, 0.39, and 0.40 kcal/mol, respectively, see Table 3 from [51]). Figure 5 shows that the helical content increases in the presence of membrane as a function of the free energy of partition for all membrane lipid compositions. A similar trend is observed between the membrane-induced helical content and the peptide valence (inset Figure 5B). Interestingly, R2Q partly deviates from this trend, suggesting that R474 significantly contributes to the formation of an α-helix upon membrane partitioning, whatever the lipid composition (Figure 5 and inset Figure 5B). Finally, as observed above for partition from solution to membrane, no correlations were observed between the hydrophobic moment, the mean hydrophobicity, and the membrane-induced increase in helical content (Figure S7), indicating that the ability of the peptides to form a helix in the membrane is not directly related to their amphipathic character.

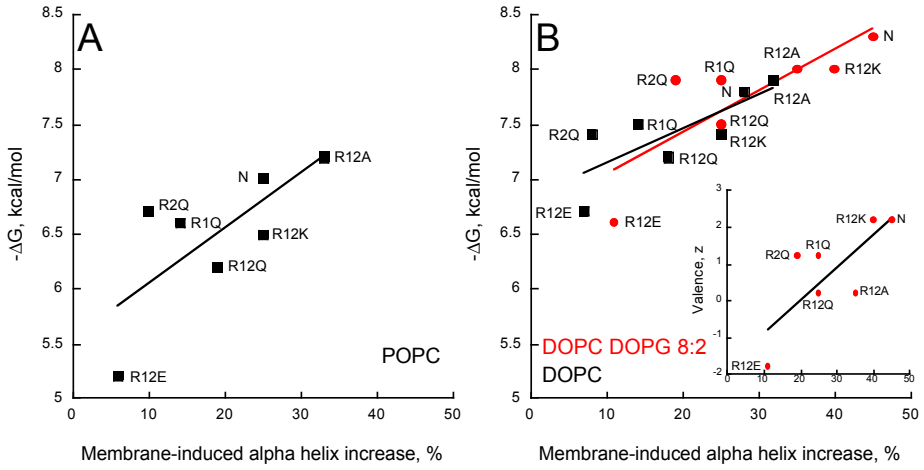

Figure 5. Partitioning-folding coupling of the P454-derived peptides. Helical content induced by the partition of peptides into POPC SUVs (**A**); DOPC SUVs (black squares) or DOPC/DOPG 8:2 SUVs (red circles) (**B**). For each peptide, the free energy of membrane partitioning is plotted as a function of the membrane-induced increase in helical content. ***Inset*** (**B**) Correlation between valence and membrane-induced helical content in the presence of DOPC/DOPG 8:2 SUVs. S.D. are ±0.1 kcal/mol.

2.7. Membrane Permeabilization

We studied membrane permeabilization induced by the P454 series by measuring the fluorescence recovery of ANTS upon vesicle efflux and dissociation from its quencher DPX. The kinetic traces are shown in supporting information (Figure S8). We then extracted the intensities of fluorescence recovery (Figure 6A,B) and the observed rate constants, k_{obs}, (Figure 6C,D), for each condition, i.e., in the presence of LUVs composed of POPC (Figure 6B,D) and POPC/POPG 8:2 (Figure 6A,C). The intensity and k_{obs} values are plotted as a function of the concentrations of the peptide partitioned into the membrane (i.e., taking into account the partition coefficient K_X (see Methods)).

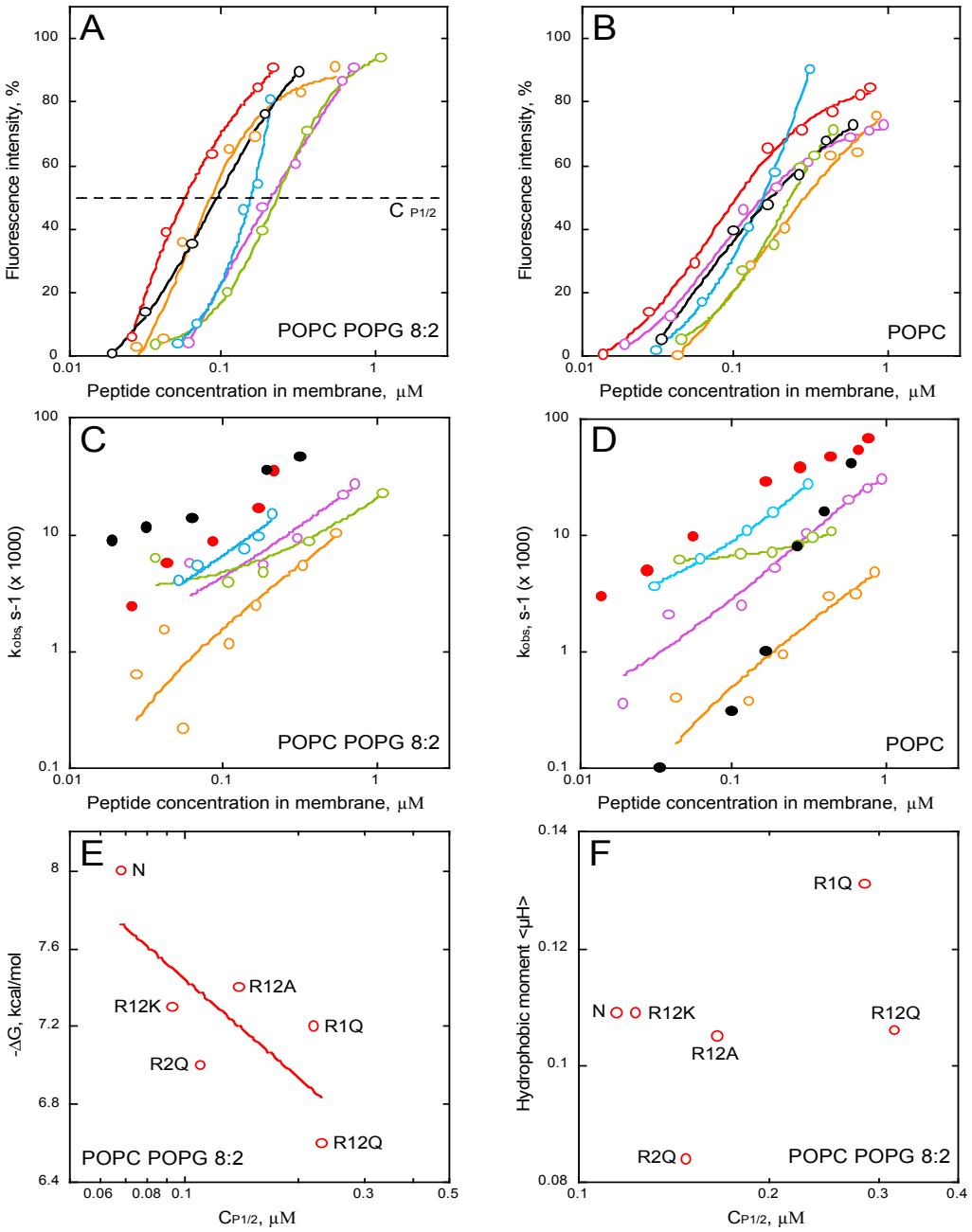

Figure 6. Membrane permeabilization by P454-derived peptides. Fluorescence intensities and observed constant rates, k_{obs}, of P454 (open and close red symbols), R1Q (purple), R2Q (orange), R12Q (green), R12A (blue), and R12K (open and close black symbols) in the presence of POPC/POPG 8:2 (**A**,**C**) or POPC (**B**,**D**) LUVs, are shown as a function of the concentration of membrane-bound peptides. (**E**) ΔG values as a function of the peptide concentration required to induce half recovery of ANTS fluorescence, $C_{P1/2}$, for the P454-derived peptides in POPC/POPG 8:2 LUVs. (**F**) Hydrophobic moment <μH> as a function of $C_{P1/2}$ in the presence of POPC/POPG LUVs. The LUVs are at a final lipid concentration of 0.45 mM. Raw data of permeabilization traces are shown in Figure S8.

The results clearly show that all P454 peptides, except R12E, are able to permeabilize anionic and neutral membranes in a concentration-dependent manner; yet, permeabilization intensities and k_{obs} values are both affected by the arginine substitutions (Figure 6A–D). The peptides that most efficiently permeabilize anionic membranes are the native P454, R12K, and R2Q, while a single arginine substitution in R1Q strongly affects P454 activity (Figure 6A, in purple). The concentrations

of membrane-bound peptides required to induce 50% of maximal ANTS fluorescence recovery, $C_{P1/2}$, are extracted from Figure 6A. The free energy of binding is then plotted as function of $C_{P1/2}$ (Figure 6E). Although the $C_{P1/2}$ values generally correlate with the free energy of membrane partitioning, some peptide variants somehow diverge from this general tendency, most particularly R1Q. Indeed, although R1Q exhibits a rather high affinity for membranes (with a ΔG value in between those of R12K and R2Q; panel 6E, left part), its $C_{P1/2}$ is relatively high, indicating that R1Q strongly partitions into membrane but is poorly efficient to destabilize lipid bilayers. Interestingly, R1Q exhibits the highest hydrophobic moment amongst the peptide series (Figure 6F) and acquires significant helical structures in membrane (Figure 5), suggesting that its weak permeabilization activity is not due to a loss of amphipathic property, nor helical content. Taken together, these results indicate that the arginine R461 of P454 specifically contributes to the anionic membrane permeabilization.

Interestingly, while the permeabilization rate constants of R12K are higher than those of WT P454 when tested on anionic membranes, they are strongly concentration-dependent when assayed on neutral membranes (Figure 6C,D, black circles). This suggests that lysines are able to induce a fast permeabilization in the presence of anionic lipids, while in the presence of neutral lipids, lysine residues are characterized by a significantly slower permeabilization than arginine ones (Figure 6D, red circles for WT P454). Although both arginine and lysine residues are positively charged, this data highlights the specific contribution of arginine side chains to membrane permeabilization (see discussion).

3. Discussion

The CyaA toxin is one of the main virulent factors produced by *Bordetella pertussis*, the bacterium responsible for whooping cough. It invades eukaryotic target cells through an original mechanism that involves a direct translocation of its AC domain across the plasma membrane. However, the conformational states and the thermodynamics of AC membrane translocation are still poorly understood. We previously identified a "translocating region", TR (see Figure 1A), which is essential for the transport of the AC domain into the cytoplasm of eukaryotic cells [10]. Indeed, deletion of this TR region selectively abolishes AC translocation across the membrane, while the cell binding and pore-forming (hemolysis) activities of the toxin are not affected. We then identified a shorter sequence, P454 (residues 454–484), which exhibits membrane-active properties, i.e., is able to both partition into and permeabilize membranes [11]. We proposed that once CyaA is inserted into the target cell membrane, this region might locally destabilize the lipid bilayer integrity, and hence, lower the energy required to translocate AC across the plasma membrane. Recently, Masin et al. showed that negatively charged residues (Asp and Glu) from TR are involved in modulating the pore-forming activity of CyaA, while mutations of positively charged residues within TR affect AC translocation [30].

Here, we further explored the structural and molecular properties of P454, the unique amphitropic peptide able to induce membrane permeabilization in the series we investigated (see below). We first characterized the effect of lipid composition on its membrane partitioning. We showed that P454 membrane interaction is favored by anionic lipid headgroups, as previously reported [11], and by acyl chain fluidity promoting liquid-disordered state (DO- vs. PO-acyl chains), while inverted hexagonal structures induced by cholesterol and PE lipids, promoting negative membrane curvature, disfavor P454 membrane interactions (Figure 3). Hence, membrane interaction of P454 is tightly regulated by the charge of the lipid head group and the physical properties of the lipid bilayer. P454 thus displays the classical properties of antimicrobial peptides (AMP) that undergo typical partition-folding coupling and shows greater affinity for negatively charged membranes than for neutral membranes. Moreover, lipid packing and order/rigidity—as induced by acyl chain saturation or cholesterol—decrease AMP membrane partitioning and permeabilization (see for instance [52] for a review), as observed here with P454 (Figures 3 and 4).

We then investigated the contributions of the arginine residues (R461 and R474) of P454 to membrane partitioning, folding, and permeabilization. P454 peptide variants were synthetized, in which R461 (called R1) and R474 (called R2) were substituted by various amino acids (A, K, Q, and E).

Our results show that both arginine residues contribute, albeit differently, to the membrane-binding and permeabilization properties of P454. Our data provides direct evidence that arginine residues, compared to other amino acids, are appropriated for interactions with both neutral and anionic lipids, helical structure formation in membranes, and local destabilization of lipid bilayers. We found that membrane insertion of P454 involves both electrostatic interactions and hydrophobic forces. On the one hand, the mean net charge of the peptides (R1Q, R2Q, R12Q, R12K, R12A, and R12E) correlates with their membrane partitioning and secondary structure formation (Figures 4 and 5). On the other, the efficient membrane partitioning of R12A, a P454 peptide with neutral charge, indicates that hydrophobic forces also significantly contribute to the peptide binding to lipid bilayer.

To further investigate the role of the guanidinium group of arginine in P454 activity, the two arginines, R461 and R474, were substituted by lysine residues in peptide R12K. Although, R12K has the same positive charge as P454, it shows weaker membrane binding than P454 with all types of lipid vesicles (Figure 4 and Table S5). Moreover, R12K is less efficient at permeabilizing neutral membranes than the native P454 peptide (Figure 6D). The higher free energy value of membrane partition measured with the native P454 peptide, as compared to R12K, highlights the contribution of the interactions established between the arginine side chains and the surrounding phospholipids. The guanidinium group from arginine forms a guanidinium-phosphate complex stabilized by a combination of bidentate hydrogen-bonding and attractive electrostatic interactions [53]. Bidentate guanidinium-phosphate complexes can be stably established between one arginine and several phospholipids, while complexes between lysine residues and lipids are unstable [54]. It has been shown by NMR that lysine side chains, unlike those of arginine, do not form long-lasting hydrogen bonds with lipid phosphates [53,55], indicating that the amino group of lysine is engaged in weaker interactions with the lipid phosphates than the guanidinium group of arginine [56]. Finally, arginine side chains are more rigid and hydrophobic than the mobile, disordered, and solvated lysine side chains. These properties of arginine side chains, i.e., aliphatic and positively charged at neutral pH, favor the location of its methyl groups in the hydrophobic core of the lipid acyl chains, and the guanidinium groups strongly bind to phosphates of lipid headgroups.

It has been shown that the network of interactions between arginine guanidinium groups and lipid phosphate groups induces distortion of the lipid bilayer [48,53,57,58], favoring membrane permeabilization, as observed with many AMPs that disrupt membrane integrity. Membrane insertion of such peptides induces a strong perturbation of lipid packing, favoring mixing of the acyl chains from the hydrophobic core with the polar groups from the lipid headgroups [59–61]. This local disorganization of the hydrophobic core and interfacial region allows the flux of molecules through the membrane. The arginine-induced membrane deformation and subsequent permeabilization is illustrated here by the comparison of the observed rate constants of P454 and R12K: in neutral membranes, WT P454, with its two native arginine residues, is able to induce a fast permeabilization at low peptide concentration while R12K requires high concentrations to speed up membrane permeabilization (Figure 6D). This highlights the strong impact on membrane binding and permeabilization of the guanidinium group of arginine as compared to the amino group of the lysine side chain.

A comparative analysis of R1Q and R2Q peptides revealed that the two arginine residues distinctly contribute to P454 interaction with membranes: R474 is primarily involved in helix formation upon membrane association, while R461 is important for membrane permeabilization. These results suggest a model in which the C-terminal part of P454 forms a helical structure in the membrane, while the N-terminal part locally destabilizes the lipid bilayer. The corresponding sequence within the full-length CyaA toxin may likely act similarly on the target cell membranes. Once the hydrophobic and acylation regions are stably inserted into the membrane, the C-terminal region of P454, containing R474, might insert into the membrane and allow its N-terminal part, containing R461, to locally disrupt the lipid bilayer. This local membrane deformation could lead to the mixing of hydrophobic core and lipid headgroups, and thus help to decrease the energy required to translocate the N-terminal

catalytic domain across the plasma membrane. In agreement with this, the protein $CyaA_{R461A}$, in which R461 was substituted by an alanine residue, exhibited a significant reduction of AC translocation compared to the WT CyaA, although toxin-binding to the cells was not affected (see Figure 3 in Masin et al. [30]). The reduced level of AC translocation measured with $CyaA_{R461A}$ may result from a lower membrane disruption capacity of R461, as evidenced by the permeabilization results obtained with R1Q (Figure 6E).

Finally, beyond the 454–484 segment from TR and the hydrophobic helical hairpins located in the hydrophobic region (500–750), we were interested in identifying other amphitropic helices that might be able to bind to membranes and destabilize lipid bilayers, and could thus contribute to the translocation process of CyaA. With this in mind, we have investigated the membrane-interacting properties of several short amphipathic segments from CyaA. They were selected according to their propensity to form helical structures, their local hydrophobicity, and their hydrophobic moment. Synthetic peptides modeled from these selected sequences were synthesized, and their abilities to partition from solution to membrane and to permeabilize membrane were analyzed by a combination of molecular dynamics, fluorescence, and circular dichroism experiments. We showed that several of these peptides exhibit membrane partitioning and secondary structure formation. However, none of them were able to permeabilize membranes (Figures 1, 2, S1 and S2). These different peptidic segments thus do not participate directly in the cell membrane destabilization, but they may contribute to appropriately docking the CyaA polypeptide chain on the surface of the plasma membrane of target cells in order to facilitate the transport of the catalytic domain across the lipid bilayer. This is particularly the case for P233, which could maintain the AC domain in close proximity to the membrane before translocation.

4. Conclusions

Many bacterial toxins need to invade eukaryotic cells to access an intracellular molecular target. Few of them carry their own translocation systems to deliver their catalytic domains into cell cytoplasm. This is the case, for example, of the diphtheria toxin, botulinum toxins, lethal toxin, and CyaA toxin [62–66]. These toxins are amphitropic, i.e., they are soluble proteins that are able to insert into membranes and translocate their catalytic domains across target membranes [67]. Interestingly, besides their hydrophobic helices, which likely favor membrane insertion of the toxins into the hydrophobic core of lipid bilayers, these proteins possess arginine rich, amphitropic segments able to locally destabilize lipid bilayers, such as TH1 to TH4 in the diphtheria toxin [14,68] and the translocation region of CyaA [10,11]. These regions thus act as membrane permeabilizing peptides embarked into bacterial toxins and are actively involved in the translocation process by locally disrupting the membrane integrity, a process that decreases the energy required to transport catalytic domains into target cells.

5. Materials and Methods

5.1. Reagents

1-palmitoyl-2-oleoyl-*sn*-glycero-3-phosphocholine (POPC, reference 850457C), 1-palmitoyl-2-oleoyl-*sn*-glycero-3-[phospho-*rac*-(1-glycerol)] (POPG, reference 840457C), 1,2-dioleoyl-*sn* -glycero-3-phosphocholine (DOPC, reference 850375C), 1,2-dioleoyl-*sn*-glycero-3-[phospho-*rac*-(1-glycerol)] (DOPG, reference 840475C), 1,2-dioleoyl-*sn*-glycero-3-phosphoethanolamine (DOPE, reference 850725C), and cholesterol (Chol, reference 700000P) were from Avanti Polar Lipids (Alabaster, AL, USA). All experiments were performed in 20 mM HEPES, 150 mM NaCl, pH 7.4 (buffer A). ANTS (A-350, 8-aminonapthalene-1,3,6 trisulfonic acid), and DPX (X-1525, p-xylene-bis-pyridinium bromide) were purchased from Molecular Probes (Eugene, OR, USA).

5.2. Peptides

All peptides were produced and purified by Genosphere Biotechnologies (Paris, France) and their purity, as their molecular weight, were controlled by HPLC and MALDI. All peptides were capped on the N-terminus with an acetyl group and on the C-terminus with an amide group. We studied 11 CyaA-derived peptides: P19, P89, P233, P414, P454, P495, P509, P626, P717, P737, and P777 peptides, as well as 6 P454-derived peptides (R1Q, R2Q, R12Q, R12A, R12K, and R12E). The peptides were selected according to their propensity to form helical structures, their local hydrophobicity, and their hydrophobic moment (Figure S1).

- The P19 peptide corresponds to the B-helix in AC, i.e., residues 19 to 35 of CyaA (IPAAVL DGIKAVAKEKNW), and a tryptophan was added at its C-terminal extremity (underlined).
- The P89 peptide corresponds to the D-helix in AC, i.e., residues 89 to 107 (APEVIAR ADNDVNSSLAHGW), with a tryptophan added at its C-terminal extremity (underlined).
- The P233 peptide corresponds to the H-helix in AC, i.e., residues 233 to 254 of CyaA (LDRERIDLLWKIARAGARSAVG), and contains the native tryptophan W242.
- The P414 peptide corresponds to residues 414 to 440 of CyaA (SW SLGEVSD-MAAVEAAELEMTRQVLHA), in which Phe-415 was substituted by a tryptophan residue (underlined).
- The P454 peptide corresponds to residues 454 to 484 of CyaA (ASAHWGQRALQG AQAVAAAQRLVHAIALMTQ) and contains the single native tryptophan W458. Several P454-derived peptides were also synthetized, in which the two arginine residues R461 (hereafter referred to as R1) or R474 (referred to as R2), or both of them (referred to R12) were substituted by either lysines (R12K), glutamines (R1Q, R2Q and R12Q), alanines (R12A), or glutamates (R12E).
- The P495 peptide corresponds to residues 495 to 524 of CyaA (QEAASLSAAVFG LGEASSAVAETVSGFFRGW), and a tryptophan was added at its C-terminal extremity (underlined).
- The P509 peptide is a shorter peptide from P495, corresponding to residues 509 to 524 of CyaA (EASSAVAETVSGFFRGW), and a tryptophan was added at its C-terminal extremity (underlined).
- The P626 peptide corresponds to residues 626 to 647 of CyaA (LVQQSHYA DQLDKLAQESSAYGW), and a tryptophan was added at its C-terminal extremity (underlined).
- The P717 peptide corresponds to residues 717 to 733 of CyaA (IIEKLANDYARKIDELGW), and a tryptophan was added at its C-terminal extremity (underlined).
- The P737 peptide corresponds to residues 737 to 771 of CyaA (AYFEKNLQA RHEQLANSDGLRKMLADLQAGWNASS) and contains the single native tryptophan W767.
- Finally, the P777 peptide corresponds to residues 777 to 793 of CyaA (TTEISKSALELAAITGNW) and a tryptophan was added at its C-terminal extremity (underlined).

The physical chemistry of these peptides is described in Tables S1 and S2.

5.3. Lipid Vesicles Preparation

Small unilamellar vesicles (SUVs) were prepared at a lipid concentration of 10 mM from POPC and POPG at a molar ratio of 10:0 or 8:2 or from DOPC, DOPE, DOPG, Chol at molar ratio 10:0:0:0, 8:0:2:0, 7:3:0:0, 7:0:0:3, 6:3:0:1, and 4:3:2:1 in buffer A, as previously described [69]. Briefly, SUVs were prepared by reverse-phase evaporation and passed through polycarbonate filters 0.8-, 0.4-, and 0.2-µm (Merck Millipore, Darmstadt, Germany). Vesicles were sonicated using a sonicator tip and their hydrodynamic diameters, dispersity, and charge were checked by dynamic light scattering (DLS) and electrophoretic mobility using a NanoZS instrument (Malvern Instruments, Orsay, France).

5.4. Tryptophan Fluorescence Titrations

Fluorescence titrations were performed with a FP-8200 Jasco spectrofluorimeter, equipped with a Peltier-thermostated ETC-272T (25 °C). A bandwidth of 5 nm was used for both excitation and emission beams. Fluorescence experiments were carried out in a 109.004F-QS cuvette (Hellma, France) with constant stirring. Fluorescence emission was recorded between 300 and 400 nm at a scan rate of 200 nm/min, with an excitation wavelength of 280 nm. Fluorescence emission spectra were corrected for SUV light scattering. Maximum emission wavelength (λ_{max}) and fluorescence intensity ratio at 330 nm over 370 nm (P454-derived peptides) or at 340 nm over 380 nm (CyaA-derived peptides) were used to report peptide-membrane interaction and to measure the partition coefficient K_X.

5.5. Peptide Partition from Solution to Membranes

The partition coefficient K_X is defined as the ratio of protein concentrations in the lipid and in buffer phases [10,11,47]. It is expressed as follows:

$K_X = \frac{P_L}{P_W} \cdot \frac{[W]}{[L]}$, providing $\frac{P_W}{P_L} = \frac{[W]}{K_X[L]}$, where P_W is the concentration of peptide in solution, P_L the concentration of peptides partitioning into lipid membrane, $[W]$ represents the concentration of water, and $[L]$ the lipid concentration.

The fraction of peptide partitioned into the membrane phase, f_{PL}, is equal to:

$$f_{PL} = \frac{P_L}{P_T} = \frac{P_L}{P_L + P_W} = \frac{1}{(P_W/P_L) + 1} = \frac{1}{\left(\frac{[W]}{K_X[L]}\right) + 1}$$

The partition coefficient is related to the apparent dissociation constant as follows: K_X * K_D = $[W]$ with K_D * P_L = P_W * $[L]$. The equation f_{PL} is fitted to the experimental data using the KaleidaGraph software, providing K_X. The free energy corresponding to the transfer of the peptide from the aqueous phase to the lipid phase is given by the equation $\Delta G = -RT \ln(K_X)$, where ΔG is the free energy in kcal/mol, R the gas constant (R = 1.98 × 10^{-3} kcal/mol/K), and T the temperature in Kelvin.

5.6. Circular Dichroism

Synchrotron radiation circular dichroism (SRCD) experiments were carried out on the DISCO beamline of Synchrotron SOLEIL (Gif-sur-Yvette, France). SRCD spectra were recorded at 25 °C with an integration time of 1.2 s and a bandwidth of 1 nm with a resolution of 1 nm. Each far-UV spectrum represents the average of three individual scans. QS cells (Hellma, France) with a path length of 100 µm were used to record SRCD signal in the far-UV (from 190 to 250 nm). Peptides were tested at 100 µM in buffer A and in the presence of 20% of trifluoroethanol (TFE). Peptides were incubated in the presence of SUVs (POPC, DOPC, or DOPC/DOPG 8:2) at final concentration of 2 mM lipids. Buffer A, in the absence or presence of SUVs, was used as blank and subtracted from far-UV CD spectra of peptides. Secondary structure content was estimated using Bestsel [49].

5.7. Membrane Permeabilization

ANTS (fluorophore probe) and DPX (quencher) were encapsulated into large unilamellar vesicles (LUVs) to monitor membrane permeabilization induced by the peptides. The LUVs were prepared at a concentration of 10 mM lipid at the following molar ratio DOPC/DOPE/DOPG/Chol 4:3:2:1, POPC/POPG 8:2, or POPC containing 20 mM ANTS and 60 mM DPX. The multilamellar vesicle suspension was passed through 0.4- and 0.2-µm polycarbonate filters to produce LUVs of 200 ± 30 nm in diameter, as measured by DLS. The unencapsulated probes were removed by gel filtration through a Sephadex G-25 column 5 mL (GE Healthcare Life Sciences, Pittsburgh, PA, USA). For permeabilization assays, LUVs were incubated in buffer at 0.45 mM lipids at 25 °C in a 101-QS cuvette (Hellma, France) and under constant stirring. The excitation wavelength was set to 390 nm and the emission of ANTS was continuously measured at 515 nm. A single exponential equation was fitted to kinetic traces

to extract fluorescence intensity and observed rate constants, k_{obs}. The percentage of fluorescence intensity was calculated using the maximum intensity measured after complete disruption of the vesicles with addition of 0.12% (2 mM) of Triton. The concentration of membrane-bound peptide required to induce half-maximal ANTS fluorescence recovery ($C_{P1/2}$) is extracted from the plot of permeabilization intensity as a function of peptide concentration (Figure 6A).

5.8. Molecular Dynamics

The coarse-grained simulations were carried out with Gromacs 4.5.5 [70] using the Martini force field [71–73] (md.chem.rug.nl). The coarse-grained model of the P233, P454, P509, and P717 were directly derived from the all-atom NMR models. Firstly, 1000 lipids were randomly mixed with water and charged beads mimicking counter-ions. Two ratios of DOPC/DOPG/Cholesterol were used: 8:1:1 and 9:0:1 in order to study the influence of negatively charged lipids. The lipid-water mixture was equilibrated over 20 ns using a 20 fs time step. The temperature was maintained to 323.15 K using velocity rescaling [74] and a coupling constant of 1 ps. The pressure was maintained to 1 bar using a semi-isotropic Berendsen barostat [75], a coupling constant of 2 ps, and a compressibility of $3e^{-4}$ bar^{-1}. Van der Waals interaction was cut off at 12 Å with a shift function applied beyond 9 Å. Electrostatics were cut-off at 14 Å with long range electrostatics treated by the particle mesh Ewald method [76,77] using a grid spacing of approximately 1 Å. The dielectric constant was set to 15. The two systems were simulated over 0.5 µs, i.e., until a lipid bilayer at equilibrium was obtained. It should be noted that bilayers were self-assembled in approximately 0.1 µs. Secondly, the resulting bilayers were extracted and the peptides P233, P454, P509, and P717 were placed at approximately 4.8 nm from the bilayer center, i.e., 0.8 nm above the bilayer surface. The systems were fully hydrated and neutralized with charged beads. The final size of the lipid-peptide systems was approximately $16 \times 20 \times 23.5$ nm^3. Each system was equilibrated over 20 ns in conditions identical to the lipid-water mixture, then simulated over 1 µs. Visualization of the trajectories was done with VMD 1.9.1 [78]. Their analysis was carried out with Gromacs 4.5.5 [70], R 2.14.1 [79], and the ggplot2 package [80].

Supplementary Materials: The following are available online at www.mdpi.com/2072-6651/9/11/369/s1: Figure S1: Hydrophobic moment <µH> as function of the mean hydrophobicity <H> of the CyaA-derived peptides; Figure S2: Far-UV circular dichroism spectra of the CyaA-derived peptides; Figure S3: Partition of CyaA-derived peptides followed by tryptophan intrinsic fluorescence; Figure S4: Free energy of partition of peptides in POPC/POPG membranes as a function of mean hydrophobicity <H> or hydrophobic moment <µH>; Figure S5: Synchrotron radiation far-UV circular dichroism of P454-derived peptides; Figure S6: Helical content of the P454-derived peptides in various environments; Figure S7: Membrane-induced helical content in the presence of DOPC/DOPG SUVs as a function of mean hydrophobicity <H> or hydrophobic moment <µH>; Figure S8: Membrane permeabilization induced by the P454-derived peptides; Table S1: Peptide names, number of residues, molecular weight, pK and charge at physiological pH of each peptide used in this study; Table S2: Maximum mean hydrophobicity <H> and hydrophobic moment <µH> of each peptide using their full sequence or a window of 12 to 18 amino acids; Table S3: Thermodynamics of peptide partitioning from solution to membrane; Table S4: Effect of lipid bilayer composition on P454 membrane partitioning; Table S5: Partition of P454-derived peptides from solution to membrane; Table S6: Estimation of the α helical content of peptides.

Acknowledgments: We thank SOLEIL for provision of synchrotron radiation facilities. We thank Frank Wien and Matthieu Refregiers for their excellent assistance in using the DISCO beamline and for optimized working conditions at DISCO. This work was supported by DIM Malinf, Région Ile-de-France, CNRS and Institut Pasteur (PasteurInnoV and PTR).

Author Contributions: A.C. designed the experiments; A.V., O.S. and N.S. made the experiments; A.V., D.L. and A.C. wrote the manuscript.

Conflicts of Interest: The authors declare no conflict of interest.

References

1. Ladant, D.; Brezin, C.; Alonso, J.M.; Crenon, I.; Guiso, N. Bordetella pertussis adenylate cyclase. Purification, characterization, and radioimmunoassay. *J. Biol. Chem.* **1986**, *261*, 16264–16269. [PubMed]
2. Bouchez, V.; Guiso, N. Bordetella pertussis, *B. parapertussis*, vaccines and cycles of whooping cough. *Pathog. Dis.* **2015**, *73*. [CrossRef] [PubMed]

3. Weiss, A.A.; Hewlett, E.L. Virulence factors of bordetella pertussis. *Annu. Rev. Microbiol.* **1986**, *40*, 661–686. [CrossRef] [PubMed]
4. Ladant, D.; Ullmann, A. Bordatella pertussis adenylate cyclase: A toxin with multiple talents. *Trends Microbiol.* **1999**, *7*, 172–176. [CrossRef]
5. Karst, J.C.; Ntsogo Enguene, V.Y.; Cannella, S.E.; Subrini, O.; Hessel, A.; Debard, S.; Ladant, D.; Chenal, A. Calcium, acylation, and molecular confinement favor folding of bordetella pertussis adenylate cyclase CyaA toxin into a monomeric and cytotoxic form. *J. Biol. Chem.* **2014**, *289*, 30702–30716. [CrossRef] [PubMed]
6. Masin, J.; Osicka, R.; Bumba, L.; Sebo, P. Bordetella adenylate cyclase toxin: A unique combination of a pore-forming moiety with a cell-invading adenylate cyclase enzyme. *Pathog. Dis.* **2015**, *73*, ftv075. [CrossRef] [PubMed]
7. Cannella, S.E.; Ntsogo Enguene, V.Y.; Davi, M.; Malosse, C.; Sotomayor Perez, A.C.; Chamot-Rooke, J.; Vachette, P.; Durand, D.; Ladant, D.; Chenal, A. Stability, structural and functional properties of a monomeric, calcium-loaded adenylate cyclase toxin, CyaA, from bordetella pertussis. *Sci. Rep.* **2017**, *7*, 42065. [CrossRef] [PubMed]
8. Ladant, D. Interaction of bordetella pertussis adenylate cyclase with calmodulin. Identification of two separated calmodulin-binding domains. *J. Biol. Chem.* **1988**, *263*, 2612–2618. [PubMed]
9. Karst, J.C.; Sotomayor Perez, A.C.; Guijarro, J.I.; Raynal, B.; Chenal, A.; Ladant, D. Calmodulin-induced conformational and hydrodynamic changes in the catalytic domain of bordetella pertussis adenylate cyclase toxin. *Biochemistry* **2010**, *49*, 318–328. [CrossRef] [PubMed]
10. Karst, J.C.; Barker, R.; Devi, U.; Swann, M.J.; Davi, M.; Roser, S.J.; Ladant, D.; Chenal, A. Identification of a region that assists membrane insertion and translocation of the catalytic domain of bordetella pertussis CyaA toxin. *J. Biol. Chem.* **2012**, *287*, 9200–9212. [CrossRef] [PubMed]
11. Subrini, O.; Sotomayor-Perez, A.C.; Hessel, A.; Spiaczka-Karst, J.; Selwa, E.; Sapay, N.; Veneziano, R.; Pansieri, J.; Chopineau, J.; Ladant, D.; et al. Characterization of a membrane-active peptide from the bordetella pertussis CyaA toxin. *J. Biol. Chem.* **2013**, *288*, 32585–32598. [CrossRef] [PubMed]
12. Rose, T.; Sebo, P.; Bellalou, J.; Ladant, D. Interaction of calcium with bordetella pertussis adenylate cyclase toxin. Characterization of multiple calcium-binding sites and calcium-induced conformational changes. *J. Biol. Chem.* **1995**, *270*, 26370–26376. [CrossRef] [PubMed]
13. Bauche, C.; Chenal, A.; Knapp, O.; Bodenreider, C.; Benz, R.; Chaffotte, A.; Ladant, D. Structural and functional characterization of an essential RTX subdomain of bordetella pertussis adenylate cyclase toxin. *J. Biol. Chem.* **2006**, *281*, 16914–16926. [CrossRef] [PubMed]
14. Chenal, A.; Prongidi-Fix, L.; Perier, A.; Aisenbrey, C.; Vernier, G.; Lambotte, S.; Haertlein, M.; Dauvergne, M.T.; Fragneto, G.; Bechinger, B.; et al. Deciphering membrane insertion of the diphtheria toxin t domain by specular neutron reflectometry and solid-state nmr spectroscopy. *J. Mol. Biol.* **2009**, *391*, 872–883. [CrossRef] [PubMed]
15. Chenal, A.; Karst, J.C.; Sotomayor Perez, A.C.; Wozniak, A.K.; Baron, B.; England, P.; Ladant, D. Calcium-induced folding and stabilization of the intrinsically disordered RTX domain of the CyaA toxin. *Biophys. J.* **2010**, *99*, 3744–3753. [CrossRef] [PubMed]
16. Sotomayor Perez, A.C.; Karst, J.C.; Davi, M.; Guijarro, J.I.; Ladant, D.; Chenal, A. Characterization of the regions involved in the calcium-induced folding of the intrinsically disordered RTX motifs from the bordetella pertussis adenylate cyclase toxin. *J. Mol. Biol.* **2010**, *397*, 534–549. [CrossRef] [PubMed]
17. Sotomayor-Perez, A.C.; Ladant, D.; Chenal, A. Calcium-induced folding of intrinsically disordered repeat-in-toxin (RTX) motifs via changes of protein charges and oligomerization states. *J. Biol. Chem.* **2011**, *286*, 16997–17004. [CrossRef] [PubMed]
18. Sotomayor-Perez, A.C.; Subrini, O.; Hessel, A.; Ladant, D.; Chenal, A. Molecular crowding stabilizes both the intrinsically disordered calcium-free state and the folded calcium-bound state of a repeat in toxin (RTX) protein. *J. Am. Chem. Soc.* **2013**, *135*, 11929–11934. [CrossRef] [PubMed]
19. O'Brien, D.P.; Hernandez, B.; Durand, D.; Hourdel, V.; Sotomayor-Perez, A.C.; Vachette, P.; Ghomi, M.; Chamot-Rooke, J.; Ladant, D.; Brier, S.; et al. Structural models of intrinsically disordered and calcium-bound folded states of a protein adapted for secretion. *Sci. Rep.* **2015**, *5*, 14223. [CrossRef] [PubMed]
20. Sotomayor-Perez, A.C.; Ladant, D.; Chenal, A. Disorder-to-order transition in the CyaA toxin RTX domain: Implications for toxin secretion. *Toxins* **2015**, *7*, 1–20. [CrossRef] [PubMed]

21. Bumba, L.; Masin, J.; Macek, P.; Wald, T.; Motlova, L.; Bibova, I.; Klimova, N.; Bednarova, L.; Veverka, V.; Kachala, M.; et al. Calcium-driven folding of RTX domain beta-rolls ratchets translocation of RTX proteins through type I secretion ducts. *Mol. Cell* **2016**, *62*, 47–62. [CrossRef] [PubMed]
22. Rogel, A.; Hanski, E. Distinct steps in the penetration of adenylate cyclase toxin of bordetella pertussis into sheep erythrocytes. Translocation of the toxin across the membrane. *J. Biol. Chem.* **1992**, *267*, 22599–22605. [PubMed]
23. Guermonprez, P.; Khelef, N.; Blouin, E.; Rieu, P.; Ricciardi-Castagnoli, P.; Guiso, N.; Ladant, D.; Leclerc, C. The adenylate cyclase toxin of bordetella pertussis binds to target cells via the alpha(m)beta(2) integrin (CD11b/CD18). *J. Exp. Med.* **2001**, *193*, 1035–1044. [CrossRef] [PubMed]
24. Paccani, S.R.; Finetti, F.; Davi, M.; Patrussi, L.; D'Elios, M.M.; Ladant, D.; Baldari, C.T. The bordetella pertussis adenylate cyclase toxin binds to T cells via lFA-1 and induces its disengagement from the immune synapse. *J. Exp. Med.* **2011**, *208*, 1317–1330. [CrossRef] [PubMed]
25. Osicka, R.; Osickova, A.; Hasan, S.; Bumba, L.; Cerny, J.; Sebo, P. Bordetella adenylate cyclase toxin is a unique ligand of the integrin complement receptor 3. *eLife* **2015**, *4*, e10766. [CrossRef] [PubMed]
26. Gonzalez-Bullon, D.; Uribe, K.B.; Martin, C.; Ostolaza, H. Phospholipase a activity of adenylate cyclase toxin mediates translocation of its adenylate cyclase domain. *Proc. Natl. Acad. Sci. USA* **2017**, *114*, E6784–E6793. [CrossRef] [PubMed]
27. Ehrmann, I.E.; Gray, M.C.; Gordon, V.M.; Gray, L.S.; Hewlett, E.L. Hemolytic activity of adenylate cyclase toxin from bordetella pertussis. *FEBS Lett.* **1991**, *278*, 79–83. [PubMed]
28. Benz, R.; Maier, E.; Ladant, D.; Ullmann, A.; Sebo, P. Adenylate cyclase toxin (CyaA) of bordetella pertussis. Evidence for the formation of small ion-permeable channels and comparison with hlyA of *Escherichia coli*. *J. Biol. Chem.* **1994**, *269*, 27231–27239. [PubMed]
29. Basler, M.; Knapp, O.; Masin, J.; Fiser, R.; Maier, E.; Benz, R.; Sebo, P.; Osicka, R. Segments crucial for membrane translocation and pore-forming activity of bordetella adenylate cyclase toxin. *J. Biol. Chem.* **2007**, *282*, 12419–12429. [CrossRef] [PubMed]
30. Masin, J.; Osickova, A.; Sukova, A.; Fiser, R.; Halada, P.; Bumba, L.; Linhartova, I.; Osicka, R.; Sebo, P. Negatively charged residues of the segment linking the enzyme and cytolysin moieties restrict the membrane-permeabilizing capacity of adenylate cyclase toxin. *Sci. Rep.* **2016**, *6*, 29137. [CrossRef] [PubMed]
31. Hackett, M.; Guo, L.; Shabanowitz, J.; Hunt, D.F.; Hewlett, E.L. Internal lysine palmitoylation in adenylate cyclase toxin from bordetella pertussis. *Science* **1994**, *266*, 433–435. [CrossRef] [PubMed]
32. Hackett, M.; Walker, C.B.; Guo, L.; Gray, M.C.; Van Cuyk, S.; Ullmann, A.; Shabanowitz, J.; Hunt, D.F.; Hewlett, E.L.; Sebo, P. Hemolytic, but not cell-invasive activity, of adenylate cyclase toxin is selectively affected by differential fatty-acylation in escherichia coli. *J. Biol. Chem.* **1995**, *270*, 20250–20253. [CrossRef] [PubMed]
33. Havlicek, V.; Higgins, L.; Chen, W.; Halada, P.; Sebo, P.; Sakamoto, H.; Hackett, M. Mass spectrometric analysis of recombinant adenylate cyclase toxin from bordetella pertussis strain 18323/phsp9. *J. Mass Spectrom.* **2001**, *36*, 384–391. [CrossRef] [PubMed]
34. Basar, T.; Havlicek, V.; Bezouskova, S.; Hackett, M.; Sebo, P. Acylation of lysine 983 is sufficient for toxin activity of bordetella pertussis adenylate cyclase. Substitutions of alanine 140 modulate acylation site selectivity of the toxin acyltransferase CyaC. *J. Biol. Chem.* **2001**, *276*, 348–354. [CrossRef] [PubMed]
35. Masin, J.; Basler, M.; Knapp, O.; El-Azami-El-Idrissi, M.; Maier, E.; Konopasek, I.; Benz, R.; Leclerc, C.; Sebo, P. Acylation of lysine 860 allows tight binding and cytotoxicity of bordetella adenylate cyclase on CD11b-expressing cells. *Biochemistry* **2005**, *44*, 12759–12766. [CrossRef] [PubMed]
36. Otero, A.S.; Yi, X.B.; Gray, M.C.; Szabo, G.; Hewlett, E.L. Membrane depolarization prevents cell invasion by bordetella pertussis adenylate cyclase toxin. *J. Biol. Chem.* **1995**, *270*, 9695–9697. [CrossRef] [PubMed]
37. Veneziano, R.; Rossi, C.; Chenal, A.; Devoisselle, J.M.; Ladant, D.; Chopineau, J. Bordetella pertussis adenylate cyclase toxin translocation across a tethered lipid bilayer. *Proc. Natl. Acad. Sci. USA* **2013**, *110*, 20473–20478. [CrossRef] [PubMed]
38. Johnson, J.E.; Cornell, R.B. Amphitropic proteins: Regulation by reversible membrane interactions (review). *Mol. Membr. Biol.* **1999**, *16*, 217–235. [CrossRef] [PubMed]
39. Cornell, R.B.; Taneva, S.G. Amphipathic helices as mediators of the membrane interaction of amphitropic proteins, and as modulators of bilayer physical properties. *Curr. Protein Peptide Sci.* **2006**, *7*, 539–552. [CrossRef]

40. Eisenberg, D.; Weiss, R.M.; Terwilliger, T.C. The helical hydrophobic moment: A measure of the amphiphilicity of a helix. *Nature* **1982**, *299*, 371–374. [CrossRef] [PubMed]
41. Mihailescu, M.; Soubias, O.; Worcester, D.; White, S.H.; Gawrisch, K. Structure and dynamics of cholesterol-containing polyunsaturated lipid membranes studied by neutron diffraction and NMR. *J. Membr. Biol.* **2011**, *239*, 63–71. [CrossRef] [PubMed]
42. Mihailescu, M.; Vaswani, R.G.; Jardon-Valadez, E.; Castro-Roman, F.; Freites, J.A.; Worcester, D.L.; Chamberlin, A.R.; Tobias, D.J.; White, S.H. Acyl-chain methyl distributions of liquid-ordered and -disordered membranes. *Biophys. J.* **2011**, *100*, 1455–1462. [CrossRef] [PubMed]
43. Dawaliby, R.; Trubbia, C.; Delporte, C.; Noyon, C.; Ruysschaert, J.M.; Van Antwerpen, P.; Govaerts, C. Phosphatidylethanolamine is a key regulator of membrane fluidity in eukaryotic cells. *J. Biol. Chem.* **2016**, *291*, 3658–3667. [CrossRef] [PubMed]
44. Epand, R.M. Detection of hexagonal phase forming propensity in phospholipid bilayers. *Biophys. J.* **1993**, *64*, 290–291. [CrossRef]
45. De Kruijff, B. Lipid polymorphism and biomembrane function. *Curr. Opin. Chem. Biol.* **1997**, *1*, 564–569. [CrossRef]
46. Toombes, G.E.; Finnefrock, A.C.; Tate, M.W.; Gruner, S.M. Determination of L(alpha)-H(II) phase transition temperature for 1,2-dioleoyl-sn-glycero-3-phosphatidylethanolamine. *Biophys. J.* **2002**, *82*, 2504–2510. [CrossRef]
47. White, S.H.; Wimley, W.C. Membrane protein folding and stability: Physical principles. *Annu. Rev. Biophys. Biomol. Struct.* **1999**, *28*, 319–365. [CrossRef] [PubMed]
48. Hristova, K.; Wimley, W.C. A look at arginine in membranes. *J. Membr. Biol.* **2011**, *239*, 49–56. [CrossRef] [PubMed]
49. Micsonai, A.; Wien, F.; Kernya, L.; Lee, Y.H.; Goto, Y.; Refregiers, M.; Kardos, J. Accurate secondary structure prediction and fold recognition for circular dichroism spectroscopy. *Proc. Natl. Acad. Sci. USA* **2015**, *112*, E3095–E3103. [CrossRef] [PubMed]
50. White, S.H.; Wimley, W.C.; Ladokhin, A.S.; Hristova, K. Protein folding in membranes: Determining energetics of peptide-bilayer interactions. *Methods Enzymol.* **1998**, *295*, 62–87. [PubMed]
51. Pace, C.N.; Scholtz, J.M. A helix propensity scale based on experimental studies of peptides and proteins. *Biophys. J.* **1998**, *75*, 422–427. [CrossRef]
52. Sani, M.A.; Separovic, F. How membrane-active peptides get into lipid membranes. *Acc. Chem. Res.* **2016**, *49*, 1130–1138. [CrossRef] [PubMed]
53. Su, Y.; Doherty, T.; Waring, A.J.; Ruchala, P.; Hong, M. Roles of arginine and lysine residues in the translocation of a cell-penetrating peptide from 13C, 31P, and 19F solid-state NMR. *Biochemistry* **2009**, *48*, 4587–4595. [CrossRef] [PubMed]
54. Schug, K.A.; Lindner, W. Noncovalent binding between guanidinium and anionic groups: Focus on biological- and synthetic-based arginine/guanidinium interactions with phosph[on]ate and sulf[on]ate residues. *Chem. Rev.* **2005**, *105*, 67–114. [CrossRef] [PubMed]
55. Tang, M.; Waring, A.J.; Hong, M. Phosphate-mediated arginine insertion into lipid membranes and pore formation by a cationic membrane peptide from solid-state NMR. *J. Am. Chem. Soc.* **2007**, *129*, 11438–11446. [CrossRef] [PubMed]
56. Su, Y.; Li, S.; Hong, M. Cationic membrane peptides: Atomic-level insight of structure-activity relationships from solid-state NMR. *Amino Acids* **2013**, *44*, 821–833. [CrossRef] [PubMed]
57. Herce, H.D.; Garcia, A.E.; Litt, J.; Kane, R.S.; Martin, P.; Enrique, N.; Rebolledo, A.; Milesi, V. Arginine-rich peptides destabilize the plasma membrane, consistent with a pore formation translocation mechanism of cell-penetrating peptides. *Biophys. J.* **2009**, *97*, 1917–1925. [CrossRef] [PubMed]
58. Tanaka, G.; Nakase, I.; Fukuda, Y.; Masuda, R.; Oishi, S.; Shimura, K.; Kawaguchi, Y.; Takatani-Nakase, T.; Langel, U.; Graslund, A.; et al. Cxcr4 stimulates macropinocytosis: Implications for cellular uptake of arginine-rich cell-penetrating peptides and HIV. *Chem. Biol.* **2012**, *19*, 1437–1446. [CrossRef] [PubMed]
59. Lohner, K.; Blondelle, S.E. Molecular mechanisms of membrane perturbation by antimicrobial peptides and the use of biophysical studies in the design of novel peptide antibiotics. *Comb. Chem. High Throughput Screen.* **2005**, *8*, 241–256. [CrossRef] [PubMed]
60. Schmidt, N.; Mishra, A.; Lai, G.H.; Wong, G.C. Arginine-rich cell-penetrating peptides. *FEBS Lett.* **2010**, *584*, 1806–1813. [CrossRef] [PubMed]

61. Bennett, W.F.; Tieleman, D.P. The importance of membrane defects-lessons from simulations. *Acc. Chem. Res.* **2014**, *47*, 2244–2251. [CrossRef] [PubMed]
62. Chenal, A.; Nizard, P.; Gillet, D. Structure and function of diphtheria toxin: From pathology to engineering. *J. Toxicol. Toxin Rev.* **2002**, *21*, 321–359. [CrossRef]
63. Galloux, M.; Vitrac, H.; Montagner, C.; Raffestin, S.; Popoff, M.R.; Chenal, A.; Forge, V.; Gillet, D. Membrane interaction of botulinum neurotoxin a translocation (t) domain. The belt region is a regulatory loop for membrane interaction. *J. Biol. Chem.* **2008**, *283*, 27668–27676. [CrossRef] [PubMed]
64. Varela Chavez, C.; Haustant, G.M.; Baron, B.; England, P.; Chenal, A.; Pauillac, S.; Blondel, A.; Popoff, M.R. The tip of the four n-terminal alpha-helices of clostridium sordellii lethal toxin contains the interaction site with membrane phosphatidylserine facilitating small GTPases glucosylation. *Toxins* **2016**, *8*, 90. [CrossRef] [PubMed]
65. Varela Chavez, C.; Hoos, S.; Haustant, G.M.; Chenal, A.; England, P.; Blondel, A.; Pauillac, S.; Lacy, D.B.; Popoff, M.R. The catalytic domains of clostridium sordellii lethal toxin and related large clostridial glucosylating toxins specifically recognize the negatively charged phospholipids phosphatidylserine and phosphatidic acid. *Cell. Microbiol.* **2015**, *17*, 1477–1493. [CrossRef] [PubMed]
66. Araye, A.; Goudet, A.; Barbier, J.; Pichard, S.; Baron, B.; England, P.; Perez, J.; Zinn-Justin, S.; Chenal, A.; Gillet, D. The translocation domain of botulinum neurotoxin a moderates the propensity of the catalytic domain to interact with membranes at acidic pH. *PLoS ONE* **2016**, *11*, e0153401.
67. Reig, N.; van der Goot, F.G. About lipids and toxins. *FEBS Lett.* **2006**, *580*, 5572–5579. [CrossRef] [PubMed]
68. Montagner, C.; Perier, A.; Pichard, S.; Vernier, G.; Menez, A.; Gillet, D.; Forge, V.; Chenal, A. Behavior of the n-terminal helices of the diphtheria toxin t domain during the successive steps of membrane interaction. *Biochemistry* **2007**, *46*, 1878–1887. [CrossRef] [PubMed]
69. Chenal, A.; Vernier, G.; Savarin, P.; Bushmarina, N.A.; Geze, A.; Guillain, F.; Gillet, D.; Forge, V. Conformational states and thermodynamics of alpha-lactalbumin bound to membranes: A case study of the effects of pH, calcium, lipid membrane curvature and charge. *J. Mol. Biol.* **2005**, *349*, 890–905. [CrossRef] [PubMed]
70. Hess, B.; Kutzner, C.; van der Spoel, D.; Lindahl, E. Gromacs 4: Algorithms for highly efficient, load-balanced, and scalable molecular simulation. *J. Chem. Theory Comput.* **2008**, *4*, 435–447. [CrossRef] [PubMed]
71. Marrink, S.J.; de Vries, A.H.; Mark, A.E. Coarse grained model for semiquantitative lipid simulations. *J. Phys. Chem. B* **2003**, *108*, 750–760. [CrossRef]
72. Marrink, S.J.; Risselada, H.J.; Yefimov, S.; Tieleman, D.P.; de Vries, A.H. The martini force field: Coarse grained model for biomolecular simulations. *J. Phys. Chem. B* **2007**, *111*, 7812–7824. [CrossRef] [PubMed]
73. Monticelli, L.; Kandasamy, S.K.; Periole, X.; Larson, R.G.; Tieleman, D.P.; Marrink, S.-J. The martini coarse-grained force field: Extension to proteins. *J. Chem. Theory Comput.* **2008**, *4*, 819–834. [CrossRef] [PubMed]
74. Bussi, G.; Donadio, D.; Parrinello, M. Canonical sampling through velocity rescaling. *J. Chem. Phys.* **2007**, *126*, 014101–014107. [CrossRef] [PubMed]
75. Berendsen, H.J.C.; Postma, J.P.M.; van Gunsteren, W.F.; DiNola, A.; Haak, J.R. Molecular dynamics with coupling to an external bath. *J. Chem. Phys.* **1984**, *81*, 3684–3690. [CrossRef]
76. Darden, T.; York, D.; Pedersen, L. Particle mesh ewald: An n.Log(n) method for ewald sums in large systems. *J. Chem. Phys.* **1993**, *98*, 10089–10092. [CrossRef]
77. Essmann, U.; Perera, L.; Berkowitz, M.L.; Darden, T.; Lee, H.; Pedersen, L.G. A smooth particle mesh ewald method. *J. Chem. Phys.* **1995**, *103*, 8577–8593. [CrossRef]
78. Humphrey, W.; Dalke, A.; Schulten, K. Vmd: Visual molecular dynamics. *J. Mol. Graph. Model.* **1996**, *14*, 27–28. [CrossRef]
79. R-Development-Core-Team. *R: A Language and Environment for Statistical Computing*; R-Development-Core-Team: Vienna, Austria, 2005.
80. Wickham, H. *Ggplot2: Elegant Graphics for Data Analysis*; Springer: New York, NY, USA, 2009.



© 2017 by the authors. Licensee MDPI, Basel, Switzerland. This article is an open access article distributed under the terms and conditions of the Creative Commons Attribution (CC BY) license (http://creativecommons.org/licenses/by/4.0/).

Supplementary Materials: Membrane-Active Properties of an Amphitropic Peptide from the CyaA Toxin Translocation Region

Alexis Voegele, Orso Subrini, Nicolas Sapay, Daniel Ladant and Alexandre Chenal

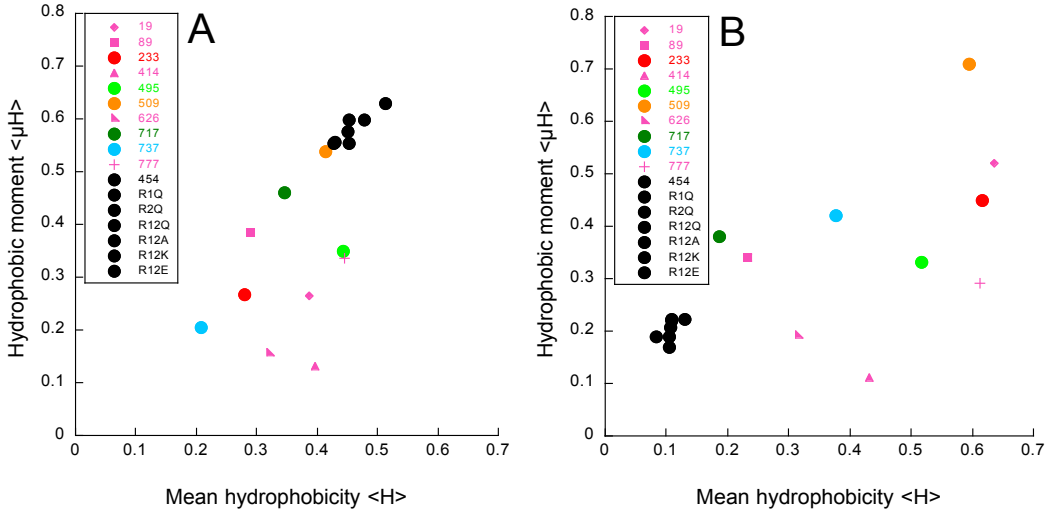

Figure S1. Hydrophobic moment <μH> as function of the mean hydrophobicity <H> of the CyaA-derived peptides. <H> and <μH> values were calculated with the Heliquest software using the sequences of the peptides (**A**) or using a window of 12 to 18 amino acids (**B**) (Table S2). Circles represent peptides interacting with membranes. Others symbols represent peptides that do not interact with membranes.

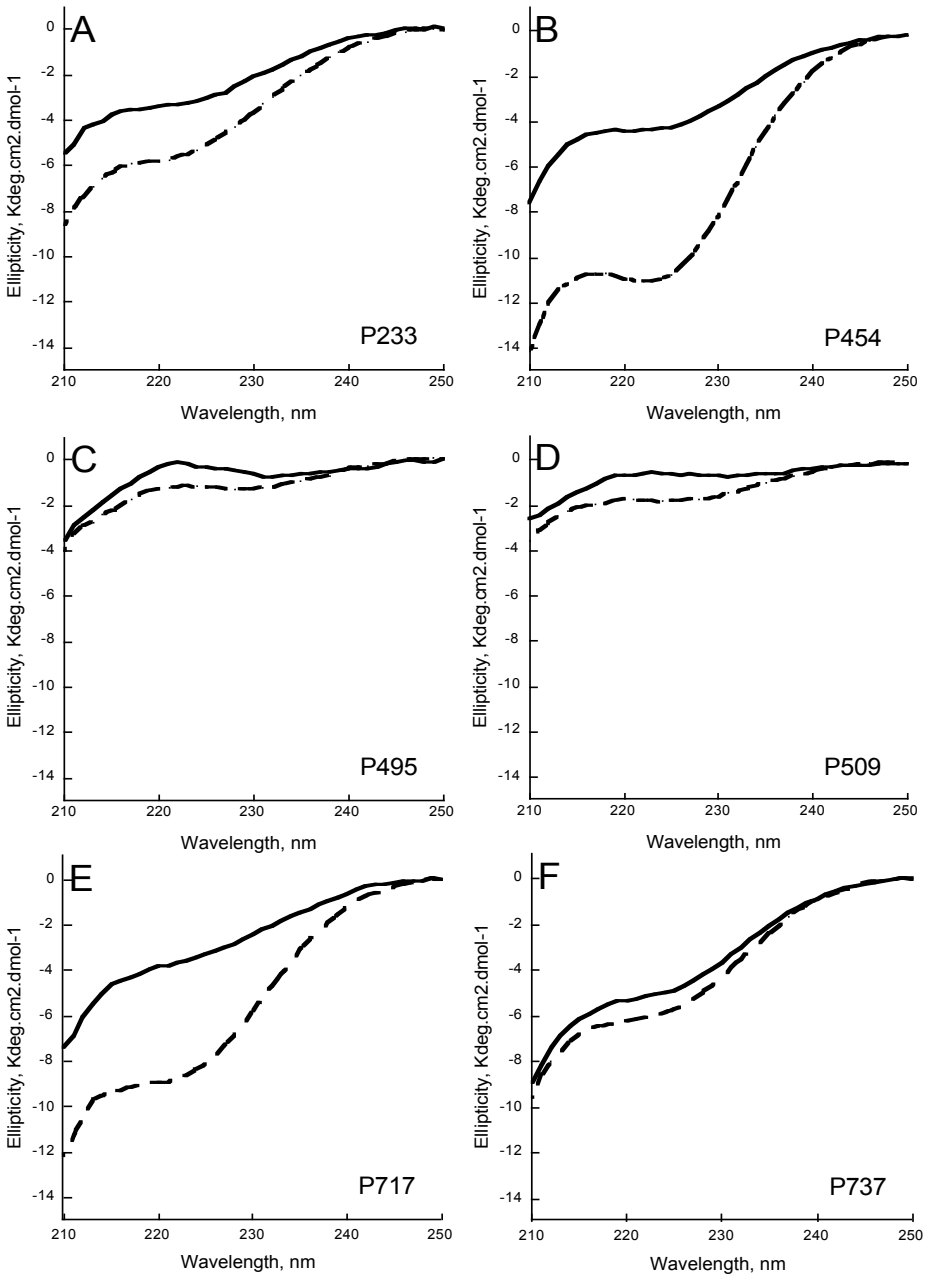

Figure S2. Far-UV circular dichroism spectra of the CyaA-derived peptides. CD spectra of P233 (**A**), P454 (**B**), P495 (**C**), P509 (**D**), P717 (**E**) and P737 (**F)** peptides at 40 μM in solution (solid lines) or in the presence of SUVs DOPC/DOPE/DOPG/Chol 4:3:2:1 at 1 mM lipids (dashed lines). CD spectra were recorded on an Aviv circular dichroism spectropolarimeter model 215. Briefly, CD measurements were carried out at a scan rate of 0.5 nm/sec (step: 0.5 nm and integration time: 1 sec) with a time constant of 100 msec and a bandwidth of 1 nm. Rectangular quartz Suprasil cells of 1 mm path lengths (110.QS, Hellma) were used for measuring CD activity in the far-UV region. Each far-UV CD spectrum represents the average of 5 scans.

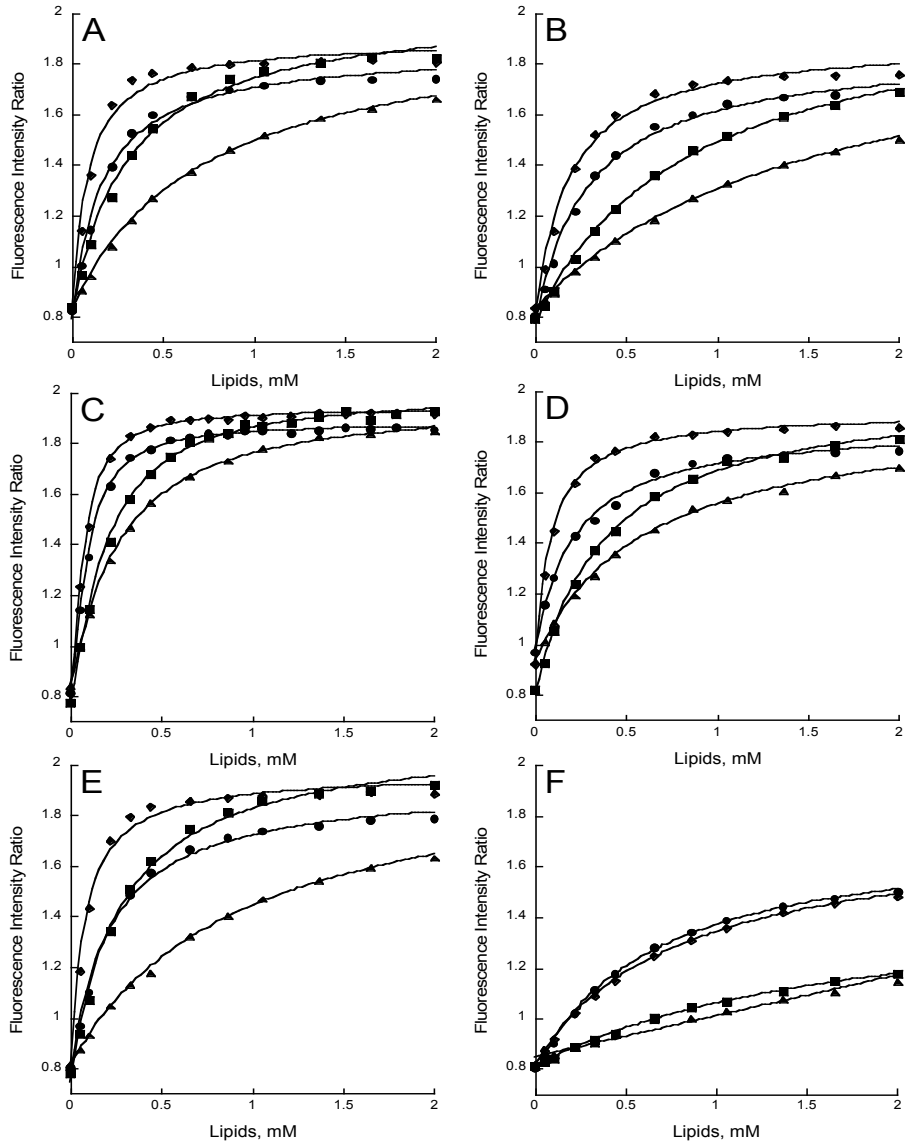

Figure S3. Partition of CyaA-derived peptides followed by tryptophan intrinsic fluorescence. Ratio of fluorescence intensity at 330 nm over 370 nm (excitation at 280 nm) as a function of lipid concentration (0 to 2 mM) for P454 R1Q (**A**), P454 R12Q (**B**), P454 R12A (**C**), P454 R2Q (**D**), P454 R12K (**E**) and P454 R12E (**F**) in POPC/POPG 8:2 (square), POPC (triangle), DOPC/DOPG 8:2 (diamond) or DOPC (circle) SUVs. The fitting procedure is described in Materials and Methods.

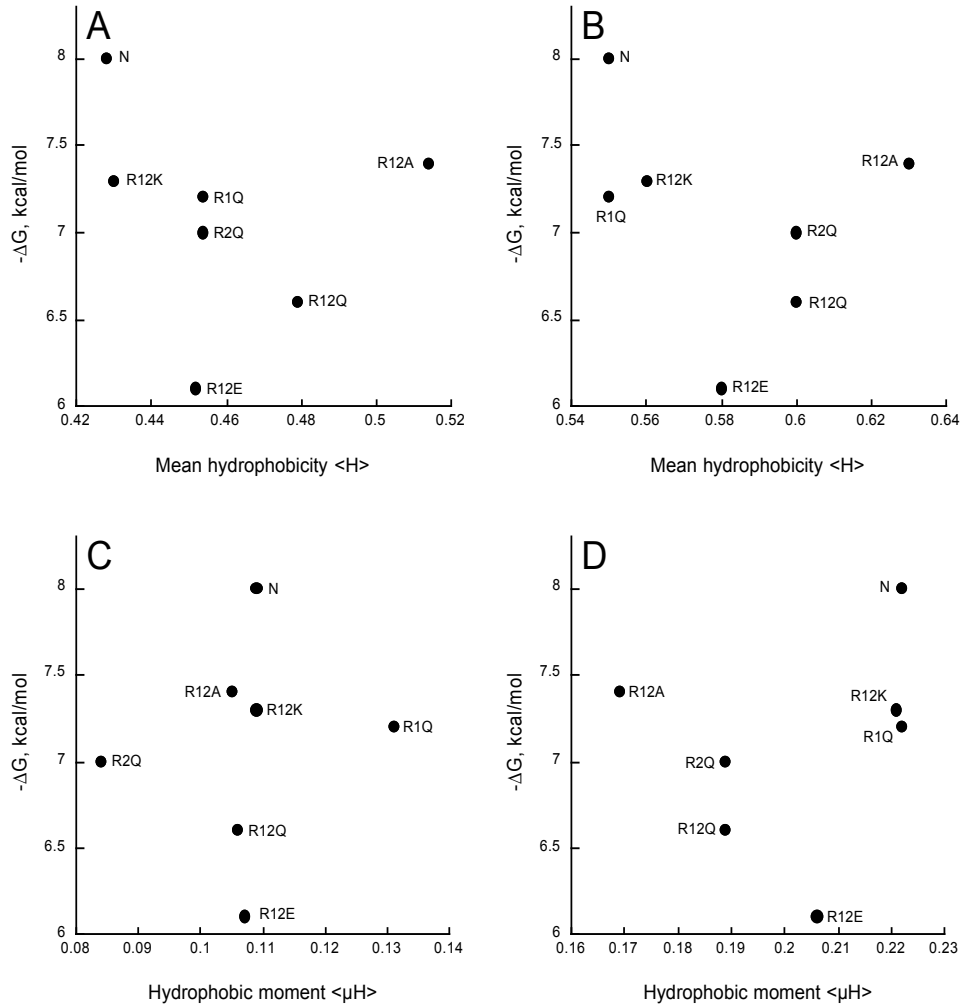

Figure S4. Free energy of partition of peptides in POPC/POPG membranes as a function of mean hydrophobicity <H> or hydrophobic moment <μH>. <H> and <μH> was extracted from Heliquest software for the sequences of the entire peptides (**A**, **C**) or for a window of 18 amino acids (**B**, **D**) corresponding to the C-terminal part of each peptide. These values are reported in Table S2.

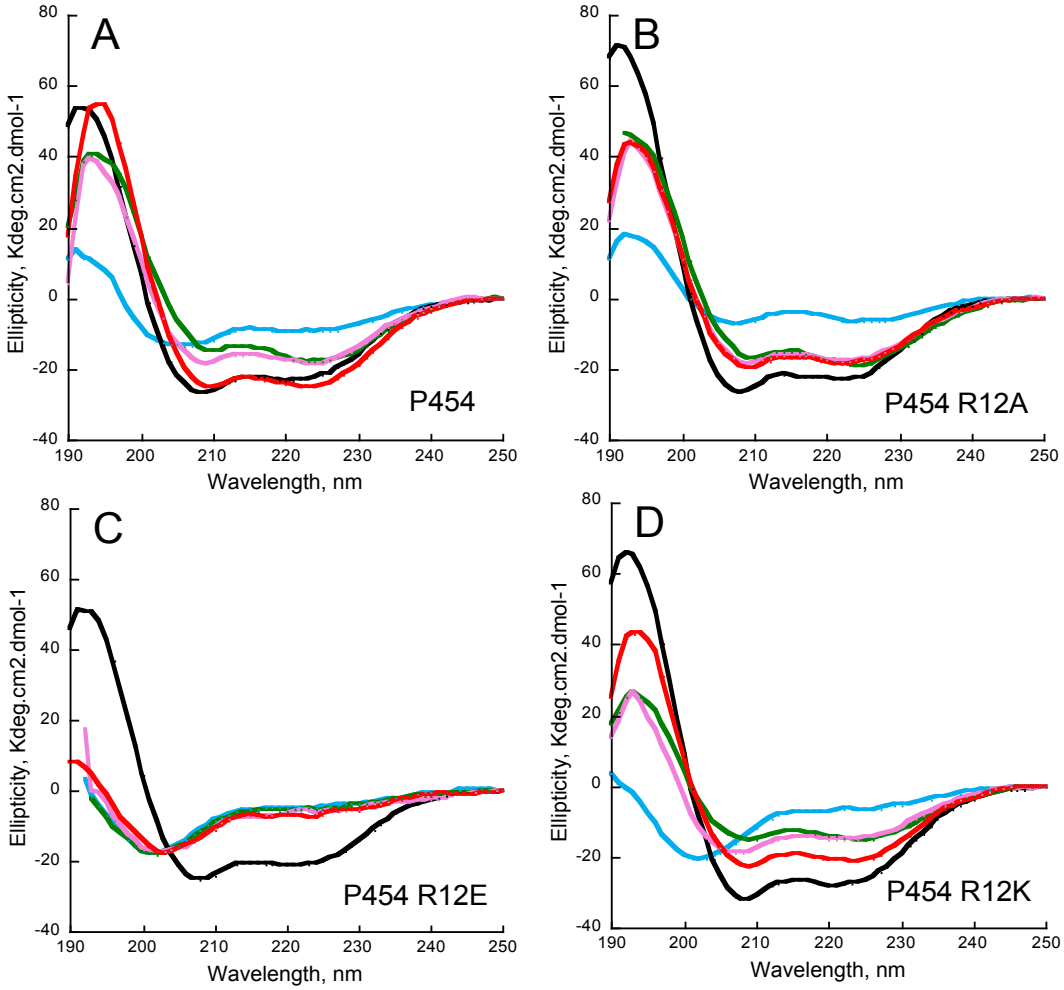

Figure S5. Synchrotron radiation far-UV circular dichroism of P454-derived peptides. The peptide concentration is 100 μM in buffer A at 25°C (blue), in the presence of 20% TFE (black) or in the presence of SUVs at 2 mM of POPC (green), DOPC/DOPG 8:2 (red) or DOPC (purple). Far-UV CD spectra of the following peptides are shown: P454 (**A**), P454 R12A (**B**), P454 R12E (**C**) and P454 R12K (**D**).

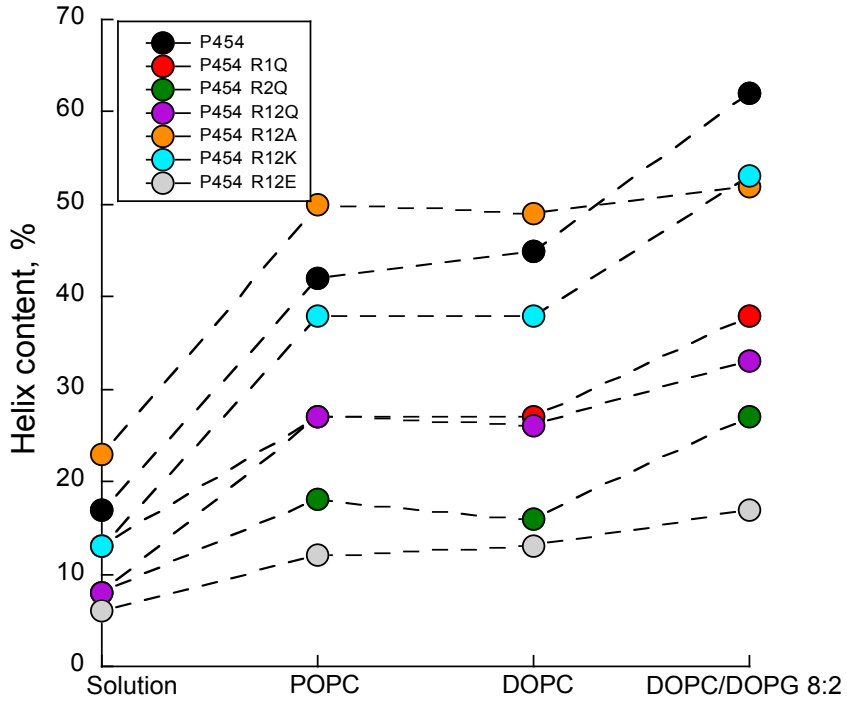

Figure S6. Helical content of the P454-derived peptides in various environments. The helical content of the peptides in solution, in the presence of POPC, DOPC and DOPC/DOPG 8:2 membranes is estimated using the BestSel software. The color code for the P454-derived peptides is the following: P454 (black), P454 R1Q (red), P454 R2Q (green), P454 R12Q (purple), P454 R12A (orange), P454 R12K (blue) and P454 R12E (grey). Bestsel estimations of the peptide helical contents are reported in Table S6.

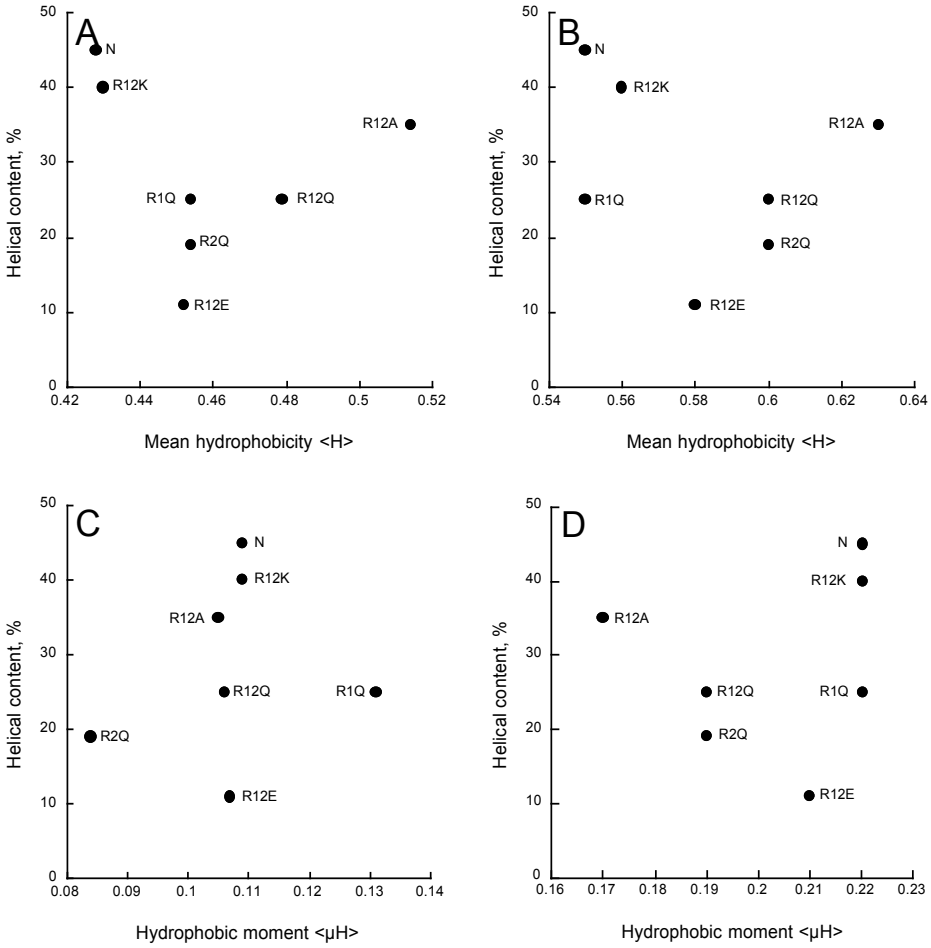

Figure S7. Membrane-induced helical content in the presence of DOPC/DOPG SUVs as a function of mean hydrophobicity <H> or hydrophobic moment <μH>. The values of <H> and <μH> were extracted from Heliquest software using the sequences of the peptides (**A**, **C**) or a window of 18 amino acids (**B**, **D**) corresponding to the C-terminal part of each peptide. These values are reported in Table S2.

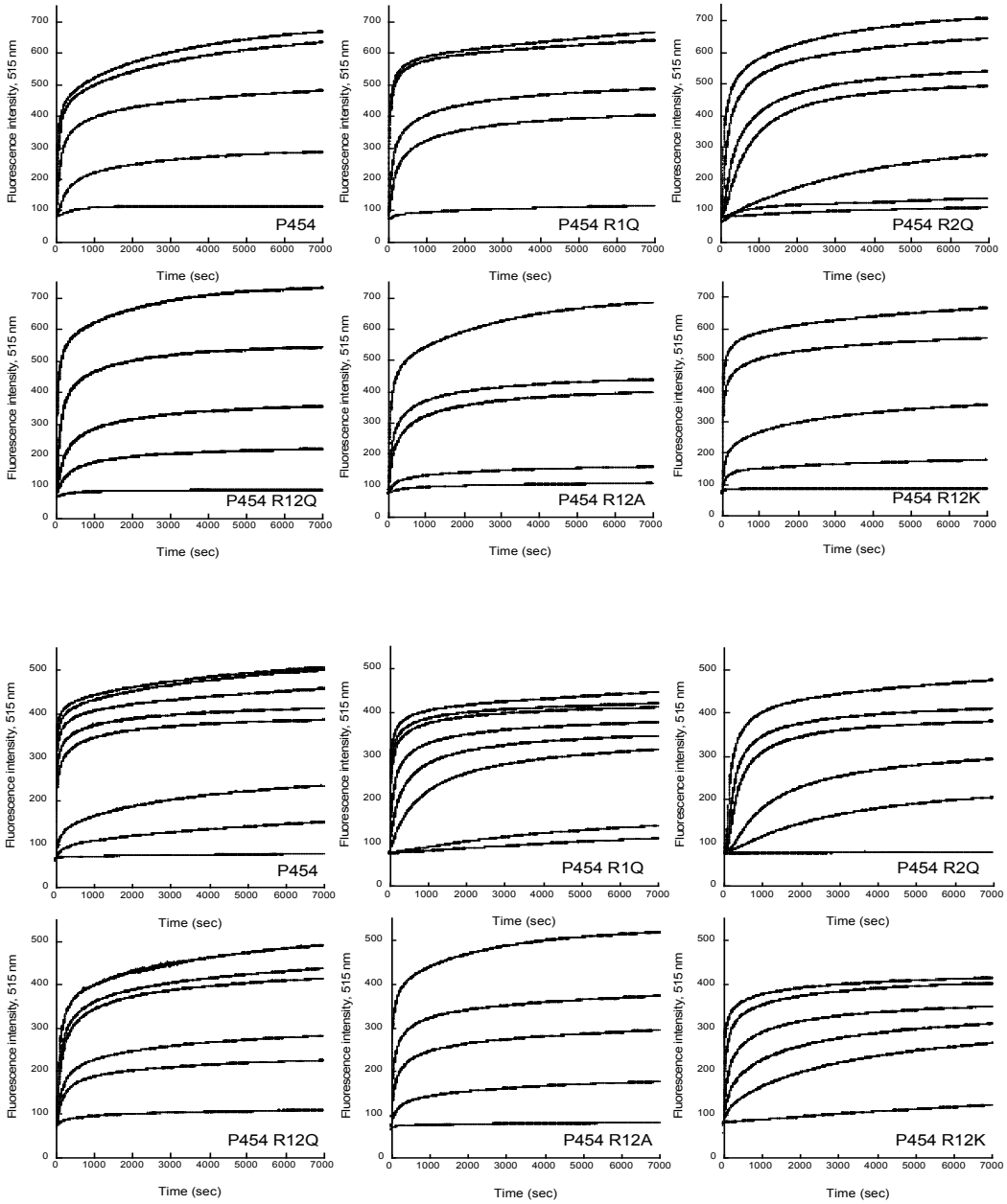

Figure S8. Membrane permeabilization induced by the P454-derived peptides. Top and bottom panels correspond to permeabilization assays performed in the presence of POPC/POPG 8:2 and POPC LUVs at 0.45 mM in solution, respectively. Each trace corresponds to a peptide at a given concentration (the peptide concentrations are reported in Figure 6). Peptide names are indicated in each panel.

Table S1. Peptide names, number of residues, molecular weight, pK and charge at physiological pH of each peptide used in this study.

Peptide	Number of residues	Molecular weight (g/mol)	pK	Charge at pH 7
P19	18	1 965	10	+1
P89	20	2 164	4.2	-2
P233	22	2 509	10.8	+2
P414	27	2 972	4	-4
P454	31	3 268	12	+2.2
P454 R1Q	31	3 240	10.9	+1
P454 R2Q	31	3 240	10.9	+1.2
P454 R12Q	31	3 211	8	+0.2
P454 R12A	31	3 097	8	+0.2
P454 R12K	31	3 212	10.7	+2.2
P454 R12E	31	3 214	5.1	-1.8
P495	31	3 101	4	-2
P509	17	1 842	4.3	-1
P626	23	2 678	4.7	-2
P717	18	2 188	4.8	-1
P737	35	3 975	7.7	0
P777	18	1 946	4.5	-1

Table S2. Maximum mean hydrophobicity <H> and hydrophobic moment <μH> of each peptide using their full sequence or a window of 12 to 18 amino acids. Values were extracted from Heliquest.

Peptide	Mean hydrophobicity <H> full peptide	Hydrophobic moment <μH> full peptide	Mean hydrophobicity <H> window of 12 to 18 amino acids	Hydrophobic moment <μH> window of 12 to 18 amino acids
P19	0.387	0.264	0.636	0.521
P89	0.29	0.385	0.233	0.341
P233	0.28	0.267	0.617	0.448
P414	0.397	0.132	0.431	0.112
P495	0.444	0.35	0.517	0.332
P509	0.415	0.537	0.596	0.71
P626	0.321	0.155	0.315	0.192
P717	0.346	0.46	0.187	0.381
P737	0.209	0.205	0.378	0.42
P777	0.445	0.336	0.613	0.292
P454	0.428	0.554	0.109	0.222
P454 R1Q	0.454	0.554	0.131	0.222
P454 R2Q	0.454	0.598	0.084	0.189
P454 R12Q	0.479	0.598	0.106	0.189
P454 R12A	0.514	0.628	0.105	0.169
P454 R12K	0.43	0.556	0.109	0.221
P454 R12E	0.452	0.575	0.107	0.206

Table S3. Thermodynamics of peptide partitioning from solution to membrane. SUVs were composed of DOPC/DOPE/DOPG/Chol at a ratio of 4:3:2:1. The P19, P89, P414, P626 and P777 peptides do not partition into membrane. *Secondary structure is inferred from both far-UV and MD results.

Peptide	Kx	ΔG, kcal/mol	Secondary structure*
P454	300 000	-7.4	α helix
P495	130 000	-6.9	non canonical
P509	80 000	-6.7	non canonical
P233	60 000	-6.5	α helix
P717	60 000	-6.5	α helix
P737	20 000	-5.8	α helix

Table S4. Effect of lipid bilayer composition on P454 membrane partitioning. All Kx and ΔG values were obtained for the WT P454 in the presence of membranes with various lipid compositions.

Membranes	Kx	ΔG, kcal/mol
DOPC/DOPG 8:2	1 200 000	-8.3
POPC/POPG 8:2	790 000	-8
DOPC	505 000	-7.8
DOPC/DOPE/DOPG/Chol 4:3:2:1	300 000	-7.4
POPC	150 000	-7
DOPC/DOPE 7:3	80 000	-6.7
DOPC/Chol 7:3	60 000	-6.5
DOPC/DOPE/Chol 6:3:1	40 000	-6.3

Table S5. Partition of P454-derived peptides from solution to membrane. The first value corresponds to the partition coefficient Kx and the second value to the free energy ΔG in kcal/mol.

Peptide	POPC/POPG 8:2	POPC	DOPC/DOPG 8:2	DOPC
P454	790 000 / -8	150 000 / -7	1 200 000 / -8.3	505 000 / -7.8
P454 R1Q	190 000 / -7.2	75 000 / -6.6	670 000 / -7.9	340 000 / -7.5
P454 R2Q	150 000 / -7	90 000 / -6.7	655 000 / -7.9	260 000 / -7.4
P454 R12Q	70 000 / -6.6	35 000 / -6.2	310 000 / -7.5	195 000 / -7.2
P454 R12A	275 000 / -7.4	195 000 / -7.2	795 000 / -8	610 000 / -7.9
P454 R12K	215 000 / -7.3	60 000 / -6.5	750 000 / -8	265 000 / -7.4
P454 R12E	30 000 / -6.1	7 000 / -5.2	70 000 / -6.6	85 000 / -6.7

Table S6. Estimation of the α helical content of peptides using Bestsel in solution, in TFE and in the presence of membranes of various lipid compositions. The last column reports the helical content predicted with the software SOPMA.

Peptide	% helix in solution	% helix in TFE 20%	% helix in POPC	% helix in DOPC	% helix in DOPC/ DOPG 8 :2	helical content (%) predicted by SOPMA
P454	17 ± 2	60 ± 2	42 ± 3	45 ± 5	62 ± 1	100
P454 R1Q	13 ± 1	41 ± 3	27 ± 1	27 ± 1	38 ± 2	80
P454 R2Q	8 ± 3	45 ± 3	18 ± 1	16 ± 1	27 ± 2	90
P454 R12Q	8 ± 4	50 ± 2	27 ± 2	26 ± 3	33 ± 3	80
P454 R12A	23 ± 2	61 ± 2	50 ± 3	49 ± 4	52 ± 2	80
P454 R12K	13 ± 2	72 ± 1	38 ± 1	38 ± 2	53 ± 3	80
P454 R12E	6 ± 1	55 ± 3	12 ± 3	13 ± 1	17 ± 2	80

Article VI (in preparation)

Coupling membrane-active and calmodulin-binding properties of the CyaA toxin translocation region for efficient delivery into cells

Alexis Voegele*, Mirko Sadi*, Darragh P. O'Brien*, Pauline Gehan*, Dorothée Raoux-Barbot, Maryline Davi, Sylviane Hoos, Sébastien Brulé, Bertrand Raynal, Patrick Weber, Ariel Mechaly, Ahmed Haouz, Nicolas Rodriguez, Patrice Vachette, Dominique Durand, Sébastien Brier, Daniel Ladant and Alexandre Chenal

* These authors contributed equally to this work

The peptide P454 shares properties with AMPs. In fact, it has the capacity to bind and destabilize membranes. Some AMPs are also able to translocate across membrane and bind a cellular target. Interestingly, P454 shows similarities with the CaM-binding peptides and was found to bind to CaM. The goal of this article was to characterize the interaction between P454 and CaM and investigate whether the complex contributes to the translocation of the catalytic domain. We first observed that P454 can translocate. We then identified crucial amino acids residues of P454 for its membrane-active properties and CaM binding. These residues were mutated in the full-length CyaA and were found to be essential for the translocation of ACD. These results are discussed in the context of the CyaA translocation and lead us to propose a mechanism of cell intoxication.

We first investigated the P454:CaM complex in solution. From ITC, SRCD (for synchrotron radiation circular dichroism) and AUC (for analytic ultracentrifugation) experiments, we found that P454 binds CaM in a 1:1 ratio with a K_D of 90 nM at 25°C, suggesting that the P454:CaM complex is favored compared to the P454-membrane (K_D of 70 μM). We then determined whether CaM could form a complex with the membrane-bound P454, to mimic the apparition of P454 in the cytosol. From tryptophan fluorescence titrations and permeabilization assays, we observed that CaM can extract P454 from the membrane in a calcium dependent manner.

We used the droplet interface bilayers approach with a fluorescent P454 peptide to investigate the translocation of P454. We clearly observed that P454 translocates in the *trans* side of the membrane only in the presence of CaM. We also examined the H-helix peptide (residues 233-254 of CyaA), corresponding to the segment binding to CaM in ACD. We found that the H-Helix is not able to translocate. This result indicates that P454 does translocate and forms a complex with CaM in the *trans* compartment of the membrane.

We performed crystallization trials of P454 with CaM. We obtained the crystal structure of P458 (a shorter P454 peptide) with CaM. The structure shows that the N-terminal of P458 binds the C-CaM and the C-terminal of the peptide to the N-CaM. Interestingly, the different crystal structures obtained illustrate that CaM is dynamic and adopts different conformations, due to the flexibility of the central helix. This structural diversity was supported by the SAXS data (for Small Angle X-ray Scattering). The SAXS data of the H:CaM complex reveal a diverse conformation of CaM than the P454:CaM complex. These data show that, although

both P454 and the H-helix bind to CaM, they adopt various conformations and exhibit different dynamic properties.

We also investigate the contributions of amino acids of P454 on its membrane-active properties and CaM binding. We identified several residues that were mutated in the P454 segment of the full-length CyaA. The functional activities (*i.e* hemolysis and cAMP production in cells) revealed that these residues are essential for the translocation of ACD. This result suggests that the P454 segment is crucial for the translocation process. We propose that the formation of the P454:CaM complex favors the translocation of ACD.

Finally, we performed the structural model of AC489 (*i.e* residues 1-489 of CyaA, comprising both the H-helix and P454 segment) in complex with CaM. Compared to AC364 (*i.e* comprising only the H-helix), HDX-MS and SRCD firstly showed that the region 345-489 contains helical structures with disordered segments.

HDX-MS experiments provided that the C-terminal extremity of AC489 showed CaM-induced protection and that only one CaM can be bound on both the H-helix and the P454 segment.

The SAXS experiments performed on AC489 in the presence of an excess of CaM has allowed modeling the complex in accordance with the previous HDX-MS and SRCD data. We propose that the C-CaM interacts with the H-helix while the N-CaM is dynamically bound to the P454 segment.

Taken together, our results allow us to propose a translocation model. After insertion of the toxin into the plasma membrane, the translocation region with the membrane-active P454 segment inserts and destabilizes the membrane. Then, P454 translocates and is trapped by N-CaM. This binding prevents back transport and the P454:CaM complex may act as a driving force pulling the catalytic domain inside the cytosol. The H-helix binds to the C-CaM, which induces a disorder-to-order transition and activation of the enzymatic activity of the toxin (see next article VII for further details).

Coupling membrane-active and calmodulin-binding properties of the CyaA toxin translocation region for efficient delivery into cells

Alexis Voegele*, Mirko Sadi*, Darragh O'Brien*, Pauline Gehan*, Dorothée Raoux-Barbot, Maryline Davi, Sylviane Hoos, Sébastien Brulé, Bertrand Raynal, Patrick Weber, Ariel Mechaly, Ahmed Haouz, Nicolas Rodriguez, Patrice Vachette, Dominique Durand, Sébastien Brier, Daniel Ladant1#, Alexandre Chenal1#

* These authors contributed equally to this work.

to whom correspondence and material requests should be addressed:
daniel.ladant@pasteur.fr; alexandre.chenal@pasteur.fr

Abstract

The molecular mechanism and the forces involved in the translocation of bacterial toxins into host cells have remained elusive thus far. We previously showed that a peptide from the translocation region of CyaA, P454 (residues 454–484), exhibits membrane-active properties. Here, we show that this peptide is able to translocate across membranes and to tightly interact with calmodulin once it reaches the *trans* compartment. The residues involved in membrane destabilization and calmodulin binding have been identified and substituted in the full-length CyaA toxin. Our data show that these residues are essential for cell intoxication. Hence, both membrane-destabilizing activity and calmodulin binding properties of this CyaA region are sequentially required to convert the stochastic process of protein translocation into an efficient, vectorial chain transfer into the cytoplasm of host cells. We also report the structure of the enzymatic complex formed in the cytosol of target cells, including the catalytic and translocation domains, both characterized by various dynamic ranges of interactions with calmodulin.

Introduction

The adenylate cyclase (CyaA) toxin is a major virulence factor produced by *Bordetella pertussis*, the causative agent of whooping cough, and is involved in the early stages of respiratory tract colonization (1-5). CyaA, a 1706-residue long protein (Figure S1), is a Repeat-in-ToXin (RTX) (6-10) multi-domain toxin (11,12), which uses an original intoxication mechanism: once secreted by *B. pertussis*, CyaA invades eukaryotic cells through a unique molecular mechanism that involves a direct translocation of its N-terminal adenyl cyclase catalytic domain (AC) across the plasma membrane. The ATP-cyclizing, calmodulin-activated AC domain is located in the 364 N-terminal residues (13-16). The translocation region (TR, residues 365 to 527) is essential for AC translocation into target cells (17). The hydrophobic region (HR, residues 528 to 710) inserts into the cell membrane and makes pores selective to cations (10,18,19); the acylation region (AR, residues 711 to 1005) contains two post-translational acylation sites, at lysines K860 and K983 (20-22), required for the refolding of the CyaA toxin (12,23) and AC translocation across membranes *in vivo* and *in vitro* (5,20,21,24). The Repeat-in-ToXin (RTX), cell-receptor binding domain of CyaA (RD, residues 1006 to 1706) is made of about 40 copies of calcium-binding RTX motifs (8-10,25). The type 1 secretion system (T1SS), made of CyaB, CyaD and CyaE proteins (26,27), recognizes a secretion signal located at the C-terminal extremity of CyaA. Once secreted through the T1SS, the toxin binds calcium and folds in the extracellular milieu. A calcium-induced disorder-to-order transition of the RTX motifs occurs upon CyaA secretion, from the low-calcium concentration of the bacterial cytosol to the calcium-rich extracellular environment (16,28-37). The folding of CyaA is calcium-driven, dependent on acylation and occurs in a sequential manner (12,23,38).

RD can bind with a high affinity to a subset of leukocytes (neutrophils, dendritic cells and macrophages) *via* a cell receptor, the CD11b/CD18 integrin (39-47). However, CyaA can also intoxicate various eukaryotic cells lacking the CD11b/CD18 (12,48-50). Irrespective of the expression on the cell surface of the CD11b/CD18 integrin, AC is directly translocated across the plasma membrane into the target cell cytoplasm (17,24,43,51-53). Once translocated, calmodulin (CaM) binding to AC does fold and stabilize the active state of the adenyl cyclase (15,16,54), which produces high amounts of cAMP at the expense of ATP, leading to host defense subversion (5,11,55,56).

Experimental results from the last decades have provided direct evidence that AC translocation requires CyaA acylation, a calcium gradient and a membrane potential across the plasma membrane (24). However, the molecular mechanism and the forces involved in the translocation of the CyaA catalytic domain across the plasma membrane have remained

elusive thus far. We previously showed that a peptide from the translocation region of CyaA, P454 (residues 454–484), exhibits membrane-active properties related to antimicrobial peptides (AMPs) (17,57,58). This peptide adopts a helical conformation upon membrane interaction and induces a local destabilization of the lipid bilayer. The peptide contains two arginine residues that are critically involved in its membrane-active properties (58), as commonly reported for AMPs. Besides membrane-lytic activity, AMPs are also able to translocate across membranes and some of them target intracellular biomolecules, such as proteins and nucleic acids, to impair cell functions (59,60). Noteworthy, several bacterial toxins hijack eukaryotic cytosolic factors to achieve the translocation of their respective catalytic domains: these toxins, such as the diphtheria toxin and botulinum toxins, contain segments able to translocate across target membranes and then bind to eukaryotic proteins (61-66). It has been proposed that the forces provided by such toxin:target complexes contribute to the energy required for the translocation of the catalytic domains across membranes.

Here we show that the P454 peptide exhibits the intrinsic propensity to translocate across lipid bilayers and forms a stable complex upon interaction with CaM. We propose that once this CyaA region (residues 454-484) is translocated across the plasma membrane, it binds to CaM and favors the translocation of the N-terminal catalytic domain. We have identified several residues from P454 involved in both membrane interaction and CaM binding. We further show in the context of the full-length CyaA toxin that these residues are essential for the efficient translocation of the catalytic domain into the cell cytoplasm and for the production of cAMP. We finally describe the structural models of the translocated CyaA regions, including the catalytic domain and the translocation region of CyaA, in complex with CaM in the cytosol, on the *trans* side of the plasma membrane. These results provide new insights into the mechanism of bacterial toxin translocation into eukaryotic host cells.

Material and methods

The material and methods section appears as supplementary file (see below).

Results

1- The P454 peptide from the CyaA toxin binds to calmodulin.

We previously showed that the P454 peptide, residues 454-484 from the CyaA translocation region, exhibits membrane-active properties similar to antimicrobial peptides (AMPs) (67). These peptides are able to locally destabilize the membrane permeability and some of them target intracellular biomolecules. Moreover, the P454 peptide shows similarities with calmodulin-binding peptides, which form amphiphilic helices, are positively charged and contain a few aromatic or hydrophobic residues involved in the complex stabilization. From these observations, we hypothesized that P454 may translocate across the plasma membrane and bind calmodulin. In the context of the full-length toxin, this interaction may constrain this CyaA segment to remain locked inside the cell, providing part of the energy required for the translocation of the catalytic domain across the plasma membrane.

Analytical ultracentrifugation and circular dichroism data show that P454 and CaM form a complex in solution (Figure S2 and Table S1). The thermodynamic parameters of the P454:CaM complex formation have been determined by isothermal titration calorimetry and reveal a calcium-dependent interaction with a dissociation constant of 90 nM at 25°C (Figure S3A, S3B and Table S2). We further characterized the P454:CaM complex at various temperatures, allowing us to determine the heat capacity change, ΔCp, upon complex formation (Figure S3C and Table S2). The values of free enthalpy, ΔH, are dependent on temperature and the ΔCp is negative, as measured for canonical CaM-binding peptides. The ΔCp value is, however, lower than that measured for globular peptide:CaM complexes, suggesting that the P454:CaM complex does not adopt a globular conformation, as confirmed below by structural biology data.

We then determined the ability of CaM to form a complex with membrane-bound P454, pre-incubated with lipid vesicles. This was done to mimic the apparition of this CyaA segment on the *trans* side of the plasma membrane and to evaluate its availability in a membrane-inserted state to bind to cytosolic CaM. Noteworthy, the affinity of P454 for membranes is K_D=70 µM (ΔG_{KD}=-5.6 kcal/mol, calculated from the partition coefficient Kx=790000, see (58) and Table S5) while the K_D value for the P454:CaM complex measured by ITC is 90 nM (ΔG_{KD}=-9.6 kcal/mol) (Figure S4A). The difference of free energy, $\Delta\Delta G_{KD}$, around -4 kcal/mol, suggests that CaM addition to membrane-inserted P454 should favor the peptide:CaM complex formation at the expense of the membrane-inserted state of P454 (Figure S4B). This is confirmed by an experiment of solution-to-membrane partition of P454 measured by fluorescence (Figure S5A and S5B): P454 is progressively partitioning from the buffer to membranes as the lipid concentration increases. Then, the shift of fluorescence polarity upon

addition of calmodulin suggests that a P454:CaM complex is formed whatever the lipid concentration (see details in figure legend of Figure S5).‡ The addition of an excess of EDTA chelates calcium ions, inducing the conversion of CaM from a holo-state to an apo-state; apo-CaM releases the P454 peptide, which reversibly interacts with membranes (Figure S5).

To confirm that calmodulin is able to bind to pre-equilibrated membrane-bound P454, we performed a modified version of the ANTS:DPX lipid vesicle permeabilization assay (57,58). We expected that addition of CaM in the presence of calcium to membrane-bound P454 would displace the peptide from the membrane and lead to the P454:CaM complex formation, preventing vesicle permeabilization. The data show that addition of holo-CaM at an early stage of membrane permeabilization immediately stops the P454-induced dye efflux (Figure S5C). Calcium chelation by EDTA converts holo-CaM to apo-CaM, leading to the release of the P454 peptide. The free peptides partition back into membranes and permeabilize the vesicles again, leading to ANTS fluorescence recovery (Figure S5C). Taken together, we show that P454 is a calmodulin-binding peptide irrespective of the peptide being in solution or inserted into membrane prior to CaM addition. These results prompted us to evaluate the intrinsic propensity of P454 to translocate across membranes.

2- P454 translocation across lipid bilayers

We investigated the ability of P454 to translocate across membranes using the droplet interface bilayers approach. The *cis* droplet population contains the dye-labelled peptide in the presence of 2 mM calcium while the *trans* droplet population contains calmodulin in the presence of 0.2 mM calcium. After mixing and random formation of pairs of droplets, a lipid bilayer is formed at the interface between two adhering droplets (Figure S6). We measure the stochastic transfer of fluorescence from a *cis* fluorescent droplet to a *trans* non-fluorescent droplet to reveal peptide translocation across the lipid bilayer formed at the droplet interface (see Figure S6A). All peptides used in the study interact with membranes as evidenced by the fluorescent rings staining the *cis* droplets at the beginning of the experiments.

In the absence of calmodulin in the *trans* droplet, no increase of fluorescent P454 is measured in the volume of the *trans* compartment after 15 minutes of incubation (Figure 1). Conversely, in the presence of CaM in the *trans* droplet, a significant amount of fluorescence is measured in the *trans* compartment (Figure 1 and Figure S6B). In the absence of a calcium gradient, *i.e.*, 0.2 mM $CaCl_2$ in both droplet populations, P454 does also translocate across the membrane and accumulate in the *trans* droplet. These results indicate that P454 is competent to translocate across membrane and to bind CaM if present. We then assayed two other peptides: the first one is the H-helix peptide, corresponding to the main binding site of AC

(residues 233-254 of CyaA) to CaM involved in adenyl cyclase activation (16). The second peptide is a P454-derived peptide with its two arginine residues substituted by glutamate residues, P454-R12E, which mainly differs from the WT peptide in CaM binding (K_D^{R12E}/K_D^{WT}=300) and partly in membrane interaction (K_X^{R12E}/K_X^{WT}=10, see below). In the presence of CaM in the *trans* compartment and a calcium gradient, the data show that both P454-R12E and H-helix peptides interact with the membrane, as evidenced by the fluorescent ring located on the *cis* lipid leaflet observed at the beginning of the experiment. However, these peptides do not accumulate in the *trans* droplet after 15 min of incubation. These results suggest that the H-helix peptide does not translocate across membrane, as this peptide strongly interact with CaM (K_D^H=10 nM, Figure S7 and Table S3) and would accumulate within a peptide:CaM complex in the *trans* compartment if translocated.

Taken together, these data indicate that P454 interacts with the *cis* lipid leaflet of the membrane, translocates across the droplet interface bilayers and forms a peptide:CaM complex in the *trans* compartment (Figure S8).

3- Structure and dynamics of P454:CaM and comparison with H:CaM and MLCK:CaM

We then performed an integrative structural biology approach, combining X-ray crystallography, size exclusion chromatography (SEC) coupled to small-angle X-ray scattering (SEC-SAXS), HDX-MS and SRCD to describe the structure and dynamics of the P454:CaM complex.

We attempted to crystallize the P454:CaM complex but all trials were unsuccessful. We shorten the peptide sequence by removing the N-terminal ASAH residues and the C-terminal MTQ residues from the P454 peptide, yielding the P458 peptide. This P458 peptide in complex with CaM provided several crystals (Figure 2A and Table S4). The stoichiometry of P458:CaM is a 1:1 complex, with the N-terminal lobe of CaM bound to the C-terminal part of the peptide and the C-terminal lobe of CaM with the N-terminal part of the peptide. The 12 X-ray structures of the P458:CaM complex illustrate the dynamics of the 2 lobes of CaM, due to the flexibility of the central helix of CaM (Figure 2A). This conformational flexibility and the overall shape of the P454:CaM complex are also evidenced by SEC-SAXS data.

The SAXS data of the P454:CaM complex is shown in figure 2B and the corresponding parameters are presented in Table S5. In a recent study of a shorter version of AC (AC364), we already analyzed CaM in complex with the H-helix peptide and MLCK by SAXS and HDX-MS (16). The distance distribution P(r) of the P454:CaM complex is intermediate between that of free CaM and H:CaM complex on the one hand, and MLCK:CaM complex

on the other hand (Figure 2C). Ab initio modelling yields a shape intermediate between the globular MLCK:CaM complex and the bi-lobed extended shape of free CaM and H:CaM complex (Figure 2D), illustrating the conformational plasticity of CaM adapted to peptide ligand diversity (68).

The calculated SAXS curves from ten out of twelve crystal structures of P458:CaM are similar to but significantly different from our experimental SAXS data, while two structures exhibit a different N and C domain arrangement and, accordingly, a different scattering pattern. Using the model with the closest agreement, we added the six missing N-terminal amino-acids of CaM and the few missing terminal residues of P454 with Modeller and used the completed complex as a starting model to fit the SAXS data using the modeling program Dadimodo. Each run of the program yielded several models, the scattering pattern of which fitted our experimental SAXS data. After superimposition of the N-CaM domain, all resulting models appeared to exhibit close but slightly different positions of the C-CaM domain (Figure 2E) that were also similar to those within crystal structures (Figure 2A). We also studied the P458:CaM complex in solution. Due to low sample concentration, the recorded SAXS data were of much lower quality, sufficient however to appear essentially identical to that of the P454:CaM complex.

We performed HDX-MS on the P454:CaM complex and compared the results to free CaM (Figures S9 and S10). The P454-induced stabilization of CaM, as expressed in the fractional differential uptake, was mapped on the structural model with the best fit to the experimental SAXS data (Figure 2F). The HDX-MS data show that P454 binding to CaM induces a strong stabilization of both N and C lobes of CaM while the central helix remains flexible, essentially unaffected by peptide binding.

We then compared the effects of the three peptides P454, H-helix and MLCK on CaM. HDX-MS data reveals that the inter-lobe helix (residues 73-84) remains flexible in the absence and in the presence of the three peptides. The MLCK and H-helix peptides induce similar deuterium uptake differences on CaM: several regions from N-CaM (residues 2-37) and C-CaM (residues 89-105 and 125-149) experience a strong protection in complex with MLCK and H-helix peptides (uptake differences increase over time) while other regions (36-48, 84-90 and 104-120) are protected from exchange but are characterized by a higher structural dynamics (uptake differences decrease over time). Noteworthy, the uptake difference induced by P454 on CaM is different from that of MLCK and the H-helix: after 1 minute of HD exchange, the uptake difference decreases over time, suggesting that the P454:CaM complex is globally characterized by a significant structural dynamics. However, despite the overall dynamics of the P454:CaM complex, HDX-MS data show that N-CaM is more strongly

stabilized by P454 than by the H-helix peptide (see amplitudes of uptake differences). This is in agreement with the crystal structures of the complex showing that P454 mostly interacts with the hydrophobic groove of N-CaM.

Taken together, the H:CaM, P454:CaM and MLCK:CaM complexes adopt various conformations and exhibit different dynamic properties: P454 mainly binds to N-CaM while the H-helix preferentially binds to C-CaM, with various affinities (K_D values of 10 nM for H:C-CaM, 380 nM for H:N-CaM and 90 nM for P454:CaM) (see Figure S3, S7 and Tables S2 and S3).

4- Mutations altering P454:CaM/mb properties *in vitro*

We then identified critical residues of P454 involved in membrane interaction and CaM binding so as to substitute the identified residues in the full-length CyaA toxin and analyze their impact on the cell intoxication process.

We mutated in the P454 peptide the unique aromatic residue, W458, both arginine residues, R461 and R474, the aliphatic residues, L463, L475, I479 and L481, and the histidine residue H477. The P454-derived peptides contain a unique or two substitutions. We characterized membrane binding of the peptides by determining their partition coefficient, K_X, and free energy of interaction with membrane, ΔG_{Kx} using fluorescence spectroscopy and ITC. The secondary structure content of the P454-derived peptides was analyzed by circular dichroism and showed a disorder-to-helical conformational transition upon membrane binding for most of the peptides (see Figure S11 for examples and Table S6). The affinity of these peptides for CaM was similarly determined (see Figure S12 for examples), providing the dissociation constant K_D and the free energy of the peptide:CaM complex, ΔG_{KD}. All thermodynamic parameters are listed in Table S7. The free energy values of the peptides for membrane interaction ΔG_{Kx} and CaM binding ΔG_{KD} are plotted in Figure 3. The results show that membrane interaction of P454-derived peptides is mainly affected by single or double point mutations of arginine residues. Their ability to permeabilize membranes is marginally affected, except, however, for R12E, I479A and WAIA, which require peptide concentrations more than 100 times higher than P454 to permeabilize vesicles (Table S8). The affinity of the P454-derived peptides for CaM is progressively affected by the single point mutations of H477S, L463A and I479A, and strongly affected by double mutations such as W458A-I479A and arginine residues substituted to glutamine and glutamate residues (R12Q and R12E). In agreement, the vesicle permeabilization induced by P454-derived peptides is blocked by calmodulin addition, except for R12E, and WAIA, which cannot be assayed as they do not permeabilize vesicles (tested up to 50 and 80 uM, respectively).

5- Mutations altering CyaA cell intoxication in cellula:

The mutational analysis of the P454-derived peptides reported above (Figure 3) has allowed us to identify the arginine residues R461 and R474, the aromatic W458, the histidine H477 and the aliphatic residues L463, L475 and I479. These residues might be crucial at various steps of the intoxication process. Consequently, several recombinant CyaA proteins have been prepared and both hemolytic activity and in-cell cAMP production have been measured (Table 1).

Up to now, the following recombinant proteins have been analyzed: $CyaA_{I479A}$, $CyaA_{W458A-I479A}$, $CyaA_{R12Q}$, $CyaA_{R12E}$, and $CyaA_{multi}$, which combines the following mutations: both arginine residues R461E and R474E, two leucine residues L463A and L475A, the histidine residue H477S and the isoleucine I479A.

The substitution of the aliphatic and arginine residues in the $CyaA_{multi}$ recombinant protein completely abolishes the ability of CyaA to translocate its catalytic domain and to produce massive amounts of cAMP, indicating that substitution of a few residues from the TR does impair CyaA cell intoxication. Interestingly, the hemolytic activity of the $CyaA_{multi}$ recombinant protein is significantly enhanced compared to the WT (Table 1), suggesting that $CyaA_{multi}$ is accumulated at a step favoring destabilization of the plasma membrane but cannot move forward in the process of AC translocation due to the mutations.

The ability of $CyaA_{I479A}$ to intoxicate cells is similar to the native CyaA toxin (Table 1), although the membrane permeabilization efficiency of its related peptide, P454-I479A, is strongly affected (Figure 3 and Table S8). Noteworthy, the substitution of both tryptophan and isoleucine residues, $CyaA_{W458A-I479A}$, partially abrogates the ability of CyaA to intoxicate cells. In agreement, both membrane destabilization activity (Cp1/2) and CaM affinity of the corresponding peptide, P454 W458A-I479A, are significantly affected (Figure 3 and Table S8).

We then focused on the arginine contribution to cell intoxication. The results show that charge reversion of arginine residues by glutamate residues in $CyaA_{R12E}$ is enough to drastically reduce the ability of CyaA to produce cAMP in cells. Neutralization of the arginine residues in $CyaA_{R12Q}$ does not prevent, however, accumulation of cAMP in erythrocytes. The study of the P454-derived peptides indicates that although P454-R12E and P454-R12Q exhibit similar affinity for membrane binding, the ability of P454-R12E to permeabilize membrane and to bind CaM are dramatically affected compared to P454-R12Q. This suggests that $CyaA_{R12E}$ is unable to produce cAMP in cells because of one or a combination of the following parameters: (i) its reduced membrane destabilization capacity,

(ii) its charge against the membrane potential (*i.e.*, against the positive inside rule), (iii) its reduced CaM binding affinity compared to $CyaA_{R12Q}$.

These data suggest that the ability of CyaA to translocate its catalytic domain correlates with both membrane permeabilization efficiency and CaM affinity. We propose that the ability of CyaA to intoxicate cells does sequentially require the ability of the translocation region to first locally destabilize and translocate across the plasma membrane, and then to interact with calmodulin, favoring the translocation of the N-terminal catalytic domain into the cytosol.

6 - Once translocated, AC489:CaM is formed and corresponds to the cytoplasmic part of the CyaA:CaM enzymatic complex.

6a - HDX-MS, SR-CD

We propose that once the CyaA translocation region reaches the cytosol, CaM binding traps this CyaA region in the cytosol, preventing its backward translocation, and most importantly, provides the energy required to translocate the catalytic domain across the membrane. Therefore, the translocated regions of CyaA would correspond to the catalytic and the translocation domains. Accordingly, we characterized by HDX-MS and SAXS the structure of the translocated N-terminal domains of CyaA, the AC489 protein (residues 1 to 489 of CyaA) in solution and in complex with CaM.

The HDX-MS data of AC489 in solution (Figure 4A and peptide map S13) shows a pattern similar to that of the isolated catalytic domain, AC364 (16). The C-terminal part of AC489, from residues 345 to 489, is characterized by structural flexibility. Circular dichroism showed that both AC364 and AC489 contain a similar helical content, *i.e.*, 27% (see Figure S14 for AC489 and see 16 for AC364). This roughly corresponds to 40 residues in helical conformation for the segment encompassing residues 345 to 489. This might correspond to the two predicted amphiphilic helices located near 418-439 and 457-485. Taken together, CD and HDX-MS suggest that the region 345-489 contains dynamic helical structures flanked by disordered segments.

The addition of CaM in excess (AC489:CaM molar ratio at 1:4) induces a significant stabilization of AC489 (highlighted in blue in Figure 4B), again, as observed for AC364 (16). Interestingly, the HDX pattern of the segment covering the region 359-470 is unaffected by calmodulin while the AC489 C-terminal extremity shows a significant calmodulin-induced protection.

The AC489:CaM complex was also investigated at 1:1 molar ratio (Figure S15). The data show that both the H-helix and the C-terminal extremity of AC489 exhibit HDX protection, suggesting that 1 CaM can be bound to both CaM-binding sites of AC489. Noteworthy, the

HDX protection is low for the peptides covering the AC489 C-terminal extremity, highlighting the dynamic nature of the interaction of this region with CaM.

6b - SAXS data and structural model(s) of AC489:CaM

AC489 SAXS: data.

Data were recorded using the SEC-SAXS setup at SWING (see Material and Methods for details). The 280 nm elution profile exhibits two peaks (Figure S16A): the main peak of monomers is preceded by a smaller peak of larger particles (most probably dimers). Identical frames on top of the monomer peak were averaged, yielding the monomer scattering pattern displayed in Figure 16B. The parameter values derived from the scattering curve are given in Table S5.

AC489 SAXS: modeling

We used as a starting point a model of AC364 determined in a previous study (16). This model was completed as explained in the Mat. Met. Section, yielding an initial configuration of AC489. We then modeled the protein keeping most of AC364 as a rigid body with the exception of the nine N-terminal residues and the 206-250 flexible region as well as the two helices using Dadimodo (see Material and Methods for details). A series of runs gave us many fitting models. Two typical models are displayed in Figure 5A; their calculated scattering patterns are superimposed over the experimental SAXS data in Figure S16B. The two models essentially differ by the position of the 471 helix, which is exposed to the solvent remote from the main protein body in model 1 in green, while it is much closer to the main protein body with the 359-470 stretch forming kind of a loop in the solvent (see model 2 in yellow, Figure 5A). A slight difference between the calculated S-value of 3.1 (model 1) and 3.2 (model 2) is obtained to be compared with an experimental value of 3.3 (Table S9).

The models obtained with Dadimodo exhibit large poorly structured regions that are likely to be very flexible. To confirm this point, we performed an analysis of our data in terms of ensemble of conformations using the program EOM 2.0 Figure S17 presents the distribution of radii of gyration of fitting ensembles compared with that of the entire pool of conformations. The width of both distributions are large and similar, supporting the high flexibility of a significant part of the molecule (mostly the 206 – 250 stretch and most of the C-terminal 130 residues).

AC489:CaM complex SAXS data

Here also data were recorded using the SEC-SAXS setup on a solution containing AC489 and CaM in a 1:4 molar ratio. The 280 nm elution profile is more complex than that of isolated AC489 with several well-defined peaks preceding that of the monomeric (with respect to AC489 content) complex eluting at 21.1 min (*vs* 22.7 min for unbound AC489) and the last peak of excess CaM at *ca* 26.3 min (Figure S16C).

We first addressed the question of the complex stoichiometry, considering that AC489 possesses two CaM binding sites: the H-helix described as the primary binding site for CaM (PBS, K_D about 10 nM for C-CaM) and the P454 region (K_D about 90 nM for N-CaM). To that aim, we determined the Rg and I(0) profiles along the elution profile using the Guinier approximation. The value of I(0), the scattered intensity extrapolated to the origin, is proportional to the molar concentration of the solution multiplied by the square of the molecular mass of the particle in solution. Comparing the I(0) values under the peak of the complex and the excess CaM peak we obtain a molar ratio of three to one, so that the complex is a 1:1 complex. Of note, the same calculation performed on a similar data set using an initial 1:3 molar ratio gave us a 1:2 ratio between complex and excess CaM respectively, confirming our conclusion (data not shown). The interpretation of the higher molecular weight peaks is easy if one considers that the concentration around the top of the peaks is of the order of a few µM, a few 100-fold the K_D value of AC489:C-CaM interaction at the PBS. In the presence of a 4-fold excess of CaM, the PBS is fully saturated by C-CaM and the P454 site, though weaker, is most likely significantly occupied even if we take into account the separation of free CaM from complex during elution. If both interactions are between one AC molecule and the two lobes of the same CaM we have a 1:1 complex. If one AC molecule interacts with two different CaM, since the PBS is saturated we have another AC489 involved, hence a dimeric complex 2:2, a trimeric 3:3 complex and so on. This explains the presence of well –resolved oligomer peaks ahead of the monomeric complex peak and the fact that all complexes exhibit a 1:1 stoichiometry. Of course, the oligomers are an experimental artefact. *In vivo*, the CaM to AC489 ratio is likely much larger and the AC489 concentration significantly lower, favoring 1:1 complexes but with no oligomers.

Complex modeling

In a similar approach to that followed for isolated AC489, we used as a starting point a model of AC364 complexed with one CaM (16). The interaction site was the PBS, the only one present within AC364, that interacted with the C-CaM domain exactly as in the crystal structure of C-CaM with AC364 (14). Since the affinity of the PBS for C-CaM is much better

than that of P454 for N-CaM (K_D=10 nM vs 90 nM respectively) we used Dadimodo to refine the flexible regions of both molecules while keeping the folded domains as rigid but mobile bodies and preserving the PBS:C-CaM interaction through contact restraints. We obtained a series of energetically plausible models all fitting the data and preserving the H:C-CaM interaction. Similarly to our observations with unbound AC489, two main types of AC conformations were obtained that primarily differed by the position of the 471 helix (Figure 5B-C).

We also tried to obtain fitting models interacting through the P454:N-CaM interaction even if, in view of the relative affinities, they could only represent a minor component in solution. Satisfactory models were produced through refinement of flexible regions by Dadimodo. Finally, we used the same approach to see whether fitting models exhibiting both interactions could fit our data. Here, models, the scattering pattern of which gave a fit to our experimental SAXS data with an acceptable c^2 value, were obtained (Figures 5D and S16D). However, upon closer examination, these models had a maximum diameter D_{max} of around 135Å, significantly smaller than the experimental estimate of 160Å. This does not mean that such doubly-bound complexes (Figure 5D) do not exist, simply that, if they are present in the solution, they coexist with a majority of AC489:CaM complexes interacting via the H-helix and C-CaM lobe which are more extended (D_{max} close to 160Å for models presented in Figure 5B-C). These observations are in agreement with the HDX-MS data described above, showing that AC489:CaM complexes interact mainly via H:C-CaM and dynamically via P454:N-CaM. This is also in agreement with the affinities measured by ITC (K_{Ds} of 10 nM for H:CaM and 90 nM for P454:CaM).

Discussion

The transport of proteins across membranes involves complex translocation machineries as in the case of protein import into mitochondria, endoplasmic reticulum, nuclei or chloroplast. Many proteins from poisonous plants or from pathogenic bacteria are secreted and then able to penetrate into target cells where they exert their toxic effects. These toxins may exploit the endogenous cellular machinery of endocytosis and intracellular sorting to gain access to the cell cytosol, while others carry their own translocation apparatus, such as the adenylate cyclase (CyaA) toxin, which is one of the major virulence factors secreted by Bordetella pertussis, the causative agent of whooping cough. CyaA, a 1706-residue long multi-domain protein, is endowed with a unique mechanism of AC delivery into eukaryotic cells: CyaA translocates its catalytic domain directly across the plasma membrane of target cells, from the extra-cellular milieu into the cytosol. Once translocated, calmodulin-induced folding of AC stimulates the production of supra physiological levels of cAMP at the expense of ATP, altering cell physiology. The molecular mechanisms involved in the CyaA toxin translocation across the plasma membrane of eukaryotic target cells remains, however, largely unknown.

The results presented herein lead us to propose a translocation model in which the segment covering residues 454-484 from the CyaA TR is required (*i*) to sequentially destabilize the lipid bilayer, favoring its translocation across the plasma membrane into the cytosol and (*ii*) to tightly interact with CaM to favor the translocation of AC into the cytosol. We have identified residues from P454 involved in membrane binding, membrane destabilization and CaM binding. These residues have been substituted in the full-length CyaA toxin and cell intoxication assay showed that these residues are essential for the efficient translocation of the catalytic domain into the cell cytoplasm and for the production of cAMP. Hence, membrane-active properties and CaM binding ability of this CyaA region are critical for an efficient catalytic delivery into host cells.

From a molecular point of view, we show that the P454 peptide (residues 454 to 484 from CyaA) is competent to translocate across lipid membranes. Moreover, once translocated, this peptide is able to form a complex with CaM. The C-terminal part of P454 strongly interacts with the N-CaM lobe via the arginine and hydrophobic residues of the peptide. This interaction displaces the P454 peptide from membrane to solution due to a favorable free energy ($\Delta\Delta G$ of 4 kcal/mol). The C-CaM lobe remains mostly free and flexible. In the context of the CyaA toxin, we propose that once this region (residues 454-484) is translocated across the plasma membrane, it binds to CaM and favors the translocation of the N-terminal catalytic domain. Indeed, after translocation, P454 interacts with the internal leaflet of the plasma membrane and may initiate kind of a ratchet effect. However, a soluble binding partner would

strongly increase the pulling force by preventing the backward flop process of this CyaA segment across the plasma membrane. It has been shown that CyaA translocation is accompanied by a Ca^{2+} influx increasing its cytoplasmic concentration close to the membrane to *ca* 1 to 2 μM (43). In view of the significant cytosolic CaM concentration close to the membrane (of the order of 5 to 10 μM), P454 rapidly changes partner from the membrane to the N-CaM domain (K_D=90 nM) of holo-CaM. This prevents the back and forth flip-flop of the P454 segment and reinforces the pulling mechanism that converts the stochastic process of protein translocation to an efficient, vectorial chain transfer into the cytoplasm of the target cell.

Once in the cytosol, the H-helix of the catalytic domain binds to CaM (K_D=10 nM), either the C-CaM of the bound CaM –this C-CaM lobe was mostly free and flexible after the P454:N-CaM complex was formed- or to that of another neighboring CaM molecule. Due to the local free C-CaM concentration, we propose that the C-CaM of the CaM already bound to the C-terminal TR region via its N-CaM does bind the AC H-helix. This double interaction of CaM with distal helices in CyaA may strengthen even more the translocation and prevent any backward chain movement. Finally, once AC translocation is achieved, CaM induces a global disorder-to-order transition in the catalytic domain, leading to the activation of the enzyme (16).

We hypothesize that the structural models of AC489 in complex with CaM reflect the conformational plasticity of the enzymatic complex formed in the cytosol, on the trans side of the plasma membrane. Due to the lower affinity of P454 for CaM (K_D=90 nM) than the H-helix for CaM (K_D=10 nM), we propose that CaM remains locked on AC via the C-CaM:H interaction, while the P454:N-CaM interaction may experience transient dissociation, leading to more open conformations, as shown in figure 5. However, such transient dissociation has not significant effect on the enzymatic activity, as the P454:N-CaM interaction is required for AC translocation, but is not required for AC activation, as AC364:CaM complex is known to constitute the fully activated enzyme (AC364:CaM kcat=2000 /sec).

Taken together, we show that the ability of CaM to interact with eukaryotic amphiphilic helical motifs is hijacked by CyaA at two steps of the cell intoxication process: we propose that the P454 and H amphiphilic helices can successively interact with CaM for the translocation and then the activation of the catalytic domain, respectively. Interestingly, several toxins hijack eukaryotic cytosolic factors to achieve the translocation of their respective catalytic domains: these toxins contain segments able to translocate across target membranes and to interact with host soluble proteins. Here, we show that the forces provided

by such toxin:target complexes significantly contribute to the energy required to achieve the translocation of the catalytic domain across membranes of host cells.

Bibliography

1. Ladant, D., Brezin, C., Alonso, J. M., Crenon, I., and Guiso, N. (1986) Bordetella pertussis adenylate cyclase. Purification, characterization, and radioimmunoassay. *J Biol Chem* **261**, 16264-16269
2. Glaser, P., Danchin, A., Ladant, D., Barzu, O., and Ullmann, A. (1988) Bordetella pertussis adenylate cyclase: the gene and the protein. *Tokai J Exp Clin Med* **13 Suppl**, 239-252
3. Glaser, P., Ladant, D., Sezer, O., Pichot, F., Ullmann, A., and Danchin, A. (1988) The calmodulin-sensitive adenylate cyclase of Bordetella pertussis: cloning and expression in Escherichia coli. *Molecular microbiology* **2**, 19-30
4. Guiso, N. (2017) Bordetella Adenylate Cyclase-Hemolysin Toxins. *Toxins (Basel)* **9**
5. Novak, J., Cerny, O., Osickova, A., Linhartova, I., Masin, J., Bumba, L., Sebo, P., and Osicka, R. (2017) Structure-Function Relationships Underlying the Capacity of Bordetella Adenylate Cyclase Toxin to Disarm Host Phagocytes. *Toxins (Basel)* **9**
6. Coote, J. G. (1992) Structural and functional relationships among the RTX toxin determinants of gram-negative bacteria. *FEMS Microbiol Rev* **8**, 137-161
7. Welch, R. A. (2001) RTX toxin structure and function: a story of numerous anomalies and few analogies in toxin biology. *Current topics in microbiology and immunology* **257**, 85-111
8. Linhartova, I., Bumba, L., Masin, J., Basler, M., Osicka, R., Kamanova, J., Prochazkova, K., Adkins, I., Hejnova-Holubova, J., Sadilkova, L., Morova, J., and Sebo, P. (2010) RTX proteins: a highly diverse family secreted by a common mechanism. *FEMS Microbiol Rev* **34**, 1076-1112
9. Chenal, A., Sotomayor Perez, A. C., and Ladant, D. (2015) Structure and function of RTX Toxins. in *The Comprehensive Sourcebook of Bacterial Protein Toxins, 4th Edition*, 4th Ed., Elsevier. pp
10. Benz, R. (2016) Channel formation by RTX-toxins of pathogenic bacteria: Basis of their biological activity. *Biochim Biophys Acta* **1858**, 526-537
11. Ladant, D., and Ullmann, A. (1999) Bordatella pertussis adenylate cyclase: a toxin with multiple talents. *Trends in microbiology* **7**, 172-176
12. Karst, J. C., Ntsogo Enguene, V. Y., Cannella, S. E., Subrini, O., Hessel, A., Debard, S., Ladant, D., and Chenal, A. (2014) Calcium, Acylation, and Molecular Confinement Favor Folding of Bordetella pertussis Adenylate Cyclase CyaA Toxin into a Monomeric and Cytotoxic Form. *J Biol Chem* **289**, 30702-30716
13. Ladant, D. (1988) Interaction of Bordetella pertussis adenylate cyclase with calmodulin. Identification of two separated calmodulin-binding domains. *J Biol Chem* **263**, 2612-2618
14. Guo, Q., Shen, Y., Lee, Y. S., Gibbs, C. S., Mrksich, M., and Tang, W. J. (2005) Structural basis for the interaction of Bordetella pertussis adenylyl cyclase toxin with calmodulin. *Embo J* **24**, 3190-3201
15. Karst, J. C., Sotomayor Perez, A. C., Guijarro, J. I., Raynal, B., Chenal, A., and Ladant, D. (2010) Calmodulin-induced conformational and hydrodynamic changes in the catalytic domain of Bordetella pertussis adenylate cyclase toxin. *Biochemistry* **49**, 318-328
16. O'Brien, D. P., Durand, D., Voegele, A., Hourdel, V., Davi, M., Chamot-Rooke, J., Vachette, P., Brier, S., Ladant, D., and Chenal, A. (2017) Calmodulin fishing with a structurally disordered bait triggers CyaA catalysis. *PLoS Biol* **15**, e2004486
17. Karst, J. C., Barker, R., Devi, U., Swann, M. J., Davi, M., Roser, S. J., Ladant, D., and Chenal, A. (2012) Identification of a region that assists membrane insertion and

translocation of the catalytic domain of Bordetella pertussis CyaA toxin. *J Biol Chem* **287**, 9200-9212
18. Knapp, O., Maier, E., Masin, J., Sebo, P., and Benz, R. (2008) Pore formation by the Bordetella adenylate cyclase toxin in lipid bilayer membranes: role of voltage and pH. *Biochim Biophys Acta* **1778**, 260-269
19. Basler, M., Knapp, O., Masin, J., Fiser, R., Maier, E., Benz, R., Sebo, P., and Osicka, R. (2007) Segments crucial for membrane translocation and pore-forming activity of Bordetella adenylate cyclase toxin. *J Biol Chem* **282**, 12419-12429
20. Barry, E. M., Weiss, A. A., Ehrmann, I. E., Gray, M. C., Hewlett, E. L., and Goodwin, M. S. (1991) Bordetella pertussis adenylate cyclase toxin and hemolytic activities require a second gene, cyaC, for activation. *J Bacteriol* **173**, 720-726
21. Hackett, M., Guo, L., Shabanowitz, J., Hunt, D. F., and Hewlett, E. L. (1994) Internal lysine palmitoylation in adenylate cyclase toxin from Bordetella pertussis. *Science* **266**, 433-435
22. Westrop, G. D., Hormozi, E. K., Da Costa, N. A., Parton, R., and Coote, J. G. (1996) Bordetella pertussis adenylate cyclase toxin: proCyaA and CyaC proteins synthesised separately in Escherichia coli produce active toxin in vitro. *Gene* **180**, 91-99
23. O'Brien, D. P., Cannella, S. E., Voegele, A., Raoux-Barbot, D., Davi, M., Douche, T., Matondo, M., Brier, S., Ladant, D., and Chenal, A. (2019) Post-translational acylation controls the folding and functions of the CyaA RTX toxin. *FASEB J* **33**, fj201802442RR
24. Veneziano, R., Rossi, C., Chenal, A., Devoisselle, J. M., Ladant, D., and Chopineau, J. (2013) Bordetella pertussis adenylate cyclase toxin translocation across a tethered lipid bilayer. *Proc Natl Acad Sci U S A* **110**, 20473-20478
25. Rose, T., Sebo, P., Bellalou, J., and Ladant, D. (1995) Interaction of calcium with Bordetella pertussis adenylate cyclase toxin. Characterization of multiple calcium-binding sites and calcium-induced conformational changes. *J Biol Chem* **270**, 26370-26376
26. Masure, H. R., Au, D. C., Gross, M. K., Donovan, M. G., and Storm, D. R. (1990) Secretion of the Bordetella pertussis adenylate cyclase from Escherichia coli containing the hemolysin operon. *Biochemistry* **29**, 140-145
27. Glaser, P., Sakamoto, H., Bellalou, J., Ullmann, A., and Danchin, A. (1988) Secretion of cyclolysin, the calmodulin-sensitive adenylate cyclase-haemolysin bifunctional protein of Bordetella pertussis. *Embo J* **7**, 3997-4004
28. O'Brien, D. P., Perez, A. C. S., Karst, J., Cannella, S. E., Enguene, V. Y. N., Hessel, A., Raoux-Barbot, D., Voegele, A., Subrini, O., Davi, M., Guijarro, J. I., Raynal, B., Baron, B., England, P., Hernandez, B., Ghomi, M., Hourdel, V., Malosse, C., Chamot-Rooke, J., Vachette, P., Durand, D., Brier, S., Ladant, D., and Chenal, A. (2018) Calcium-dependent disorder-to-order transitions are central to the secretion and folding of the CyaA toxin of Bordetella pertussis, the causative agent of whooping cough. *Toxicon : official journal of the International Society on Toxinology* **149**, 37-44
29. Sotomayor-Perez, A. C., Ladant, D., and Chenal, A. (2015) Disorder-to-order transition in the CyaA toxin RTX domain: implications for toxin secretion. *Toxins (Basel)* **7**, 1-20
30. O'Brien, D. P., Hernandez, B., Durand, D., Hourdel, V., Sotomayor-Perez, A. C., Vachette, P., Ghomi, M., Chamot-Rooke, J., Ladant, D., Brier, S., and Chenal, A. (2015) Structural models of intrinsically disordered and calcium-bound folded states of a protein adapted for secretion. *Sci Rep* **5**, 14223
31. Sotomayor-Perez, A. C., Subrini, O., Hessel, A., Ladant, D., and Chenal, A. (2013) Molecular Crowding Stabilizes Both the Intrinsically Disordered Calcium-Free State

and the Folded Calcium-Bound State of a Repeat in Toxin (RTX) Protein. *Journal of the American Chemical Society* **135**, 11929-11934
32. Sotomayor-Perez, A. C., Ladant, D., and Chenal, A. (2011) Calcium-induced folding of intrinsically disordered repeat-in-toxin (RTX) motifs via changes of protein charges and oligomerization states. *J Biol Chem* **286**, 16997-17004
33. Sotomayor Perez, A. C., Karst, J. C., Davi, M., Guijarro, J. I., Ladant, D., and Chenal, A. (2010) Characterization of the regions involved in the calcium-induced folding of the intrinsically disordered RTX motifs from the bordetella pertussis adenylate cyclase toxin. *Journal of molecular biology* **397**, 534-549
34. Chenal, A., Karst, J. C., Sotomayor Perez, A. C., Wozniak, A. K., Baron, B., England, P., and Ladant, D. (2010) Calcium-induced folding and stabilization of the intrinsically disordered RTX domain of the CyaA toxin. *Biophys J* **99**, 3744-3753
35. Chenal, A., Guijarro, J. I., Raynal, B., Delepierre, M., and Ladant, D. (2009) RTX calcium binding motifs are intrinsically disordered in the absence of calcium: implication for protein secretion. *J Biol Chem* **284**, 1781-1789
36. Bauche, C., Chenal, A., Knapp, O., Bodenreider, C., Benz, R., Chaffotte, A., and Ladant, D. (2006) Structural and functional characterization of an essential RTX subdomain of Bordetella pertussis adenylate cyclase toxin. *J Biol Chem* **281**, 16914-16926
37. O'Brien, D. P., Brier, S., Ladant, D., Durand, D., Chenal, A., and Vachette, P. (2018) SEC-SAXS and HDX-MS: A powerful combination. The case of the calcium-binding domain of a bacterial toxin. *Biotechnol Appl Biochem* **65**, 62-68
38. Cannella, S. E., Ntsogo Enguene, V. Y., Davi, M., Malosse, C., Sotomayor Perez, A. C., Chamot-Rooke, J., Vachette, P., Durand, D., Ladant, D., and Chenal, A. (2017) Stability, structural and functional properties of a monomeric, calcium-loaded adenylate cyclase toxin, CyaA, from Bordetella pertussis. *Sci Rep* **7**, 42065
39. Guermonprez, P., Khelef, N., Blouin, E., Rieu, P., Ricciardi-Castagnoli, P., Guiso, N., Ladant, D., and Leclerc, C. (2001) The adenylate cyclase toxin of Bordetella pertussis binds to target cells via the alpha(M)beta(2) integrin (CD11b/CD18). *J Exp Med* **193**, 1035-1044
40. Guermonprez, P., Fayolle, C., Rojas, M. J., Rescigno, M., Ladant, D., and Leclerc, C. (2002) In vivo receptor-mediated delivery of a recombinant invasive bacterial toxoid to CD11c + CD8 alpha -CD11bhigh dendritic cells. *Eur J Immunol* **32**, 3071-3081
41. El-Azami-El-Idrissi, M., Bauche, C., Loucka, J., Osicka, R., Sebo, P., Ladant, D., and Leclerc, C. (2003) Interaction of Bordetella pertussis adenylate cyclase with CD11b/CD18: Role of toxin acylation and identification of the main integrin interaction domain. *J Biol Chem* **278**, 38514-38521
42. Masin, J., Basler, M., Knapp, O., El-Azami-El-Idrissi, M., Maier, E., Konopasek, I., Benz, R., Leclerc, C., and Sebo, P. (2005) Acylation of lysine 860 allows tight binding and cytotoxicity of Bordetella adenylate cyclase on CD11b-expressing cells. *Biochemistry* **44**, 12759-12766
43. Fiser, R., Masin, J., Basler, M., Krusek, J., Spulakova, V., Konopasek, I., and Sebo, P. (2007) Third activity of Bordetella adenylate cyclase (AC) toxin-hemolysin. Membrane translocation of AC domain polypeptide promotes calcium influx into CD11b+ monocytes independently of the catalytic and hemolytic activities. *J Biol Chem* **282**, 2808-2820
44. Adkins, I., Holubova, J., Kosova, M., and Sadilkova, L. (2012) Bacteria and their toxins tamed for immunotherapy. *Curr Pharm Biotechnol* **13**, 1446-1473
45. Svedova, M., Masin, J., Fiser, R., Cerny, O., Tomala, J., Freudenberg, M., Tuckova, L., Kovar, M., Dadaglio, G., Adkins, I., and Sebo, P. (2016) Pore-formation by adenylate cyclase toxoid activates dendritic cells to prime CD8+ and CD4+ T cells. *Immunol Cell Biol* **94**, 322-333

46. Fedele, G., Schiavoni, I., Adkins, I., Klimova, N., and Sebo, P. (2017) Invasion of Dendritic Cells, Macrophages and Neutrophils by the Bordetella Adenylate Cyclase Toxin: A Subversive Move to Fool Host Immunity. *Toxins (Basel)* **9**
47. Chenal, A., and Ladant, D. (2018) Bioengineering of Bordetella pertussis Adenylate Cyclase Toxin for Antigen-Delivery and Immunotherapy. *Toxins (Basel)* **10**
48. Angely, C., Nguyen, N. M., Andre Dias, S., Planus, E., Pelle, G., Louis, B., Filoche, M., Chenal, A., Ladant, D., and Isabey, D. (2017) Exposure to Bordetella pertussis adenylate cyclase toxin affects integrin-mediated adhesion and mechanics in alveolar epithelial cells. *Biol Cell* **109**, 293-311
49. Hasan, S., Kulkarni, N. N., Asbjarnarson, A., Linhartova, I., Osicka, R., Sebo, P., and Gudmundsson, G. H. (2018) Bordetella pertussis Adenylate Cyclase Toxin Disrupts Functional Integrity of Bronchial Epithelial Layers. *Infection and immunity* **86**
50. Roderova, J., Osickova, A., Sukova, A., Mikusova, G., Fiser, R., Sebo, P., Osicka, R., and Masin, J. (2019) Residues 529 to 549 participate in membrane penetration and pore-forming activity of the Bordetella adenylate cyclase toxin. *Scientific Reports* **9**
51. Uribe, K. B., Martin, C., Etxebarria, A., Gonzalez-Bullon, D., Gomez-Bilbao, G., and Ostolaza, H. (2013) Ca2+ influx and tyrosine kinases trigger Bordetella adenylate cyclase toxin (ACT) endocytosis. Cell physiology and expression of the CD11b/CD18 integrin major determinants of the entry route. *PLoS One* **8**, e74248
52. Uribe, K. B., Etxebarria, A., Martin, C., and Ostolaza, H. (2013) Calpain-Mediated Processing of Adenylate Cyclase Toxin Generates a Cytosolic Soluble Catalytically Active N-Terminal Domain. *PLoS One* **8**, e67648
53. Bumba, L., Masin, J., Fiser, R., and Sebo, P. (2010) Bordetella adenylate cyclase toxin mobilizes its beta2 integrin receptor into lipid rafts to accomplish translocation across target cell membrane in two steps. *PLoS Pathog* **6**, e1000901
54. Voegele, A., O'Brien, D. P., Subrini, O., Sapay, N., Cannella, S. E., Enguene, V. Y. N., Hessel, A., Karst, J., Hourdel, V., Perez, A. C. S., Davi, M., Veneziano, R., Chopineau, J., Vachette, P., Durand, D., Brier, S., Ladant, D., and Chenal, A. (2018) Translocation and calmodulin-activation of the adenylate cyclase toxin (CyaA) of Bordetella pertussis. *Pathog Dis* **76**
55. Sakamoto, H., Bellalou, J., Sebo, P., and Ladant, D. (1992) Bordetella pertussis adenylate cyclase toxin. Structural and functional independence of the catalytic and hemolytic activities. *J Biol Chem* **267**, 13598-13602
56. Vojtova, J., Kamanova, J., and Sebo, P. (2006) Bordetella adenylate cyclase toxin: a swift saboteur of host defense. *Curr Opin Microbiol* **9**, 69-75
57. Subrini, O., Sotomayor-Perez, A. C., Hessel, A., Spiaczka-Karst, J., Selwa, E., Sapay, N., Veneziano, R., Pansieri, J., Chopineau, J., Ladant, D., and Chenal, A. (2013) Characterization of a membrane-active peptide from the Bordetella pertussis CyaA toxin. *J Biol Chem* **288**, 32585-32598
58. Voegele, A., Subrini, O., Sapay, N., Ladant, D., and Chenal, A. (2017) Membrane-Active Properties of an Amphitropic Peptide from the CyaA Toxin Translocation Region. *Toxins (Basel)* **9**
59. Shah, P., Hsiao, F. S., Ho, Y. H., and Chen, C. S. (2016) The proteome targets of intracellular targeting antimicrobial peptides. *Proteomics* **16**, 1225-1237
60. Le, C. F., Fang, C. M., and Sekaran, S. D. (2017) Intracellular Targeting Mechanisms by Antimicrobial Peptides. *Antimicrob Agents Chemother* **61**
61. Ratts, R., Zeng, H., Berg, E. A., Blue, C., McComb, M. E., Costello, C. E., vanderSpek, J. C., and Murphy, J. R. (2003) The cytosolic entry of diphtheria toxin catalytic domain requires a host cell cytosolic translocation factor complex. *The Journal of cell biology* **160**, 1139-1150
62. Lemichez, E., and Boquet, P. (2003) To be helped or not helped, that is the question. *The Journal of cell biology* **160**, 991-992

63. Ratts, R., Trujillo, C., Bharti, A., vanderSpek, J., Harrison, R., and Murphy, J. R. (2005) A conserved motif in transmembrane helix 1 of diphtheria toxin mediates catalytic domain delivery to the cytosol. *Proc Natl Acad Sci U S A* **102**, 15635-15640
64. Trujillo, C., Ratts, R., Tamayo, A., Harrison, R., and Murphy, J. R. (2006) Trojan horse or proton force: finding the right partner(s) for toxin translocation. *Neurotoxicity research* **9**, 63-71
65. Ernst, K., Liebscher, M., Mathea, S., Granzhan, A., Schmid, J., Popoff, M. R., Ihmels, H., Barth, H., and Schiene-Fischer, C. (2016) A novel Hsp70 inhibitor prevents cell intoxication with the actin ADP-ribosylating Clostridium perfringens iota toxin. *Sci Rep* **6**, 20301
66. Ernst, K., Schnell, L., and Barth, H. (2016) Host Cell Chaperones Hsp70/Hsp90 and Peptidyl-Prolyl Cis/Trans Isomerases Are Required for the Membrane Translocation of Bacterial ADP-Ribosylating Toxins. *Current topics in microbiology and immunology*
67. Last, N. B., Schlamadinger, D. E., and Miranker, A. D. (2013) A common landscape for membrane-active peptides. *Protein science : a publication of the Protein Society* **22**, 870-882
68. Villarroel, A., Taglialatela, M., Bernardo-Seisdedos, G., Alaimo, A., Agirre, J., Alberdi, A., Gomis-Perez, C., Soldovieri, M. V., Ambrosino, P., Malo, C., and Areso, P. (2014) The ever changing moods of calmodulin: how structural plasticity entails transductional adaptability. *Journal of molecular biology* **426**, 2717-2735

Materials

1-palmitoyl-2-oleoyl-sn-glycero-3-phosphocholine (POPC, reference 850457C), 1-palmitoyl-2-oleoyl-sn-glycero-3-[phospho-rac-(1-glycerol)] (POPG, reference 840457C) were purchased from Avanti Polar Lipids (Alabaster, AL, USA). ANTS (A-350, 8-aminonapthalene-1,3,6 trisulfonic acid), and DPX (X-1525, p-xylene-bis-pyridinium bromide) were purchased from Molecular Probes (Eugene, OR, USA). Squalene was from Sigma-Aldrich. Experiments were performed in 20 mM HEPES, 150 mM NaCl pH 7.4 (buffer A) or in 20 mM HEPES, 150 mM NaCl, 2 mM $CaCl_2$ pH 7.4 (buffer B) or in 20 mM HEPES, 150 mM NaCl, 4 mM $CaCl_2$ pH 7.4 (buffer C) or in 20 mM HEPES, 150 mM NaCl, 8 mM $MgCl_2$, 2 mM $CaCl_2$ pH 7.4 (buffer D) or 20 mM HEPES, 150 mM NaCl, 9.8 mM $MgCl_2$, 0.2 mM $CaCl_2$ (buffer E).

Peptides synthesis

The peptide P454 corresponds to residues 454 to 484 of CyaA (ASAHWGQRALQGAQAVAAAQRLVHAIALMTQ) and contains a single native tryptophan W458. The P454-derived peptides were produced and purified by Genosphere Biotechnologies (Paris, France). All peptides were capped on the N-terminus with an acetyl group and on the C-terminus with an amide group, except for the P458 peptide (uncapped N-terminus). The native W458 is present in all peptides (except in P454 W458A-I458A). Their molecular weight was determined by MALDI-TOF and purity analyzed by HPLC.

The sequences of P454-derived peptides are described as follows:

- P454 L463A corresponds to the substitution of L463 by an alanine
(ASAHWGQRAAQGAQAVAAAQRLVHAIALMTQ)
- P454 L475A peptide corresponds to the substitution of L475 by an alanine
(ASAHWGQRALQGAQAVAAAQRAVHAIALMTQ)
- P454 L481A corresponds to the substitution of L481 by an alanine
(ASAHWGQRALQGAQAVAAAQRLVHAIAAMTQ)
- P454 I479L, I479V and I479A correspond to the substitution of I479 by a leucine, a valine or an alanine, respectively.
(ASAHWGQRALQGAQAVAAAQRLVHALALMTQ)
(ASAHWGQRALQGAQAVAAAQRLVHAVALMTQ)
(ASAHWGQRALQGAQAVAAAQRLVHAAALMTQ)
- P454 H477S corresponds to the substitution of H477 by a serine
(ASAHWGQRALQGAQAVAAAQRLVSAIALMTQ)

- P454 W458A-I479A corresponds to the substitution of both W458 and I479 by an alanine. (ASAHAGQRALQGAQAVAAAQRLVHAAALMTQ)
- P458 peptide corresponds to a shorter P454 peptide, from residue 458 to 481. (WGQRALQGAQAVAAAQRLVHAIAL)

The two arginine residues R461 (referred as R1) or R474 (referred as R2), or both of them (referred as R12) were substituted by lysine (R12K), glutamine (R1Q, R2Q and R12Q), alanine (R12A) or glutamate (R12E) residues (1), given the following sequences:
P454 R1Q (ASAHWGQQALQGAQAVAAAQRLVHAIALMTQ)
P454 R2Q (ASAHWGQRALQGAQAVAAAQQLVHAIALMTQ)
P454 R12Q (ASAHWGQQALQGAQAVAAAQQLVHAIALMTQ)
P454 R12A (ASAHWGQAALQGAQAVAAAQALVHAIALMTQ)
P454 R12K (ASAHWGQRKALQGAQAVAAAQKLVHAIALMTQ)
P454 R12E (ASAHWGQEALQGAQAVAAAQELVHAIALMTQ)

The P454, P454 R12E and H-helix (corresponding to residues 233-254 of CyaA) peptides were also synthetized with a 5-carboxytetramethylrhodamine (TAMRA) linked to their N-terminus and capped on the C-terminus with an amide group for the droplet interface bilayer experiments.

Proteins production and purification

The adenylate cyclase catalytic domain (AC364) corresponds to residues 1-364 of CyaA. A longer form, encompassing the catalytic domain and the translocation region (AC489), corresponds to residues 1-489 of CyaA (2). The proteins were produced in *E. coli* strain BLR (Novagen) as previously described (2,3).

AC364

AC364 was purified as previously described (3). Briefly, inclusions bodies were resuspended in 6 M GdnHCl, 20 mM HEPES to prevent carbamylation from urea. They were then buffer exchanged on prepacked G25SF desalting columns equilibrated with 6 M urea. AC364 was purified by two consecutive IEX (ion exchange chromatography) followed by a SEC (size exclusion chromatography) (2). The protein was concentrated on Amicon 10 kDa and purity was checked by SDS-PAGE and mass spectrometry. Protein concentration was determined by absorbance at 280 nm (ε_{280} = 28,880 M^{-1} cm^{-1})

AC489

AC489 was purified as described previously (2). Briefly, the urea extract of AC489 was loaded on a DEAE-Sepharose column and eluted with 20 mM HEPES, 8 M urea, 0.5 M NaCl. Then the eluate was diluted in 20 mM HEPES, 0.1 mM $CaCl_2$ and further purified on a calmodulin-agarose column. AC489 was eluted with 20 mM HEPES, 8 M urea. Finally, the protein was loaded onto a Sephacryl S300 and eluted as a refolded soluble form in 20 mM HEPES, 50 mM NaCl. Protein concentration was determined by absorbance at 280 nm (ε_{280} = 35,870 M^{-1} cm^{-1})

CaM

CaM was produced in *E. coli* as previously described (4). Briefly, ammonium sulfate precipitation followed by a glacial acetic acid precipitation and a phenyl-Speharose chromatography were used to purify CaM. Protein concentration was determined by absorbance at 280 nm (ε_{280} = 2,980 M^{-1} cm^{-1}).

CyaA recombinant proteins

All the CyaA recombinant proteins were produced in *E. coli* BLR. The proteins were produced and purified as previously described (5,6). Briefly, inclusion bodies were resuspended overnight in 8 M urea, 20 mM HEPES. Proteins were purified by two consecutive IEX Q-Sepharose equilibrated with 6 M urea, 20 mM HEPES, 150 mM NaCl, pH 7.4. Proteins were eluted with a NaCl gradient. Proteins were further purified onto a HIC Phenyl-Sepharose column. Proteins were eluted with 6 M urea, 20 mM HEPES, pH 7.4. Finally, proteins were loaded on a Sephacryl S500 equilibrated with 6 M urea, 20 mM HEPES, 50 mM NaCl, pH 7.4. Proteins were concentrated on Amicon 50 kDa. Protein concentration was determined by absorbance at 280 nm (ε_{280} = 144,000 M^{-1} cm^{-1}).

The following recombinant proteins has been produced and purified:

$CyaA_{I479A}$: substitution of I479 by an alanine residue,

$CyaA_{W458A-I479A}$: substitutions of W458 and I479 by alanine residues

$CyaA_{R12Q}$: substitutions of R461 and R474 by glutamine residues

$CyaA_{R12E}$: substitutions of R461 and R474 by glutamate residues

$CyaA_{multi}$: substitutions of R461 and R474 by glutamate residues; substitutions of L463, L475 and I479 by alanine residues; substitution of H477 by a serine residue.

Lipid vesicles preparation

Small unilamellar vesicles (SUVs) and large unilamellar vesicles (LUVs) were prepared with POPC and POPG at a molar ratio of 8:2, at a lipid concentration of 10 mM in buffer A, as previously described (1). Briefly, SUVs and LUVs were prepared by reverse phase evaporation and filtered through polycarbonate filters of 1 µm and 0.2 µm of pore size diameter to obtain LUV. SUVs were further sonicated. The hydrodynamic diameters and mean net charge of the vesicles were measured by dynamic light scattering (DLS) and electrophoretic mobility, respectively, using a ZetaSizer NanoZS (Malvern Instruments, Orsay, France) (7).

Peptide titrations by SUVs and CaM followed by tryptophan fluorescence

Titrations were carried out with a FP-8200 Jasco spectrofluorimeter, equipped with a Peltier-thermostated ETC-272T at 25°C. A bandwidth of 5 nm was used for both excitation and emission beams. Fluorescence experiments were carried out in a 109.004F-QS cuvette (Hellma, France) with constant stirring. Fluorescence emission was recorded between 300 and 400 nm at a scan rate of 100 nm/min, with an excitation wavelength of 280 nm. Fluorescence emission spectra were corrected for SUV or CaM baselines. Fluorescence intensity ratio at 330 nm over 370 nm was used to measure the partition coefficient (K_X) of peptides for membrane and the affinity (K_D) of peptides for CaM (see (8) for details).

Partition coefficient

The partition coefficient K_X is defined as the ratio of protein in the lipid (P_L) and in buffer (P_W) phases (9,10), expressed by: $K_X = \frac{P_L}{P_W} \times \frac{[W]}{[L]}$, giving $\frac{P_W}{P_L} = \frac{[W]}{K_X[L]}$, where [W] the concentration of water (55.5 M) and [L] the lipid concentration.

The fraction of peptide partitioned into the membrane, f_{PL}, is equal to:

$$f_{P_L} = \frac{P_L}{P_T} = \frac{P_L}{P_L + P_W} = \frac{1}{1 + (\frac{P_W}{P_L})} = \frac{1}{1 + (\frac{[W]}{[L]K_X})}$$

where P_T is the total concentration of peptides $P_T = P_L + P_W$.

The equation is fitted to the experimental data using the software KaleidaGraph, providing the K_X value. The partition coefficient is related to the apparent dissociation constant: $K_X \times K_D = [W]$ and to the free energy of partition $\Delta G = -RT\ln(K_X)$, where ΔG is the free energy in kcal/mol, R the gas constant ($R = 1.98 \times 10^{-3}$ kcal/mol/K) and T the temperature in Kelvin.

The conversion of ΔG_{Kx} to ΔG_{KD} is done using the following relations:

$K_X \times K_D = [W]$ => $-RT\ln(K_D) = -RT\ln(W) + RT\ln(K_x)$, from which $\Delta G_{KD} = -\Delta G_{Kx} - 2.4$

Sedimentation velocity-Analytical ultracentrifugation (SV-AUC)

SV-AUC experiments were carried out in a ProteomeLab XL-I analytical ultracentrifuge (Beckman Coulter, Brea, CA, USA). Samples of 400 µL and 410 µL buffer were loaded in cells equipped with 12-mm thick double-sector epoxy centerpieces and sapphire windows. P454 and CaM were tested alone (at 57 µM and 72 µM, respectively) or mixed in a molar ratio 1:1 (at 70 µM each). Samples were incubated 2h at 20°C in the ultracentrifuge and, then span at 42,000 rpm in an An-50 Ti rotor. Detection of protein concentration as a function of radial position and time was monitored with the ProteomeLab software (Beckman Coulter, Brea, CA, USA) by both absorbance at 280 nm and interferometry. Four hundred scans were collected at 3-min intervals with a radial step size of 0.003 cm. SV scans were analyzed using the continuous size distribution model c(s) of the software Sedfit (11). All the c(s) distributions were calculated with a fitted frictional ratio f/f0 and a maximum entropy regularization procedure with a confidence level of 0.68. All partial specific volumes were theoretically calculated with the software Sednterp (Spin Analytical, Berwick, ME, USA). Buffer density and viscosity at 20°C of 1.0310 $g.mL^{-1}$ and 1.0061 cP respectively were also determined with Sednterp for the buffer B.

Sedimentation equilibrium-Analytical ultracentrifugation (SE-AUC)

SE experiments (AUC-SE) were performed at 20°C in a Optima XL-I analytical ultracentrifuge (Beckman Coulter, Brea, CA, USA). AC489 and CaM were mixed at a molar ratio 1:4. 120 µL of sample at three concentrations (for a final absorbance of 0.5; 0.35 and 0.17) were loaded into 12-mm thick double-sector epoxy centerpieces. Six increasing rotor speeds (8000, 10000, 14000, 20000, 24000, 42000 rpm) were used over 72 hours and equilibrium was monitored using absorbance at 280 nm and interference profiles. The software SEDPHAT was used to perform a global fit of the data with a 3 species model in order to determine the molar mass (12). A Monte-carlo statistical analysis of 1000 run was performed to determine the standard deviation. Buffer viscosity and density, and partial specific volumes were determined with Sednterp.

Isothermal titration calorimetry

ITC experiments were performed using a VP-ITC colorimeter (Malvern Panalytical). The standard ITC condition was buffer B or buffer A complemented with 2 mM EDTA. For a typical titration, the solution of analyte (ranging from 0.2 to 10 µM) was loaded in the reaction cell. The titrants (ranging from 4 to 430 µM) were loaded into the syringe and then the titrant was injected into the reaction cell, usually at 3.5-minute intervals. Heats of

dilutions were measured by injecting the titrant into the protein-free buffer, and were subtracted from the heat of reaction. To obtain the thermodynamic parameters ΔH, ΔS and ΔG, titration profiles were analyzed using the single- or two-site models with Origin7 software (OriginLab). Changes of heat capacity (ΔCp) for the P454:CaM complex formation was obtained from the slope of ΔH values versus temperature. ITC experiments were performed at 10, 20, 25, 30 and 38°C.

Synchrotron Radiation Circular Dichroism

Synchrotron radiation circular dichroism (SRCD) was performed on the DISCO beamline of the synchrotron SOLEIL (Saint-Aubin, France). Spectra were recorded at 25°C with an integration time of 1.2 s and a bandwidth of 1 nm with a resolution of 1 nm. A far-UV spectrum represents the average of four individual scans. QS cells (Hellma, France) with a pathlength of 20, 50, 100 or 200 µm (depending on final protein concentrations) were used to record spectra in the far-UV range (from 190 to 250 nm). CD spectra of peptides and proteins were measured in buffers A and B, 20% of trifluoroethanol (TFE), in the presence of SUVs (POPC POPG 8:2) or CaM. Secondary structure content was estimated using Bestsel (13,14).

Membrane permeabilization

To monitor membrane permeabilization induced by peptides, ANTS (fluorophore probe) and DPX (quencher) were encapsulated into large unilamellar vesicles (LUVs). The LUVs were prepared at a concentration of 10 mM lipid at a POPC POPG molar ratio of 8:2 containing 20 mM ANTS and 60 mM DPX. The multilamellar vesicle suspension was extruded through 0.4- and 0.2 µm polycarbonate filters to produce LUVs. The unencapsulated ANTS and DPX were removed by gel filtration with a 5 mL Sephadex G-25 column (GE Healthcare Life Sciences). For permeabilization assays, LUVs were incubated in buffer A at 0.45 mM lipid concentration at 25°C in a 101-QS cuvette (Hellma, France) and under constant stirring. The excitation wavelength was set at 390 nm and the emission of ANTS was continuously measured at 515 nm. Maximum intensity of permeabilization, corresponding to the maximum recovery of ANTS fluorescence, was measured after addition of 0.1% of Triton X100. The concentration of membrane-bound peptides required to induce half of the ANTS florescence recovery ($C_{P1/2}$) was extracted from the permeabilization intensity as a function of peptide concentration (1).

Membrane permeabilization with CaM and EDTA

LUVs were incubated in buffer B at a lipid concentration of 0.45 mM. P454 was added at a concentration inducing vesicle permeabilization. After a few seconds of permeabilization, holo-CaM was added in solution at a peptide:CaM molar ratio of 1:3. Then EDTA was added in excess to chelate calcium and convert holo-CaM to apo-CaM.

Hemolysis

Hemolytic activity of CyaA recombinant proteins was performed on sheep erythrocytes, as previously described (5). Briefly, erythrocytes were washed several times in buffer B and resuspended in this buffer at 5 x 10^8 cells/mL. Hemolytic activity of the CyaA proteins was measured after 20 min and overnight incubation at 37°C by measuring the hemoglobin release at 405 nm. Complete lysis was obtained after addition of 0.1% Trtion X-100.

Cell intoxication assays

The CyaA proteins were diluted from the urea stock solutions to a final concentration of 5.6 nM (1 μg/mL) into sheep erythrocytes (5 x 10^8 cells/mL) in buffer B or in buffer A complemented with 2 mM EDTA, and incubated at 30°C for 20 min. An aliquot was taken to measure the total activity. The cell suspensions were chilled on ice and centrifuged at 4°C. The pelleted cells were resuspended in buffer A and separated into 2 different batches. One is centrifuged again and pelleted cells were lysed with 0.1% Tween 20. The enzymatic activity measured corresponds to the toxin bound to the cells and was expressed as a percentage of total activity added to the cells. The second batch is digested with 20 μg of TPCK-treated trypsin (MilliporeSigma, Burlington, MA, USA) for 10 min at 30°C. A 5-fold excess of soybean trypsin inhibitor was added and cells were washed with buffer A and lysed with 0.1% Tween 20. The activity protected from trypsin digestion corresponds to the internalized toxin. It was measured and expressed as percentage of total activity. Activities are expressed as percentages of total toxin added to the erythrocytes (taken as 100%) and represent average values from at least 3 independent measurements. One unit of CyaA activity corresponds to 1 μmol of cAMP formed per min at 30°C pH 8.0.

Peptide translocation followed by droplet interface bilayer experiments

An aqueous phase is prepared with buffer D or E and the oil phase is prepared with 15 % (v/v) of chloroform and 0,08 % (w/v) of lipids (POPC POPG 9:1 molar ratio) in squalene. A population of droplets is obtained by adding 2 μL of the aqueous phase to 20 μL of the oil phase, and then the mixture is briefly shaken to create the invert emulsion. Two droplet

populations were prepared: one containing the TAMRA-labeled peptide in buffer D, the "source", cis-droplets and the other one containing buffer D or E, or in the presence or in the absence of calmodulin, the "capture", trans-droplets. The two droplet populations were deposed successively on a glass slide (covered with a thin layer of polydimethylsiloxane, PDMS), which allows their mixing and the random formation of pairs of droplets. A lipid bilayer is thus formed at the interface between the two adhering droplets. We then track the possible translocation of the TAMRA-labeled peptides through this bilayer. The fluorescence signals of the "source" and the "capture" droplets were monitored by epi-fluorescence microscopy for 15 minutes with an Olympus microscope and a MicroMax camera (Princeton Instrument). Fluorescent probes were excited by illumination with a mercury lamp with an excitation filter (515-555nm).

Image analysis

Quantification of the translocation process is possible thanks to the analysis of the fluorescence images of the droplet pairs. Even if fluorescence is not directly proportional to peptide concentration due to photo-bleaching and small volume variations, one can hypothesize that the fluorescence intensities of the "source" and the "capture" droplets are proportional to the ratio of their concentrations. Moreover, as the initial concentration in the "source" droplet is known and as the total amount of peptide is conserved during the experience, we can write that: $C_s(t=0)\times V_s = C_s(t)\times V_s + C_c(t)\times V_c$, where C_i is the concentration of the droplet i, V_i its volume, which was determined from microscopy images (i="s" for the source droplet and "c" for the capture droplet). We can thus estimate C_c, the concentration of the "capture" droplet at any time as:

$$C_c = \frac{C_s(t=0)\times V_s}{V_c + \frac{V_s \times F_s}{F_c}}$$

where F_i is the fluorescence intensity measured on droplet i.

For each experiment, background fluorescence was subtracted from the fluorescence of the droplet pair. Furthermore, during experiments we observed that a certain amount of peptide was able to exit the droplets, reaching the oil phase and possibly go back inside another droplet. To take into account this amount of peptide that could go inside the "capture" droplet without crossing the bilayer, we performed all experiments with a control droplet, or "dark" droplet, initially peptide-free and we subtracted its fluorescence from the one of the "capture" droplet of the pair so that the remaining fluorescence increase of the capture droplet was from

translocation through the bilayer only and not contaminated by the oil-mediated peptide diffusion phenomenon.

SAXS

Data acquisition

X-ray scattering data were collected at the SWING beamline of the SOLEIL Synchrotron (Saint-Aubin, France). All measurements were performed using a size-exclusion HPLC column on-line with the SAXS measuring cell, a 1.5 mm diameter quartz capillary contained in an evacuated vessel (15). All experimental details are given in Table S5 in accordance with the guidelines given in (16).

We studied solutions of AC489 alone and in the presence of a 4-fold molar excess of CaM (similar experiments were performed with AC489:CaM 1:1 molar ratio) as well as CaM in the presence of a 2-fold excess of P454. All proteins were analyzed in buffer C. Scattering of the elution buffer before void volume was recorded and used as buffer scattering for subtraction from all protein patterns. For each frame, the protein concentration (about 1-2 mg/mL at the top of elution peak) was estimated from UV absorption at 280 nm using a spectrometer located immediately upstream of the SAXS measuring cell.

Data analysis

SAXS data were normalized to the intensity of the incident beam and background subtracted using the programs FoxTrot (courtesy of SWING beamline) and Primus (https://www.embl-hamburg.de/biosaxs/primus.html) (17). Identical frames under the main elution peak were selected using Cormap (18) and averaged for further analysis. The radius of gyration (R_g) was evaluated using the Guinier approximation (19) and also derived from the distance distribution function P(r) calculated by the program GNOM (20). Two independent molecular masses M estimates were obtained using the using SAXSMoW2 and ScÅtter available at the URLs http://saxs.ifsc.usp.br/ and https://bl1231.als.lbl.gov/scatter/, respectively. Both mass determination donot depend on the value of the protein concentration c, a feature of particular interest in the case of CaM containing samples since CaM does not possess any tryptophan.

Modeling

Ab initio shape determination

The shape or envelope of the complex of CaM with P454 peptide was determined using the *ab initio* program DAMMIF (21). 20 runs yielded as many shapes that were compared using the DAMAVER suite of routines based on the calculation of the Normalized Spatial

Discrepancy (NSD) that is lower than 0.7 if all 20 models are similar. The final envelope is obtained using DAMMIN (22) that uses the envelope of all superimposed DAMMIF models (the union of all models) as initial volume.

Rigid-body modeling

All scattering patterns calculated from atomic coordinates were obtained using CRYSOL (23). AC489 alone was first modeled starting from a model of AC364 obtained in a previous study (3). That in turn was derived from the crystal structure of AC364 in complex with the C-terminal domain of CaM (24) using AllosModFoxs (25) to refine the position of flexible protein regions (see (3) for details). Secondary structure analyses of the 365-489 amino-acid sequence as well as the modeling program Phyre 2 (ref) predict two helical stretches in the 410 – 444 region and in the 458 – 482 region. Analysis of the far-UV CD spectrum of peptide P454-489 suggests the presence of *ca* 20% α-helices while the comparison of CD measurements of AC364 and AC484 suggests that the C-terminal part (365-489) contains, like the rest of the molecule, about 27% α-helices. Using all information we restricted the helices to 417-439 and 471-478 stretches and produced an initial configuration for the flexible linkers using Modeller (26). The resulting model was used as input to the DADIMODO modelling program (27) that uses an all atom description of the molecule and explores conformational space by random modifications of the internal degrees of freedom ϕ and ψ angles within flexible regions. Models fitting experimental data are selected using a genetic algorithm that includes after each modification an energy minimization step so as to yield energetically plausible models. A similar approach was used for AC:CaM complexes.

Ensemble of conformations

Finally, AC489 was modeled in terms of an ensemble of conformations using the program EOM 2.0 (28). The program first creates a large pool of 10,000 conformations by varying the conformation of the stretch 200-234 of AC a well as 359-416, 440-470 and 479-489. Subsequently the program determines ensembles of conformations from the pool, the average scattering pattern of which fits our experimental data. Beyond fitting ensembles, the program yields distributions of R_g and of D_{max} of both the pool and the fitting ensembles, the comparison of which informs about the global extension of the models and their likely degree of flexibility expressed in the R_{flex} parameter (28).

Crystallography

Crystallization and diffraction data collection

Crystallization screening trials of calmodulin in complex with different peptides (molar ratio 1:2) were carried out by the sitting drop vapor-diffusion method with a Mosquito automated nanoliter dispensing system (TTP Labtech, Melbourn, UK) at 291K. Sitting drops of 400 nL were set up in Greiner plates for 672 commercially available screening solutions using a 1:1 mixture of protein sample and reservoir well solution (150 nL). The plates were stored in a RockImager (Formulatrix, Bedford, USA) automated imaging system to monitor crystal growth. Manual optimizations of the different obtained hits were performed in Linbro plates with the hanging-drop method by mixing 2 µl of protein with 2 µl of reservoir solution. The best crystals were obtained with the conditions shown in Table S4. For data collection, the crystals were flash-cooled in liquid nitrogen using a condition of crystallization supplemented by 30% (v/v) of glycerol as a cryoprotectant. The X-ray diffraction data were collected on beamline PROXIMA-1 (Synchrotron SOLEIL, St Aubin, France) or on beamline MASIFF (Synchrotron ESRF, Grenoble, France) and processed with autoPROC (Global Phasing Ltd.) (29).

Structure determination and model refinement

The crystal structures of the calmodulin in complex with the synthetic peptides P458 were solved by the molecular replacement technique using separately, the N-ter and C-ter lobes of calmodulin (from the PDB entry 1CTR) as search models with program Phaser (30). Peptides were manually traced into Fourier difference electron density maps. Final models of the complexes were obtained through interactive cycles of manual model building with Coot (31) and reciprocal space refinement with Buster (32). X-ray data collection and model refinement statistics are summarized in Table S4. Figures showing the crystallographic model were generated and rendered with Pymol (Schrodinger, LLC) and/or Chimera (33).

HDX-MS analysis

A summary of the Hydrogen/Deuterium eXchange – Mass Spectrometry (HDX-MS) experiments is provided in Table S10.

Biological samples

Two experimental conditions were analyzed; A: to monitor the effects of CaM binding on AC489, the uptake behavior of AC489 was both measured alone, and in the presence of a four-fold molar excess of CaM (similar experiments were performed for AC489:CaM 1:1 molar ratio); B: to determine the effect of P454 binding on CaM, the labeling was performed

on CaM alone, and in the presence of a two-fold molar excess P454. All protein solutions contained 20 mM HEPES, 150 mM NaCl, pH 7.4, supplemented with 2 mM $CaCl_2$ (unlabeled buffer). The quality of each protein and peptide was assessed prior to labeling by intact mass measurement.

Sample preparation for HDX-MS

The P454:CaM complex was formed by mixing 10 µL of P454 (20 µM) in buffer B with 10 µL of CaM solution (10 µM) in buffer B. The labeling control (*i.e.,* CaM alone) was prepared by mixing 10 µL of CaM solution (10 µM) with 10 µL of unlabeled buffer B. Prior to addition of the deuterated buffer (99.98% D_2O in 20 mM HEPES, 150 mM NaCl, 2 mM $CaCl_2$, pD 7.4), all solutions were equilibrated for 1 h at room temperature. Continuous labeling was initiated at 20˚C by adding 80 µL of deuterated buffer (80% final excess deuterium). Considering a K_D of 90 nM, 92.3% of CaM remains bound to P454 during labeling. The exchange reaction was quenched after 0.16, 1, 10, 30, 60 and 120 min by mixing 14 µL of the labeling reaction (*i.e.,* 14 pmoles CaM) with 56 µL of quench buffer (0.6% formic acid; final D_20/H_20 ratio = 1/4) maintained at 4 ˚C to achieve a final pH of 2.5. Quenched samples were immediately snap-frozen in liquid nitrogen and stored at -80 ˚C.

The AC489:CaM complex was formed at room temperature by mixing 131.5 µL of AC489 (48 µM in buffer B) with 38.5 µL of CaM (656 µM in buffer B). After 10 min incubation time, a 2 µL aliquote was removed and diluted with 26 µL of unlabeled buffer to adjust the complex concentration to 2.6 µM. The labeling control (*i.e.,* AC489 alone) was prepared by mixing 2.5 µL of AC489 (48 µM in buffer B) with 42.5 µL of unlabeled buffer B. After 1 h equilibration at room temperature, continuous labeling was initiated at 20˚C as described above with the following modification: the quench was performed after 0.16, 1, 10, 30 and 120 min by mixing 20 µL of labeling reaction (*i.e.,* 10.4 pmoles AC489) with 40 µL of ice-cold quench buffer (2.5% formic acid, 4 M urea; final D_20/H_20 ratio = 1/2). Considering a AC489:CaM K_D at 1 nM, no dissociation of the complex should occurs during labeling. Undeuterated CaM and AC489 controls were treated using an identical procedure to generate the peptide maps. A fully-deuterated AC489 control was prepared in 8 M urea using the following buffer: 20 mM HEPES, 150 mM NaCl, 2 mM $CaCl_2$, 8M d4-urea, pD 7.4. The exchange reaction was quenched after 24 h incubation at room temperature by mixing 20 µL of fully deuterated sample with 40 µL of ice-cold quench buffer (2.5% formic acid). Triplicate labelling experiments were performed for each time point and condition for all HDX-MS analyses (independent technical replicates).

Data acquisition

HDX-MS analyses were performed with the aid of an HDX manager (Waters Corporation) maintained at 0 ºC. Prior to mass analysis, samples were rapidly thawed and 50 µL were digested for 2 min at 20 ºC using an in-house prepared column (2.0 X 20 mm, 66 µL bead volume) of immobilized pepsin beads (Thermo Scientific). Peptides were trapped, concentrated and desalted using a VanGuard™ CSH C18 pre-column (1.7 µm, 2.1 x 5 mm; Waters), and separated using an ACQUITY UPLC™ CSH C18 column (1.7 µm, 1 x 100 mm). Labeled peptides were eluted with a 8 min gradient of 5-30% acetonitrile at 40 µL/min and 0°C. After each run, the pepsin column was manually cleaned with two consecutive washes of 1.5% formic acid, 5% acetonitrile, 1.5 M guanidinium chloride, pH 1.6. Blank injections were performed after each sample to confirm the absence of carry-over.

The LC flow was directed to a Synapt™ G2-Si HDMS™ mass spectrometer (Waters Corporation) equipped with a standard electrospray ionization source (ESI). Mass accuracy was ensured by continuously infusing a Glu-1-Fibrinogen solution (100 fmol/µL in 50% acetonitrile, 0.1% formic acid) through the reference probe of the ESI source at a flow rate of 2.5 µL/min. Mass spectra were acquired in positive-ion and resolution mode over the 50–1950 *m/z* range. Peptides were identified in undeuterated samples using a combination of data-independent acquisition scheme (MS^E; trap collision energy ramp: 15.0 to 45.0) and exact mass measurement (<5.0 ppm mass error) using the same chromatographic settings than for the deuterated samples.

Data processing

Peptide maps were generated by database searching in ProteinLynx Global Server 3.0 (Waters corporation) using the following processing and workflow parameters: low and elevated intensity thresholds set to 100.0 and 50.0 counts; intensity threshold sets to 750.0 counts; automatic peptide and fragment tolerance; non-specific primary digest reagent; false discovery rate sets to 4%. Each fragmentation spectrum was manually inspected for assignment confirmation. Peptide map were refined in DynamX 3.0 (Waters corporation, Milford, MA) using the following Import PLGS results filter: minimum products per amino acid value = 0.4. DynamX 3.0 HDX software (Waters) was used to extract the centroid masses of all peptides selected for local HDX-analyses; only one charge state was considered per peptide. No adjustment was made for back-exchange and the results are reported as relative deuterium exchange levels expressed in either mass unit or fractional exchange. Fractional exchange data was calculated by dividing the experimentally measured uptake by the theoretically maximum number of exchangeable backbone amide hydrogens that could be

replaced into each peptide (taking into account the final excess of deuterium present in the labeling mixture). MEMHDX was used to visualize and statistically validate HDX results (Wald test, false discovery rate sets to 5%) (34).

The presence of bimodal *m/z* envelopes was determined by visually inspecting the shape of the isotopic distribution for all peptides. HX-Express2 software was used to extract the uptake value of bimodal *m/z* envelopes using a Double-Gaussian fitting and to plot the peak width of the isotopic envelop (distribution width sets at 15% of the base peak chromatogram) as a function of labeling time.

Bibliography

1. Voegele, A., Subrini, O., Sapay, N., Ladant, D., and Chenal, A. (2017) Membrane-Active Properties of an Amphitropic Peptide from the CyaA Toxin Translocation Region. *Toxins (Basel)* **9**
2. Karst, J. C., Barker, R., Devi, U., Swann, M. J., Davi, M., Roser, S. J., Ladant, D., and Chenal, A. (2012) Identification of a region that assists membrane insertion and translocation of the catalytic domain of Bordetella pertussis CyaA toxin. *J Biol Chem* **287**, 9200-9212
3. O'Brien, D. P., Durand, D., Voegele, A., Hourdel, V., Davi, M., Chamot-Rooke, J., Vachette, P., Brier, S., Ladant, D., and Chenal, A. (2017) Calmodulin fishing with a structurally disordered bait triggers CyaA catalysis. *PLoS Biol* **15**, e2004486
4. Karst, J. C., Sotomayor Perez, A. C., Guijarro, J. I., Raynal, B., Chenal, A., and Ladant, D. (2010) Calmodulin-induced conformational and hydrodynamic changes in the catalytic domain of Bordetella pertussis adenylate cyclase toxin. *Biochemistry* **49**, 318-328
5. Karst, J. C., Ntsogo Enguene, V. Y., Cannella, S. E., Subrini, O., Hessel, A., Debard, S., Ladant, D., and Chenal, A. (2014) Calcium, Acylation, and Molecular Confinement Favor Folding of Bordetella pertussis Adenylate Cyclase CyaA Toxin into a Monomeric and Cytotoxic Form. *J Biol Chem* **289**, 30702-30716
6. Cannella, S. E., Ntsogo Enguene, V. Y., Davi, M., Malosse, C., Sotomayor Perez, A. C., Chamot-Rooke, J., Vachette, P., Durand, D., Ladant, D., and Chenal, A. (2017) Stability, structural and functional properties of a monomeric, calcium-loaded adenylate cyclase toxin, CyaA, from Bordetella pertussis. *Sci Rep* **7**, 42065
7. Sotomayor-Perez, A. C., Karst, J. C., Ladant, D., and Chenal, A. (2012) Mean net charge of intrinsically disordered proteins: experimental determination of protein valence by electrophoretic mobility measurements. *Methods in molecular biology* **896**, 331-349
8. Sotomayor Perez, A. C., Karst, J. C., Davi, M., Guijarro, J. I., Ladant, D., and Chenal, A. (2010) Characterization of the regions involved in the calcium-induced folding of the intrinsically disordered RTX motifs from the bordetella pertussis adenylate cyclase toxin. *Journal of molecular biology* **397**, 534-549
9. White, S. H., and Wimley, W. C. (1999) Membrane protein folding and stability: physical principles. *Annual review of biophysics and biomolecular structure* **28**, 319-365
10. Subrini, O., Sotomayor-Perez, A. C., Hessel, A., Spiaczka-Karst, J., Selwa, E., Sapay, N., Veneziano, R., Pansieri, J., Chopineau, J., Ladant, D., and Chenal, A. (2013) Characterization of a membrane-active peptide from the Bordetella pertussis CyaA toxin. *J Biol Chem* **288**, 32585-32598
11. Schuck, P. (2000) Size-distribution analysis of macromolecules by sedimentation velocity ultracentrifugation and lamm equation modeling. *Biophys J* **78**, 1606-1619
12. Schuck, P. (2003) On the analysis of protein self-association by sedimentation velocity analytical ultracentrifugation. *Anal Biochem* **320**, 104-124
13. Micsonai, A., Wien, F., Kernya, L., Lee, Y. H., Goto, Y., Refregiers, M., and Kardos, J. (2015) Accurate secondary structure prediction and fold recognition for circular dichroism spectroscopy. *Proc Natl Acad Sci U S A* **112**, E3095-3103

14. Micsonai, A., Wien, F., Bulyaki, E., Kun, J., Moussong, E., Lee, Y. H., Goto, Y., Refregiers, M., and Kardos, J. (2018) BeStSel: a web server for accurate protein secondary structure prediction and fold recognition from the circular dichroism spectra. *Nucleic Acids Res* **46**, W315-W322
15. David, G., and Pérez, J. (2009) Combined sampler robot and high-performance liquid chromatography: a fully automated system for biological small-angle X-ray scattering experiments at the Synchrotron SOLEIL SWING beamline. *J. Appl. Cryst.* **42**, 892-900.
16. Trewhella, J., Duff, A. P., Durand, D., Gabel, F., Guss, J. M., Hendrickson, W. A., Hura, G. L., Jacques, D. A., Kirby, N. M., Kwan, A. H., Perez, J., Pollack, L., Ryan, T. M., Sali, A., Schneidman-Duhovny, D., Schwede, T., Svergun, D. I., Sugiyama, M., Tainer, J. A., Vachette, P., Westbrook, J., and Whitten, A. E. (2017) 2017 publication guidelines for structural modelling of small-angle scattering data from biomolecules in solution: an update. *Acta Crystallogr D Struct Biol* **73**, 710-728
17. Franke, D., Petoukhov, M. V., Konarev, P. V., Panjkovich, A., Tuukkanen, A., Mertens, H. D. T., Kikhney, A. G., Hajizadeh, N. R., Franklin, J. M., Jeffries, C. M., and Svergun, D. I. (2017) ATSAS 2.8: a comprehensive data analysis suite for small-angle scattering from macromolecular solutions. *J Appl Crystallogr* **50**, 1212-1225
18. Franke, D., Jeffries, C. M., and Svergun, D. I. (2015) Correlation Map, a goodness-of-fit test for one-dimensional X-ray scattering spectra. *Nature methods* **12**, 419-422
19. Guinier, A. (1939) La diffraction des rayons X aux très petits angles; application à l'étude de phénomènes ultramicroscopiques. *Ann Phys (Paris)* **12**, 161–237
20. Svergun, D. I. (1992) Determination of the Regularization Parameter in Indirect - Transform Methods Using Perceptual Criteria. *J. Appl. Cryst.* **25**, 495-503
21. Franke, D., and Svergun, D. I. (2009) DAMMIF, a program for rapid ab-initio shape determination in small-angle scattering. *J Appl Crystallogr* **42**, 342-346
22. Svergun, D. I. (1999) Restoring low resolution structure of biological macromolecules from solution scattering using simulated annealing. *Biophysical Journal* **76**, 2879-2886
23. Svergun, D. I., Barberato, C., and Koch, M. H. J. (1995) CRYSOL - a program to evaluate X-ray solution scattering of biological macromolecules from atomic coordinates. *J. Appl. Crystallogr.* **28**, 768-773
24. Guo, Q., Shen, Y., Lee, Y. S., Gibbs, C. S., Mrksich, M., and Tang, W. J. (2005) Structural basis for the interaction of Bordetella pertussis adenylyl cyclase toxin with calmodulin. *Embo J* **24**, 3190-3201
25. Guttman, M., Weinkam, P., Sali, A., and Lee, K. K. (2013) All-atom ensemble modeling to analyze small-angle x-ray scattering of glycosylated proteins. *Structure* **21**, 321-331
26. Brookes, E., Demeler, B., Rosano, C., and Rocco, M. (2010) The implementation of SOMO (SOlution MOdeller) in the UltraScan analytical ultracentrifugation data analysis suite: enhanced capabilities allow the reliable hydrodynamic modeling of virtually any kind of biomacromolecule. *Eur Biophys J* **39**, 423-435
27. Evrard, G., Mareuil, F., Bontems, F., Sizun, C., and Perez, J. (2011) DADIMODO: a program for refining the structure of multidomain proteins and complexes against small-angle scattering data and NMR-derived restraints. *J Appl Crystallogr* **44**, 1264-1271

28. Tria, G., Mertens, H. D. T., Kachala, M., and Svergun, D. I. (2015) Advanced ensemble modelling of flexible macromolecules using X-ray solution scattering. *IUCrJ* **2**, 207-217.
29. Vonrhein, C., Flensburg, C., Keller, P., Sharff, A., Smart, O., Paciorek, W., Womack, T., and Bricogne, G. (2011) Data processing and analysis with the autoPROC toolbox. *Acta Crystallogr D Biol Crystallogr* **67**, 293-302
30. Mccoy, A. J., Grosse-Kunstleve, R. W., Adams, P. D., Winn, M. D., Storoni, L. C., and Read, R. J. (2007) Phaser crystallographic software. *J Appl Crystallogr* **40**, 658-674
31. Emsley, P., and Cowtan, K. (2004) Coot: model-building tools for molecular graphics. *Acta Crystallogr D* **60**, 2126-2132
32. Bricogne, G., Blanc, E., Brandl, M., Flensburg, C., and Keller, P. (2011) BUSTER version 2.11.1. *Cambridge, UK: Global Phasing Ltd.*
33. Pettersen, E. F., Goddard, T. D., Huang, C. C., Couch, G. S., Greenblatt, D. M., Meng, E. C., and Ferrin, T. E. (2004) UCSF chimera - A visualization system for exploratory research and analysis. *Journal of Computational Chemistry* **25**, 1605-1612
34. Hourdel, V., Volant, S., O'Brien, D. P., Chenal, A., Chamot-Rooke, J., Dillies, M. A., and Brier, S. (2016) MEMHDX: An interactive tool to expedite the statistical validation and visualization of large HDX-MS datasets. *Bioinformatics (Oxford, England)*

Figures

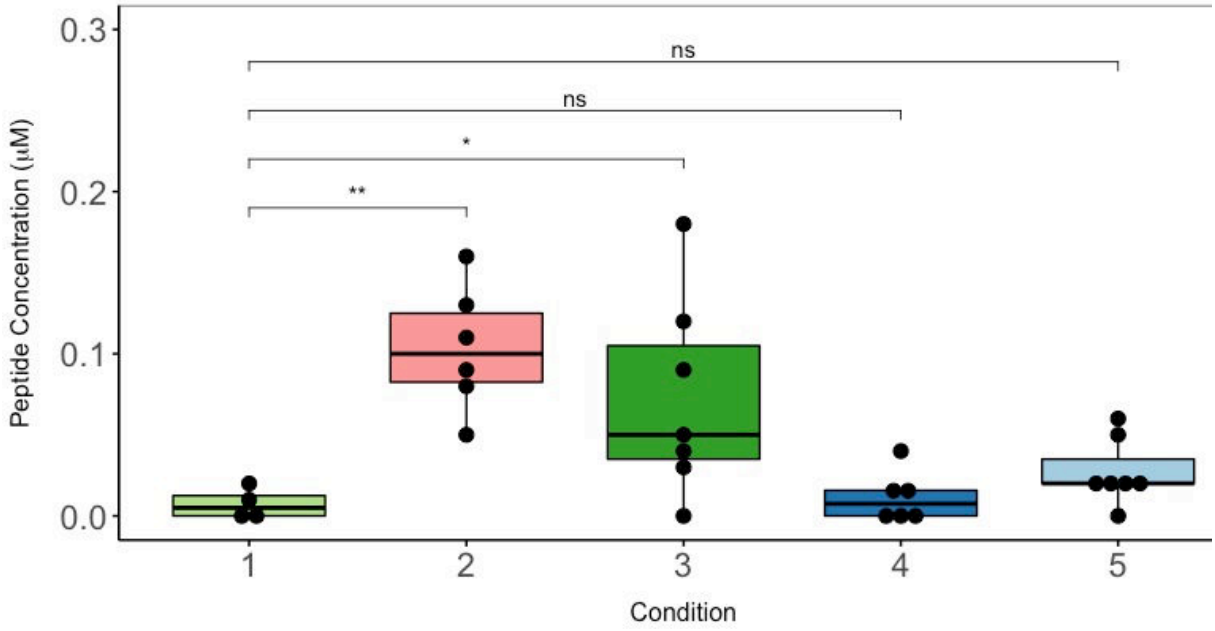

Figure 1. Peptide translocation across droplet interface bilayer. TAMRA-peptide concentration (μM) in the *trans* droplet 15 min (see Material and Methods for details). Peptide concentration was tested in the absence (1) and in the presence of CaM (2-5) in the *trans* droplet; in the absence (3) and in the presence (1,2,4,5) of a calcium gradient across the *cis* and *trans* droplets. Translocation of P454 (1-3), P454 R12E (4) and the H-helix (5) peptides was investigated.

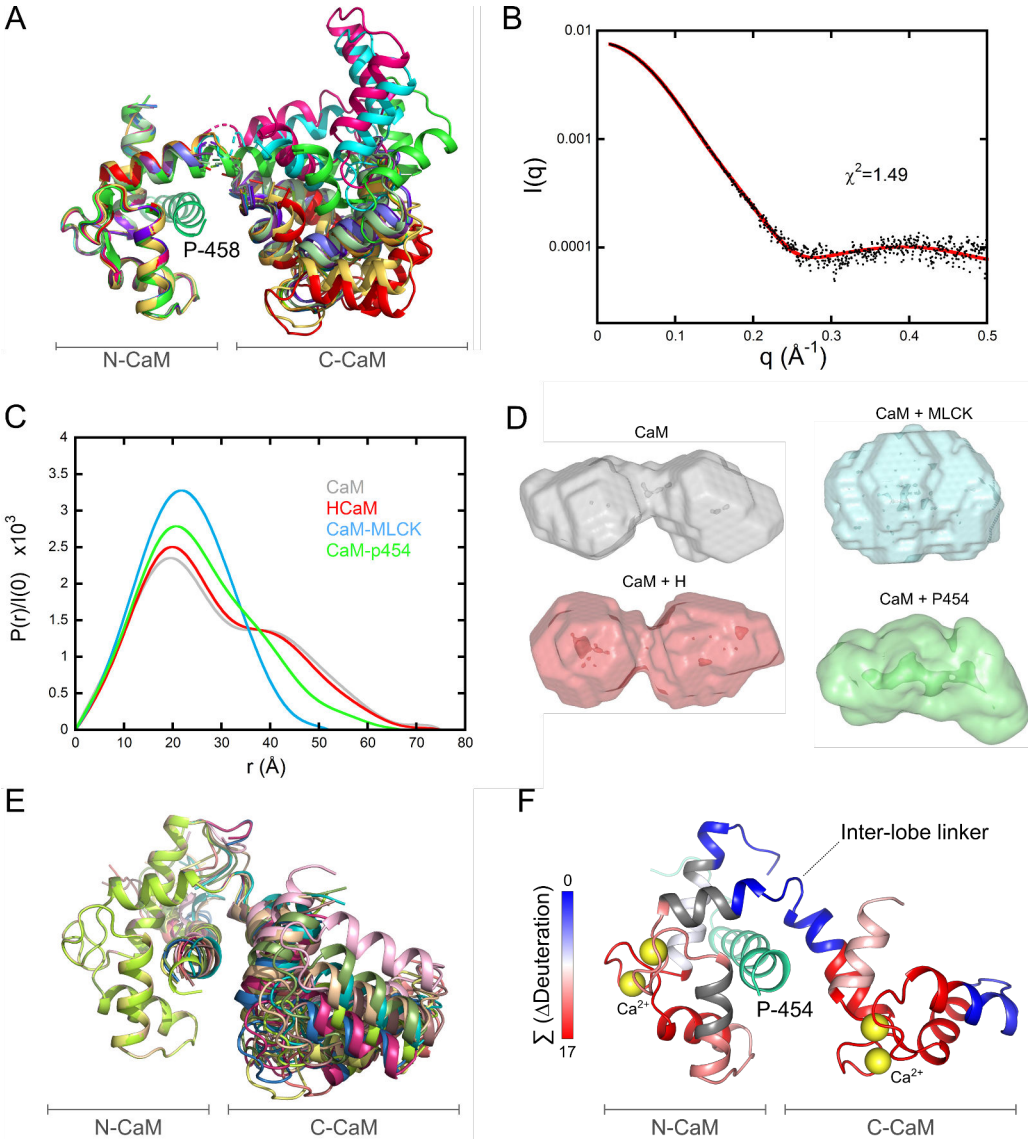

Figure 2. Structure and dynamics of the P454:CaM complex. (**A**) Superimposition of the twelve peptide:CaM crystal structures. The crystal structure 1CLL of the extended conformation of CaM is shown in light green. (**B**) Experimental SAXS curve of the P454:CaM complex (black dots) superimposed over the best fit (red curve) obtained from the structural model shown on Fig 2F. (**C**) Comparison of the four distance distribution functions obtained using the program GNOM for CaM alone (grey), H:CaM (red), MLCK:CaM (cyan) and P454:CaM (green) complexes. (**D**) DAMMIN models of CaM alone, H:CaM, MLCK:CaM and P454:CaM complexes, shown with the same color code. (**E**) Superimposition of ten models fitting the SAXS curve shown on Fig. 2B obtained using the program Dadimodo. (**F**) Effects of P454 on the HDX behavior of CaM. The uptake differences (ΔDeuteration) measured between the free- and P454-bound CaM were extracted for each peptide at each time point, summed, and plotted on the best-fitted structural model of CaM (red curve in 2B). The summed ΔDeuteration values [Σ (ΔDeuteration)] are colored from blue (no variation of deuterium uptake) to red (major reductions of deuterium uptake).

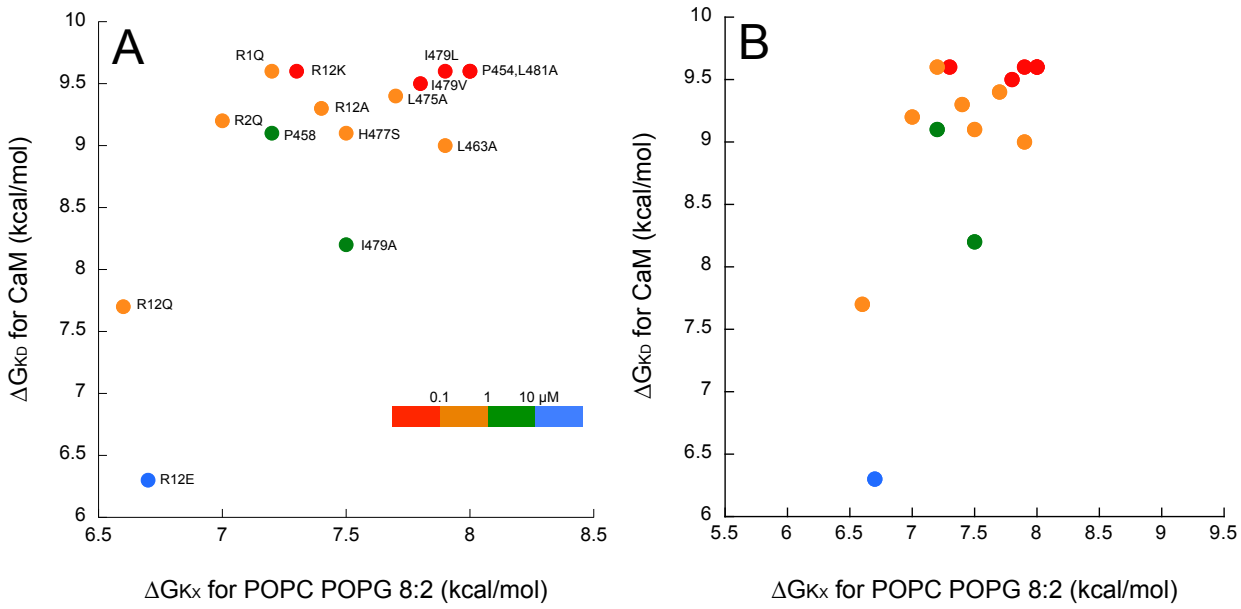

Figure 3. **Representation of the free energy values for peptide:CaM binding and peptide:membrane interaction**. (**A**) The inserted box represents the window of peptide concentration (µM) required to induce half recovery of ANTS fluorescence (see Table S8). Red peptides correspond to the most permeabilizing peptides while green one are the lowest. Free energy values (ΔG_{Kx} and ΔG_{KD} are indicated in Table S7). (**B**) Same data as in A but with the same range on both x- and y-axes. This representation highlights that large free energy changes occur for CaM binding ($\Delta\Delta G \sim 3.5$ kcal/mol) while free energy changes for membrane interaction is less affected ($\Delta\Delta G \sim 1.5$ kcal/mol).

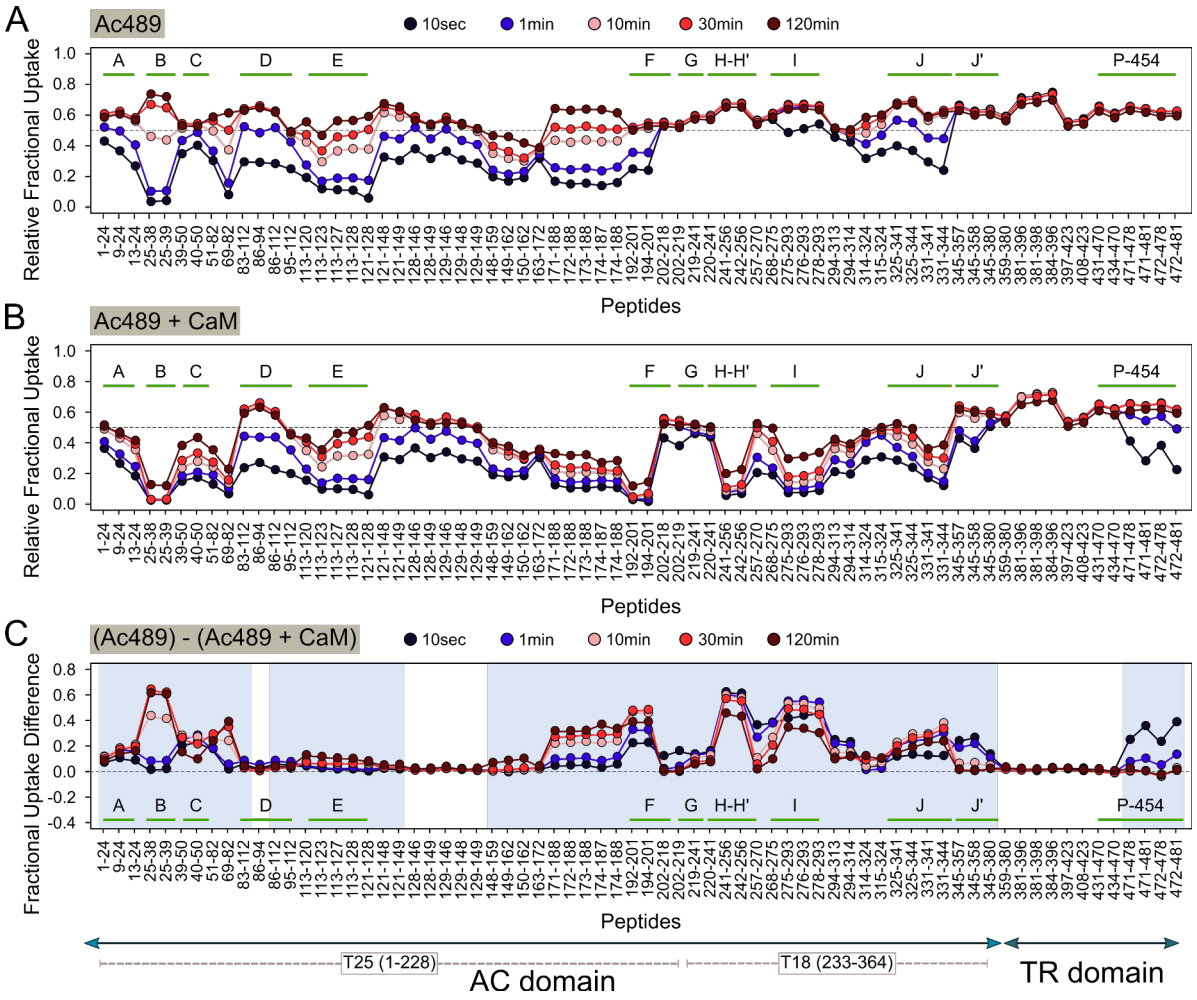

Figure 4. HDX-MS behavior of AC489 in the presence and absence of a 4-fold molar excess of human CaM. Fractional uptake profiles of AC489 alone (**A**) and in the presence of CaM (**B**). The deuterium content calculated for each peptide and condition and at each time point is plotted as a function of peptide position. Each dot corresponds to the average value of three independent replicates. The position of helices A to J' within the AC domain and of the P454 region within the TR domain is indicated. (**C**) Differential fractional uptake plot showing the uptake difference between AC489 alone and in the presence of a 4-fold molar excess CaM for all peptides and labeling time points. CaM binding to AC489 induces major reductions of deuterium uptake within helices B, C and F of the T25 region and within helices H-H', I and J/J' of the T18 region of the AC domain. A slight but significant reduction of incorporation is observed within the P454 region of the TR domain. Regions displaying statistically significant variations of deuterium uptake in the presence of CaM (Wald test, $p < 0.05$) are highlighted in light blue.

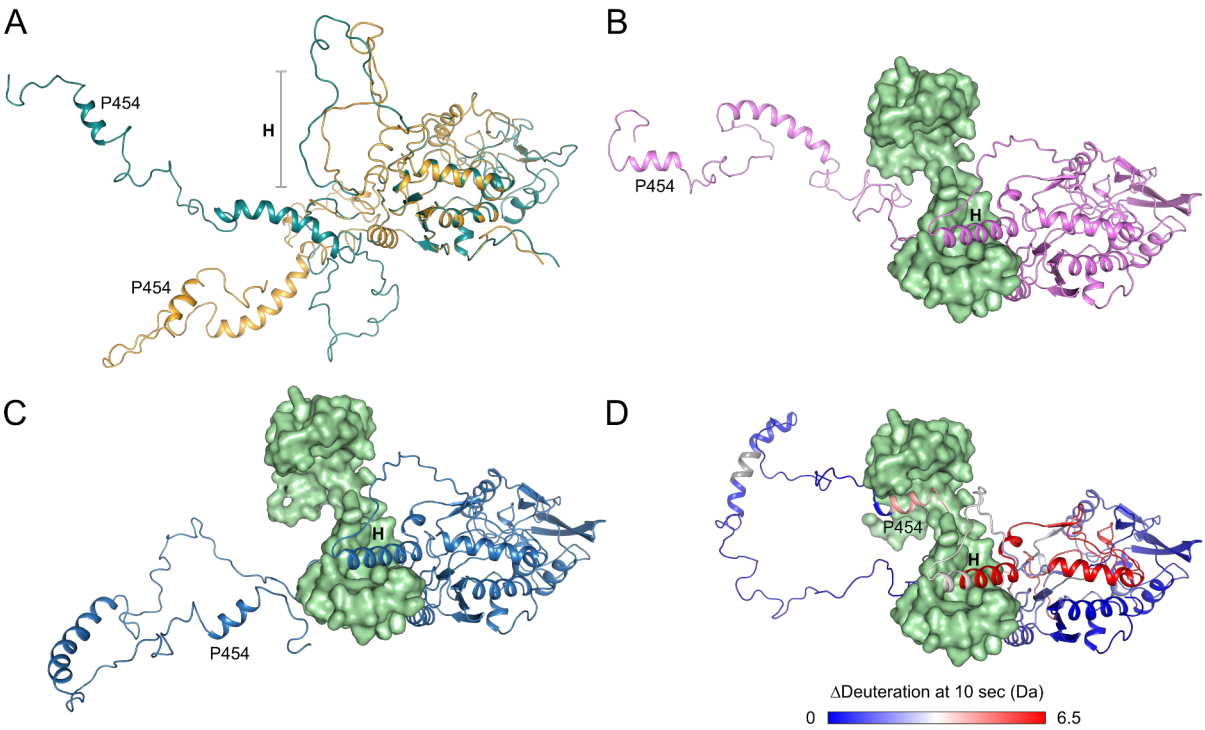

Figure 5. Structural models of AC489 isolated and in complex with calmodulin. Typical structural models of AC489 alone (**A**) and AC489 in complex with CaM (**B**, **C** and **D**) obtained using the program Dadimodo, which refines the flexible regions by fitting the experimental SAXS curve. CaM is shown in green, with the N-terminal lobe (N-CaM, top) and the C-terminal lobe (C-CaM, bottom) interacting with the AC489 H-helix. (**A**) Models of AC489 with its C-terminal helix exposed to the solvent (model 1, blue) or with the 359-470 region forming a loop (model 2, orange). These two models illustrate the structural plasticity of AC489. (**B**), (**C**) and (**D**) C-CaM interacts with the H-helix of AC489. The 359-470 region of AC489 is extended (**B**) or more folded (**C**). In Fig. D, in addition to the C-CaM bound to the H-helix, the N-CaM lobe interacts with the C-terminal helix of AC489. The CaM-induced HDX protection of AC489 is mapped on the structural model of the AC489:CaM complex in 5D. The variations of deuterium incorporation monitored after 10 sec labeling are colored from blue (no change) to red (major changes).

Table 1. Hemolytic and cytotoxic activities of the different recombinant CyaA proteins. Hemolytic activity was measured after overnight incubation at 37°C. The concentration of CyaA required to induce half-hemolysis is indicated. cAMP production was assayed on sheep erythrocytes as described in the Material and Methods section. The proteins were directly diluted (final concentration of 5.6 nM) in sheep erythrocyte solutions in buffer B. Activity of the recombinant proteins was expressed as a function of the total activity of WT CyaA and represents the average value of at least 3 independent measurements.

Proteins	[CyaA] of half hemolysis (nM)	cAMP production in cell (% of WT)
CyaA	10 ± 2	100
$CyaA_{multi}$	3 ± 1	< 10
$CyaA_{R12Q}$	10 ± 2	100
$CyaA_{R12E}$	4 ± 1	< 10
$CyaA_{I479A}$	7 ± 1	100
$CyaA_{W458A-I479A}$	5 ± 1	55 ± 10

Supplementary Figures

A

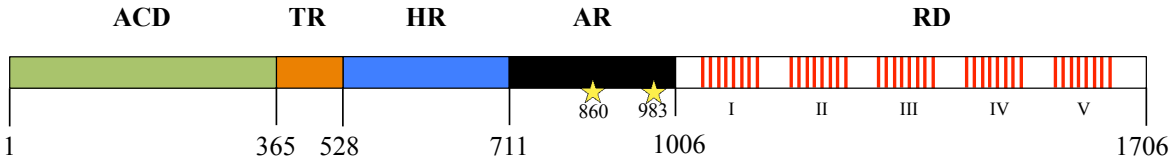

B

MQQSHQAGYANAADRESGIPAAVLDGIKAVAKEKNATLMFRLVNPHSTSLIAEGVATKGLGVHAKSSD
WGLQAGYIPVNPNLSKLFGRAPEVIARADNDVNSSLAHGHTAVDLTLSKERLDYLRQAGLVTGMADGV
VASNHAGYEQFEFRVKETSDGRYAVQYRRKGGDDFEAVKVIGNAAGIPLTADIDMFAIMPHLSNFRDS
ARSSVTSGDSVTDYLARTRRAASEATGGLDRERIDLLWKIARAGARSAVGTEARRQFRYDGDMNIGVI
TDFELEVRNALNRRAHAVGAQDVVQHGTEQNNPFPEADEKIFVVSATGESQMLTRGQLKEYIGQQRGE
GYVFYENRAYGVAGKSLFDDGLGAAPGVPSGRSKFSPDVLETVPASPGLRRPSLGAVERQDSGYDSLD
GVGSRSFSLGEVSDMAAVEAAELEMTRQVLHAGARQDDAEPGVSGASAHWGQRALQGAQAVAAAQRLV
HAIALMTQFGRAGSTNTPQEAASLSAAVFGLGEASSAVAETVSGFFRGSSRWAGGFGVAGGAMALGGG
IAAAVGAGMSLTDDAPAGQKAAAGAEIALQLTGGTVELASSIALALAAARGVTSGLQVAGASAGAAAG
ALAAALSPMEIYGLVQQSHYADQLDKLAQESSAYGYEGDALLAQLYRDKTAAEGAVAGVSAVLSTVGA
AVSIAAAASVVGAPVAVVTSLLTGALNGILRGVQQPIIEKLANDYARKIDELGGPQAYFEKNLQARHE
QLANSDGLRKMLADLQAGWNASSVIGVQTTEISKSALELAAITGNADNLKSVDVFVDRFVQGERVAGQ
PVVLDVAAGGIDIASRKGERPALTFITPLAAPGEEQRRRTKTGKSEFTTFVEIVGKQDRWRIRDGAAD
TTIDLAKVVSQLVDANGVLKHSIKLDVIGGDGDDVVLANASRIHYDGGAGTNTVSYAALGRQDSITVS
ADGERFNVRKQLNNANVYREGVATQTTAYGKRTENVQYRHVELARVGQLVEVDTLEHVQHIIGGAGND
SITGNAHDNFLAGGSGDDRLDGGAGNDTLVGGEGQNTVIGGAGDDVFLQDLGVWSNQLDGGAGVDTVK
YNVHQPSEERLERMGDTGIHADLQKGTVEKWPALNLFSVDHVKNIENLHGSRLNDRIAGDDQDNELWG
HDGNDTIRGRGGDDILRGGLGLDTLYGEDGNDIFLQDDETVSDDIDGGAGLDTVDYSAMIHPGRIVAP
HEYGFGIEADLSREWVRKASALGVDYYDNVRNVENVIGTSMKDVLIGDAQANTLMGQGGDDTVRGGDG
DDLLFGGDGNDMLYGDAGNDTLYGGLGDDTLEGGAGNDWFGQTQAREHDVLRGGDGVDTVDYSQTGAH
AGIAAGRIGLGILADLGAGRVDKLGEAGSSAYDTVSGIENVVGTELADRITGDAQANVLRGAGGADVL
AGGEGDDVLLGGDGDDQLSGDAGRDRLYGEAGDDWFFQDAANAGNLLDGGDGRDTVDFSGPGRGLDAG
AKGVFLSLGKGFASLMDEPETSNVLRNIENAVGSARDDVLIGDAGANVLNGLAGNDVLSGGAGDDVLL
GDEGSDLLSGDAGNDDLFGGQGDDTYLFGVGYGHDTIYESGGGHDTIRINAGADQLWFARQGNDLEIR
ILGTDDALTVHDWYRDADHRVEIIHAANQAVDQAGIEKLVEAMAQYPDPGAAAAAPPAARVPDTLMQS
LAVNWR

Figure S1. (**A**) Schematic representation of the CyaA toxin. The toxin is composed of the following domains: a N-terminal catalytic domain (ACD, residues 1-364), a translocation region (TR, 365-527), a hydrophobic region (HR, 528-710), an acylation region (AR, 711-1005) with acylated K860 and K983 labeled with yellow stars, and a C-terminal receptor-binding domain (RD, 1006-1706) containing the RTX motifs (red bars). (**B**) Sequence of the full-length CyaA from *Bordetella pertussis*. The segment AC364 is in bold, AC489 is colored in gray and the region corresponding to the P454 peptide is underlined.

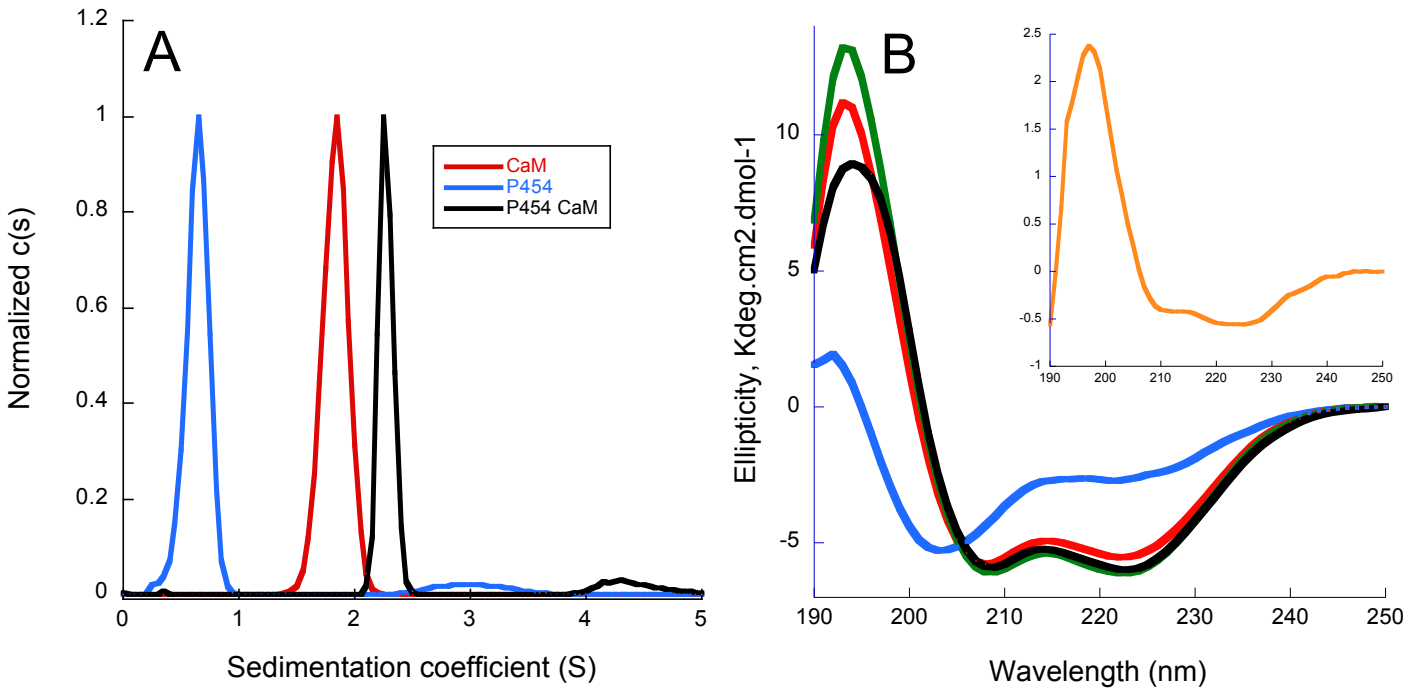

Figure S2. (**A**) Sedimentation coefficient distributions of P454 (blue), CaM (red) and the P454:CaM complex (black). Sedimentation coefficients are listed in Table S1. (**B**) Synchrotron radiation circular dichroism in the far-UV region of P454 and CaM. Spectra were recorded in 100 µm cell. Far-UV spectra of P454 (blue), CaM (green) or P454/CaM at a 1:1 molar ratio (black) in buffer B. The red curve is the sum of the spectra of P454 and CaM. The inset corresponds to the subtraction of the spectrum of the P454:CaM complex by the sum of the two individual spectra of (red spectrum defined above). The subtraction spectrum shows that the P454:CaM complex formation induces an increase of secondary structure content.

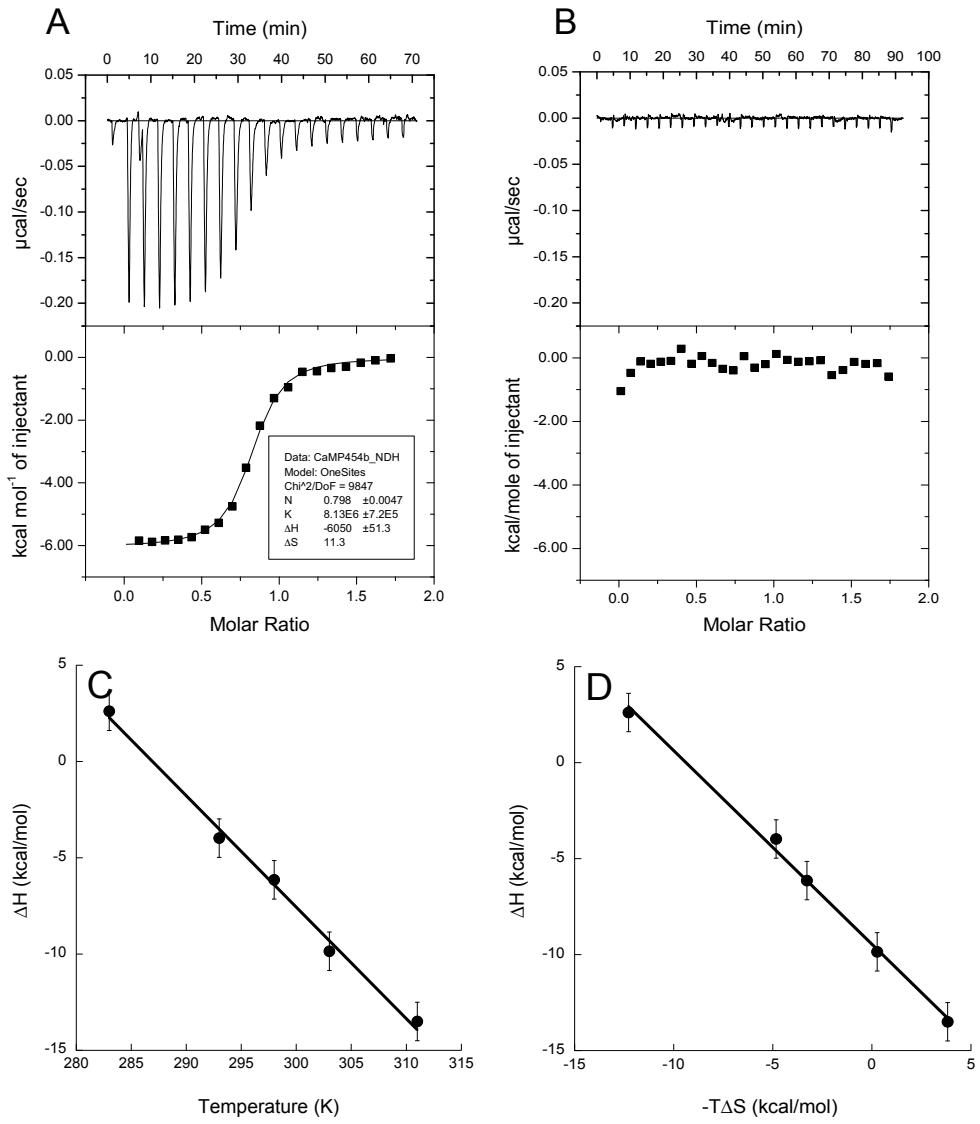

Figure S3. (**A**) Isothermal titration calorimetry of CaM by P454 in buffer B at 25°C. P454 is loaded in the syringe at 90 µM and CaM in the cell at 10 µM. Titration was performed on VP-ITC 500 by injections of 13 µL. (**B**) Isothermal titration calorimetry of CaM by P454 in buffer A complemented with 0.2 mM EDTA at 25°C. P454 is loaded in the syringe at 90 µM and CaM in the cell at 10 µM. Titration was performed on VP-ITC 500 by injections of 10 µL. (**C**) The slope of ΔH=f(T) provides us the heat capacity ΔCp of the P454/CaM complex. The enthalpy and temperature values are listed in Table S2. (**D**) Representation of the enthalpy-entropy compensation (EEC) plot derived from ITC experiments of P454/CaM titrations at different temperatures. Values are listed in Table S2. S.D for ΔH is ± 1 kcal/mol.

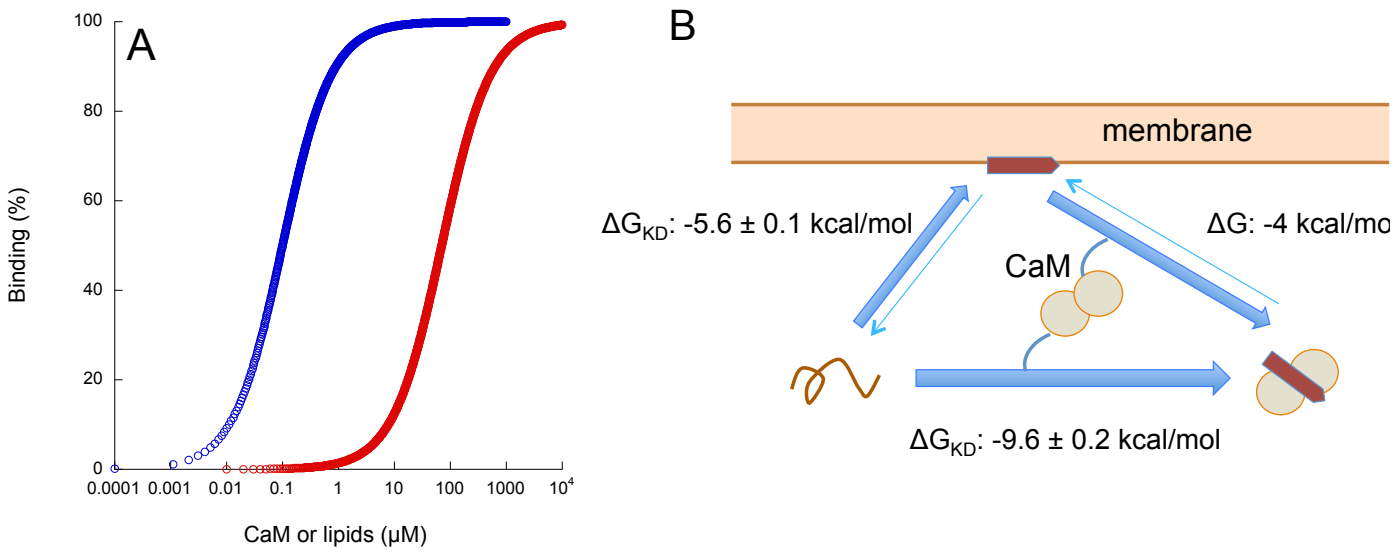

Figure S4. (**A**) Fraction of P454 bound to CaM and membrane, calculated from the affinity constants for CaM (K_D=90 nM, blue trace) and POPC POPG 8:2 (K_D=70 μM, red trace). (**B**) Representation of the free energy of interaction of P454 with membrane and CaM. The peptide P454 is represented in red and CaM by two lobes. Free energy ΔG_{KD} of interaction of P454 with membrane was determined from its K_X, as described in the Material and Methods section.

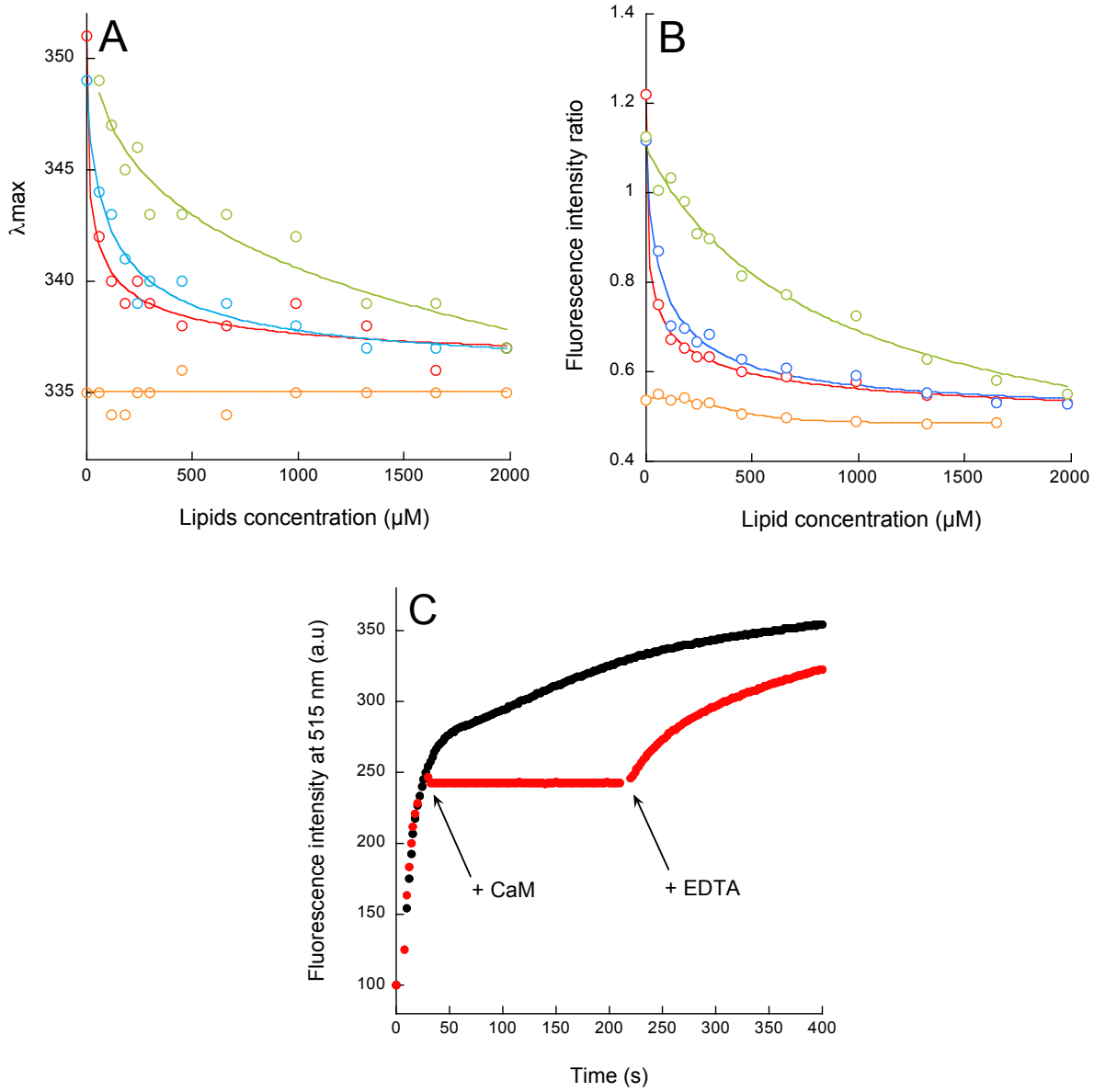

Figure S5. Titration of P454 followed by tryptophan fluorescence. Maximum wavelength of emission (**A**) and ratio of fluorescence intensity (**B**) as a function of lipid concentration. P454 was first titrated in buffer A with SUVs composed of POPC POPG 8:2 (red circles). An excess of apo-CaM is added (blue circles, molar ratio P454:CaM 1:3), followed by 1 mM of calcium (orange circles) and finally 2 mM EDTA (green circles). (**C**) Membrane permeabilization assay. Time course of ANTS and DPX efflux from LUVs made of POPC POPG 8:2 (0.45 mM lipids concentration) in buffer B. Experiment was performed in the presence of P454 at 100 nM (black curve). In red, the same experiment is performed but CaM is added (molar ratio P454:CaM 1:3) at 40 sec, followed by addition of 5 mM EDTA (red curve).

Figure S6. DIB images of translocated and non-translocated P454

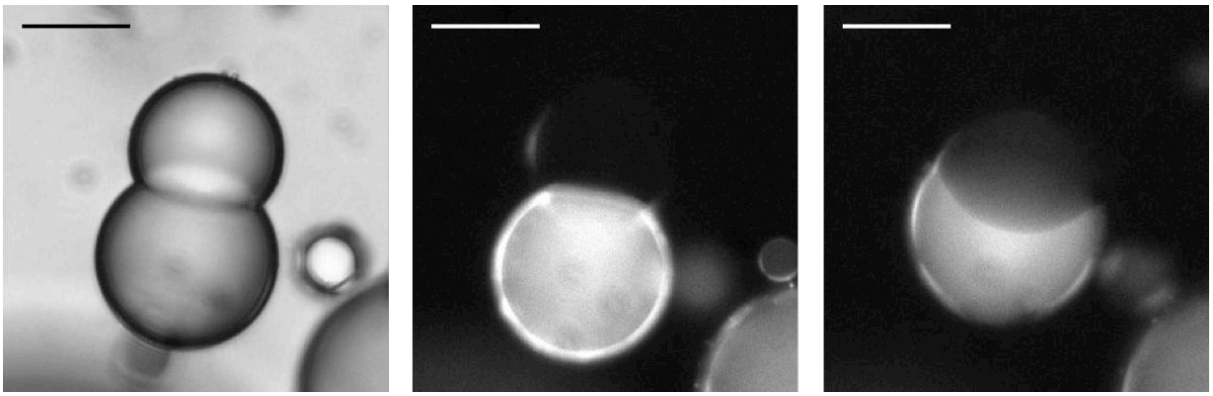

S6A: Images of a DIB made of 10% POPG 90% POPC with P454 (2 μM) in the bottom droplet and CaM (5μM) in the upper droplet. On the left: brightfield microscopy image. In the middle: fluorescence microscopy image at the beginning of the experiment (t=0min). On the right: fluorescence microscopy image after 15 minutes of experiment. Translocation was observed in this experiment. Scale bar represents 30 μm.

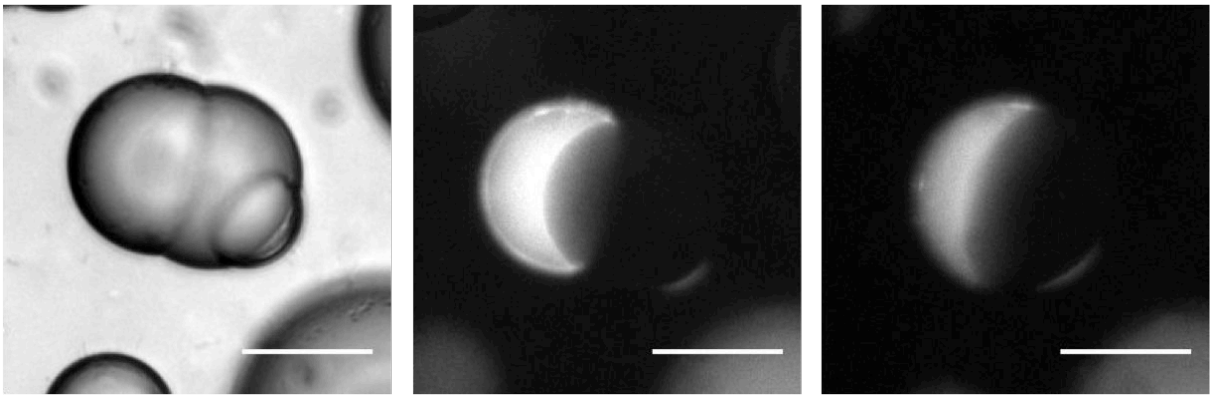

S6B: Pictures of a DIB made of 10% POPG 90% POPC with P454 (2 μM) in the left droplet and without CaM in the right droplet. On the left: brightfield microscopy image. In the middle: fluorescence microscopy image at the beginning of the experiment (t=0min). On the right: fluorescence microscopy image after 15 minutes of experiment. No translocation was observed in this experiment. Scale bar represents 30 μm.

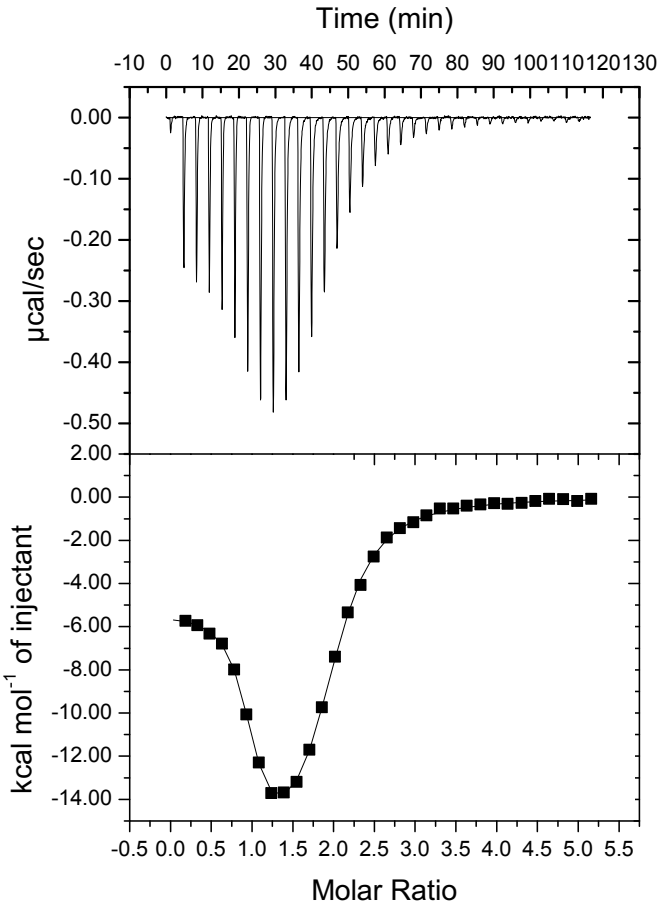

Figure S7. Isothermal titration calorimetry of CaM by the H-helix in buffer B at 25°C. The H-helix is loaded in the syringe at 130 µM and CaM in the cell at 5 µM. Titration was performed on VP-ITC 500 with injections of 8 µL. Thermodynamic parameters are listed in Table S3.

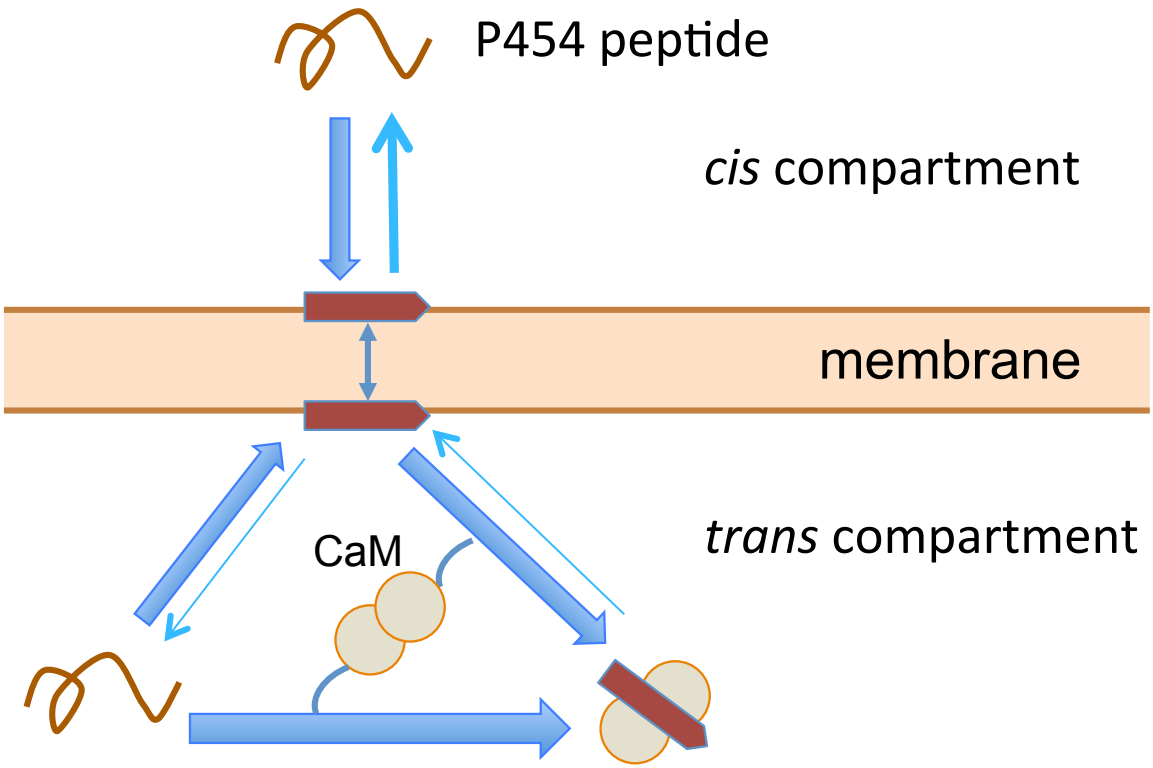

Figure S8. Scheme of the P454 translocation and CaM binding inferred from the *in vitro* experiments based on the ITC, fluorescence, SRCD and DIB experiments described in this study.

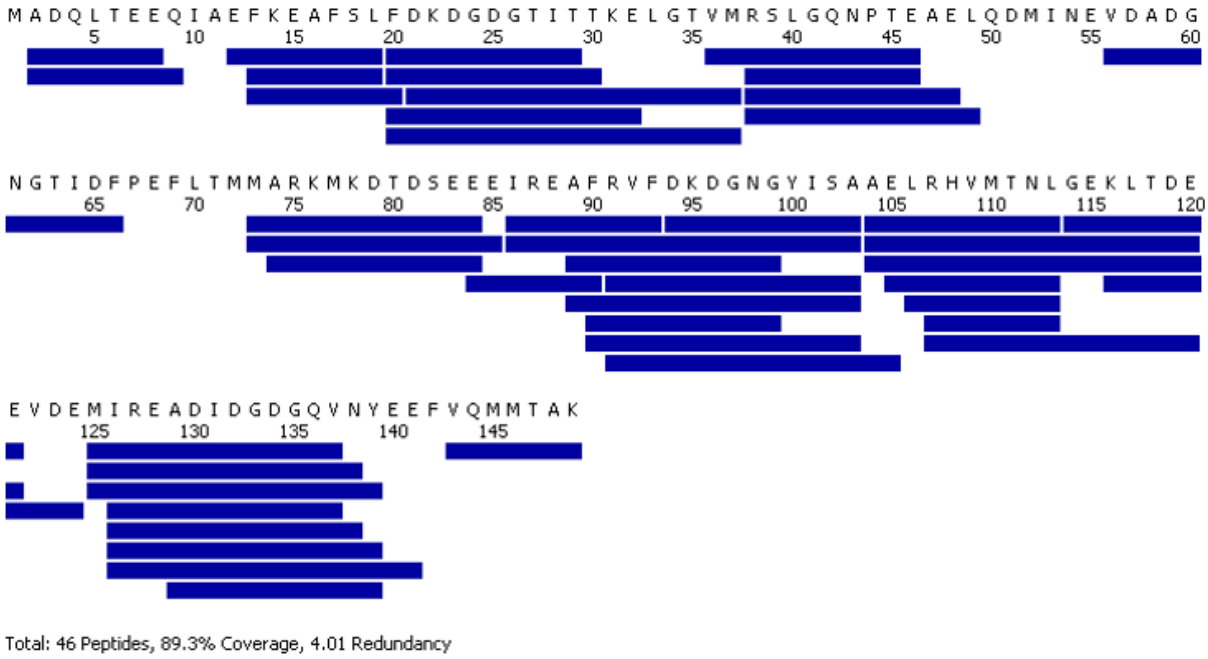

Figure S9. Peptide map used to analyze the deuterium content in full-length human CaM. CaM was digested with immobilized pig pepsin at 20°C and pH 2.5 for 2 min. Each blue bar corresponds to a unique peptide selected for HDX-MS analysis. A final linear sequence coverage 89.3% (4.01 redundancy) was achieved.

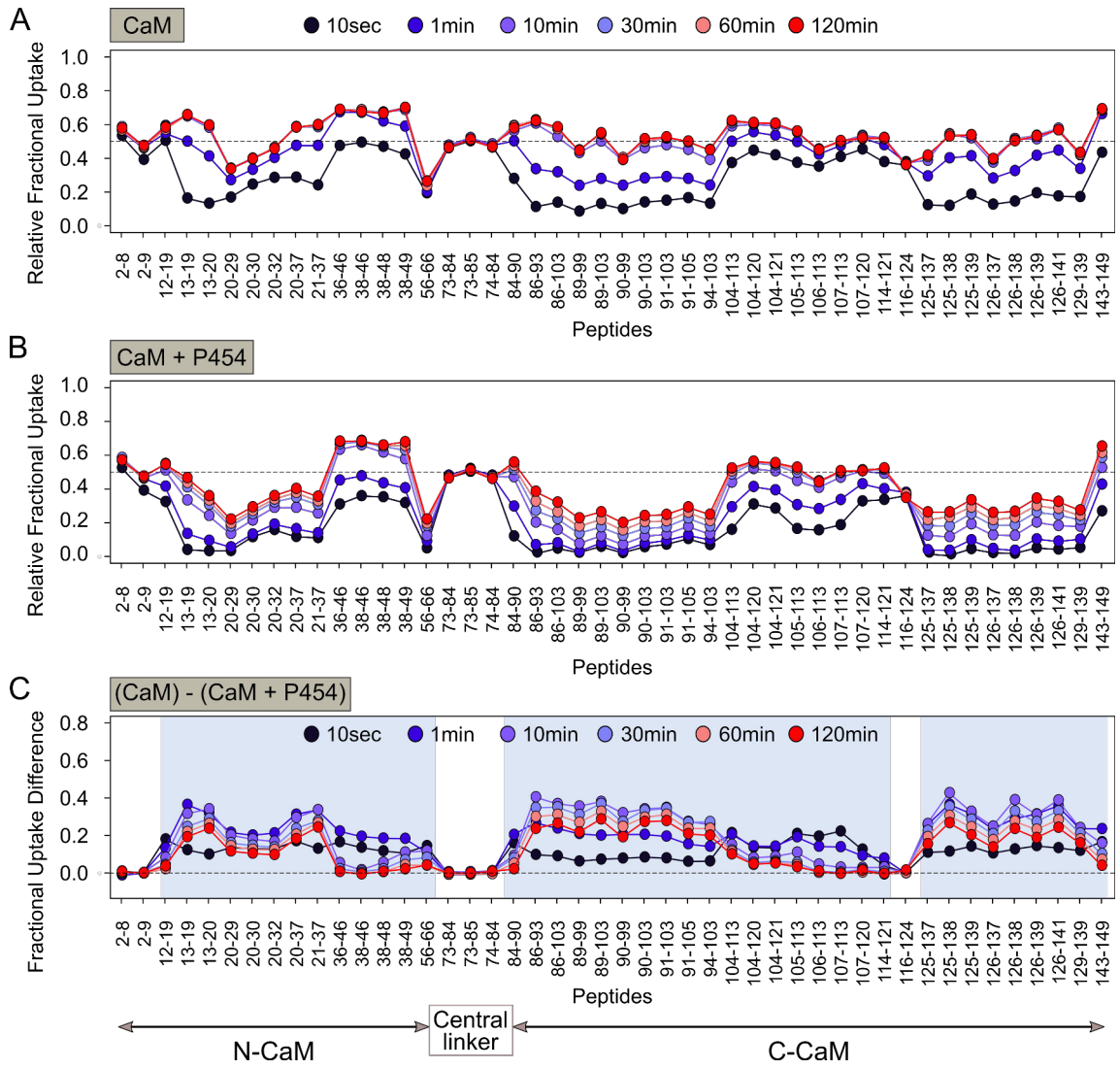

Figure S10. Effect of P454 binding on the HDX-MS behavior of CaM. Fractional uptake profiles of CaM alone (**A**) and in the presence of a 4-fold molar excess P454 (**B**). The deuterium content calculated for each peptide and condition and at each time point is plotted as a function of peptide position. Each dot corresponds to the average value of three independent replicates. (**C**) Differential fractional uptake plot showing the uptake difference between CaM alone and in the presence of a 4-fold molar excess P454 for all peptides and labeling time points. The binding of P454 induces significant reduction of deuterium uptake throughout both N- and C-terminal lobes of CaM. Regions displaying statistically significant variations of deuterium uptake in the presence of P454 (Wald test, $p< 0.05$) are highlighted in light blue.

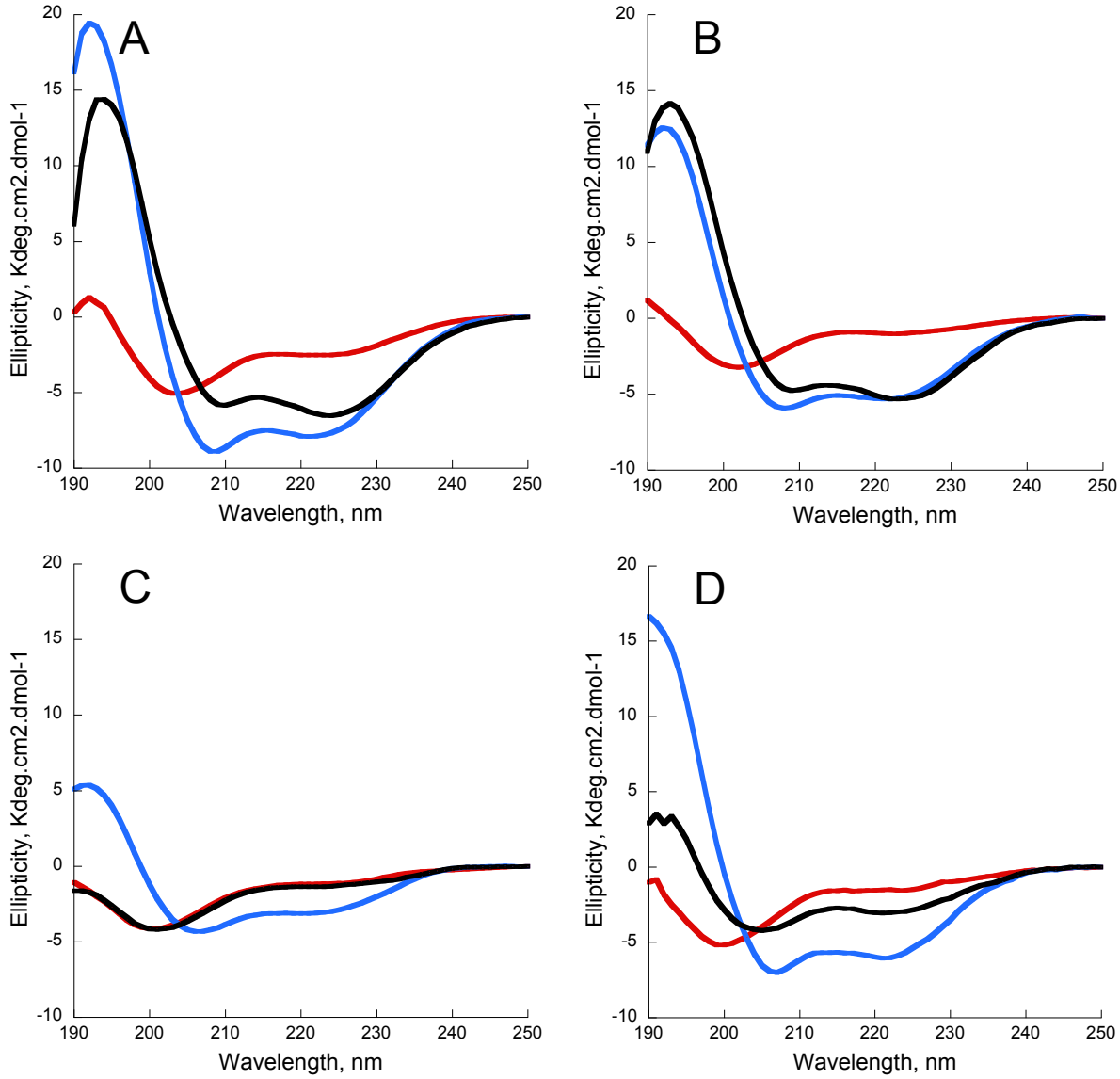

Figure S11. Synchrotron radiation circular dichroism in the far-UV region of P454-derived peptides. The peptides were in buffer A at 25°C (red), in the presence of 20% TFE (blue) or in the presence of SUVs at 2 mM of POPC:POPG 8:2 (black). Far-UV CD spectra of the following peptides are shown: P454 (**A**), P454 L481A (**B**), P454 I479A (**C**) and P454 R12Q (**D**).

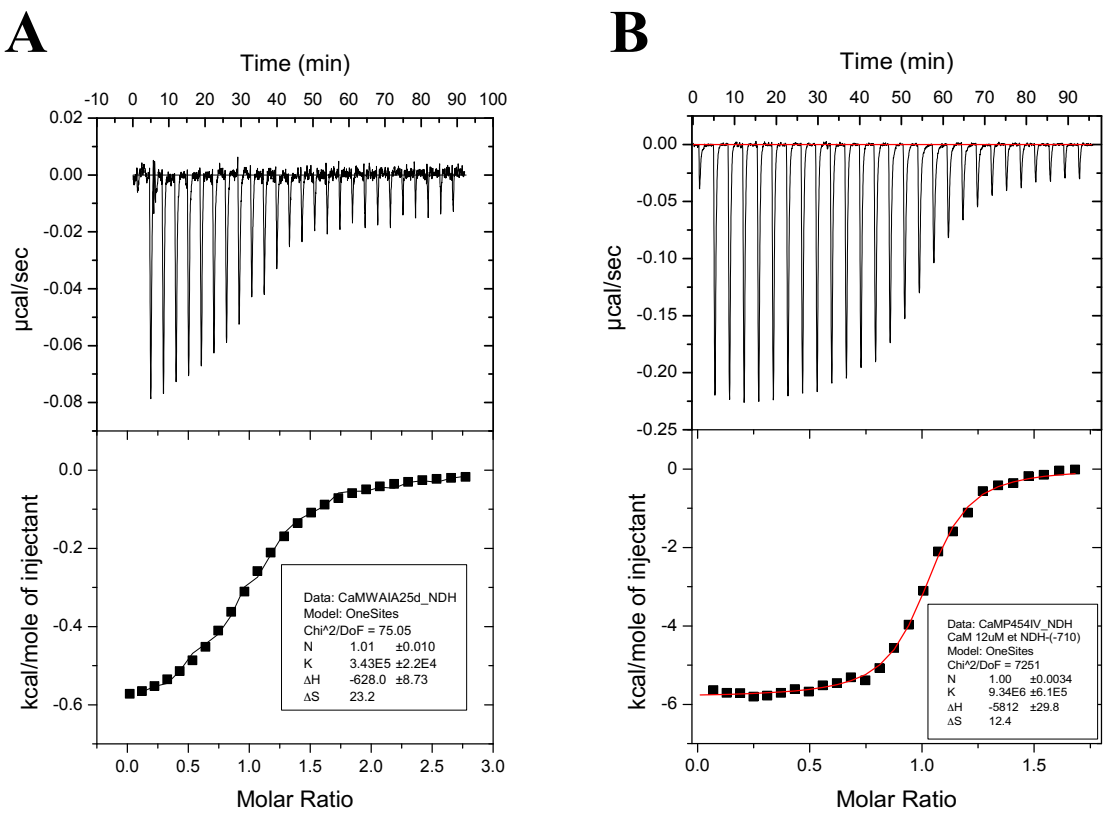

Figure S12. Isothermal titration calorimetry of P454-derived peptides. Illustration of low (**A**, P454 W458A-I479A) and high (**B**, P454 I479V) affinity of P454-derived peptides for CaM.

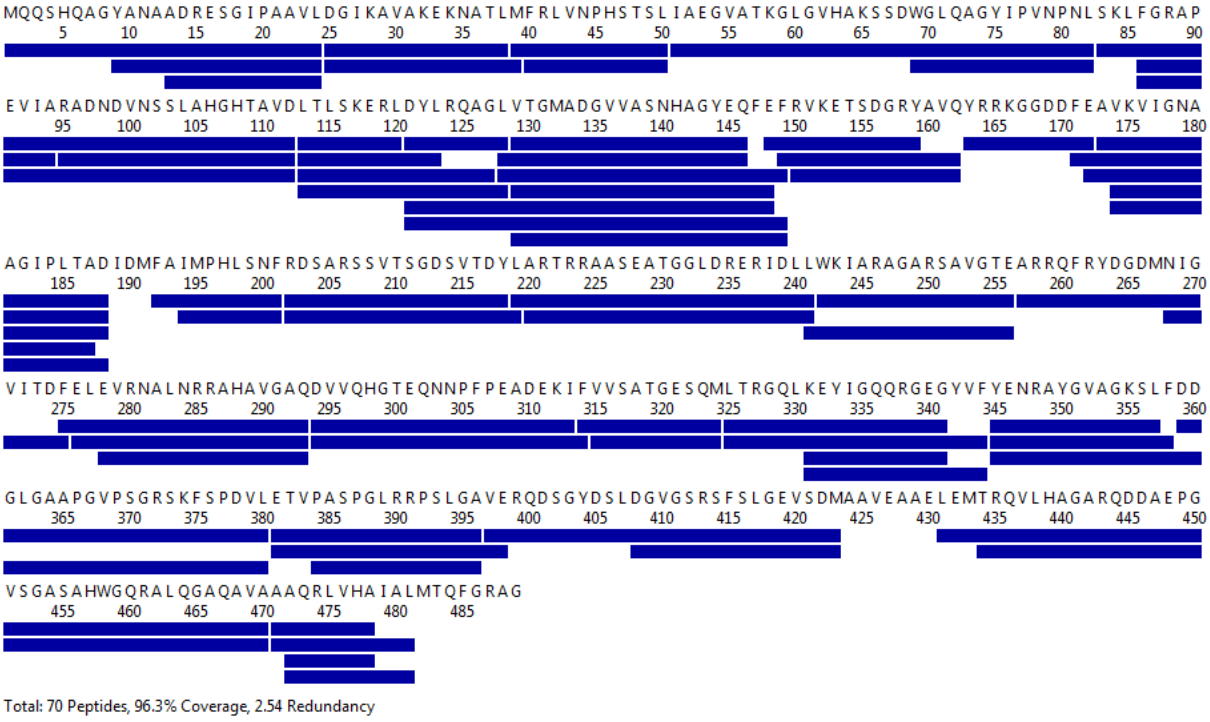

Figure S13. Peptide map used to analyze the deuterium content in AC489. AC489 was digested with immobilized pig pepsin at 20°C and pH 2.5 for 2 min. Each blue bar corresponds to a unique peptide selected for HDX-MS analysis. A final linear sequence coverage of 96.3% (2.54 Redundancy) was achieved.

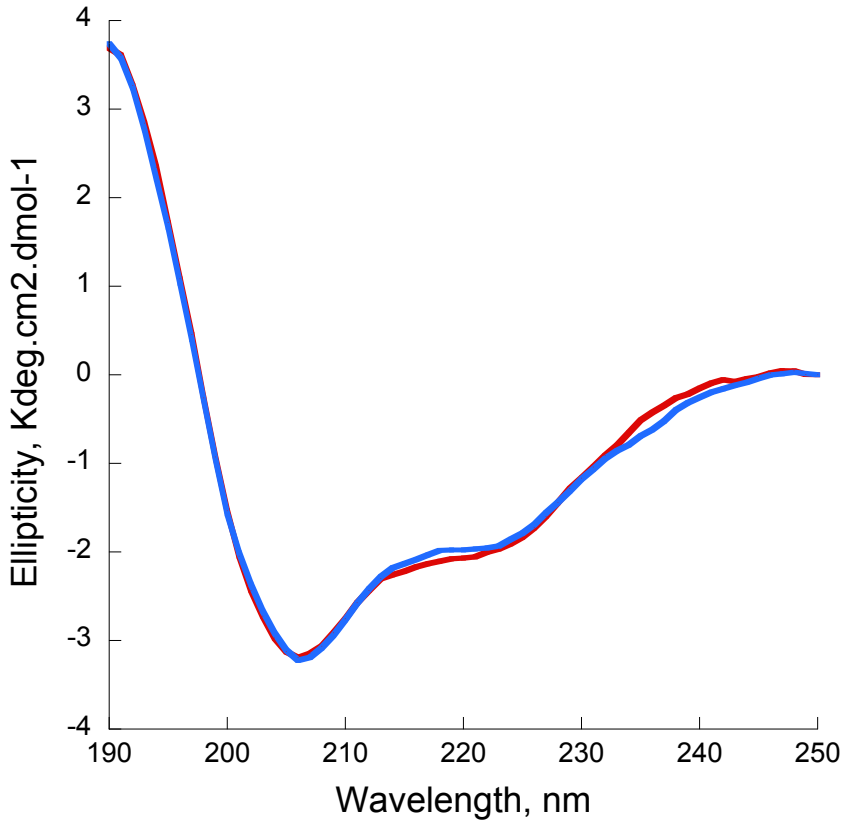

Figure S14. Synchrotron radiation circular dichroism in the far-UV region of AC489 in buffer A (red) and in buffer B (blue). Percentage of secondary structures content was determined using Bestsel. AC489 exhibits 27% of α-helical content in both conditions.

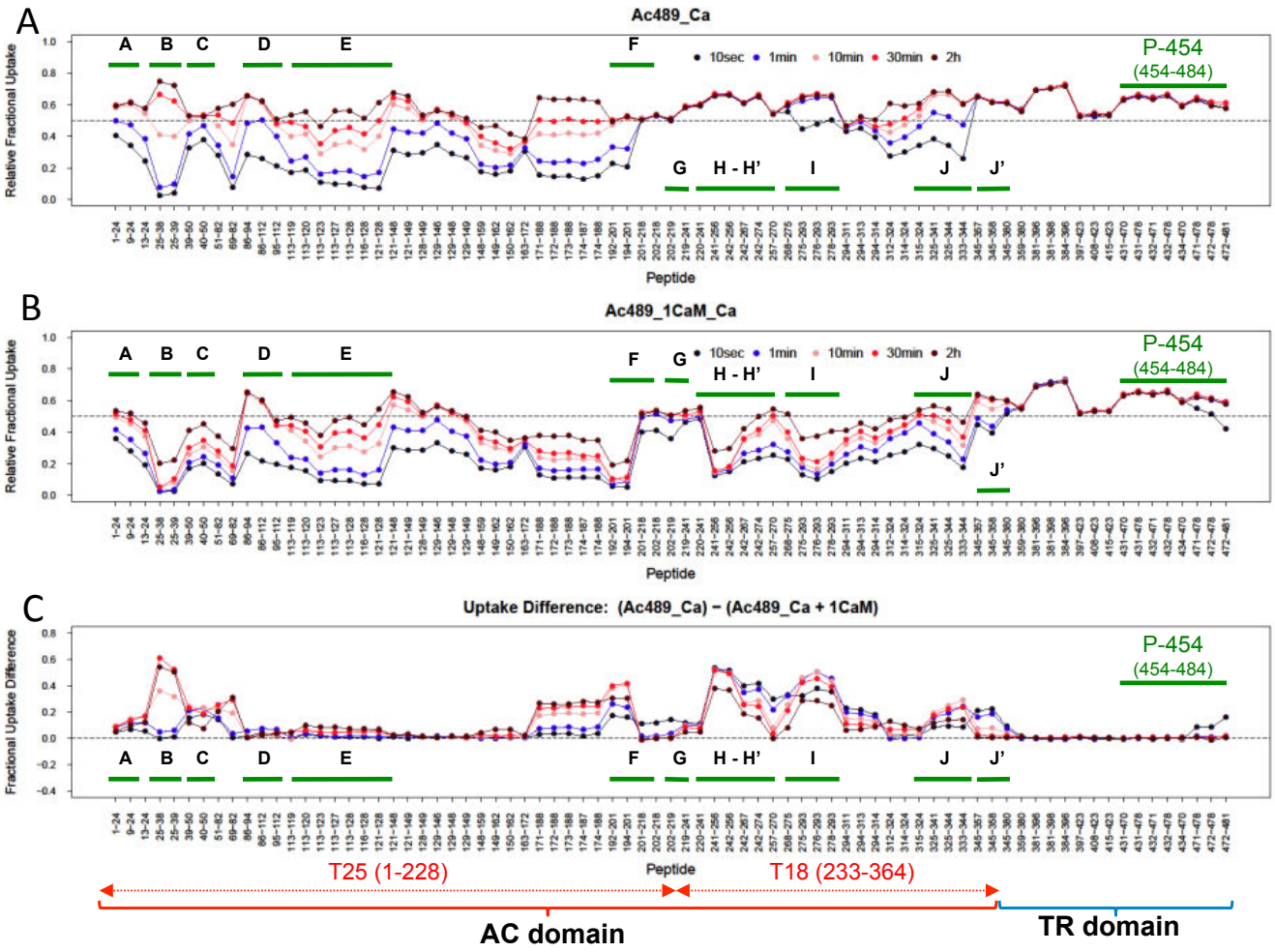

Figure S15. HDX-MS behavior of AC489 in the presence and absence of an equimolar concentration of CaM. Fractional uptake profiles of AC489 alone (**A**) and in the presence of CaM (**B**). The deuterium content calculated for each peptide and condition and at each time point is plotted as a function of peptide position. Each dot corresponds to the average value of three independent replicates. Peptides displaying a bimodal pattern in the absence of CaM are highlighted in yellow. The position of helices A to J' within the AC domain and of the P454 region within the TR domain is indicated. (**C**) Differential fractional uptake plot showing the uptake difference between AC489 alone and in the presence of an equimolar concentration of CaM for all peptides and labeling time points. CaM binding to AC489 induces major reductions of deuterium uptake within helices B, C and F of the T25 region and within helices H-H', I and J/J' of the T18 region of the AC domain. A slight but significant reduction of incorporation is observed within the P454 region of the TR domain.

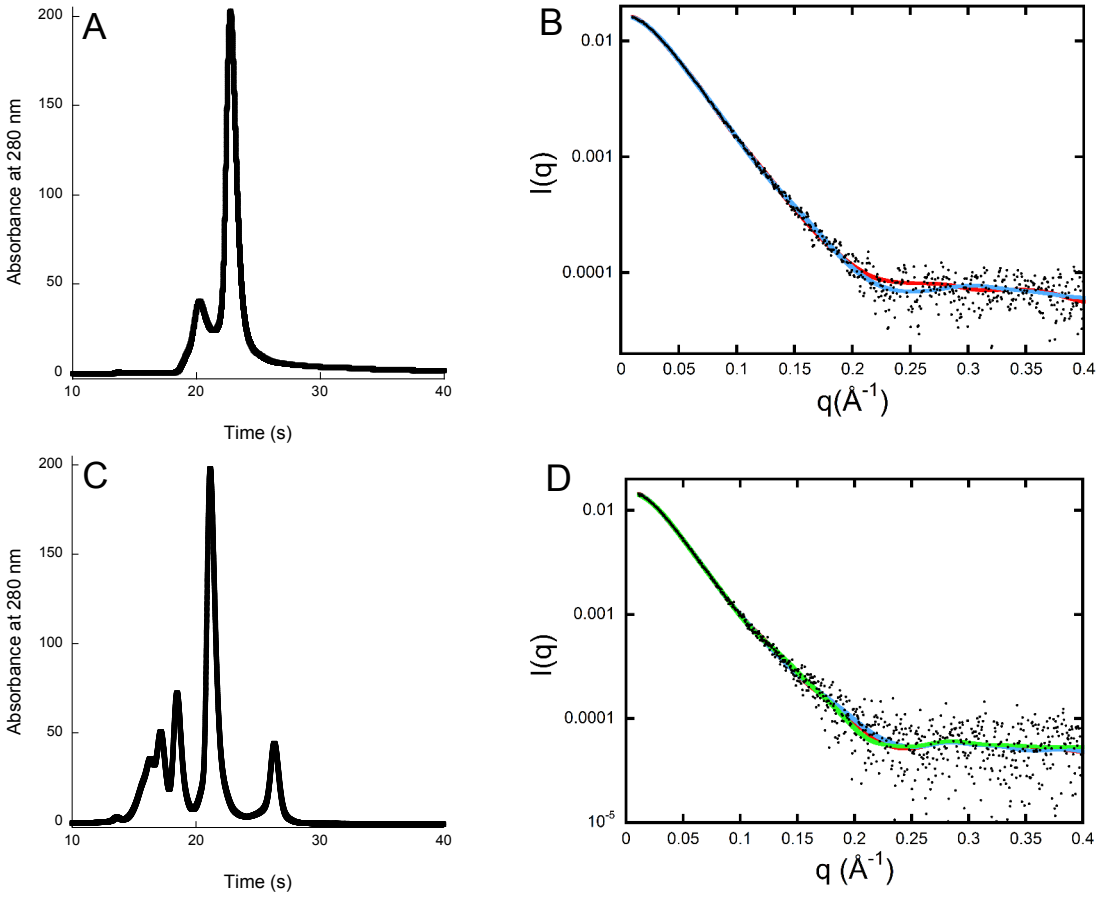

Figure S16. SEC-SAXS of AC489 in the absence and in the presence of CaM. (**A**) Elution profile of AC489 in buffer C. (**B**) Calculated scattering curves (solid lines) for the two typical structural models of AC489 shown on Fig. 5A, superimposed over the experimental SAXS curve (black dots). The red/blue lines correspond to the models 1/2, respectively. (**C**) Elution profile of AC489:CaM at a 1:4 molar ratio in buffer C. (**D**) Calculated scattering curves (solid lines) for the three typical structural models of AC489:CaM complexes shown on Fig. 5B, C and D, superimposed over the experimental SAXS curve (black dots). The red/blue/green lines correspond to the models shown in figure 5B/C/D, respectively.

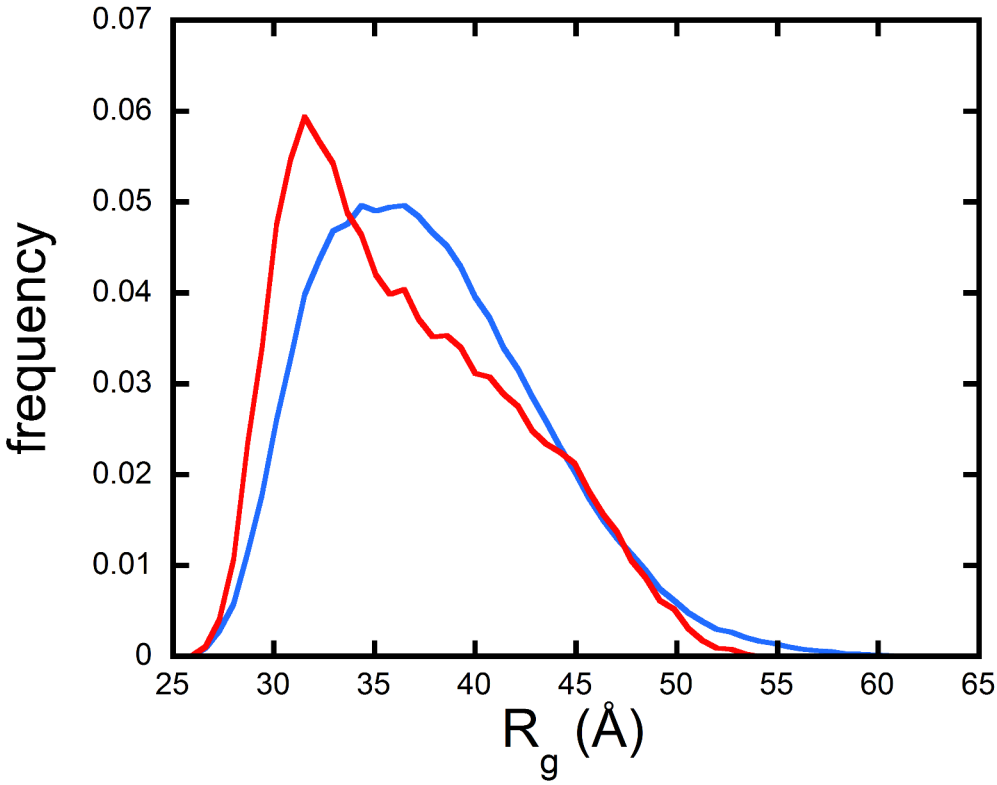

Figure S17. Ensemble Optimization Method analysis on SAXS data of AC489. Distribution of radius of gyration values of conformations from ensembles selected by the program EOM so that the average scattering curve fits the experimental data (red line); corresponding distribution for the complete pool of 10,000 randomly generated conformations (blue line).

Table S1. Sedimentation coefficient of P454, CaM and P454:CaM complex at a 1:1 molar ratio. P454 and CaM were investigated alone (at 57 μM and 72 μM, respectively) and mixed in a 1:1 molar ratio (at 70 μM each). Experiments were performed at 20°C in buffer B with density at 1.0310 $g.mL^{-1}$ and viscosity at 1.0061 cP.

	P454	CaM	P454:CaM
Sedimentation coefficient (S)	0.65	1.85	2.25

Table S2. Thermodynamic parameters of P454:CaM titrations at different temperatures extracted from isothermal titrations calorimetry experiments.

Temperature (K)	K_A (10^7 M^{-1})	K_D (nM)	ΔH (kcal/mol)	ΔS (kcal/mol/K)	-TΔS (kcal/mol)	ΔG (kcal/mol)
283	2.8	35	2.6	0.043	-12.3	-9.6
293	0.3	270	-3.9	0.016	-4.8	-8.8
298	0.8	120	-6.1	0.011	-3.3	-9.4
303	0.8	120	-9.8	-0.0009	0.3	-9.5
311	0.6	160	-13.5	-0.012	3.8	-9.6

Table S3. Thermodynamic parameters of the H:CaM titration at 25°C. The two sites binding model was used to extract the ITC isothermal titration calorimetry parameters.

	Stoichiometry (n)	K_A (10^7 M^{-1})	K_D (nM)	ΔH (kcal/mol)	ΔS (kcal/mol/K)	-TΔS (kcal/mol)	ΔG (kcal/mol)
Site 1	0.9	11.4	10	-5.4	0.02	-5.6	-10.9
Site 2	1.03	0.26	380	-17.7	-0.03	8.9	-8.7

Table S4: Data collection and refinement statistics of P458:CaM crystal structures

	P458:CaM (form 1)	P458:CaM (form 2)*
Wavelength		
Resolution range	67.6 - 3.127 (3.238 - 3.127)	48.46 - 3.591 (3.72 - 3.591)
Space group	C 2 2 21	P 21 21 21
Unit cell	73.342 174.348 97.844 90 90 90	96.92 106.91 221.46 90 90 90
Total reflections	102689 (10270)	133842 (13289)
Unique reflections	11438 (1102)	27453 (2629)
Multiplicity	9.0 (9.3)	4.9 (5.1)
Completeness (%)	99.40 (99.37)	99.38 (96.80)
Mean I/sigma(I)	23.09 (3.38)	5.75 (1.18)
Wilson B-factor	99.26	102.02
R-merge	0.05535 (0.5995)	0.2127 (1.252)
R-meas	0.05866 (0.634)	0.2388 (1.398)
R-pim	0.01896 (0.2026)	0.1063 (0.6107)
CC1/2	1 (0.955)	0.995 (0.552)
CC*	1 (0.989)	0.999 (0.843)
Reflections used in refinement	11380 (1096)	27415 (2628)
Reflections used for R-free	588 (51)	1372 (131)
R-work	0.2801 (0.4586)	0.2899 (0.3685)
R-free	0.2836 (0.4726)	0.3380 (0.3826)
CC(work)	0.890 (0.886)	0.930 (0.667)
CC(free)	0.868 (0.812)	0.860 (0.621)

Number of non-hydrogen atoms	2665	17014
macromolecules	2656	16987
ligands	9	27
solvent		
Protein residues	340	2214
RMS(bonds)	0.013	0.012
RMS(angles)	1.70	1.59
Ramachandran favored (%)	98.49	97.45
Ramachandran allowed (%)	1.51	2.46
Ramachandran outliers (%)	0.00	0.09
Rotamer outliers (%)	3.60	5.61
Clashscore	5.38	6.41
Average B-factor	101.88	115.67
macromolecules	101.92	115.75
ligands	91.84	60.88
solvent		

Statistics for the highest-resolution shell are shown in parentheses.

Table S5: **Data collection and scattering derived parameters from SAXS.**

	CaM	P454-CaM	AC489	AC489-CaM
Data collection parameters				
Instrument	SWING (SOLEIL)			
Detector	CCD-based AVIEX			Eiger4M(Dectris)
Beam geometry	0.8 mm x 0.15 mm			
Wavelength [Å]	1.0			
q-range [$Å^{-1}$]	$0.006 < q < 0.50$			
Absolute scaling	Comparison with scattering from pure H_2O			
Exposure (Dead) time [s]	1/0.5			2.49/0.01
Temperature [K]	288			
SEC-SAXS column	Biosec 3 Agilent			S200 Increase
Loading concentration [mM]	409	136 (CaM)-272(P454)	83	53 (AC489)-212(CaM)
Injection volume [µL]	50			95
Buffer	20 mM Hepes, 150 mM NaCl, 4 mM CaCl2, pH 7.4			
Flow rate [$mL.min^{-1}$]	0.2			0.6
Software employed for SAXS data reduction and analysis				
Foxtrot	Swing in-house software			
PRIMUS	ATSAS 2.8 suite, Franke et al. J. Appl. Cryst. 2017			
DADIMODO	Roudenko O., Thureau A. & Pérez J., 2018			
DAMMIF/DAMMIN	D. Franke and D. I. Svergun, J. Appl. Cryst. 2009			
Structural parameters				
I(0) Guinier [cm^{-1}]	0.02571±0.00002	0.00782±0.00001	0.01675±0.0001	0.01537±0.0001
R_g Guinier [Å]	22.2±0.1	19.7±0.1	35.1±0.3	39.4±0.4
qRg-range	0.287-1.02	0.256-1.30	0.356 - 1.13	0.431-1.03
I(0) p(r) [cm^{-1}]	0.02571±0.00002	0.00783±0.00001	0.01693±0.0001	0.01547±0.0001
R_g p(r) [Å]	22.3±0.1	19.9±0.1	36.9±0.3	40.8±0.4
q-range [$Å^{-1}$]	0.013 - 0.35	0.013 - 0.35	0.010 - 0.40	0.011 - 0.4
D_{Max} [Å]	75	67	145	160
Molecular mass determination				
$MM_{sequence}$ [kDa] [a]	16.8	20.1	52.2	69.1
$MM_{SAXS\ MoW}$ [kDa] [b]	17.8	19.5	57.1	68.8
$MM_{SAXS\ QR}$ [kDa] [c]	16.8	18.7	56.5	71.5
DAMMIF/DAMMIN analysis				
Model number	20	20		
NSD	0.56	0.74		
χ^2 (Dammin)	1.56	1.34		
DADIMODO analysis				
Model number		20	20	20
q-range [$Å^{-1}$]		0.016-0.50	0.010 - 0.40	0.011-0.4
χ^2 (Crysol)		1.49-1.70	1.19-1.37	1.14-1.26

[a] The calculated masses were derived from the sequences.

[b] Molecular mass M obtained from the whole I(q) curve (q_{max} = 0.3-0.4 $Å^{-1}$) using the SAXS-MoW2 program, available at http://saxs.ifsc.usp.br/.

[c] Molecular mass M obtained from the whole I(q) curve (q_{max} = 0.25 $Å^{-1}$) using the ScÅtter3 program, available at https://bl1231.als.lbl.gov/scatter/.

Table S6. Estimation of the α-helical content of P454-derived peptides using Bestsel in solution, in 20% TFE and in the presence of POPC POPG 8:2 at 2 mM lipids concentration.

P454 derived peptide	Solution (%)	TFE 20% (%)	POPC POPG 8:2 (%)
P454	17 ± 2	60 ± 2	50 ± 1
P454 R12Q	8 ± 4	50 ± 2	23 ± 1
P454 R12K	13 ± 2	45 ± 4	26 ± 1
P454 R12E	6 ± 1	55 ± 3	10 ± 1
P454 L463A	14 ± 2	48 ± 3	19 ± 2
P454 L475A	5 ± 2	45 ± 1	15 ± 1
P454 L481A	5 ± 1	49 ± 1	44 ± 3
P454 I479A	8 ± 2	29 ± 1	12 ± 3
P454 I479V	2 ± 1	47 ± 6	37 ± 2
P454 I479L	13 ± 1	51 ± 1	51 ± 5
P454 H477S	4 ± 2	40 ± 1	20 ± 2
P458	10 ± 4	50	23 ± 2
P454 W458A-I479A	10 ± 3	55 ± 1	7 ± 3

Table S7. Affinity constants of the P454-derived peptides for POPC POPG SUVs and CaM. The free energy ΔG_{Kx} for POPC POPG was calculated from the partition coefficient K_x. The K_D for CaM was calculated from fluorescent titrations and ITC experiments. Note that the K_D for CaM and for membranes are expressed in nM and μM, respectively.

*Not yet determined

Peptides	K_D for CaM (nM)	ΔG_{KD} for CaM (kcal/mol)	Partition coefficient K_X ($\times 10^3$)	ΔG_{Kx} for POPC POPG 8:2 (kcal/mol)	K_D for POPC POPG 8:2 (μM)
P454	90	-9.6	790	-8	70
P454 R1Q	90	-9.6	190	-7.2	290
P454 R2Q	180	-9.2	150	-7	370
P454 R12Q	2000	-7.7	70	-6.6	790
P454 R12A	130	-9.3	280	-7.4	200
P454 R12K	90	-9.6	220	-7.3	260
P454 R12E	90	-9.6	80	-6.7	690
P454 L463A	200	-9	630	-7.9	90
P454 L475A	120	-9.4	350	-7.7	160
P454 L481A	90	-9.6	780	-8	70
P454 I479A	1000	-8.2	330	-7.5	170
P454 I479V	100	-9.5	560	-7.8	100
P454 I479L	90	-9.6	700	-7.9	80
P454 H477S	190	-9.1	340	-7.5	160
P458	200	-9.1	190	-7.2	290
P454 W458A-I479A	3000	-7.5	*	*	*

Table S8. Concentration of P454-derived peptides required to induce half permeabilization of ANTS-encapsulated LUVs ($C_{P1/2}$) (see Material and Methods for details).

Peptide	$C_{P1/2}$ (μM)
P454	0.068
P454 R1Q	0.218
P454 R2Q	0.110
P454 R12Q	0.23
P454 R12A	0.139
P454 R12K	0.092
P454 R12E	> 50
P454 L463A	0.414
P454 L475A	0.645
P454 L481A	0.065
P454 I479A	7.862
P454 I479V	0.091
P454 I479L	0.043
P454 H477S	0.251
P458	1.263
P454 W458A-I479A	> 80

Table S9. Sedimentation equilibrium of AC489 and CaM at a 1:4 molar ratio. Mass values are indicated in kDa. Monte-Carlo error analysis provides us with the standard deviation values (see Material and Methods for details).

	Pic 1	Pic 2	Pic 3
Mass, kDa	16.8 ± 0.4	69.2 ± 0.5	142.8 ± 1.3
Expected mass, kDa	16.7	68.9	137.8
Species	CaM	AC489:CaM 1:1	AC489:CaM 2:2

Extended Table S10: **HDX Data Summary**

EXPERIMENT	**CaM BINDING TO AC489**		**P-454 BINDING TO CaM**	
Dat set :	AC489_Ca	AC489_Ca_CaM	CaM_Ca	CaM_Ca_P-454
HDX reaction details				
- *pD*	7.4	7.4	7.4	7.4
- *T°C*	20°C	20°C	20°C	20°C
- *Excess deuterium*	80%	80%	80%	80%
HDX time course analyzed (min)	0.16, 1, 10, 30, 120	0.16, 1, 10, 30, 120	0.16, 1, 10, 30, 60, 120	0.16, 1, 10, 30, 60, 120
HDX control samples	Fully-labeled control	Fully-labeled control	/	/
Number of peptides	70	70	46	46
Sequence coverage	96.3	96.3	89.3	89.3
Average peptide length	17.1	17.1	11.7	11.7
Redundancy	2.54	2.54	4.01	4.01
Replicates	3 (technical)	3 (technical)	3 (technical)	3 (technical)
Repeatability (pooled standard deviation)[#]	0.05 Da	0.05 Da	0.07 Da	0.07 Da
Significant difference between state[$]	Wald test, $p < 0.05$			

[#] One unique charge state was used per peptide
[$] MEMHDX (www. memhdx.c3bi.pasteur.fr)

Article VII

Calmodulin fishing with a structurally disordered bait triggers CyaA catalysis

Darragh P. O'Brien, Dominique Durand, Alexis Voegele, Véronique Hourdel, Maryline Davi, Julia Chamot-Rooke, Patrice Vachette, Sébastien Brier, Daniel Ladant and Alexandre Chenal

PLOS Biology
Volume 15(12)
December 2017

When translocated across the plasma membrane, the catalytic domain of CyaA (ACD, residues 1-364) binds to calmodulin (CaM) and produces supraphysiological levels of cAMP that disrupts cellular signaling pathways and leads to cell death (Ladant and Ullmann, 1999). Guo and co-workers solved the crystal structure of ACD with the C-terminal part of CaM (C-CaM) (Guo et al., 2005). However, how CaM activates ACD remains unclear. From a combination of biophysical and structural approaches, the aim of this study was to characterize the conformational changes occurring in ACD upon CaM binding, which could explain how CaM regulates and activates ACD.

We performed a model using SAXS, HDX-MS and SRCD structural data. Interestingly, the HDX-MS data indicated that the N-terminal part of ACD, corresponding to the T25 (*i.e* residues 1-224 of ACD where the catalytic site is identified), exhibited secondary structures, indicating that T25 is well folded. On the contrary, the C-terminal part of ACD, corresponding to the T18 (*i.e* residues 225-364 of ACD where the CaM-binding site is identified), was mainly unstructured. Particularly, a segment covering residues 201-275 was completely disordered. These results were unexpected because in the crystal structure, this region of 75 residues is partly helical and corresponds to the main contact between ACD and CaM. The contact occurs with the amphipathic H-helix peptide of ACD, spanning residues 233-254. SRCD data confirmed that ACD in solution is more disordered than in the complex.

All together, the SAXS, HDX-MS and SRCD data allowed proposing a structural model of ACD in solution.

It is well described that CaM is a highly flexible protein that can have different conformations in solution and in complex with peptides. CaM adopts a global dumbbell shape linked by an inter-domain helix. The main site of interaction of ACD with CaM occurs with the H-helix peptide. We performed SAXS with the H:CaM complex. We found that the overall shape of CaM remains the same as CaM alone and thus that the H-helix binding does not cause structural rearrangement of the CaM. Our SRCD data showed that more than 20 residues underwent a disorder to α-helix transition upon interaction. Finally, the HDX-MS data of the complex indicated that this disorder-to-order transition did not occur in CaM, suggesting that the H-helix peptide acquires a helical conformation upon CaM binding.

We undertook equivalent experiments with the MLCK:CaM: complex (for Myosin Light Chain Kinase peptide) to compare with the H:CaM one. MLCK is known to induce structural rearrangements of CaM, which on end adopts a compact structure (Gsponer et al., 2008). Our data were equivalent to those observed with the known crystal structure of the complex.

These SAXS data provide evidence that CaM adopt various conformations upon interaction with amphiphilic peptides.

Finally the ACD:CaM complex in solution was investigated by HDX-MS. As we observed with ACD in solution, the N-terminal T25 was mainly stabilized. Some regions of the C-terminal T18 were stabilized and others like the H-helix peptide region, acquired structure upon CaM binding. We also examined the effect of ACD binding on CaM. We found that C-CaM was strongly stabilized. In contrast, the inter-lobe helix and the N-CaM were unaffected. The SRCD data showed that CaM binding induces an increase of helical content of about 40 residues in ACD and was proposed to occur in the H-helix region upon interaction, as supported by the HDX-MS data.

Taken together, our data demonstrate how the ACD of CyaA can be activated by its endogenous factor CaM. Although the T25 catalytic site remains mainly folded, the T18 CaM binding site undergoes secondary structures acquisitions. Especially, the H-helix region of 75 residues (201-275) is disordered in solution and acquires helical content upon CaM interaction. It serves as a bait for CaM capture. This binding stabilizes and reorganizes adjacent segments, which contributes to the shaping of the catalytic site.

This structural disorder in ACD may explain the biological functions of the molecule. Firstly, the disorder destabilizes the catalytic site and may prevent overproduction of cAMP production in the bacteria lacking of CaM (k_{cat} of about 2 s^{-1}) while in the presence of CaM, the catalytic activity is uncontrollable (k_{cat} of about 2000 s^{-1}). Secondly, this instability of ACD may help for its secretion out of the bacteria. Thirdly, this disorder could facilitate its passage across the plasma membrane of target cells and the unfolded H-helix facilitates the CaM binding, promotes folding and structural reorganization of some regions of ACD and enzymatic activation.

PLOS BIOLOGY

RESEARCH ARTICLE

Calmodulin fishing with a structurally disordered bait triggers CyaA catalysis

Darragh P. O'Brien[1], Dominique Durand[2]*, Alexis Voegele[1], Véronique Hourdel[3], Marilyne Davi[1], Julia Chamot-Rooke[3], Patrice Vachette[2], Sébastien Brier[3]*, Daniel Ladant[1]*, Alexandre Chenal[1]*

1 Institut Pasteur, UMR CNRS 3528, Chemistry and Structural Biology Department, Paris, France, **2** Institute for Integrative Biology of the Cell (I2BC), CEA, CNRS, Univ. Paris-Sud, Université Paris-Saclay, Gif-sur-Yvette cedex, France, **3** Institut Pasteur, USR CNRS 2000, Chemistry and Structural Biology Department, CITECH, Paris, France

* alexandre.chenal@pasteur.fr (A.C.); daniel.ladant@pasteur.fr (D.L.); dominique.durand@i2bc.paris-saclay.fr (D.D.); sebastien.brier@pasteur.fr (S.B.)

Check for updates

OPEN ACCESS

Citation: O'Brien DP, Durand D, Voegele A, Hourdel V, Davi M, Chamot-Rooke J, et al. (2017) Calmodulin fishing with a structurally disordered bait triggers CyaA catalysis. PLoS Biol 15(12): e2004486. https://doi.org/10.1371/journal.pbio.2004486

Academic Editor: Ann Stock, UMDNJ/Robert Wood Johnson Medical School, United States of America

Received: October 10, 2017

Accepted: December 7, 2017

Published: December 29, 2017

Copyright: © 2017 O'Brien et al. This is an open access article distributed under the terms of the Creative Commons Attribution License, which permits unrestricted use, distribution, and reproduction in any medium, provided the original author and source are credited.

Data Availability Statement: All relevant HDX-MS and SR-CD data are available in the S1 to S5 Data files and in the Supporting Information files. The molecular models and experimental SAXS data have been deposited on SASBDB (Small Angle Scattering Biological Data Bank, http://www.sasbdb.org/aboutSASBDB/) under the SAS codes SASDCK9 and SASDCL9.

Funding: Fondation pour la Recherche Médicale (FRM) https://www.frm.org/ (grant number DBS

Abstract

Once translocated into the cytosol of target cells, the catalytic domain (AC) of the adenylate cyclase toxin (CyaA), a major virulence factor of *Bordetella pertussis*, is potently activated by binding calmodulin (CaM) to produce supraphysiological levels of cAMP, inducing cell death. Using a combination of small-angle X-ray scattering (SAXS), hydrogen/deuterium exchange mass spectrometry (HDX-MS), and synchrotron radiation circular dichroism (SR-CD), we show that, in the absence of CaM, AC exhibits significant structural disorder, and a 75-residue-long stretch within AC undergoes a disorder-to-order transition upon CaM binding. Beyond this local folding, CaM binding induces long-range allosteric effects that stabilize the distant catalytic site, whilst preserving catalytic loop flexibility. We propose that the high enzymatic activity of AC is due to a tight balance between the CaM-induced decrease of structural flexibility around the catalytic site and the preservation of catalytic loop flexibility, allowing for fast substrate binding and product release. The CaM-induced dampening of AC conformational disorder is likely relevant to other CaM-activated enzymes.

Author summary

Calmodulin is a widespread and highly conserved protein that interacts with a wide variety of eukaryotic proteins and enzymes, controlling their activities in response to calcium. The adenylate cyclase toxin (CyaA) of *Bordetella pertussis*, the causative agent of whooping cough, is one such calmodulin target. Once transported across the plasma membrane of eukaryotic cells, the catalytic domain (AC) of CyaA is activated by calmodulin, producing high levels of cAMP, which can induce cell death. We use an integrative structural biology approach combining several biophysical techniques to characterize the structural rearrangements in AC upon calmodulin binding and to elucidate their relationship to CyaA activation. We show that a disordered stretch of 75 amino acid residues in AC serves as a bait for calmodulin capture. Binding induces significant folding within this region, a prerequisite for CyaA activation. Calmodulin binding promotes the stabilization of the

20140930771). Received By DOB, AV, MD, DL, and AC. The funder had no role in study design, data collection and analysis, decision to publish, or preparation of the manuscript. Agence Nationale de la Recherche (grant number CACSICE Equipex ANR-11-EQPX-0008). DOB, AV, VH, MD, JCR, SB, DL, and AC. The funder had no role in study design, data collection and analysis, decision to publish, or preparation of the manuscript. Region Ile de France (grant number DIM MalInf 2016). AV and AC. The funder had no role in study design, data collection and analysis, decision to publish, or preparation of the manuscript. CNRS. DOB, DD, AV, VH, MD, JCR, PV, SB, DL, and AC. The funder had no role in study design, data collection and analysis, decision to publish, or preparation of the manuscript. Institut Pasteur (grant number PasteurInnoV15006-01A and PTR451). DOB and AC. The funder had no role in study design, data collection and analysis, decision to publish, or preparation of the manuscript.

Competing interests: The authors have declared that no competing interests exist.

Abbreviations: AC, adenylate cyclase catalytic domain; ACN, acetonitrile; AID, auto-inhibitory domain; CaM, calmodulin; CBS, CaM-binding site; C-CaM, C-terminal domain of CaM; CR1, catalytic region 1; CR2, catalytic region 2; CR3, catalytic region 3; CyaA, adenylate cyclase toxin; D_{max}, maximal dimension; DSSP, Dictionary of Secondary Structure of Proteins; EOM, ensemble optimization method; far-UV, far-ultraviolet; FDR, false discovery rate; HDX-MS, hydrogen/deuterium exchange mass spectrometry; IDR, intrinsically disordered region; LHL, loop-helix-loop; MEMHDX, Mixed-Effects Model for HDX experiments; MLCK, myosin light chain kinase; MoRF, molecular recognition feature; MRE, mean residual ellipticity; MS, mass spectrometry; MS^E, data-independent acquisition scheme; N-CaM, N-terminal domain of CaM; NSD, normalized spatial discrepancy; PA, protective antigen; pdb, Protein Data Bank; PLGS, Protein Lynx Global Server; P_{MLCK}, myosin light-chain kinase peptide; R_g, radius of gyration; SASBDB, Small Angle Scattering Biological Data Bank; SAXS, small-angle X-ray scattering; SEC, size exclusion chromatography; SLIM, short linear motif; SR-CD, synchrotron radiation circular dichroism; T18, C-terminal trypsin-cleavage fragment of CyaA (amino acids 225–364); T18b1, first beta-sheet of the T18 fragment; T18b2, second beta-sheet of the T18 fragment; T1SS, type I secretion system; T25, N-terminal trypsin-cleavage fragment of CyaA (amino acids 1–224).

distant catalytic site, whilst maintaining its catalytic loop in a flexible and exposed state. Both phenomena contribute to the high enzymatic activity of AC, allowing for fast substrate binding and cAMP release. The calmodulin-induced reduction of AC conformational disorder is likely relevant to other calmodulin-activated enzymes.

Introduction

Calmodulin (CaM) is a major mediator of calcium signaling in eukaryotic cells, ubiquitously distributed and highly conserved in the whole eukaryotic kingdom. This small acidic protein of 148 amino acids interacts with a wide variety of target proteins or enzymes to control their activities in response to calcium. CaM is made of two pairs of calcium-binding EF-hand motifs that are connected by a long flexible helix, adopting a dumbbell shape in solution. The binding of calcium ions to each EF hand triggers conformational changes that result in the exposure of hydrophobic patches, altering the association of CaM with its target proteins.

Typically, CaM interacts with its targets by binding a short segment, or CaM-binding site (CBS), of about 20–30 residues that are positively charged and can adopt an amphipathic helical structure. CaM binding to the CBS is associated with a large conformational change as the protein bends from its extended dumbbell shape into a more globular structure in which its two N- and C-lobes wrap around the target helical sequence. In many instances (e.g., myosin light chain kinase [MLCK], CaM kinases, calcineurin, CaM-activated Ca-ATPase/pumps), the CBS sequence is proximal in the primary structure to an auto-inhibitory domain (AID), which occupies the catalytic site of the enzyme in the resting state, thus inhibiting enzymatic activity. Binding of CaM to the CBS induces a conformational change that displaces the AID from the enzymatic site to release the full catalytic activity.

An original mechanism of CaM regulation has been uncovered in two toxins produced by two pathogenic bacteria, *Bacillus anthracis*, the causative agent of anthrax, and *B. pertussis*, responsible for whooping cough. These toxins, the edema factor and the adenylate cyclase toxin (CyaA), respectively, are adenylate cyclases secreted by the bacteria and are able to invade eukaryotic target cells, in which they are potently activated by CaM to produce cytotoxic, supraphysiological levels of cAMP [1, 2]. CyaA is essential for the early steps of colonization of the respiratory tract by *B. pertussis*, selectively targeting the innate immune cells to favor bacterial survival. CyaA is a 1,706-residue-long bifunctional protein; the CaM-activated, catalytic domain (AC) is located in the 364 amino-proximal residues, while the carboxy-terminal 1,342 residues are involved in toxin binding to target cells and delivery of the AC domain across the plasma membrane to the cell cytosol [3–5].

How CaM binding regulates the activity of the edema factor toxin has been illuminated by a series of structural studies carried out by W.J. Tang and colleagues, who solved the structures of both the CaM-free and -bound forms [6]. Edema factor consists of an N-terminal protective antigen (PA)-binding domain; a catalytic core made up of two globular subdomains, C_A and C_B; and a C-terminal helical domain. The latter makes substantial contacts with the catalytic core in the absence of CaM and locks the enzyme in an inactive state. Most of these contacts are disrupted upon CaM binding, which inserts in an extended conformation between the catalytic core and the helical domain. Through a series of conformational changes, CaM indirectly stabilizes the conformation of a substrate-binding loop that is fully disordered in the CaM-free form.

In contrast to edema factor, the exact mechanism of CyaA activation by CaM is unclear. To date, the structures of AC in the absence of CaM and of AC bound to full-length CaM remain

unsolved; Guo and colleagues [7] have determined the structure of AC in complex with the C-terminal domain of CaM (C-CaM) only. Although AC and the edema factor display limited sequence identity, their catalytic cores share substantial structural similarity: like edema factor, AC is organized into two globular subdomains, C_A and C_B. The catalytic site, located at the interface between these two domains, is essentially identical to that of the edema factor: it is made of three highly conserved regions (catalytic region 1 [CR1], residues 54–77; catalytic region 2 [CR2], residues 184–198; and catalytic region 3 [CR3], residues 295–315) that are directly involved in substrate binding and catalysis. Nevertheless, the edema factor and AC significantly differ in CaM binding. AC has no equivalent of the edema factor C-terminal helical domain that is involved in CaM binding and activation. Instead, C-CaM binds mainly to the H-helix (spanning residues 234–254 [7]), with typical characteristics of classical CBS, i.e., a basic and amphipathic sequence, which protrudes from the C_A subdomain. C-CaM also interacts with a loop-helix-loop (LHL) motif (residues 341–364) located at the very C-terminal end of AC. As this segment directly contacts the CR3 catalytic loop, C-CaM could thus indirectly stabilize it in a configuration favorable for catalysis [7, 8].

Herein, we have characterized the conformational changes of AC upon binding to its CaM activator through a combination of structural studies in solution, including synchrotron radiation circular dichroism (SR-CD), hydrogen/deuterium exchange mass spectrometry (HDX-MS), and small-angle X-ray scattering (SAXS). Our results indicate that, in the absence of CaM, AC exhibits a large intrinsically disordered region (IDR) of about 75 residues (circa 20% of the AC domain) encompassing the main CBS. CaM binding triggers the folding of the CBS and a strong overall reduction in disorder that is likely crucial for AC activation. The presence of a large IDR in AC may facilitate intoxication (translocation across the membrane) of target cells and subsequently favor its association with the CaM activator via a "fly-casting" mechanism [9].

Results

We performed parallel studies of five different samples using both HDX-MS and SAXS: CaM and AC alone, CaM in complex with the H-helix peptide from AC, and a peptide from myosin light-chain kinase (MLCK) as a reference, and finally, the AC-CaM complex. SAXS measurements were recorded using the size exclusion chromatography followed by SAXS (SEC-SAXS) setup available on the SWING beamline at the SOLEIL synchrotron (a succinct description of instrumental conditions is given in Materials and methods and [10]). All SAXS experimental and analytical details are given in S1 Table, together with the values of global structural parameters (radius of gyration [R_g], maximal dimension [D_{max}], and molecular mass) derived from the scattering data. Of note, all molecular mass values indicate that the investigated particles are present as monomers of AC or CaM in solution. HDX-MS experimental details are to be found in the relevant section of Materials and methods.

Structural model of the isolated AC domain

SAXS data from the free AC protein were initially modeled, starting from the atomic coordinates of AC extracted from the Protein Data Bank (pdb) dataset 1YRU of the crystal structure of AC in complex with the C-CaM [7]. Using AllosModFoxs [11], we adjusted the calculated scattering profile against experimental SAXS data by refining the proposed position of the missing residues in 1YRU (residues 226–232, defined as the Hom-loop, and the first six N-terminal residues), while keeping the AC structure unchanged. An example of one of the fits (χ^2 = 2.57) obtained in this way is shown in Fig 1A. The corresponding model, shown in blue in Fig 1D, suggests that AC adopts a conformation roughly similar to that of the crystal, albeit

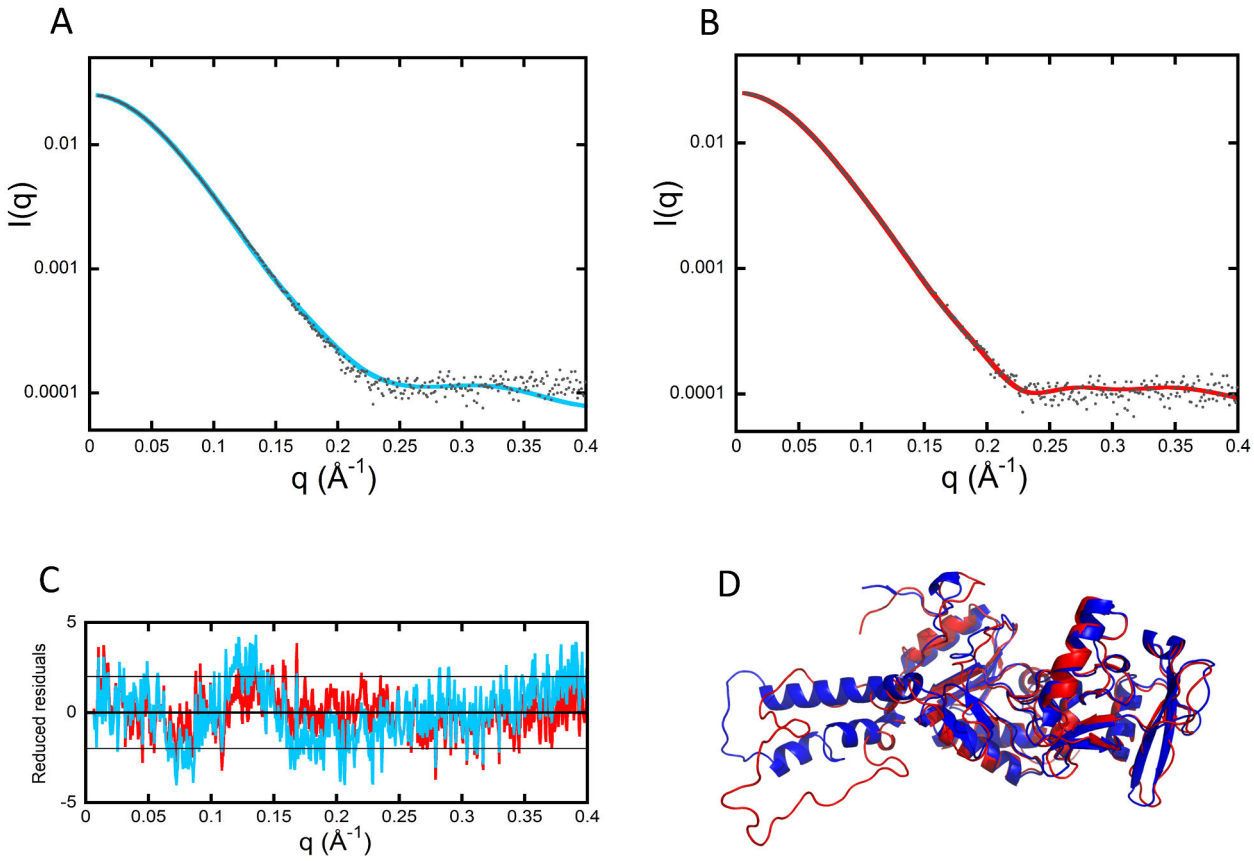

Fig 1. SAXS models of isolated AC. (A) Adjustment of the curve calculated from the crystal structure of AC extracted from the pdb dataset 1YRU (blue curve) against experimental data (black dots). (B) Adjustment obtained by releasing the residues comprising helices F through H′ (red curve). (C) Distribution of reduced residuals corresponding to the two fits shown in panels (A) and (B), using the same color code. (D) Crystal structure (blue) and conformation with relaxed F–H′-helices (red). AC, adenylate cyclase catalytic domain; pdb, Protein Data Bank; SAXS, small-angle X-ray scattering.

https://doi.org/10.1371/journal.pbio.2004486.g001

with significant differences. Using the same degrees of freedom and a description in terms of ensemble of conformations did not allow us to further improve the agreement with our experimental data.

We therefore undertook a second cycle of SAXS modeling by incorporating the structural data deduced from HDX-MS and far-ultraviolet (far-UV) SR-CD data. Regarding local-level HDX-MS analysis, pepsin digestion of AC yielded 181 unique peptides identified from their accurate masses and production spectra. A total of 36 peptides covering 100% of the AC sequence were included in the final data analysis (S1 Fig; the nomenclature of secondary structures from W.J. Tang [7] is used throughout this work and reported in the legend of S1 Fig). HDX-MS experiments performed on the isolated AC protein show a significant difference in structural content between the N-terminal (T25 trypsin-cleavage fragment of CyaA, from residues 1–224) and C-terminal (T18 trypsin-cleavage fragment of CyaA, from residues 225–364) regions of the protein (Fig 2A, top panel; S1 Data). Dynamic HDX-MS behavior, indicative of the presence of secondary structural elements, was observed throughout the N-terminal moiety of AC (specifically, in A–E-helices and the beta-sheets of T25), confirming that T25 domain is well folded. Two peptides, namely 51–68 and 163–172, give no dynamic HDX-MS pattern and correspond to loops between structural elements. The C-terminal moiety, on the

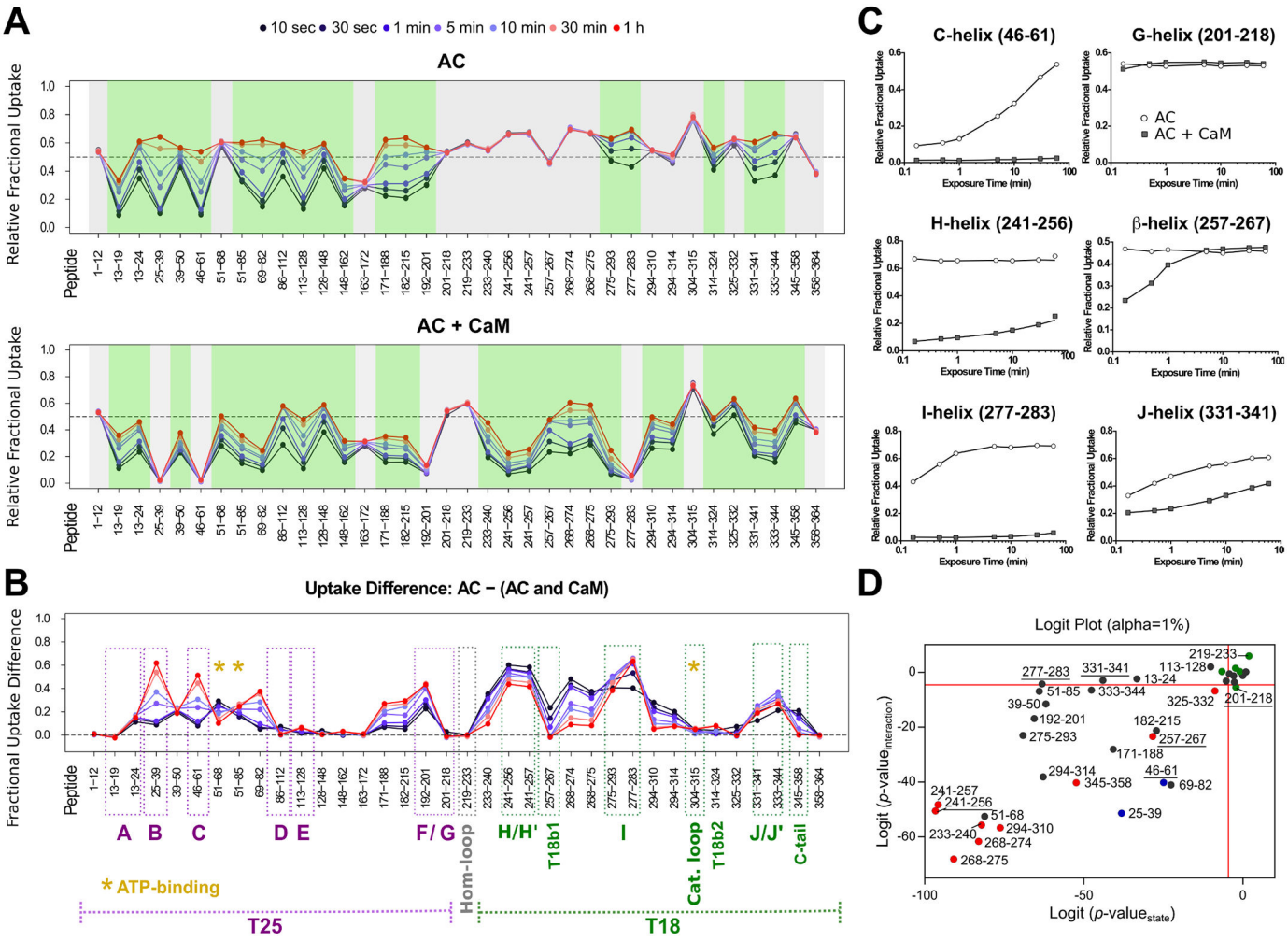

Fig 2. AC dynamics are significantly altered upon CaM interaction. HDX-MS was performed at the peptide level to improve the spatial resolution. Panel (A) displays relative fractional uptake maps of AC alone and upon CaM binding. The presence of dynamic HDX-MS indicative of structure formation is colored green, whereas non-dynamic events are colored gray. CaM binding to AC results in an overall reduction in the solvent accessibility and structure formation in several regions. (B) Multiple regions of AC are altered upon CaM binding, as determined by the uptake difference chart. Major modifications of the AC T25 region are observed within helices B, C, and F. For the T18 region, primary sites of alteration are found within the H/H″-, I-, and J/J′-helices as well as within the T18b1 and C-tail regions of the protein. No changes in accessibility were observed at the Hom- and catalytic loops in either state. Sites of ATP-binding are also given. (C) Several types of HDX-MS behavior were observed upon AC:CaM complex formation. All AC peptides selected for final HDX-MS analysis are displayed in S10 Fig. (D) Logit representation of the statistical results generated for each peptide by MEMHDX. Peptides colored red display nondynamic behavior in the AC alone state only, while those in blue give nondynamic behavior in the AC + CaM state only. Green peptides are those that have nondynamic HDX-MS behavior in both states, while those peptides colored black are dynamic in both states. The FDR value was set to 0.01 (red lines). The data used to generate the figure can be found in S1 Data. AC, adenylate cyclase catalytic domain; CaM, calmodulin; FDR, false discovery rate; MEMHDX, Mixed-Effects Model for HDX experiments; T18, C-terminal trypsin-cleavage fragment of CyaA (amino acids 225–364); T25, N-terminal trypsin-cleavage fragment of CyaA (amino acids 1–224); T18b1, first beta-sheet of the T18 fragment.

https://doi.org/10.1371/journal.pbio.2004486.g002

other hand, appears poorly structured: the few regions exhibiting dynamic HDX-MS behavior cover the I- and J/J′-helices and the second beta-sheet of the T18 fragment (T18b2) region, respectively. Strikingly, the amide hydrogens from the region covering residues 201–275 are fully exchanged from the first time point of the HDX experiment to the last, indicating that this region of circa 75 amino acids is essentially disordered (Fig 2A and 2C). This result provides direct evidence that the F-, G-, H-, and H′-helices, the Hom-loop, and the first beta-sheet of the T18 fragment (T18b1) are disordered in the isolated AC protein. This is somewhat

unexpected, as in the X-ray structure of AC:C-CaM, this region is predominantly helical [7]. Finally, the catalytic loop (residues 300–315) is fully exposed to the solvent.

In view of the major differences observed between our HDX-MS results and the crystal structure in a helix-rich part of the crystal structure, we decided to complement our experimental approach using the spectroscopic far-UV SR-CD method, which constitutes a very sensitive probe of a protein helical content in solution. The helical content of AC was estimated from the SR-CD spectrum (S2 Fig) using the BestSel software [12] and compared to that of the crystal structure using the Dictionary of Secondary Structure of Proteins (DSSP) algorithm [13, 14] (S2–S4 Tables and S2 Data). The analysis of SR-CD data indicate that 27% of all residues are part of helical secondary structures, a value significantly lower than the 36% value derived from the X-ray structure using DSSP. However, the SR-CD value favorably compares with HDX-MS results, in which the region corresponding to F-, G-, H- and H′-helices and the T18b1 appear to be disordered in solution (Fig 2A).

Taking into account these results from HDX-MS and far-UV SR-CD, the residues from 200–270 were released and allowed to move in SAXS modeling to obtain a new set of models and associated fits, an example of which is shown in Fig 1B ($\chi^2 = 1.36$). The distributions of reduced residuals corresponding to the two fits are shown in Fig 1C, while the conformation with relaxed F–H′-helices is shown in red in Fig 1D. This model exhibits a much better fit to the SAXS data and also displays a helical content close to that experimentally determined by SR-CD (S2 Fig and S2 Table). Overall, our model of AC in solution accounts for all three sets of experimental data.

Structural model of CaM

CaM has been the object of many SAXS studies over the last few decades [15–19]. Ab initio modeling of our CaM data using the DAMMIF/DAMMIN programs [20] yields the well-known dumbbell shape shown in Fig 3A. Yet, the experimental scattering pattern differed significantly from that calculated from the crystal structure of CaM (1CLL [21]) (Fig 3D, $\chi^2 = 37$, green curve)—not surprisingly, given the flexibility of the inter-domain helix, as revealed previously by nuclear magnetic resonance (NMR) studies and corroborated by our present HDX-MS data (see Fig 4, described later). This flexibility makes more difficult the ab initio modeling of the protein on the basis of the SAXS data. Hence, CaM was first described as an ensemble of conformations using the Ensemble Optimization Method (EOM) suite of programs [22]. Ten thousand conformations were generated by the Ranch program, starting from the structures of each Ca^{2+}-bound domain determined in solution from NMR data by Chou and colleagues (pdb files 1J7O and 1J7P for N- and C-terminal domains, respectively [23]). Residues in the center of the inter-domain helix were described as dummy residues with variable positions. These dummy residues were substituted by a full-atom description using the program PD2 [24]. At this point, the Gajoe program was used to select ensembles of conformations, the average scattering pattern of them being fitted against our experimental data using a genetic algorithm. Fig 3D shows a typical ensemble of conformations that yields a good fit to the experimental data ($\chi^2 = 2.15$, red curve). This ensemble of conformations illustrates that CaM is made of two folded lobes connected by a highly flexible hinge.

Pepsin digestion of CaM yielded 64 unique peptides, covering approximately 88% of the protein sequence. From these, 20 peptides were selected for HDX-MS analysis (S3 Fig). The dynamic HDX-MS pattern of the isolated CaM protein is typical of a folded protein (Fig 4A, S4 Fig and S3 Data). Notably, however, the central part of the inter-lobe helix (residues 66–92, represented here by peptide 74–85) is fully exchanged, indicating that these residues do not adopt a stable helical conformation but rather behave as a flexible link between the N-terminal

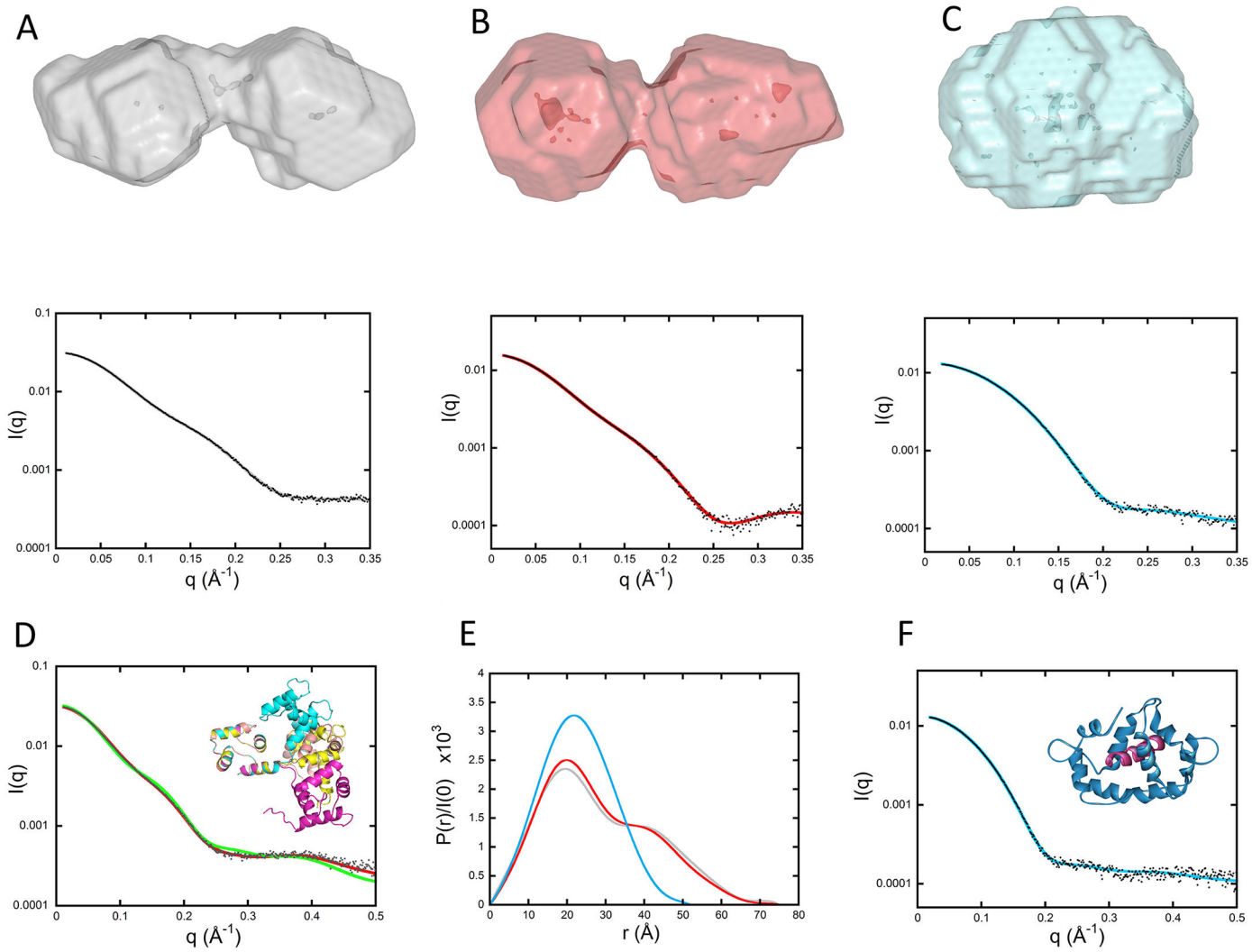

Fig 3. SAXS envelopes of CaM alone and in the presence of H-helix and P_{MLCK} peptides. (A, B, and C [top panels]) DAMMIN models of CaM alone, CaM:H-helix, and CaM:P_{MLCK} complexes, respectively. (A, B, and C [bottom panels]) Corresponding fits (color curves) to experimental data (black dots). (D) Green curve: comparison of experimental data (black dots) to the scattering pattern of the crystal structure of CaM (pdb 1CLL) calculated using Crysol. Red curve: fit obtained using the program EOM and corresponding to the ensemble of four conformations shown in the inset after superimposition of the N-terminal domain of each conformation. (E) Comparison of the three distance distribution functions obtained using the program GNOM for CaM alone (grey), CaM:H-helix (red), and CaM-P_{MLCK} (cyan) complexes. (F) Comparison of experimental data (black dots) to the scattering pattern of the crystal structure of CaM: P_{MLCK} (pdb 2K0F shown in the inset) calculated using Crysol (blue line). The P_{MLCK} peptide is shown in purple. CaM, calmodulin; EOM, Ensemble Optimization Method; pdb, Protein Data Bank; P_{MLCK}, myosin light-chain kinase peptide; SAXS, small-angle X-ray scattering.

https://doi.org/10.1371/journal.pbio.2004486.g003

domain of CaM (N-CaM) and C-CaM. The α-helical structural content of the isolated CaM protein inferred from SR-CD experiments (S2 Fig, S2 Table, and S2 Data) is 51 ± 3%. This is, however, significantly lower than that observed in the CaM X-ray structure (62%) and most likely due to the disordered segment within the central part of the inter-lobe helix observed in our HDX-MS results.

CaM:H-helix complex

The H-helix region of AC represents the primary site of interaction with CaM, as seen in the crystal structure of AC with C-CaM [7]. Accordingly, the complex of CaM with the H-helix

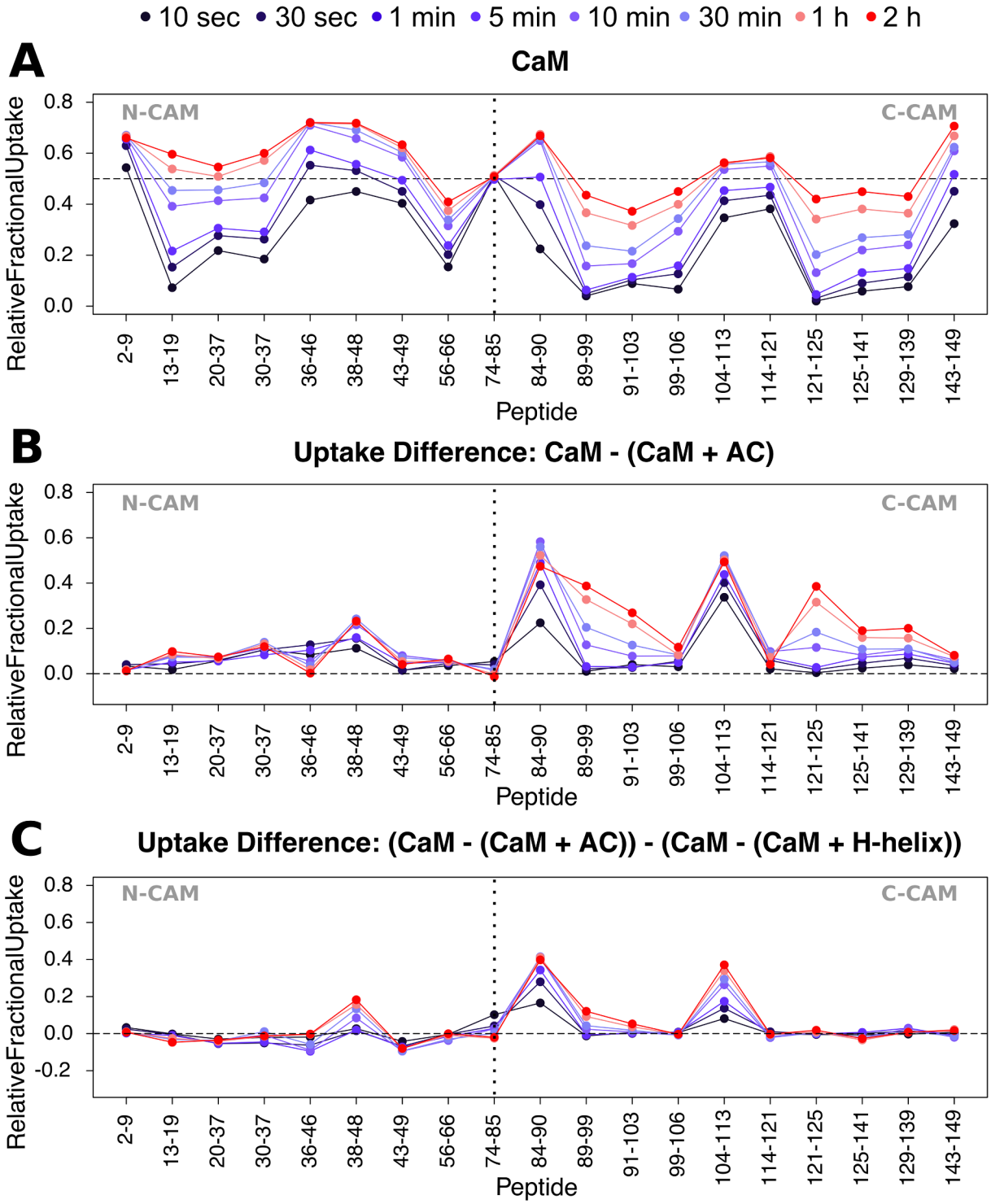

Fig 4. Differential HDX-MS patterns within CaM upon H-helix and AC binding. (A) Relative fractional exchange data were calculated at each point and plotted as a function of peptide position for full-length CaM. (B) Uptake difference plot for CaM in the presence of AC. AC-induced differences in deuterium exchange are principally located in C-CaM. (C) Uptake "difference of uptake differences" plot of CaM in the presence of AC and H-helix peptide. Addition of the full-length catalytic domain results in much greater differences in the deuteration of both N- and C-CaM compared to the H-helix region alone, e.g., in peptides 84–90 and 104–113. Uptake plots of all CaM peptides selected for final HDX-MS analysis are given in S11 Fig. The data used to generate the figure can be found in S3 and S4 Data. AC, adenylate cyclase catalytic domain; C-CaM, C-terminal domain of CaM; CaM, calmodulin; HDX-MS, hydrogen/deuterium exchange mass spectrometry; N-CaM, N-terminal domain of CaM.

https://doi.org/10.1371/journal.pbio.2004486.g004

peptide was investigated in parallel. This allowed us to decipher those additional regions of AC that are involved in AC:CaM complex formation and stabilization. Although the joint presence in solution of both 1:1 and 1:2 CaM:H-helix peptide complexes severely limits modeling attempts, ab initio modeling indicated that the global dumbbell shape of CaM was not altered in the complex, as shown in Fig 3B, which presents a typical envelope obtained with DAMMIF/DAMMIN. This is clearly apparent when examining the two distance distribution functions P(r) that exhibit similar maximal extensions with or without the H-helix peptide bound (Fig 3E). These data suggest that H-helix peptide binding does not cause any significant modification of the CaM dumbbell shape and its inter-domain helix.

Far-UV SR-CD indicates that more than 20 amino acids undergo a disorder-to-helix transition upon CaM:H-helix complex formation (S2 Fig, S4 Table and S2 Data). The binding of the H-helix peptide does not create any additional dynamic HDX-MS activity within CaM (S4 Fig and S4 Data). Consequently, the observed increase in helical content can be attributed to the disorder-to-order transition within the H-helix peptide itself. The H-helix peptide appears to stabilize the C-CaM helices of CaM (Fig 4C and S4 Fig) and to acquire a helical conformation upon CaM binding (S2B Fig, S2 and S4 Tables).

CaM:P_{MLCK} complex

Ab initio modeling of SAXS data indicated that the global dumbbell shape of CaM was not altered upon binding of the H-helix peptide. We therefore undertook equivalent experiments on the CaM protein in complex with the myosin light-chain kinase peptide (P_{MLCK}), which is known to reshape CaM from its extended dumbbell conformation into a compact globular structure. In marked contrast to the H-helix peptide, the shape of the CaM:P_{MLCK} complex determined ab initio using the programs DAMMIF/DAMMIN was clearly globular and isometric (Fig 3C). Noticeably, the experimental scattering curve of CaM:P_{MLCK} is very similar to the scattering pattern calculated from the known crystal structure of this complex (2K0F.pdb) (Fig 3F), in which the two domains of CaM are wrapped around the P_{MLCK} peptide. Altogether, these SAXS studies confirm the distinct modes of interaction of CaM with the H-helix peptide of AC and the P_{MLCK} peptide from MLCK. This difference is also clearly evident when comparing the distance distribution functions P(r) (Fig 3E): CaM:P_{MLCK} exhibits a bell-shaped curve with a single maximum, while the CaM:H-helix profile presents an extra shoulder characteristic of a two-domain structure.

Finally, P_{MLCK} binding exerts a more pronounced reduction in solvent accessibility than the H-helix throughout the full-length CaM protein, with both N- and C-CaM lobes affected (S5 Fig and S5 Data). However, the linker connecting both domains remains solvent exposed throughout, as previously observed with both the H-helix peptide and the full-length AC domain.

AC-CaM complex in solution

The HDX-MS data indicate that the binding of CaM induces several statistically significant ($p \leq 0.01$) changes in AC (Fig 2A and 2D and S1 Data). Globally, the N-terminal moiety is stabilized, while the C-terminal domain now exhibits several regions characterized by HDX dynamic patterns, indicative of secondary structure acquisition within T18. The main effects in the N-terminal part of AC are the stabilization of both B- and C-helices and of the embedded T25 antiparallel beta-sheet (peptides 25–39, 46–61, and 192–201), as highlighted in Fig 2B. These structural elements become completely resistant to deuteration over the experimental timescale (Fig 2A and 2C). The internal loop (51–68), which was fully accessible in the isolated AC, exhibits a dynamic HDX-MS behavior in AC:CaM. In contrast, the regions corresponding

to the G-helix as well as the Hom-loop are unaffected by CaM binding, suggesting that these solvent-exposed regions in the isolated AC protein remain accessible throughout (Fig 2A–2C). Upon complex formation, the majority of the C-terminal half of AC acquires secondary structure elements, except the catalytic loop (residues 304–315 from CR3), which remains completely solvent exposed. Most notably, the regions encompassing the H/H′-helices and T18b1, which were fully exposed in AC alone, are structured in the presence of CaM (see dynamic HDX behavior in Fig 2A–2C). The I- and J/J′-helices, which were already structured in the absence of CaM, are further stabilized, as evidenced by the observed reduction in deuteration level.

Reciprocally, we examined the consequences of AC binding for CaM structural dynamics. HDX-MS data show that AC binding induces a strong stabilization of C-CaM, as evidenced by the dramatic reduction in accessibility imposed by the wrapping of C-CaM helices around the H-helix region of AC (Fig 4B and S6 Fig). The loop between the first two helices, H5 and H6, of C-CaM is also significantly stabilized, likely via interactions with the J/J′-helices and the C-terminal loop of AC. The involvement, beyond the CBS-containing H-helix, of various regions of AC in CaM stabilization is best illustrated by the "difference of uptake differences" plot (Fig 4C). In contrast, the majority of N-CaM is unaffected, besides peptide 38–48, which covers the loop connecting helices H2 and H3. Notably, the central part of the inter-lobe helix of CaM is also unaffected by AC binding and remains solvent exposed upon complex formation.

Finally, we recorded the far-UV SR-CD spectrum of the AC-CaM complex (S2 Fig) to estimate the CaM-induced helical content increase of AC. Assuming a constant helical content of CaM, we derive for AC an increase in its helical content from 27% to 42 ± 3% upon CaM binding (S2–S4 Tables). This increase, corresponding to about 40 amino acids (S3 Table), is proposed to be primarily due to the CaM-induced folding of the H/H′ regions, as reported by the HDX-MS results (Fig 2).

The first modeling attempt of the AC-CaM complex from our SEC-SAXS data made use of the BUNCH program, which considers that the particle adopts a unique conformation in solution and searches for one conformation that yields a good fit to the experimental data. More specifically, AC and each CaM domain were handled as rigid bodies while the program searched an optimal conformation of the inter-domain helix of CaM, the only variable part of the complex. We started from the crystal structure 1YRU of the complex of AC with the C-CaM and the solution structure 1J7O of the N-CaM. Furthermore, the central residues of the inter-domain helix were described as dummy residues, the positions of which were varied by the program in order to adjust the calculated scattering pattern to experimental data. We made one change to the 1YRU structure based on our experimental HDX-MS data: residues 200–234, corresponding to helices F and G together with the disordered Hom-loop, remain unfolded in the AC:CaM complex. Indeed, examination of the crystal structure and of its contacts with neighboring molecules shows that these two helices are interacting with their counterpart from an adjacent molecule within the crystal. Moreover, these residues are not predicted to adopt a helical conformation by secondary structure predictions. Accordingly, we assumed that the two helices are strongly stabilized within the crystal but may only transiently exist in solution. Therefore, we released the position of residues 200–234 of AC so that this stretch was also variable during the refinement process. Thirty runs of the program BUNCH yielded models similar to that shown in S7 Fig. The corresponding fit to the experimental data is also shown in S7 Fig ($\chi^2 = 2.0$). Noticeably, the N-CaM is immersed in the solvent at a distance from the rest of the complex, without any contact with AC (S7 Fig).

The high flexibility of the central CaM linker suggests that a better description of the complex would make use of an ensemble of conformations (as opposed to a unique structural model). Accordingly, we undertook a second round of complex modeling using the program

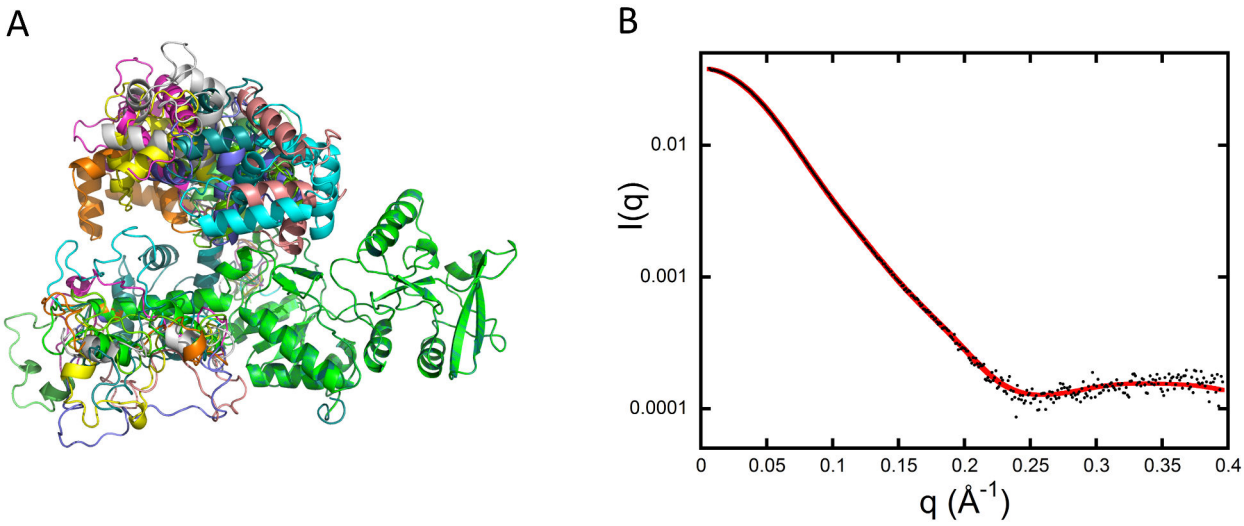

Fig 5. Modeling of the AC:CaM complex. (A) Typical ensemble of conformations describing the AC:CaM complex, obtained using the program EOM and displayed after superimposition of the AC moiety of each conformation (green) (see main text for details). (B) Corresponding fit (red curve) to experimental data (black dots). AC, adenylate cyclase catalytic domain; CaM, calmodulin; EOM, Ensemble Optimization Method.

https://doi.org/10.1371/journal.pbio.2004486.g005

EOM. The 10,000 conformations of the initial pool differ in the relative position of the two CaM domains as well as in the conformation of the region 200–234 of AC. An example of the resulting ensemble of conformations is displayed in Fig 5A, with the corresponding fit to the SAXS data shown in Fig 5B ($\chi^2 = 1.41$). Interestingly, the SAXS data are compatible with a description of the complex in which the flexibility of the CaM inter-domain helix makes possible transient interactions of the CaM N-terminal domain with AC, as suggested by the results of HDX-MS experiments (CaM peptide 38–48, see Fig 4B).

Discussion

Exploiting an integrative structural biology approach, the present study proposes detailed and novel structural descriptions of the catalytic AC domain of the CyaA toxin, both in isolation and in the presence of its activator, CaM, and describes how specific conformational rearrangements within each molecule may be requisite to trigger the enzymatic activity. The isolated AC protein appears significantly less folded in solution than in the crystal structure of the AC:C-CaM complex [7]. Although the N-terminal T25 domain is folded, the C-terminal T18 moiety contains few structural elements: most noticeably, HDX-MS identifies a large region of 75 amino acids (residues 201–275) in T18, which is predominantly structurally disordered. This IDR includes the H-helix region, which is the main CBS of AC, as well as its flanking regions, namely the Hom-loop and the F-, G-, and H′-helices (Fig 6A). This is in agreement with prior studies that showed that the isolated AC domain is partially folded [25–27].

AC:CaM complex formation primarily takes place between the H/H′-helix region of T18 and C-CaM, inducing the folding of T18 as well as establishing long-distance stabilization of structural elements within the T25 moiety (Fig 6B and 6C, S8 and S9 Figs; [7, 28–30]). The SR-CD and HDX-MS data of both AC:CaM and H-helix:CaM complexes strongly suggest that CaM binding triggers the folding of the H- and H′-helices (S1–S4 Tables). However, the area upstream of the H-helix region clearly remains highly flexible in the AC:CaM complex. Several regions of T18, including the I- and J/J′-helices (residues 273–290 and 331–344, respectively)

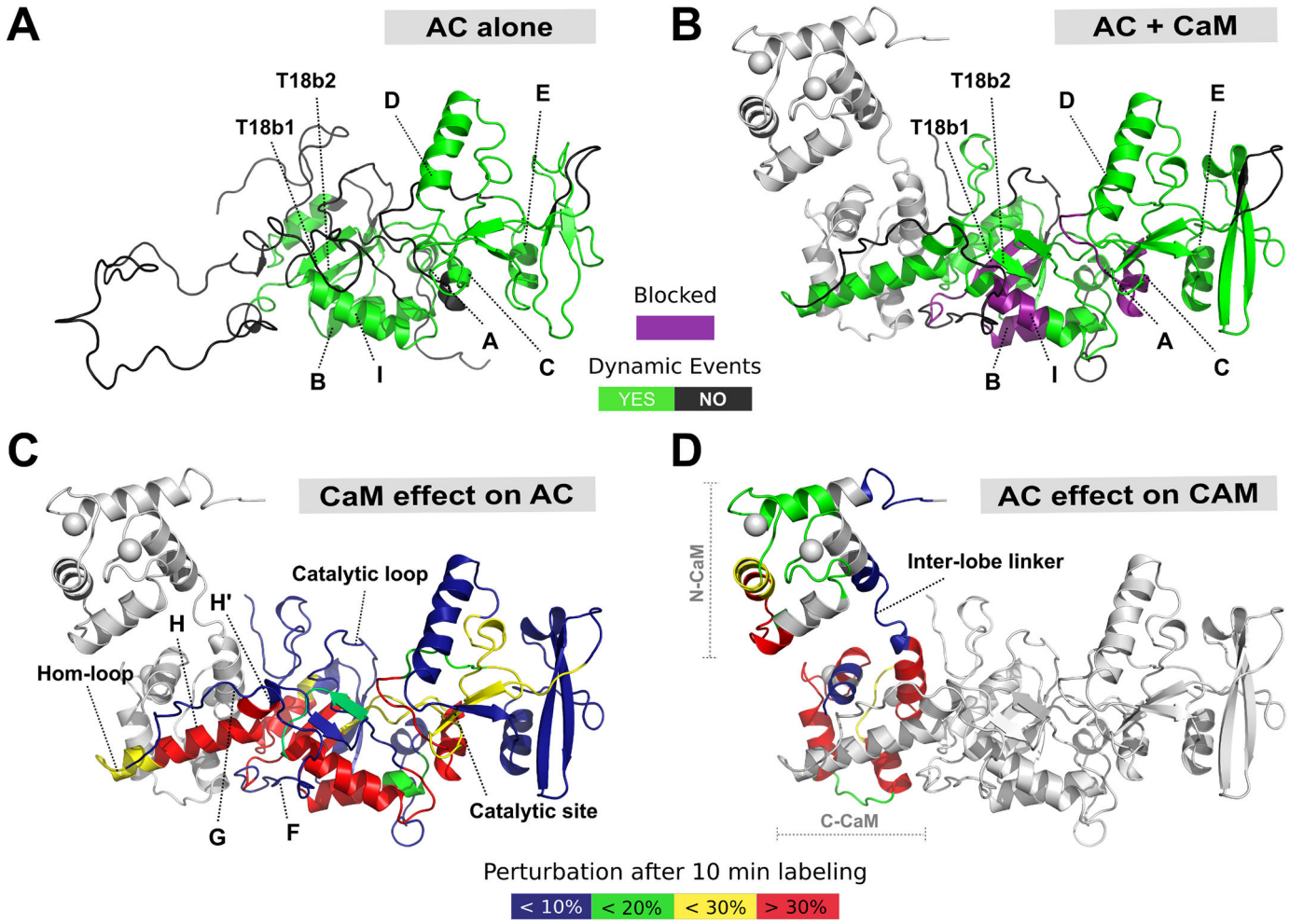

Fig 6. The structural interplay of AC and CaM complex formation. Specific regions within the AC T18 domain serve as a MoRF for CaM recognition, binding, and activation of AC itself. (A) In the absence of CaM, the F-, G-, H-, and H′-helices and Hom-loop are found as an extended disordered coil, acting as a bait for CaM capture. (B) An interplay between protein structural disorder and order is requisite for activation by CaM of AC catalytic function. Upon CaM binding, the H- and H′-helices undergo extensive structure formation, resulting in a conformation that is appropriate for catalytic activation. Helices F and G and the Hom-loop remain unstructured throughout. Some regions become "blocked" and resistant to deuteration (highlighted in purple). (C) The effect of CaM binding on AC. (D) The effect of AC on CaM. CaM binding to AC results in widespread perturbations, primarily within the T18 region of the protein, while AC primarily binds to C-CaM, with only a transient interaction in N-CaM. In addition to those effects occurring in the H/H′ region, long-range allosteric remodeling is observed at the site of catalysis, which becomes more stable and rigid. Meanwhile, the catalytic loop does not undergo any dramatic structural rearrangement, remaining unstructured and exposed regardless of CaM availability. This is suited to a maximal turnover of ATP substrate and thus maximal toxicity in the form of cAMP production. The data used to generate the figure can be found in S1, S3 and S4 Data. AC, adenylate cyclase catalytic domain; C-CaM, C-terminal domain of CaM; CaM, calmodulin; MoRF, molecular recognition feature; N-CaM, N-terminal domain of CaM; T18, C-terminal trypsin-cleavage fragment of CyaA (amino acids 225–364); T18b1, first beta-sheet of the T18 fragment; T18b2, second beta-sheet of the T18 fragment.

https://doi.org/10.1371/journal.pbio.2004486.g006

as well as the C-terminal LHL motif (residues 345–358, which interact with the AC catalytic loop [8]) are significantly stabilized upon CaM binding. These different interactions may contribute to the shaping of the catalytic site through the correct positioning of the CR3 loop, which directly interacts with the purine moiety of the ATP substrate. CaM binding also induces significant modifications in the T25 region of AC, including the B- and C-helices, and the conserved catalytic regions CR1 and CR2, which contact the ribose and triphosphate moieties of ATP [7] (Figs 2 and 6). In contrast, the G-helix region remains highly flexible in the AC: CaM complex in solution, and it is likely that the helix is stabilized in the crystal structure of

AC:CaM through interactions with its counterpart in symmetry mates. Our experimental SAXS data are indeed fully compatible with AC:CaM models in which all AC residues from 200–234 remain largely disordered.

The significant level of structural disorder observed in AC alone, with a large IDR of about 75 residues, has major implications for the biological functions of the molecule. In the first instance, the IDR and global structural disorder of the T18 moiety may contribute via an "entropic chain effect" to destabilizing the catalytic site and thus preventing cAMP synthesis in the absence of the activator—most importantly, at the time of CyaA production in *B. pertussis*, when any significant basal activity would be deleterious to the bacterial host, as illustrated by the high toxicity observed when CaM and AC are co-expressed in recombinant *Escherichia coli* [31]. Secondly, the weak stability of significant parts of the AC structure is favorable for toxin delivery from the bacterial host to eukaryotic target cells. CyaA is secreted outside the bacteria by a type I secretion system (T1SS), and then, upon binding to target cells, AC is delivered across the plasma membrane to reach the eukaryotic cell cytosol [32]. There is evidence to suggest that both the secretion through the T1SS and the translocation across the eukaryotic cell membrane are critically dependent upon the ability of the polypeptide chain to adopt partially unfolded states [5, 33–36]. The disordered region and overall low structural content of AC in solution should clearly facilitate these key steps of the intoxication process. Thirdly, the intrinsic disorder of the central region of AC, which harbors the main CBS, namely the H-helix, potentially plays a crucial role in molecular recognition of the activator [37, 38]. Indeed, the CBS located within the IDR of AC (see the long loop in Fig 6A) exemplifies the canonical properties of so-called molecular recognition features (MoRFs) or short linear motifs (SLIMs), which are short and conserved motifs involved in recognition (in silico analysis in S8 Fig). MoRFs often comprise a few hydrophobic residues amidst charged residues and are frequently embedded within IDRs that serve as flexible linkers to efficiently expose the MoRFs to the solvent, thereby favoring their potential interactions with partner biomolecules [37]. The MoRF in AC is typical of eukaryotic CaM-binding targets: it is 10–20 residues long and is flanked by disordered regions, with a high net charge and a propensity for structural disorder in the CaM-free state (S8 Fig). Moreover, it undergoes a disorder-to-helix transition upon complex formation [39]. Such coupled binding and folding processes appear to be a common mechanism by which CaM activates its target enzymes, including, for example, the CaM-dependent protein kinases and calcineurin [40]. The AID of these latter proteins occludes access to the catalytic site in the resting state. A CaM-induced conformational change physically shifts the AID from the enzymatic site, allowing catalysis. In the case of AC, the structural disorder of the catalytic site induced by the IDR replaces the steric hindrance of the AID.

Once AC has been delivered across the target cell plasma membrane, the long IDR may facilitate the efficient capture of the intracellular CaM through a "fly-casting" mechanism [9]. CaM binding promotes folding of the H/H′ region and stabilization of several structural elements of T18 (Figs 2 and 6). The reduction of disorder is then propagated to the core of the T25 domain to allosterically stabilize other key regions shaping the catalytic site (Fig 6B and 6C). This suggests that the overall dampening of disorder triggered by CaM-binding is crucial for AC activation. Interestingly, our HDX-MS data indicate that, although CaM binding imposes a strong entropy reduction and steric restrictions on regions flanking the CR3 catalytic loop, the loop itself (residues 300–314) remains largely dynamic and solvent exposed, as indicated by the rapid and high deuterium uptake (S10 Fig). The high flexibility and structural dynamics of this catalytic loop that binds the purine ring of ATP are likely crucial for the efficient catalysis of AC, which has a turnover number higher than 1,000 s^{-1}, i.e., one ATP converted to cAMP in less than a ms.

A striking property of AC is that it is fully activated by the C-terminal lobe of CaM, with an affinity that is only 10–20-fold lower than that of the full-length CaM protein [7]. As only the structure of AC in complex with C-CaM has been reported thus far, the structure and mode of interaction of AC with the full-length CaM molecule has remained elusive. Our HDX-MS analysis indicates that the C-CaM lobe is strongly stabilized upon complex formation (Fig 6D and S11 Fig), while the N-CaM domain remains mostly dynamic and essentially unaffected by the presence of AC (Figs 4 and 5). This is in good agreement with the Springer and colleagues NMR study, which also showed that AC binding primarily affects C-CaM, with minimal structural changes to N-CaM [41]. Notably, when bound to either AC or the H-helix peptide, CaM remains in an extended conformation (Figs 3 and 5), with high flexibility of the central CaM inter-lobe helix (Fig 4, S4 and S6 Figs). Our SAXS data are in excellent agreement with structural models in which CaM interacts with AC essentially via its C-terminal lobe, while its N-terminal lobe, connected through the flexible central linker region (residues 77–83), remains highly dynamic, without establishing stable contacts with AC (Fig 5), although transient interactions are likely, as suggested by both our EOM analysis of SAXS data and our HDX-MS results. Interestingly, these models are reminiscent of those proposed by Guo and colleagues [30] on the basis of molecular dynamics simulations, although these authors further suggested that the β-hairpin region (residues 259–273) of AC directly contacts the second calcium-binding motif of the extended CaM. To probe this model, the group performed cross-linking experiments between AC and CaM variants harboring a unique cysteine at positions 260 and 50, respectively (AC-Q260C and CaM-D50C). However, only a very faint disulfide bond cross-link was detected, indicating that the proposed conformations with the two cysteines in proximity are weakly populated in solution. From our point of view, these data support the view of a fairly dynamic N-CaM lobe that samples a variety of conformations, restricted only by the flexibility of the central hinge (Fig 4). How the N-CaM lobe may contribute to the 10–20-fold higher affinity of native CaM as compared to that of C-CaM [42, 43] remains an intriguing question. One attractive hypothesis could be that the mere presence of the N-CaM module, acting as a "local crowder," may stabilize the complex by restricting the conformational dynamic of the AC polypeptide chain (mainly the T18 region). Additional stabilization may also be provided by global electrostatic interactions between the overall negatively charged N-CaM and the positively charged cluster of residues around 221–224 of AC [29].

Interestingly, our combined SAXS, HDX-MS, and SR-CD analyses also show that the CaM dumbbell shape [44, 45] is not significantly modified upon binding to the AC H-helix peptide. This is in marked contrast to what is observed with the classical CaM-binding peptide from MLCK, P_{MLCK} (Fig 3), around which both N- and C-CaM are seen to wrap in a conformation that requires a sharp bending of the CaM central helix (Fig 3C, S5 and S12 Figs) [46]. The ability of individual N- and C-terminal lobes of CaM to independently associate to either distinct sites on the same protein or to the same site on two distinct polypeptides, thus facilitating their dimerization, have been described for numerous CaM targets, although in many instances, the affinity of individual lobes with their target sequence is lower than that with the AC H-helix. Our data further highlight the remarkable conformational diversity of CaM upon binding to its targets [44–49].

Conclusions

In the bacterial cytosol, there is no chaperone, inhibitor, or antitoxin available to prevent cAMP production, and thus we propose that structural disorder acts as the inhibitor of CyaA catalytic activity. Once translocated into eukaryotic cells, bacterial toxins such as CyaA hijack CaM, which is used as a disorder dampener to activate the enzyme. The disorder-to-order

transition observed in the MoRF region of AC is not directly involved in catalysis but rather transduces the stabilization toward the enzymatic region. This CaM-induced folding and stabilization, from local to distal regions, allosterically tunes the enzymatic activity of bacterial toxins.

Materials and methods

Buffer A composition is 20 mM HEPES, 150 mM NaCl, pH 7.4, and 2 mM (HDX-MS and SR-CD experiments) or 4 mM (SEC-SAXS experiments) $CaCl_2$ (final calcium concentration), unless otherwise stated.

Protein production and purification

The H-helix peptide corresponds to residue numbers 234–254 of AC (LDRERIDLLWKIARAGARSAVG). H-helix peptide molecular mass deduced from mass spectrometry (MS) was 2,509 g/mol, its pI was 11 and it contained +2 charges at neutral pH, and its molar epsilon at 280 nm was 5,600 M^{-1} cm^{-1}. The CaM-binding peptide (P_{MLCK}) from the smooth muscle MLCK corresponds to residues RRKWQKTGHAVRAIGRLSS (Em: 5,600 M^{-1} cm^{-1}). All peptides contain an N-terminal acetyl and C-terminal amide as capping groups. All peptides were purchased from Genosphere Biotechnologies (Paris, France).

Human CaM protein was produced in *E. coli*, as previously described [27]. MS confirmed the integrity and identity of all proteins in the study. MS analysis of CaM gave a single peak of 16,706.25 Da (expected mass = 16,706.30 Da). A molar epsilon at 280 nm of 2,980 M^{-1} cm^{-1} and a pI of 4.1 were derived from the CaM sequence using ProtParam.

The adenylate cyclase catalytic domain (AC) toxin under investigation corresponds to residues 1–364 of *B. pertussis* CyaA. The protein was produced in *E. coli* and purified as follows: protein-containing inclusion bodies from the bacterial cell pellet were resuspended in 6 M GdnHCl, 20 mM HEPES, pH 7.4, overnight at 4˚C, and then buffer exchanged from 6 M GdnHCl to 6 M urea on prepacked G25SF desalting columns. Inclusion body solubilization was performed in GdnHCl instead of urea to prevent AC364 carbamylation. AC364 was purified by two successive chromatographic separations on DEAE-Sepharose [4]. The protein was initially eluted in 8 M urea, 20 mM HEPES, and 500 mM NaCl, pH 7.4, followed by a second elution in 20 mM HEPES and 100 mM NaCl, pH 7.4. AC364 was further purified on a Sephacryl S200 column equilibrated with Buffer A and concentrated on an Amicon 10 kDa MWCO filter. The identity and purity of protein batches was monitored by SDS-PAGE and MS. AC364 gave a single MS peak of 39,380.90 Da (expected mass = 39,381.50 Da). A molar epsilon at 280 nm of 28,880 M^{-1} cm^{-1} and a pI of 6.2 were derived from the AC364 sequence. All proteins and peptides, whether in solution or lyophilized, were stored at −20˚C.

HDX-MS

Sample preparation. Five experimental conditions were analyzed. In the first instance, AC was incubated in both the presence and absence of a twofold molar excess of CaM. Furthermore, CaM was incubated alone or in a twofold molar excess of either H-helix or P_{MLCK} peptide. The excess of peptide or protein ensured that all complexes were fully formed and maintained over the labeling reaction (AC:CaM $K_D < 0.1$ nM, P_{MLCK}:CaM and H-helix:CaM K_D are in the nM range). Prior to addition of the deuterated buffer, all solutions were equilibrated for 1 h at room temperature. Continuous labeling was performed at 20˚C for $t = 0.16$, 0.5, 1, 5, 10, 30, 60, 120, and 240 min in D_2O containing Buffer A. A D_2O/H_2O ratio of 80:20% was selected such that the kinetics favored unidirectional exchange. Aliquots of 10–20 pmol of protein were withdrawn at each time point and quenched upon mixing of the deuterated

sample with ice-cold 0.5% formic acid solution to achieve a final pH of 2.5. Quenched samples were immediately snap frozen in liquid nitrogen and stored at −80˚C for approximately 12 h. Undeuterated controls were treated using an identical procedure. All MS-analyses were performed in triplicate for each time point and condition.

HDX-MS data acquisition. Prior to MS analysis, samples were rapidly thawed. To minimize back exchange, the LC solvent line, injection valve, columns, and sample loop were maintained at 0˚C. To achieve this, HDX-MS analyses were performed with the aid of a cooled HDX Manager (Waters Corporation, Milford, MA). Labeled samples were digested using an in-house prepared cartridge of immobilized pepsin beads (Thermo Scientific, Rockford, IL) for 2 min at 70 μL/min and 20˚C. Peptic peptides were rapidly desalted, as described above, using a VanGuard C18 pre-column (1.7 μm, 2.1 × 5 mm; Waters) and separated using an ACQUITY UPLC BEH C18 column (1.7 μm, 1 × 100 mm). AC and CaM peptides were separated over an 8-min gradient of 5%–40% acetonitrile (ACN) at 40 μL/min and at 0˚C. After each run, the pepsin column was manually cleaned with two washes of 0.8% formic acid, 5% ACN, 1.5 M guanidinium chloride, pH 2.5. Blank injections were performed after each sample to confirm the absence of carryover. The LC flow was directed to a Synapt G2-Si HDMS mass spectrometer (Waters), which was equipped with ESI and lock-mass correction using Glu-Fibrinogen peptide (100 fmol/μL in 50% ACN). Mass spectra were acquired in positive-ion and resolution mode over the m/z range of 50–1,800 using a data-independent acquisition scheme (MS^E), whereby exact mass information is collected at both low and high collisional energies for collisional-induced dissociation. For local-level analysis, unlabeled AC and CaM samples were digested in triplicate to obtain a peptide coverage map of both proteins.

HDX-MS data processing. Peptide identification was via the Protein Lynx Global Server (PLGS) 3.0 (Waters Corporation). Oxidation of methionines and carbamylation of N-terminal and lysine residues were set as variable modifications. The sequence coverage map was plotted using DynamX 3.0 HDX software (Waters Corporation). D_2O uptake at the peptide level was extracted and visualized in DynamX; only one charge state was considered per peptide. No adjustment was made for back exchange, and the results were reported as relative deuterium exchange levels expressed in either mass unit or fractional exchange. Fractional exchange data were calculated by dividing the experimentally measured uptake by the theoretically maximum number of exchangeable backbone amide hydrogens that could be replaced within each peptide. This number corresponds to the number of amino acid residues present in the peptide minus the number of proline residues and minus one for the N-terminus that back exchanges too rapidly to be measured by MS [50]. HDX-MS results were further analyzed using mixed-effects model for HDX experiments (MEMHDX), using a Wald test ($p < 0.01$) and with a false discovery rate (FDR) of 1% [51].

Small angle X-ray scattering

Data acquisition. X-ray scattering data were collected at the SWING beamline of the SOLEIL Synchrotron (Saint-Aubin, France). All measurements were performed using a size-exclusion HPLC column (Agilent BioSEC-3, 300 Å, 4.6*300 mm) online with the SAXS measuring cell, a 1.5-mm diameter quartz capillary contained in an evacuated vessel [52]. The sample to detector distance was 1,988 mm, allowing useful data collection in the q range 0.006 $Å^{-1} < q < 0.5$ $Å^{-1}$, for which $q = 4\pi\sin\theta/\lambda$, 2θ is the scattering angle, and $\lambda = 1.00$ Å, the wavelength of the X-rays. We first studied solutions of isolated AC364 and CaM proteins. We then examined solutions of CaM in complex with either H-helix peptide (both 5:1 and 3:1 ratios of peptide:CaM), P_{MLCK} (3:1 ratio of peptide:CaM), or AC364 (1:2 and 1:4 ratios of AC364:CaM). All proteins were analyzed in Buffer A. Scattering of the elution buffer before void volume was

recorded and used as buffer scattering for subtraction from all protein patterns. Successive frames of 1 s were recorded and separated by a 0.5-s interval. The elution flow of 0.200 mL/min ensured that no protein was irradiated for more than 0.4 s. For each frame, the protein concentration (about 1–2 mg/mL at the top of elution peak) was estimated from UV absorption at 280 and 295 nm using a spectrometer located immediately upstream of the SAXS measuring cell.

Data analysis. Scattered intensities were put on an absolute scale using water scattering. SAXS data were normalized to the intensity of the incident beam and background subtracted using the programs FoxTrot (courtesy of SWING beamline) and Primus (https://www.embl-hamburg.de/biosaxs/primus.html) [53]. Identical frames under the main elution peak were selected using Cormap [54] and averaged for further analysis. The R_g was evaluated using the Guinier approximation [55] and also derived from the distance distribution function P(r) calculated by the program GNOM [56]. Two independent determinations of the molecular mass were obtained using the programs SAXSMow2 and ScÅtter, available at URLs http://saxs.ifsc.usp.br/ and https://bl1231.als.lbl.gov/scatter/, respectively. A third determination was also obtained from the value of I(0)/c, in which c is the protein concentration for the two samples containing AC364. This could not be generated for the CaM, CaM:H-helix, and CaM-P_{MLCK} samples, as CaM does not possess any tryptophan. The molecular mass of the CaM/H-peptide complex derived from the SAXS data was intermediate between that of the 1:1 and that of the 1:2 complex. This was confirmed by the estimate of the stoichiometry derived from the amount of free H-helix peptide eluting from the column using the 280-nm elution profiles of the CaM:H-helix complex, CaM alone, and the H-helix peptide alone. A 1:1 stoichiometry was observed for the CaM:P_{MLCK} complex, as judged from the SAXS-derived molecular mass.

Modeling

Ab initio shape determination. Regarding CaM and its complexes with H-helix and P_{MLCK} peptides, the structural effect of peptide binding was investigated by determining the shape or envelope of each scattering particle. For all three systems, 20 shapes were determined using the ab initio program DAMMIF [20] and compared using the DAMAVER suite of routines based on the calculation of the normalized spatial discrepancy (NSD), which is lower than 0.7 if all 20 models are similar. The final envelope is obtained using DAMMIN [57], which uses the envelope of all superimposed DAMMIF models (the union of all models) as initial volume.

Rigid-body modeling. All scattering patterns calculated from atomic coordinates were obtained using CRYSOL [58]. AC alone was first modeled using its crystal structure in complex with C-CaM [7]. The scattering pattern was calculated using AllosModFoxs [11], which refines the position of missing residues. For the sake of consistency, the scattering intensities of the resulting models were recalculated using CRYSOL. The complex of AC with CaM was modeled using the BUNCH program [59]. Starting from the crystal structure of AC:C-CaM (1YRU), the program refines the position of the N-CaM domain by modifying the position of the central linker residues so as to fit the data. Modifications to 1YRU were authorized in the 200–234 stretch of AC (helices F and G), a region that appears to be essentially disordered in HDX-MS studies.

Ensemble of conformations. Finally, CaM and AC:CaM were modeled in terms of an ensemble of conformations using the program EOM [22]. The routine Ranch first creates a large pool of 10,000 conformations by varying the conformation of the central linker of CaM (hence, the position of the N-CaM domain) and that of the stretch 200–234 of AC (in the case

of the complex). The subsequent Gajoe routine determines ensembles of conformations from the pool, the average scattering pattern of which fits our experimental data.

SR-CD

SR-CD experiments were carried out at the synchrotron facility SOLEIL (DISCO beamline, Saint-Aubin, France). SR-CD spectra were recorded in the far-UV region from 180–260 nm with an integration time of 1.2 s, a bandwidth of 1 nm with a 1 nm resolution-step at 20˚C in QS cells (Hellma), with a path length of 50 μm. Each far-UV spectrum represents the average of 3 individual scans. Experimental details on the procedure are described elsewhere [33, 35]. Protein and peptide concentrations ranged from 50–200 μM. The far-UV CD spectra were processed using BestSel to estimate the alpha-helical content of proteins, peptides, and complexes [12].

Supporting information

S1 Fig. Peptide map of AC. A sequence coverage map of AC was determined after 2 min digestion with pepsin. Each blue bar represents a single AC peptide. Only those peptides selected for HDX-MS data analysis after filtering the complete dataset are displayed. Linear sequence coverage of 100% was achieved. The secondary structure architecture of AC is as follows: A-helix (residues 11–17), B-helix (residues 20–34), C-helix (residues 44–53), D-helix (residues 89–106), E-helix (residues 116–126), F-helix (198–210), G-helix (214–223), Hom-loop (residues 226–232), H-helix (residues 234–253), H′-helix (residues 255–259), T18b1 (residues 262–270), I-helix (residues 274–289), catalyic loop (residues 300–312), T18b2 (residues 313–325), J-helix (residues 326–340), and an LHL motif (residues 341–364). The catalytic site is made of three highly conserved regions that are directly involved in substrate binding and catalysis: CR1 (residues 54–77), CR2 (residues 184–198), and CR3 (residues 295–315). AC, catalytic domain; CR1, catalytic region 1; CR2, catalytic region 2; CR3, catalytic region 3; LHL, loop-helix-loop; T18b1, first beta-sheet of the T18 fragment; T18b2, second beta-sheet of the T18 fragment.
(PDF)

S2 Fig. Far-UV SR-CD spectra of isolated AC, CaM, H-helix peptide, and their complexes. (A) AC (blue), CaM (red), and AC:CaM complex (dark). (B) H-helix peptide (blue), CaM (red), and H-helix:CaM complex (dark). The buffer is 20 mM HEPES, 150 mM NaCl, 2 mM $CaCl_2$, pH 7.4. kMRE corresponds to MRE × 10^3. AC, adenylate cyclase catalytic domain; CaM, calmodulin; far-UV, far-ultraviolet; MRE, mean residual ellipticity; SR-CD, synchrotron radiation circular dichroism.
(PDF)

S3 Fig. Peptide map of CaM. A sequence coverage map of CaM was determined after 2 min digestion with pepsin. Each blue bar represents a single CaM peptide. Only those peptides selected for HDX-MS data analysis after filtering the complete dataset are displayed. Linear sequence coverage of 87.9% was achieved. CaM, calmodulin; HDX-MS, hydrogen/deuterium exchange mass spectrometry.
(PDF)

S4 Fig. HDX-MS behavior of CaM in the presence of H-helix peptide. Relative fractional exchange data were calculated at each point and plotted as a function of peptide position for CaM and CaM + H-helix. Each dot corresponds to the average of three independent replicates. The fractional uptake difference plot shows the differences in uptake calculated between CaM alone and in the presence of H-helix. Uptake plots of all peptides selected for final HDX-MS

analysis are displayed in S11 Fig. The data used to generate the figure can be found in S4 Data. CaM, calmodulin; HDX-MS, hydrogen/deuterium exchange mass spectrometry.
(PDF)

S5 Fig. HDX-MS behavior of CaM in the presence of P_{MLCK} peptide. Relative fractional exchange data were calculated at each point and plotted as a function of peptide position for CaM and CaM + P_{MLCK} peptide. Each dot corresponds to the average of three independent replicates. The fractional uptake difference plot shows the differences in uptake calculated between CaM alone and in the presence of P_{MLCK}. Uptake plots of all peptides selected for final HDX-MS analysis are displayed in S12 Fig. The data used to generate the figure can be found in S5 Data. CaM, calmodulin; HDX-MS, hydrogen/deuterium exchange mass spectrometry; P_{MLCK}, myosin light-chain kinase peptide.
(PDF)

S6 Fig. HDX-MS behavior of CaM in the presence of full-length AC. Relative fractional exchange data were calculated at each point and plotted as a function of peptide position for CaM and CaM + full-length AC. Each dot corresponds to the average of three independent replicates. The fractional uptake difference plot shows the differences in uptake calculated between CaM alone and in the presence of AC. Uptake plots of all peptides selected for final HDX-MS analysis are displayed in S10 Fig. The data used to generate the figure can be found in S3 Data. AC, adenylate cyclase catalytic domain; CaM, calmodulin; HDX-MS, hydrogen/deuterium exchange mass spectrometry.
(PDF)

S7 Fig. Small angle X-ray scattering of the AC:CaM complex. (A) Calculated scattering curve of the BUNCH model shown in panel (B) (blue line) and experimental data (black dots). (B) Typical model of AC-CaM complex obtained using the program BUNCH. The AC domain is shown in green while CaM is shown in red, interacting through its C-terminal domain (see text for details). AC, adenylate cyclase catalytic domain; CaM, calmodulin.
(PDF)

S8 Fig. Intrinsic disorder prediction within the AC364 protein. AC HDX-MS results upon CaM binding, and regions of predicted disorder within the AC were mapped to the sequence of the protein. X-labeled residues correspond to the site of partner (CaM) binding. Areas of highest solvent protection in the AC correspond to those involved in partner binding and are flanked by regions of structural disorder. Gray areas correspond to those in which CaM does not induce changes in HDX-MS. For the complete nomenclature of secondary structure elements, please see the legend of S1 Fig. AC, adenylate cyclase catalytic domain; CaM, calmodulin; HDX-MS, hydrogen/deuterium exchange mass spectrometry.
(PDF)

S9 Fig. Intrinsic disorder prediction within CaM. CaM HDX-MS results upon AC binding and those residues involved in protein/protein interactions were mapped to the sequence of the protein. Areas of highest solvent protection in the protein correspond to those involved in partner binding, as determined by X-ray Crystallography (X-labels). Gray areas correspond to those in which the AC does not induce changes in HDX-MS, or in which there is a lack of HDX-MS data. AC, adenylate cyclase catalytic domain; CaM, calmodulin; HDX-MS, hydrogen/deuterium exchange mass spectrometry.
(PDF)

S10 Fig. HDX-MS results for individual AC peptides, both from AC in isolation and in complex with CaM. Black indicates the AC alone state, while red indicates AC in complex

with CaM. AC, adenylate cyclase catalytic domain; CaM, calmodulin; HDX-MS, hydrogen/deuterium exchange mass spectrometry.
(PDF)

S11 Fig. HDX-MS results for individual CaM peptides in complex with AC and H-helix peptide. For each peptide, CaM alone is colored black and CaM in the presence of H-helix is colored red, while CaM in the presence of AC is colored blue. AC, adenylate cyclase catalytic domain; CaM, calmodulin; HDX-MS, hydrogen/deuterium exchange mass spectrometry.
(PDF)

S12 Fig. HDX-MS results for individual CaM peptides in complex with P_{MLCK}. Black indicates the CaM alone state, while purple indicates CaM in complex with P_{MLCK}. CaM, calmodulin; HDX-MS, hydrogen/deuterium exchange mass spectrometry; P_{MLCK}, myosin light-chain kinase peptide.
(PDF)

S1 Table. SAXS data collection and scattering derived parameters.

[a] R_g obtained with the Guinier approximation in the range $qR_g < 1$.

[b] The calculated masses were derived from the sequences.

[b1] Corresponds to the 1H:1CaM complex.

[b2] Corresponds to the 2H:1CaM complex.

[c] Calculated from the sequence using the program sednterp, available at http://rasmb.org/sednterp/.

[d] Molecular mass M obtained from the whole I(q) curve (q_{max} = 0.4 $Å^{-1}$) using the SAXS--MoW2 program, available at http://saxs.ifsc.usp.br/.

[e] Molecular mass M obtained from the whole I(q) curve (q_{max} = 0.2–0.25 $Å^{-1}$) using the ScÅtter3 program, available at https://bl1231.als.lbl.gov/scatter/.
These two mass determinations do not depend on the value of the protein concentration, c. In general, they provide a useful complement to the derivation of M from the I(0)/c value but are especially relevant in cases such as CaM, which does not possess any tryptophan. CaM, calmodulin; q, momentum transfer; R_g, radius of gyration; SAXS, small-angle X-ray scattering.
(PDF)

S2 Table. Structural content of the isolated proteins and complexes derived from SR-CD data. The helical content from SR-CD was estimated using the BestSel software [12]. The helical content of AC364 (36%) in the AC:C-CaM complex [7] was computed using DSSP [13, 14]. AC, adenylate cyclase catalytic domain; C-CaM, C-terminal domain of CaM; DSSP, Dictionary of Secondary Structure of Proteins; SR-CD, synchrotron radiation circular dichroism.
(PDF)

S3 Table. Estimation of the CaM-induced helical content increase in AC364 from SR-CD. The helical content increase ("difference in residues" column) provides an estimation of 41 amino acids that undergo a conversion from a disordered to a helical structure. AC364 and CaM contain 364 and 148 amino acids, respectively. CaM, calmodulin; SR-CD, synchrotron radiation circular dichroism.
(PDF)

S4 Table. Estimation of the CaM-induced helical content increase in the H:CaM complex from SR-CD data. Assuming that the helical structure content does not change upon H:CaM complex formation, the number of amino acids in helical conformation would be 80 for a complex of 171 residues, (i.e., 76 + 4 residues from CaM and H-helix peptide, respectively; 47 ± 4% of helices in H:CaM complex). The helical content of the H:CaM complex estimated by BestSel from the SR-CD data is 60 ± 5, corresponding to 102 residues. Therefore, the H:CaM complex formation induces the conversion of approximately 22 residues in helical conformation. CaM, calmodulin; SR-CD, synchrotron radiation circular dichroism.
(PDF)

S1 Data.
(XLSX)

S2 Data.
(XLSX)

S3 Data.
(XLSX)

S4 Data.
(XLSX)

S5 Data.
(XLSX)

Acknowledgments

We acknowledge SOLEIL for provision of synchrotron radiation facilities. We thank Franck Wien for assistance in using the DISCO beamline and for optimized working conditions at DISCO. We thank the staff of the SWING beamline for constant support and help.

SAXS data and structural models

The molecular models and experimental SAXS data have been deposited on Small Angle Scattering Biological Data Bank (SASBDB, http://www.sasbdb.org/aboutSASBDB/) under the SAS codes SASDCK9 and SASDCL9.

Author Contributions

Conceptualization: Dominique Durand, Julia Chamot-Rooke, Patrice Vachette, Sébastien Brier, Daniel Ladant, Alexandre Chenal.

Data curation: Darragh P. O'Brien, Dominique Durand, Patrice Vachette, Sébastien Brier, Alexandre Chenal.

Formal analysis: Darragh P. O'Brien, Dominique Durand, Alexis Voegele, Patrice Vachette, Sébastien Brier, Daniel Ladant, Alexandre Chenal.

Funding acquisition: Julia Chamot-Rooke, Daniel Ladant, Alexandre Chenal.

Investigation: Darragh P. O'Brien, Dominique Durand, Alexis Voegele, Marilyne Davi, Patrice Vachette, Sébastien Brier, Alexandre Chenal.

Methodology: Darragh P. O'Brien, Dominique Durand, Véronique Hourdel, Marilyne Davi, Patrice Vachette, Sébastien Brier, Alexandre Chenal.

Project administration: Sébastien Brier, Alexandre Chenal.

Resources: Dominique Durand, Marilyne Davi, Julia Chamot-Rooke, Patrice Vachette, Daniel Ladant, Alexandre Chenal.

Software: Darragh P. O'Brien, Dominique Durand, Véronique Hourdel, Patrice Vachette, Sébastien Brier.

Supervision: Sébastien Brier, Alexandre Chenal.

Validation: Darragh P. O'Brien, Dominique Durand, Patrice Vachette, Sébastien Brier, Alexandre Chenal.

Visualization: Darragh P. O'Brien, Dominique Durand, Véronique Hourdel, Patrice Vachette, Sébastien Brier, Alexandre Chenal.

Writing – original draft: Darragh P. O'Brien, Dominique Durand, Patrice Vachette, Sébastien Brier, Daniel Ladant, Alexandre Chenal.

Writing – review & editing: Darragh P. O'Brien, Dominique Durand, Patrice Vachette, Sébastien Brier, Daniel Ladant, Alexandre Chenal.

References

1. Ladant D, Ullmann A. Bordetella pertussis adenylate cyclase: a toxin with multiple talents. Trends in microbiology. 1999; 7(4):172–6. PMID: 10217833.
2. Tang WJ, Guo Q. The adenylyl cyclase activity of anthrax edema factor. Mol Aspects Med. 2009; 30 (6):423–30. https://doi.org/10.1016/j.mam.2009.06.001 PMID: 19560485.
3. Guermonprez P, Khelef N, Blouin E, Rieu P, Ricciardi-Castagnoli P, Guiso N, et al. The adenylate cyclase toxin of Bordetella pertussis binds to target cells via the alpha(M)beta(2) integrin (CD11b/CD18). J Exp Med. 2001; 193(9):1035–44. PMID: 11342588.
4. Karst JC, Barker R, Devi U, Swann MJ, Davi M, Roser SJ, et al. Identification of a region that assists membrane insertion and translocation of the catalytic domain of Bordetella pertussis CyaA toxin. J Biol Chem. 2012; 287(12):9200–12. Epub 2012/01/14. https://doi.org/10.1074/jbc.M111.316166 PMID: 22241477.
5. Cannella SE, Ntsogo Enguene VY, Davi M, Malosse C, Sotomayor Perez AC, Chamot-Rooke J, et al. Stability, structural and functional properties of a monomeric, calcium-loaded adenylate cyclase toxin, CyaA, from Bordetella pertussis. Sci Rep. 2017; 7:42065. https://doi.org/10.1038/srep42065 PMID: 28186111.
6. Shen Y, Zhukovskaya NL, Guo Q, Florian J, Tang WJ. Calcium-independent calmodulin binding and two-metal-ion catalytic mechanism of anthrax edema factor. EMBO J. 2005; 24(5):929–41. https://doi.org/10.1038/sj.emboj.7600574 PMID: 15719022.
7. Guo Q, Shen Y, Lee YS, Gibbs CS, Mrksich M, Tang WJ. Structural basis for the interaction of Bordetella pertussis adenylyl cyclase toxin with calmodulin. Embo J. 2005; 24(18):3190–201. https://doi.org/10.1038/sj.emboj.7600800 PMID: 16138079.
8. Selwa E, Davi M, Chenal A, Sotomayor-Perez AC, Ladant D, Malliavin TE. Allosteric Activation of Bordetella pertussis Adenylyl Cyclase by Calmodulin: MOLECULAR DYNAMICS AND MUTAGENESIS STUDIES. J Biol Chem. 2014; 289(30):21131–41. https://doi.org/10.1074/jbc.M113.530410 PMID: 24907274.
9. Mollica L, Bessa LM, Hanoulle X, Jensen MR, Blackledge M, Schneider R. Binding Mechanisms of Intrinsically Disordered Proteins: Theory, Simulation, and Experiment. Front Mol Biosci. 2016; 3:52. https://doi.org/10.3389/fmolb.2016.00052 PMID: 27668217.
10. O'Brien DP, Brier S, Ladant D, Durand D, Chenal A, Vachette P. SEC-SAXS and HDX-MS: a powerful combination. The case of the calcium-binding domain of a bacterial toxin. Biotechnol Appl Biochem. 2017. https://doi.org/10.1002/bab.1577 PMID: 28770577.
11. Guttman M, Weinkam P, Sali A, Lee KK. All-atom ensemble modeling to analyze small-angle x-ray scattering of glycosylated proteins. Structure. 2013; 21(3):321–31. https://doi.org/10.1016/j.str.2013.02.004 PMID: 23473666.
12. Micsonai A, Wien F, Kernya L, Lee YH, Goto Y, Refregiers M, et al. Accurate secondary structure prediction and fold recognition for circular dichroism spectroscopy. Proc Natl Acad Sci U S A. 2015; 112 (24):E3095–103. https://doi.org/10.1073/pnas.1500851112 PMID: 26038575.

13. Kabsch W, Sander C. Dictionary of protein secondary structure: pattern recognition of hydrogen-bonded and geometrical features. Biopolymers. 1983; 22(12):2577–637. https://doi.org/10.1002/bip.360221211 PMID: 6667333.

14. Touw WG, Baakman C, Black J, te Beek TA, Krieger E, Joosten RP, et al. A series of PDB-related databanks for everyday needs. Nucleic Acids Res. 2015; 43(Database issue):D364–8. https://doi.org/10.1093/nar/gku1028 PMID: 25352545.

15. Kataoka M, Head JF, Vorherr T, Krebs J, Carafoli E. Small-angle X-ray scattering study of calmodulin bound to two peptides corresponding to parts of the calmodulin-binding domain of the plasma membrane Ca2+ pump. Biochemistry. 1991; 30(25):6247–51. PMID: 1647818.

16. Knott R, Hansen S, Henderson S. A small angle X-ray scattering study of the binding of cyclosporin-A to calmodulin. J Struct Biol. 1994; 112(3):192–8. https://doi.org/10.1006/jsbi.1994.1020 PMID: 7986646.

17. Majava V, Kursula P. Domain swapping and different oligomeric States for the complex between calmodulin and the calmodulin-binding domain of calcineurin a. PLoS ONE. 2009; 4(4):e5402. https://doi.org/10.1371/journal.pone.0005402 PMID: 19404396.

18. Grishaev A, Anthis NJ, Clore GM. Contrast-matched small-angle X-ray scattering from a heavy-atom-labeled protein in structure determination: application to a lead-substituted calmodulin-peptide complex. Journal of the American Chemical Society. 2012; 134(36):14686–9. https://doi.org/10.1021/ja306359z PMID: 22908850.

19. Ye Q, Feng Y, Yin Y, Faucher F, Currie MA, Rahman MN, et al. Structural basis of calcineurin activation by calmodulin. Cell Signal. 2013; 25(12):2661–7. https://doi.org/10.1016/j.cellsig.2013.08.033 PMID: 24018048.

20. Franke D, Svergun DI. DAMMIF, a program for rapid ab-initio shape determination in small-angle scattering. J Appl Crystallogr. 2009; 42(Pt 2):342–6. https://doi.org/10.1107/S0021889809000338 PMID: 27630371.

21. Chattopadhyaya R, Meador WE, Means AR, Quiocho FA. Calmodulin structure refined at 1.7 A resolution. Journal of molecular biology. 1992; 228(4):1177–92. PMID: 1474585.

22. Bernado P, Mylonas E, Petoukhov MV, Blackledge M, Svergun DI. Structural characterization of flexible proteins using small-angle X-ray scattering. Journal of the American Chemical Society. 2007; 129 (17):5656–64. Epub 2007/04/07. https://doi.org/10.1021/ja069124n PMID: 17411046.

23. Chou JJ, Delaglio F, Bax A. Measurement of one-bond 15N-13C' dipolar couplings in medium sized proteins. Journal of biomolecular NMR. 2000; 18(2):101–5. PMID: 11101214.

24. Moore BL, Kelley LA, Barber J, Murray JW, MacDonald JT. High-quality protein backbone reconstruction from alpha carbons using Gaussian mixture models. J Comput Chem. 2013; 34(22):1881–9. Epub 2013/05/25. https://doi.org/10.1002/jcc.23330 PMID: 23703289.

25. Bouhss A, Vincent M, Munier H, Gilles AM, Takahashi M, Barzu O, et al. Conformational transitions within the calmodulin-binding site of Bordetella pertussis adenylate cyclase studied by time-resolved fluorescence of Trp242 and circular dichroism. European journal of biochemistry / FEBS. 1996; 237 (3):619–28. PMID: 8647105.

26. Gallay J, Vincent M, Li de la Sierra IM, Munier-Lehmann H, Renouard M, Sakamoto H, et al. Insight into the activation mechanism of Bordetella pertussis adenylate cyclase by calmodulin using fluorescence spectroscopy. European journal of biochemistry / FEBS. 2004; 271(4):821–33. PMID: 14764099.

27. Karst JC, Sotomayor Perez AC, Guijarro JI, Raynal B, Chenal A, Ladant D. Calmodulin-induced conformational and hydrodynamic changes in the catalytic domain of Bordetella pertussis adenylate cyclase toxin. Biochemistry. 2010; 49(2):318–28. Epub 2009/12/17. https://doi.org/10.1021/bi9016389 PMID: 20000337.

28. Ladant D, Michelson S, Sarfati R, Gilles AM, Predeleanu R, Barzu O. Characterization of the calmodulin-binding and of the catalytic domains of Bordetella pertussis adenylate cyclase. J Biol Chem. 1989; 264(7):4015–20. PMID: 2537301.

29. Bouhss A, Krin E, Munier H, Gilles AM, Danchin A, Glaser P, et al. Cooperative phenomena in binding and activation of Bordetella pertussis adenylate cyclase by calmodulin. J Biol Chem. 1993; 268 (3):1690–4. PMID: 8420945.

30. Guo Q, Jureller JE, Warren JT, Solomaha E, Florian J, Tang WJ. Protein-protein docking and analysis reveal that two homologous bacterial adenylyl cyclase toxins interact with calmodulin differently. J Biol Chem. 2008; 283(35):23836–45. https://doi.org/10.1074/jbc.M802168200 PMID: 18583346.

31. Ladant D, Glaser P, Ullmann A. Insertional mutagenesis of Bordetella pertussis adenylate cyclase. J Biol Chem. 1992; 267(4):2244–50. PMID: 1733931.

32. Karst JC, Ntsogo Enguene VY, Cannella SE, Subrini O, Hessel A, Debard S, et al. Calcium, Acylation, and Molecular Confinement Favor Folding of Bordetella pertussis Adenylate Cyclase CyaA Toxin into a

Monomeric and Cytotoxic Form. J Biol Chem. 2014; 289(44):30702–16. https://doi.org/10.1074/jbc.M114.580852 PMID: 25231985.

33. Subrini O, Sotomayor-Perez AC, Hessel A, Spiaczka-Karst J, Selwa E, Sapay N, et al. Characterization of a membrane-active peptide from the Bordetella pertussis CyaA toxin. J Biol Chem. 2013; 288 (45):32585–98. Epub 2013/09/26. https://doi.org/10.1074/jbc.M113.508838 PMID: 24064217.

34. Veneziano R, Rossi C, Chenal A, Devoisselle JM, Ladant D, Chopineau J. Bordetella pertussis adenylate cyclase toxin translocation across a tethered lipid bilayer. Proc Natl Acad Sci U S A. 2013; 110 (51):20473–8. Epub 2013/12/04. https://doi.org/10.1073/pnas.1312975110 PMID: 24297899.

35. Sotomayor-Perez AC, Subrini O, Hessel A, Ladant D, Chenal A. Molecular Crowding Stabilizes Both the Intrinsically Disordered Calcium-Free State and the Folded Calcium-Bound State of a Repeat in Toxin (RTX) Protein. Journal of the American Chemical Society. 2013; 135(32):11929–34. Epub 2013/08/15. https://doi.org/10.1021/ja404790f PMID: 23941183.

36. O'Brien DP, Hernandez B, Durand D, Hourdel V, Sotomayor-Perez AC, Vachette P, et al. Structural models of intrinsically disordered and calcium-bound folded states of a protein adapted for secretion. Sci Rep. 2015; 5:14223. https://doi.org/10.1038/srep14223 PMID: 26374675.

37. Mohan A, Oldfield CJ, Radivojac P, Vacic V, Cortese MS, Dunker AK, et al. Analysis of molecular recognition features (MoRFs). Journal of molecular biology. 2006; 362(5):1043–59. https://doi.org/10.1016/j.jmb.2006.07.087 PMID: 16935303.

38. Hsu WL, Oldfield C, Meng J, Huang F, Xue B, Uversky VN, et al. Intrinsic protein disorder and protein-protein interactions. Pacific Symposium on Biocomputing Pacific Symposium on Biocomputing. 2012:116–27. PMID: 22174268.

39. Radivojac P, Vucetic S, O'Connor TR, Uversky VN, Obradovic Z, Dunker AK. Calmodulin signaling: analysis and prediction of a disorder-dependent molecular recognition. Proteins. 2006; 63(2):398–410. https://doi.org/10.1002/prot.20873 PMID: 16493654.

40. Rumi-Masante J, Rusinga FI, Lester TE, Dunlap TB, Williams TD, Dunker AK, et al. Structural basis for activation of calcineurin by calmodulin. Journal of molecular biology. 2012; 415(2):307–17. https://doi.org/10.1016/j.jmb.2011.11.008 PMID: 22100452.

41. Springer TI, Goebel E, Hariraju D, Finley NL. Mutation in the beta-hairpin of the Bordetella pertussis adenylate cyclase toxin modulates N-lobe conformation in calmodulin. Biochemical and biophysical research communications. 2014; 453(1):43–8. https://doi.org/10.1016/j.bbrc.2014.09.048 PMID: 25251320.

42. Wolff J, Newton DL, Klee CB. Activation of Bordetella pertussis adenylate cyclase by the carboxyl-terminal tryptic fragment of calmodulin. Biochemistry. 1986; 25(24):7950–5. PMID: 2879560.

43. Shen Y, Lee YS, Soelaiman S, Bergson P, Lu D, Chen A, et al. Physiological calcium concentrations regulate calmodulin binding and catalysis of adenylyl cyclase exotoxins. EMBO J. 2002; 21(24):6721–32. https://doi.org/10.1093/emboj/cdf681 PMID: 12485993.

44. Barbato G, Ikura M, Kay LE, Pastor RW, Bax A. Backbone dynamics of calmodulin studied by 15N relaxation using inverse detected two-dimensional NMR spectroscopy: the central helix is flexible. Biochemistry. 1992; 31(23):5269–78. PMID: 1606151.

45. Wall ME, Clarage JB, Phillips GN. Motions of calmodulin characterized using both Bragg and diffuse X-ray scattering. Structure. 1997; 5(12):1599–612. PMID: 9438860.

46. Ikura M, Barbato G, Klee CB, Bax A. Solution structure of calmodulin and its complex with a myosin light chain kinase fragment. Cell Calcium. 1992; 13(6–7):391–400. PMID: 1505004.

47. Tripathi S, Wang Q, Zhang P, Hoffman L, Waxham MN, Cheung MS. Conformational frustration in calmodulin-target recognition. Journal of molecular recognition: JMR. 2015; 28(2):74–86. https://doi.org/10.1002/jmr.2413 PMID: 25622562.

48. Jang H, Banerjee A, Chavan T, Gaponenko V, Nussinov R. Flexible-body motions of calmodulin and the farnesylated hypervariable region yield a high-affinity interaction enabling K-Ras4B membrane extraction. J Biol Chem. 2017; 292(30):12544–59. https://doi.org/10.1074/jbc.M117.785063 PMID: 28623230.

49. Liu F, Chu X, Lu HP, Wang J. Molecular mechanism of multispecific recognition of Calmodulin through conformational changes. Proc Natl Acad Sci U S A. 2017; 114(20):E3927–E34. https://doi.org/10.1073/pnas.1615949114 PMID: 28461506.

50. Englander SW, Kallenbach NR. Hydrogen exchange and structural dynamics of proteins and nucleic acids. Q Rev Biophys. 1983; 16(4):521–655. PMID: 6204354.

51. Hourdel V, Volant S, O'Brien DP, Chenal A, Chamot-Rooke J, Dillies MA, et al. MEMHDX: An interactive tool to expedite the statistical validation and visualization of large HDX-MS datasets. Bioinformatics (Oxford, England). 2016. https://doi.org/10.1093/bioinformatics/btw420 PMID: 27412089.

52. David G, Pérez J. Combined sampler robot and high-performance liquid chromatography: a fully automated system for biological small-angle X-ray scattering experiments at the Synchrotron SOLEIL SWING beamline. J Appl Cryst. 2009; 42:892–900.

53. Konarev PV, Volkov VV, Sokolova AV, Koch MHJ, Svergun DI. PRIMUS—a Windows-PC based system for small-angle scattering data analysis. J Appl Crystallogr. 2003; 36:1277–82.

54. Franke D, Jeffries CM, Svergun DI. Correlation Map, a goodness-of-fit test for one-dimensional X-ray scattering spectra. Nature methods. 2015; 12(5):419–22. https://doi.org/10.1038/nmeth.3358 PMID: 25849637.

55. Guinier A. Diffraction of X-rays of very small angles—application to the study of ultramicroscopic phenomenon. Ann Phys 1939; 12: 161–237.

56. Svergun DI. Determination of the Regularization Parameter in Indirect -Transform Methods Using Perceptual Criteria. J Appl Cryst. 1992; 25:495–503.

57. Svergun DI. Restoring low resolution structure of biological macromolecules from solution scattering using simulated annealing. Biophysical Journal. 1999; 76(6):2879–86. https://doi.org/10.1016/S0006-3495(99)77443-6 PMID: 10354416

58. Svergun DI, Barberato C, Koch MHJ. CRYSOL—a program to evaluate X-ray solution scattering of biological macromolecules from atomic coordinates. J Appl Crystallogr. 1995; 28:768–73.

59. Petoukhov MV, Svergun DI. Global rigid body modeling of macromolecular complexes against small-angle scattering data. Biophys J. 2005; 89(2):1237–50. Epub 2005/06/01. https://doi.org/10.1529/biophysj.105.064154 PMID: 15923225.

Supplementary figures: Calmodulin fishing with a structurally disordered bait triggers CyaA catalysis.

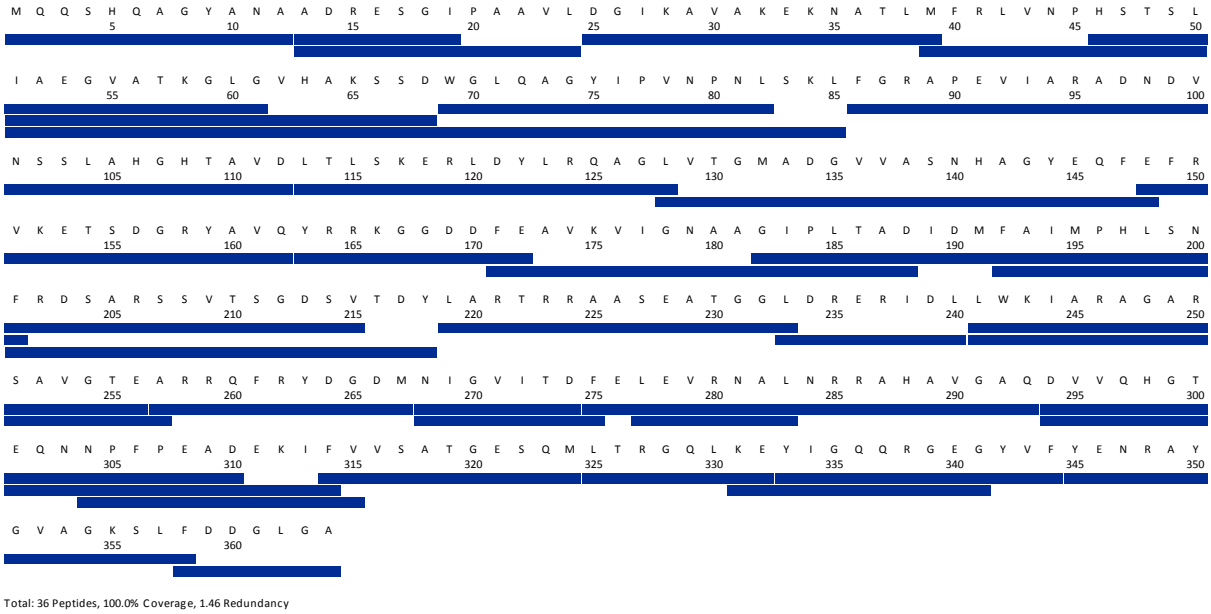

Figure S1: Peptide map of AC

A sequence coverage map of AC was determined after 2 min digestion with pepsin. Each blue bar represents a single AC peptide. Only those peptides selected for HDX-MS data analysis after filtering the complete dataset are displayed. Linear sequence coverage of 100% was achieved. The secondary structure architecture of AC is as follows: A-helix (residues 11–17), B-helix (residues 20–34), C-helix (residues 44–53), D-helix (residues 89–106), E-helix (residues 116–126), F-helix (198–210), G-helix (214–223), Hom-loop (residues 226–232), H-helix (residues 234–253), H′-helix (residues 255–259), T18b1 (residues 262–270), I-helix (residues 274–289), catalyic loop (residues 300–312), T18b2 (residues 313–325), J-helix (residues 326–340), and an LHL motif (residues 341–364). The catalytic site is made of three highly conserved regions that are directly involved in substrate binding and catalysis: CR1 (residues 54–77), CR2 (residues 184–198), and CR3 (residues 295–315). AC, catalytic domain; CR1, catalytic region 1; CR2, catalytic region 2; CR3, catalytic region 3; LHL, loop-helix-loop; T18b1, first beta-sheet of the T18 fragment; T18b2, second beta-sheet of the T18 fragment.

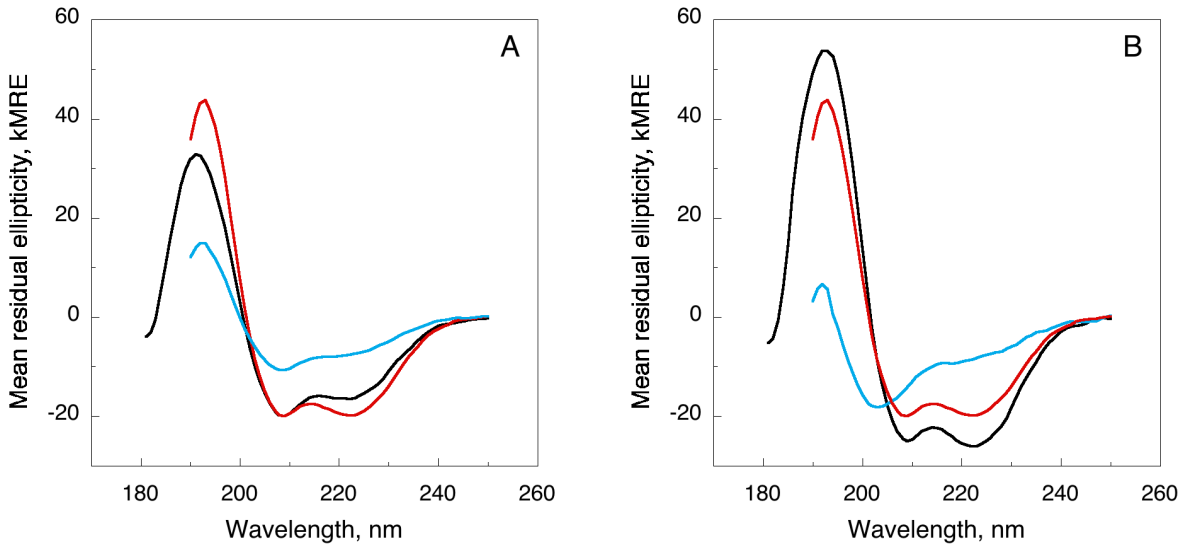

Figure S2: Far-UV SR-CD spectra of isolated AC, CaM, H-helix peptide, and their complexes

(**A**) AC (blue), CaM (red), and AC:CaM complex (dark). (**B**) H-helix peptide (blue), CaM (red), and H-helix:CaM complex (dark). The buffer is 20 mM HEPES, 150 mM NaCl, 2 mM $CaCl_2$, pH 7.4. kMRE corresponds to MRE × 10^3. AC, adenylate cyclase catalytic domain; CaM, calmodulin; far-UV, far-ultraviolet; MRE, mean residual ellipticity; SR-CD, synchrotron radiation circular dichroism.

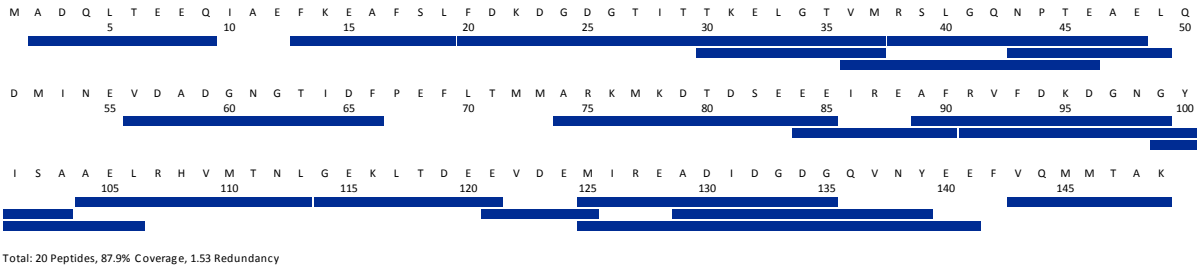

Figure S3: Peptide map of CaM

A sequence coverage map of CaM was determined after 2 min digestion with pepsin. Each blue bar represents a single CaM peptide. Only those peptides selected for HDX-MS data analysis after filtering the complete dataset are displayed. Linear sequence coverage of 87.9% was achieved. CaM, calmodulin; HDX-MS, hydrogen/deuterium exchange mass spectrometry.

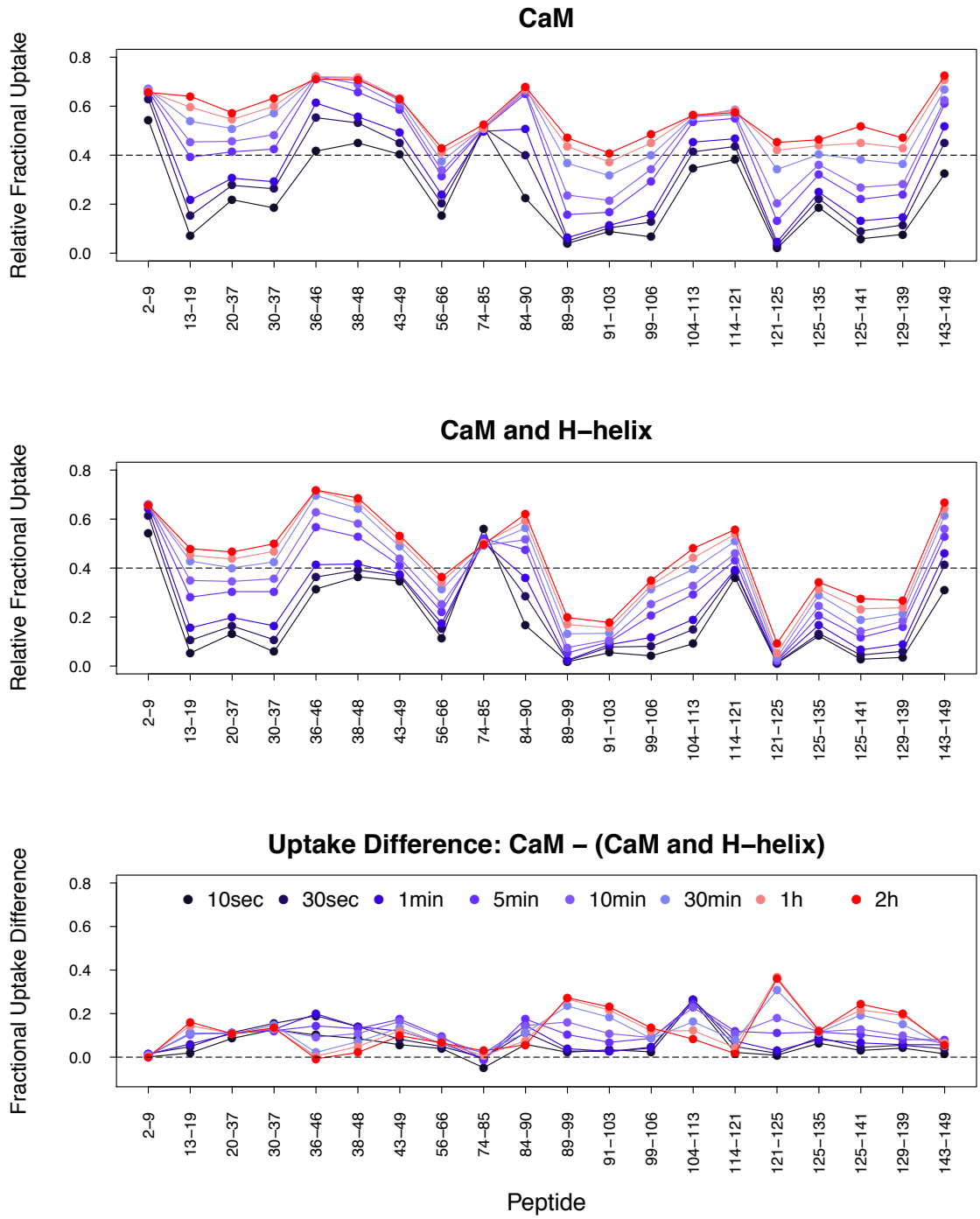

Figure S4: HDX-MS behavior of CaM in the presence of H-helix pepitde

Relative fractional exchange data were calculated at each point and plotted as a function of peptide position for CaM and CaM + H-helix. Each dot corresponds to the average of three independent replicates. The fractional uptake difference plot shows the differences in uptake calculated between CaM alone and in the presence of H-helix. Uptake plots of all peptides selected for final HDX-MS analysis are displayed in S11. The data used to generate the figure can be found in S4. CaM, calmodulin; HDX-MS, hydrogen/deuterium exchange mass spectrometry.

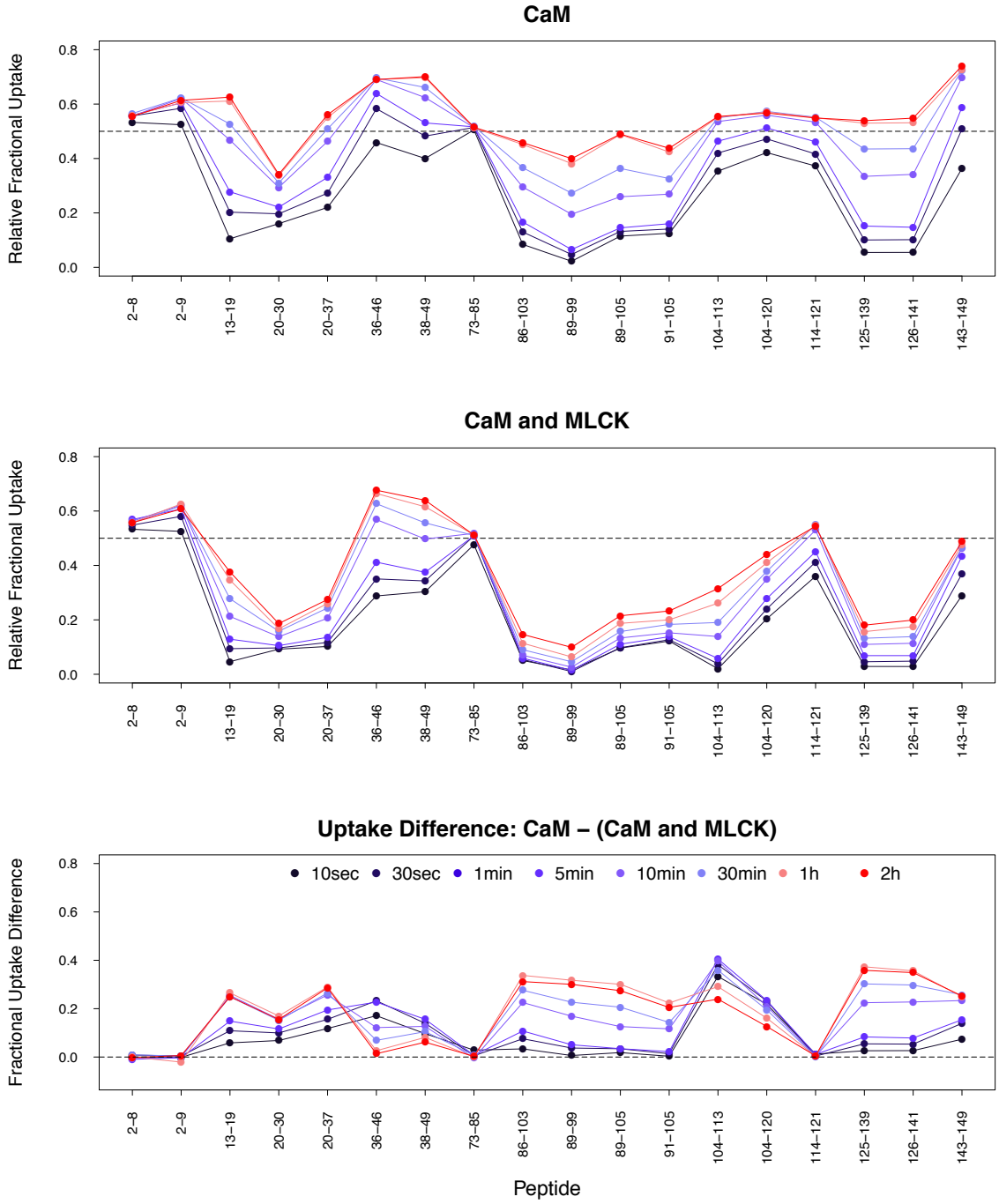

Figure S5: HDX-MS behavior of CaM in the presence of P_{MLCK} peptide

Relative fractional exchange data were calculated at each point and plotted as a function of peptide position for CaM and CaM + P_{MLCK} peptide. Each dot corresponds to the average of three independent replicates. The fractional uptake difference plot shows the differences in uptake calculated between CaM alone and in the presence of P_{MLCK}. Uptake plots of all peptides selected for final HDX-MS analysis are displayed in S12. The data used to generate the figure can be found in S5. CaM, calmodulin; HDX-MS, hydrogen/deuterium exchange mass spectrometry; P_{MLCK}, myosin light-chain kinase peptide.

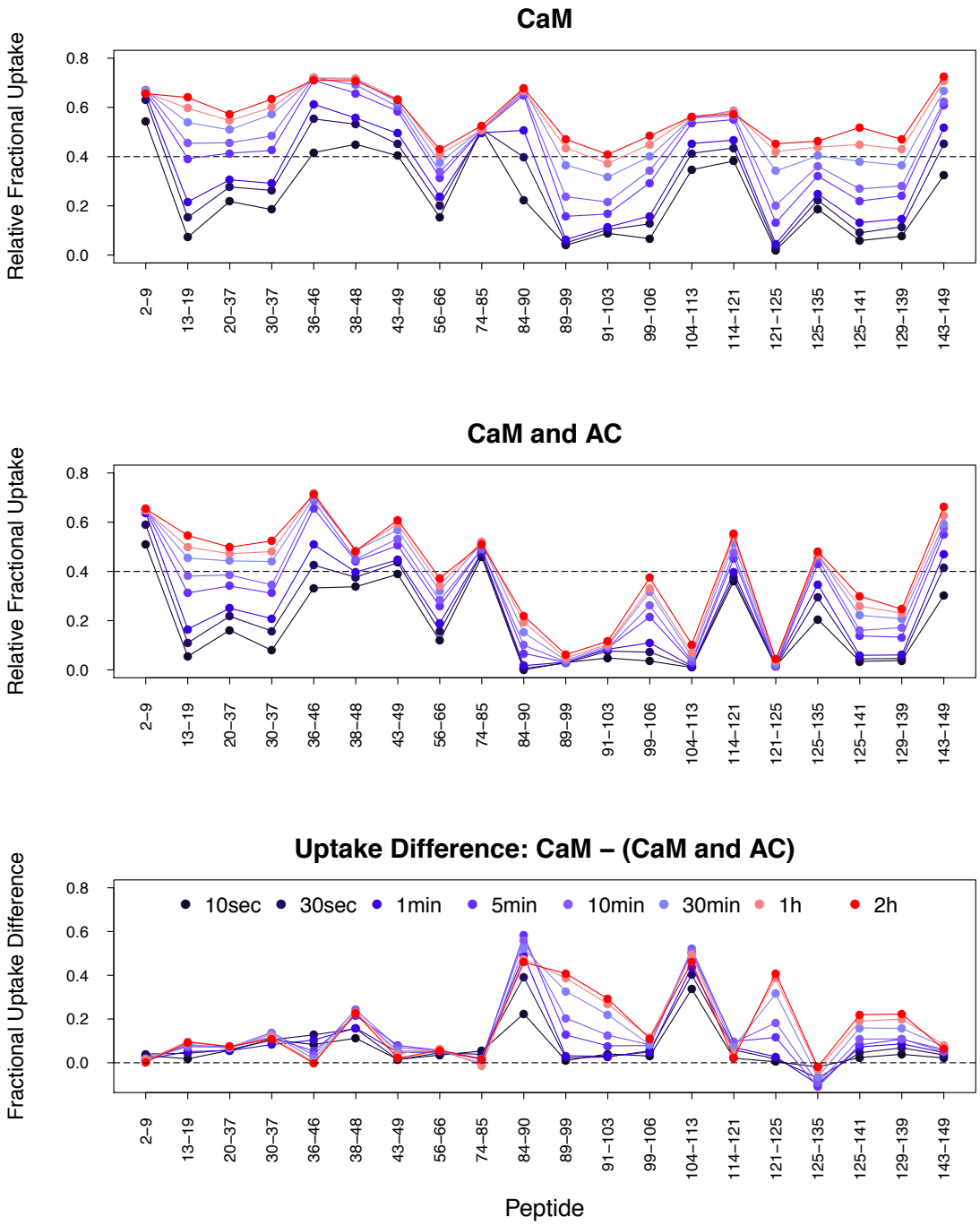

Figure S6: HDX-MS behavior of CaM in the presence of full-length AC

Relative fractional exchange data were calculated at each point and plotted as a function of peptide position for CaM and CaM + full-length AC. Each dot corresponds to the average of three independent replicates. The fractional uptake difference plot shows the differences in uptake calculated between CaM alone and in the presence of AC. Uptake plots of all peptides selected for final HDX-MS analysis are displayed in S10. The data used to generate the figure can be found in S3. AC, adenylate cyclase catalytic domain; CaM, calmodulin; HDX-MS, hydrogen/deuterium exchange mass spectrometry.

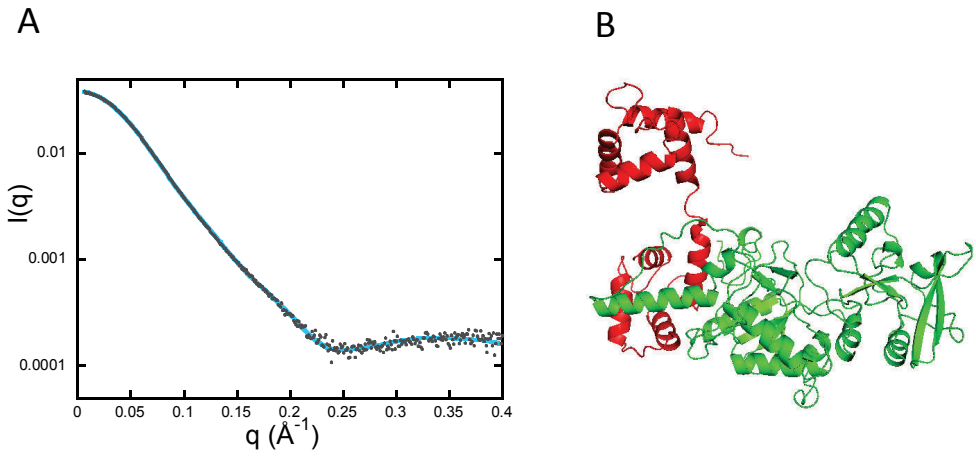

Figure S7: Small angle X-ray scattering of the AC:CaM complex

(**A**) Calculated scattering curve of the BUNCH model shown in panel (B) (blue line) and experimental data (black dots). (**B**) Typical model of AC-CaM complex obtained using the program BUNCH. The AC domain is shown in green while CaM is shown in red, interacting through its C-terminal domain (see text for details). AC, adenylate cyclase catalytic domain; CaM, calmodulin.

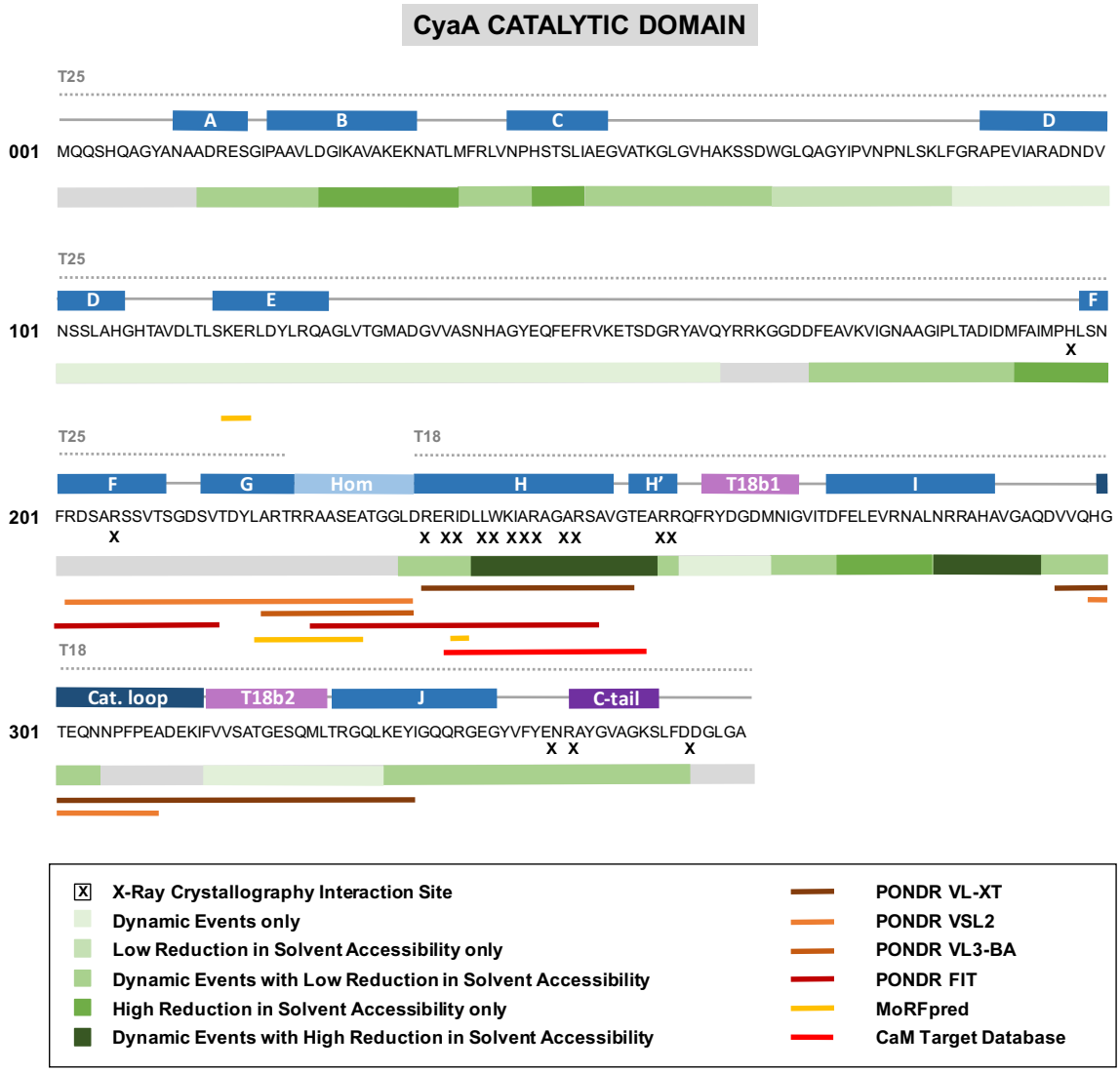

Figure S8: Intrinsic disorded prediction within the AC364 protein

AC HDX-MS results upon CaM binding, and regions of predicted disorder within the AC were mapped to the sequence of the protein. X-labeled residues correspond to the site of partner (CaM) binding. Areas of highest solvent protection in the AC correspond to those involved in partner binding and are flanked by regions of structural disorder. Gray areas correspond to those in which CaM does not induce changes in HDX-MS. For the complete nomenclature of secondary structure elements, please see the legend of S1. AC, adenylate cyclase catalytic domain; CaM, calmodulin; HDX-MS, hydrogen/deuterium exchange mass spectrometry.

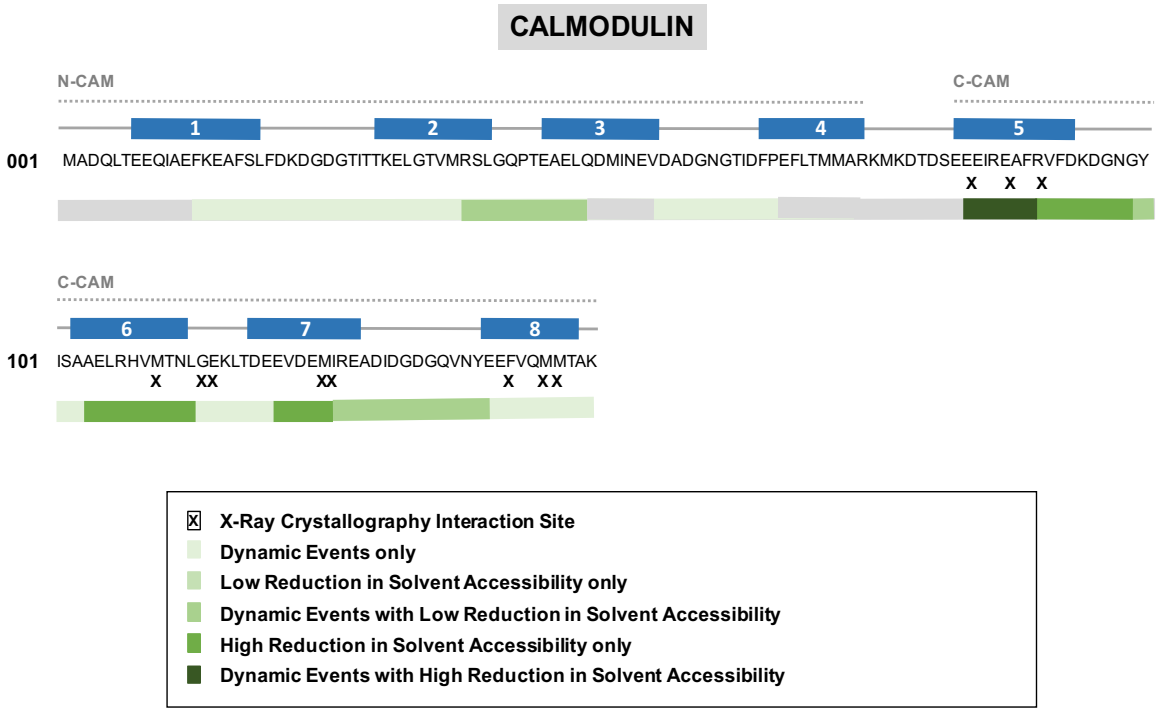

Figure S9: Intrinsic disorded prediction within CaM

CaM HDX-MS results upon AC binding and those residues involved in protein/protein interactions were mapped to the sequence of the protein. Areas of highest solvent protection in the protein correspond to those involved in partner binding, as determined by X-ray Crystallography (X-labels). Gray areas correspond to those in which the AC does not induce changes in HDX-MS, or in which there is a lack of HDX-MS data. AC, adenylate cyclase catalytic domain; CaM, calmodulin; HDX-MS, hydrogen/deuterium exchange mass spectrometry.

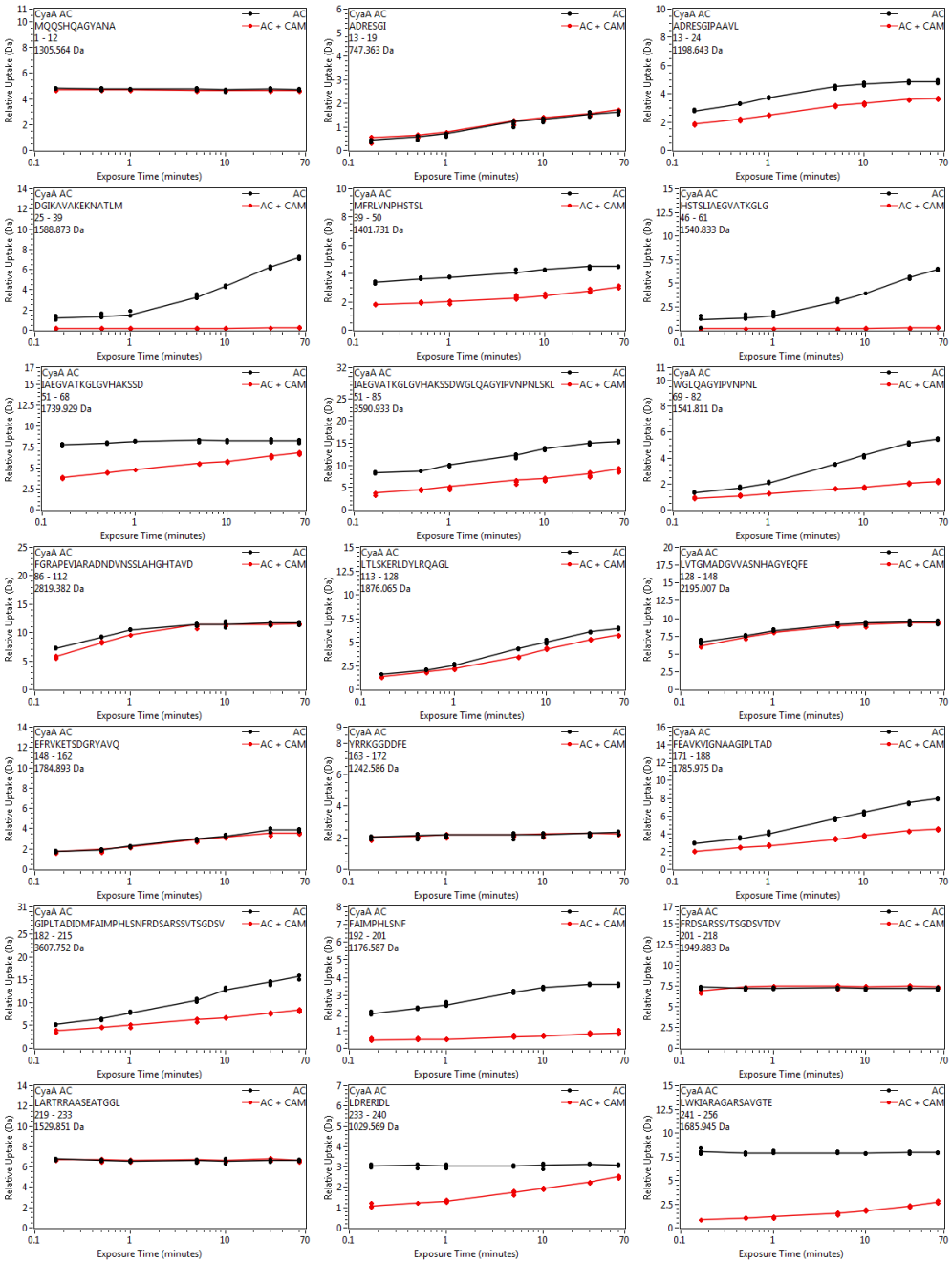

Figure S10: HDX-MS results for individual AC peptides, both from AC in isolation and in complex with CaM

Black indicates the AC alone state, while red indicates AC in complex with CaM. AC, adenylate cyclase catalytic domain; CaM, calmodulin; HDX-MS, hydrogen/deuterium exchange mass spectrometry.

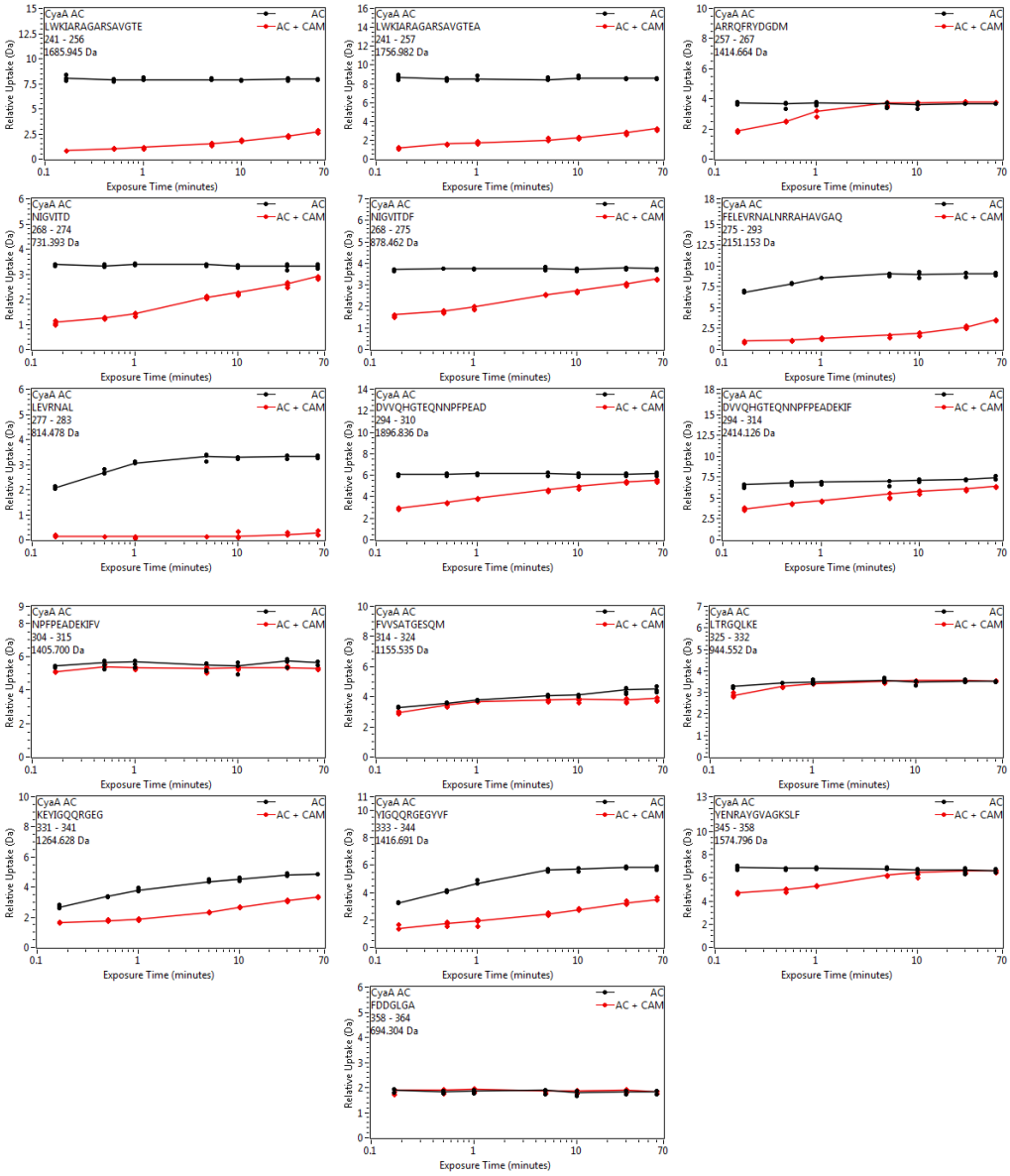

Figure S10: HDX-MS results for individual AC peptides, both from AC in isolation and in complex with CaM

Black indicates the AC alone state, while red indicates AC in complex with CaM. AC, adenylate cyclase catalytic domain; CaM, calmodulin; HDX-MS, hydrogen/deuterium exchange mass spectrometry.

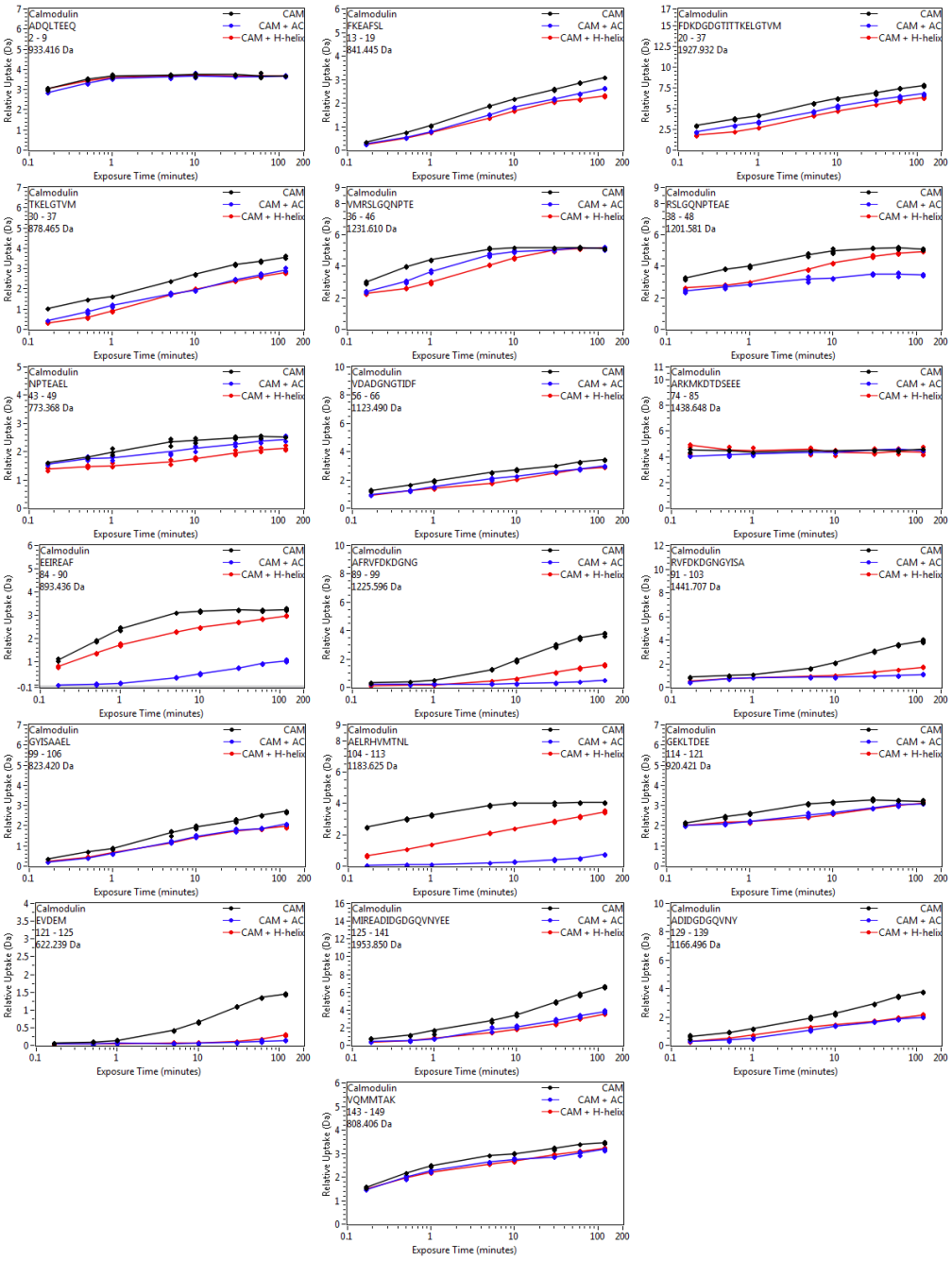

Figure S11: HDX-MS results for individual CaM peptides in complex with AC and H-helix peptide

For each peptide, CaM alone is colored black and CaM in the presence of H-helix is colored red, while CaM in the presence of AC is colored blue. AC, adenylate cyclase catalytic domain; CaM, calmodulin; HDX-MS, hydrogen/deuterium exchange mass spectrometry.

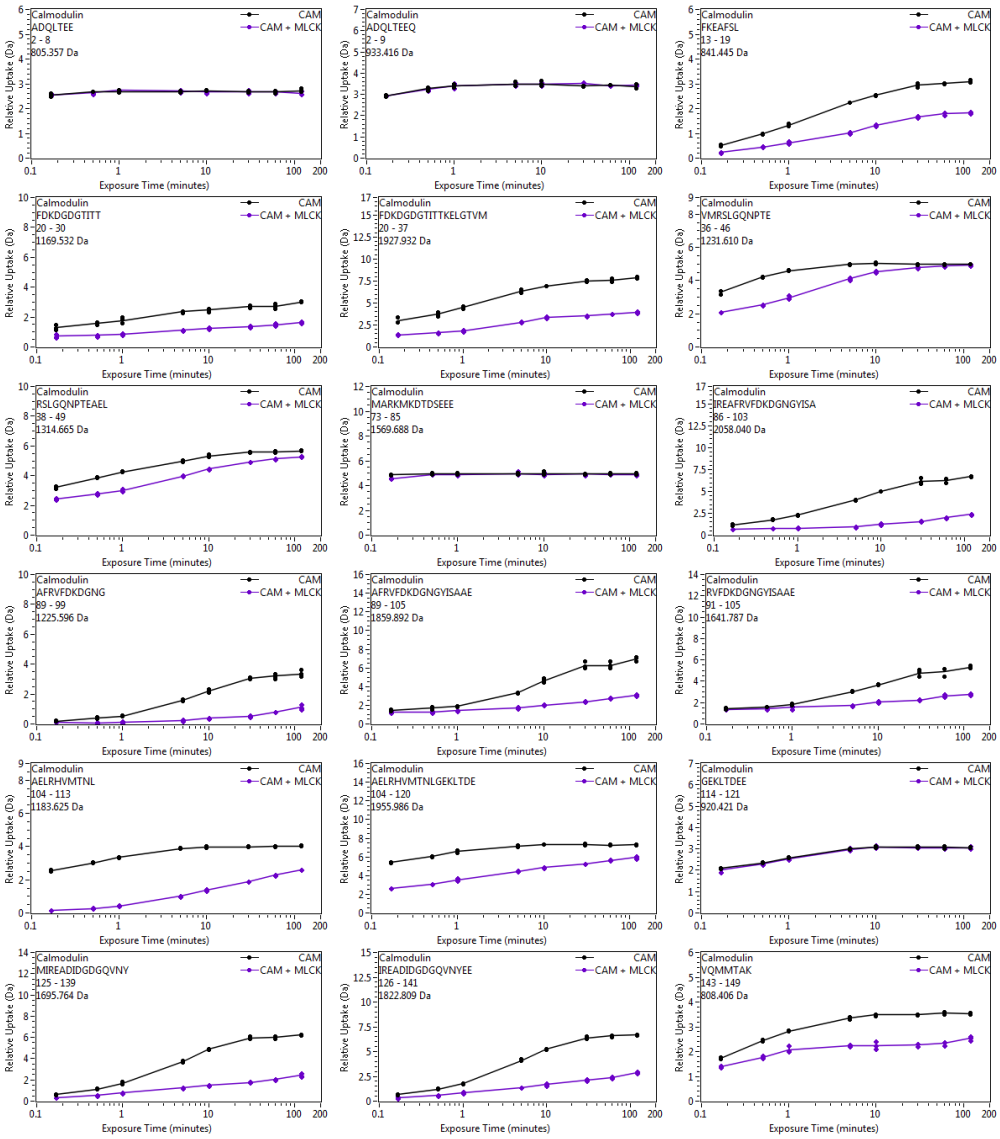

Figure S12: HDX-MS results for individual CaM peptides in complex with PMLCK

Black indicates the CaM alone state, while purple indicates CaM in complex with P_{MLCK}. CaM, calmodulin; HDX-MS, hydrogen/deuterium exchange mass spectrometry; P_{MLCK}, myosin light-chain kinase peptide.

	CaM	H-CaM	P_{MLCK}-CaM	AC364	AC364-CaM
Data collection parameters					
Instrument	Beamline SWING (synchrotron SOLEIL)				
Detector	CCD-based AVIEX				
Beam geometry	0.8 mm x 0.15 mm				
Wavelength [Å]	1.0				
q-range [$Å^{-1}$]	$0.0064 < q < 0.50$				
Exposure time [s]	2				
Temperature [K]	288				
Structural parameters					
I(0) Guinier [cm^{-1}]	0.0317	0.0159	0.0134	0.0252	0.0381
R_g Guinier [Å] [a]	22.2	21.9	17.4	25.9	29.2
I(0) p(r) [cm^{-1}]	0.0319	0.0159	0.0134	0.0252	0.0383
R_g p(r) [Å]	22.7	22.1	17.3	26.2	29.7
D_{Max} [Å]	78	75	52	91	98
Molecular mass determination					
$MM_{sequence}$ [kDa] [b]	16.8	19.3 [b1]-21.7 [b2]	19.0	39.4	56.2
Partial specific volume [$cm^3.g^{-1}$] [c]	0.7174	0.7210	0.7191	0.7233	0.7215
Concentration [$g.L^{-1}$]	ND*	ND*	ND*	0.80	0.82
$MM_{I(0)/c}$ [kDa]	ND*	ND*	ND*	38.6	56.3
$MM_{SAXS\ MoW}$ [kDa] [d]	17.9	21.9	18.6	41.9	58.3
$MM_{SAXS\ QR}$ [kDa] [e]	16.8	19.7	19.2	40.2	54.3
Dammif/Dammin analysis					
Dammif Model number	20	20	20		
NSD	0.56	0.53	0.46		
c^2 (Dammin)	1.56	1.10	1.90		

Table S1: SAXS data collection and scattering derived parameters

[a] R_g obtained with the Guinier approximation in the range $qR_g < 1$.

[b] The calculated masses were derived from the sequences.

[b1] Corresponds to the 1H:1CaM complex.

[b2] Corresponds to the 2H:1CaM complex.

[c] Calculated from the sequence using the program sednterp, available at http://rasmb.org/sednterp/.

[d] Molecular mass M obtained from the whole I(q) curve (q_{max} = 0.4 $Å^{-1}$) using the SAXS-MoW2 program, available at http://saxs.ifsc.usp.br/.

[e] Molecular mass M obtained from the whole I(q) curve (q_{max} = 0.2–0.25 $Å^{-1}$) using the ScÅtter3 program, available at https://bl1231.als.lbl.gov/scatter/.

These two mass determinations do not depend on the value of the protein concentration, c. In general, they provide a useful complement to the derivation of M from the I(0)/c value but are especially relevant in cases such as CaM, which does not possess any tryptophan. CaM, calmodulin; q, momentum transfer; R_g, radius of gyration; SAXS, small-angle X-ray scattering.

Sample	SR-CD
	Helical Content, % ± S.D.
holo-AC alone	27 ± 2
holo-CaM	51 ± 3
holo-AC:CaM	42 ± 3
holo-H	19 ± 1
holo-H:CaM	60 ± 5

Table S2: Structural content of the isolated proteins and complexes derived from SR-CD data

The helical content from SR-CD was estimated using the BestSel software. The helical content of AC364 (36%) in the AC:C-CaM complex was computed using DSSP. AC, adenylate cyclase catalytic domain; C-CaM, C-terminal domain of CaM; DSSP, Dictionary of Secondary Structure of Proteins; SR-CD, synchrotron radiation circular dichroism.

Sample	SR-CD	
	Helical Content, %	Residues
1 AC	27	98
2 CaM	51	76
3 AC + CaM*	34	174
4 AC: CaM complex	42	215
Difference 4 - 3	8	41

* average of the two previous values weighted by the respective residue number.

Table S3: Estimation of the CaM-induced helical content increase in AC364 from SR-CD

The helical content increase ("difference in residues" column) provides an estimation of 41 amino acids that undergo a conversion from a disordered to a helical structure. AC364 and CaM contain 364 and 148 amino acids, respectively. CaM, calmodulin; SR-CD, synchrotron radiation circular dichroism.

Sample	Helical Content, % ± S.D.	Total no. of residues	No. of AA in helices
CaM	51 ± 3	148	76
H-helix peptide	19 ± 1	22	4
Sum of H:CaM assuming no helical structure changes	47 ± 4	171	80
H-helix:CaM	60 ± 5	171	102

Table S4: Estimation of the CaM-induced helical content increase in H:CaM complex from SR-CD data

Assuming that the helical structure content does not change upon H:CaM complex formation, the number of amino acids in helical conformation would be 80 for a complex of 171 residues, (i.e., 76 + 4 residues from CaM and H-helix peptide, respectively; 47 ± 4% of helices in H:CaM complex). The helical content of the H:CaM complex estimated by BestSel from the SR-CD data is 60 ± 5, corresponding to 102 residues. Therefore, the H:CaM complex formation induces the conversion of approximately 22 residues in helical conformation. CaM, calmodulin; SR-CD, synchrotron radiation circular dichroism.

Chapter VI. Discussion & Perspectives

Chapter VI. Discussion & Perspectives

CyaA is one of the major virulence factor produced by *B. pertussis*, the agent of whooping cough. Among bacterial toxins, CyaA invades eukaryotic cells with an original mechanism (Ladant and Ullmann, 1999). Indeed, CyaA is able to translocate its catalytic domain directly across the plasma membrane. Despite several research groups are working on CyaA, the translocation process remains poorly understood. The recent data obtained in the lab about the translocation mechanism are discussed below.

Role of calcium on CyaA folding

Our recent HDX-MS data (see Article II) provide further insights into the calcium involvement on the folding of the entire CyaA. Interestingly, in the absence of calcium, the CyaA does not contain structural elements whatever the urea concentrations investigated. The RD domain alone represents almost half of the toxin. In the absence of calcium, the structural disorder of RD prevents the folding of CyaA.

The disordered state may explain how the whole CyaA toxin can be exported through the T1SS. In the presence of calcium, a progressive folding occurs from RD to the N-terminal domains of the protein. This HDX-MS result is in agreement with the observations made previously in the lab by Cannella and colleagues suggesting that, once secreted and folded, RD may act as a scaffold for the folding of the upstream N-terminal domains of CyaA (Cannella et al., 2017; O'Brien et al., 2015). However, although RD folding prevents back transport, we have no evidences that it triggers the secretion of the rest of the toxin. *In vivo*, we do not know whether *B. pertussis* secretes the CyaA toxin by itself or whether other partners facilitate the secretion. As the RD domain binds the CD11b/CD18 receptor, we can speculate that an immune cell harboring the receptor and trying to phagocyte the bacteria, may bind to the partially secreted CyaA, exposing the RD domain at the bacterial surface. The binding and the cell mobility may act as a force pulling the rest of the CyaA domains through the T1SS.

Role of the acylation on structural and stability properties of CyaA

CyaA possesses two acylation on its residues K860 and K983. Acylation is required in the RTX toxins for their cytotoxicity and we showed that they play a central role in the refolding of CyaA. Remarkably, using the molecular confinement developed by Karst and colleagues (Karst et al., 2014), it has been observed that the yield of proCyaA monomers was lower than CyaA monomers. This indicates that the acyl chains have a thermodynamic contribution on the CyaA refolding and reduce multimers formation. Using AUC and ANS fluorescence, we showed that CyaA exhibits a more compact and stable state with hydrophobic regions less solvent-exposed than proCyaA. We show that the acyl chains of CyaA favor a collapse of the hydrophobic regions and its overall stability. These data suggest that upon secretion and progressive folding of the different domains from the C- to the N-terminal, the acylation favors a faster folding of the HR and AR domains, leading to a more compact state of CyaA, and decreases the time of solvent-exposed hydrophobic regions, prone to aggregate as observed with proCyaA.

P454 membrane interaction

My PhD was mainly focused on how CyaA can deliver its adenylate cyclase domain across the plasma membrane. Recently our team identified the so-called translocation region (TR, residues 365-527 of CyaA) (Karst et al., 2012). Deletion of the TR does not prevent cell hemolysis but abrogates the toxin's ability to produce cAMP in cells. Subrini and colleagues further identified in this region the amphiphilic peptide P454 (residues 454 to 484), exhibiting membrane-active properties, *i.e* membrane interaction, α-helical folding upon membrane insertion and permeabilization (Subrini et al., 2013).

During my thesis, we first investigated whether CyaA possessed other amphiphilic peptides that might have membrane-active properties such as P454. Based on their hydrophobic moment, hydrophobicity and helical propensity, we identified up to 10 others peptides distributed throughout CyaA. Interestingly, some are able to interact with the membranes and adopt a α-helical conformation upon membrane binding. This indicates that these amphiphilic peptides distributed in CyaA may contribute to membrane insertion and stabilization of the toxin into the plasma membrane. However, among all, P454 was found to be the unique peptide competent for membrane permeabilization. Therefore, in the context of the CyaA translocation, we propose that the membrane active properties of P454 peptide may contribute to the catalytic domain delivery. It has been proposed that P454 could locally destabilize the membrane and decrease the energy required for the ACD delivery into the

cytosol (Subrini et al., 2013). However, this description remains elusive. In fact, how about 400 amino could be transported across the plasma membrane with just a membrane destabilization? The main objective of the PhD was to investigate more precisely the structural and molecular properties of P454 in the translocation process.

P454 is a cationic peptide and we observed that its interaction is favored in the presence of negatively charged lipids headgroups, as already reported (Subrini et al., 2013). Usually, anionic lipids are in the inner leaflet of the plasma membrane. Interestingly, Martin and colleagues previously demonstrated that CyaA possesses a lipid flip-flop activity in the HR (Martin et al., 2004). This activity may expose anionic lipids in the outer leaflet and hence may contribute to the P454 membrane interaction during the early stages of membrane insertion. Usually, in the lab, we investigate P454 membrane interaction with lipid vesicles as source of membrane, which are homogeneous in lipids composition in both leaflets. It would be interesting to investigate the P454 membrane insertion in the presence of asymmetric membranes, to mimic as much as possible a plasma membrane. Several techniques are available such as the Langmuir-Blodgett/Langmuir-Schaefer to make asymmetric lipid bilayers (Clifton et al., 2013; Crane et al., 2005) and the cyclodextrin-mediated lipid exchange of the outer membrane leaflet (Cheng et al., 2009). The constitution of such lipid membrane would allow inferring whether the lipid flip-flop activity of CyaA could favor the interaction of the P454 segment with the plasma membrane.

We also investigated membrane fluidity and found that the P454 partition is favored by fluidic membrane. The proximity between the TR (where belongs the P454 segment) and ACD suggests that the interaction of the TR with the membrane and ACD translocation would occur in a same membrane area. Furthermore, from a thermodynamic point of view, a fluidic membrane facilitates membrane insertion and translocation in general compared to rigid membranes (Wallbrecher et al., 2017). Our hypothesis is in contradiction with the previous observations made by Bumba and colleagues (Bumba et al., 2010; Vojtova et al., 2006). They claimed that the CyaA translocation occurs in lipid rafts, which are composed of lipids that confer membrane rigidity (*i.e* cholesterol, sphingolipids and saturated lipids). They also identified five putative CRAC (for Cholesterol Recognition/interaction Amino acid Consensus) involved in the translocation of ACD, which may explain why CyaA inserts in lipid rafts (Masin et al., 2017). However, none of these CRAC seem to be involved in membrane activity of CyaA. A future approach would be to investigate the effect of lipid composition on the membrane insertion and translocation of the entire CyaA toxin *in vitro*,

to provide answers to these contradictory data. For that, we propose to use the method developed by Veneziano and colleagues to follow the translocation of ACD across a tethered lipid bilayer (tBLM) (Veneziano et al., 2013). The tBLM allows us to control the buffers in the *cis* and *trans* sides as well as the composition of the lipid bilayer and the membrane potential. Hence, it is possible to partly mimic the physiological conditions and only vary the membrane composition to examine the effect on the overall translocation process. Another approach would be to use the dual polarization interferometry method (DPI). This technic studies the interactions of proteins with planar single lipid bilayers (Swann et al., 2004). The DPI monitors the mass and thickness changes occurring upon addition of interacting proteins (Karst et al., 2012). As the tBLM, we can control the lipid composition. Furthermore, we can extract the kinetic of penetration of CyaA into the membrane and it would allow discriminating which type of lipids affect the kinetics of interaction of the toxin with the membranes.

Hence, these two methods would be interesting approaches for investigation of the effects of the lipid composition on membrane insertion and translocation of the CyaA toxin. Potentially, these data could give a hint on which lipids are crucial for toxin interaction with a cellular membrane.

Finally, we focused on the effect of lipid polymorphism on P454 membrane interaction. We observed that a local membrane curvature affects the P454 partition. Interestingly, a negative curvature (*i.e* membrane invagination) reduces and even abolishes the P454-membrane interaction compared to plane membrane. This kind of curvature can be observed in lipids rafts (Martin et al., 2004) and may further support that the ACD translocation may not occur in these membrane regions. On the contrary, we observed that a positive curvature considerably increases the P454 membrane-active properties. Our results might have nicely fit with the pretended phospholipase activity (PLA) identified by Gonzalez-Bullon and colleagues (Gonzalez-Bullon et al., 2018, 2017). In fact, the supposed PLA activity of CyaA may induce a membrane remodeling (*i.e* generation of lysophospholipids) with formation of a local membrane positive curvature. It would have explained why such membrane curvature increases the P454 interaction and permeabilization. However, their work was not rigorous and a number of experiments carried out were lacking PLA positive control. Bumba and co-workers published a contradictory article about the non-existing PLA activity of CyaA (Bumba et al., 2018). We also examined the PLA activity of CyaA and clearly observed that CyaA has no detectable PLA activity. Hence, we do not know which phenomenon may induce this positive membrane curvature that increases the P454

interaction and if it has a contribution in the CyaA intoxication process. Lysophospholipids are present as minor lipids in the cell membrane (less than 3%) (White, 1973; Hill and Lands, 1970), which implicates that such lipids may be recruited by the CyaA toxin. It would be interesting to introduce in a cell membrane some labeled lysophospholipids and investigate whether they are recruited in a membrane area and/or co-localize with CyaA. Another hypothesis would be that the membrane insertion and the local destabilization performed by the HR may induce a membrane remodeling in the plasma membrane and favor the formation of a positive curvature. Numerous proteins are known to induce positive curvature. The amphiphilic peptides of CyaA may induce a positive membrane curvature, which may increase the P454 segment activity.

Involvement of the arginine residues on the P454 membrane active properties

As described in part 3.4.1, P454 exhibits common features with AMPs and CPPs and possesses two arginine residues R461 and R474. Arginine residues are well described in literature for their membrane-active properties, especially for AMPs in membrane permeabilization. From the different experiments performed, we clearly observe that the presence of the two arginine residues is appropriated for the membrane-active properties of P454. Among the P454-derived peptides, the peptide P454 R12K (*i.e* substitution of both arginine by lysine residues) is interesting. Concerning the contribution of arginine, P454 R12K has the same charge than P454 but exhibits a weaker interaction and permeabilization, although the overall folding is not affected. This indicates that not only the positive net charge but also the guanidinium group of the arginine's side chain is required for the membrane-active properties of P454. Arginine residues form a bidentate guanidinium-phosphate complex with lipids, which allows membrane insertion of the peptide into the acyl chains and increases membrane destabilization compared to lysine. It would be interesting to study two new P454-derived peptides with the substitution of only one arginine by a lysine and investigate more precisely the implication of each arginine residue on the membrane-active properties.

P454 can be divided into two regions: the C-terminal part of the peptide with R474 allows peptide membrane insertion and folding while the N-terminal part with R461 inserts into and destabilizes the membrane. We also tried to separate these two domains to investigate whether they can operate independently. We used a N-terminal peptide (454-474) and a C-terminal peptide (residues 464-484). Interestingly, the N-terminal peptide

interacts weakly with membranes (ΔG = -5 kcal/mol) while the C-terminal peptide does not. However, none of them folds and permeabilizes membranes. This suggests that both domains are interdependent for the membrane-active properties of P454.

Our results are in agreement with the previous data obtained by Masin and colleagues (Masin et al., 2016). They previously observed that a single mutation of R461 or R474 in CyaA reduces translocation of the toxin. Furthermore, the mutation of R474 significantly decreases the toxin binding. Our data bring more insights on the arginine contributions of P454 during translocation: the C-terminal part of P454 with the R474 would allow anchoring and folding of the P454 segment into the plasma membrane. Then, the N-terminal part, more flexible, would destabilize the membrane. However, it is difficult to extrapolate results from a peptide to the full length CyaA toxin. Our hypothesis shall to be tested in the full-length protein.

Implication of the P454:CaM complex for the translocation of CyaA

P454 shares similar properties with AMPs peptides. It has been described that some AMPs are able translocate across membranes to reach the cytosol and bind to intracellular targets to impair cell pathways (Mahlapuu et al., 2016; Hancock and Sahl, 2006). Alternatively, these sequences may be involved in translocation and binding to eukaryotic targets in order to help the translocation of a larger cargo. Noteworthy, some toxins, such as the botulinium and diphtheria toxins, possess their own translocating machineries able to translocate and bind to an eukaryotic factor. Such binding may act as a driving force for the translocation of their catalytic domain. We show that P454 binds to CaM and may contribute to the driving force for the translocation of ACD.

The cellular entry of CyaA is unique compared to others toxins. However, the overall translocation process to reach the cytosol is quite similar. Indeed, the toxin requires the help from an eukaryotic partner to translocate its catalytic domain. Hence, although the biological processes are different, they require common physical processes.

From our titrations and permeabilizing assays, we also observed that CaM can remove P454 from the membrane but only in a calcium dependent manner. However, CaM is mainly in apo-state (*i.e* without bound calcium) in the cytosol of the cell due to the low calcium concentration (around 100 nM) (Bogdanova et al., 2013). Hence, the translocation of the P454 segment would not be favorable for the formation of the P454:CaM complex. Interestingly, Cannella and colleagues observed that the translocation of the monomeric

CyaA occurs only in the presence of free calcium in solution *(i.e* > 0.3 mM) (Cannella et al., 2017). In the absence of calcium, the toxin is still able to hemolyse cells but not to translocate ACD. This observation supports that the free calcium in the extracellular medium is required for the transport of ACD. From the membrane-active properties of P454, we can speculate that the local membrane destabilization of P454 may create an influx of calcium into the cytosol. Hence, the local calcium concentration may increase. Apo-CaM is present in excess in eukaryotic cells (~ 5 to 10 μM) and the burst of calcium may favor calcium binding and structural reorganization toward holo-CaM. The holo-CaM is now competent to bind to the translocating segment and trap P454 inside the cytosol.

From the droplet interface bilayers experiments, we could characterize the translocation of P454. Interestingly, if CaM is not present, any increase of fluorescence is observed in the *trans* droplet. This result suggests that P454 can be accumulated in the buffer of the *trans* droplet only if CaM is present. Otherwise it is not able to diffuse and remains bound to the membrane. Thus, as we observed before, CaM is able to bind the peptide from the membrane and keep it in solution.

We also assayed to monitor the translocation of the H-helix, which possesses a higher K_d than P454 for CaM and can thus be accumulated in *trans* droplet if translocated. In the same conditions, we observed that the H-helix interacts with the membrane but does not accumulate in the *trans* droplet. Our data suggest that, although the H-helix corresponds to the main binding site of ACD for CaM, it does not translocate by itself. As observed by Karst and colleagues in 2012, the H-helix and the rest of ACD need the TR and the full toxin to translocate (Karst et al., 2012).

However, in these experiments, we are not in the physiological conditions. It would be interesting to impose a membrane potential across the interfacial bilayer of the two droplets to further investigate the ability of the H-helix to reach the *trans* side of the DIB.

To confirm the hypothesis that the P454:CaM complex drives the ACD translocation, we analyses several substitutions and identified seven critical residues of P454 for membrane interaction and CaM binding : W458, R461, L463, R474, L475, H477 and I479. We previously identified that the two arginine residues are important for the membrane active properties of P454. The remaining residues are hydrophobic and are thus important for the insertion of the peptide into the membrane. From the crystal structure of P454:CaM, we observe that these residues make close contact with some CaM residues and may contribute

to stabilize the overall structure. Hence, we suggested that these residues are important for the overall translocation process, *i.e*, membrane destabilization and CaM binding.

We then investigated these mutations on the full-length protein. The first recombinant CyaA, $CyaA_{multi}$ (R461E, L463A, R474E, L475A, H477S and I479A) exhibits an enzymatic activity similar to the wild type *in vitro*, but it is not able to produce cAMP *in vivo*. This first recombinant protein indicates that mutations in the P454 segment abolish the ACD translocation, confirming that the P454 segment is actively involved in the CyaA translocation. Another interesting observation is that the $CyaA_{multi}$ hemolytic activity is enhanced. As it cannot translocate its ACD, we propose that the P454 segment within the $CyaA_{multi}$ may not be trap by CaM. Instead, it remains in the membrane and acts as a permeabilizing segment, which may explain why $CyaA_{multi}$ is more hemolytic.

To be less drastic than the $CyaA_{multi}$, we only mutated the two arginine residues with the recombinants $CyaA_{R12E}$ and $CyaA_{R12Q}$, corresponding to lowest affinity of the arginine-substituted peptides for membrane and CaM interactions. Interestingly, the recombinant $CyaA_{R12Q}$ does translocates its ACD while $CyaA_{R12E}$ does not. Mutation of only the two arginine is sufficient to abolish translocation. Yet, both P454-derived peptides exhibit similar membrane affinity. Their dissimilarities are observed in the permeabilization process and CaM binding. Indeed, the P454 R12E does not permeabilize membranes (not up to 50 µM in solution) while P454 R12Q does. Furthermore the P454 R12E affinity for CaM is above 30 µM and close to 2 µM for P454 R12Q. The CaM concentration varies from 1 to 10 µM in a eukaryotic cell (Jurado et al., 1999). Hence, it is possible that even if the P454 segment of $CyaA_{R12E}$ translocates, the K_d for CaM is too much affected for the formation of the peptide:CaM complex in the cytosol.

Our results are in accordance with the observations of Masin and colleagues (Masin et al., 2016). Indeed, they previously observed that single mutation of R461A or R474A reduces significantly but does not abolish the translocation of CyaA. Our results show that $CyaA_{R12Q}$ does translocate while P454 R12Q exhibits lower membrane actives properties and CaM affinity that P454 R12A (2 µM and 150 nM, respectively). Hence, it would be interesting to mutate both arginine residues by alanine and investigate the effect on the translocation process.

We then focused on the contributions of hydrophobic amino acids. In the crystal structure, the I479 is buried into the hydrophobic pocket of the N-CaM while the W458A is

into the hydrophobic pocket of the C-CaM. The recombinant $CyaA_{I479A}$ was found to intoxicate cells similarly to the native toxin while $CyaA_{W458A-I479A}$ partially abrogates the translocation. The affinities of the P454-derived peptides I479A and W458A-I479A for CaM are close to 1 μM and 3 μM, respectively. This is in the concentration range of CaM in the cytosol. However, the P454 I479A still permeabilizes membranes (although it is strongly affected) while P454 W458A-I479A does not (no permeabilization up to 80 μM in solution). Hence W458 is involved in the permeabilization process as well as the translocation.

Our data suggest that although the P454-derived peptides bind to the membrane and have an affinity in the concentration range of the cytosolic CaM concentration, the permeabilization efficiency seems to be correlated with the translocation event. It would be interesting to identify a P454-derived peptide exhibiting membrane-active properties, endowed with the capacity to translocate but not to bind CaM. Such recombinant CyaA would serve as a proof of concept that, although the P454 segment translocates across the plasma membrane, the binding to CaM is crucial to trigger ACD translocation.

In AC489 (*i.e* comprising both the H-helix and the P454 segment), our *in vitro* structural model supports a AC489:CaM complex of 1:1 with the C-CaM bound to the H-helix and the N-CaM to the P454 segment. *In vivo*, the P454 would translocate and bind to a N-CaM. Hence, the C-CaM is free and moves around the P454:N-CaM complex. Thereby, the increase of the local CaM concentration suggests that the H-helix binds to the C-CaM coming from the P454:N-CaM complex and not from another CaM.

The crystal structure by Guo and colleagues of ACD:C-CaM clearly shows that the H-helix is well folded (Guo et al., 2005). From our recent data, we observe that the H-helix segment is completely unfolded in solution and acquires structure upon CaM binding. This result suggests that the H-helix segment is presented in the cytosol in a disordered state. In general, the low structural content decreases the energy required to cross the membrane. For the diphtheria, anthrax and botulinum toxins, their catalytic domains are partially unfolded in the endosomes upon pH acidification (*i.e* molten globule state) and it is favorable for translocation (Araye et al., 2016; Lai et al., 2010; Galloux et al., 2008; Montagner et al., 2007; Chenal et al., 2002). Yet, we observed that the H-helix could interact with membranes and folds in α-helix upon membrane interaction. This suggests that the H-helix may be presented in the *trans* side of the membrane in a folded conformation. Furthermore, as observed for P454, we observed that CaM can remove and trap the H-helix from the

membrane. Hence, we suggest that, in the *trans* side, the H-helix is removed from the membrane by the free C-CaM.

This is no evidence that all the ACD is translocated when the H-helix reaches the cytosol and binds to the CaM. From our results, we observed that the H:CaM complex possesses an higher affinity than the P454:CaM complex (10 nM and 90 nM, respectively). Hence, the H:CaM complex may also act as a force for the translocation of the rest of the catalytic domain. Furthermore, our SAXS and HDX-MS models of AC489:CaM indicate that the H:CaM complex remains bound while the P454:CaM complex is dynamic. Hence, the H:CaM complex may help the translocation of the remaining segments of ACD into the cytosol and then allows the folding and activation of the catalytic site.

Perspectives on the translocation process of the CyaA toxin

The research performed during the PhD brings more details on the translocation process of the CyaA toxin. We propose that the P454 segment of the TR translocates and binds to CaM. The complex constitutes the driving force, based on the entropic pulling model (see part 3.3.3) and/or molecular ratchet for the translocation of ACD. However, several points are still missing.

We identified CaM as eukaryotic partner for both P454 and the H-helix binding. However, the diphtheria, botulinum and cholera toxins bind to several eukaryotic proteins (Azarnia Tehran et al., 2017; Burress et al., 2014; Taylor et al., 2010; Ratts et al., 2005, 2003) to favor their translocation into the cytosol. Hence, it is not excluded that others eukaryotic partners may participate to the translocation process of the CyaA toxin.

We identified some P454 residues as crucial for the translocation of ACD. However the inter segments as well as the length of the polypeptide chain (around 200 amino acids) between the H-helix and P454 may contribute to the translocation. In 2016, Masin and colleagues studied the implication of arginine and negatively charged residues between residues 390 and 500, in the translocation and hemolytic activities of CyaA (Masin et al., 2016). They found that mutation of some residues (not from P454) decrease the invasive capacity of CyaA. Hence, not only the P454 residues but also others contribute to the translocation. It would be interesting to further investigate the role of these 200 amino acids on the overall translocation process of CyaA.

We mainly focused on the TR and ACD concerning the translocation process. It is important to consider that the others domains, *i.e*, HR, AR and RD, might participate to the translocation process. They allow the folding of the toxin and its insertion into the plasma membrane. We are currently setting up experiments on erythrocytes to characterize the translocation of CyaA . The objective is to identify the different localizations (extracellular, membrane-bound or intracellular) of the different segments when CyaA is translocated.

We also plan to perform HDX-MS on membrane-inserted CyaA in order to shed light on the folding of CyaA when inserted into the membrane. To mimic as much as possible the physiological conditions, we would use Valinomycin. Valinomycin is a cyclic ionophore interacting with membranes and able to transport potassium ions through the membrane to induce an artificial "membrane potential".

Other perspectives

Crystallography of CyaA

Several efforts have been done over the years to get a high-resolution crystal structure of the full-length CyaA. The structure of the toxin is still lacking and currently, the only structures available are ACD with the C-CaM and the RTX block V of the RD (Bumba et al., 2016; Guo et al., 2005). The main problem is the structural disorder and flexibility of CyaA, which constitute a limit for crystallization in general. An approach would be to carry out proteolysis of unfolded regions with different proteases, as performed recently by Khanppnavar and Datta to get the partial structure of ExoY from *P. aeruginosa* (Khanppnavar and Datta, 2018). Another problem is that CyaA is a hydrophobic protein which multimerizes easily upon dilution from urea to conventional buffers. Now, we can purify CyaA into a monomeric state without chaotropes (Karst et al., 2014). This method paves the way for new trials of crystallization of the monomeric state of CyaA. Henceforth, the main objective is to stabilize flexible regions of the monomeric CyaA. In this perspective, we have recently selected 8 VHHs against the monomeric CyaA, in collaboration with the plateforme d'ingénieries des anticorps of the Institut Pasteur (see part 2.7). In parallel, in collaboration with the Institut de biologie integrative de la cellule (Gif-sur-Yvette, France), 9 αReps have been selected against the monomeric CyaA. αReps is a family of artificial repeat proteins. They are well produced, soluble, natively folded and extremely stable. αReps can stabilize unstable proteins, acting as "chaperones" and may favor crystallization (Chevrel et al., 2018).

Our objective is to crystallize CyaA in complex with VHHs and/or αReps.

P454 as an AMP

As P454 shares several similarities with AMPs, we also investigated whether P454 could have an antimicrobial activity on living bacteria. The bacteria were grown until exponential phase and an aliquot was incubated with P454 (final concentration around 150 µM). After 1h incubation at 30°C, several dilutions were carried out and bacterial growth was investigated. We first tried on *Escherichia coli*, *Staphylococcus aureus* and *Streptococcus agalactiae*. We did not observe any effects on bacterial growth on these bacteria. On contrary, we observed a complete inhibition of growth on the Gram-positive *Bacillus subtilis*, which indicates that P454 acts as an AMP peptide on this strain. Why P454 have an activity on this Gram-positive bacterium and not the others remains unknown. The answer may come from the composition of cell wall. These results are preliminary but it indicates that P454 has an AMP activity. We need to further investigate the AMP property of P454 on other bacteria strains.

Conclusion of the thesis

The work carried out during this thesis brings several molecular details about the translocation process of the catalytic domain of CyaA. Although CyaA possesses a unique cellular entry, we observed that the translocation requires a common process with the contribution of an eukaryotic partner for the passage of the catalytic domain into the cytosol. We identified the P454 peptide as a membrane-active peptide able to translocate and bind to CaM. This interaction is proposed to favor the translocation of the catalytic domain and then activation of the catalytic site. However, several questions need be to answer. Our model proposes a general translocation process. We need to further investigate the contributions of the P454 amino acids as well as those from the adjacent segments on the overall translocation process.

The cellular entry of CyaA is unique compared to others toxins. However, the overall translocation process to reach the cytosol is quite similar. Indeed, the toxin requires the help from an eukaryotic partner to translocate its catalytic domain. Hence, although the biological processes are different, they require common physical processes.

Chapter VII. Annex

Chapter VII. Annex

During the PhD, I had the opportunity to contribute to a project in collaboration with the Unité de Microbiologie Structurale of the Institut Pasteur, Paris. The team was interested to determine whether a protein, Bklc, was able to bind membrane and favor the anchoring of the cytoskeleton in *Prosthecobacter*. My contribution to this study was to prepare the lipid vesicles for AUC and Cryo-EM experiments. The publication is presented below.

Article

Bacterial kinesin light chain (Bklc) links the Btub cytoskeleton to membranes

Lurlène Akendengue, Sylvain Trépout, Martin Grana, Alexis Voegele, Carsten Janke, Bertrand Raynal, Alexandre Chenal, Sergio Marco and Anne Marie Wehenkel

Scientific Reports
Volume 7
Pages 45668
March 2017

It was long though that tubulin, a major component of the cytoskeleton, was only present in eukaryotic cells. However, bacterial tubulins (Btubs) exist in some *Prosthecobacter* species. The BtubA and B assemble into heterodimers in a GTP dependent manner like their eukaryotic homologous. A third protein, the bacterial kinesin light chain (Bklc) is present in the genetic cluster of the *btub* genes and very little is known about its functional role. The aim of this study was to characterize the functional role of Bklc with respect to Btubs.

Bklc is 256 amino acids protein, which showed a significant sequence identity with the eukaryotic kinesin light chain proteins. Also, the protein seems to have the propensity to form an α-helix, with an amphipathic character identified in its N-terminal part (residues 1-29). Circular dichroism confirmed that Bklc has mainly a α-helical conformation.

The next step was to figure out whether Bklc could bind BtubA and B. Using sedimentation assays, it was found that when BtubA/B are not polymerized, Blkc does not bind. On the contrary, in polymerizing conditions, Bklc binds to Btubs filaments with a stoichiometry of one Bklc per heterodimer. To confirm these results, cryo-electron microscopy (cryo-EM) was carried out with the His-tag marker Bklc and Ni-NTA nanogold beads. It was observed that Bklc largely decorates the Btubs filaments and their polymerization is not affected by the presence of the protein.

The presence of the N-terminal amphipathic helix suggested that Bklc could bind membranes and may anchor the Btub filaments. Analytical ultracentrifugation provided evidence for the interaction of Bklc with lipid vesicles, which was confirmed by cryo-EM. Interestingly, it was also found that Bklc induces a resizing of lipids with the presence of smaller vesicles. Finally, to evaluate whether Bklc could bind both Btubs and lipid vesicles, they were incubated together. It was found that the protein mediates both interactions.

In summary, Bklc forms a ternary complex linking Btubs and membranes, suggesting an important role in membrane anchor of Btubs in the prosthecae (*i.e* appendage, natural prolongation of the cellular membrane) of *Prosthecobacter*.

SCIENTIFIC REPORTS

OPEN

Bacterial kinesin light chain (Bklc) links the Btub cytoskeleton to membranes

Received: 23 November 2016
Accepted: 01 March 2017
Published: 30 March 2017

Lurlène Akendengue[1,2,†,*], Sylvain Trépout[3,4,*], Martín Graña[5], Alexis Voegele[6], Carsten Janke[1,2], Bertrand Raynal[7], Alexandre Chenal[6], Sergio Marco[3,4] & Anne Marie Wehenkel[1,2,‡]

Bacterial kinesin light chain is a TPR domain-containing protein encoded by the *bklc* gene, which co-localizes with the bacterial tubulin (*btub*) genes in a conserved operon in *Prosthecobacter*. Btub heterodimers show high structural homology with eukaryotic tubulin and assemble into head-to-tail protofilaments. Intriguingly, Bklc is homologous to the light chain of the microtubule motor kinesin and could thus represent an additional eukaryotic-like cytoskeletal element in bacteria. Using biochemical characterization as well as cryo-electron tomography we show here that Bklc interacts specifically with Btub protofilaments, as well as lipid vesicles and could thus play a role in anchoring the Btub filaments to the membrane protrusions in *Prosthecobacter* where they specifically localize *in vivo*. This work sheds new light into possible ways in which the microtubule cytoskeleton may have evolved linking precursors of microtubules to the membrane via the kinesin moiety that in today's eukaryotic cytoskeleton links vesicle-packaged cargo to microtubules.

Tubulin is one of the major components of the eukaryotic cytoskeleton and assembles as an obligate heterodimer into protofilaments that in turn form microtubules, which are generally made up of 13 protofilaments. Although tubulin has long been considered exclusively eukaryotic, bacterial tubulins (Btubs) exist in several *Prosthecobacter* species[1]. *Prosthecobacter* are gram-negative bacteria and belong to the division of *Verrucomicrobia* within the PVC (*Planctomycetes*, *Verrucomicrobia* and *Chlamydiae*) superphylum and are ubiquitiously present in soil, but also in aquatic environments[2,3]. They all present a single prosthecae (narrow extension of the cell wall) that may be required to decrease sedimentation in aquatic environments[2]. A unique feature of these bacteria is the presence of eukaryotic-like tubulin genes, *btubA* and *btubB*, that show high structural homology with eukaryotic tubulin[4]. BtubA and B assemble just like their eukaryotic counterparts as heterodimers in a GTP dependent manner[1,5] and have been shown to localize to the base of the prosthecae of several *Prosthecobacter* species[6]. The *btub* genes coexist with the bacterial tubulin homologue *ftsZ*[7], suggesting that they are not replacing FtsZ function, but their physiological role remains unclear. Whereas FtsZ forms individual protofilaments, Btubs seem to assemble in more complex bundle structures involving a different number of protofilaments both *in vitro*[4,5] and *in vivo*[6].

The *in vitro* assembly of BtubA/B protofilaments has been thoroughly studied[5,8,9] but very little is known about a third protein, Bklc (Bacterial kinesin light chain), that is systematically present within the genetic cluster that contains the *btub* genes[10]. Interestingly eukaryotic kinesins are a large family of microtubule motors subdivided into about 50 superfamilies (KIFs)[11]. Kinesins are generally composed of a motor domain and a coiled coil domain. Moreover KIF-specific adaptors can be found all over the kinesin families. Kinesin light chains (KLC1–4)

[1]Institut Curie, PSL Research University, CNRS UMR3348, F-91405 Orsay, France. [2]Université Paris Sud, Université Paris-Saclay, CNRS UMR3348, F-91405 Orsay, France. [3]INSERM, U1196, Université Paris Sud, Université Paris-Saclay, F-91405 Orsay, France. [4]Institut Curie, PSL Research University, CNRS UMR9187, F-91405 Orsay, France. [5]Institut Pasteur Montevideo, Unidad de Bioinformática, Mataojo 2020, 11400 Montevideo, Uruguay. [6]Institut Pasteur, Unité de Biochimie des Interactions Macromoléculaires, CNRS UMR3528, 28 rue du Dr Roux, 75724 Paris, France. [7]Institut Pasteur, Plateforme de Biophysique Moléculaire, CNRS UMR3528, 28 rue du Dr Roux, 75724 Paris, France. [†]Present address: Laboratoire de Biologie et Pharmacologie Appliquée, CNRS UMR8113, Ecole Normale Supérieure Paris-Saclay, 94235 Cachan, France. [‡]Present address: Institut Pasteur, Unité de Microbiologie Structurale, CNRS UMR3528, Université Paris Diderot, 25 rue du Dr Roux, 75724 Paris, France. [*]These authors contributed equally to this work. Correspondence and requests for materials should be addressed to A.M.W. (email: annemarie.wehenkel@pasteur.fr)

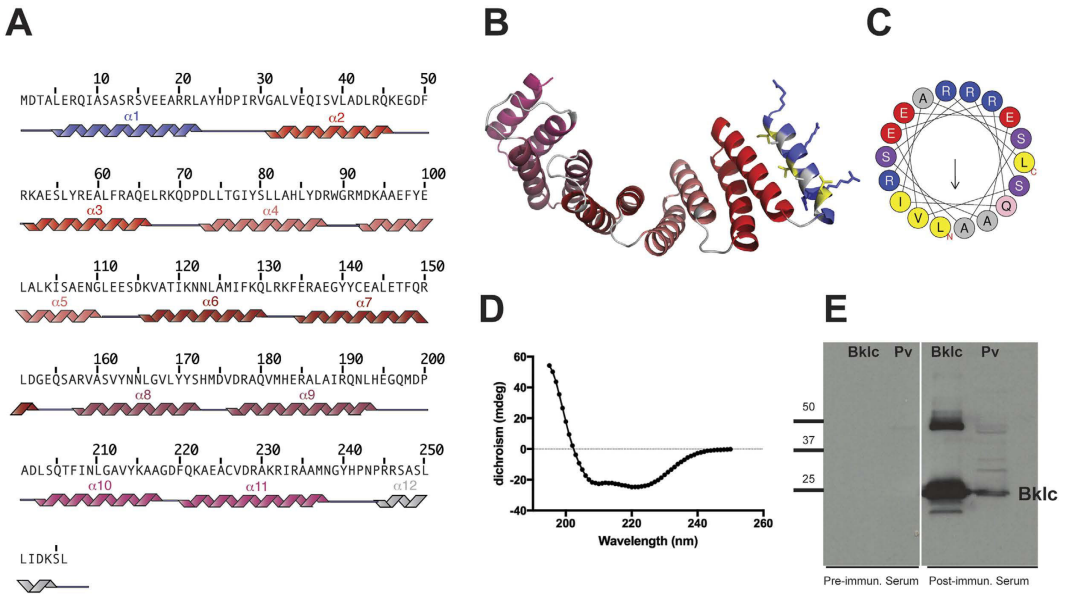

Figure 1. Bklc characterization (**A**). Secondary structure prediction of Bklc from P. vanneervenii (GenBank accession number: CAP16140.1). The 5 predicted TPR domains cover the following sequences: TPR1: 34–67; TPR2: 76–109; TPR3: 118–151; TPR4: 160–193; TPR5: 204–237 (**B**). 3D model of Bklc generated using Phyre2[30]. The N-terminal helix is shown in blue; the positively charged arginine residues are highlighted in blue and the hydrophobic residues in yellow (in accordance with the colors used in Fig. 1C) (**C**). Helical wheel representation of the N-terminal helix generated using Heliquest[31]. The arrow indicates the hydrophobic moment (**D**). Far-UV CD spectrum of Bklc showing a typical profile of an alpha-helical protein (**E**). Bklc is expressed *in vivo* in Prosthecobacter cell extracts. Lanes labeled Bklc correspond to purified recombinant Bklc protein. Lanes labeled Pv correspond to *Prosthecobacter vanneervenii* cell extracts.

are cargo adaptors for some of the KIF5 superfamily kinesin motors that are involved in axonal transport of synaptic vesicles, membrane organelles, as well as tubulin dimers[11].

The *btub* and *bklc* genes are co-transcribed and are thought to form a *bona fide* operon[1,10] but a functional link between the Btubs and Bklc has not yet been described. In order to understand whether *btubAB* and *bklc* form a functional operon we set out to characterize Bklc with respect to the bacterial tubulins. Here we show that the 3 proteins do indeed interact when Btubs are polymerized. Moreover Bklc was found to bind to lipid vesicles, and cryo-electron tomography allowed us to visualize a ternary complex between Btub filaments, Bklc and lipids, strongly suggesting a role in the membrane anchorage of the Btub filaments within the prosthecae. This work provides new elements towards understanding possible ways in which the microtubule cytoskeleton may have evolved linking precursors of microtubules to the membrane via the kinesin moiety.

Results and Discussion

Bklc characterization. Bklc had previously been described as a tetratricopeptide repeat (TPR)-containing protein with homology to eukaryotic kinesin light chain proteins[10]. TPR repeats are ubiquitously present in nature and play a major role in scaffolding and protein-protein interactions[12]. The entire central region of Bklc (residues 30–238) displays significant sequence identity (24%) with the experimental structure of human kinesin light chain HKLC2 (PDB code 3ceq), indicating that the central core of Bklc is an all alpha-helical protein with 5 central TPRs (10 helices, Fig. 1A,B). The additional N-terminal (residues 1–29) and C-terminal (239–256) segments of Bklc also have a high alpha-helix propensity (Fig. 1A) and might correspond to the flanking helices that are thought to have a "capping" or solubilizing function in TPRs[12]. The analysis of the hydrophobic and polar properties of these helices shows an amphipathic character for the N-terminal helix, with a hydrophobic and a polar face (with positive mean net charge, Fig. 1B,C).

Homologues of Bklc are found in all domains of life. This is in contrast with Btubs for which all detectable homologues out of a high similarity zone (*Prosthecobacter* genus) are from eukaryotic organisms. More sensitive profile-based searches confirmed this tendency and we were able to collect a diverse set of distant homologues against non-redundant databases. Although the promiscuity and ubiquity of TPR repeats in nature preclude extracting a clear evolutionary path for the origin of Bklc, some consistent results are noteworthy. First, eukaryotic homologues are found in simple unicellular eukaryotes (including *Ostreococcus tauri*, a marine green alga and the smallest free-living eukaryote) as well as higher eukaryotes. We also confirmed homology to kinesin light chains from vertebrates, including human kinesin light chain as well as the ciliary protein nephrocystin-3 (NPHP3).

In order to biochemically characterize Bklc we produced the C-terminal poly-histidine-tagged recombinant protein from *Prosthecobacter vanneervenii*. Bklc is a soluble protein and could be purified as a monomer using size exclusion chromatography. The secondary structure content of Bklc was analyzed by far-UV circular dichroism

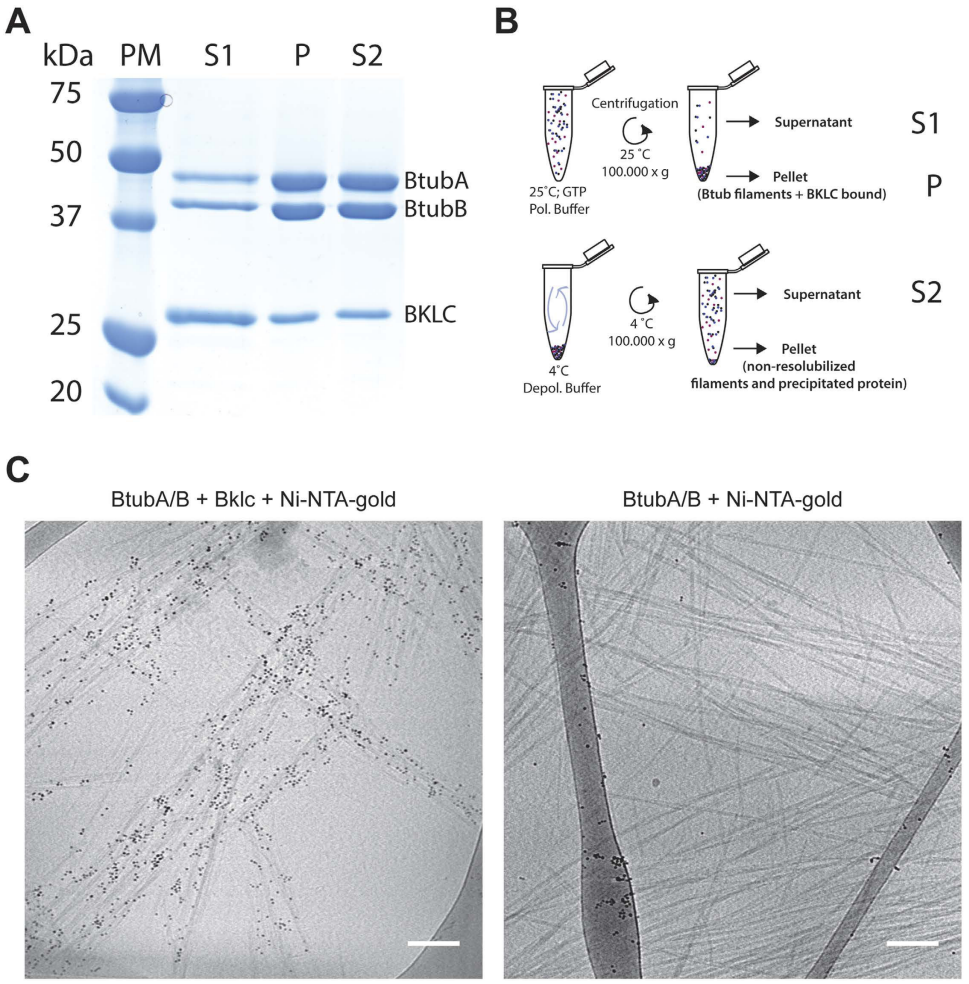

Figure 2. Btub-Bklc interaction (**A**). Coomassie stained SDS-PAGE showing that Bklc reversibly binds to Btub polymers in co-sedimentation assays (**B**). Schematic representation of the experimental procedure corresponding to fractions S1, P and S2 of the co-sedimentation assay (**C**). Ni-NTA-gold labeling of Bklc bound to Btubs in cryo-electron microscopy (left) Btub filaments without Bklc (right) Scale bar: 100 nm.

spectroscopy, which confirmed the predominantly alpha helical nature of the protein (Fig. 1D). We also wanted to verify that Bklc has a biological relevance and tested for its presence *in vivo* in *P. vanneervenii* cell extracts obtained from late exponential cultures. We produced polyclonal antibodies against recombinant Bklc in order to detect the protein in cell culture extracts. Using Western blot analysis with anti-Bklc antibodies we were indeed able to detect a band specifically recognized by the antibody and corresponding to the size of recombinant Bklc (Fig. 1E). We were thus able to confirm that the *bklc* gene is expressed and the protein present in *Prosthecobacter* cultures.

Bklc binds to polymerized Btubs. As *bklc* systematically co-localizes with the *btub* genes we set out to understand whether Bklc is functionally related to the Btubs by testing for the interaction between BtubA/B and Bklc. We could not detect an interaction of Bklc with non-polymerized Btub proteins neither by size exclusion chromatography (Supplementary Figure S1) nor by pull-down experiments suggesting very low or no affinity of Bklc for soluble Btubs. In order to detect binding of Bklc to polymerized Btubs we carried out sedimentation assays. In brief, purified and stoichiometric amounts of BtubA/B (generally 10 μM of the heterodimer) were incubated with an excess of Bklc per Btub monomer (10 or 20 μM) in polymerizing conditions. After high-speed centrifugation the Btub polymers were recovered in the pellet (P) together with Bklc, suggesting an interaction of the latter with the assembled Btub filaments (Fig. 2A). As a further control we tested for the reversibility of the binding (to exclude protein precipitation) by depolymerizing the Btub filaments present in the pellet and recovering the soluble fraction after depolymerization (Supernatant 2 (S2); Fig. 2B). Bklc as well as the Btubs were recovered in the soluble fraction and consecutive co-polymerization cycles could be carried without losing Bklc. Visual inspection of the SDS PAGE bands from the sedimentation assay suggests sub-stoichiometric binding of Bklc to Btub polymers.

Considering the technical difficulties to accurately measure polymer-associated stoichiometry in solution, we used the ImageJ software for densitometric quantification of gel band intensities of Btub and Bklc. A total of 10 μM of BtubA/B was used in all the gels analyzed where BtubA and B were present in stoichiometric amounts

as shown by Sontag and colleagues[8]. Bklc was added at a concentration of 10 or 20 μM. We thus quantified the relative intensities for BtubA, BtubB and Bklc from the gel bands (knowing that S1 + P1 correspond to the total amount of protein input) and calculated the intensity that would correspond to the amount of protein loaded. For the same amount of protein, the signal from the Btubs on the Coomassie stained gel was about twice that of Bklc. Relating these values to the S2 fraction of the sedimentation assay, the stoichiometry thus estimated corresponds to about 1 Bklc monomer per BtubA/B heterodimer.

Under the conditions used in our study Bklc interacted with polymerized Btubs but not monomeric or dimeric proteins, suggesting that the binding mode of Bklc may be sensitive to a particular environment only found within the context of the Btub polymer. Several microtubule-associated proteins (MAPs) have been shown to discriminate between assembled microtubules and unpolymerized tubulin. Two structurally characterized examples are the plus end tracking protein EB3[13] and doublecortin (DXC[14]), both proteins binding between two protofilaments making longitudinal as well as lateral contacts with the tubulin dimers and thus fully relying on the assembled microtubule for binding[15]. A second possibility for Btub-Bklc interaction would be the recognition of a polymer-specific conformation of the Btub heterodimer. In the case of tubulin, it is known that tubulin dimers can adopt different conformations depending on which nucleotide is bound and whether they are incorporated into a microtubule or are free in solution[14,16]. While the observed stoichiometry of 1 Bklc per BtubA/B heterodimer would be compatible with both models above, we observed that Bklc binds several BtubA/B filament bundles with different lateral assemblies (that co-exist *in vitro,* see results below), suggesting the recognition of a polymer-associated conformation rather than a polymer specific interface.

To confirm the results obtained from the sedimentation assay and to visualize any potential changes to the Btub filament assembly we carried out cryo-electron microscopy analysis of the assembly. Btubs and Bklc were co-polymerized and Ni-NTA nanogold beads were added just prior to freezing in order to label the poly-histidine tag of Bklc. The Btub filaments in the presence of Bklc were largely decorated by Ni-NTA beads whereas the negative control of Btubs with Ni-NTA beads alone were not (Fig. 2C), further confirming the functional relationship between the 3 proteins of the operon. Using a light scattering assay to follow Btub assembly we could not observe significant changes in assembly or critical concentration in the presence of Bklc (Supplementary Figure S2), suggesting that Bklc does not affect polymerization properties of the Btubs.

Btubs have been suggested to assemble as 5-protofilament bacterial microtubules (bMTs)[6] *in vivo*, so we asked if Bklc could induce different inter-filament assemblies. Our images of Btub filaments alone did not show evidence for bMTs, in fact all of our polymers appeared to be helical polymers of 2 or 4 protofilaments, as previously seen in negative stain EM[4,5]. We analyzed the 3D structures of some representative filament assemblies made up of 2 or 4 filaments and determined their periodicity (Fig. 3 and Supplemental Movie S1 and S2). For double filaments a cross over was observed every 110 to 130 nm corresponding to a periodicity of 250 nm. The helical periodicity increases with 4 filaments to 310 nm suggesting a flattening out as filament numbers increase. Indeed we observed 6 filament assemblies (Supplemental Movie S3), but we were not able to accurately measure the periodicity due to fiber crowding on the images. However, based on half-repeats, which are 370 nm long, we can estimate the periodicity to be around 740 nm. In the presence of Bklc we did not observe any significant changes in the assembly properties of the filaments with respect to each other (Supplementary Movies S4 and S5).

Purified Bklc binds to lipid membranes. The above results showed that Bklc directly interacts with Btub filaments but its physiological role remains unclear. The presence of an N-terminal amphipathic helix as well as previous localization studies of Btubs within the base of the prosthecae and near the plasma membrane of *P. vanneervenii*[6] suggested that Bklc could bind to membranes and play a functional role in membrane tethering of the Btub filaments. To determine if Bklc interacted with membranes, we performed AUC sedimentation velocity experiments. Experiments were carried out using a double optical detection system by absorbance at 280 nm (ABS; specific to proteins such as Bklc) and interferometry (IF) that can detect both protein and lipids. Bklc on its own sediments as a main species with a sedimentation coefficient of 2.8 S and frictional ratio of 1.2 giving a calculated molecular mass of 30.3 kDa in accordance with a monomeric state of the protein (Fig. 4A insert). The small unilamellar vesicles (SUVs) were run separately and showed a main peak at 2.4 S (Fig. 4A insert). Upon incubation of both SUVs and Bklc a new peak appears at 2.0 S with a signal for both Bklc (ABS and IF) and lipids (IF) providing direct experimental evidence for their interaction (Fig. 4A). Integration of absorbance and interference signals showed that the peak contains lipids as well as proteins. The decrease in sedimentation of Bklc from 2.8 S to 2.0 S is in accordance with a higher buoyancy and thus "floatation" of Bklc in interaction with lipid vesicles. We confirmed the Bklc-SUV interaction using cryo-EM where Ni-NTA nano-gold beads that label the C-terminal His-tag of Bklc were co-localized with lipid vesicles (Fig. 4B). An additional new peak was detected by interference only, at a sedimentation value of 1.3 S suggesting the presence of small lipid assemblies. Indeed our cryo-EM data showed that Bklc induces a resizing of lipid vesicles and we observed small objects (about 14 nm; Fig. 4C) that were not found when SUVs were imaged alone. It is likely that these vesicles correspond to the peak of 1.3 S.

Btub filaments have been described in close vicinity to the plasma membrane of *P. vanneervenii*[6]. Our sedimentation and AUC data above suggest that Bklc could therefore tether the Btubs to the membrane. To understand if Bklc could mediate both Btub and SUV interactions simultaneously we incubated BtubAB (5 μM) with Bklc (5 μM) and SUVs (4 mM lipid) in polymerizing conditions for 10 to 20 minutes for subsequent EM imaging. Just prior to flash-freezing the mixture was diluted in polymerization buffer with Ni-NTA nanogold beads. Gold labeling of the Bklc His tag localized the protein to the area between the filaments and the lipid vesicles, indicating that the protein could mediate their interaction. A 3D reconstitution showed the direct interaction of all 3 partners (Fig. 5). Taken together our results point to a physiological role of Bklc as a membrane tether of Btub filaments in *Prosthecobacter*.

From an evolutionary point of view the Btub operon seems to be clearly related to the eukaryotic kingdom from which *Prosthecobacter* have acquired it via horizontal gene transfer. The ubiquitous presence of TPR domains

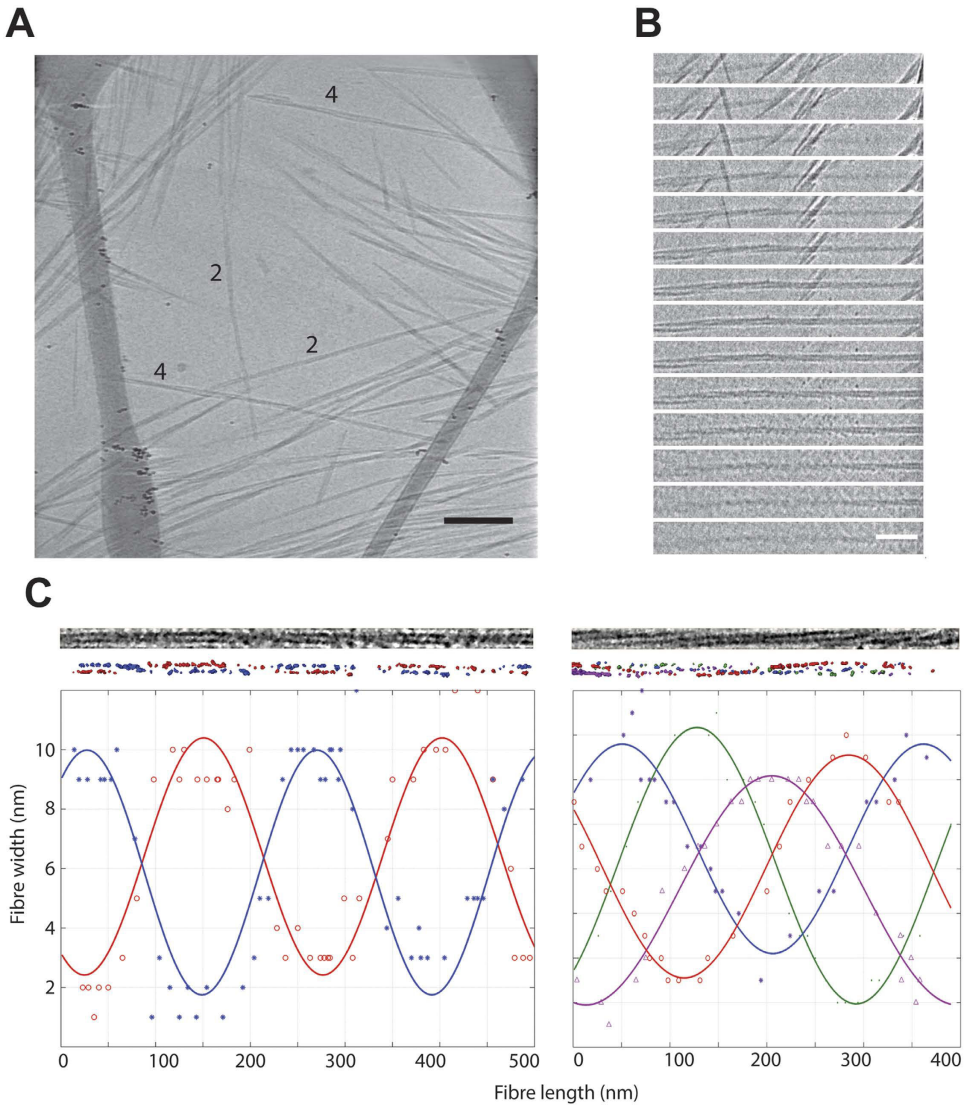

Figure 3. Structural characterization of Btub filaments (**A**). The image shows a 2D projection from a tomogram of BtubA/B fiber (see also Supplementary Movie S4 for corresponding tomogram). Some representative filaments of 2 and 4 are highlighted in the figure. Scale bar: 100 nm (**B**). A sequential view through a tomogram of a 2 filament assembly is shown in Fig. 3C (left) Scale bar: 50 nm (**C**). 3D structures of Btub filament assemblies. Top, experimental images of Btubs extracted from two cryo-tomograms. Middle, rendering of threshold-based manually segmented tomograms showing each filament in a single color (red, blue, violet and green). Bottom, distance (width and length) plot of each filament depicting their periodicity. For the helical reconstruction and periodicity the mean squared error (MSE) for each curve is as follows: Left plot: blue curve (*) = 1.96; red curve (○) = 1.52; Right plot: blue curve (*) = 0.53; red curve (○) = 0.41; green curve (•) = 0.39; purple curve (Δ) = 1.01.

in all domains of life hampers determination of Bklc origin. Yet Bklc is probably a molecular partner since the Btub transfer event. Supporting this hypothesis is the abrupt decay in sequence identity (from >80% to <40%) for the three proteins out of the '*Verrucomicrobia*' zone as well as our functional characterization. Our work shows that Bklc can bind both Btubs and SUVs, leading us to speculate that an early eukaryotic MAP could have been involved in membrane tethering of microtubules. It is interesting to note that kinesin motors were postulated to be present in the last eukaryotic common ancestor (LECA)[17]. One possibility may be that Btub-Bklc complex represents a transition period in eukaryotic tubulin evolution where the microtubule cytoskeleton acquired its complexity. Indeed membrane tethering of microtubules is thought to be an important step in the evolution of the eukaryotic cell, evolving from vesicle binding modules to more sophisticated microtubule-membrane compartment such as the cilium[18]. Interestingly, the second close homologue we found for Bklc in higher eukaryotes is NPHP3, a multi-domain ciliary protein that apart from the TPR domains also includes a tubulin modifying domain (tubulin tyrosine Ligase, TTL) and is thus likely to directly interact with tubulin or microtubules[19]. If our hypothesis were correct the early link between membranes and microtubules would have consisted of a TPR domain-containing protein. TPR domains are helical tandem repeats, that when present as multiple copies,

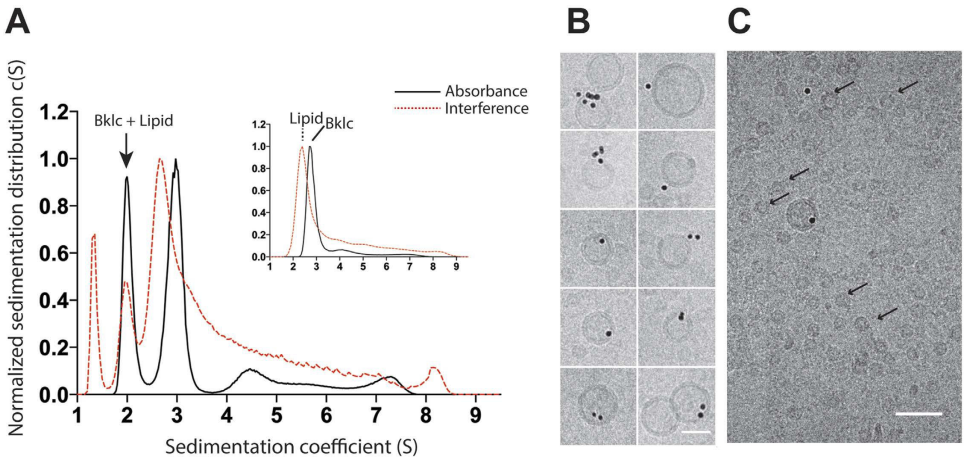

Figure 4. Bklc binding to lipid vesicles (**A**). Sedimentation profiles of Bklc + SUVs (main graph) detected by absorbance at 280 nm and interference; control Bklc alone detected by absorbance at 280 nm (inset, black continuous line) and SUVs alone detected by interference (inset, red dotted line) (**B**). SUV-Bklc co-localization as indicated by the Ni-NTA-gold beads directed against the His-tag of Bklc (scale bar: 30 nm) (**C**). Upon incubation of SUVs with Bklc, small lipid assemblies are formed (some highlighted by arrows) that could correspond to the lowest sedimenting species of Fig. 4A main graph (scale bar: 50 nm).

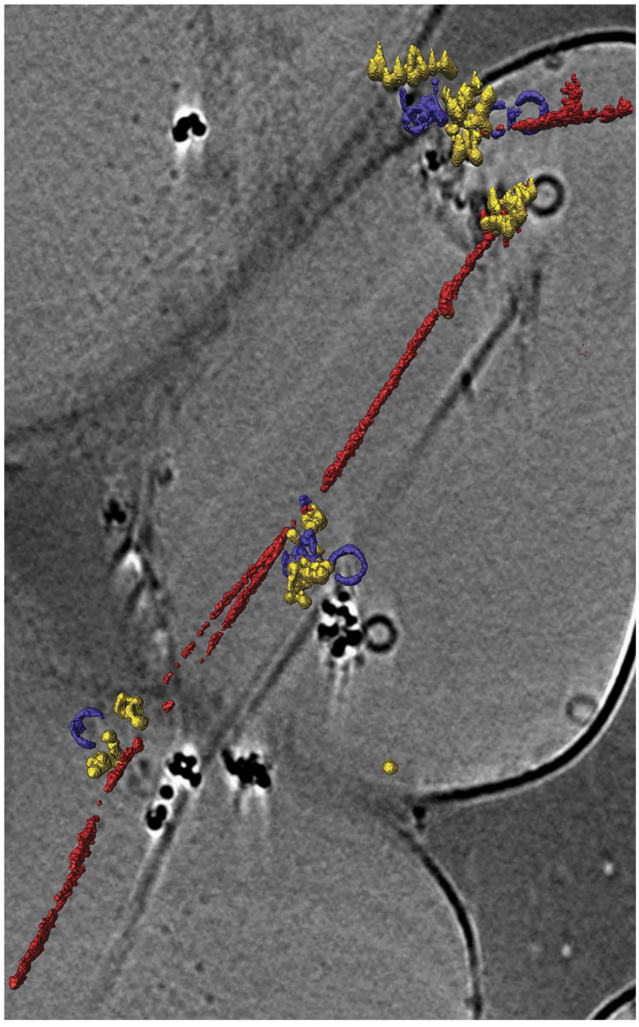

Figure 5. Cryo-EM image and 3D representation of the ternary complex between Btub fibers (red), SUVs (purple) and Bklc + Ni-NTA-Gold (yellow). The 3D iso-surfaces are overlaid on a 2D image corresponding to one z-plane from the tomogram.

can form alpha solenoids similar to Heat or Armadillo (ARM) domains. The latter are predominantly found in eukaryotes whereas TPRs are widespread in both eukaryotes and prokaryotes[20]. Alpha-solenoid based architectures are evolutionary conserved modules involved in membrane trafficking and shaping[20] and it is thought that membrane-curving protein modules were required to evolve the endomembrane system[21].

Materials and Methods

Protein Expression and Purification. The *btubA* and *btubB* genes from *P. dejongeii* were co-expressed without an affinity tag in a pHis17 vector from a biscistronic gene construct where the native intergenic region remained intact (gift from JM. Andreu). Transformed *E. coli* C41 (DE3) cells were grown to an optical density (OD_{600nm}) of 0.4 at 37 °C and protein expression was induced with 0.25 mM IPTG for 3 hours at 37 °C. Cell pellets were harvested and flash frozen in liquid nitrogen. BtubA and BtubB proteins were purified by an initial cycle of polymerization/depolymerization, followed by size exclusion chromatography. In brief, bacterial cell pellets from 1-liter cultures were resuspended in 20 ml lysis buffer (50 mM Tris-HCl pH 8 supplemented with EDTA-free protease inhibitor cocktails (ROCHE)). Cells were disrupted by sonication and the lysate was centrifuged for 30 min at 30.000 rpm. The cleared lysate was completed with the polymerization buffer (300 mM potassium glutamate, 5 mM $MgCl_2$, 2 mM GTP, 1 mM EGTA) and incubated for 10 minutes at 25 °C. The mixture was centrifuged for 30 min at 100,000 × g at 25 °C (in a pre-warmed Ti-70 rotor). The semi-transparent protein pellet (P1) corresponding to the polymerized Btubs was carefully dissolved in a small volume (1.5 ml) of cold depolymerization buffer (20 mM Tris-HCl, 1 mM EGTA, pH 7.5) for 20 minutes on ice to allow for complete depolymerization of the BtubA/B-assembled polymers. The sample was centrifuged 30 minutes at 100,000 × g at 4 °C in a precooled rotor (TLA-55). BtubA and BtubB were now recovered in the supernatant (S2). The supernatant (S2) containing Btub A/B was concentrated and loaded onto a size exclusion column (GE Healthcare - Hiload Superdex 200 PG 16–60) pre-equilibrated at 4 °C in the gel filtration buffer (20 mM Tris-HCl, 1 mM EDTA pH 7.5). The fractions containing BtubA and BtubB were then pooled and concentrated to about 20 mg/ml, flash frozen in liquid nitrogen and stored at −80 °C.

The *bklc* gene from *P. vanneervenii* was expressed from pHis17 with a C-terminal His-tag (gift from M. Pilhofer). Transformed *E. coli* C41 (DE3) cells were grown to an optical density (OD_{600nm}) of 0.4 at 37 °C followed by an equilibration at 16 °C for 20 minutes. Protein expression was induced with 0.25 mM IPTG for 20 hours at 16 °C. Cell pellets were harvested and flash frozen in liquid nitrogen, and resuspended in lysis buffer (50 mM Tris-HCl pH 7.5, 500 mM NaCl, 5% glycerol, 1 mM DTT, EDTA-free protease inhibitor cocktail). The resuspension was sonicated, and the lysate was centrifuged for 30 minutes at 30,000 rpm. The cleared lysate was loaded onto a Ni-NTA affinity chromatography column (HisTrap FF, GE Healthcare). Nonspecific proteins were removed by washing the column with buffer A (20 mM Tris-HCl, 200 mM NaCl, 5% glycerol, 1 mM DTT and 10 mM imidazole, pH 7.5). Bklc-His was eluted with a linear gradient of imidazole (Buffer B, 20 mM Tris-HCl pH 7.5, 200 mM NaCl, 5% glycerol, 1 mM DTT, 1 M imidazole). The eluted fractions containing Bklc were concentrated and loaded onto a size exclusion column (GE Healthcare, Superdex 200 10/300) pre-equilibrated at 4 °C in the gel filtration buffer (20 mM TrisHCl pH 7.5, 200 mM NaCl, 5% glycerol 1 mM DTT). The final elution peak was concentrated to 2 mg/ml, flash frozen in liquid nitrogen and stored at −80 °C.

Circular Dichroism. Far-UV spectra (195–250 nm) of Bklc in solution were obtained by circular dichroism on an AVIV 215 machine. Bklc was used at a concentration of 17.5 μM in its storage Buffer (20 mM TrisHCl pH 7.5, 200 mM NaCl, 5% glycerol 1 mM DTT) in a cuvette with optical path length of 0.2 mm.

Analyical Ultracentrifugation. Bklc, SUVs, as well as Bklc-SUV complexes at the following final concentration [Bklc] 27 μM, [Lipid] 2 mM were centrifuged at 42 000 rpm in a Beckman Coulter XL-1 analytical ultracentrifuge, at 20 °C in a four-hole AN 60–Ti rotor equipped with 12-mm double-sector epoxy centerpieces. Detection of the protein and SUV concentration as a function of radial position and time was performed by optical density measurements at 280 nm and interferometry. Ultracentrifugation experiments were performed in 25 mM Tris-HCl buffer (pH 7.5) containing 150 mM NaCl. The following parameters were calculated with Sednterp software and used for the results analysis: partial specific volumes 0.729 $ml.g^{-1}$ for Bklc, 0.979 $ml.g^{-1}$ for lipid, viscosity 0.01023 poise, and density 1.0053 $g.ml^{-1}$. Sedimentation velocity data analysis was performed by continuous size distribution analysis c(s) using Sedfit 15.01 software[22].

Prosthecobacter cultures. *Prosthecobacter vanneervenii* strain 12252 was purchased from DSMZ (Leibniz-Institut DSMZ-Deutsche Sammlung von Mikroorganismen und Zellkulturen GmbH, www.dsmz.de) and grown in liquid MMB medium as described in DSMZ recipe 628 (https://www.dsmz.de/microorganisms/medium/pdf/DSMZ_Medium628.pdf). Cultures were grown at 26 °C in an orbital shaker and reached a maximal optical density $OD_{600nm} = 0.7$ after 65 hours of culture. Cell pellets were harvested by extended centrifugation (90 minutes at 20.000 × g).

Antibody production and Western Blot. Rabbit polyclonal antibodies were generated against recombinant Bklc-His from *P. vanneervenii* by PTL (Pettinghill Technology, London). The specific recognition of anti-Bklc antibodies was validated by testing pre-immunized and different post-immunization bleeds against purified recombinant protein (0.2 μg per lane) used for immunization as well as total cell extracts from *P. vanneervenii* (70 μg total protein per lane). The sera were diluted at a ratio of 1:2000 and HRP-conjugated anti-rabbit secondary antibodies (1:10 000, GE Healthcare NA934) were used for chemiluminescent detection (Luminata Forte, Millipore) on film (Amersham Hyperfilm ECL). The pre-immune sera and anti-Bklc antibody were blotted on separate membranes (from a single gel transferred to a single membrane, and then cut in two). The two membranes were laid side by side to reconstitute the original gel for chemiluminescent exposure on film.

Sedimentation assay. Purified BtubA/B (generally at a concentration of 10 μM) were polymerized as described in ref. 23. In brief BtubA/B were incubated for 10 minutes at 25 °C in polymerization buffer (20 mM TrisHCl pH 7.5, 300 mM potassium glutamate, 5 mM $MgCl_2$, 1 mM EGTA, 2 mM GTP). Polymerized Btub filaments were sedimented into the pellet after ultracentrifugation for 30 minutes at 100.000 × g at 25 °C. In order to check for reversibility of the polymerization, the pellet was resuspended in depolymerization buffer (20 mM TrisHCl pH 7.5, 1 mM EGTA) at 4 °C for 20 minutes. The sample was centrifuged at 100.000 × g for 20 minutes at 4 °C and the depolymerized Btubs were recovered in the soluble fraction. Co-polymerization with Bklc (varying concentrations) was carried out according to the same protocol as Btubs alone.

Densitometric quantification of gel bands. The SDS-PAGE gels to be analyzed were scanned and loaded into ImageJ software (Rasband, W.S., ImageJ, U. S. National Institutes of Health, Bethesda, Maryland, USA, http://imagej.nih.gov/ij/, 1997–2016). The Images were converted to 32 bit grayscale images and rectangles were drawn around the area of the lanes to analyze and the band intensity was plotted per lane. The peaks corresponding to the band intensities were quantified and the ratios of Btub:Bklc were calculated on an average of 3 independent gels from three independent experiments.

Small unilamellar vesicle preparation. Small unilamellar vesicles (SUVs) were prepared by reverse phase evaporation[24] from a chloroform solution made of an 8:2 mixture of 1-palmitoyl-2-oleoyl phosphatidylcholine (POPC) and 1-palmitoyl-2-oleoylglycero-3-phosphoglycerol (POPG) to a final concentration of 10 mM lipids. The chloroform was removed by evaporation in a rotavapor under vacuum. The dried phospholipid film was protected from oxidation by a layer of argon and then resuspended in a mixture of diethyl ether and buffer solution (25 mM TrisHCl, pH 7.6, 150 mM NaCl), followed by sonication to make an emulsion of lipid, ether and buffer. The reverse phase evaporation was performed by slowly evaporating the ether in the rotavapor by slowly decreasing the pressure down to the vacuum to avoid ether boiling. The lipid suspension was then extruded through polycarbonate filters (from 0.8 to 0.2 μm pore sizes) to obtain large unilamellar vesicles (LUVs). The SUVs were obtained by further sonication of the LUV solution. The diameter and charge of SUV were measured by dynamic light scattering (DLS) and electrophoretic mobility on a Zetasizer Nano instrument (Malvern Instruments)[25]

Sample preparation for electron microscopy. The images obtained for Btub filaments in absence or presence of Bklc were obtained by 2 consecutive cycles of polymerization in order to remove protein noise that could be generated from non-polymerization competent molecules. The Ni-NTA-nanogold beads (5 nm; purchased from Nanoprobes) were added after the second polymerization and used at a final concentration of 50 nM.

For the SUV images with or without Bklc, experiments were carried out at room temperature, and the SUVs were incubated with or without Bklc for 45–60 minutes using concentrations of 2.5 mM and 4 M for SUVs and Bklc respectively in 20 mM TrisHCl pH 7.5 and 150 mM NaCl. The Ni-NTA-nanogold beads (5 nm; purchased from Nanoprobes) were added just prior to sample freezing and used at a final concentration of 50 nM.

For plunge freezing of samples, a 5 μl drop of sample was deposited onto 300 mesh holey carbon copper grids (Ted Pella). The excess of solution was manually blotted using a Whatman filter paper and the grid was plunge-frozen in liquid ethane using a Leica EM-CPC.

Electron microscopy imaging and data processing. Data acquisition was performed on a 200 kV field emission gun JEOL 2200FS electron microscope equipped with a Gatan US1000 slow scan CCD camera and an in-column energy-filter. Zero-loss (slit: 20 eV) high magnification images were acquired at pixel sizes between 7 and 2 Å at the specimen level with nominal defocus between 1 and 4 μm depending on the experiment. Tilt-series dataset were collected under zero-loss conditions (slit: 25 eV) at a pixel size of 7 Å at the specimen level with nominal defocus varying from 5 to 10 μm depending on the experiment using an in-house developed software.

For data processing of the Btub fibers Tilt-series were aligned and reconstructed using TomoJ v2.32[26]. The alignments were performed using the local minima algorithm[27] and reconstruction was generated using OS-SART-GPU (iterations: 100, relaxation coefficient: 0.01, volume update: every 4 images).

The periodicity of the helical filament repeats was calculated on the electron densities of the 3D reconstructed filaments that were semi-automatically segmented with Amira which corresponds to threshold-based method. The computation was performed in Matlab using a non-linear least-squares regression algorithm nlinfit[28]. The animations showing the filament densities presented in the Supplementary Data have been generated with Amira.

Bioinformatic analysis. TPR predictions were done using the TPRpred program[29] and the secondary structure and closest structural homologues were inferred from Phyre 2[30]. The pdb entry 3CEQ of the Human kinesin light chain 2 was used to obtain the Bklc model with highest confidence over the largest sequence coverage with highest sequence identity and the model in Fig. 1B was done using Pymol (http://www.pymol.org). The amphipathic nature and hydrophobic characteristics of the N-terminal helix were predicted using the HELIquest software[31].

Blast[32] searches using Bklc from *Prosthecobacter vanneervenii* (Uniprot id: A8Y5U5_9BACT) as query were performed over several databases, including: Uniprot, non-redundant and IMG complete genomes and metagenomic databases. For all searches, an inclusion e-value threshold of 10^{-10} was used. Blast outputs showed a high rate of false positives, due in part to sequence divergence but also to variable number of TPR motifs associated with diverse protein functions. For this reason we turned to profile-based searches to search for eukaryotic homologues, using HHblits[33] against the Uniprot database and HHsearch[34] against the PDB. We also turned to transitive profile searches as implemented in HHsenser[35] to explore distant homologues, as this method has proved to gather few false positive rates.

References

1. Jenkins, C. *et al.* Genes for the cytoskeletal protein tubulin in the bacterial genus Prosthecobacter. *Proc Natl Acad Sci USA* **99,** 17049–17054 (2002).
2. Hedlund, B. P., Gosink, J. J. & Staley, J. T. Verrucomicrobia div. nov., a new division of the bacteria containing three new species of Prosthecobacter. *Antonie Van Leeuwenhoek* **72,** 29–38 (1997).
3. Bergmann, G. T. *et al.* The under-recognized dominance of Verrucomicrobia in soil bacterial communities. *Soil Biology and Biochemistry* **43,** 1450–1455 (2011).
4. Schlieper, D., Oliva, M. A., Andreu, J. M. & Löwe, J. Structure of bacterial tubulin BtubA/B: evidence for horizontal gene transfer. *Proc Natl Acad Sci USA* **102,** 9170–9175 (2005).
5. Sontag, C. A., Staley, J. T. & Erickson, H. P. *In vitro* assembly and GTP hydrolysis by bacterial tubulins BtubA and BtubB. *Journal of Cell Biology* **169,** 233–238 (2005).
6. Pilhofer, M., Ladinsky, M. S., McDowall, A. W., Petroni, G. & Jensen, G. J. Microtubules in bacteria: Ancient tubulins build a five-protofilament homolog of the eukaryotic cytoskeleton. *PLoS Biol* **9,** e1001213 (2011).
7. Pilhofer, M., Rosati, G., Ludwig, W., Schleifer, K.-H. & Petroni, G. Coexistence of tubulins and ftsZ in different Prosthecobacter species. *Mol. Biol. Evol.* **24,** 1439–1442 (2007).
8. Sontag, C. A., Sage, H. & Erickson, H. P. BtubA-BtubB heterodimer is an essential intermediate in protofilament assembly. *PLoS ONE* **4,** e7253 (2009).
9. Martin-Galiano, A. J. *et al.* Bacterial tubulin distinct loop sequences and primitive assembly properties support its origin from a eukaryotic tubulin ancestor. *J Biol Chem* **286,** 19789–19803 (2011).
10. Pilhofer, M. *et al.* Characterization of bacterial operons consisting of two tubulins and a kinesin-like gene by the novel Two-Step Gene Walking method. *Nucleic Acids Res.* **35,** e135 (2007).
11. Hirokawa, N., Noda, Y., Tanaka, Y. & Niwa, S. Kinesin superfamily motor proteinsand intracellular transport. *Nat Rev Mol Cell Biol* **10,** 682–696 (2009).
12. D'Andrea, L. TPR proteins: the versatile helix. *Trends Biochem. Sci.* **28,** 655–662 (2003).
13. Fourniol, F. J. *et al.* Template-free 13-protofilament microtubule-MAP assembly visualized at 8 A resolution. *J Cell Biol* **191,** 463–470 (2010).
14. Zhang, R., Alushin, G. M., Brown, A. & Nogales, E. Mechanistic Origin of Microtubule Dynamic Instability and Its Modulation by EB Proteins. *Cell* **162,** 849–859 (2015).
15. Nogales, E. & Zhang, R. Visualizing microtubule structural transitions and interactions with associated proteins. *Curr Opin Struct Biol* **37,** 90–96 (2016).
16. Brouhard, G. J. & Rice, L. M. The contribution of ab-tubulin curvature to microtubule dynamics. *J Cell Biol* **207,** 323–334 (2014).
17. Wickstead, B. & Gull, K. The evolution of the cytoskeleton. *J Cell Biol* **194,** 513–525 (2011).
18. Satir, P., Guerra, C. & Bell, A. J. Evolution and persistence of the cilium. *Cell Motil Cytoskeleton* **64,** 906–913 (2007).
19. Prota, A. E. *et al.* Structural basis of tubulin tyrosination by tubulin tyrosine ligase. *J Cell Biol* **200,** 259–270 (2013).
20. Fournier, D. *et al.* Functional and Genomic Analyses of Alpha-Solenoid Proteins. *PLoS ONE* **8,** e79894 (2013).
21. Devos, D. *et al.* Components of coated vesicles and nuclear pore complexes share a common molecular architecture. *PLoS Biol* **2,** e380 (2004).
22. Schuck, P. Size-Distribution Analysis of Macromolecules by Sedimentation Velocity Ultracentrifugation and Lamm Equation Modeling. *Biophysj* **78,** 1606–1619 (2000).
23. Andreu, J. M. & Oliva, M. A. *Purification and Assembly*. *Microtubules, in vitro 2E* **115,** 269–281 (© Elsevier 2013).
24. Subrini, O. *et al.* Characterization of a Membrane-active Peptide from the Bordetella pertussis CyaA Toxin. *Journal of Biological Chemistry* **288,** 32585–32598 (2013).
25. Sotomayor-Pérez, A. C., Ladant, D. & Chenal, A. Calcium-induced Folding of Intrinsically Disordered Repeat-in-Toxin (RTX) Motifs via Changes of Protein Charges and Oligomerization States. *Journal of Biological Chemistry* **286,** 16997–17004 (2011).
26. Messaoudi, C., Boudier, T., Sorzano, C. & Marco, S. TomoJ: tomography software for three-dimensional reconstruction in transmission electron microscopy. *BMC Bioinformatics* **8,** 288 (2007).
27. Sorzano, C. *et al.* Marker-free image registration of electron tomography tilt-series. *BMC Bioinformatics* **10,** 124 (2009).
28. Seber, G. & Wild, C. J. Computational Methods for Nonlinear Least squares. *Wiley Series in Probability and Statistics* (1989).
29. Karpenahalli, M. R., Lupas, A. N. & Söding, J. TPRpred: a tool for prediction of TPR-, PPR- and SEL1-like repeats from protein sequences. *BMC Bioinformatics* **8,** 2 (2007).
30. Mezulis, S., Yates, C. M., Wass, M. N., Sternberg, M. J. E. & Kelley, L. A. The Phyre2 web portal for protein modeling,prediction and analysis. *Nat Protoc* **10,** 845–858 (2015).
31. Gautier, R., Douguet, D., Antonny, B. & Drin, G. HELIQUEST: a web server to screen sequences with specific -helical properties. *Bioinformatics* **24,** 2101–2102 (2008).
32. Altschul, S. F., Gish, W., Miller, W., Myers, E. W. & Lipman, D. J. Basic local alignment search tool. *Journal of Molecular Biology* **215,** 403–410 (1990).
33. Remmert, M., Biegert, A., Hauser, A. & Söding, J. HHblits: lightning-fast iterative protein sequence searching by HMM-HMM alignment. *Nat Methods* **9,** 173–175 (2011).
34. Soding, J. Protein homology detection by HMM-HMM comparison. *Bioinformatics* **21,** 951–960 (2005).
35. Soding, J., Remmert, M., Biegert, A. & Lupas, A. N. HHsenser: exhaustive transitive profile search using HMM-HMM comparison. *Nucleic Acids Res.* **34,** W374–W378 (2006).

Acknowledgements

We would like to thank Jose Manuel Andreu and Martin Pilhofer for providing the plasmids used in this work and Patricia Duchambon for her assistance and access to equipment. We are grateful to Martin Pilhofer and Pedro Alzari for critical reading of the manuscript and discussions. We also thank Bruno Baron, Sebastien Brulé, Patrick England from the Molecular Biophysics facility (PFBM) at the Institut Pasteur (Paris) for AUC and CD measurements and discussions, as well as the PICT-IBiSA for providing access to the chemical imaging facility. This work was supported by the Institut Curie, the Institut Pasteur, the CNRS, INSERM, DIM MALINF and the French National Research Agency, ANR (HetTub 12-PDOC-0021-01; ANR-10-LBX-0038, ANR-10-IDEX-0001-02 PSL).

Author Contributions

L.A., S.T., A.C. and A.W. designed the experiments. L.A. carried our protein purifications, polymerization assays. A.W. carried out Western Blot analysis. L.A. and A.W. prepared samples for cryo-EM. S.T. carried out sample freezing, cryo-EM data acquisition and data processing. M.G. and A.W. carried out structure and sequence analysis. A.V. prepared the SUVs. B.R. carried out the AUC experiments and data analysis. S.M. and C.J. provided constructive input to the work. A.W. coordinated the team and wrote the manuscript with input from all the authors.

Additional Information

Supplementary information accompanies this paper at http://www.nature.com/srep

Competing Interests: The authors declare no competing financial interests.

How to cite this article: Akendengue, L. *et al.* Bacterial kinesin light chain (Bklc) links the Btub cytoskeleton to membranes. *Sci. Rep.* **7**, 45668; doi: 10.1038/srep45668 (2017).

Publisher's note: Springer Nature remains neutral with regard to jurisdictional claims in published maps and institutional affiliations.

This work is licensed under a Creative Commons Attribution 4.0 International License. The images or other third party material in this article are included in the article's Creative Commons license, unless indicated otherwise in the credit line; if the material is not included under the Creative Commons license, users will need to obtain permission from the license holder to reproduce the material. To view a copy of this license, visit http://creativecommons.org/licenses/by/4.0/

© The Author(s) 2017

Chapter VIII. Bibliography

Chapter VIII. Bibliography

A

Abrami, L., Liu, S., Cosson, P., Leppla, S.H., and van der Goot, F.G. (2003). Anthrax toxin triggers endocytosis of its receptor via a lipid raft–mediated clathrin-dependent process. J. Cell Biol. *160*, 321.

Abrami, L., Lindsay, M., Parton, R.G., Leppla, S.H., and van der Goot, F.G. (2004). Membrane insertion of anthrax protective antigen and cytoplasmic delivery of lethal factor occur at different stages of the endocytic pathway. J. Cell Biol. *166*, 645–651.

Abrami, L., Reig, N., and van der Goot, F.G. (2005). Anthrax toxin: the long and winding road that leads to the kill. Trends Microbiol. *13*, 72–78.

Abramson, T., Kedem, H., and Relman, D.A. (2001). Proinflammatory and proapoptotic activities associated with Bordetella pertussis filamentous hemagglutinin. Infect. Immun. *69*, 2650–2658.

Adkins, I., Kamanova, J., Kocourkova, A., Svedova, M., Tomala, J., Janova, H., Masin, J., Chladkova, B., Bumba, L., Kovar, M., et al. (2014). Bordetella adenylate cyclase toxin differentially modulates toll-like receptor-stimulated activation, migration and T cell stimulatory capacity of dendritic cells. PloS One *9*, e104064.

Agarraberes, F.A., and Dice, J.F. (2001). Protein translocation across membranes. Biochim. Biophys. Acta *1513*, 1–24.

Albitar-Nehme, S., Basheer, S.M., Njamkepo, E., Brisson, J.-R., Guiso, N., and Caroff, M. (2013). Comparison of lipopolysaccharide structures of Bordetella pertussis clinical isolates from pre- and post-vaccine era. Carbohydr. Res. *378*, 56–62.

Alfano, M., Schmidtmayerova, H., Amella, C.A., Pushkarsky, T., and Bukrinsky, M. (1999). The B-oligomer of pertussis toxin deactivates CC chemokine receptor 5 and blocks entry of M-tropic HIV-1 strains. J. Exp. Med. *190*, 597–605.

Almagro-Molto, M., Eder, W., and Schubert, S. (2015). Bordetella trematum in chronic ulcers: report on two cases and review of the literature. Infection *43*, 489–494.

Amano, K., Fukushi, K., and Watanabe, M. (1990). Biochemical and immunological comparison of lipopolysaccharides from Bordetella species. J. Gen. Microbiol. *136*, 481–487.

Aminian, M., Salehi, E., and Khafri, A. (2007). Regulation of pertussis toxin and lipopolysaccharide levels of Bordetella pertussis 134 in response to modulators. Arch. Razi Inst. *62*, 135–144, 177.

Andreasen, C., and Carbonetti, N.H. (2009). Role of Neutrophils in Response to Bordetella pertussis Infection in Mice. Infect. Immun. *77*, 1182.

Andreasen, C., Powell, D.A., and Carbonetti, N.H. (2009). Pertussis toxin stimulates IL-17 production in response to Bordetella pertussis infection in mice. PloS One *4*, e7079.

Araye, A., Goudet, A., Barbier, J., Pichard, S., Baron, B., England, P., Perez, J., Zinn-Justin, S., Chenal, A., and Gillet, D. (2016). The Translocation Domain of Botulinum Neurotoxin A Moderates the Propensity of the Catalytic Domain to Interact with Membranes at Acidic pH. PloS One *11*, e0153401.

Arico, B., Gross, R., Smida, J., and Rappuoli, R. (1987). Evolutionary relationships in the genus Bordetella. Mol. Microbiol. *1*, 301–308.

Armstrong, G.D., Clark, C.G., and Heerze, L.D. (1994). The 70-kilodalton pertussis toxin-binding protein in Jurkat cells. Infect. Immun. *62*, 2236–2243.

Arp, L., and Cheville, N. (1984). Tracheal lesions in young turkeys infected with Bordetella avium. Am. J. Vet. Res. *45*, 2196—2200.

Arvand, M., Feldhues, R., Mieth, M., Kraus, T., and Vandamme, P. (2004). Chronic cholangitis caused by Bordetella hinzii in a liver transplant recipient. J. Clin. Microbiol. *42*, 2335–2337.

Aude Fabre, Clarisse Dupin, François Bénézit, Julien Goret, Caroline Piau, Stéphane Jouneau, Sophie Guillot, Francis Mégraud, Samer Kayal, Benoit Desrues, et al. (2015). Opportunistic Pulmonary Bordetella hinzii Infection after Avian Exposure. Emerg. Infect. Dis. J. *21*, 2122.

Azarnia Tehran, D., Pirazzini, M., Leka, O., Mattarei, A., Lista, F., Binz, T., Rossetto, O., and Montecucco, C. (2017). Hsp90 is involved in the entry of clostridial neurotoxins into the cytosol of nerve terminals. Cell. Microbiol. *19*.

B

Babu, Y.S., Sack, J.S., Greenhough, T.J., Bugg, C.E., Means, A.R., and Cook, W.J. (1985). Three-dimensional structure of calmodulin. Nature *315*, 37–40.

Bachelet, M., Richard, M.J., Francois, D., and Polla, B.S. (2002). Mitochondrial alterations precede Bordetella pertussis-induced apoptosis. FEMS Immunol. Med. Microbiol. *32*, 125–131.

Bakas, L., Chanturiya, A., Herlax, V., and Zimmerberg, J. (2006). Paradoxical lipid dependence of pores formed by the Escherichia coli alpha-hemolysin in planar phospholipid bilayer membranes. Biophys. J. *91*, 3748–3755.

Banerjee, T., Cilenti, L., Taylor, M., Showman, A., Tatulian, S.A., and Teter, K. (2016). Thermal Unfolding of the Pertussis Toxin S1 Subunit Facilitates Toxin Translocation to the Cytosol by the Mechanism of Endoplasmic Reticulum-Associated Degradation. Infect. Immun. *84*, 3388.

Barbato, G., Ikura, M., Kay, L.E., Pastor, R.W., and Bax, A. (1992). Backbone dynamics of calmodulin studied by 15N relaxation using inverse detected two-dimensional NMR spectroscopy: the central helix is flexible. Biochemistry. *31*, 5269–5278.

Barnes, M.G., and Weiss, A.A. (2001). BrkA protein of Bordetella pertussis inhibits the classical pathway of complement after C1 deposition. Infect. Immun. *69*, 3067–3072.

Barry, E.M., Weiss, A.A., Ehrmann, I.E., Gray, M.C., Hewlett, E.L., and Goodwin, M.S. (1991). Bordetella pertussis adenylate cyclase toxin and hemolytic activities require a second gene, cyaC, for activation. J. Bacteriol. *173*, 720–726.

Barth, H., Aktories, K., Popoff, M.R., and Stiles, B.G. (2004). Binary bacterial toxins: biochemistry, biology, and applications of common Clostridium and Bacillus proteins. Microbiol. Mol. Biol. Rev. MMBR *68*, 373–402, table of contents.

Basar, T., Havlicek, V., Bezouskova, S., Halada, P., Hackett, M., and Sebo, P. (1999). The conserved lysine 860 in the additional fatty-acylation site of Bordetella pertussis adenylate cyclase is crucial for toxin function independently of its acylation status. J. Biol. Chem. *274*, 10777–10783.

Basar, T., Havlicek, V., Bezouskova, S., Hackett, M., and Sebo, P. (2001). Acylation of lysine 983 is sufficient for toxin activity of Bordetella pertussis adenylate cyclase. Substitutions of alanine 140 modulate acylation site selectivity of the toxin acyltransferase CyaC. J. Biol. Chem. *276*, 348–354.

Basler, M., Knapp, O., Masin, J., Fiser, R., Maier, E., Benz, R., Sebo, P., and Osicka, R. (2007). Segments crucial for membrane translocation and pore-forming activity of Bordetella adenylate cyclase toxin. J. Biol. Chem. *282*, 12419–12429.

Bassinet, L., Gueirard, P., Maitre, B., Housset, B., Gounon, P., and Guiso, N. (2000). Role of adhesins and toxins in invasion of human tracheal epithelial cells by Bordetella pertussis. Infect. Immun. *68*, 1934–1941.

Bassinet, L., Fitting, C., Housset, B., Cavaillon, J.-M., and Guiso, N. (2004). Bordetella pertussis adenylate cyclase-hemolysin induces interleukin-6 secretion by human tracheal epithelial cells. Infect. Immun. *72*, 5530–5533.

Bauche, C., Chenal, A., Knapp, O., Bodenreider, C., Benz, R., Chaffotte, A., and Ladant, D. (2006). Structural and functional characterization of an essential RTX subdomain of Bordetella pertussis adenylate cyclase toxin. J. Biol. Chem. *281*, 16914–16926.

Baumann, U., Wu, S., Flaherty, K.M., and McKay, D.B. (1993). Three-dimensional structure of the alkaline protease of Pseudomonas aeruginosa: a two-domain protein with a calcium binding parallel beta roll motif. EMBO J. *12*, 3357–3364.

Bechara, C., and Sagan, S. (2013). Cell-penetrating peptides: 20 years later, where do we stand? FEBS Lett. *587*, 1693–1702.

Belcher, C.E., Drenkow, J., Kehoe, B., Gingeras, T.R., McNamara, N., Lemjabbar, H., Basbaum, C., and Relman, D.A. (2000). The transcriptional responses of respiratory epithelial cells to Bordetella pertussis reveal host defensive and pathogen counter-defensive strategies. Proc. Natl. Acad. Sci. *97*, 13847.

Bellalou, J., Sakamoto, H., Ladant, D., Geoffroy, C., and Ullmann, A. (1990a). Deletions affecting hemolytic and toxin activities of Bordetella pertussis adenylate cyclase. Infect. Immun. *58*, 3242–3247.

Bellalou, J., Ladant, D., and Sakamoto, H. (1990b). Synthesis and secretion of Bordetella pertussis adenylate cyclase as a 200-kilodalton protein. Infect. Immun. *58*, 1195–1200.

Belyy, A., Raoux-Barbot, D., Saveanu, C., Namane, A., Ogryzko, V., Worpenberg, L., David, V., Henriot, V., Fellous, S., Merrifield, C., et al. (2016). Actin activates Pseudomonas aeruginosa ExoY nucleotidyl cyclase toxin and ExoY-like effector domains from MARTX toxins. Nat. Commun. *7*, 13582.

Belyy, A., Mechold, U., Renault, L., and Ladant, D. (2018). ExoY, an actin-activated nucleotidyl cyclase toxin from P. aeruginosa: A minireview. Toxicon Off. J. Int. Soc. Toxinology *149*, 65–71.

Benz, R., Schmid, A., Wagner, W., and Goebel, W. (1989). Pore formation by the Escherichia coli hemolysin: evidence for an association-dissociation equilibrium of the pore-forming aggregates. Infect. Immun. *57*, 887–895.

Benz, R., Maier, E., Ladant, D., Ullmann, A., and Sebo, P. (1994). Adenylate cyclase toxin (CyaA) of Bordetella pertussis. Evidence for the formation of small ion-permeable channels and comparison with HlyA of Escherichia coli. J. Biol. Chem. *269*, 27231–27239.

Berggard, K., Johnsson, E., Mooi, F.R., and Lindahl, G. (1997). Bordetella pertussis binds the human complement regulator C4BP: role of filamentous hemagglutinin. Infect. Immun. *65*, 3638–3643.

Bernardi, K.M., Forster, M.L., Lencer, W.I., and Tsai, B. (2008). Derlin-1 facilitates the retro-translocation of cholera toxin. Mol. Biol. Cell *19*, 877–884.

Bernardi, K.M., Williams, J.M., Kikkert, M., van Voorden, S., Wiertz, E.J., Ye, Y., and Tsai, B. (2010). The E3 ubiquitin ligases Hrd1 and gp78 bind to and promote cholera toxin retro-translocation. Mol. Biol. Cell *21*, 140–151.

Betsou, F., Sebo, P., and Guiso, N. (1993). CyaC-mediated activation is important not only for toxic but also for protective activities of Bordetella pertussis adenylate cyclase-hemolysin. Infect. Immun. *61*, 3583–3589.

Binz, T., and Rummel, A. (2009). Cell entry strategy of clostridial neurotoxins. J. Neurochem. *109*, 1584–1595.

Blanchard Rohner, G., Chatzis, O., Chinwangso, P., Rohr, M., Grillet, S., Salomon, C., Lemaître, B., Boonrak, P., Lawpoolsri, S., and Clutterbuck, E. (2018). Boosting Teenagers With Acellular Pertussis Vaccines Containing Recombinant or Chemically Inactivated Pertussis Toxin: A Randomized Clinical Trial. Clin. Infect. Dis.

Bock, A., and Gross, R. (2001). The BvgAS two-component system of Bordetella spp.: a versatile modulator of virulence gene expression. Int. J. Med. Microbiol. IJMM *291*, 119–130.

Bogdanova, A., Makhro, A., Wang, J., Lipp, P., and Kaestner, L. (2013). Calcium in red blood cells-a perilous balance. Int. J. Mol. Sci. *14*, 9848–9872.

Bordet, J. (1906). Le microbe de la coqueluche. Ann Inst Pasteur *20*, 48–68.
Bordet, J., and Gengou, O. (1909). L'endotoxine coquelucheuse. Ann Ist Pasteur *23*, 415–419.

Bouchez, V., Douche, T., Dazas, M., Delaplane, S., Matondo, M., Chamot-Rooke, J., and Guiso, N. (2017). Characterization of Post-Translational Modifications and Cytotoxic Properties of the Adenylate-Cyclase Hemolysin Produced by Various Bordetella pertussis and Bordetella parapertussis Isolates. Toxins *9*.

Boyd, A.P., Ross, P.J., Conroy, H., Mahon, N., Lavelle, E.C., and Mills, K.H.G. (2005). Bordetella pertussis adenylate cyclase toxin modulates innate and adaptive immune responses: distinct roles for acylation and enzymatic activity in immunomodulation and cell death. J. Immunol. Baltim. Md 1950 *175*, 730–738.

Bradford, W.L., and Slavin, B. (1937). An Organism Resembling Hemophilus Pertussis: With Special Reference to Color Changes Produced by Its Growth Upon Certain Media. Am. J. Public Health Nations Health *27*, 1277–1282.

Bradley, K.A., Mogridge, J., Mourez, M., Collier, R.J., and Young, J.A.T. (2001). Identification of the cellular receptor for anthrax toxin. Nature *414*, 225–229.

Breakwell, L., Kelso, P., Finley, C., Schoenfeld, S., Goode, B., Misegades, L.K., Martin, S.W., and Acosta, A.M. (2016). Pertussis Vaccine Effectiveness in the Setting of Pertactin-Deficient Pertussis. PEDIATRICS *137*, e20153973–e20153973.

Brennan, M.J., David, J.L., Kenimer, J.G., and Manclark, C.R. (1988). Lectin-like binding of pertussis toxin to a 165-kilodalton Chinese hamster ovary cell glycoprotein. J. Biol. Chem. *263*, 4895–4899.

Brodsky, J.L. (2007). The protective and destructive roles played by molecular chaperones during ERAD (endoplasmic-reticulum-associated degradation). Biochem. J. *404*, 353–363.

Brogden, K.A. (2005). Antimicrobial peptides: pore formers or metabolic inhibitors in bacteria? Nat. Rev. Microbiol. *3*, 238–250.

Brookes, C., Freire-Martin, I., Cavell, B., Alexander, F., Taylor, S., Persaud, R., Fry, N., Preston, A., Diavatopoulos, D., and Gorringe, A. (2018). Bordetella pertussis isolates vary in their interactions with human complement components. Emerg. Microbes Infect. *7*, 1–11.

Brown, M.F. (2012). Curvature forces in membrane lipid-protein interactions. Biochemistry. *51*, 9782–9795.

Bumba, L., Masin, J., Fiser, R., and Sebo, P. (2010). Bordetella adenylate cyclase toxin mobilizes its beta2 integrin receptor into lipid rafts to accomplish translocation across target cell membrane in two steps. PLoS Pathog. *6*, e1000901.

Bumba, L., Masin, J., Macek, P., Wald, T., Motlova, L., Bibova, I., Klimova, N., Bednarova, L., Veverka, V., Kachala, M., et al. (2016). Calcium-Driven Folding of RTX Domain beta-Rolls Ratchets Translocation of RTX Proteins through Type I Secretion Ducts. Mol. Cell *62*, 47–62.

Bumba, L., Masin, J., Osickova, A., Osicka, R., and Sebo, P. (2018). Bordetella Pertussis Adenylate Cyclase Toxin Does Not Possess a Phospholipase A Activity; Serine 606 and Aspartate 1079 Residues Are Not Involved in Target Cell Delivery of the Adenylyl Cyclase Enzyme Domain. Toxins *10*.

Burress, H., Taylor, M., Banerjee, T., Tatulian, S.A., and Teter, K. (2014). Co- and post-translocation roles for HSP90 in cholera Intoxication. J. Biol. Chem. *289*, 33644–33654.

Burstyn, D.G., Baraff, L.J., Peppler, M.S., Leake, R.D., St Geme, J., and Manclark, C.R. (1983). Serological response to filamentous hemagglutinin and lymphocytosis-promoting toxin of Bordetella pertussis. Infect. Immun. *41*, 1150.

C

Cannella, S.E., Ntsogo Enguene, V.Y., Davi, M., Malosse, C., Sotomayor Perez, A.C., Chamot-Rooke, J., Vachette, P., Durand, D., Ladant, D., and Chenal, A. (2017). Stability, structural and functional properties of a monomeric, calcium-loaded adenylate cyclase toxin, CyaA, from Bordetella pertussis. Sci. Rep. *7*, 42065.

Carbonetti, N.H. (2010). Pertussis toxin and adenylate cyclase toxin: key virulence factors of Bordetella pertussis and cell biology tools. Future Microbiol. *5*, 455–469.

Carbonetti, N.H. (2015). Contribution of pertussis toxin to the pathogenesis of pertussis disease. Pathog. Dis. *73*.

Carbonetti, N.H., Artamonova, G.V., Mays, R.M., and Worthington, Z.E.V. (2003). Pertussis toxin plays an early role in respiratory tract colonization by Bordetella pertussis. Infect. Immun. *71*, 6358–6366.

Carbonetti, N.H., Artamonova, G.V., Andreasen, C., and Bushar, N. (2005). Pertussis toxin and adenylate cyclase toxin provide a one-two punch for establishment of Bordetella pertussis infection of the respiratory tract. Infect. Immun. *73*, 2698–2703.

Cerny, O., Kamanova, J., Masin, J., Bibova, I., Skopova, K., and Sebo, P. (2015). Bordetella pertussis Adenylate Cyclase Toxin Blocks Induction of Bactericidal Nitric Oxide in Macrophages through cAMP-Dependent Activation of the SHP-1 Phosphatase. J. Immunol. Baltim. Md 1950 *194*, 4901–4913.

Charles, I., Fairweather, N., Pickard, D., Beesley, J., Anderson, R., Dougan, G., and Roberts, M. (1994). Expression of the Bordetella pertussis P.69 pertactin adhesin in Escherichia coli: fate of the carboxy-terminal domain. Microbiol. Read. Engl. *140 (Pt 12)*, 3301–3308.

Chassaing, A., Pichard, S., Araye-Guet, A., Barbier, J., Forge, V., and Gillet, D. (2011). Solution and membrane-bound chaperone activity of the diphtheria toxin translocation domain towards the catalytic domain. FEBS J. *278*, 4516–4525.

Chenal, A., and Ladant, D. (2018). Bioengineering of Bordetella pertussis Adenylate Cyclase Toxin for Antigen-Delivery and Immunotherapy. Toxins *10*.

Chenal, A., Savarin, P., Nizard, P., Guillain, F., Gillet, D., and Forge, V. (2002). Membrane Protein Insertion Regulated by Bringing Electrostatic and Hydrophobic Interactions into Play. A Case Study with the Translocation Domain of the Diphtheria Toxin. J. Biol. Chem. *277*, 43425–43432.

Chenal, A., Guijarro, J.I., Raynal, B., Delepierre, M., and Ladant, D. (2009a). RTX calcium binding motifs are intrinsically disordered in the absence of calcium: implication for protein secretion. J. Biol. Chem. *284*, 1781–1789.

Chenal, A., Prongidi-Fix, L., Perier, A., Aisenbrey, C., Vernier, G., Lambotte, S., Haertlein, M., Dauvergne, M.-T., Fragneto, G., Bechinger, B., et al. (2009b). Deciphering membrane insertion of the diphtheria toxin T domain by specular neutron reflectometry and solid-state NMR spectroscopy. J. Mol. Biol. *391*, 872–883.

Chenal, A., Karst, J.C., Sotomayor Perez, A.C., Wozniak, A.K., Baron, B., England, P., and Ladant, D. (2010). Calcium-induced folding and stabilization of the intrinsically disordered RTX domain of the CyaA toxin. Biophys. J. *99*, 3744–3753.

Cheng, H.-T., Megha, and London, E. (2009). Preparation and properties of asymmetric vesicles that mimic cell membranes: effect upon lipid raft formation and transmembrane helix orientation. J. Biol. Chem. *284*, 6079–6092.

Cheung, G.Y.C., Xing, D., Prior, S., Corbel, M.J., Parton, R., and Coote, J.G. (2006). Effect of different forms of adenylate cyclase toxin of Bordetella pertussis on protection afforded by an acellular pertussis vaccine in a murine model. Infect. Immun. *74*, 6797–6805.

Chevalier, N., Moser, M., Koch, H.-G., Schimz, K.-L., Willery, E., Locht, C., Jacob-Dubuisson, F., and Muller, M. (2004). Membrane targeting of a bacterial virulence factor harbouring an extended signal peptide. J. Mol. Microbiol. Biotechnol. *8*, 7–18.

Chevrel, A., Mesneau, A., Sanchez, D., Celma, L., Quevillon-Cheruel, S., Cavagnino, A., Nessler, S., Li de la Sierra-Gallay, I., van Tilbeurgh, H., Minard, P., et al. (2018). Alpha repeat proteins (alphaRep) as expression and crystallization helpers. J. Struct. Biol. *201*, 88–99.

Chinnapen, D.J.-F., Hsieh, W.-T., te Welscher, Y.M., Saslowsky, D.E., Kaoutzani, L., Brandsma, E., D'Auria, L., Park, H., Wagner, J.S., and Drake, K.R. (2012). Lipid sorting by ceramide structure from plasma membrane to ER for the cholera toxin receptor ganglioside GM1. Dev. Cell *23*, 573–586.

Cho, J.A., Chinnapen, D.J.-F., Aamar, E., te Welscher, Y.M., Lencer, W., and Massol, R. (2012). Insights on the trafficking and retro-translocation of glycosphingolipid-binding bacterial toxins. Front. Cell. Infect. Microbiol. *2*, 51.

Clifton, L.A., Skoda, M.W.A., Daulton, E.L., Hughes, A.V., Le Brun, A.P., Lakey, J.H., and Holt, S.A. (2013). Asymmetric phospholipid: lipopolysaccharide bilayers; a Gram-negative bacterial outer membrane mimic. J. R. Soc. Interface *10*, 20130810.

Coenye, T., Goris, J., Spilker, T., Vandamme, P., and LiPuma, J.J. (2002). Characterization of unusual bacteria isolated from respiratory secretions of cystic fibrosis patients and description of Inquilinus limosus gen. nov., sp. nov. J. Clin. Microbiol. *40*, 2062–2069.

Colasante, C., Rossetto, O., Morbiato, L., Pirazzini, M., Molgó, J., and Montecucco, C. (2013). Botulinum Neurotoxin Type A is Internalized and Translocated from Small Synaptic Vesicles at the Neuromuscular Junction. Mol. Neurobiol. *48*, 120–127.

Confer, D.L., and Eaton, J.W. (1982). Phagocyte impotence caused by an invasive bacterial adenylate cyclase. Science *217*, 948–950.

Connelly, C.E., Sun, Y., and Carbonetti, N.H. (2012). Pertussis Toxin Exacerbates and Prolongs Airway Inflammatory Responses during Bordetella pertussis Infection. Infect. Immun. *80*, 4317.

Cookson, B.T., Cho, H.-L., Herwaldt, L.A., and Goldman, W.E. (1989). Biological activities and chemical composition of purified tracheal cytotoxin of Bordetella pertussis. Infect. Immun. *57*, 2223–2229.

Cookson, B.T., Vandamme, P., Carlson, L.C., Larson, A.M., Sheffield, J.V., Kersters, K., and Spach, D.H. (1994). Bacteremia caused by a novel Bordetella species, "B. hinzii". J. Clin. Microbiol. *32*, 2569–2571.

Cooper, D.M., Mons, N., and Karpen, J.W. (1995). Adenylyl cyclases and the interaction between calcium and cAMP signalling. Nature *374*, 421–424.

Coulie, P.G., Van den Eynde, B.J., van der Bruggen, P., and Boon, T. (2014). Tumour antigens recognized by T lymphocytes: at the core of cancer immunotherapy. Nat. Rev. Cancer *14*, 135–146.

Coutte, L., and Locht, C. (2015). Investigating pertussis toxin and its impact on vaccination. Future Microbiol. *10*, 241–254.

Coutte, L., Antoine, R., Drobecq, H., Locht, C., and Jacob-Dubuisson, F. (2001). Subtilisin-like autotransporter serves as maturation protease in a bacterial secretion pathway. EMBO J. *20*, 5040–5048.

Coutte, L., Willery, E., Antoine, R., Drobecq, H., Locht, C., and Jacob-Dubuisson, F. (2003). Surface anchoring of bacterial subtilisin important for maturation function. Mol. Microbiol. *49*, 529–539.

Cowell, J.L., Hewlett, E.L., and Manclark, C.R. (1979). Intracellular localization of the dermonecrotic toxin of Bordetella pertussis. Infect. Immun. *25*, 896–901.

Craig, E.A. (2018). Hsp70 at the membrane: driving protein translocation. BMC Biol. *16*, 11.

Crane, J.M., Kiessling, V., and Tamm, L.K. (2005). Measuring lipid asymmetry in planar supported bilayers by fluorescence interference contrast microscopy. Langmuir ACS J. Surf. Colloids *21*, 1377–1388.

Cullinane, L.C., Alley, M.R., Marshall, R.B., and Manktelow, B.W. (1987). Bordetella parapertussis from lambs. N. Z. Vet. J. *35*, 175.

Cundell, D.R., Kanthakumar, K., Taylor, G.W., Goldman, W.E., Flak, T., Cole, P.J., and Wilson, R. (1994). Effect of tracheal cytotoxin from Bordetella pertussis on human neutrophil function in vitro. Infect. Immun. *62*, 639–643.

Cutrona, K.J., Kaufman, B.A., Figueroa, D.M., and Elmore, D.E. (2015). Role of arginine and lysine in the antimicrobial mechanism of histone-derived antimicrobial peptides. FEBS Lett. *589*, 3915–3920.

D

Dadaglio, G., Moukrim, Z., Lo-Man, R., Sheshko, V., Sebo, P., and Leclerc, C. (2000). Induction of a polarized Th1 response by insertion of multiple copies of a viral T-cell epitope into adenylate cyclase of Bordetella pertussis. Infect. Immun. *68*, 3867–3872.

Dadaglio, G., Morel, S., Bauche, C., Moukrim, Z., Lemonnier, F.A., Van Den Eynde, B.J., Ladant, D., and Leclerc, C. (2003). Recombinant adenylate cyclase toxin of Bordetella pertussis induces cytotoxic T lymphocyte responses against HLA*0201-restricted melanoma epitopes. Int. Immunol. *15*, 1423–1430.

Dal Molin, F., Tonello, F., Ladant, D., Zornetta, I., Zamparo, I., Di Benedetto, G., Zaccolo, M., and Montecucco, C. (2006). Cell entry and cAMP imaging of anthrax edema toxin. EMBO J. *25*, 5405–5413.

Dalby, T., Fry, N.K., Krogfelt, K.A., Jensen, J.S., and He, Q. (2013). Evaluation of PCR methods for the diagnosis of pertussis by the European surveillance network for vaccine-preventable diseases (EUVAC.NET). Eur. J. Clin. Microbiol. Infect. Dis. Off. Publ. Eur. Soc. Clin. Microbiol. *32*, 1285–1289.

Dalet, K., Weber, C., Guillemot, L., Njamkepo, E., and Guiso, N. (2004). Characterization of adenylate cyclase-hemolysin gene duplication in a Bordetella pertussis isolate. Infect. Immun. *72*, 4874–4877.

Dautin, N., Karimova, G., Ullmann, A., and Ladant, D. (2000). Sensitive genetic screen for protease activity based on a cyclic AMP signaling cascade in Escherichia coli. J. Bacteriol. *182*, 7060–7066.

Dautin, N., Karimova, G., and Ladant, D. (2002). Bordetella pertussis adenylate cyclase toxin: a versatile screening tool. Toxicon Off. J. Int. Soc. Toxinology *40*, 1383–1387.

Daxboeck, F., Goerzer, E., Apfalter, P., Nehr, M., and Krause, R. (2004). Isolation of Bordetella trematum from a diabetic leg ulcer. Diabet. Med. J. Br. Diabet. Assoc. *21*, 1247–1248.

De Ley, J., Segers, P., Kersters, K., Mannheim, W., and Lievens, A. (1986). Intra- and Intergeneric Similarities of the Bordetella Ribosomal Ribonucleic Acid Cistrons: Proposal for a New Family, Alcaligenaceae. *36*, 405–414.

De Los Rios, P., Ben-Zvi, A., Slutsky, O., Azem, A., and Goloubinoff, P. (2006). Hsp70 chaperones accelerate protein translocation and the unfolding of stable protein aggregates by entropic pulling. Proc. Natl. Acad. Sci. U. S. A. *103*, 6166–6171.

Delaroche, D., Aussedat, B., Aubry, S., Chassaing, G., Burlina, F., Clodic, G., Bolbach, G., Lavielle, S., and Sagan, S. (2007). Tracking a New Cell-Penetrating (W/R) Nonapeptide, through an Enzyme-Stable Mass Spectrometry Reporter Tag. Anal. Chem. *79*, 1932–1938.

Delattre, A.-S., Saint, N., Clantin, B., Willery, E., Lippens, G., Locht, C., Villeret, V., and Jacob-Dubuisson, F. (2011). Substrate recognition by the POTRA domains of TpsB transporter FhaC. Mol. Microbiol. *81*, 99–112.

Delepelaire, P. (2004). Type I secretion in gram-negative bacteria. Protein Export. Bact. *1694*, 149–161.

Delepelaire, P., and Wandersman, C. (1990). Protein secretion in gram-negative bacteria. The extracellular metalloprotease B from Erwinia chrysanthemi contains a C-terminal secretion signal analogous to that of Escherichia coli alpha-hemolysin. J. Biol. Chem. *265*, 17118–17125.

Delisse-Gathoye, A.-M., Locht, C., Jacob, F., Raaschou-Nielsen, M., Heron, I., Ruelle, J.L., De Wilde, M., and Cabezon, T. (1990). Cloning, partial sequence, expression, and antigenic analysis of the filamentous hemagglutinin gene of Bordetella pertussis. Infect. Immun. *58*, 2895–2905.

Deshayes, S., Decaffmeyer, M., Brasseur, R., and Thomas, A. (2008). Structural polymorphism of two CPP: An important parameter of activity. Biochim. Biophys. Acta BBA - Biomembr. *1778*, 1197–1205.

Diavatopoulos, D.A., Cummings, C.A., Schouls, L.M., Brinig, M.M., Relman, D.A., and Mooi, F.R. (2005). Bordetella pertussis, the causative agent of whooping cough, evolved from a distinct, human-associated lineage of B. bronchiseptica. PLoS Pathog. *1*, e45.

Dietz, G.P.H., and Bähr, M. (2004). Delivery of bioactive molecules into the cell: the Trojan horse approach. Mol. Cell. Neurosci. *27*, 85–131.

Dmochewitz, L., Lillich, M., Kaiser, E., Jennings, L.D., Lang, A.E., Buchner, J., Fischer, G., Aktories, K., Collier, R.J., and Barth, H. (2011). Role of CypA and Hsp90 in membrane translocation mediated by anthrax protective antigen. Cell. Microbiol. *13*, 359–373.

Dobereiner, A., Schmid, A., Ludwig, A., Goebel, W., and Benz, R. (1996). The effects of calcium and other polyvalent cations on channel formation by Escherichia coli alpha-hemolysin in red blood cells and lipid bilayer membranes. Eur. J. Biochem. *240*, 454–460.

Domenech de Celles, M., Magpantay, F.M.G., King, A.A., and Rohani, P. (2018). The impact of past vaccination coverage and immunity on pertussis resurgence. Sci. Transl. Med. *10*.

Domenighini, M., Relman, D., Capiau, C., Falkow, S., Prugnola, A., Scarlato, V., and Rappuoli, R. (1990). Genetic characterization of Bordetella pertussis filamentous haemagglutinin: a protein processed from an unusually large precursor. Mol. Microbiol. *4*, 787–800.

Dominguez, D.C. (2004). Calcium signalling in bacteria. Mol. Microbiol. *54*, 291–297.

Donato, G.M., Hsia, H.-L.J., Green, C.S., and Hewlett, E.L. (2005). Adenylate cyclase toxin (ACT) from Bordetella hinzii: characterization and differences from ACT of Bordetella pertussis. J. Bacteriol. *187*, 7579–7588.

Drum, C.L., Yan, S.-Z., Bard, J., Shen, Y.-Q., Lu, D., Soelaiman, S., Grabarek, Z., Bohm, A., and Tang, W.-J. (2002). Structural basis for the activation of anthrax adenylyl cyclase exotoxin by calmodulin. Nature *415*, 396–402.

E

Ebenhan, T., Gheysens, O., Kruger, H.G., Zeevaart, J.R., and Sathekge, M.M. (2014). Antimicrobial peptides: their role as infection-selective tracers for molecular imaging. BioMed Res. Int. *2014*, 867381.

Eby, J.C., Ciesla, W.P., Hamman, W., Donato, G.M., Pickles, R.J., Hewlett, E.L., and Lencer, W.I. (2010). Selective translocation of the Bordetella pertussis adenylate cyclase toxin across the basolateral membranes of polarized epithelial cells. J. Biol. Chem. *285*, 10662–10670.

Ehrmann, I.E., Gray, M.C., Gordon, V.M., Gray, L.S., and Hewlett, E.L. (1991). Hemolytic activity of adenylate cyclase toxin from Bordetella pertussis. FEBS Lett. *278*, 79–83.

El-Azami-El-Idrissi, M., Bauche, C., Loucka, J., Osicka, R., Sebo, P., Ladant, D., and Leclerc, C. (2003). Interaction of Bordetella pertussis adenylate cyclase with CD11b/CD18: Role of toxin acylation and identification of the main integrin interaction domain. J. Biol. Chem. *278*, 38514–38521.

Eldering, G., and Kendrick, P. (1938). Bacillus para-pertussis: a species ressembling both bacillus pertussis and bacillus bronchisepticus but identical with neither. J. Bacteriol. *35*, 561–572.

Emsley, P., Charles, I.G., Fairweather, N.F., and Isaacs, N.W. (1996). Structure of Bordetella pertussis virulence factor P. 69 pertactin. Nature *381*, 90.

Endoh, M., Amitani, M., and Nakase, Y. (1986). Effect of purified heat-labile toxin of Bordetella bronchiseptica on the peripheral blood vessels in guinea pigs or suckling mice. Microbiol. Immunol. *30*, 1327–1330.

F

Falnes, P.O., and Olsnes, S. (1995). Cell-mediated reduction and incomplete membrane translocation of diphtheria toxin mutants with internal disulfides in the A fragment. J. Biol. Chem. *270*, 20787–20793.

Falnes, P.O., and Sandvig, K. (2000). Penetration of protein toxins into cells. Curr. Opin. Cell Biol. *12*, 407–413.

Falnes, P.Ø., Choe, S., Madshus, I.H., Wilson, B.A., and Olsnes, S. (1994). Inhibition of membrane translocation of diphtheria toxin A-fragment by internal disulfide bridges. J. Biol. Chem. *269*, 8402–8407.

Farfel, Z., Friedman, E., and Hanski, E. (1987). The invasive adenylate cyclase of Bordetella pertussis. Intracellular localization and kinetics of penetration into various cells. Biochem. J. *243*, 153–158.

Farfel, Z., Konen, S., Wiertz, E., Klapmuts, R., Addy, P.A., and Hanski, E. (1990). Antibodies to Bordetella pertussis adenylate cyclase are produced in man during pertussis infection and after vaccination. J. Med. Microbiol. *32*, 173–177.

Farizo, K.M., Cafarella, T.G., and Burns, D.L. (1996). Evidence for a ninth gene, ptlI, in the locus encoding the pertussis toxin secretion system of Bordetella pertussis and formation of a PtlI-PtlF complex. J. Biol. Chem. *271*, 31643–31649.

Fayolle, C., Sebo, P., Ladant, D., Ullmann, A., and Leclerc, C. (1996). In vivo induction of CTL responses by recombinant adenylate cyclase of Bordetella pertussis carrying viral CD8+ T cell epitopes. J. Immunol. Baltim. Md 1950 *156*, 4697–4706.

Fayolle, C., Bauche, C., Ladant, D., and Leclerc, C. (2004). Bordetella pertussis adenylate cyclase delivers chemically coupled CD8+ T-cell epitopes to dendritic cells and elicits CTL in vivo. Vaccine *23*, 604–614.

Fedele, G., Spensieri, F., Palazzo, R., Nasso, M., Cheung, G.Y.C., Coote, J.G., and Ausiello, C.M. (2010). Bordetella pertussis commits human dendritic cells to promote a Th1/Th17 response through the activity of adenylate cyclase toxin and MAPK-pathways. PloS One *5*, e8734.

Fedele, G., Schiavoni, I., Adkins, I., Klimova, N., and Sebo, P. (2017). Invasion of Dendritic Cells, Macrophages and Neutrophils by the Bordetella Adenylate Cyclase Toxin: A Subversive Move to Fool Host Immunity. Toxins *9*.

Felmlee, T., Pellett, S., Lee, E.Y., and Welch, R.A. (1985). Escherichia coli hemolysin is released extracellularly without cleavage of a signal peptide. J. Bacteriol. *163*, 88–93.

Fernandez, R.C., and Weiss, A.A. (1994). Cloning and sequencing of a Bordetella pertussis serum resistance locus. Infect. Immun. *62*, 4727–4738.

Ferry, N.S. (1912). Bacillus Bronchisepticus (Bronchicanis): The Cause of Distemper in Dogs and a Similar Disease in other Animals. Vet. J. 1900 *68*, 376–391.

Filion, R., Cloutier, S., Vrancken, E.R., and Bernier, G. (1967). Infection respiratoire du dindonneau causée par un microbe apparenté au Bordetella bronchiseptica. Can. J. Comp. Med. Vet. Sci. *31*, 129–134.

Finn, O.J. (2018). The dawn of vaccines for cancer prevention. Nat. Rev. Immunol. *18*, 183–194.

Finn, T.M., and Amsbaugh, D.F. (1998). Vag8, a Bordetella pertussis bvg-regulated protein. Infect. Immun. *66*, 3985–3989.

Finn, T.M., and Stevens, L.A. (1995). Tracheal colonization factor: a Bordetella pertussis secreted virulence determinant. Mol. Microbiol. *16*, 625–634.

Finn, B.E., Evenas, J., Drakenberg, T., Waltho, J.P., Thulin, E., and Forsen, S. (1995). Calcium-induced structural changes and domain autonomy in calmodulin. Nat. Struct. Biol. *2*, 777–783.

Fischer, A., and Montal, M. (2007). Single molecule detection of intermediates during botulinum neurotoxin translocation across membranes. Proc. Natl. Acad. Sci. U. S. A. *104*, 10447–10452.

Fiser, R., and Konopasek, I. (2009). Different modes of membrane permeabilization by two RTX toxins: HlyA from Escherichia coli and CyaA from Bordetella pertussis. Biochim. Biophys. Acta *1788*, 1249–1254.

Fiser, R., Masin, J., Basler, M., Krusek, J., Spulakova, V., Konopasek, I., and Sebo, P. (2007). Third activity of Bordetella adenylate cyclase (AC) toxin-hemolysin. Membrane translocation of AC domain polypeptide promotes calcium influx into CD11b+ monocytes independently of the catalytic and hemolytic activities. J. Biol. Chem. *282*, 2808–2820.

Fishbain, J.T., Riederer, K., Sawaf, H., and Mody, R. (2015). Invasive Bordetella holmesii infections. Infect. Dis. Lond. Engl. *47*, 65–68.

Flak, T.A., and Goldman, W.E. (1996). Autotoxicity of nitric oxide in airway disease. Am. J. Respir. Crit. Care Med. *154*, S202-206.

Flak, T.A., and Goldman, W.E. (1999). Signalling and cellular specificity of airway nitric oxide production in pertussis. Cell. Microbiol. *1*, 51–60.

Friedman, R.L., Fiederlein, R.L., Glasser, L., and Galgiani, J.N. (1987). Bordetella pertussis adenylate cyclase: effects of affinity-purified adenylate cyclase on human polymorphonuclear leukocyte functions. Infect. Immun. *55*, 135–140.

Fry, N.K., Duncan, J., Malnick, H., Warner, M., Smith, A.J., Jackson, M.S., and Ayoub, A. (2005). Bordetella petrii clinical isolate. Emerg. Infect. Dis. *11*, 1131–1133.

Fry, N.K., Duncan, J., Malnick, H., and Cockcroft, P.M. (2007). The first UK isolate of "Bordetella ansorpii" from an immunocompromised patient. J. Med. Microbiol. *56*, 993–995.

Fukui, A., and Horiguchi, Y. (2004). Bordetella dermonecrotic toxin exerting toxicity through activation of the small GTPase Rho. J. Biochem. (Tokyo) *136*, 415–419.

Fukui-Miyazaki, A., Toshima, H., Hiramatsu, Y., Okada, K., Nakamura, K., Ishigaki, K., Shinzawa, N., Abe, H., and Horiguchi, Y. (2018). The Eukaryotic Host Factor 14-3-3 Inactivates Adenylate Cyclase Toxins of Bordetella bronchiseptica and B. parapertussis, but Not B. pertussis. mBio *9*.

Futaki, S., Suzuki, T., Ohashi, W., Yagami, T., Tanaka, S., Ueda, K., and Sugiura, Y. (2001). Arginine-rich peptides. An abundant source of membrane-permeable peptides having potential as carriers for intracellular protein delivery. J. Biol. Chem. *276*, 5836–5840.

G

Gabutti, G., Azzari, C., Bonanni, P., Prato, R., Tozzi, A.E., Zanetti, A., and Zuccotti, G. (2015). Pertussis: Current perspectives on epidemiology and prevention. Hum. Vaccines Immunother. *11*, 108–117.

Galan, J.E., and Collmer, A. (1999). Type III secretion machines: bacterial devices for protein delivery into host cells. Science *284*, 1322–1328.

Galloux, M., Vitrac, H., Montagner, C., Raffestin, S., Popoff, M.R., Chenal, A., Forge, V., and Gillet, D. (2008). Membrane Interaction of Botulinum Neurotoxin A Translocation (T) Domain: The Bel Region is a Regulatory Loop For Membrane Interaction. J. Biol. Chem. *283*, 27668–27676.

Gancedo, J.M., Mazón, M.J., and Eraso, P. (1985). Biological roles of cAMP: similarities and differences between organisms. Trends Biochem. Sci. *10*, 210–212.

Gendlina, I., Held, K.G., Bartra, S.S., Gallis, B.M., Doneanu, C.E., Goodlett, D.R., Plano, G.V., and Collins, C.M. (2007). Identification and type III-dependent secretion of the Yersinia pestis insecticidal-like proteins. Mol. Microbiol. *64*, 1214–1227.

Gentile, F., Knipling, L.G., Sackett, D.L., and Wolff, J. (1990). Invasive adenylyl cyclase of Bordetella pertussis. Physical, catalytic, and toxic properties. J. Biol. Chem. *265*, 10686–10692.

Geourjon, C., and Deleage, G. (1995). SOPMA: significant improvements in protein secondary structure prediction by consensus prediction from multiple alignments. Comput. Appl. Biosci. CABIOS *11*, 681–684.

Geuijen, C.A., Willems, R.J., and Mooi, F.R. (1996). The major fimbrial subunit of Bordetella pertussis binds to sulfated sugars. Infect. Immun. *64*, 2657–2665.

Geuijen, C.A., Willems, R.J., Bongaerts, M., Top, J., Gielen, H., and Mooi, F.R. (1997). Role of the Bordetella pertussis minor fimbrial subunit, FimD, in colonization of the mouse respiratory tract. Infect. Immun. *65*, 4222–4228.

Gilles, A.M., Munier, H., Rose, T., Glaser, P., Krin, E., Danchin, A., Pellecuer, C., and Barzu, O. (1990). Intrinsic fluorescence of a truncated Bordetella pertussis adenylate cyclase expressed in Escherichia coli. Biochemistry. *29*, 8126–8130.

Gillet, D., and Barbier, J. (2015). Diphtheria toxin. Compr. Sourceb. Bact. Protein Toxins 111.

Glaser, P., Ladant, D., Sezer, O., Pichot, F., Ullmann, A., and Danchin, A. (1988a). The calmodulin-sensitive adenylate cyclase of Bordetella pertussis: cloning and expression in Escherichia coli. Mol. Microbiol. *2*, 19–30.

Glaser, P., Sakamoto, H., Bellalou, J., Ullmann, A., and Danchin, A. (1988b). Secretion of cyclolysin, the calmodulin-sensitive adenylate cyclase-haemolysin bifunctional protein of Bordetella pertussis. EMBO J. *7*, 3997–4004.

Glaser, P., Elmaoglou-Lazaridou, A., Krin, E., Ladant, D., Barzu, O., and Danchin, A. (1989). Identification of residues essential for catalysis and binding of calmodulin in Bordetella pertussis adenylate cyclase by site-directed mutagenesis. EMBO J. *8*, 967–972.

Glaser, P., Munier, H., Gilles, A.-M., Krin, E., Porumb, T., Bârzu, O., Sarfati, R., Pellecuer, C., and Danchin, A. (1991). Functional consequences of single amino acid substitutions in calmodulin-activated adenylate cyclase of Bordetella pertussis. EMBO J. *10*, 1683–1688.

Glick, B.S. (1995). Can Hsp70 proteins act as force-generating motors? Cell *80*, 11–14.

Glick, B.S., Wachter, C., and Schatz, G. (1992). The energetics of protein import into mitochondria. Biochim. Biophys. Acta *1101*, 249–251.

Gmira, S., Karimova, G., and Ladant, D. (2001). Characterization of recombinant Bordetella pertussis adenylate cyclase toxins carrying passenger proteins. Res. Microbiol. *152*, 889–900.

Goebel, E.M., Zhang, X., and Harvill, E.T. (2009). Bordetella pertussis infection or vaccination substantially protects mice against B. bronchiseptica infection. PloS One *4*, e6778.

Goldman, W.E., Klapper, D.G., and Baseman, J.B. (1982). Detection, isolation, and analysis of a released Bordetella pertussis product toxic to cultured tracheal cells. Infect. Immun. *36*, 782–794.

Goloubinoff, P., and De Los Rios, P. (2007). The mechanism of Hsp70 chaperones:(entropic) pulling the models together. Trends Biochem. Sci. *32*, 372–380.

Gonzalez-Bullon, D., Uribe, K.B., Martin, C., and Ostolaza, H. (2017). Phospholipase A activity of adenylate cyclase toxin mediates translocation of its adenylate cyclase domain. Proc. Natl. Acad. Sci. U. S. A. *114*, E6784–E6793.

Gonzalez-Bullon, D., Martin, C., and Ostolaza, H. (2018). Characterization of the Intrinsic Phospholipase A1 Activity of Bordetella pertussis Adenylate Cyclase Toxin. Toxins *10*.

Gonzalez-Bullon, D., Uribe, K.B., Largo, E., Guembelzu, G., Garcia-Arribas, A.B., Martin, C., and Ostolaza, H. (2019). Membrane Permeabilization by Bordetella Adenylate Cyclase Toxin Involves Pores of Tunable Size. Biomolecules *9*.

Goodnow, R.A. (1980). Biology of Bordetella bronchiseptica. Microbiol. Rev. *44*, 722–738.

Goodwin, M.S., and Weiss, A.A. (1990). Adenylate cyclase toxin is critical for colonization and pertussis toxin is critical for lethal infection by Bordetella pertussis in infant mice. Infect. Immun. *58*, 3445–3447.

Gordon, V.M., Leppla, S.H., and Hewlett, E.L. (1988). Inhibitors of receptor-mediated endocytosis block the entry of Bacillus anthracis adenylate cyclase toxin but not that of Bordetella pertussis adenylate cyclase toxin. Infect. Immun. *56*, 1066–1069.

Gordon, V.M., Young, W.W.J., Lechler, S.M., Gray, M.C., Leppla, S.H., and Hewlett, E.L. (1989). Adenylate cyclase toxins from Bacillus anthracis and Bordetella pertussis. Different processes for interaction with and entry into target cells. J. Biol. Chem. *264*, 14792–14796.

Gray, M., Szabo, G., Otero, A.S., Gray, L., and Hewlett, E. (1998). Distinct mechanisms for K+ efflux, intoxication, and hemolysis by Bordetella pertussis AC toxin. J. Biol. Chem. *273*, 18260–18267.

Gray, M.C., Ross, W., Kim, K., and Hewlett, E.L. (1999). Characterization of binding of adenylate cyclase toxin to target cells by flow cytometry. Infect. Immun. *67*, 4393–4399.

Gray, M.C., Lee, S.J., Gray, L.S., Zaretzky, F.R., Otero, A.S., Szabo, G., and Hewlett, E.L. (2001). Translocation-specific conformation of adenylate cyclase toxin from Bordetella pertussis inhibits toxin-mediated hemolysis. J. Bacteriol. *183*, 5904–5910.

Gray, M.C., Donato, G.M., Jones, F.R., Kim, T., and Hewlett, E.L. (2004). Newly secreted adenylate cyclase toxin is responsible for intoxication of target cells by Bordetella pertussis. Mol. Microbiol. *53*, 1709–1719.

Gross, R. (1995). Domain structure of the outer membrane transporter protein CyaE of Bordetella pertussis. Mol. Microbiol. *17*, 1219–1220.

Gross, R., and Rappuoli, R. (1989). Pertussis toxin promoter sequences involved in modulation. J. Bacteriol. *171*, 4026–4030.

Gross, M.K., Au, D.C., Smith, A.L., and Storm, D.R. (1992). Targeted mutations that ablate either the adenylate cyclase or hemolysin function of the bifunctional cyaA toxin of Bordetella pertussis abolish virulence. Proc. Natl. Acad. Sci. U. S. A. *89*, 4898–4902.

Gsponer, J., Christodoulou, J., Cavalli, A., Bui, J.M., Richter, B., Dobson, C.M., and Vendruscolo, M. (2008). A coupled equilibrium shift mechanism in calmodulin-mediated signal transduction. Struct. Lond. Engl. 1993 *16*, 736–746.

Guedin, S., Willery, E., Locht, C., and Jacob-Dubuisson, F. (1998). Evidence that a globular conformation is not compatible with FhaC-mediated secretion of the Bordetella pertussis filamentous haemagglutinin. Mol. Microbiol. *29*, 763–774.

Gueirard, P., Druilhe, A., Pretolani, M., and Guiso, N. (1998). Role of adenylate cyclase-hemolysin in alveolar macrophage apoptosis during Bordetella pertussis infection in vivo. Infect. Immun. *66*, 1718–1725.

Guermonprez, P., Ladant, D., Karimova, G., Ullmann, A., and Leclerc, C. (1999). Direct delivery of the Bordetella pertussis adenylate cyclase toxin to the MHC class I antigen presentation pathway. J. Immunol. Baltim. Md 1950 *162*, 1910–1916.

Guermonprez, P., Fayolle, C., Karimova, G., Ullmann, A., Leclerc, C., and Ladant, D. (2000). Bordetella pertussis adenylate cyclase toxin: a vehicle to deliver CD8-positive. Methods Enzymol. *326*, 527–542.

Guermonprez, P., Khelef, N., Blouin, E., Rieu, P., Ricciardi-Castagnoli, P., Guiso, N., Ladant, D., and Leclerc, C. (2001). The adenylate cyclase toxin of Bordetella pertussis binds to target cells via the alpha(M)beta(2) integrin (CD11b/CD18). J. Exp. Med. *193*, 1035–1044.

Guiso, N., Rocancourt, M., Szatanik, M., and Alonso, J.M. (1989). Bordetella adenylate cyclase is a virulence associated factor and an immunoprotective antigen. Microb. Pathog. *7*, 373–380.

Guiso, N., Szatanik, M., and Rocancourt, M. (1991). Protective activity of Bordetella adenylate cyclase-hemolysin against bacterial colonization. Microb. Pathog. *11*, 423–431.

Guo, Q., Shen, Y., Lee, Y.-S., Gibbs, C.S., Mrksich, M., and Tang, W.-J. (2005). Structural basis for the interaction of Bordetella pertussis adenylyl cyclase toxin with calmodulin. EMBO J. *24*, 3190–3201.

Gupta, B., Levchenko, T.S., and Torchilin, V.P. (2005). Intracellular delivery of large molecules and small particles by cell-penetrating proteins and peptides. Protein- Pept.-Mediat. Transduct. Mech. Implic. Drug Deliv. *57*, 637–651.

H

Hackett, M., Guo, L., Shabanowitz, J., Hunt, D.F., and Hewlett, E.L. (1994). Internal lysine palmitoylation in adenylate cyclase toxin from Bordetella pertussis. Science *266*, 433–435.

Hackett, M., Walker, C.B., Guo, L., Gray, M.C., Van Cuyk, S., Ullmann, A., Shabanowitz, J., Hunt, D.F., Hewlett, E.L., and Sebo, P. (1995). Hemolytic, but not cell-invasive activity, of adenylate cyclase toxin is selectively affected by differential fatty-acylation in Escherichia coli. J. Biol. Chem. *270*, 20250–20253.

Hancock, R.E. (2000). Cationic antimicrobial peptides: towards clinical applications. Expert Opin. Investig. Drugs *9*, 1723–1729.

Hancock, R.E., and Chapple, D.S. (1999). Peptide antibiotics. Antimicrob. Agents Chemother. *43*, 1317–1323.

Hancock, R.E.W., and Sahl, H.-G. (2006). Antimicrobial and host-defense peptides as new anti-infective therapeutic strategies. Nat. Biotechnol. *24*, 1551–1557.

Hannah, J.H., Menozzi, F.D., Renauld, G., Locht, C., and Brennan, M.J. (1994). Sulfated glycoconjugate receptors for the Bordetella pertussis adhesin filamentous hemagglutinin (FHA) and mapping of the heparin-binding domain on FHA. Infect. Immun. *62*, 5010–5019.

Hanski, E., and Farfel, Z. (1985). Bordetella pertussis invasive adenylate cyclase. Partial resolution and properties of its cellular penetration. J. Biol. Chem. *260*, 5526–5532.

Harper, C.B., Martin, S., Nguyen, T.H., Daniels, S.J., Lavidis, N.A., Popoff, M.R., Hadzic, G., Mariana, A., Chau, N., McCluskey, A., et al. (2011). Dynamin inhibition blocks botulinum neurotoxin type A endocytosis in neurons and delays botulism. J. Biol. Chem. *286*, 35966–35976.

Harrington, A.T., Castellanos, J.A., Ziedalski, T.M., Clarridge, J.E., 3rd, and Cookson, B.T. (2009). Isolation of Bordetella avium and novel Bordetella strain from patients with respiratory disease. Emerg. Infect. Dis. *15*, 72–74.

Harvill, E.T., Cotter, P.A., and Miller, J.F. (1999). Pregenomic comparative analysis between bordetella bronchiseptica RB50 and Bordetella pertussis tohama I in murine models of respiratory tract infection. Infect. Immun. *67*, 6109–6118.

Harvill, E.T., Preston, A., Cotter, P.A., Allen, A.G., Maskell, D.J., and Miller, J.F. (2000). Multiple roles for Bordetella lipopolysaccharide molecules during respiratory tract infection. Infect. Immun. *68*, 6720–6728.

Hasan, S., Osickova, A., Bumba, L., Novak, P., Sebo, P., and Osicka, R. (2015). Interaction of Bordetella adenylate cyclase toxin with complement receptor 3 involves multivalent glycan binding. FEBS Lett. *589*, 374–379.

Hauser, A.R. (2009). The type III secretion system of Pseudomonas aeruginosa: infection by injection. Nat. Rev. Microbiol. *7*, 654–665.

Havlicek, V., Higgins, L., Chen, W., Halada, P., Sebo, P., Sakamoto, H., and Hackett, M. (2001). Mass spectrometric analysis of recombinant adenylate cyclase toxin from Bordetella pertussis strain 18323/pHSP9. J. Mass Spectrom. JMS *36*, 384–391.

Hazenbos, W.L., van den Berg, B.M., Geuijen, C.W., Mooi, F.R., and van Furth, R. (1995). Binding of FimD on Bordetella pertussis to very late antigen-5 on monocytes activates complement receptor type 3 via protein tyrosine kinases. J. Immunol. Baltim. Md 1950 *155*, 3972–3978.

Hazes, B., and Read, R.J. (1997). Accumulating evidence suggests that several AB-toxins subvert the endoplasmic reticulum-associated protein degradation pathway to enter target cells. Biochemistry. *36*, 11051–11054.

Heck, D.V., Trus, B.L., and Steven, A.C. (1996). Three-dimensional structure of Bordetella pertussis fimbriae. J. Struct. Biol. *116*, 264–269.

Heiss, L.N., Moser, S.A., Unanue, E.R., and Goldman, W.E. (1993). Interleukin-1 is linked to the respiratory epithelial cytopathology of pertussis. Infect. Immun. *61*, 3123–3128.

Heiss, L.N., Lancaster, J.R., Corbett, J.A., and Goldman, W.E. (1994). Epithelial autotoxicity of nitric oxide: role in the respiratory cytopathology of pertussis. Proc. Natl. Acad. Sci. *91*, 267–270.

Hellwig, S.M., Rodriguez, M.E., Berbers, G.A., van De Winkel, J.G., and Mooi, F.R. (2003). Crucial role of antibodies to pertactin in Bordetella pertussis immunity. J. Infect. Dis. *188*, 738–742.

Heveker, N., and Ladant, D. (1997). Characterization of mutant Bordetella pertussis adenylate cyclase toxins with reduced affinity for calmodulin. Implications for the mechanism of toxin entry into target cells. Eur. J. Biochem. *243*, 643–649.

Heveker, N., Bonnaffe, D., and Ullmann, A. (1994). Chemical fatty acylation confers hemolytic and toxic activities to adenylate cyclase protoxin of Bordetella pertussis. J. Biol. Chem. *269*, 32844–32847.

Hewlett, E.L., Urban, M.A., Manclark, C.R., and Wolff, J. (1976). Extracytoplasmic adenylate cyclase of Bordetella pertussis. Proc. Natl. Acad. Sci. U. S. A. *73*, 1926–1930.

Hewlett, E.L., Wolff, J., and Manclark, C.R. (1978). Regulation of Bordetella pertussis extracytoplasmic adenylate cyclase. Adv. Cyclic Nucleotide Res. *9*, 621–628.

Hewlett, E.L., Underhill, L.H., Cook, G.H., Manclark, C.R., and Wolff, J. (1979). A protein activator for the adenylate cyclase of Bordetella pertussis. J. Biol. Chem. *254*, 5602–5605.

Hewlett, E.L., Gordon, V.M., McCaffery, J.D., Sutherland, W.M., and Gray, M.C. (1989). Adenylate cyclase toxin from Bordetella pertussis. Identification and purification of the holotoxin molecule. J. Biol. Chem. *264*, 19379–19384.

Hewlett, E.L., Gray, L., Allietta, M., Ehrmann, I., Gordon, V.M., and Gray, M.C. (1991). Adenylate cyclase toxin from Bordetella pertussis. Conformational change associated with toxin activity. J. Biol. Chem. *266*, 17503–17508.

Hewlett, E.L., Gray, M.C., Ehrmann, I.E., Maloney, N.J., Otero, A.S., Gray, L., Allietta, M., Szabo, G., Weiss, A.A., and Barry, E.M. (1993). Characterization of adenylate cyclase toxin from a mutant of Bordetella pertussis defective in the activator gene, cyaC. J. Biol. Chem. *268*, 7842–7848.

Hewlett, E.L., Donato, G.M., and Gray, M.C. (2006). Macrophage cytotoxicity produced by adenylate cyclase toxin from Bordetella pertussis: more than just making cyclic AMP! Mol. Microbiol. *59*, 447–459.

Hickey, F.B., Brereton, C.F., and Mills, K.H.G. (2008). Adenylate cycalse toxin of Bordetella pertussis inhibits TLR-induced IRF-1 and. J. Leukoc. Biol. *84*, 234–243.

Hill, E.E., and Lands, W.E.M. (1970). Chapter VI - Phospholipid Metabolism. In Lipid Metabolism, S.J. Wakil, ed. (Academic Press), pp. 185–277.

Hinz, K.H., Glunder, G., and Luders, H. (1978). Acute respiratory disease in turkey poults caused by Bordetella bronchiseptica-like bacteria. Vet. Rec. *103*, 262–263.

Holland, I.B., Blight, M.A., and Kenny, B. (1990). The mechanism of secretion of hemolysin and other polypeptides from gram-negative bacteria. J. Bioenerg. Biomembr. *22*, 473–491.

Holmgren, J., Lönnroth, I., M\a ansson, J., and Svennerholm, L. (1975). Interaction of cholera toxin and membrane GM1 ganglioside of small intestine. Proc. Natl. Acad. Sci. *72*, 2520–2524.

Honjo, T., Nishizuka, Y., and Hayaishi, O. (1968). Diphtheria toxin-dependent adenosine diphosphate ribosylation of aminoacyl transferase II and inhibition of protein synthesis. J. Biol. Chem. *243*, 3553–3555.

Horiguchi, Y., Nakai, T., and Kume, K. (1989). Purification and characterization of Bordetella bronchiseptica dermonecrotic toxin. Microb. Pathog. *6*, 361–368.

Horiguchi, Y., Nakai, T., and Kume, K. (1991). Effects of Bordetella bronchiseptica dermonecrotic toxin on the structure and function of osteoblastic clone MC3T3-e1 cells. Infect. Immun. *59*, 1112.

Horiguchi, Y., Sugimoto, N., and Matsuda, M. (1993). Stimulation of DNA synthesis in osteoblast-like MC3T3-E1 cells by Bordetella bronchiseptica dermonecrotic toxin. Infect. Immun. *61*, 3611.

Horiguchi, Y., Senda, T., Sugimoto, N., Katahira, J., and Matsuda, M. (1995). Bordetella bronchiseptica dermonecrotizing toxin stimulates assembly of actin stress fibers and focal adhesions by modifying the small GTP-binding protein rho. J. Cell Sci. *108*, 3243.

Horiguchi, Y., Inoue, N., Masuda, M., Kashimoto, T., Katahira, J., Sugimoto, N., and Matsuda, M. (1997). Bordetella bronchiseptica dermonecrotizing toxin induces reorganization of actin stress fibers through deamidation of Gln-63 of the GTP-binding protein Rho. Proc. Natl. Acad. Sci. U. S. A. *94*, 11623–11626.

Hovingh, E.S., Mariman, R., Solans, L., Hijdra, D., Hamstra, H.-J., Jongerius, I., van Gent, M., Mooi, F., Locht, C., and Pinelli, E. (2018). Bordetella pertussis pertactin knock-out strains reveal immunomodulatory properties of this virulence factor. Emerg. Microbes Infect. *7*, 1–13.

Hristov, A.C., Auwaerter, P.G., Romagnoli, M., and Carroll, K.C. (2008). Bordetella hinzii septicemia in association with Epstein-Barr virus viremia and an Epstein-Barr virus-associated diffuse large B-cell lymphoma. Diagn. Microbiol. Infect. Dis. *61*, 484–486.

Hviid, A., Stellfeld, M., Andersen, P.H., Wohlfahrt, J., and Melbye, M. (2004). Impact of routine vaccination with a pertussis toxoid vaccine in Denmark. Vaccine *22*, 3530–3534.

I

Iglesias-Bartolomé, R., Trenchi, A., Comín, R., Moyano, A.L., Nores, G.A., and Daniotti, J.L. (2009). Differential endocytic trafficking of neuropathy-associated antibodies to GM1 ganglioside and cholera toxin in epithelial and neural cells. Biochim. Biophys. Acta BBA-Biomembr. *1788*, 2526–2540.

Iida, T., and Okonogi, T. (1971). Lienotoxicity of Bordetella pertussis in mice. J. Med. Microbiol. *4*, 51–61.

Ikura, M., Clore, G.M., Gronenborn, A.M., Zhu, G., Klee, C.B., and Bax, A. (1992). Solution structure of a calmodulin-target peptide complex by multidimensional NMR. Science *256*, 632–638.

Iriarte, M., and Cornelis, G.R. (1998). YopT, a new Yersinia Yop effector protein, affects the cytoskeleton of host cells. Mol. Microbiol. *29*, 915–929.

Ishibashi, Y., Claus, S., and Relman, D.A. (1994). Bordetella pertussis filamentous hemagglutinin interacts with a leukocyte signal transduction complex and stimulates bacterial adherence to monocyte CR3 (CD11b/CD18). J. Exp. Med. *180*, 1225–1233.

Ishibashi, Y., Yoshimura, K., Nishikawa, A., Claus, S., Laudanna, C., and Relman, D.A. (2002). Role of phosphatidylinositol 3-kinase in the binding of Bordetella pertussis to human monocytes. Cell. Microbiol. *4*, 825–833.

Issartel, J.P., Koronakis, V., and Hughes, C. (1991). Activation of Escherichia coli prohaemolysin to the mature toxin by acyl carrier protein-dependent fatty acylation. Nature *351*, 759–761.

Ivanov, Y.V., Linz, B., Register, K.B., Newman, J.D., Taylor, D.L., Boschert, K.R., Le Guyon, S., Wilson, E.F., Brinkac, L.M., Sanka, R., et al. (2016). Identification and taxonomic characterization of Bordetella pseudohinzii sp. nov. isolated from laboratory-raised mice. Int. J. Syst. Evol. Microbiol. *66*, 5452–5459.

J

Jacobs, C., Joris, B., Jamin, M., Klarsov, K., Van Beeumen, J., Mengin-Lecreulx, D., van Heijenoort, J., Park, J.T., Normark, S., and Frère, J.-M. (1995). AmpD, essential for both β-lactamase regulation and cell wall recycling, is a novel cytosolic N-acetylmuramyl-L-alanine amidase. Mol. Microbiol. *15*, 553–559.

Järver, P., Langel, K., El-Andaloussi, S., and Langel, Ü. (2007). Applications of cell-penetrating peptides in regulation of gene expression. Biochem. Soc. Trans. *35*, 770.

Jiyipong, T., Morand, S., Jittapalapong, S., Raoult, D., and Rolain, J.-M. (2013). Bordetella hinzii in rodents, Southeast Asia. Emerg. Infect. Dis. *19*, 502–503.

Jo, I., Kim, J.-S., Xu, Y., Hyun, J., Lee, K., and Ha, N.-C. (2019). Recent paradigm shift in the assembly of bacterial tripartite efflux pumps and the type I secretion system. J. Microbiol. Seoul Korea *57*, 185–194.

Jonson, A.-B., Normark, S., and Rhen, M. (2005). Fimbriae, pili, flagella and bacterial virulence. Contrib. Microbiol. *12*, 67–89.

Junker, M., Schuster, C.C., McDonnell, A.V., Sorg, K.A., Finn, M.C., Berger, B., and Clark, P.L. (2006). Pertactin β-helix folding mechanism suggests common themes for the secretion and folding of autotransporter proteins. Proc. Natl. Acad. Sci. *103*, 4918–4923.

Juntapremjit, S., Thamwiriyasati, N., Kurehong, C., Prangkio, P., Shank, L., Powthongchin, B., and Angsuthanasombat, C. (2015). Functional importance of the Gly cluster in transmembrane helix 2 of the Bordetella pertussis CyaA-hemolysin: Implications for toxin oligomerization and pore formation. Toxicon Off. J. Int. Soc. Toxinology *106*, 14–19.

Jurado, L.A., Chockalingam, P.S., and Jarrett, H.W. (1999). Apocalmodulin. Physiol. Rev. *79*, 661–682.

K

Kaczorek, M., Delpeyroux, F., Chenciner, N., Streeck, R.E., Murphy, J.R., Boquet, P., and Tiollais, P. (1983). Nucleotide sequence and expression of the diphtheria tox228 gene in Escherichia coli. Science *221*, 855–858.

Kajava, A.V., Cheng, N., Cleaver, R., Kessel, M., Simon, M.N., Willery, E., Jacob-Dubuisson, F., Locht, C., and Steven, A.C. (2001). Beta-helix model for the filamentous haemagglutinin adhesin of Bordetella pertussis and related bacterial secretory proteins. Mol. Microbiol. *42*, 279–292.

Kamanova, J., Kofronova, O., Masin, J., Genth, H., Vojtova, J., Linhartova, I., Benada, O., Just, I., and Sebo, P. (2008). Adenylate cyclase toxin subverts phagocyte function by RhoA inhibition and unproductive ruffling. J. Immunol. Baltim. Md 1950 *181*, 5587–5597.

Kanonenberg, K., Spitz, O., Erenburg, I.N., Beer, T., and Schmitt, L. (2018). Type I secretion system-it takes three and a substrate. FEMS Microbiol. Lett. *365*.

Kapil, P., Papin, J.F., Wolf, R.F., Zimmerman, L.I., Wagner, L.D., and Merkel, T.J. (2018). Maternal Vaccination With a Monocomponent Pertussis Toxoid Vaccine Is Sufficient to Protect Infants in a Baboon Model of Whooping Cough. J. Infect. Dis. *217*, 1231–1236.

Karimova, G., and Ullmann, A. (1997). Characterization of DNA binding sites for the BvgA protein of Bordetella pertussis. J. Bacteriol. *179*, 3790–3792.

Karimova, G., Bellalou, J., and Ullmann, A. (1996). Phosphorylation-dependent binding of BvgA to the upstream region of the cyaA gene of Bordetella pertussis. Mol. Microbiol. *20*, 489–496.

Karimova, G., Fayolle, C., Gmira, S., Ullmann, A., Leclerc, C., and Ladant, D. (1998a). Charge-dependent translocation of Bordetella pertussis adenylate cyclase toxin into eukaryotic cells: implication for the in vivo delivery of CD8(+) T cell epitopes into antigen-presenting cells. Proc. Natl. Acad. Sci. U. S. A. *95*, 12532–12537.

Karimova, G., Pidoux, J., Ullmann, A., and Ladant, D. (1998b). A bacterial two-hybrid system based on a reconstituted signal transduction pathway. Proc. Natl. Acad. Sci. U. S. A. *95*, 5752–5756.

Karimova, G., Ullmann, A., and Ladant, D. (2000a). Bordetella pertussis adenylate cyclase toxin as a tool to analyze molecular interactions in a bacterial two-hybrid system. Int. J. Med. Microbiol. IJMM *290*, 441–445.

Karimova, G., Ullmann, A., and Ladant, D. (2000b). A bacterial two-hybrid system that exploits a cAMP signaling cascade in Escherichia coli. Methods Enzymol. *328*, 59–73.

Karimova, G., Dautin, N., and Ladant, D. (2005). Interaction network among Escherichia coli membrane proteins involved in cell division as revealed by bacterial two-hybrid analysis. J. Bacteriol. *187*, 2233–2243.

Karimova, G., Robichon, C., and Ladant, D. (2009). Characterization of YmgF, a 72-residue inner membrane protein that associates with the Escherichia coli cell division machinery. J. Bacteriol. *191*, 333–346.

Karst, J.C., Sotomayor Perez, A.C., Guijarro, J.I., Raynal, B., Chenal, A., and Ladant, D. (2010). Calmodulin-induced conformational and hydrodynamic changes in the catalytic domain of Bordetella pertussis adenylate cyclase toxin. Biochemistry. *49*, 318–328.

Karst, J.C., Barker, R., Devi, U., Swann, M.J., Davi, M., Roser, S.J., Ladant, D., and Chenal, A. (2012). Identification of a region that assists membrane insertion and translocation of the catalytic domain of Bordetella pertussis CyaA toxin. J. Biol. Chem. *287*, 9200–9212.

Karst, J.C., Ntsogo Enguene, V.Y., Cannella, S.E., Subrini, O., Hessel, A., Debard, S., Ladant, D., and Chenal, A. (2014). Calcium, acylation, and molecular confinement favor folding of Bordetella pertussis adenylate cyclase CyaA toxin into a monomeric and cytotoxic form. J. Biol. Chem. *289*, 30702–30716.

Katada, T., Tamura, M., and Ui, M. (1983). The A protomer of islet-activating protein, pertussis toxin, as an active peptide catalyzing ADP-ribosylation of a membrane protein. Arch. Biochem. Biophys. *224*, 290–298.

Kerr, J.R., and Preston, N.W. (2001). Current pharmacotherapy of pertussis. Expert Opin. Pharmacother. *2*, 1275–1282.

Kersters, K., Hinz, K.-H., Hertle, A., Segers, P., Lievens, A., Siegmann, O., and De Ley, J. (1984). Bordetella avium sp. nov., Isolated from the Respiratory Tracts of Turkeys and Other Birds. Int. J. Syst. Evol. Microbiol. *34*, 56–70.

Khanppnavar, B., and Datta, S. (2018). Crystal structure and substrate specificity of ExoY, a unique T3SS mediated secreted nucleotidyl cyclase toxin from Pseudomonas aeruginosa. Biochim. Biophys. Acta BBA - Gen. Subj. *1862*, 2090–2103.

Khelef, N., and Guiso, N. (1995). Induction of macrophage apoptosis by Bordetella pertussis adenylate cyclase-hemolysin. FEMS Microbiol. Lett. *134*, 27–32.

Khelef, N., Sakamoto, H., and Guiso, N. (1992). Both adenylate cyclase and hemolytic activities are required by Bordetella pertussis to initiate infection. Microb. Pathog. *12*, 227–235.

Khelef, N., Zychlinsky, A., and Guiso, N. (1993). Bordetella pertussis induces apoptosis in macrophages: role of adenylate cyclase-hemolysin. Infect. Immun. *61*, 4064–4071.

Khelef, N., Bachelet, C.M., Vargaftig, B.B., and Guiso, N. (1994). Characterization of murine lung inflammation after infection with parental Bordetella pertussis and mutants deficient in adhesins or toxins. Infect. Immun. *62*, 2893–2900.

Khelef, N., Gounon, P., and Guiso, N. (2001). Internalization of Bordetella pertussis adenylate cyclase–haemolysin into endocytic vesicles contributes to macrophage cytotoxicity. Cell. Microbiol. *3*, 721–730.

Killian, J.A., and von Heijne, G. (2000). How proteins adapt to a membrane–water interface. Trends Biochem. Sci. *25*, 429–434.

Kimura, A., Mountzouros, K.T., Relman, D.A., Falkow, S., and Cowell, J.L. (1990). Bordetella pertussis filamentous hemagglutinin: evaluation as a protective antigen and colonization factor in a mouse respiratory infection model. Infect. Immun. *58*, 7.

Klein, N.P. (2014). Licensed pertussis vaccines in the United States: history and current state. Hum. Vaccines Immunother. *10*, 2684–2690.

Kloos, W.E., Mohapatra, N., Dobrogosz, W.J., Ezzell, J.W., and Manclark, C.R. (1981). Deoxyribonucleotide Sequence Relationships Among Bordetella Species. Int. J. Syst. Bacteriol. *31*, 173–176.

Kloss, E., Courtemanche, N., and Barrick, D. (2008). Repeat-protein folding: New insights into origins of cooperativity, stability, and topology. Highlight Issue Protein Fold. *469*, 83–99.

Knapp, O., Maier, E., Polleichtner, G., Masin, J., Sebo, P., and Benz, R. (2003). Channel formation in model membranes by the adenylate cyclase toxin of Bordetella pertussis: effect of calcium. Biochemistry. *42*, 8077–8084.

Knapp, O., Maier, E., Masin, J., Sebo, P., and Benz, R. (2008). Pore formation by the Bordetella adenylate cyclase toxin in lipid bilayer membranes: role of voltage and pH. Biochim. Biophys. Acta *1778*, 260–269.

Ko, K.S., Peck, K.R., Oh, W.S., Lee, N.Y., Lee, J.H., and Song, J.-H. (2005). New species of Bordetella, Bordetella ansorpii sp. nov., isolated from the purulent exudate of an epidermal cyst. J. Clin. Microbiol. *43*, 2516–2519.

Koriazova, L.K., and Montal, M. (2003). Translocation of botulinum neurotoxin light chain protease through the heavy chain channel. Nat. Struct. Biol. *10*, 13–18.

Koronakis, V., Eswaran, J., and Hughes, C. (2004). Structure and function of TolC: the bacterial exit duct for proteins and drugs. Annu. Rev. Biochem. *73*, 467–489.

Krantz, B.A., Melnyk, R.A., Zhang, S., Juris, S.J., Lacy, D.B., Wu, Z., Finkelstein, A., and Collier, R.J. (2005). A Phenylalanine Clamp Catalyzes Protein Translocation Through the Anthrax Toxin Pore. Science *309*, 777.

Kurehong, C., Powthongchin, B., Thamwiriyasati, N., and Angsuthanasombat, C. (2011). Functional significance of the highly conserved Glu(570) in the putative pore-forming helix 3 of the Bordetella pertussis haemolysin toxin. Toxicon Off. J. Int. Soc. Toxinology *57*, 897–903.

Kurehong, C., Kanchanawarin, C., Powthongchin, B., Katzenmeier, G., and Angsuthanasombat, C. (2015). Membrane-Pore Forming Characteristics of the Bordetella pertussis CyaA-Hemolysin Domain. Toxins *7*, 1486–1496.

Kurehong, C., Kanchanawarin, C., Powthongchin, B., Prangkio, P., Katzenmeier, G., and Angsuthanasombat, C. (2017). Functional Contributions of Positive Charges in the Pore-Lining Helix 3 of the Bordetella pertussis CyaA-Hemolysin to Hemolytic Activity and Ion-Channel Opening. Toxins *9*.

L

Lacey, B.W. (1960). Antigenic modulation of Bordetella pertussis. Epidemiol. Infect. *58*, 57–93.

Lacy, D.B., Tepp, W., Cohen, A.C., DasGupta, B.R., and Stevens, R.C. (1998). Crystal structure of botulinum neurotoxin type A and implications for toxicity. Nat. Struct. Biol. *5*, 898–902.

Ladant, D. (1988). Interaction of Bordetella pertussis adenylate cyclase with calmodulin. Identification of two separated calmodulin-binding domains. J. Biol. Chem. *263*, 2612–2618.

Ladant, D., and Ullmann, A. (1999). Bordatella pertussis adenylate cyclase: a toxin with multiple talents. Trends Microbiol. *7*, 172–176.

Ladant, D., Michelson, S., Sarfati, R., Gilles, A.M., Predeleanu, R., and Barzu, O. (1989). Characterization of the calmodulin-binding and of the catalytic domains of Bordetella pertussis adenylate cyclase. J. Biol. Chem. *264*, 4015–4020.

Ladant, D., Glaser, P., and Ullmann, A. (1992). Insertional mutagenesis of Bordetella pertussis adenylate cyclase. J. Biol. Chem. *267*, 2244–2250.

Lai, B., Agarwal, R., Nelson, L.D., Swaminathan, S., and London, E. (2010). Low pH-induced pore formation by the T domain of botulinum toxin type A is dependent upon NaCl concentration. J. Membr. Biol. *236*, 191–201.

Laoide, B.M., and Ullmann, A. (1990). Virulence dependent and independent regulation of the Bordetella pertussis cya operon. EMBO J. *9*, 999–1005.

Lapin, J.H. (1943). Whooping Cough. (Springfield, Ill. : Baltimore, Md.).

Lavine, J., Broutin, H., Harvill, E.T., and Bjornstad, O.N. (2010). Imperfect vaccine-induced immunity and whooping cough transmission to infants. Vaccine *29*, 11–16.

Le Coustumier, A., Njamkepo, E., Cattoir, V., Guillot, S., and Guiso, N. (2011). Bordetella petrii infection with long-lasting persistence in human. Emerg. Infect. Dis. *17*, 612–618.

Le Dur, A., Chaby, R., and Szabo, L. (1980). Isolation of two protein-free and chemically different lipopolysaccharides from Bordetella pertussis phenol-extracted endotoxin. J. Bacteriol. *143*, 78–88.

Lee, S.-J., Gray, M.C., Zu, K., and Hewlett, E.L. (2005). Oligomeric behavior of Bordetella pertussis adenylate cyclase toxin in solution. Arch. Biochem. Biophys. *438*, 80–87.

Lehrer, R.I., and Ganz, T. (1999). Antimicrobial peptides in mammalian and insect host defence. Curr. Opin. Immunol. *11*, 23–27.

Lehto, T., Kurrikoff, K., and Langel, Ü. (2012). Cell-penetrating peptides for the delivery of nucleic acids. Expert Opin. Drug Deliv. *9*, 823–836.

Leininger, E., Roberts, M., Kenimer, J.G., Charles, I.G., Fairweather, N., Novotny, P., and Brennan, M.J. (1991). Pertactin, an Arg-Gly-Asp-containing Bordetella pertussis surface protein that promotes adherence of mammalian cells. Proc. Natl. Acad. Sci. *88*, 345–349.

Leininger, E., Ewanowich, C.A., Bhargava, A., Peppler, M.S., Kenimer, J.G., and Brennan, M.J. (1992). Comparative roles of the Arg-Gly-Asp sequence present in the Bordetella pertussis adhesins pertactin and filamentous hemagglutinin. Infect. Immun. *60*, 2380–2385.

Leppla, S.H. (1982). Anthrax toxin edema factor: a bacterial adenylate cyclase that increases cyclic AMP concentrations of eukaryotic cells. Proc. Natl. Acad. Sci. *79*, 3162.

Leslie, P.H., and Gardner, A.D. (1931). The phases of Haemophilus pertussis. Epidemiol. Infect. *31*, 423–434.

Létoffé, S., Delepelaire, P., and Wandersman, C. (1996). Protein secretion in gram-negative bacteria: assembly of the three components of ABC protein-mediated exporters is ordered and promoted by substrate binding. EMBO J. *15*, 5804–5811.

Linhartová, I., Bumba, L., Mašín, J., Basler, M., Osička, R., Kamanová, J., Procházková, K., Adkins, I., Hejnová-Holubová, J., Sadílková, L., et al. (2010). RTX proteins: a highly diverse family secreted by a common mechanism. FEMS Microbiol. Rev. *34*, 1076–1112.

Linhartova, I., Osicka, R., Bumba, L., Masin, J., and Sebo, P. (2016). RTX Toxins: A Review. In Microbial Toxins, P. Gopalakrishnakone, B. Stiles, A. Alape-Girón, J.D. Dubreuil, and M. Mandal, eds. (Dordrecht: Springer Netherlands), pp. 1–29.

Litvak, A.M., and Gibel, H. (1948). Cerebral complications in pertussis. J. Pediatr. *32*, 357–379.

Liu, S., and Leppla, S.H. (2003). Cell surface tumor endothelium marker 8 cytoplasmic tail-independent anthrax toxin binding, proteolytic processing, oligomer formation, and internalization. J. Biol. Chem. *278*, 5227–5234.

Liu, D.F., Phillips, E., Wizemann, T.M., Siegel, M.M., Tabei, K., Cowell, J.L., and Tuomanen, E. (1997). Characterization of a recombinant fragment that contains a carbohydrate recognition domain of the filamentous hemagglutinin. Infect. Immun. *65*, 3465.

Liu, S., Moayeri, M., Pomerantsev, A.P., and Leppla, S.H. (2015). Bacillus anthracis toxins. Compr. Sourceb. Bact. Protein Toxins 361.

Livey, I., and Wardlaw, A.C. (1984). Production and properties of Bordetella pertussis heat-labile toxin. J. Med. Microbiol. *17*, 91–103.

Livey, I., Duggleby, C.J., and Robinson, A. (1987). Cloning and nucleotide sequence analysis of the serotype 2 fimbrial subunit gene of Bordetella pertussis. Mol. Microbiol. *1*, 203–203.

Locht, C. (1999). Molecular aspects of Bordetella pertussis pathogenesis. Int. Microbiol. Off. J. Span. Soc. Microbiol. *2*, 137–144.

Locht, C., Bertin, P., Menozzi, F.D., and Renauld, G. (1993). The filamentous haemagglutinin, a multifaceted adhesion produced by virulent Bordetella spp. Mol. Microbiol. *9*, 653–660.

Locht, C., Leininger, E., Menozzi, F.D., Renauld-Mongénie, G., Heron, I., Rouse, J.H., Brennan, M.J., and Bowen, S. (1997). Immunodominant Domains Present on the Bordetella pertussis Vaccine Component Filamentous Hemagglutinin. J. Infect. Dis. *175*, 1423–1431.

London, E. (1992). Diphtheria toxin: membrane interaction and membrane translocation. Biochim. Biophys. Acta BBA - Rev. Biomembr. *1113*, 25–51.

Lord, J.M., Smith, D.C., and Roberts, L.M. (1999). Toxin entry: how bacterial proteins get into mammalian cells. Cell. Microbiol. *1*, 85–91.

Loucká, J., Schlecht, G., Vodolánová, J., Leclerc, C., and Sebo, P. (2002). Delivery of a MalE CD4(+)-T-cell epitope into the major histocompatibility complex class II antigen presentation pathway by Bordetella pertussis adenylate cyclase. Infect. Immun. *70*, 1002–1005.

Luker, K.E., Tyler, A.N., Marshall, G.R., and Goldman, W.E. (1995). Tracheal cytotoxin structural requirements for respiratory epithelial damage in pertussis. Mol. Microbiol. *16*, 733–743.

M

Mäe, M., and Langel, Ü. (2006). Cell-penetrating peptides as vectors for peptide, protein and oligonucleotide delivery. Anti-Infect. Technol. *6*, 509–514.

Mahlapuu, M., Håkansson, J., Ringstad, L., and Björn, C. (2016). Antimicrobial Peptides: An Emerging Category of Therapeutic Agents. Front. Cell. Infect. Microbiol. *6*, 194–194.

Majlessi, L., Simsova, M., Jarvis, Z., Brodin, P., Rojas, M.-J., Bauche, C., Nouze, C., Ladant, D., Cole, S.T., Sebo, P., et al. (2006). An increase in antimycobacterial Th1-cell responses by prime-boost protocols of immunization does not enhance protection against tuberculosis. Infect. Immun. *74*, 2128–2137.

Makhov, A.M., Hannah, J.H., Brennan, M.J., Trus, B.L., Kocsis, E., Conway, J.F., Wingfield, P.T., Simon, M.N., and Steven, A.C. (1994). Filamentous hemagglutinin of Bordetella pertussis. A bacterial adhesin formed as a 50-nm monomeric rigid rod based on a 19-residue repeat motif rich in beta strands and turns. J. Mol. Biol. *241*, 110–124.

Malenbaum, S.E., Collier, R.J., and London, E. (1998). Membrane Topography of the T Domain of Diphtheria Toxin Probed with Single Tryptophan Mutants. Biochemistry. *37*, 17915–17922.

Malliavin, T.E. (2017). Molecular Modeling of the Catalytic Domain of CyaA Deepened the Knowledge of Its Functional Dynamics. Toxins *9*.

Marr, A.K., Gooderham, W.J., and Hancock, R.E. (2006). Antibacterial peptides for therapeutic use: obstacles and realistic outlook. Curr. Opin. Pharmacol. *6*, 468–472.

Marr, N., Shah, N.R., Lee, R., Kim, E.J., and Fernandez, R.C. (2011). Bordetella pertussis autotransporter Vag8 binds human C1 esterase inhibitor and confers serum resistance. PloS One *6*, e20585.

Martin, C., Requero, M.-A., Masin, J., Konopasek, I., Goni, F.M., Sebo, P., and Ostolaza, H. (2004). Membrane restructuring by Bordetella pertussis adenylate cyclase toxin, a member of the RTX toxin family. J. Bacteriol. *186*, 3760–3765.

Martín, C., Gómez-Bilbao, G., and Ostolaza, H. (2010). Bordetella adenylate cyclase toxin promotes calcium entry into both CD11b+ and CD11b- cells through cAMP-dependent L-type-like calcium channels. J. Biol. Chem. *285*, 357–364.

Martin, S.W., Pawloski, L., Williams, M., Weening, K., DeBolt, C., Qin, X., Reynolds, L., Kenyon, C., Giambrone, G., Kudish, K., et al. (2015). Pertactin-Negative Bordetella pertussis Strains: Evidence for a Possible Selective Advantage. Clin. Infect. Dis. *60*, 223–227.

Mascarell, L., Fayolle, C., Bauche, C., Ladant, D., and Leclerc, C. (2005). Induction of neutralizing antibodies and Th1-polarized and CD4-independent CD8+. J. Virol. *79*, 9872–9884.

Mascarell, L., Bauche, C., Fayolle, C., Diop, O.M., Dupuy, M., Nougarede, N., Perraut, R., Ladant, D., and Leclerc, C. (2006). Delivery of the HIV-1 Tat protein to dendritic cells by the CyaA vector induces specific Th1 responses and high affinity neutralizing antibodies in non human primates. Vaccine *24*, 3490–3499.

Masin, J., Konopasek, I., Svobodova, J., and Sebo, P. (2004). Different structural requirements for adenylate cyclase toxin interactions with erythrocyte and liposome membranes. Biochim. Biophys. Acta *1660*, 144–154.

Masin, J., Basler, M., Knapp, O., El-Azami-El-Idrissi, M., Maier, E., Konopasek, I., Benz, R., Leclerc, C., and Sebo, P. (2005). Acylation of lysine 860 allows tight binding and cytotoxicity of Bordetella adenylate cyclase on CD11b-expressing cells. Biochemistry. *44*, 12759–12766.

Masin, J., Osickova, A., Sukova, A., Fiser, R., Halada, P., Bumba, L., Linhartova, I., Osicka, R., and Sebo, P. (2016). Negatively charged residues of the segment linking the enzyme and cytolysin moieties restrict the membrane-permeabilizing capacity of adenylate cyclase toxin. Sci. Rep. *6*, 29137.

Masin, J., Roderova, J., Osickova, A., Novak, P., Bumba, L., Fiser, R., Sebo, P., and Osicka, R. (2017). The conserved tyrosine residue 940 plays a key structural role in membrane interaction of Bordetella adenylate cyclase toxin. Sci. Rep. *7*, 9330.

Masuda, M., Betancourt, L., Matsuzawa, T., Kashimoto, T., Takao, T., Shimonishi, Y., and Horiguchi, Y. (2000). Activation of Rho through a cross-link with polyamines catalyzed by Bordetella dermonecrotizing toxin. EMBO J. *19*, 521–530.

Masure, H.R., Au, D.C., Gross, M.K., Donovan, M.G., and Storm, D.R. (1990). Secretion of the Bordetella pertussis adenylate cyclase from Escherichia coli containing the hemolysin operon. Biochemistry. *29*, 140–145.

Matsuzawa, T., Kashimoto, T., Katahira, J., and Horiguchi, Y. (2002). Identification of a receptor-binding domain of Bordetella dermonecrotic toxin. Infect. Immun. *70*, 3427–3432.

Matsuzawa, T., Fukui, A., Kashimoto, T., Nagao, K., Oka, K., Miyake, M., and Horiguchi, Y. (2004). Bordetella dermonecrotic toxin undergoes proteolytic processing to be translocated from a dynamin-related endosome into the cytoplasm in an acidification-independent manner. J. Biol. Chem. *279*, 2866–2872.

Mattoo, S., and Cherry, J.D. (2005). Molecular pathogenesis, epidemiology, and clinical manifestations of respiratory infections due to Bordetella pertussis and other Bordetella subspecies. Clin. Microbiol. Rev. *18*, 326–382.

Mattoo, S., Yuk, M.H., Huang, L.L., and Miller, J.F. (2004). Regulation of type III secretion in Bordetella. Mol. Microbiol. *52*, 1201–1214.

McGuirk, P., and Mills, K.H. (2000). Direct anti-inflammatory effect of a bacterial virulence factor: IL-10-dependent suppression of IL-12 production by filamentous hemagglutinin from Bordetella pertussis. Eur. J. Immunol. *30*, 415–422.

Meade, B.R., and Dowdy, S.F. (2008). Enhancing the cellular uptake of siRNA duplexes following noncovalent packaging with protein transduction domain peptides. Membr. Permeable Pept. Vectors Chem. Funct. Des. Ther. Appl. *60*, 530–536.

Meador, W., Means, A., and Quiocho, F. (1992). Target enzyme recognition by calmodulin: 2.4 A structure of a calmodulin-peptide complex. Science *257*, 1251.

Meetum, K., Imtong, C., Katzenmeier, G., and Angsuthanasombat, C. (2017). Acylation of the Bordetella pertussis CyaA-hemolysin: Functional implications for efficient membrane insertion and pore formation. Biochim. Biophys. Acta Biomembr. *1859*, 312–318.

Melvin, J.A., Scheller, E.V., Miller, J.F., and Cotter, P.A. (2014). Bordetella pertussis pathogenesis: current and future challenges. Nat. Rev. Microbiol. *12*, 274–288.

Melvin, J.A., Scheller, E.V., Noël, C.R., and Cotter, P.A. (2015). New Insight into Filamentous Hemagglutinin Secretion Reveals a Role for Full-Length FhaB in Bordetella Virulence. mBio *6*, e01189-15.

Ménétrey, J., Gillet, D., and Ménez, A. (2005). Structural features common to intracellularly acting toxins from bacteria. Toxicon *45*, 129–137.

Merkel, T.J., and Stibitz, S. (1995). Identification of a locus required for the regulation of bvg-repressed genes in Bordetella pertussis. J. Bacteriol. *177*, 2727–2736.

Merkel, T.J., Boucher, P.E., Stibitz, S., and Grippe, V.K. (2003). Analysis of bvgR Expression in Bordetella pertussis. J. Bacteriol. *185*, 6902–6912.

Merritt, E.A., Sarfaty, S., van den Akker, F., L'Hoir, C., Martial, J.A., and Hol, W.G. (1994). Crystal structure of cholera toxin B-pentamer bound to receptor GM1 pentasaccharide. Protein Sci. Publ. Protein Soc. *3*, 166–175.

Mitchell, D.J., Steinman, L., Kim, D.T., Fathman, C.G., and Rothbard, J.B. (2000). Polyarginine enters cells more efficiently than other polycationic homopolymers. J. Pept. Res. *56*, 318–325.

Moayeri, M., and Leppla, S.H. (2004). The roles of anthrax toxin in pathogenesis. Curr. Opin. Microbiol. *7*, 19–24.

Mobberley-Schuman, P.S., and Weiss, A.A. (2005). Influence of CR3 (CD11b/CD18) expression on phagocytosis of Bordetella pertussis by human neutrophils. Infect. Immun. *73*, 7317–7323.

Montagner, C., Perier, A., Pichard, S., Vernier, G., Menez, A., Gillet, D., Forge, V., and Chenal, A. (2007). Behavior of the N-terminal helices of the diphtheria toxin T domain during the successive steps of membrane interaction. Biochemistry. *46*, 1878–1887.

Montecucco, C., Schiavo, G., Gao, Z., Bauerlein, E., Boquet, P., and DasGupta, B.R. (1988). Interaction of botulinum and tetanus toxins with the lipid bilayer surface. Biochem. J. *251*, 379–383.

Montecucco, C., Schiavo, G., and Dasgupta, B.R. (1989). Effect of pH on the interaction of botulinum neurotoxins A, B and E with liposomes. Biochem. J. *259*, 47–53.

Mooi, F.R., Jansen, W.H., Brunings, H., Gielen, H., van der Heide, H.G., Walvoort, H.C., and Guinee, P.A. (1992). Construction and analysis of Bordetella pertussis mutants defective in the production of fimbriae. Microb. Pathog. *12*, 127–135.

Mooi, F.R., Van Loo, I.H., and King, A.J. (2001). Adaptation of Bordetella pertussis to vaccination: a cause for its reemergence? Emerg. Infect. Dis. *7*, 526.

Mooi, F.R., van Loo, I.H.M., van Gent, M., He, Q., Bart, M.J., Heuvelman, K.J., de Greeff, S.C., Diavatopoulos, D., Teunis, P., Nagelkerke, N., et al. (2009). Bordetella pertussis strains with increased toxin production associated with pertussis resurgence. Emerg. Infect. Dis. *15*, 1206–1213.

Moreno Lopez, M. (1990). [The genus Bordetella. By Manuel Moreno Lopez, 1952]. Enferm. Infecc. Microbiol. Clin. *8*, 480–485.

Morova, J., Osicka, R., Masin, J., and Sebo, P. (2008). RTX cytotoxins recognize beta2 integrin receptors through N-linked oligosaccharides. Proc. Natl. Acad. Sci. U. S. A. *105*, 5355–5360.

Morse, S.I., and Morse, J.H. (1976). Isolation and properties of the leukocytosis- and lymphocytosis-promoting factor of Bordetella pertussis. J. Exp. Med. *143*, 1483–1502.

Mouallem, M., Farfel, Z., and Hanski, E. (1990). Bordetella pertussis adenylate cyclase toxin: intoxication of host cells by bacterial invasion. Infect. Immun. *58*, 3759–3764.

Moya, M., Dautry-Varsat, A., Goud, B., Louvard, D., and Boquet, P. (1985). Inhibition of coated pit formation in Hep2 cells blocks the cytotoxicity of diphtheria toxin but not that of ricin toxin. J. Cell Biol. *101*, 548.

Munier, H., Gilles, A.M., Glaser, P., Krin, E., Danchin, A., Sarfati, R., and Barzu, O. (1991). Isolation and characterization of catalytic and calmodulin-binding domains of Bordetella pertussis adenylate cyclase. Eur. J. Biochem. *196*, 469–474.

Munier, H., Bouhss, A., Krin, E., Danchin, A., Gilles, A.M., Glaser, P., and Barzu, O. (1992). The role of histidine 63 in the catalytic mechanism of Bordetella pertussis adenylate cyclase. J. Biol. Chem. *267*, 9816–9820.

Munoz, J.J., Arai, H., Bergman, R.K., and Sadowski, P.L. (1981). Biological activities of crystalline pertussigen from Bordetella pertussis. Infect. Immun. *33*, 820–826.

Munoz, J.J., Peacock, M.G., and Hadlow, W.J. (1987). Anaphylaxis or so-called encephalopathy in mice sensitized to an antigen with the aid of pertussigen (pertussis toxin). Infect. Immun. *55*, 1004–1008.

Musser, J.M., Hewlett, E.L., Peppler, M.S., and Selander, R.K. (1986). Genetic diversity and relationships in populations of Bordetella spp. J. Bacteriol. *166*, 230–237.

N

Naglich, J.G., Metherall, J.E., Russell, D.W., and Eidels, L. (1992). Expression cloning of a diphtheria toxin receptor: Identity with a heparin-binding EGF-like growth factor precursor. Cell *69*, 1051–1061.

Nakai, T., Sawata, A., and Kume, K. (1985). Intracellular locations of dermonecrotic toxins in Pasteurella multocida and in Bordetella bronchiseptica. Am. J. Vet. Res. *46*, 870–874.

Nakase, Y., Tateishi, M., Sekiya, K., and Kasuga, T. (1970). Chemical and biological properties of the purified O antigen of Bordetella pertussis. Jpn. J. Microbiol. *14*, 1–8.

Nasso, M., Fedele, G., Spensieri, F., Palazzo, R., Costantino, P., Rappuoli, R., and Ausiello, C.M. (2009). Genetically detoxified pertussis toxin induces Th1/Th17 immune response through MAPKs and IL-10-dependent mechanisms. J. Immunol. Baltim. Md 1950 *183*, 1892–1899.

Needham, P.G., and Brodsky, J.L. (2013). How early studies on secreted and membrane protein quality control gave rise to the ER associated degradation (ERAD) pathway: the early history of ERAD. Biochim. Biophys. Acta *1833*, 2447–2457.

Neupert, W., and Brunner, M. (2002). The protein import motor of mitochondria. Nat. Rev. Mol. Cell Biol. *3*, 555–565.

Nguyen, L.T., Haney, E.F., and Vogel, H.J. (2011). The expanding scope of antimicrobial peptide structures and their modes of action. Trends Biotechnol. *29*, 464–472.

Nicaud, J.M., Mackman, N., Gray, L., and Holland, I.B. (1985). Characterisation of HlyC and mechanism of activation and secretion of haemolysin from E. coli 2001. FEBS Lett. *187*, 339–344.

Notredame, C., Higgins, D.G., and Heringa, J. (2000). T-coffee: a novel method for fast and accurate multiple sequence alignment 1 1Edited by J. Thornton. J. Mol. Biol. *302*, 205–217.

Novotny, P., Chubb, A.P., Cownley, K., and Montaraz, J.A. (1985). Adenylate cyclase activity of a 68,000-molecular-weight protein isolated from the outer membrane of Bordetella bronchiseptica. Infect. Immun. *50*, 199–206.

O

O'Brien, D.P., Hernandez, B., Durand, D., Hourdel, V., Sotomayor-Pérez, A.-C., Vachette, P., Ghomi, M., Chamot-Rooke, J., Ladant, D., Brier, S., et al. (2015). Structural models of intrinsically disordered and calcium-bound folded states of a protein adapted for secretion. Sci. Rep. *5*, 14223–14223.

O'Brien, D.P., Durand, D., Voegele, A., Hourdel, V., Davi, M., Chamot-Rooke, J., Vachette, P., Brier, S., Ladant, D., and Chenal, A. (2017). Calmodulin fishing with a structurally disordered bait triggers CyaA catalysis. PLoS Biol. *15*, e2004486.

O'Brien, D.P., Perez, A.C.S., Karst, J., Cannella, S.E., Enguene, V.Y.N., Hessel, A., Raoux-Barbot, D., Voegele, A., Subrini, O., Davi, M., et al. (2018). Calcium-dependent disorder-to-order transitions are central to the secretion and folding of the CyaA toxin of Bordetella pertussis, the causative agent of whooping cough. Toxicon Off. J. Int. Soc. Toxinology *149*, 37–44.

Oldenburg, D.J., Gross, M.K., Wong, C.S., and Storm, D.R. (1992). High-affinity calmodulin binding is required for the rapid entry of Bordetella pertussis adenylyl cyclase into neuroblastoma cells. Biochemistry. *31*, 8884–8891.

Oliver, D.C., and Fernandez, R.C. (2001). Antibodies to BrkA augment killing of Bordetella pertussis. Vaccine *20*, 235–241.

Oliver, D.C., Huang, G., and Fernandez, R.C. (2003). Identification of secretion determinants of the Bordetella pertussis BrkA autotransporter. J. Bacteriol. *185*, 489–495.

Olson, M.G., Goldammer, M., Gauliard, E., Ladant, D., and Ouellette, S.P. (2018). A Bacterial Adenylate Cyclase-Based Two-Hybrid System Compatible with Gateway((R)) Cloning. Methods Mol. Biol. Clifton NJ *1794*, 75–96.

O'Neal, C.J., Jobling, M.G., Holmes, R.K., and Hol, W.G.J. (2005). Structural basis for the activation of cholera toxin by human ARF6-GTP. Science *309*, 1093–1096.

Oropeza-Wekerle, R.L., Muller, S., Briand, J.P., Benz, R., Schmid, A., and Goebel, W. (1992). Haemolysin-derived synthetic peptides with pore-forming and haemolytic activity. Mol. Microbiol. *6*, 115–121.

Osicka, R., Osickova, A., Basar, T., Guermonprez, P., Rojas, M., Leclerc, C., and Sebo, P. (2000). Delivery of CD8(+) T-cell epitopes into major histocompatibility complex class I antigen presentation pathway by Bordetella pertussis adenylate cyclase: delineation of cell invasive structures and permissive insertion sites. Infect. Immun. *68*, 247–256.

Osickova, A., Osicka, R., Maier, E., Benz, R., and Sebo, P. (1999). An amphipathic alpha-helix including glutamates 509 and 516 is crucial for membrane translocation of adenylate cyclase toxin and modulates formation and cation selectivity of its membrane channels. J. Biol. Chem. *274*, 37644–37650.

Osickova, A., Masin, J., Fayolle, C., Krusek, J., Basler, M., Pospisilova, E., Leclerc, C., Osicka, R., and Sebo, P. (2010). Adenylate cyclase toxin translocates across target cell membrane without forming a pore. Mol. Microbiol. *75*, 1550–1562.

Ostrowski, M., Porowinska, D., Prochnicki, T., Prevost, M., Raynal, B., Baron, B., Sauguet, L., Corringer, P.-J., and Faure, G. (2016). Neurotoxic phospholipase A2 from rattlesnake as a new ligand and new regulator of prokaryotic receptor GLIC (proton-gated ion channel from G. violaceus). Toxicon Off. J. Int. Soc. Toxinology *116*, 63–71.

Otero, A.S., Yi, X.B., Gray, M.C., Szabo, G., and Hewlett, E.L. (1995). Membrane depolarization prevents cell invasion by Bordetella pertussis adenylate cyclase toxin. J. Biol. Chem. *270*, 9695–9697.

Otto, T., Lummen, G., Kalble, T., Recker, F., Krege, S., Bex, A., Noll, F., and Rubben, H. (1999). Intravesical therapy with pertussis toxin before radical cystectomy in patients with bladder cancer: a Phase I study. Urology *54*, 458–460.

P

Paddock, C.D., Sanden, G.N., Cherry, J.D., Gal, A.A., Langston, C., Tatti, K.M., Wu, K.-H., Goldsmith, C.S., Greer, P.W., Montague, J.L., et al. (2008). Pathology and pathogenesis of fatal Bordetella pertussis infection in infants. Clin. Infect. Dis. Off. Publ. Infect. Dis. Soc. Am. *47*, 328–338.

Parkhill, J., Sebaihia, M., Preston, A., Murphy, L.D., Thomson, N., Harris, D.E., Holden, M.T.G., Churcher, C.M., Bentley, S.D., Mungall, K.L., et al. (2003). Comparative analysis of the genome sequences of Bordetella pertussis, Bordetella parapertussis and Bordetella bronchiseptica. Nat. Genet. *35*, 32–40.

Parkinson, J.S., and Kofoid, E.C. (1992). Communication modules in bacterial signaling proteins. Annu. Rev. Genet. *26*, 71–112.

Parton, R. (1985). Effect of prednisolone on the toxicity of Bordetella pertussis for mice. J. Med. Microbiol. *19*, 391–400.

Passerini de Rossi, B.N., Friedman, L.E., González Flecha, F.L., Castello, P.R., Franco, M.A., and Rossi, J.P.F.. (1999). Identification of Bordetella pertussis virulence-associated outer membrane proteins. FEMS Microbiol. Lett. *172*, 9–13.

Peppler, M.S. (1984). Two physically and serologically distinct lipopolysaccharide profiles in strains of Bordetella pertussis and their phenotype variants. Infect. Immun. *43*, 224–232.

Perraud, A.L., Weiss, V., and Gross, R. (1999). Signalling pathways in two-component phosphorelay systems. Trends Microbiol. *7*, 115–120.

Pilon, M., Schekman, R., and Römisch, K. (1997). Sec61p mediates export of a misfolded secretory protein from the endoplasmic reticulum to the cytosol for degradation. EMBO J. *16*, 4540–4548.

Pittet, L.F., Emonet, S., Schrenzel, J., Siegrist, C.-A., and Posfay-Barbe, K.M. (2014). Bordetella holmesii: an under-recognised Bordetella species. Lancet Infect. Dis. *14*, 510–519.

Pittman, M. (1979). Pertussis toxin: the cause of the harmful effects and prolonged immunity of whooping cough. A hypothesis. Rev. Infect. Dis. *1*, 401–412.

Pittman, M., and Wardlaw, A.C. (1981). The Genus Bordetella. In The Prokaryotes: A Handbook on Habitats, Isolation, and Identification of Bacteria, M.P. Starr, H. Stolp, H.G. Trüper, A. Balows, and H.G. Schlegel, eds. (Berlin, Heidelberg: Springer Berlin Heidelberg), pp. 1075–1085.

Plaut, R.D., and Carbonetti, N.H. (2008). Retrograde transport of pertussis toxin in the mammalian cell. Cell. Microbiol. *10*, 1130–1139.

Porter, J.F., Connor, K., and Donachie, W. (1994). Isolation and characterization of Bordetella parapertussis-like bacteria from ovine lungs. Microbiol. Read. Engl. *140 (Pt 2)*, 255–261.

Porter, J.F., Connor, K., and Donachie, W. (1996). Differentiation between human and ovine isolates of Bordetella parapertussis using pulsed-field gel electrophoresis. FEMS Microbiol. Lett. *135*, 131–135.

Poulain, B., Popoff, M.R., and Molgo, J. (2008). How do the Botulinum Neurotoxins block neurotransmitter release: from botulism to the molecular mechanism of action. Botulinum J. *1*, 14–87.

Powthongchin, B., and Angsuthanasombat, C. (2009). Effects on haemolytic activity of single proline substitutions in the Bordetella pertussis CyaA pore-forming fragment. Arch. Microbiol. *191*, 1–9.

Prangkio, P., Juntapremjit, S., Koehler, M., Hinterdorfer, P., and Angsuthanasombat, C. (2018). Contributions of the Hydrophobic Helix 2 of the Bordetella pertussis CyaA-hemolysin to Membrane Permeabilization. Protein Pept. Lett. *25*, 236–243.

Prasad, S.M., Yin, Y., Rodzinski, E., Tuomanen, E.I., and Masure, H.R. (1993). Identification of a carbohydrate recognition domain in filamentous hemagglutinin from Bordetella pertussis. Infect. Immun. *61*, 2780–2785.

Preville, X., Ladant, D., Timmerman, B., and Leclerc, C. (2005). Eradication of established tumors by vaccination with recombinant Bordetella pertussis adenylate cyclase carrying the human papillomavirus 16 E7 oncoprotein. Cancer Res. *65*, 641–649.

R

Rainey, G.J.A., Wigelsworth, D.J., Ryan, P.L., Scobie, H.M., Collier, R.J., and Young, J.A.T. (2005). Receptor-specific requirements for anthrax toxin delivery into cells. Proc. Natl. Acad. Sci. U. S. A. *102*, 13278.

Rambow, A.A., Fernandez, R.C., and Weiss, A.A. (1998). Characterization of BrkA expression in Bordetella bronchiseptica. Infect. Immun. *66*, 3978–3980.

Ratts, R., Zeng, H., Berg, E.A., Blue, C., McComb, M.E., Costello, C.E., vanderSpek, J.C., and Murphy, J.R. (2003). The cytosolic entry of diphtheria toxin catalytic domain requires a host cell cytosolic translocation factor complex. J. Cell Biol. *160*, 1139.

Ratts, R., Trujillo, C., Bharti, A., vanderSpek, J., Harrison, R., and Murphy, J.R. (2005). A conserved motif in transmembrane helix 1 of diphtheria toxin mediates catalytic domain delivery to the cytosol. Proc. Natl. Acad. Sci. *102*, 15635.

Ray, A., Redhead, K., Selkirk, S., and Poole, S. (1991). Variability in LPS composition, antigenicity and reactogenicity of phase variants of Bordetella pertussis. FEMS Microbiol. Lett. *63*, 211–217.

Reddy, K.V.R., Yedery, R.D., and Aranha, C. (2004). Antimicrobial peptides: premises and promises. Int. J. Antimicrob. Agents *24*, 536–547.

Reig, N., and van der Goot, F.G. (2006). About lipids and toxins. Lipidome Dis. *580*, 5572–5579.

Relman, D., Tuomanen, E., Falkow, S., Golenbock, D.T., Saukkonen, K., and Wright, S.D. (1990). Recognition of a bacterial adhesion by an integrin: macrophage CR3 (alpha M beta 2, CD11b/CD18) binds filamentous hemagglutinin of Bordetella pertussis. Cell *61*, 1375–1382.

Rhodes, C.R., Gray, M.C., Watson, J.M., Muratore, T.L., Kim, S.B., Hewlett, E.L., and Grisham, C.M. (2001). Structural consequences of divalent metal binding by the adenylyl cyclase toxin of Bordetella pertussis. Arch. Biochem. Biophys. *395*, 169–176.

Roderova, J., Osickova, A., Sukova, A., Mikusova, G., Fiser, R., Sebo, P., Osicka, R., and Masin, J. (2019). Residues 529 to 549 participate in membrane penetration and pore-forming activity of the Bordetella adenylate cyclase toxin. Sci. Rep. *9*, 5758.

Rodgers, L., Martin, S.W., Cohn, A., Budd, J., Marcon, M., Terranella, A., Mandal, S., Salamon, D., Leber, A., Tondella, M.-L., et al. (2013). Epidemiologic and laboratory features of a large outbreak of pertussis-like illnesses associated with cocirculating Bordetella holmesii and Bordetella pertussis--Ohio, 2010-2011. Clin. Infect. Dis. Off. Publ. Infect. Dis. Soc. Am. *56*, 322–331.

Rogel, A., and Hanski, E. (1992). Distinct steps in the penetration of adenylate cyclase toxin of Bordetella pertussis into sheep erythrocytes. Translocation of the toxin across the membrane. J. Biol. Chem. *267*, 22599–22605.

Rogel, A., Schultz, J.E., Brownlie, R.M., Coote, J.G., Parton, R., and Hanski, E. (1989). Bordetella pertussis adenylate cyclase: purification and characterization of the toxic form of the enzyme. EMBO J. *8*, 2755–2760.

Rogel, A., Meller, R., and Hanski, E. (1991). Adenylate cyclase toxin from Bordetella pertussis. The relationship between induction of cAMP and hemolysis. J. Biol. Chem. *266*, 3154–3161.

Ropele, M., and Menestrina, G. (1989). Electrical properties and molecular architecture of the channel formed by Escherichia coli hemolysin in planar lipid membranes. Biochim. Biophys. Acta *985*, 9–18.

Rose, T., Sebo, P., Bellalou, J., and Ladant, D. (1995). Interaction of calcium with Bordetella pertussis adenylate cyclase toxin. Characterization of multiple calcium-binding sites and calcium-induced conformational changes. J. Biol. Chem. *270*, 26370–26376.

Rosenthal, R.S., Nogami, W., Cookson, B.T., Goldman, W.E., and Folkening, W.J. (1987). Major fragment of soluble peptidoglycan released from growing Bordetella pertussis is tracheal cytotoxin. Infect. Immun. *55*, 2117–2120.

Rossi Paccani, S., Benagiano, M., Capitani, N., Zornetta, I., Ladant, D., Montecucco, C., D'Elios, M.M., and Baldari, C.T. (2009). The adenylate cyclase toxins of Bacillus anthracis and Bordetella pertussis promote Th2 cell development by shaping T cell antigen receptor signaling. PLoS Pathog. *5*, e1000325.

Rydberg, H.A., Matson, M., Åmand, H.L., Esbjörner, E.K., and Nordén, B. (2012). Effects of Tryptophan Content and Backbone Spacing on the Uptake Efficiency of Cell-Penetrating Peptides. Biochemistry. *51*, 5531–5539.

S

Sakamoto, H., Bellalou, J., Sebo, P., and Ladant, D. (1992). Bordetella pertussis adenylate cyclase toxin. Structural and functional independence of the catalytic and hemolytic activities. J. Biol. Chem. *267*, 13598–13602.

Sandvig, K., Skotland, T., van Deurs, B., and Klokk, T.I. (2013). Retrograde transport of protein toxins through the Golgi apparatus. Histochem. Cell Biol. *140*, 317–326.

Saron, M.F., Fayolle, C., Sebo, P., Ladant, D., Ullmann, A., and Leclerc, C. (1997). Anti-viral protection conferred by recombinant adenylate cyclase toxins from Bordetella pertussis carrying a CD8+ T cell epitope from lymphocytic choriomeningitis virus. Proc. Natl. Acad. Sci. U. S. A. *94*, 3314–3319.

Saukkonen, K., Burnette, W.N., Mar, V.L., Masure, H.R., and Tuomanen, E.I. (1992). Pertussis toxin has eukaryotic-like carbohydrate recognition domains. Proc. Natl. Acad. Sci. U. S. A. *89*, 118–122.

Scarlato, V., Arico, B., Prugnola, A., and Rappuoli, R. (1991). Sequential activation and environmental regulation of virulence genes in Bordetella pertussis. EMBO J. *10*, 3971–3975.

Scheller, E.V., and Cotter, P.A. (2015). Bordetella filamentous hemagglutinin and fimbriae: critical adhesins with unrealized vaccine potential. Pathog. Dis. *73*, ftv079.

Scheller, E.V., Melvin, J.A., Sheets, A.J., and Cotter, P.A. (2015). Cooperative Roles for Fimbria and Filamentous Hemagglutinin in Bordetella Adherence and Immune Modulation. mBio *6*, e00500-15.

Schlecht, G., Loucka, J., Najar, H., Sebo, P., and Leclerc, C. (2004). Antigen targeting to CD11b allows efficient presentation of CD4+ and CD8+ T cell epitopes and in vivo Th1-polarized T cell priming. J. Immunol. Baltim. Md 1950 *173*, 6089–6097.

Schmidt, G., Goehring, U.M., Schirmer, J., Lerm, M., and Aktories, K. (1999). Identification of the C-terminal part of Bordetella dermonecrotic toxin as a transglutaminase for rho GTPases. J. Biol. Chem. *274*, 31875–31881.

Schmidt, N., Mishra, A., Lai, G.H., and Wong, G.C.L. (2010). Arginine-rich cell-penetrating peptides. FEBS Lett. *584*, 1806–1813.

Scobie, H.M., Rainey, G.J.A., Bradley, K.A., and Young, J.A.T. (2003). Human capillary morphogenesis protein 2 functions as an anthrax toxin receptor. Proc. Natl. Acad. Sci. *100*, 5170.

Sealey, K.L., Belcher, T., and Preston, A. (2016). Bordetella pertussis epidemiology and evolution in the light of pertussis resurgence. Infect. Genet. Evol. *40*, 136–143.

Sebaihia, M., Preston, A., Maskell, D.J., Kuzmiak, H., Connell, T.D., King, N.D., Orndorff, P.E., Miyamoto, D.M., Thomson, N.R., Harris, D., et al. (2006). Comparison of the genome sequence of the poultry pathogen Bordetella avium with those of B. bronchiseptica, B. pertussis, and B. parapertussis reveals extensive diversity in surface structures associated with host interaction. J. Bacteriol. *188*, 6002–6015.

Sebo, P., and Ladant, D. (1993). Repeat sequences in the Bordetella pertussis adenylate cyclase toxin can be recognized as alternative carboxy-proximal secretion signals by the Escherichia coli alpha-haemolysin translocator. Mol. Microbiol. *9*, 999–1009.

Sebo, P., Glaser, P., Sakamoto, H., and Ullmann, A. (1991). High-level synthesis of active adenylate cyclase toxin of Bordetella pertussis in a reconstructed Escherichia coli system. Gene *104*, 19–24.

Sebo, P., Fayolle, C., d'Andria, O., Ladant, D., Leclerc, C., and Ullmann, A. (1995). Cell-invasive activity of epitope-tagged adenylate cyclase of Bordetella pertussis allows in vitro presentation of a foreign epitope to CD8+ cytotoxic T cells. Infect. Immun. *63*, 3851–3857.

Selwa, E., Laine, E., and Malliavin, T.E. (2012). Differential role of calmodulin and calcium ions in the stabilization of the catalytic domain of adenyl cyclase CyaA from Bordetella pertussis. Proteins *80*, 1028–1040.

Selwa, E., Davi, M., Chenal, A., Sotomayor-Perez, A.-C., Ladant, D., and Malliavin, T.E. (2014). Allosteric activation of Bordetella pertussis adenylyl cyclase by calmodulin: molecular dynamics and mutagenesis studies. J. Biol. Chem. *289*, 21131–21141.

Shen, Y., Lee, Y.-S., Soelaiman, S., Bergson, P., Lu, D., Chen, A., Beckingham, K., Grabarek, Z., Mrksich, M., and Tang, W.-J. (2002). Physiological calcium concentrations regulate calmodulin binding and catalysis of adenylyl cyclase exotoxins. EMBO J. *21*, 6721–6732.

Shen, Y., Zhukovskaya, N.L., Zimmer, M.I., Soelaiman, S., Bergson, P., Wang, C.-R., Gibbs, C.S., and Tang, W.-J. (2004). Selective inhibition of anthrax edema factor by adefovir, a drug for chronic hepatitis B virus infection. Proc. Natl. Acad. Sci. *101*, 3242–3247.

Shen, Y., Zhukovskaya, N.L., Guo, Q., Florian, J., and Tang, W.-J. (2005). Calcium-independent calmodulin binding and two-metal-ion catalytic mechanism of anthrax edema factor. EMBO J. *24*, 929–941.

Shen, Y., Maupetit, J., Derreumaux, P., and Tufféry, P. (2014). Improved PEP-FOLD Approach for Peptide and Miniprotein Structure Prediction. J. Chem. Theory Comput. *10*, 4745–4758.

Simmons, D.G., Rose, L.P., and Gray, J.G. (1980). Some Physical, Biochemic, and Pathologic Properties of Alcaligenes faecalis, the Bacterium Causing Rhinotracheitis (Coryza) in Turkey Poults. Avian Dis. *24*, 82–90.

Sixma, T.K., Kalk, K.H., van Zanten, B.A., Dauter, Z., Kingma, J., Witholt, B., and Hol, W.G. (1993). Refined structure of Escherichia coli heat-labile enterotoxin, a close relative of cholera toxin. J. Mol. Biol. *230*, 890–918.

Skinner, J.A., Reissinger, A., Shen, H., and Yuk, M.H. (2004). Bordetella type III secretion and adenylate cyclase toxin synergize to drive dendritic cells into a semimature state. J. Immunol. Baltim. Md 1950 *173*, 1934–1940.

Smith, A.M., Guzman, C.A., and Walker, M.J. (2001). The virulence factors of Bordetella pertussis: a matter of control. FEMS Microbiol. Rev. *25*, 309–333.

Smith, M.H., Ploegh, H.L., and Weissman, J.S. (2011). Road to Ruin: Targeting Proteins for Degradation in the Endoplasmic Reticulum. Science *334*, 1086.

Sory, M.P., and Cornelis, G.R. (1994). Translocation of a hybrid YopE-adenylate cyclase from Yersinia enterocolitica into HeLa cells. Mol. Microbiol. *14*, 583–594.

Sory, M.P., Boland, A., Lambermont, I., and Cornelis, G.R. (1995). Identification of the YopE and YopH domains required for secretion and internalization into the cytosol of macrophages, using the cyaA gene fusion approach. Proc. Natl. Acad. Sci. U. S. A. *92*, 11998–12002.

Sotomayor Perez, A.-C., Karst, J.C., Davi, M., Guijarro, J.I., Ladant, D., and Chenal, A. (2010). Characterization of the regions involved in the calcium-induced folding of the intrinsically disordered RTX motifs from the bordetella pertussis adenylate cyclase toxin. J. Mol. Biol. *397*, 534–549.

Sotomayor-Perez, A.C., Ladant, D., and Chenal, A. (2011). Calcium-induced folding of intrinsically disordered repeat-in-toxin (RTX) motifs via changes of protein charges and oligomerization states. J. Biol. Chem. *286*, 16997–17004.

Sotomayor-Perez, A.C., Karst, J.C., Ladant, D., and Chenal, A. (2012). Mean net charge of intrinsically disordered proteins: experimental determination of protein valence by electrophoretic mobility measurements. Methods Mol. Biol. Clifton NJ *896*, 331–349.

Sotomayor-Perez, A.-C., Ladant, D., and Chenal, A. (2014). Disorder-to-order transition in the CyaA toxin RTX domain: implications for toxin secretion. Toxins *7*, 1–20.

Sousa, R., and Lafer, E.M. (2006). Keep the traffic moving: mechanism of the Hsp70 motor. Traffic Cph. Den. *7*, 1596–1603.

Spensieri, F., Fedele, G., Fazio, C., Nasso, M., Stefanelli, P., Mastrantonio, P., and Ausiello, C.M. (2006). Bordetella pertussis inhibition of interleukin-12 (IL-12) p70 in human monocyte-derived dendritic cells blocks IL-12 p35 through adenylate cyclase toxin-dependent cyclic AMP induction. Infect. Immun. *74*, 2831–2838.

Spilker, T., Liwienski, A.A., and LiPuma, J.J. (2008). Identification of Bordetella spp. in respiratory specimens from individuals with cystic fibrosis. Clin. Microbiol. Infect. Off. Publ. Eur. Soc. Clin. Microbiol. Infect. Dis. *14*, 504–506.

Spilker, T., Leber, A.L., Marcon, M.J., Newton, D.W., Darrah, R., Vandamme, P., and Lipuma, J.J. (2014). A simplified sequence-based identification scheme for Bordetella reveals several putative novel species. J. Clin. Microbiol. *52*, 674–677.

Stanley, P., Packman, L.C., Koronakis, V., and Hughes, C. (1994). Fatty acylation of two internal lysine residues required for the toxic activity of Escherichia coli hemolysin. Science *266*, 1992–1996.

Stark, D., Riley, L., Harkness, J., and Marriott, D. (2007). Bordetella petrii from a clinical sample in Australia: isolation and molecular identification. J. Med. Microbiol. *56*, 435—437.

Stefanelli, P., Fazio, C., Fedele, G., Spensieri, F., Ausiello, C.M., and Mastrantonio, P. (2009). A natural pertactin deficient strain of Bordetella pertussis shows improved entry in human monocyte-derived dendritic cells. New Microbiol. *32*, 159.

Steffen, P., Goyard, S., and Ullmann, A. (1996). Phosphorylated BvgA is sufficient for transcriptional activation of virulence-regulated genes in Bordetella pertussis. EMBO J. *15*, 102–109.

Stein, P.E., Boodhoo, A., Armstrong, G.D., Heerze, L.D., Cockle, S.A., Klein, M.H., and Read, R.J. (1994). Structure of a pertussis toxin–sugar complex as a model for receptor binding. Nat. Struct. Biol. *1*, 591–596.

Steven, A.C., Bisher, M.E., Trus, B.L., Thomas, D., Zhang, J.M., and Cowell, J.L. (1986). Helical structure of Bordetella pertussis fimbriae. J. Bacteriol. *167*, 968–974.

Stibitz, S., and Yang, M.-S. (1991). Subcellular localization and immunological detection of proteins encoded by the vir locus of Bordetella pertussis. J. Bacteriol. *173*, 4288–4296.

Strnad, C.F., and Carchman, R.A. (1987). Human T lymphocyte mitogenesis in response to the B oligomer of pertussis toxin is associated with an early elevation in cytosolic calcium concentrations. FEBS Lett. *225*, 16–20.

Subrini, O., Sotomayor-Perez, A.-C., Hessel, A., Spiaczka-Karst, J., Selwa, E., Sapay, N., Veneziano, R., Pansieri, J., Chopineau, J., Ladant, D., et al. (2013). Characterization of a membrane-active peptide from the Bordetella pertussis CyaA toxin. J. Biol. Chem. *288*, 32585–32598.

Sun, J. (2012). Roles of cellular redox factors in pathogen and toxin entry in the endocytic pathways. In Molecular Regulation of Endocytosis, (IntechOpen).

Swann, M.J., Peel, L.L., Carrington, S., and Freeman, N.J. (2004). Dual-polarization interferometry: an analytical technique to measure changes in protein structure in real time, to determine the stoichiometry of binding events, and to differentiate between specific and nonspecific interactions. Anal. Biochem. *329*, 190–198.

Syed, M.A., Jamil, B., and Bokhari, H. (2016). Shattering a myth - Whooping cough susceptible to antibiotics. Pak. J. Pharm. Sci. *29*, 985–990.

Szabo, G., Gray, M.C., and Hewlett, E.L. (1994). Adenylate cyclase toxin from Bordetella pertussis produces ion conductance across artificial lipid bilayers in a calcium- and polarity-dependent manner. J. Biol. Chem. *269*, 22496–22499.

T

Tamura, M., Nogimori, K., Murai, S., Yajima, M., Ito, K., Katada, T., Ui, M., and Ishii, S. (1982). Subunit structure of islet-activating protein, pertussis toxin, in conformity with the A-B model. Biochemistry. *21*, 5516–5522.

Tang, Y.W., Hopkins, M.K., Kolbert, C.P., Hartley, P.A., Severance, P.J., and Persing, D.H. (1998). Bordetella holmesii-like organisms associated with septicemia, endocarditis, and respiratory failure. Clin. Infect. Dis. Off. Publ. Infect. Dis. Soc. Am. *26*, 389–392.

Taranger, J., Trollfors, B., Bergfors, E., Knutsson, N., Lagergard, T., Schneerson, R., and Robbins, J.B. (2001). Immunologic and epidemiologic experience of vaccination with a monocomponent pertussis toxoid vaccine. Pediatrics *108*, E115.

Tatti, K.M., Wu, K.-H., Sanden, G.N., Greer, P., Sumner, J., Guarner, J., Paddock, C.D., and Zaki, S.R. (2006). Molecular Diagnosis of Bordetella pertussis Infection by Evaluation of Formalin-Fixed Tissue Specimens. J. Clin. Microbiol. *44*, 1074.

Taylor, M., Navarro-Garcia, F., Huerta, J., Burress, H., Massey, S., Ireton, K., and Teter, K. (2010). Hsp90 is required for transfer of the cholera toxin A1 subunit from the endoplasmic reticulum to the cytosol. J. Biol. Chem. *285*, 31261–31267.

Tazato, N., Handa, Y., Nishijima, M., Kigawa, R., Sano, C., and Sugiyama, J. (2015). Novel environmental species isolated from the plaster wall surface of mural paintings in the Takamatsuzuka tumulus: Bordetella muralis sp. nov., Bordetella tumulicola sp. nov. and Bordetella tumbae sp. nov. Int. J. Syst. Evol. Microbiol. *65*, 4830–4838.

Teter, K. (2013). Toxin instability and its role in toxin translocation from the endoplasmic reticulum to the cytosol. Biomolecules *3*, 997–1029.

Thamwiriyasati, N., Powthongchin, B., Kittiworakarn, J., Katzenmeier, G., and Angsuthanasombat, C. (2010). Esterase activity of Bordetella pertussis CyaC-acyltransferase against synthetic substrates: implications for catalytic mechanism in vivo. FEMS Microbiol. Lett. *304*, 183–190.

Thanabalu, T., Koronakis, E., Hughes, C., and Koronakis, V. (1998). Substrate-induced assembly of a contiguous channel for protein export from E.coli: reversible bridging of an inner-membrane translocase to an outer membrane exit pore. EMBO J. *17*, 6487–6496.

Thierry-Carstensen, B., Dalby, T., Stevner, M.A., Robbins, J.B., Schneerson, R., and Trollfors, B. (2013). Experience with monocomponent acellular pertussis combination vaccines for infants, children, adolescents and adults—A review of safety, immunogenicity, efficacy and effectiveness studies and 15 years of field experience. Vaccine *31*, 5178–5191.

Torgersen, M.L., Skretting, G., van Deurs, B., and Sandvig, K. (2001). Internalization of cholera toxin by different endocytic mechanisms. J. Cell Sci. *114*, 3737–3747.

Trent, M.S., Worsham, L.M., and Ernst-Fonberg, M.L. (1999). HlyC, the internal protein acyltransferase that activates hemolysin toxin: role of conserved histidine, serine, and cysteine residues in enzymatic activity as probed by chemical modification and site-directed mutagenesis. Biochemistry. *38*, 3433–3439.

Tsai, B., Rodighiero, C., Lencer, W.I., and Rapoport, T.A. (2001). Protein disulfide isomerase acts as a redox-dependent chaperone to unfold cholera toxin. Cell *104*, 937–948.

Tsuneoka, M., Nakayama, K., Hatsuzawa, K., Komada, M., Kitamura, N., and Mekada, E. (1993). Evidence for involvement of furin in cleavage and activation of diphtheria toxin. J. Biol. Chem. *268*, 26461–26465.

Tuomanen, E., and Weiss, A. (1985). Characterization of two adhesins of Bordetella pertussis for human ciliated respiratory-epithelial cells. J. Infect. Dis. *152*, 118–125.

U

Uhl, M.A., and Miller, J.F. (1994). Autophosphorylation and phosphotransfer in the Bordetella pertussis BvgAS signal transduction cascade. Proc. Natl. Acad. Sci. *91*, 1163–1167.

Uhl, M.A., and Miller, J.F. (1996). Central role of the BvgS receiver as a phosphorylated intermediate in a complex two-component phosphorelay. J. Biol. Chem. *271*, 33176–33180.

Ui, J. (1990). Pertussis toxin as a valuable probe for G-protein involvement in signal transduction. Am. Soc. Microbiol. 45–77.

Ullmann, A., and Danchin, A. (1980). Role of cyclic AMP in regulatory mechanisms in bacteria. Trends Biochem. Sci. *5*, 95–96.

Ullmann, A., Joseph, E., and Danchin, A. (1979). Cyclic AMP as a modulator of polarity in polycistronic transcriptional units. Proc. Natl. Acad. Sci. U. S. A. *76*, 3194–3197.

Ulmer, T.S., Soelaiman, S., Li, S., Klee, C.B., Tang, W.-J., and Bax, A. (2003). Calcium Dependence of the Interaction between Calmodulin and Anthrax Edema Factor. J. Biol. Chem. *278*, 29261–29266.

V

Vandamme, P., Hommez, J., Vancanneyt, M., Monsieurs, M., Hoste, B., Cookson, B., Wirsing von Konig, C.H., Kersters, K., and Blackall, P.J. (1995). Bordetella hinzii sp. nov., isolated from poultry and humans. Int. J. Syst. Bacteriol. *45*, 37–45.

Vandamme, P., Heyndrickx, M., Vancanneyt, M., Hoste, B., De Vos, P., Falsen, E., Kersters, K., and Hinz, K.H. (1996). Bordetella trematum sp. nov., isolated from wounds and ear infections in humans, and reassessment of Alcaligenes denitrificans Ruger and Tan 1983. Int. J. Syst. Bacteriol. *46*, 849–858.

Vandamme, P.A., Peeters, C., Cnockaert, M., Inganas, E., Falsen, E., Moore, E.R.B., Nunes, O.C., Manaia, C.M., Spilker, T., and LiPuma, J.J. (2015). Bordetella bronchialis sp. nov., Bordetella flabilis sp. nov. and Bordetella sputigena sp. nov., isolated from human respiratory specimens, and reclassification of Achromobacter sediminum Zhang et al. 2014 as Verticia sediminum gen. nov., comb. nov. Int. J. Syst. Evol. Microbiol. *65*, 3674–3682.

van der Zee, A., Groenendijk, H., Peeters, M., and Mooi, F.R. (1996). The differentiation of Bordetella parapertussis and Bordetella bronchiseptica from humans and animals as determined by DNA polymorphism mediated by two different insertion sequence elements suggests their phylogenetic relationship. Int. J. Syst. Bacteriol. *46*, 640–647.

van der Zee, A., Mooi, F., Van Embden, J., and Musser, J. (1997). Molecular evolution and host adaptation of Bordetella spp.: phylogenetic analysis using multilocus enzyme electrophoresis and typing with three insertion sequences. J. Bacteriol. *179*, 6609–6617.

van Gent, M., Bart, M.J., van der Heide, H.G.J., Heuvelman, K.J., and Mooi, F.R. (2012). Small Mutations in Bordetella pertussis Are Associated with Selective Sweeps. PLoS ONE *7*, e46407.

Veneziano, R., Rossi, C., Chenal, A., Devoisselle, J.-M., Ladant, D., and Chopineau, J. (2013). Bordetella pertussis adenylate cyclase toxin translocation across a tethered lipid bilayer. Proc. Natl. Acad. Sci. U. S. A. *110*, 20473–20478.

Villarino Romero, R., Osicka, R., and Sebo, P. (2014). Filamentous hemagglutinin of Bordetella pertussis: a key adhesin with immunomodulatory properties? Future Microbiol. *9*, 1339–1360.

Vojtova, J., Kofronova, O., Sebo, P., and Benada, O. (2006). Bordetella adenylate cyclase toxin induces a cascade of morphological changes of sheep erythrocytes and localizes into clusters in erythrocyte membranes. Microsc. Res. Tech. *69*, 119–129.

von Wintzingerode, F., Schattke, A., Siddiqui, R.A., Rosick, U., Gobel, U.B., and Gross, R. (2001). Bordetella petrii sp. nov., isolated from an anaerobic bioreactor, and emended description of the genus Bordetella. Int. J. Syst. Evol. Microbiol. *51*, 1257–1265.

Vougier, S., Mary, J., Dautin, N., Vinh, J., Friguet, B., and Ladant, D. (2004). Essential Role of Methionine Residues in Calmodulin Binding to Bordetella pertussis Adenylate Cyclase, as Probed by Selective Oxidation and Repair by the Peptide Methionine Sulfoxide Reductases. J. Biol. Chem. *279*, 30210–30218.

W

W. C. Rucker (1912). Whooping Cough. Its Nature and Prevention: A Popular Discussion of a Widespread and Dangerous Disease for Which Familiarity Has Bred Contempt. Public Health Rep. 1896-1970 *27*, 1736–1739.

Wagner, W., Kuhn, M., and Goebel, W. (1988). Active and inactive forms of hemolysin (HlyA) from Escherichia coli. Biol. Chem. Hoppe. Seyler *369*, 39–46.

Walker, K.E., and Weiss, A.A. (1994). Characterization of the dermonecrotic toxin in members of the genus Bordetella. Infect. Immun. *62*, 3817–3828.

Wallbrecher, R., Ackels, T., Olea, R.A., Klein, M.J., Caillon, L., Schiller, J., Bovée-Geurts, P.H., van Kuppevelt, T.H., Ulrich, A.S., Spehr, M., et al. (2017). Membrane permeation of arginine-rich cell-penetrating peptides independent of transmembrane potential as a function of lipid composition and membrane fluidity. J. Controlled Release *256*, 68–78.

Walrant, A., Correia, I., Jiao, C.-Y., Lequin, O., Bent, E.H., Goasdoué, N., Lacombe, C., Chassaing, G., Sagan, S., and Alves, I.D. (2011). Different membrane behaviour and cellular uptake of three basic arginine-rich peptides. Biochim. Biophys. Acta BBA - Biomembr. *1808*, 382–393.

Wandersman, C., and Delepelaire, P. (1990). TolC, an Escherichia coli outer membrane protein required for hemolysin secretion. Proc. Natl. Acad. Sci. U. S. A. *87*, 4776–4780.

Wang, C., Liu, L., Zhang, Z., Yan, Z., Yu, C., Shao, M., Jiang, X., Chi, S., Wei, K., and Zhu, R. (2015a). Immunological and protective effects of Bordetella bronchiseptica subunit vaccines based on the recombinant N-terminal domain of dermonecrotic toxin. Int. Immunopharmacol. *28*, 952–959.

Wang, X., Gray, M.C., Hewlett, E.L., and Maynard, J.A. (2015b). The Bordetella adenylate cyclase repeat-in-toxin (RTX) domain is immunodominant and elicits neutralizing antibodies. J. Biol. Chem. *290*, 3576–3591.

Watanabe, M., Takimoto, H., Kumazawa, Y., and Amano, K. (1990). Biological properties of lipopolysaccharides from Bordetella species. J. Gen. Microbiol. *136*, 489–493.

Weingart, C.L., and Weiss, A.A. (2000). Bordetella pertussis virulence factors affect phagocytosis by human neutrophils. Infect. Immun. *68*, 1735–1739.

Weingart, C.L., Mobberley-Schuman, P.S., Hewlett, E.L., Gray, M.C., and Weiss, A.A. (2000). Neutralizing antibodies to adenylate cyclase toxin promote phagocytosis of Bordetella pertussis by human neutrophils. Infect. Immun. *68*, 7152–7155.

Weiss, A.A., and Goodwin, M.S. (1989). Lethal infection by Bordetella pertussis mutants in the infant mouse model. Infect. Immun. *57*, 3757.

Weiss, A.A., Hewlett, E.L., Myers, G.A., and Falkow, S. (1984). Pertussis toxin and extracytoplasmic adenylate cyclase as virulence factors of Bordetella pertussis. J. Infect. Dis. *150*, 219–222.

Weiss, A.A., Johnson, F.D., and Burns, D.L. (1993). Molecular characterization of an operon required for pertussis toxin secretion. Proc. Natl. Acad. Sci. U. S. A. *90*, 2970–2974.

Welch, R.A. (2001). RTX toxin structure and function: a story of numerous anomalies and few analogies in toxin biology. Curr. Top. Microbiol. Immunol. *257*, 85–111.

Wender, P.A., Mitchell, D.J., Pattabiraman, K., Pelkey, E.T., Steinman, L., and Rothbard, J.B. (2000). The design, synthesis, and evaluation of molecules that enable or enhance cellular uptake: Peptoid molecular transporters. Proc. Natl. Acad. Sci. *97*, 13003.

Westrop, G.D., Hormozi, E.K., Da Costa, N.A., Parton, R., and Coote, J.G. (1996). Bordetella pertussis adenylate cyclase toxin: proCyaA and CyaC proteins synthesised separately in Escherichia coli produce active toxin in vitro. Gene *180*, 91–99.

Weyant, R.S., Hollis, D.G., Weaver, R.E., Amin, M.F., Steigerwalt, A.G., O'Connor, S.P., Whitney, A.M., Daneshvar, M.I., Moss, C.W., and Brenner, D.J. (1995). Bordetella holmesii sp. nov., a new gram-negative species associated with septicemia. J. Clin. Microbiol. *33*, 1–7.

White, D.A. (1973). The phospholipid composition of mammalian tissues. Form Funct. Phospholipids 441–482.

White, S.H., and Wimley, W.C. (1999). Membrane Protein Folding and Stability: Physical Principles. Annu. Rev. Biophys. Biomol. Struct. *28*, 319–365.

Wiertz, E.J., Tortorella, D., Bogyo, M., Yu, J., Mothes, W., Jones, T.R., Rapoport, T.A., and Ploegh, H.L. (1996). Sec61-mediated transfer of a membrane protein from the endoplasmic reticulum to the proteasome for destruction. Nature *384*, 432–438.

Willems, R., Paul, A., van der Heide, H.G., ter Avest, A.R., and Mooi, F.R. (1990). Fimbrial phase variation in Bordetella pertussis: a novel mechanism for transcriptional regulation. EMBO J. *9*, 2803–2809.

Williams, J.M., Inoue, T., Banks, L., and Tsai, B. (2013). The ERdj5-Sel1L complex facilitates cholera toxin retrotranslocation. Mol. Biol. Cell *24*, 785–795.

Williamson, M.P. (1994). The structure and function of proline-rich regions in proteins. Biochem. J. *297*, 249.

Wilson, R., Read, R., Thomas, M., Rutman, A., Harrison, K., Lund, V., Cookson, B., Goldman, W., Lambert, H., and Cole, P. (1991). Effects of Bordetella pertussis infection on human respiratory epithelium in vivo and in vitro. Infect. Immun. *59*, 337–345.

Winkeler, A., Gödderz, D., Herzog, V., and Schmitz, A. (2003). BiP-dependent export of cholera toxin from endoplasmic reticulum-derived microsomes. FEBS Lett. *554*, 439–442.

Witvliet, M.H., Burns, D.L., Brennan, M.J., Poolman, J.T., and Manclark, C.R. (1989). Binding of pertussis toxin to eucaryotic cells and glycoproteins. Infect. Immun. *57*, 3324–3330.

Wolff, J., Cook, G.H., Goldhammer, A.R., and Berkowitz, S.A. (1980). Calmodulin activates prokaryotic adenylate cyclase. Proc. Natl. Acad. Sci. U. S. A. *77*, 3841–3844.

Woolfrey, B.F., and Moody, J.A. (1991). Human infections associated with Bordetella bronchiseptica. Clin. Microbiol. Rev. *4*, 243–255.

World Health Organization (2015). Pertussis vaccines: WHO position paper—August 2015. Wkly. Epidemiol. Rec. Relevé Épidémiologique Hebd. *90*, 433–458.

Worsham, L.M., Trent, M.S., Earls, L., Jolly, C., and Ernst-Fonberg, M.L. (2001). Insights into the catalytic mechanism of HlyC, the internal protein acyltransferase that activates Escherichia coli hemolysin toxin. Biochemistry. *40*, 13607–13616.

X

Xu, Y., and Barbieri, J.T. (1995). Pertussis toxin-mediated ADP-ribosylation of target proteins in Chinese hamster ovary cells involves a vesicle trafficking mechanism. Infect. Immun. *63*, 825–832.

Y

Yahr, T.L., Vallis, A.J., Hancock, M.K., Barbieri, J.T., and Frank, D.W. (1998). ExoY, an adenylate cyclase secreted by the Pseudomonas aeruginosa type III system. Proc. Natl. Acad. Sci. U. S. A. *95*, 13899–13904.

Yeaman, M.R., and Yount, N.Y. (2003). Mechanisms of antimicrobial peptide action and resistance. Pharmacol. Rev. *55*, 27–55.

Yuk, M.H., Heininger, U., Martinez de Tejada, G., and Miller, J.F. (1998). Human but not ovine isolates of Bordetella parapertussis are highly clonal as determined by PCR-based RAPD fingerprinting. Infection *26*, 270–273.

Z

Zaitsev, E.M., Poddubikov, A.V., Britsina, M.V., Mertsalova, N.U., Ozeretskovskaia, M.N., Bazhanova, I.G., and Plekhanova, N.G. (2014). Immunobiological properties of Bordetella pertussis lipopolysaccharide in the acellular pertussis vaccine. Zh. Mikrobiol. Epidemiol. Immunobiol. 20–24.

Zaretzky, F.R., Gray, M.C., and Hewlett, E.L. (2002). Mechanism of association of adenylate cyclase toxin with the surface of Bordetella pertussis: a role for toxin-filamentous haemagglutinin interaction. Mol. Microbiol. *45*, 1589–1598.

Zeddeman, A., Gent, M. van, Heuvelman, C., Heide, H., Bart, M., Advani, A., Hallander, H., Wirsing von Konig, C., Riffelman, M., and Storsaeter, J. (2014). Investigations into the emergence of pertactin-deficient Bordetella pertussis isolates in six European countries, 1996 to 2012.

Zhang, X., Rodriguez, M.E., and Harvill, E.T. (2009a). O antigen allows B. parapertussis to evade B. pertussis vaccine-induced immunity by blocking binding and functions of cross-reactive antibodies. PloS One *4*, e6989.

Zhang, X., Goebel, E.M., Rodriguez, M.E., Preston, A., and Harvill, E.T. (2009b). The O antigen is a critical antigen for the development of a protective immune response to Bordetella parapertussis. Infect. Immun. *77*, 5050–5058.

Zu, T., Manetti, R., Rappuoli, R., and Scarlato, V. (1996). Differential binding of BvgA to two classes of virulence genes of Bordetella pertussis directs promoter selectivity by RNA polymerase. Mol. Microbiol. *21*, 557–565.

Abstract

The adenylate cyclase toxin (CyaA) is one of the major virulence factor produced by *Bordetella pertussis*, the causative agent of whopping cough. CyaA has the unique capacity to translocate its catalytic domain directly across the plasma membrane. Then, the catalytic domain binds to calmodulin (CaM) to produce high levels of cAMP, leading to cell intoxication. Although several models have been proposed, the molecular mechanism and the forces involved in the translocation of CyaA remain elusive. The calcium gradient, the membrane potential across the plasma membrane and post-translational acylation are required for an efficient CyaA translocation. During my PhD, I mainly investigated the translocation process. It has been previously shown that deletion of the translocation region abolishes the delivery of the catalytic domain into the cytosol of target cells. In this region, the peptide P454 (residues 454 to 484 of CyaA) was identified and exhibits membrane-active properties related to antimicrobial peptides, *i.e* membrane interaction, α-helical folding upon membrane insertion and membrane permeabilization. We have investigated the role of P454 on the translocation process. We observed that negatively charged and fluidic membrane favor P454 membrane insertion. The peptide contains two arginine residues that are critically involved in its membrane-active properties. We further identified that P454 exhibits the intrinsic propensity to translocate across lipid bilayers and forms a stable complex with CaM. We identified several residues from P454 involved in both membrane interaction and CaM binding. We showed in the context of the full-length CyaA toxin that these residues are essential for the efficient translocation of the catalytic domain into the cell and production of cAMP. We propose a translocation model in which the membrane-active P454 segment from the translocation region destabilizes the membrane, favoring its translocation. In the cytosol, the P454 segment is trapped by CaM and the formation of the complex may act as a driving force pulling the catalytic domain across the plasma membrane. We further showed that CaM binding to the main CaM-binding site in the catalytic domain induces local and long-range allosteric effects that stabilize the enzymatic site, allowing fast ATP catalysis to cAMP, leading to host subversion. The relevance of these results for the translocation and activation of CyaA are discussed.

Key words: Adenylate cyclase toxin, calmodulin, membrane-active peptide, translocation

Résumé

La toxine adénylcyclase (CyaA) est un des principaux facteurs de virulence produite par *Bordetella pertussis*, l'agent de la coqueluche. CyaA a l'unique capacité de transloquer son domaine catalytique directement à travers la membrane plasmique. Puis le domaine catalytique lie la calmoduline (CaM) pour produire de grandes quantités d'AMPc, conduisant à l'intoxication de la cellule. Bien que plusieurs modèles aient été proposés, le mécanisme moléculaire et les forces impliquées dans la translocation de CyaA restent peu connus. Un gradient de calcium, un potentiel de membrane et des acylations post-traductionnelles sont requis pour la translocation de CyaA. Pendant mon doctorat, je me suis principalement intéressé au processus de translocation. Il a été montré précédemment que la suppression de la région de translocation abolit le passage du domaine catalytique. Dans cette région, le peptide P454 (résidus 454 à 484 de CyaA) a été identifié et montre des propriétés membranaires, *i.e* interaction avec la membrane, repliement en hélice α au contact de la membrane et perméabilisation membranaire. Nous avons étudié le rôle de P454 dans le processus de translocation. Nous avons observé que des lipides fluides et chargés négativement favorisent l'insertion de P454 dans les membranes. Le peptide possède deux arginines qui sont impliquées dans ses activités membranaires. P454 possède aussi la capacité de transloquer à travers la membrane et de former un complexe avec la CaM. Nous avons identifié plusieurs résidus de P454 impliqués dans la liaison à la membrane et la CaM. Dans le contexte de la toxine entière, ces résidus sont essentiels pour la translocation du domaine catalytique et la production d'AMPc. On propose un modèle de translocation dans lequel le segment P454 de la région de translocation déstabilise la membrane, favorisant sa translocation. Dans le cytosol, le segment P454 est piégé par la CaM et le complexe pourrait agir comme une force tirant le domaine catalytique à travers la membrane. Nous avons aussi montré que la liaison à la CaM du peptide liant la CaM dans le domaine catalytique induit des effets allostériques qui stabilisent le site catalytique, permettant la catalyse rapide d'ATP en AMPc. La pertinence de ces résultats pour la translocation et l'activation de CyaA sont discutées.

Mots clés: Toxine adenylate cyclase, calmoduline, propriétés membranaires, translocation